Publié avec le concours
du Ministère de la Recherche
et de la Technologie

PHYSICAL COSMOLOGY

Second "Rencontres de Blois"
Château de Blois, France - August 28 - Sept. 1, 1990

"25th Anniversary of the Cosmic Background Radiation Discovery"
"Physical Cosmology"

ISBN 2-86332-094-7

EDITIONS FRONTIERES
B. P. 33
91192 Gif-sur-Yvette Cedex - France

Printed in Singapore by Fong & Sons Printers Pte Ltd.

PHYSICAL COSMOLOGY

edited by

A. Blanchard
L. Celnikier
M. Lachièze-Rey
J. Trân Thanh Vân

EDITIONS
FRONTIERES

"25th Anniversary of the Cosmic Background Radiation Discovery"
"Physical Cosmology"

International Advisory Committee

Audouze J. *(Paris)*
Fowler W. A. *(Pasadena)*
Longair M. *(Edinburgh)*
Lynden Bell D. *(Cambridge)*
Novikov I. *(Moscow)*
Partridge R. B. *(Haverford)*
Peebles J. *(Princeton)*
Pellat R. *(Palaiseau)*
Rees M. *(Cambridge)*
Reeves H. *(Saclay)*
Salam A. *(Trieste)*
Schatzman E. *(Paris)*
Silk J. *(Berkeley)*
Sunyaev R. *(Moscow)*
Szalay A. *(Budapest)*
Weinberg S. *(Austin)*

International Program Committee

Blanchard A. *(Meudon)*
Bouquet A. *(Paris)*
Celnikier L. *(Meudon)*
da Costa L. *(Rio Janeiro)*
Icke V. *(Leiden)*
Jones B. *(Copenhagen)*
Kunth D. *(Paris)*
Lachièze-Rey M. *(Saclay)*
Linde A. *(Moscow)*
Melchiorri F. *(Rome)*
Peacock J. *(Edinburgh)*
Sanz J. *(Santander)*
Schramm D. *(Chicago)*
Steigman G. *(Columbus)*
Thuân T. X. *(Charlottesville)*
Trân Thanh Vân J. *(Orsay)*
Vittorio N. *(Rome)*
Wilkinson D. *(Princeton)*

Sponsors :

La Commission des Communautés Européennes
Le Ministère de la Recherche et de la Technologie
Le Centre National de la Recherche Scientifique
Le Commissariat à l'Energie Atomique
Le Centre National d'Etudes Spatiales
L'Observatoire de Paris, Meudon

Le Conseil Régional de la Région Centre
Le Conseil Général du Loir-et-Cher
La Ville de Blois

Aérospatiale
Framatome

We aknowledge the help of :

Monsieur Alain Voindrot, Mairie de Blois
Monsieur Jacques Laemle, Mairie de Blois
Monsieur Frank Trouilloud, Mairie de Blois

Madame Martine Tissier de Mallerais, Château de Blois
Monsieur Franck Boitel, Château de Blois

Madame Martine Rebière, Palais des Congrès de Blois
Madame Anne Liny, Palais des Congrès de Blois

Madame Jeanne Lorenzo, Office de Tourisme de Blois

Madame Chantal Balkowski, Meudon

Madame Catherine Cesarsky, Saclay

Monsieur André Rousset, Aérospatiale
Monsieur Patrice de Lanversin, Aérospatiale

Monsieur Pierre Clauzon, Framatome
Monsieur Luc de Rancourt, Framatome

Monsieur Gilbert Cotteau
Monsieur Dominique Lê van Truoc

Monsieur Alain Pasquier
Monsieur Jean Girard

AVANT PROPOS

La Seconde Rencontre de Blois s'est tenue au Château de Blois, du 28 Août au 1er Septembre 1990 ; elle a réuni 175 astrophysiciens venant d'une vingtaine de pays des cinq continents.

La Rencontre avait pour but de faire le point sur les progrès réalisés en Cosmologie Physique depuis la découverte, il y a 25 ans, du rayonnement cosmique fossile par A. Penzias et R. Wilson. Elle a bénéficié des remarquables résultats obtenus par le satellite COBE (Cosmic Background Explorer) lancé en Novembre 1989.

La journée inaugurale a été consacrée à l'histoire de la découverte et à la synthèse des développements de la cosmologie physique des dernières années. Il a été fascinant d'écouter le cheminement de cette découverte et la floraison des idées qui finalement ont conduit à la forme actuelle de la théorie du Big Bang, par les acteurs même de cette avancée extraordinaire : Robert Wilson, Jim Peebles et David Wilkinson.

Le rayonnement cosmique du fond du ciel qui est l'un des témoins les plus directs des conditions primitives de l'Univers a été discuté en détail. De nouveaux résultats, en particulier ceux de COBE qui montrent un spectre parfait du corps noir avec une très grande isotropie, ont été présentés. Ils confirment l'origine cosmologique du rayonnement fossile comme cela est prédit dans la théorie du Big Bang.

L'interconnection entre la cosmologie et la physique des particules est présentée sous l'angle de la nucléosynthèse, de la matière noire et des lentilles gravitationnelles. En particulier, on peut déduire de la nucléosynthèse que le nombre de familles de neutrinos légers dans la nature ne doit pas dépasser 3 : ce qui fut vérifié par des expériences de physique de hautes énergies au CERN à Genève grâce à l'accélérateur de particules "LEP". Comment détecter la matière noire? de quoi est-elle formée? de WIMPS (Weakly Interacting Massive Particles) ou de MACHOS (MAssive Compact Halo Objects) ou d' autres objets plus ou moins exotiques, toutes ces questions ont été longuement débattues.

Le modèle cosmologique standard mène cependant à une énigme : comment concilier l'isotropie apparemment parfaite du rayonnement fossile avec la distribution hétérogène des galaxies ou des amas de galaxies. Des résultats récents concernant les structures à grande échelle ont été obtenus par le satellite IRAS et par des observations optiques, donnant en particulier les positions et les vitesses d'un grand nombre de galaxies. Ces études ont été discutées en relation avec la dynamique de la formation des galaxies et la structure à grande échelle de l'univers.

La diversité des opinions concernant les structures à grande échelle a été largement représentée au colloque et souligne la nécessité de bien comprendre les désaccords entre les résultats des mesures effectuées selon de méthodes différentes.

Une revue des missions spatiales futures a donné un aperçu des sources possibles de nouvelles données dans ce domaine. En particulier, la mise en service imminente de l'ISO permettra d'enrichir les données déjà acquises par les satellites IRAS et COBE/ DIRBE. Le VLT (Very Large Telescope) montre le grand potentiel d'une nouvelle technologie optique; il permet, en particulier, d'observer des objets ayant un grand décalage vers le rouge, à la frontière de l'univers visible, ce qui est très important pour étudier l'évolution de l'Univers.

De cette conférence, il apparait clairement que, si les modèles du Big Bang forment un schéma relativement attrayant, il reste un certain nombre de problèmes non

résolus, d'ordre soit théorique, soit observationnel. De nouveaux résultats ont été obtenus récemment. De nouvelles idées ont été proposées. La cosmologie physique est en pleine évolution.

L'intérêt et l'enthousiasme manifestés tout au long de la conférence, nous le devons aux membres du Comité Scientifique International pour leur suggestion des thèmes et aux membres du Comité de Programme pour la coordination du programme scientifique. En particulier, je suis très reconnaissant à Alain Blanchard, Alain Bouquet, Ludwik Celnikier et Marc Lachièze-Rey de l'aide qu'ils ont apportée.

La conférence a été honorée par le précieux soutien de Monsieur Jack Lang, Ministre de la Culture et Maire de Blois, de Monsieur Hubert Curien, Ministre de la Recherche et de la Technologie, de Monsieur Maurice Dousset, Président du Conseil Régional de la Région Centre et de Monsieur Roger Goemaere, Président du Conseil Général du Loir-et-Cher.

L'organisation de cette conférence n'aurait pas été possible sans le concours financier et logistique de la Commission des Communautés Européenne, du Ministère de la Recherche et de l'Industrie, du Centre National de la Recherche Scientifique, du Commissariat à l'Energie Atomique, du Centre National d'Etudes Spatiales, de l'Observatoire de Paris, du Conseil Régional de la Région Centre, du Conseil Général du Loir-et-Cher et de la Mairie de Blois qui nous a accueilli dans le magnifique Château de Blois. La contribution de la NASA qui a permis à de jeunes astrophysiciens de participer à la conférence a été particulièrement appréciée. Je remercie aussi les Chocolats Poulain et Infoprism pour leur contribution.

L'aide financière de l'Aérospatiale et de Framatome fut déterminante. Ma profonde gratitude va à Monsieur Henri Martre, Président de l'Aérospatiale et à Monsieur Jean Claude Lény, Président de Framatome pour leurs encouragements au développement de la recherche scientifique.

Messieurs Trân van Khê et Trân Quang Hai, Madame Bach Yên et Mademoiselle Trân Thi Thuy Ngoc nous ont offert une soirée mémorable d'évasion vers la musique traditionnelle du Vietnam, au cours de laquelle la ville de Blois et les scientifiques des cinq continents ont vibré au même diapason.

L'organisation matérielle a été prise en charge par les Rencontres de Moriond. Je remercie vivement Christian Bareille, Aida Cherkaoui, Françoise Eschenbrenner, Francine Lefevre, Laurence Massiot, Lê van Suu, Noëlle Nguyên, Lucienne Norry, Trân Dai Thanh Binh, Emmanuelle Trân Thanh Tâm et Anne Claire Trân Thanh Binh Minh qui ont consacré beaucoup d'énergie et de temps à la réussite et au caractère chaleureux de cette rencontre.

J. Trân Thanh Vân

FOREWORD

The second of the "Rencontres de Blois" was held in the Château de Blois from the 28th of August to the 1st of September 1990, and brought together 175 astrophysicists from about 20 countries spanning 5 continents.

Twenty-five years ago Penzias and Wilson discovered the cosmic background radiation ; this conference has reviewed the progress made in physical cosmology since that time. The remarkable results of the COBE satellite (Cosmic Background Explorer), launched in November 1989, were a particular highlight.

The opening sessions traced the history of the discovery of the background radiation, and gave an overview of the recent developments in physical cosmology. It was a remarkable experience indeed to listen to some of the principal actors - Robert Wilson, Jim Peebles and David Wilkinson - of this extraordinary episode of modern science talking about their work and the breakthroughs which finally led to the present form of the "Big Bang".

The cosmic background radiation, one of the most direct sources of information about the physical conditions of the early universe, was discussed in considerable detail. The latest measurements, and in particular those of COBE which show the spectrum to be that of a perfect black body with a very high degree of isotropy, confirm the cosmological origin of the radiation and its identification as the relict radiation foreseen by the theory of the Big Bang.

Nucleosynthesis, dark matter searches and the gravitational lensing phenomenon constitute growth points around which is crystallizing a synthesis of cosmology and particle physics. If primordial nucleosynthesis is to produce the observed light element abundances within the context of the Big Bang, there should be no more than three families of neutrinos : this was convincingly proven by the high energy experiments at LEP. Of what is dark matter made ? Is it made of WIMPS (Weakly Interacting Particles), MACHOS (Massive Compact Halo Objects) or other more or less exotic objects : such questions stimulated long and vigorous discussions.

A profound problem is related to the seemingly perfect isotropy of the relict radiation, since the distribution of galaxies and clusters of galaxies is far from isotropic. New information on large scale structures has come from the infra-red satellite IRAS and from ground based optical studies ; we now have the velocities and positions of statistically interesting samples of galaxies. This work was discussed in the context of theories of galaxy formation and the large scale structure of the universe ; the wide spectrum of opinions was well represented at the conference and emphasizes the importance of understanding why measurements made using different techniques lead to different conclusions.

Emerging technologies will surely revolutionize our picture of the Universe.

A presentation of the VLT (Very Large Telescope) showed what new optical techniques could bring : this instrument will, in particular, enable us to observe very high red shift objects, at the very limits of the visible universe, work which is essential to understanding the evolution of the universe.

A survey of forthcoming space missions indicated another source of potentially new data ; the imminent lauch of ISO (Infrared Space Observatory) will allow the continuation of the work begun by the IRAS and COBE/DIRBE instruments.

The various models of the Big Bang provide a rather pleasing intellectual structure ; there are, however, a certain number of unsolved problems, theoretical as well as observational. New results are interlaced with new ideas ; from the conference emerges an image of cosmology as a lively and evolving domain.

The stimulating atmosphere of the conference was due in no small measure to the subjects suggested by the members of the International Scientific Committee, and to the overall organization of the session by the Programme Committee. I am particularly grateful to Alain Blanchard, Alain Bouquet, Ludwik Celnikier and Marc Lachièze-Rey for their help.

The conference is proud to acknowledge the irreplaceable support of Mr Jack Lang, Minister for Culture and the Mayor of Blois, Mr Hubert Curien, Minister of Research and Technology, of Mr Maurice Dousset, President of the Conseil Régional de la Région Centre, and of Mr Roger Goemaere, President of the Conseil Général du Loir-et-Cher.

This conference could not have taken place without the financial aid of the Commission of the European Communities, of the Ministry for Research and Industry, of the Centre National de la Recherche Scientifique, of the Commissariat à l'Energie Atomique, of the Centre National d'Etudes Spatiales, of the Observatoire de Paris, of the Conseil Régional de la Région Centre, of the Conseil Général du Loir-et-Cher and of the Mairie de Blois who welcomed us in the magnificent Château de Blois. The financial help of NASA, which allowed a certain number of young astrophysicists to participate, was much appreciated, and I would like to thank the Chocolats Poulain and Infoprism for their contributions.

Finally, I wish to extend my thanks to Aérospatiale and to Framatome, whose financial assistance was a determining factor in the organisation of the Conference. A vote of gratitude is due to Mr Henri Martre, President of Aérospatiale and to Mr Jean Claude Lény, President of Framatome, for their encouragement of scientific research.

Messrs. Trân Van Khê and Trân Quang Hai, Mrs. Bach Yên and Miss Trân Thi Thuy Ngoc provided a memorable evening of traditional vietnamese music, during which the inhabitants of Blois and the scientists of five continents vibrated in time to the traditional rythm of Vietnam.

The Rencontres de Moriond took care of the infrastructure of the conference. I am grateful to Christian Bareille, Aïda Cherkaoui, Françoise Eschenbrenner, Francine Lefevre, Laurence Massiot, Lê Van Suu, Noëlle Nguyên, Lucienne Norry, Trân Dai Thanh Binh, Emmanuelle Trân Thanh Tâm and Anne Claire Trân Thanh Binh Minh who devoted much time and energy to making such a successful and pleasant meeting.

J. Trân Thanh Vân

SCIENTIFIC PROGRAM

Tuesday August 28, 1990

Morning session : Opening session

CELEBRATION AND HISTORICAL ASPECTS

***Chairman* : G. Steigman**

R. Wilson	Discovery of the Cosmic Microwave Background

***Chairman* : C. Cesarsky**

J. Peebles	The emergence of physical cosmology
Fang Li Zhi	Cosmology and Particles

Afternoon session

***Chairman* : D. G. R. Morrison**

A. Linde	Inflation and Quantum Cosmology
G. Burbidge	The scale of the Universe

***Chairman* : F. Melchiorri**

D. Wilkinson	Ground based measurement of the CBR spectrum

Wednesday August 29, 1990

Morning session

COSMIC BACKGROUNDS

Chairman **: J. Peoples**

E. Cheng	The signicance of COBE (microwave and infrared)
G. Smoot	COBE DMR maps of the CMB - large angular scale isotropy measurements

Chairman **: B. Jones**

M. Halpern	Rocket measurements of the CBR
F. Melchiorri	European contribution to CBR studies

Afternoon session

Chairman **: B. Carr**

N. Vittorio	How fluctuations in the microwave background constrain cosmological models
B. Partridge	Fluctuations : first measurements and recent results

Chairman **: R. Schaeffer**

M. Birkinshaw	Measurement of the Sunyaev-Zeldovitch effect
X. Barcons	High energy backgrounds

Thursday August 30, 1990

Morning session

PARTICLES AND COSMOLOGY, DARK MATTER

Chairman **: G. Steigman**

F. Englert	The very early Universe
D. Schramm	Cosmological nucleosynthesis

Chairman **: J. P. Luminet**

M. Spiro	Dark matter searches
L. Nottale	Application of gravitational lensing
A. de Rujula	Why the galactic dark mass is in H/He balls and how to measure their mass function

Friday August 31, 1990

Morning session

LARGE SCALE STRUCTURES

***Chairman* : B. Jones**

M. Davis	IRAS galaxies
Trinh Xuan Thuan	Dwarf galaxies

***Chairman* : C. Frenk**

E. Bertschinger	Large scale motion
M. Geller	Large scale structures

Afternoon session

***Chairman* : B. Rocca-Volmerange**

R. Fong	Pencil beam redshift survey
A. Doroshkevich	A new method of analysing deep redshift surveys
A. Dekel	Reconstruction methods for cosmological gravitating systems

***Chairman* : B. Fort**

C. Collins	Clustering results from the Edinburgh-Durham Survey
S. Maddox	Normal galaxies in the APM survey
F. Bouchet	Cosmic strings and cosmological consequences

Saturday September 1, 1990

Morning session

GALAXY FORMATION, SPACE PROJECTS RELATING TO COSMOLOGY

- **Galaxy formation**

***Chairman* : R. Carlberg**

J. Peacock	Observational constraints on galaxy formation
S. White	Numerical simulation in cosmology

- **Space projects relating to cosmology**

Chairman :

E. Groth	Cosmological applications of the Hubble telescope
P. Léna	The European Very Large Telescope

Afternoon session

***Chairman* : J. Trân Thanh Vân**

M. Lachièze-Rey	Overview of European space projects
C. Cesarsky	ISO and other infrared projects
	Summary and conclusions

End of the conference

Contents

IV. GALAXIES : PROPERTIES AND DISTRIBUTIONS

V. FUTURE PROSPECTS

Posters

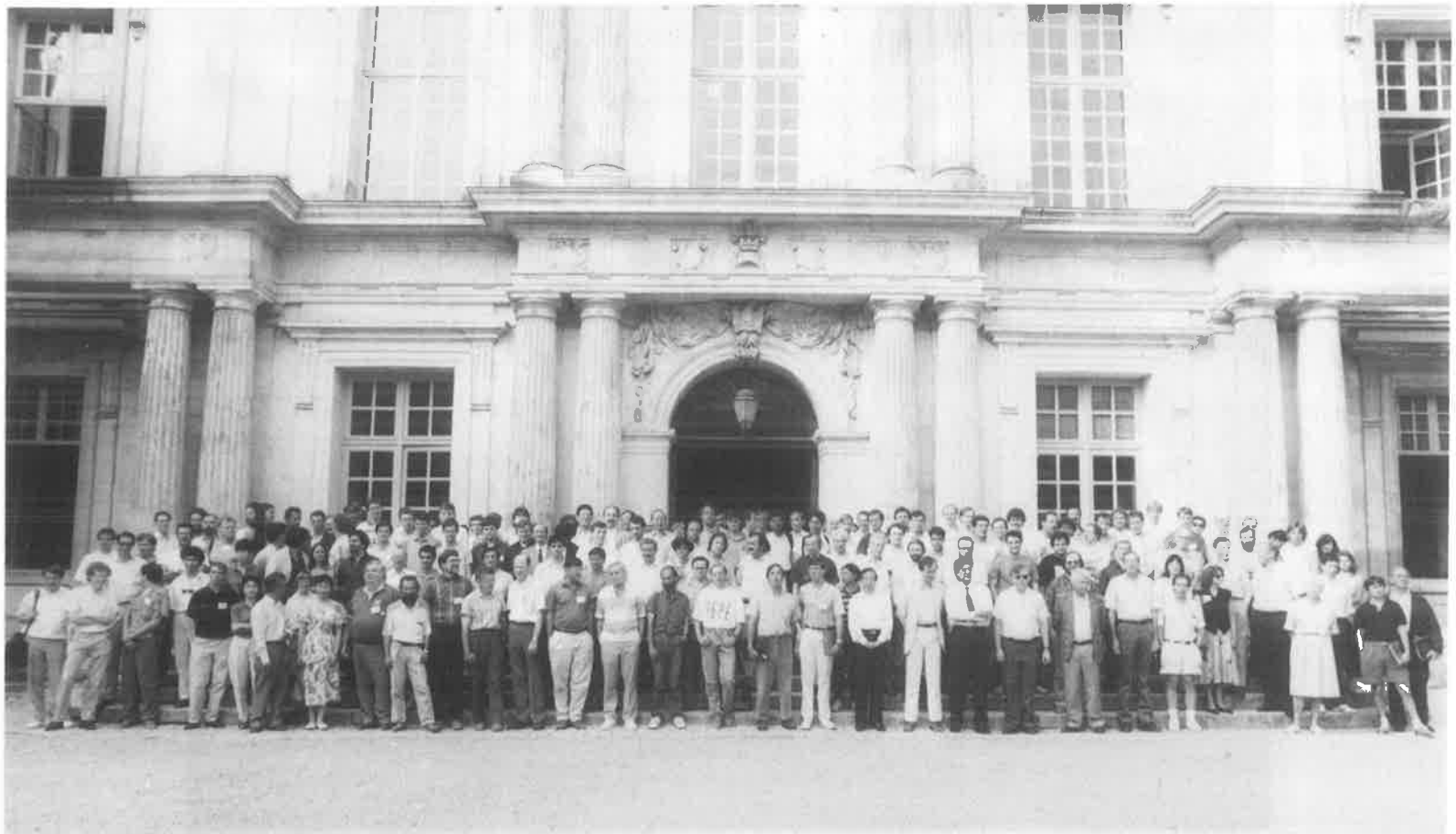

Participants in front of the Gaston d'Orléans wing of the Château de Blois.

To the conference room.

25th anniversary cake.
From left : Robert Wilson, Jim Peebles and Jean Trân Thanh Vân.

Press conference at the Château de Blois.
From left : Douglas Morrisson, Jim Peebles, Robert Wilson, Jean Trân Thanh Vân and André Berroir.

Reception at the City Hall.
From left : Ms Li Shuxian, Fang Li Zhi, Jack Lang, Jean and Kim Trân Thanh Vân.

Reception at the City Hall.
From left : Ms Li Shuxian, Jack Lang, Robert Wilson and Jean Trân Thanh Vân.

Conference dinner.
From left : André Berroir, Robert Wilson and Ms Madeleine Nash.

Conference dinner.
From left : Gary Steigman, John Peoples, Ms Judith Schramm, Jim Peebles,
Ms Alison Peebles, David Schramm, Ms Eunice Wilkinson and David Wilkinson.

Physical Cosmology

Conference room

DISCOVERY OF THE COSMIC MICROWAVE BACKGROUND

Robert W. Wilson
AT&T Bell Laboratories
Crawford Hill Laboratory
Holmdel, New Jersey 07733

In the late 1950's plans were made to start working on communication satellites at Bell Labs, particularly at Holmdel. The first satellite tests were planned with NASA's Echo balloon. It was known that the return signal from Echo would be very weak because a sphere scatters the incoming radiation in all directions. In contemplating the weak signal, they decided that one should have a very low noise receiver system to receive that signal. It was very convenient that there were two Bell Labs devices which would go together and should make a very low noise receiving system: One of them was the traveling wave maser which Derrick Scovil and his group at Murray Hill were making (De Grasse et al. 1959a). This worked at liquid helium temperatures and had a noise temperature of a few Kelvin. Even after making a room temperature connection to it, you could have a receiver with a noise temperature of 10 K.

The other device which seemed to fit with the traveling wave maser was a horn reflector antenna. The horn-reflector was invented by Al Beck and Harold Friis for use in a microwave relay system. In addition to turning the corner between the waveguide going up a tower and the horizontal communication path, it has the distinct advantage that when two of are put them back-to-back on a tower and have a very weak signal coming in on one side, a strong regenerated signal can be transmitted from the other side without interference. Its front-to-back ratio is very high. The corollary of this is that a horn-reflector is put on its back, it will not pick up much radiation from the earth and will be a very low noise antenna. Therefore, Art Crawford (1961) built a large (20-foot aperture) horn reflector to be used with a traveling wave maser to receive the weak signals from Echo.

Figure 1 shows the 20 foot horn-reflector with its parabolic reflector on the left and cab on the right. Since the cab does not tilt, almost any kind of receiver can be conveniently put at the focus of this antenna (apex of the horn). It is fairly obvious that the horn shields the receiver from the ground, especially when it is looking up.

Just to convince the engineers how good the shielding is, Figure 2 shows a polar diagram of a rather smaller horn reflector antenna compared with the gain of a theoretical isotropic (uniform response) antenna. If we take an isotropic antenna and put it on a field with the 300 K ground down below and zero degree sky up above, we expect it to pick up 150 K; half of its response comes from the ground. Now look at this horn-reflector. It is certainly at least 35 db less responsive to the ground than the isotropic antenna would be. So we take 150 K and divide it by a few thousand and we expect under a tenth of a Kelvin for the ground pickup from the horn-reflector.

In 1963, knowing of the existence of this antenna, I accepted a job at Bell Labs, leaving a postdoc position at Caltech. Arno had been there a year or so at that time, and obviously the only two radio astronomers in the place were going to work together because making a radio telescope do any kind of an observation is a job for at least two people. One might ask why two young astronomers wanted to work with such a tiny little antenna, with a collecting area of maybe 25 square meters, when there were much bigger antennas around. We knew it had very special properties. First it is a small enough antenna that one could measure its gain very accurately. It was necessary only to be about a kilometer away to be in the far field, for making an accurate gain measurement. And that, in fact, had already been started by Dave Hogg.

The availability of the traveling wave masers at several frequencies made this small antenna sensitive enough for work even with small diameter sources, and for sources which were of a diameter large enough diameter to fill its beam, it would have been the most sensitive radio telescope in existence at the time. The other important thing about

horn-reflectors I have pointed out before; the good shielding of the antenna leads to the conclusion that we ought to be able to understand all the sources of noise. Radio astronomers don't often understand the background temperature when they do the usual on-off experiment (subtracting a measurement pointing away from the source from the measurement on the source), but the 20-foot horn-reflector offered the possibility of absolute temperature measurement.

My interest in that possibility came directly from my thesis work at Caltech. There, with John Bolton, I had made a survey of the Milky Way. We had done it in the standard way of doing such things at the time; we pointed the antenna to the west of the Milky Way and let the earth's rotation sweep the antenna beam through it and to the other side. Of course, we are inside the Galaxy, and there is no possibility of pointing completely away from the Galaxy to do an on-off measurement. What we observed was a simple curve in which the power goes up as we approach the Milky Way and comes back down on the other side, and has a fairly steady level more than 10° from the plane. I did the usual thing; I drew a linear baseline from one side to the other and measured levels above it. That was enough to see the radiation from the plane of the galaxy but it was clearly somewhat unsatisfying because I knew that there was a possible large-scale component, the halo that people were talking about, which my measurement was not at all sensitive to.

After I went to Bell Laboratories, the 20-foot horn reflector was released from the various satellite jobs it was doing. It had been designed for the Echo experiment which required operation at 13 cm wavelength, but it had later been used to receive a beacon from the Telstar® satellite, so when Arno and I inherited it there was a 7.3 cm. maser receiver on it (Tabor and Sibilia 1963). It had a communications receiver which a radio astronomer would find hard to believe. The maser was followed by a low-noise nitrogen cooled parametric amplifier which was followed by a low noise traveling wave tube

amplifier, and the gain stability was unbelievably bad. Our jobs were to turn all of this into a radio telescope by making a radiometer, finish up the gain measurement, and then proceed to do some astronomy projects.

We thought about what astronomy we ought to do and laid out a plan, which would take a few years. The first project was the absolute flux measurement. If we could measure the gain of the antenna to a few percent, which we thought we could, and then understand the temperature scale of the receiver very well, we could measure the standard calibration sources more accurately then had been done before. I planned to follow up on my thesis by taking a few selected cuts across the Milky Way and then confirm the spectrum of some of the sources that I had looked at. Next we wanted to check our ability to measure the galactic halo radiation. Extrapolating from a lower frequency, we did not expect to see any galactic halo at 7 cm. We wanted to prove that when we did try to make such a measurement we got a null result. After doing these projects, our plan was to build a 21-cm receiver scaled from our 7-cm receiver. We already had the maser in hand We would then make the halo measurement and do a number of 21-cm line projects including reworking Arno's thesis of looking for hydrogen in clusters of galaxies.

At one point during that time John Bolton came for a visit and we laid out this plan of attack in front of him and asked his opinion, and he said, "Well, obviously the most important thing to do in that list is the 21-cm background measurement." He thought that it was an unexplored area and something that we really ought to do.

Actually by the time I joined Bell Laboratories, Arno had started making a liquid Helium-cooled noise source (Penzias 1965). In Figure 3 we see it; a piece of ordinary C-band waveguide, 90% copper, which runs down inside the dewar which has a six-inch inside diameter. About halfway down, the waveguide is thinned to reduce its heat conductivity and finally there is a carefully designed absorber in the bottom. There's a

sheet of mylar in the flange near the bottom which keeps the liquid helium out of the upper part of the waveguide. There are some holes in the bottom section so that the liquid helium can surround the absorber and there will be no question of the physical temperature of the absorber. The cryogenics has been taken care of with the baffles which make a heat exchange between the cold Helium gas and the waveguide. We realized that we had to know the radiation from the walls of the waveguide, so there are a series of diode thermometers on the waveguide for measuring its physical temperature distribution. We calculated the radiation of the walls using these temperatures and the measured loss in the waveguide.

When we first transferred the contents of a 25-liter dewar of liquid helium into the cold load, it would fill up to a fairly high level and we calculated the radiation temperature at the top to be approximately 5 K - just eight-tenths of a Kelvin above the temperature of the liquid helium. Fifteen hours later or so (we usually ran down before the helium did), the liquid helium level would be down near the absorber and we would calculate the flange temperature to be about 6 K. Comparing it to the horn reflector, the change agreed within something like a tenth of a degree over that period, so we felt we had a reasonably good calibration of what was going on in our cold load.

While Arno was doing that, I set up the radiometer shown in Figure 4 (Penzias and Wilson 1965a). As with most of our astronomical equipment at Bell Laboratories, this is somewhat unusual. The horn-reflector has a circular waveguide at its output, and so we decided to use that property in a scheme which Doug Ring and others at Crawford Hill had used in the past. It takes advantage of the fact that two orthogonal polarizations will pass through round waveguide. The polarization coupler near the antenna couples the signal from the reference ncise source into the horizontal polarization mode traveling toward the maser and allows vertical polarization from the antenna to go straight through. The polarization rotator is the equivalent of a half-wave plate. It is a squeezed

piece of waveguide with two rotary joints; another polarization coupler at the back picks one polarization off and sends it over to the maser. By rotating the squeezed waveguide, we could switch between the reference noise and the antenna. The noise tube was a secondary temperature standard in our measurement of Cas A and other sources. An important aspect of this radiometer design is that except for the unused port, all ports of the waveguide were terminated at approximately the same low radiation temperature. Thus small reflections would not have a large effect. All parts of the system, however, were well matched and the unused port could be opened to room temperature with no effect on measurements.

Figure 5 shows a picture of the actual installation including the rotary joint which allowed the horn reflector to turn while the receiver stayed stationary in the cab. The cold load was connected to the reference port through an adjustable 0.11 dB attenuator which could add a well-calibrated additional noise. You can see that having the output of the horn-reflector in a cab which moves only in azimuth was very important for this experiment.

Before we started making measurements with this system, there had been careful measurements of horn-reflectors with traveling wave masers at Bell Laboratories. First, before going to the trouble of building a 20-foot horn-reflector, the antenna and maser groups had put together a test system (De Grasse et al. 1959b). They had a 6 GHz maser and a small horn-reflector antenna. They hooked the two up with a calibrating noise lamp and saw that indeed they got a system temperature of something like 18½ K which was very nice, but they had expected to do a little better. You see in Figure 6 that contrary to the prediction I made before, they have assigned 2 K to the antenna for the back lobe and other pickup from the antenna, 2½ K for atmosphere, and 10.5 K for the temperature of the maser. The makers of the maser were not very happy with that number. They thought they had made a better maser than that, but within the accuracy

of what they knew about all the components, they solved the problem in making things add up by assigning additional noise to those components. Arno had used this horn-reflector for another astronomy project and was aware of the extra 2 K that had been assigned to it. One of the reasons that he built the cold load was to improve on their experiment.

This group had measured the atmospheric radiation (sky noise) by the same technique that Dicke had first reported on in 1946. Figure 7 shows a chart of a measurement such as Arno and I made with the 20-foot horn-reflector. It shows the radiometer output as the antenna is scanned from a fairly high elevation angle down to 10° elevation angle. This is a chart with power increasing to the right, and you can see what the power out of the receiver did. The circles correspond to the expected change if the zenith sky brightness is 2.2 K and the crosses to 2.4 K. You can see that the curve is a very good fit to the expected curve down to at least 10° elevation, so a well-shielded antenna makes the measurement of the atmospheric radiation very easy.

After the 20-foot horn-reflector was built and was being used with the Echo satellite, Ed Ohm, who was a very careful experimenter (Ohm 1961), added up the noise contribution of all the components of the system and compared it to his measured total. In Figure 8 we see that from the sum of the components he predicted a total system temperature of 18.9 K, but he found that he consistently measured 22.2, or 3.3 K more than what he had expected. However, that was within the measurement errors of his summation, so he did not take it to be significant.

Well, our first observations were somewhat of a disappointment because we had naturally hoped that these things I have mentioned were just errors in the experiments. Figure 9 is the first measurement with our receiver. At the bottom and top, the receiver is switched to the antenna and in between to the cold load. The level from the antenna at 90° elevation matched that from the cold load with .04 dB of attenuation ($\sim$7.5 K

total radiation temperature). At the bottom I recorded measurements of the temperature-sensing diodes on the cold load.

That was a direct confrontation. We expected 2.3 K from the sky, 1 K from the absorption in the walls of the antenna, and we saw something that was obviously considerably more than that. It was really a qualitative thing rather than just quantitative because the antenna was hotter than the helium reference and it should have been colder. But we knew that the problem was either in the antenna or beyond. Arno's initial reaction was "Well, I made a pretty good cold load!" The most likely problem in such an experiment is that you do not understand all the sources of extra radiation in your reference noise source, but it is not possible to make it have a lower temperature than the liquid helium.

It initially looked like we could not do the Galactic halo experiment, but at that time our measurements of the gain of the antenna had started (Hogg and Wilson 1965) and we wanted to go on with the absolute flux measurements before taking anything apart or trying to change anything. So we ended up waiting for almost a year before doing anything about our antenna temperature problem; however, we were thinking about it all that time.

We thought of several possible explanations of the excess antenna temperature. Many radio astronomers at the time thought the centimeter wave atmospheric radiation was about twice what we were saying. That would have gone a long way toward explaining our problem. However, the curve for the zenith angle dependence in Fig. 7 indicates that we were measuring the atmospheric absorption or emission correctly. It turned out later that the centimeter astronomers had applied refraction corrections to their measurements of radio sources in the wrong sense. John Shakeshaft finally straightened this out.

Crawford Hill overlooks New York City; perhaps man-made interference was causing trouble. Therefore we turned our antenna down and scanned around the horizon. We found a little bit of superthermal radiation, but, given the horn-reflector's rejection of back radiation, nothing that would explain the sort of thing that we were seeing.

Could it be the Milky Way? Not according to extrapolations from low frequencies. The galactic poles should have a very small brightness at 7 cm and our actual measurements of the plane of the Milky Way did fit very well with the extrapolations.

Perhaps it was discrete sources. The strongest discrete source we could see was Cas A and it had an antenna temperature of 7K. Point sources extrapolate in frequency in about the same way as the radiation from the Galaxy, so they seemed a very unlikely explanation.

That left radiation from the walls of the antenna itself. We calculated nine-tenths of a degree Kelvin for that, taking into account the actual construction of the throat section of the antenna which is the most important. It was a piece of electroformed copper and we could measure similar sorts of waveguides in the lab.

We had to wait sometime to finish the flux measurement, but in the spring of 1965, almost a year later, we had completed it (Penzias and Wilson, 1965a). The earth had made a complete cycle around the sun and nothing had changed in what we were measuring. We pointed to many different parts of the sky, and unless we had a known source or the plane of the Galaxy in our beam, we had never seen anything other than the usual antenna temperature. In 1962 there had been a high altitude nuclear explosion over the Pacific which had filled up the van Allen belts. We were initially worried that something strange was going on there, but after a year, the population of van Allen belts had gone down considerably and we'd not seen any change.

There was a pair of pigeons living in the antenna at the time, and they had deposited

the usual white dielectric in the part of the horn where they roosted. So we cleaned up the antenna, disposed of the pigeons, and put some aluminum tape over the joints between the separate pieces of aluminum that made it up. All of this made only a minor improvement.

We were really scratching our heads about what to do until one day Arno happened to be talking to Bernie Burke about other matters. After they had finished talking about what Arno had called for, he mentioned our problems, our dilemma that the Galactic halo experiment was not ever going to work, and that we could not understand what was going on. Bernie had heard about Jim Peebles' calculations of microwave radiation from a hot big bang and suggested that we get in touch with Dicke's group at Princeton. So of course Arno called Dicke. Dicke was thinking about oscillating big bangs which he concluded should be hot. After a discussion on the phone, they sent us a preprint and agreed to come for a visit. When they came and saw what we had done, I'm sure they were thoroughly disappointed, but agreed that what we had done was probably right. Afterword the two groups wrote separate letters to the Astrophysical Journal (Dicke et al. 1965; Penzias and Wilson 1965b).

We made one last check before actually sending off our letter for publication. We took a signal generator, attached it to a small horn and took it around the top of Crawford Hill to artificially increase the temperature of the ground and measure the back lobe level of the 20-foot horn, maybe there was something wrong with it. But the result was as low as we expected. So we sent the letter in!

Arno and I of course were very happy to have any sort of an answer to our dilemma. Any reasonable explanation would have probably made us happy. In fact, I do not think either of us took the cosmology very seriously at first. We had been used to the idea of steady-state cosmology; I had come from Caltech and had been there during many of Fred Hoyle's visits. Philosophically, I liked the steady-state cosmology. So I thought

that we should report our result as a simple measurement; the measurement might be true after the cosmology was no longer true!

After our meeting, the Princeton experimental group returned to complete their apparatus and make their measurement, with the expectation that the background temperature would be about 3 K.

The first confirmation of the microwave cosmic background that we knew of, however, came from a totally different, indirect measurement. This measurement had, in fact, been made 30 years earlier by Adams (1941, 1943), Dunham (1937, 1939, 1941), and Dunham and Adams (1937) had discovered several faint optical interstellar absorption lines which were later identified with the molecules CH, CH^+, and CN. In the case of CN, in addition to the ground state, absorption was seen from the first rotationally excited state. McKellar (1941) using Adams' data on the populations of these two states calculated that the excitation temperature of CN was 2.3 K. The rotational transition occurs at 2.64 mm wavelength, near the peak of a 3 K blackbody spectrum. Shortly after the discovery of the background radiation, G. B. Field *et al.* (1965, 1966), Field and Hitchcock (1966), I. S. Shklovsky (1966), and P. Thaddeus (1966) (following a suggestion by N. J. Woolf) independently realized that the CN is in equilibrium with the background radiation. (We now know enough about the interstellar medium to say that there is no other significant source of excitation where these molecules are located). In addition to confirming that the background was not zero, this idea immediately confirmed that the spectrum of the background radiation was close to that of a blackbody source for wave-lengths larger than the peak. It also gave a hint that, at short wavelengths, the intensity was departing from the $1/\lambda^2$ dependence expected in the long wavelength (Raleigh-Jeans) region of the spectrum and following the true blackbody (Planck) distribution.

In December 1965 Roll and Wilkinson (1965) completed their measurement of 3.0 ± 0.5 K at 3.2 cm, the first confirming microwave measurement. This was followed shortly by Howell and Shakeshaft's (1966) value of 2.8 ± 0.6 K at 20.7 cm and then by our measurement of 3.2 ± 1 K at 21.1 cm (Penzias and Wilson 1967). (Half of the difference between these two results comes from a difference in the corrections used for the galactic halo and integrated discrete sources.) By mid-1966, the intensity of the microwave background radiation had been shown to be close to 3 K between 21 cm and 2.6 mm, almost two orders of magnitude in wavelength.

Earlier Theory

I have mentioned that the first experimental evidence for cosmic microwave background radiation was obtained (but unrecognized) long before 1965. We soon learned that the theoretical prediction of it had been made at least 16 years before our detection. George Gamow (1948) had made calculations of the conditions in the early universe in an attempt to understand element formation. Although these calculations were not strictly correct, Gamow and his collaborators calculated that the density of radiation in the hot early universe was much higher than the density of matter. In this early work, the present remnants of this radiation were not considered. However, in 1949, Alpher and Herman (1949) followed the evolution of the temperature of the hot radiation in the early universe up to the present epoch and predicted a value of 5 K. They noted that the present density of radiation was not well known experimentally. In 1953 Alpher, Follin, and Herman (1953) reported what has been called the first thoroughly modern analysis of the early history of the universe, but failed to recalculate or mention the present radiation temperature of the universe.

In 1964, Doroshkevich and Novikov (1964a, 1964b) had also calculated the relic radiation and realized that it would have a blackbody spectrum. They quoted E. A. Ohm's article on the Echo receiver, but misunderstood it and concluded that the

present radiation temperature of the universe is near zero.

Cosmology is a science which has only a few observable facts to work with. The discovery of the cosmic microwave background radiation added one - the present radiation temperature of the universe. This, however, was a significant increase in our knowledge since it requires a cosmology with a source for the radiation at an early epoch and is a new probe of that epoch. More sensitive measurements of the background radiation in the future will allow us to discover additional facts about the universe.

References

Adams, W. S. (1941). Results with the Coudé Spectrograph of the Mt. Wilson Observatory. *Astrophysical Journal,* **93**, 11-23.
(1943). The Structure of Interstellar H. & K Lines in 50 Stars. *Astrophysical Journal,* **97**, 105.

Alpher, R. A. and Herman, R. C. (1949). Remarks on the Evolution of the Expanding Universe. *Physical Review,* **75**, 1089-1095.

Alpher, R. A., Follin, J. W., and Herman, R. C. (1953). Physical Conditions in the Initial Stages of the Expanding Universe. *Physical Review,* **92**, 1347-1361.

Crawford, A. B., Hogg, D. C., and Hunt, L. E. (1961). A Horn-Reflector Antenna for Space Communication. *Bell Systems Technical Journal,* **40**, 1095.

DeGrasse, R. W., Schultz-Dubois, E. O., and Scovil, H. E. D. (1959a). Three-Level Solid-State Traveling-wave Maser. *Bell System Technical Journal,* **38**, 305.

DeGrasse, R. W., Hogg, D. C., Ohm, E. A., and Scovil, H. E. D. (1959b). Ultra Low Noise Antenna and Receiver Combination for Satellite or Space Communication. *National Electronics Conference,* **15**, 370.

Dicke, R. H., Peebles, P. J. E., Roll, P. G., and Wilkinson, T. D. (1965). Cosmic Black-Body Radiation. *Astrophysical Journal,* **142**, 414-419.

Doroshkevtch, A. G. and Novikov, I. D. (1964). Mean Density of Radiation in the Metagalaxy and Certain Problems in Relativistic Cosmology. Doklady Akademii Nauk SSSR, **154**, 809; also in *Soviet Physics Doklady,* **9**, 111-113.

Dunham, T. (1937). Interstellar Neutron Potassium and Neutron Calcium. *Publications of the Astronomical Society of the Pacific,* **49**, 26
(1939). *Proceedings of American* Philosophical Society. **81**, 277. The Material of Interstellar Space.
(1941). Concentration of Interstellar Molecules. *Publications of the American Astronomical Soc.* **10**, 123.

Dunham, T. Jr and Adams, W. S. (1937). New Interstellar Lines in the Ultra-violet Spectrum. *Publications of the American Astronomical Society.* **9**, 5.

Field, G. B. and Hitchcock, J. L. (1966). Cosmic Black-Body Radiation at $\lambda = 2.6$ *mm* (from Observations of Interstellar CN). *Physical Review Letters,* **16**, 817-818.

Field, G. B., Herbig, G. H., and Hitchcock, J. L. (1965). Radiation Temperature of Space at λ 2.6 *mm*. *Astronomical Journal,* **71**, 161.

Gamow, G. (1948). The Evolution of the Universe. *Nature,* **162**, 680-682.

Hogg, D. C. and Wilson, R. W. (1965). A Precise Measurement of the Gain of a Large Horn-Reflector Antenna. *Bell System Technical Journal,* **44**, 1019.

Howell, T. F. and Shakeshaft, Jr. R. (1966). Measurement of the Minimum Cosmic Background Radiation at 207-cm Wavelength. *Nature,* **210**, 1318-1319.

McKellar, A. (1941). Molecular Lines from the Lowest States of the Atomic Molecules Composed of Atoms Probably Present in Interstellar Spaces. *Publications Dominion Astrophysical Observatory Victoria B. C.,* **7**, 251-272.

Ohm, E. A. (1961). Project Echo Receiving System. *Bell Systems Technical Journal,* **40**, 1065.

Penzias, A.A. (1965). Helium-Cooled Reference Noise Source in a 4-kMc Waveguide. *Review of Scientific Instruments,* **36**, 68.

Penzias, A. A. and Wilson, R. W. (1965a). Measurement of the Flux Density of CasA at 4080 MHz. *Astrophysical Journal,* **142**, 1149.
(1965b). A Measurement of Excess Antenna Temperature at 4080 Mc/s. *Astrophysical Journal,* **142**, 419.
(1967). Measurement of Background Temperature at 1415 MHz. *Astronomical Journal,* **72**, 315.

Roll, P. G. and Wilkinson, D. T. (1966). Measurement of Cosmic Background Radiation at 3.2 cm Wavelength - Support for Cosmic Black-Body Radiation. *Physical Review Letters,* **16**, 405-407.

Shklovsky, I. S. (1966). Astronomical Circular No. 364. Academy of Sciences of the U.S.S.R.: Moscow.

Tabor, W. J. and Sibilia, J. T. (1963). Masers for the Telstar® Satellite Communications Experiment. *Bell System Technical Journal* **42**, 1863.

Thaddeus, P. and Clauser, J. F. (1966). Cosmic Microwave Radiation at 263 mm from Observation of Interstellar CN. *Physical Review Letters,* **16**, 819-822.

THE EMERGENCE OF PHYSICAL COSMOLOGY

"plus ça change, plus c'est la même chose"

P. J. E. Peebles

Institute for Advanced Study
and
Princeton University
Princeton NJ USA

ABSTRACT

A review of the evolution of research in physical cosmology over the past several decades can be a useful guide to where we seem to be making progress, where some of the older less fashionable ideas might be reconsidered, and where a more concerted search for new ideas might be in order. My conclusion is that although there is a healthy amount of confusion over the possible resolution of outstanding problems such as the origin of galaxies and the large-scale structure of the galaxy distribution, the nature and amount of the dark matter, and the parameters of the cosmological model, one can see distinct signs of progress.

INTRODUCTION

I mean by physical cosmology an observational/experimental science, in which definite physical models are used to interpret and predict the results of measurements. In a mature physical science the models, or paradigms, are believable because they account for the relations among a network of experiments and/or observations that is substantially larger than what was used to develop the paradigms. The purpose of this review is to offer some opinions on the state of progress toward this goal in physical cosmology. My historical remarks may be of some use to those who are interested in the origins of our subject, but the main goal is to draw some morals for the way the work is progressing. I shall argue that although many of the basic elements of physical cosmology still are in a confused state the subject is showing distinct signs of developing into a mature science.

I discuss only the relativistic Friedmann-Lemaître model, because in my opinion we have no serious alternative. I shall not discuss physics at redshifts greater than those relevant for light element nucleosynthesis, because although current ideas on the very early universe have had a strong and on the whole arguably beneficial effect, they have not yet generated any new positive observational results. Finally, I adopt as a benchmark for the state of thinking in cosmology 20 years ago the book *Physical Cosmology*[1] (hereafter PC). It was written in 1969-70, a few years after the discovery of the microwave cosmic background radiation (CBR), and at about the time physical cosmology began to become popular. It gives just one person's view, but I think it is a useful measure of the opinions of an appreciable fraction of the principals. (There were after all not that many.) But let us begin with a short statement of the establishment of the hot Big Bang cosmology as the standard model.

THE ORIGINS OF THE STANDARD PICTURE

The main steps in the discovery of the standard Big Bang cosmological model are well known. Einstein[2] gave us general relativity theory, and the bold assumption that the universe is homogeneous and isotropic in the large-scale average. Friedman[3] found the evolving solution to Einstein's field equations for a homogeneous isotropic universe. This solution predicts a linear relation between galaxy distance and redshift, and Hubble[4] hit on the linear relation on observational grounds. But I identify Lemaître[5] as the founder of cosmology as a subject in physics. His 1927 paper was the first to to make the now standard connection between physical theory and observation in the Big Bang model. (It is difficult to decide whether in 1927 Lemaître knew of Hubble's law, but he certainly understood that there would have to be a linear relation between distance and redshift in a homogeneous expanding universe. It is interesting that Lemaître's 1927 estimate of the constant of proportionality, based on Hubble's distance estimates, is close to the value given by Hubble in 1929.) Lemaître[6] recognized that in general relativity theory the expanding universe is gravitationally unstable, and that this instability is likely to have something to do with the tendency of galaxies to be found in groups and clusters, a subject that much exercises us today.

In the decade following World War II, George Gamow was the master of the Big Bang physical cosmology. He and his colleagues saw the connection between a hot Big Bang and

element production, as the universe expands and cools, and they had the right order of magnitude for the primeval entropy per baryon, and so the present CBR temperature.[7)]

The other major theme in post World War II cosmology was the Steady State theory developed by Bondi, Gold and Hoyle.[8)] This theory was an important stimulus to observational work, much of it with the goal of disproving the Steady State theory. To quote a more positive example, the Steady State theory predicts that galaxies have a broad range of ages, some much younger than the Hubble time. The paper in 1963 by Burbidge, Burbidge and Hoyle on this point foreshadows the recent debate on whether galaxies could be as young as is suggested by the Cold Dark Matter theory.[9)]

The great challenge to the the Steady State theory was the discovery of the microwave cosmic background radiation, or CBR, or what we used to call the Primeval Fireball. Bob Dicke (who ranks in my pantheon with the above master physical cosmologists) initiated a search for this radiation. As Bob Wilson describes in these Proceedings, that is what led Penzias and Wilson to recognize in 1965 that the radiation may already have been detected in their radio telescope.

The test of the interpretation of the microwave background as the thermal radiation left over from the early dense stages of expansion of the universe is the prediction that the spectrum is very close to a thermal Planck function. The prediction is robust because the heat capacity of the radiation is so large that it is difficult to think of processes that could appreciably perturb it. Progress in measuring the spectrum at wavelengths longer than ~ 3 mm was rapid; by 1970 there was strong evidence for consistency with the Rayleigh-Jeans part of the spectrum, and a reasonable case for detection of the predicted break away from a power law at $\lambda \sim 3$ mm (as illustrated in Fig. V-1 in PC). However, as one sees in Figure V-2 in PC, the observational situation at shorter wavelengths was quite confused. Only recently, with the beautiful work described in these Proceedings by Cheng and Halpern, has it become clear that the CBR does have the closely thermal spectrum predicted by the hot Big Bang interpretation.

The thermal form of the spectrum of this radiation is considered to be almost tangible evidence that the universe expanded from a state considerably denser than it is now, because it is exceedingly difficult to see any other way to make the spectrum so close to thermal. Consider for example the classical Steady State theory, in which the mean mass density of the universe is constant in time. It is not unreasonable to conjecture that radiation is created along with baryons, but it would be absurd to supose the spectrum of the spontaneously created radiation is just such that the integrated background (taking account of the redshift suffered by distant radiation) is very nearly thermal. Instead, one looks for a relaxation mechanism, that makes the universe optically thick at centimeter through submillimeter wavelengths. And the optical depth must reach unity at very low redshifts. For example, if the optical depth reached unity at $z \sim 0.1$, the integrated background would be a superposition of Planck functions with a roughly 10% percent spread in temperatures, which would disagree with the new submillimeter spectrum measurements. But of course we know from radio astronomy that the universe is optically thin to considerably higher redshifts than $z \sim 0.1$.

The discovery of the microwave CBR naturally revived interest in element production in the early universe.[10] The predicted light element production depends on the present baryon density. It is encouraging that in the simplest homogeneous model the required baryon density is in the acceptable range, somewhat greater than what is observed in stars in the bright parts of galaxies, somewhat less than dynamical estimates of the total mass density. The computation also depends on the contribution to the mass density at the epoch of element production by relativistic weakly interacting matter such as gravitational radiation, or new species of low mass neutrinos. Such additional relativistic matter would be difficult to detect today because the energy density would be suppressed by redshift. Its effect at high redshifts is to increase the expansion rate at a given temperature. The increased expansion rate reduces the relaxation of the neutron-proton abundance ratio to its low equilibrium value, so there are more neutrons to make deuterium to burn to helium. This means that adding relativistic species increases helium production. It was already clear in 1970 that the existence of a substantial number of new neutrino families would cause problems by predicting excessive helium production (PC p. 267). As described in Schramm's contribution to these Proceedings, several groups continued honing the argument, and harvesting and refining the interpretation of the observational results. This has led to what appears to be an elegant positive test of the standard model.

The general moral of this story is that we are past the days when the invention of cosmologies could be based on physical or philosophical principles alone. If you want people to pay attention to your alternative cosmology, you are going to have to face up to the precision tests the standard model passes so well, in particular the thermal spectrum of the CBR, but including also the other fundamental tests, such as light element production, the isotropy of the radiation backgrounds and deep counts of objects, and the linearity of the redshift-distance relation.

The specific moral is that within the standard model the CBR temperature is a key parameter in fixing the thermal and dynamical history of the universe. The measurement of this parameter made physical cosmology much more definite, and the detection of the radiation made the Big Bang cosmology a good deal more credible. These are the major factors in the explosion of interest in physical cosmology over the last 25 years.

LARGE-SCALE STRUCTURE

Hubble[11] introduced two tests of Einstein's assumption of large-scale homogeneity: galaxy counts away from the zone of avoidance are predicted to be isotropic across the sky and to vary with apparent magnitude m as $dN/dm \propto 10^{0.6m}$. The latter is unlikely ever to be a precision test because the K-correction for redshift at the faint end overlaps the correction for local clustering at the bright end, with the result that the counts vary more nearly as $N(m) \propto 10^{0.45m}$. Hubble was well aware that the fluctuations of galaxy counts across the sky are larger than would be expected for a homogeneous random Poisson process; yet another of Hubble's laws is that the galaxy counts within a given limiting magnitude and angular field size have a lognormal frequency distribution, a result of the clustering of

galaxies. As Shapley[12] emphasized, one can identify major nearby concentrations as clouds or supergalaxies or superclusters of galaxies.

For the purpose of physical cosmology one wants to have numerical measures of the clustering. An obvious first choice for a point process is the two-point correlation function, $\xi(r)$, the analog of an autocorrelation function. Rubin[13] Limber[14] and Totsuji and Kihara[15] found the first estimates of $\xi(r)$, with values for the clustering length r_o (such that $\xi(x_o) = 1$) close to the modern value,

$$r_o = 5.4 \pm 0.5\, h^{-1} \text{ Mpc} , \tag{1}$$

for Hubble constant $H = 100h$ km s^{-1} Mpc^{-1}. By the early 1980s we had satisfactory tests of reproducibility of measures of the low order correlation functions derived from angular catalogs of different depths, and from the CfA redshift catalog. The results showed that the small-scale galaxy distribution is well approximated as a fractal with dimension $D = 3 - \gamma = 1.23 \pm 0.04$, and that at $r \sim 2r_o$ the two-point function breaks down from the power law observed on smaller scales. A handy measure of the degree of large-scale fluctuations in the galaxy counts is that the rms fluctuation in the count within a randomly placed sphere of diameter $d = 2r = 40h^{-1}$ Mpc is

$$\frac{\delta N}{N} = \int \frac{d^2V}{V^2} \xi(r_{12}) \sim \frac{3}{r^3} J_3(r) \sim 0.5 . \tag{2}$$

The integral $J_3(r) = \int_o^r r^2 dr\, \xi(r)$ is taken from Clutton-Brock and Peebles;[16] a similar value for $\delta N/N$ is found in the recent study of Efstathiou *et al.*[17] The length 40 h^{-1} Mpc is a reasonable measure of the scale of the transition from the non-linear fluctuations observed on small scales to the nearly homogeneous large-scale distribution.

In the 1980s there was some debate on the reliability of these results. This was an appropriate challenge, that led to a thorough reevaluation of the old work, and left me feeling even more confident that the results as summarized above are believable. All this is chronicled Groth and Peebles[18] and references therein. But of course the best argument is an independent measurement, and I find it comforting that the two-point function from the Cambridge-Oxford APM galaxy survey is in excellent agreement with the earlier results at small scales and through the break in $\xi(r)$.[19] Beyond the break $\xi(r)$ is small and hard to measure. Here the new APM estimates are above the old results. That may well be because the older work overcorrected for variable obscuration in our galaxy, but it is also possible the APM result underestimates the correction. My bet is that $\xi(r)$ is somewhere between the two!

One can test how well the fractal model captures the character of the galaxy distribution, by using it as a prescription for the construction of point distributions that can be compared to maps of the observed galaxy distribution. Angular maps of the model distributions look reasonably similar to the observations, though the model lacks a certain crispness.[20] A model redshift map from Soneira's thesis is shown in Figure 1. The peculiar velocities assume virial equilibrium within the small-scale clustering hierarchy. The map covers polar angles

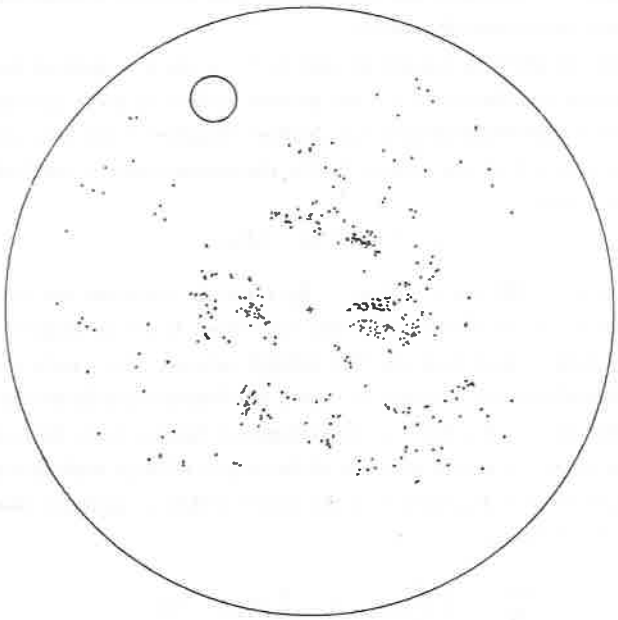

Fig. 1. Redshift map in a model distribution that matches the observed low order galaxy correlation functions at $r \lesssim 2r_o$, with statistically independent positions at separations $r \gtrsim 4r_o$. The radial position coordinate is proportional to the redshift, with peculiar velocities based on virial equilibrium within the clustering hierarchy. The slice has a depth of 10°. The radius of the large circle is 70 h^{-1} Mpc. The small circle has a diameter of 10 h^{-1} Mpc.

$30 < \theta < 40°$ to redshift $cz < 7000$ km s^{-1}. The limiting magnitude in the model is $m \sim 14$, in a magnitude system where the limit is $m = 14.5$ in the CfA galaxy redshift survey.[21] The small circle has diameter $10h^{-1}$ Mpc. As one would anticipate from equation (2), it is not hard to find voids in the model map three times this size.

The model map in Figure 1 was made some five years before the CfA galaxy redshift survey.[21] I have since regretted that I never pushed Ray Soneira to publish it, because the model redshift maps give a good illustration of what we expected the redshift surveys to show, and what turned out to be new in them. As I have indicated, the $\sim 30h^{-1}$ Mpc voids were no surprise: to produce the observed small-scale clustering one must collect galaxies into clumps, leaving voids. What became clear to me (though others certainly anticipated it) only in still more densely sampled redshift surveys[22] is that the voids tend to have sharp smooth walls.

There are of course many ways to measure the galaxy distribution. My guess is that alternatives to N-point correlation functions will increasingly come into play as people analyze the new deeper redshift surveys, that sample the galaxy distribution on scales where the two-point correlation function is close to zero.

What is the theoretical significance of the numerical measures of galaxy clustering? I

have been surprised at the number of different theories for galaxy formation that are said to give reasonable approximations to the galaxy two-point function, and in some cases also the three-point function. Perhaps there is something generic about the observed forms of the low order correlation functions; perhaps there has been some filtering of the theories that reach publication. The simple forms of the low order correlation functions led to the dream that they could be explained by simple physics. I have not yet given up hope but must admit that we do not seem to be close to realizing the dream. I would rate the state of physical cosmology in this subject as "emerging."

MISSING MASS

The phrase "missing mass" has fallen out of style, perhaps because it is the starlight that is missing, but the phrase has an honorable history and a definite meaning: we seem to have missed mass in our accounting of the contents of galaxies and clusters of galaxies. In the 1960s people were well aware of the missing mass puzzle; you can read in PC (pp. 115-117) and elsewhere familiar-sounding themes, on "dead" galaxies, "massive faint halos of galaxies," and the possibility that the missing mass might bring the total to the critical Einstein-de Sitter mass density.

In the 1970s the idea of massive faint halos of galaxies became a good deal more definite with the discovery of the nearly flat rotation curves of the outer parts of spiral galaxies,[23] and, on the theoretical side, with the recognition that massive dark halos would be a good way to account for the stability of disc galaxies[24] and for the systematics of structures and motions of systems of galaxies.[25]

In the 1970s I indulged in a good deal of wishful argumentation about the possibility of reaching the critical Einstein-de Sitter density (density parameter $\Omega = 1$). My faith was shaken by the analysis of the CfA redshift catalog, that showed that the rms relative velocity $\sigma(r_p)$ as a function of galaxy separation r_p has a shape that agrees with the assumption that galaxies trace mass, but an amplitude well below the Einstein-de Sitter prediction.[26] We were careful to note that our low estimate of Ω from the CfA catalog applies only to mass clustered with galaxies on scales $\lesssim 1h^{-1}$ Mpc, but I remember that this is what led me to start thinking about alternatives to Einstein-de Sitter.

In the 1980s Kaiser, Bardeen, and the team of Davis, Efstathiou, Frenk and White pioneered the biasing concept,[27] that "dead" galaxies might reasonably be expected to be in the voids, and so missed from the dynamical measures of the mean mass density. This has been an influential idea, and may even be right, but we should bear in mind that there is not much observational evidence in support of it. To the contrary, as mentioned above, the statistic $\sigma(r_p)$ is consistent with the assumption that optically bright galaxies are an unbiased tracer of mass. Also, I consider it a serious problem that the biasing picture surely would predict that galaxies in voids show signs of their development under adverse conditions — a tendency to be irregular, or to have low luminosity — but that the effect not very prominent in the observations.

It is worth pausing to consider the test of the biasing picture using the galaxies in our immediate neighborhood, where we have a complete survey well into the faint end of the luminosity function. At distances $\lesssim 4h^{-1}$ Mpc there are a dozen or so bright galaxies, most of which lie in the plane of the de Vaucouleurs Local Supercluster. There are over 200 faint galaxies known within the same distance, and most lie in the plane defined by the bright ones. In the Einstein-de Sitter model, most of the mass within $4h^{-1}$ Mpc would have to be in the local voids away from the plane, because it is difficult to see how the mass could be concentrated with the seen galaxies in our neighborhood without making the virial motions larger than the observations. Under the biasing picture, with most of the mass in the voids, there would be many hundreds of the seeds of failed galaxies within $4h^{-1}$ Mpc distance. It surely is reasonable to expect that among all these failed seeds some would have developed into visible galaxies, and that such galaxies would bear the stigmata of an unhealthy youth. There are a few galaxies in the nearby voids. The brightest nearby one is NGC 6946. But it looks like a normal giant spiral. Another interesting case is DDO 154, which Carignan and Freeman[28] call a Dark Galaxy, because if it were a little fainter, or a little farther away, it would be an optically invisible massive object. This is just the sort of thing the biasing picture would suggest is present in great numbers in the voids. However, DDO 154 is in the plane of the Local Supercluster, with most of the other galaxies, and there are not many candidates for objects like it in the local voids.

The biasing picture is a bold conjecture that, like the Steady State theory, has had a beneficial effect on research in physical cosmology. Perhaps, unlike the Steady State theory, the biasing picture will prove to be right. However, following the rules of experimental/observational science, my conclusion is that biasing must be treated with reservation unless or until we find some positive evidence that the obvious reading of the clues so far thrown our way has been misleading.

Whatever the value of the mean mass density, it is clear either that we have the wrong gravity physics or else the mass of the universe is dominated by dark matter. The definite and exciting challenge is to discover the nature of the dark mass. The standard computation of light element production in the hot Big Bang suggests some of the dark mass is baryonic, but not all. The ongoing experimental and observational searches for signatures of the dark mass, whether baryonic or exotic, are exciting examples of physical cosmology in progress.

COSMOLOGICAL TESTS

The purpose of the classical cosmological tests is to measure the curvature parameter $(HR)^{-2}$, the density parameter $\Omega = 8\pi G\rho/3H^2$, and the parameter $\Lambda/3H^2$ associated with a cosmological constant. And one would like to have redundant measurements, so as to test the theory and the measurements. The chances for doing this did not seem very high in the 1970s, because of the problems of separating cosmological effects in the observations from those due to evolution of the galaxies (as discussed for example by Tinsley[29] in 1972). That is why there is not much discussion of the classical tests in PC, and why I ruled out a discussion of Λ, on the grounds that we had more than enough unknowns without it.

It was of course apparent that the situation could change if advances in technology permitted observations of galaxies at redshifts on the order of unity, where the observational differences among the predictions of different choices of the cosmological parameters can be large. Recent milestones in this direction are the extension of the redshift-infrared magnitude diagram to redshifts greater than unity,[30] and deep galaxy counts as a function of redshift.[31] I think we should not emphasize too much the preliminary estimates of the cosmological parameters from these pioneering studies. The key point is that the advances in ability to observe galaxies at high redshifts might be expected to stimulate a new cycle of application of the classical cosmological tests, as I think we already are seeing happen, because the increase in redshift causes a qualitative change in the effects one looks for.

The theoretical side also has seen some pronounced cycles of activity. It is amusing to note Robertson's[32] remark from 1955: the Einstein-de Sitter model is "of some passing interest." In the 1980s the Einstein-de Sitter case often was called the "standard model." One reason is that inflation argues against appreciable space curvature. I suspect another is that the inflation concept was partially inspired by and in turn popularized the Dicke coincidence argument against appreciable values for space curvature or the cosmological constant. Coincidence arguments have worked in other contexts, and we rightly pay attention to this one, but we should also recognize that a coincidence argument is not the same as an observational test. My impression (perhaps wishful) is that as we enter the 1990s we are starting to see a little more negotiation on the cosmological parameters.

GALAXY FORMATION

In the 1970s discussions of how galaxy might have formed tended to be phenomenological and schematic. In the 1980s inflation and other ideas from particle physics led to the invention and study of rather explicit scenarios involving hypothetical objects such as cold dark matter and cosmic strings. Dekel[33] has given an amusing and instructive account of the evolving fortunes of the leading theories during the 1980s. Dekel predicts this activity will continue into the 1990s, and that certainly agrees with experience to date. However, I hope we may also see some more stabs at phenomenology, of which we have a much larger store now. To conclude this review, I present the following example of what I have in mind.

Let us consider, within conventional physics, what might be a straightforward interpretation of the observations that seem relevant to the origin of galaxies.

I think the straightforward conclusion from the studies of the dynamics of galaxies is that the density parameter is $\Omega \sim 0.1$. The standard model for nucleosynthesis in the hot Big Bang (together with the large Hubble constant I am going to adopt) indicates the baryon density is a third of this dynamical estimate. Possibilities are that the dynamical approach overestimates Ω, or inhomogeneous nucleosynthesis somehow increases the allowed baryon density, or there is a soupçon of non-baryonic matter. For the purpose of this exploratory discussion I adopt the first possibility, and take

$$\Omega = \Omega_{\rm baryonic} = 0.03 \ . \qquad (3)$$

(This would say that $\sim$ 20 % of the mass of the universe is within the Abell radius of an Abell cluster, which does seem high. A systematic study of options at Ω closer to 0.1 would be in order, but this is not the place to do it.)

Under general relativity theory, and with Ω in moveable matter less than unity, we have to have nonzero space curvature or a nonzero cosmological constant (but not both in the simplest case). The latter option has the advantage that the rate of growth of mass density fluctuations is almost as large as in the Einstein-de Sitter model.[34] It also may be relevant that in the best picture we have for the very early universe, inflation, space curvature has to be negligible. I assume therefore that space curvature has negligible effect on the expansion rate, and that there is a cosmological constant that contributes the fraction $\Omega_\Lambda = 0.97$ to H^2. (A Λ term that is slowly rolling toward zero maybe is more elegant, and would not much affect the story.)

With Hubble parameter

$$H_o = 100 \text{ km s}^{-1} \text{ Mpc}^{-1} , \tag{4}$$

the age of the universe in this cosmology is[34]

$$t_o = 16 \text{ by} . \tag{5}$$

These values for H_o and t_o are within the ranges now under discussion.

The background radiation drag on ionized matter became unimportant at redshift $z \sim 100$. Let us consider the situation a little later, at expansion factor $1 + z = 30$. At this epoch Hubble's constant is

$$H = 2800 \text{ km s}^{-1} \text{ Mpc}^{-1} , \tag{6}$$

and the mean density is

$$n \sim 0.01 \text{ protons cm}^{-3} . \tag{7}$$

The present mean luminosity density is 2×10^8 $L_\odot$ Mpc^{-3}, and a characteristic galaxy luminosity is 10^{10} $L_\odot$, so a characteristic present number density of bright galaxies is $n_o \sim 0.02$ Mpc^{-3}. The mean distance between bright galaxies scaled back to $1 + z = 30$ is

$$n^{-1/3} = l \sim 100 \text{ kpc} , \tag{8}$$

so at this redshift the typical relative velocity of neighboring galaxies is

$$Hl \sim 300 \text{ km s}^{-1} . \tag{9}$$

If each of these galaxies had a dark halo, with circular velocity 200 km s^{-1}, the halo radius needed to produce the assumed mean mass density in equation (3) is

$$R_{\max} \sim 50 \text{ kpc} . \tag{10}$$

Now we note that the mean density in equation (7) at $1 + z = 30$ is well below the mean density within the bright parts of galaxies, consistent with the fact that the mean distance between bright galaxies (eq. [8]) is considerably larger than the size of the bright part of a galaxy. The halo radius $R_{\rm max}$ in equation (10) is compararable to the distance l between galaxies (eq. [8]). That is, protogalaxies with mass structures and comoving number density comparable to present day giant galaxies could have existed at $1 + z = 30$ (though not much earlier). The straightforward assumption is that the universe yesterday was much like the universe today, lumpy on small scales, smooth in the large-scale average. By this extrapolation, or by the argument that what is not forbidden is required, the straightforward assumption within the cosmology adopted here is that mass concentrations with mass structures comparable to present galaxies existed at $1 + z = 30$.

The galaxies observed at expansion factors $1 + z \sim 2$ to 4 look irregular, and it is reasonable to guess that galaxies at $z \sim 30$ were quite untidy objects, still in the process of accreting a good deal of mass in gas and stars. The collapse factor from the characteristic length l in equation (8) to a disc radius ~ 5 kpc is roughly what is thought to be needed to spin up a rotationally supported disc made from accreted gas, so we could imagine that at $z \sim 30$ discs are starting to form out of intergalactic gas as the period of heavy accretion comes to an end. We can imagine star formation already had raised the level of heavy elements in this accreted material. We must also imagine that star formation is converting the larger part of it into a dissipationless state out of which the extended massive halos are forming. Since we have abandoned exotic matter, we must assume that star formation in the relatively low density intergalactic medium at $z \sim 30$ favored massive comets, or Jupiters, or very low mass stars, or other relatively dark objects. Since the halo radius $R_{\rm max}$ is comparable to l (eqs. [8] and [10]), the massive halos would be just in the process of forming at $z \sim 30$. Consistent with this, the characteristic velocity in equation (9) is typical of the motions within halos.

Now let us consider the CBR anisotropy to be expected in this scenario. The Hubble length at $z \sim 30$ is

$$L = ct = \frac{2}{3}\frac{c}{H} \sim 70 \text{ Mpc} , \tag{11}$$

about the present distance to the Coma cluster. If observers had been present they would only have needed modest telescopes to observe galaxies at the Hubble distance. However, if much of the mass at $z \sim 30$ were still in optically thin plasma, concentrated in and around the protogalaxies, the optical depth for electron scattering at the Hubble length would be

$$\tau = \sigma n L \sim 1.3 . \tag{12}$$

That is, galaxies at redshift near unity would tend to be obscured by electron scattering. The same effect would erase primeval irregularities in the CBR on scales much smaller than the Hubble length L in equation (11).

To translate this smoothing by electron scattering into what would be observed today, we need the relation between the physical diameter d of an object at redshift z and the angular

size θ it subtends at the present epoch:

$$\theta = \frac{H_o d}{c} \frac{1+z}{(H_o a_o x/c)} . \tag{13}$$

In the present cosmological model the coordinate distance x at $1 + z = 30$ is

$$H_o a_o x/c = 6.9 . \tag{14}$$

Equation (12) says that the smoothing length of the CBR could be comparable to the Hubble length L in equation (11). By equations (13) and (14) the smoothing angle in this case is

$$\theta_s \sim 6^\circ , \tag{15}$$

at the present epoch.

At angular scales $\gtrsim \theta_s$ the fluctuations in the CBR are unaffected by the scattering. However, this probes the primeval mass fluctuations on comoving scales

$$R \gtrsim (1+z)L \sim 2000 \text{ Mpc} , \tag{16}$$

considerably larger than the scales on which we have observations from which to estimate the amplitude of the mass density fluctuation spectrum.

On scales substantially smaller than θ_s, free electron scattering removes the primeval fluctuations in the CBR and inserts anisotropy due to the coherent motion of plasma within clouds. Since a gas cloud in a protogalaxy with the diameter $\sim$ 10 kpc characteristic of a galaxy subtends an angle of only $\sim$ 3 arc sec, and the amplitude of the inserted anisotropy due to motions within the protogalaxy is not large,[35] the reinserted anisotropy in this picture seems to be below the present observational limits. That is, it does not seem to be difficult to reconcile early galaxy formation with the small anisotropy of the CBR.

This discussion is meant to show that, by following the path of least resistance through the observations, one can arrive at a galaxy formation scenario of some substance. The approach is semiempirical, in the sense that the analysis is strongly guided by conventional physical ideas. The result certainly is speculative, but I like the fact that the speculation is pretty closely guided by the phenomena. I also like the resulting picture, with what I would consider reasonable collapse factors for halos and discs, and galaxy formation at relatively high redshift so one is comfortable with the observation that the intergalactic medium is in place at expansion factor $1 + z \sim 6$.

CONCLUDING REMARKS

The CBR and light element production are by no means the only pieces of evidence for the standard hot Big Bang model; a more thorough review would include the homogeneity measurements, Hubble's law, the order of magnitude prediction of the age of the universe, and so on. However, it is the successful predictions of the CBR thermal spectrum and the

light element abundances that strongly argue for the Big Bang model and against any known alternative.

The physics of light element production is straightforward and has been understood for several decades. The important recent developments have been the improved understanding of the light elements, including abundances and astrophysical sources, and the constraints from particle physics on the contribution of neutrinos to the mass density at high redshifts. If the consistency of observed and computed abundances continues to stand up this will be a shining example of the success of cosmology as a physical science.

Even older than the idea of light element production is the search for measures of the parameters of the standard cosmological model: the mean mass density, space curvature, and the cosmological constant. The observational difficulties are well known, and the record of theoretical opinions is not inspiring. However, there is a new development, the ability to apply the classical cosmological tests at high redshifts where the cosmological effects are large. I think we will do well to be alert to what comes of this new round of applications of the classical tests.

It may be that inspired guesses about the nature of the dark matter, and the physics of the very early universe, will lead us to the correct theory for the origin of galaxies and the large-scale structure of the galaxy distribution. Progress in this direction during the 1980s was mixed. An alternative is the semiempirical approach, an example of which was presented in the last section. I believe this approach is worth further discussion. For the more distant future, the reasonable guess is that a fully satisfactory theory of the origin of galaxies will be informed by a definite physical model for the early universe, because the behaviour of a protogalaxy is strongly influenced by the background cosmology. Someone may hit on the appropriate model for the early universe by the *ab initio* methods of the 1980s, or it may be that the semiempirical approach will turn up a scenario that seems compelling, and that the scenario is what guides us to the early universe.

My conclusion is that cosmology has developed into an active physical science. The paradigm has given us a network of successful predictions and, to keep us occupied, a set of well defined puzzles with lots of clues.

This work was supported in part at Princeton University by the US National Science Foundation, and at the Institute for Advanced Study by the Ambrose Monell Foundation.

REFERENCES

1) Peebles, P. J. E. 1971, *Physical Cosmology* (Princeton: Princeton University Press).
2) Einstein, A. 1917, S.-B. Preuss. Akad. Wiss., 142.
3) Friedman, A. 1922, *Z. Phys.*, **10**, 377.
4) Hubble, E. 1929, *Proc. N. A. S.*, **15**, 168.
5) Lemaître, G. 1927, *Ann. Soc. Sci. Bruxelles*, **47A**, 49.
6) Lemaître, G. 1931, *M. N. R. A. S.*, **91**, 490.
7) Gamow, G. 1948, *Phys. Rev.*, **74**, 505; Alpher, R. A. and Herman, R. C. 1948, *Nature*, **162**, 774.

8) Bondi, H. and Gold, T. 1948, *M. N. R. A. S.*, **108**, 252; Hoyle, F. 1948, *M. N. R. A. S.*, **108**, 372.
9) Burbidge, E. M., Burbidge, G. R. and Hoyle, F. 1963, *Ap. J.*, **138**, 873; Frenk, C. S. *et al.* 1989, *The Epoch of Galaxy Formation* (Dordrecht: Kulwer Publishers).
10) Peebles, P. J. E. 1966, *Ap. J.*, **146**, 542; Wagoner, R. V., Fowler, W. A. and Hoyle, F. 1967, *Ap. J.*, **148**, 3.
11) Hubble, E. 1926, *Ap. J.*, **64**, 321; 1934, *Ap. J.*, **79**, 8.
12) Shapley, H. 1935, *Proc. N. A. S.*, **21**, 587.
13) Rubin, V. C. 1954, *Proc. N. A. S.*, **40**, 541.
14) Limber, D. N. 1954, *Ap. J.*, **119**, 655.
15) Totsuji, H. and Kihara, T. 1969, *Publ. Astron. Soc. Japan*, **21**, 221.
16) Clutton-Brock, M. and Peebles, P. J. E. 1981, *A. J.*, **86**, 1115.
17) Efstathiou, G., Kaiser, N., Saunders, W., Rowan-Robinson, M., Lawrence, A., Ellis, R. S. and Frenk, C. S. 1990, *M. N. R. A. S.*, in press.
18) Groth, E. J. and Peebles, P. J. E. 1986, *Ap. J.*, **310**, 507.
19) Maddox, S. J., Efstathiou, G., Sutherland, W. and Loveday, J. 1990, *M. N. R. A. S.*, **242**, 43p.
20) Soneira, R. M. and Peebles, P. J. E. 1978, *A. J.*, **83**, 845; Soneira, R. M. 1978, PhD. dissertation, Princeton University.
21) Davis, M., Huchra, J., Latham, D. W. and Tonry, J. 1982, *Ap. J.*, **253**, 423.
22) Geller, M. J. and Huchra, J. P. 1990, *Science*, **246**, 897; Haynes, M. P. and Giovanelli, R. 1986, *Ap. J. Letters*, **306**, L55.
23) Shostak, G. S. and Rogstad, D. H. 1973, *Astron. Astrophys.*, **24**, 405; Rubin, V. C., Thonnard, N. and Ford, W. K. 1977, *Ap. J. Lett.*, **217**, L1; Bosma, A. 1981, *A. J.*, **86**, 1791.
24) Ostriker, J. P. and Peebles, P. J. E. 1973, *Ap. J.*, **186**, 467.
25) Einasto, J., Kaasik, A. and Saar, E. 1974, *Nature*, **250**, 309; Ostriker, J. P., Peebles, P. J. E. and Yahil, A. 1974, *Ap. J. Letters*, **193**, L1.
26) Davis, M. and Peebles, P. J. E. 1983, *Ap. J.*, **267**, 465.
27) Kaiser, N. 1986, in *Inner Space/Outer Space* (Chicago: Univ. of Chicago Press), eds. E. W. Kolb *et al.*, p. 258; Bardeen, J. M. 1986, in *Inner Space/Outer Space* (Chicago: Univ. of Chicago Press), eds. E. W. Kolb *et al.*, p. 212; Davis, M., Efstathiou, G., Frenk, C. S. and White, S. D. M. 1985, *Ap. J.*, **292**, 394.
28) Carignan, C. and Freeman, K. C. 1988, *Ap. J.*, **332**, L33.
29) Tinsley, B. M. 1972, *Ap. J. Lett.*, **173**, L93.
30) Lilly, S. J. and Longair, M. S. 1984, *M.N.R.A.S.*, **211**, 833; Spinrad, H. and Djorgovski, S. 1987, in *Observational Cosmology*, eds. A. Hewitt, G. Burbidge and Li Zhi Fang (Dordrecht: Reidel) p. 129.
31) Loh, E. D. and Spillar, E. J. 1986, *Ap. J.*, **307**, L1; Koo, D. C. 1989, in *The Epoch of Galaxy Formation* (eds. Frenk, C. S. *et al.*) Kluwer Publishers, p. 71; Lilly, S. J., Cowie, L. L and Gardner, J. P. 1990, *Ap. J.*, in the press.
32) Robertson, H. P. 1955, *Pub. A. S. P.*, **67**, 82.
33) Dekel, A. 1988, in *Large-Scale Motions in the Universe*, eds V. C. Rubin and G. V. Coyne (Princeton: Princeton University Press) p. 567.
34) Peebles, P. J. E. 1984, *Ap. J.*, **284**, 439.
35) Peebles, P. J. E. 1990, in *The Galactic and Extragalactic Background Radiation* eds. S. Bowyer and C. Leinert (Dordrecht: Kulwer Academic Publisher) p. 295.

INFLATIONARY COSMOLOGY

Andrei Linde[1]

Department of Physics, Stanford University, Stanford CA 94305-4060, USA[2]

ABSTRACT

We discuss an interplay between elementary particle physics, quantum cosmology and inflation. It is shown that domains of the inflationary universe with sufficiently large energy density permanently produce new inflationary domains. Therefore the evolution of the universe in the inflationary scenario has no end and may have no beginning. After inflation the universe becomes divided into different exponentially large domains inside which properties of elementary particles and dimension of space-time may be different. It is argued that the simplest and the most natural realization of the idea of inflation is given by the chaotic inflation scenario. Some other models of the inflationary universe scenario are also discussed, including extended inflation based on the Jordan-Brans-Dicke theory of gravity.

[1]On leave of absence from: Lebedev Physical Institute, Moscow 117924, USSR and CERN, CH-1211 Geneva 23, Switzerland

[2]Bitnet address LINDE@SLACVM

1 Introduction

The standard Big Bang hot universe theory asserts that the universe was born at some moment $t = 0$ about 15 billion years ago, in a state of infinitely large density. With the rapid expansion of the universe, the average energy of particles, given by the temperature, decreases rapidly, and the universe becomes cold. This theory became especially popular after the discovery of the microwave background radiation, which is the main topic of this conference.

However, in the end of 70's it was understood that this theory is hardly compatible with the present theory of elementary particles (primordial monopole problem, Polonyi fields problem, gravitino problem, domain wall problem) and it has many internal difficulties (flatness problem, horizon problem, homogeneity and isotropy problem, etc.).

Fortunately, all these problems can be solved simultaneously in the context of a relatively simple scenario of the universe evolution - the inflationary universe scenario [1] - [6]. The invention of this scenario has modified considerably the standard cosmological paradigm [7]. The main idea of this scenario is that the universe at the very early stages of its evolution expanded quasi-exponentially (the stage of inflation) in a state with energy density dominated by the potential energy density $V(\phi)$ of some scalar field ϕ. This rapid expansion made the universe flat, homogeneous and isotropic and decreased exponentially the density of monopoles, gravitinos and domain walls. Later, the potential energy density of the scalar field transformed into thermal energy and still later, the universe was correctly described by the standard hot universe theory predicting the existence of the microwave background radiation.

The main idea of the inflationary universe scenario is very simple and it can be realized in a wide class of realistic theories of elementary particles. On the other hand, despite many efforts, no other solution of all problems mentioned above has been suggested during the last 10 years. Therefore many cosmologists believe that something like inflation actually has taken place at the very early stages of the evolution of the universe. One should note though, that *inflation* is not a magic word which can save all theories of elementary particles from being in a contradiction with cosmology. In many theories it is impossible to obtain inflation. Such theories typically lead to unacceptable cosmological consequences and, perhaps, should be abandoned. Many other theories can support inflation but still lead to disastrous cosmological consequences. Therefore cosmological considerations can be very useful for imposing strong constraints on various parameters of the theories of elementary particles and even on the classes of the cosmologically acceptable theories.

Historically, there were several different versions of the inflationary universe scenario [1]-[6]. One of the most important stages of the development of the inflationary cosmology was related to the old inflationary universe scenario of Guth [3]. This scenario was based on three fundamental propositions:

1. The universe initially expands in a state with a very high temperature, which leads to the symmetry restoration in the early universe, $\varphi(T) = 0$, where φ is some scalar field driving inflation (the inflaton field).

2. The effective potential $V(\varphi, T)$ of the scalar field φ has a deep local minimum at $\varphi = 0$ even at a very low temperature T. As a result, the universe remains in a supercooled vacuum state $\varphi = 0$ (false vacuum) for a long time. The energy-momentum tensor of such a state rapidly becomes equal to $T_{\mu\nu} = g_{\mu\nu}V(0)$, and the universe expands exponentially (inflates) until the false vacuum decays.

3. The decay of the false vacuum proceeds by forming bubbles containing the field φ_o corresponding to the minimum of the effective potential $V(\varphi)$. Reheating of the universe occurs due to the bubble-wall collisions.

Unfortunately, as it was pointed out by Guth in [3], this scenario had a major defect. If the rate of the bubble formation is bigger than the speed of the universe expansion, then the phase transition occurs very rapidly and inflation does not take place. On the other hand, if the vacuum decay rate is small, then the universe after the phase transition becomes extremely inhomogeneous, and in a considerable part of the physical volume of the universe the phase transition to the minimum of $V(\varphi)$ never completes. This is called the graceful exit problem.

The main idea of the old inflationary universe scenario was very simple and attractive. However, all attempts to solve or avoid the graceful exit problem and to suggest a successful inflationary universe scenario failed until cosmologists managed to surmount a certain psychological barrier and renounce all three of the aforementioned assumptions, while retaining the main idea of ref. [3] that the universe has undergone inflation during the early stages of its evolution. The invention of the new inflationary universe scenario [4] marked the departure from the assumptions (2), (3). Later it was shown that the assumption (1) also does not hold in all realistic models of inflation, for two main reasons. First of all, the time which is necessary for the field φ to roll down to the minimum of $V(\varphi, T)$ typically is too large, so that either inflation occurs before the field rolls to the minimum of $V(\varphi, T)$, or it does not occur at all. On the other hand, even if the field φ occasionally was near the minimum of $V(\varphi, T)$ from the very beginning, inflation typically starts very late, when thermal energy drops from M_p^4 down to $V(0, T)$. In all realistic models of inflation $V(0, T) < 10^{-10}M_p^4$, hence inflation may start in a state with $\varphi = 0$ not earlier than at $t \sim 10^4 M_p^{-1}$. During such a time a typical closed universe would collapse before the conditions necessary for inflation could be realized [7].

The assumption (1) was finally given up with the invention of the chaotic inflation scenario [5]. The main idea of this scenario was that instead of making the *assumption* that the scalar field from the very beginning should be in a state corresponding to a minimum of $V(\varphi, T)$, one should study various initial distributions of the scalar field φ and investigate in which case the inflationary regime may occur. The result of this investigation is that there

exists a wide class of theories where inflation occurs under quite natural initial conditions during a slow rolling of the scalar field down to the absolute minimum of its effective potential (for a review see [7]). This class includes all theories of a scalar field φ minimally coupled to gravity, with a polynomial effective potential $V(\varphi)$, or even with an exponential effective potential $V \sim \exp\frac{c\varphi}{M_p}$ with $c \lesssim 5$. The graceful exit problem in this scenario just does not appear. Recently it was shown that it is possible to solve the graceful exit problem of the old inflation in the context of the Jordan-Brans-Dicke theory [9]. The new scenario is called extended inflation [6]. It has an intermediate position between the old and the chaotic inflation scenario, but it is slightly more complicated since it requires a modification of the standard Einstein gravity theory and consideration of the theories containing at least two different scalar fields.

In this article we give a review of the present status of inflationary cosmology. We start with the discussion of a simplest version of the chaotic inflation scenario [5]. Then we discuss some recent developments in the inflationary cosmology, including the theory of a self-reproducing inflationary universe (eternal chaotic inflation) [10,11]. We will show that the universe containing at least one inflationary domain filled with a sufficiently big scalar field ϕ unceasingly produces inflationary domains of all possible types. According to this theory, there is no end (and there may be no unique beginning) of the evolution of the universe. The universe after inflation becomes divided into many exponentially large domains, inside which the laws of low energy physics and even the dimensionality of space-time may be different.

Many of these results remain valid for the extended inflation scenario as well. We develop the eternal extended inflation scenario and compare extended and chaotic inflation. We show in particular that the graceful exit problem can be solved in the theory of two scalar fields without any need to modify the Einstein gravity theory [12].

2 Chaotic Inflation

2.1 The stage of inflation

In our opinion, the simplest and, simultaneously, the most general version of the inflationary universe scenario is the chaotic inflation scenario [5]. To describe it, let us consider the simplest model based on the theory of a massive non-interacting scalar field ϕ with the Lagrangian

$$L = \frac{M_P^2}{16\pi}R + \frac{1}{2}\partial_\mu\phi\partial^\mu\phi - \frac{m^2}{2}\phi^2 \qquad (1)$$

Here $M_P^{-2} = G$ is the gravitational constant, $M_P \sim 10^{19}GeV$ is the Planck mass, R is the curvature scalar, m is the mass of the scalar field $\phi, m \ll M_P$. If the classical field ϕ is sufficiently homogeneous in some domain of the universe (see below), then its behavior inside

this domain is governed by the equations

$$\ddot{\phi} + 3H\dot{\phi} = -dV/d\phi, \tag{2}$$

$$H^2 + \frac{k}{a^2} = \frac{8\pi}{3M_P^2}(\frac{1}{2}\dot{\phi}^2 + V(\phi)). \tag{3}$$

Here $V(\phi)$ is the effective potential of the field ϕ (in our case $V(\phi) = \frac{1}{2}m^2\phi^2$), $H = \dot{a}/a, a(t)$ is the scale factor of the locally Friedmannian universe (inside the domain under consideration), $k = +1, -1$, or 0 for a closed, open or flat universe, respectively. If the field ϕ initially is sufficiently large ($\phi \geq M_P$), then the functions $\phi(t)$ and $a(t)$ rapidly approach the asymptotic regime

$$\phi(t) = \phi_0 - \frac{mM_P}{2(3\pi)^{1/2}}t, \tag{4}$$

$$a(t) = a_0 exp(\frac{2\pi}{M_P^2}(\phi_0^2 - \phi^2(t))). \tag{5}$$

According to (4) and (5), during a time $\tau \sim \phi/mM_P$ the value of the field ϕ remains almost unchanged and the universe expands quasi-exponentially:

$$a(t + \Delta t) \sim a(t)exp(H\Delta t) \tag{6}$$

for $\Delta t \leq \tau = \phi/mM_P$. Here

$$H = \frac{2\pi^{1/2}}{\sqrt{3}}\frac{m\phi}{M_P} \tag{7}$$

Note that $H \gg \tau^{-1}$ for $\phi \gg M_P$.

The regime of quasi-exponential expansion (inflation) occurs for $\phi \geq \frac{1}{5}M_P$. For $\phi \leq \frac{1}{5}M_P$ the field ϕ oscillates rapidly, and if this field interacts with other matter fields (which are not written explicitly in eq. (1)), its potential energy $V(\phi) \sim \frac{m^2\phi^2}{2} \sim m^2M_P^2$ is transformed into heat. The reheating temperature T_R may be of the order $(mM_P)^{1/2}$ or somewhat smaller, depending on the strength of the interaction of the field ϕ with other fields. It is important that T_R does not depend on the initial value ϕ_0 of the field ϕ. The only parameter which depends on ϕ_0 is the scale factor $a(t)$, which grows $\exp((2\pi/M_P^2)\phi_0^2)$ times during inflation.

If, as is usually assumed, a classical description of the universe becomes possible only when the energy-momentum tensor of matter becomes smaller than M_P^4, then at this moment $\partial_\mu\phi\partial^\mu\phi \leq M_P^4$ and $V(\phi) \leq M_P^4$.

Therefore, the only constraint on the initial amplitude of the field ϕ is given by $\frac{1}{2}m^2/\phi^2 \leq M_P^4$. This gives a typical initial value of the field ϕ:

$$\phi_0 \sim \frac{M_P^2}{m} \tag{8}$$

Let us consider for definiteness a closed universe of a typical initial size $O(M_P^{-1})$. It can be shown that if initially $\partial_\mu\phi\partial^\mu\phi$ becomes much smaller than $V(\phi)$, the evolution of the universe becomes describable by (2)-(7), and after inflation the total size of the universe becomes larger than

$$l \sim M_P^{-1} exp(\frac{2\pi}{M_P^2}\phi_0^2) \sim M_P^{-1} exp(\frac{2\pi M_P^2}{m^2}) \tag{9}$$

For $m \sim 10^{-6} M_P$ (which is necessary to produce density perturbations $\frac{\delta\rho}{\rho} \sim 10^{-5}$, see below)

$$l \sim M_P^{-1} \exp(2\pi 10^{12}) \geq 10^{10^{12}} cm, \tag{10}$$

which is much greater than the size of the observable part of the universe $\sim 10^{28} cm$.

After such a large inflation the term k/a^2 in (3) becomes negligibly small compared with H^2, which means that the universe becomes flat and its geometry locally Euclidean. This implies that the total density of the universe ρ becomes almost exactly equal to the critical density $\rho_c = \frac{3M_P^2}{8\pi}H^2$, i.e.

$$\Omega = \frac{\rho}{\rho_c} \sim 1. \tag{11}$$

For similar reasons the universe becomes locally homogeneous and isotropic. The density of all 'undesirable' objects (monopoles, domain walls, gravitinos) created before or during inflation becomes exponentially small. After inflation the universe becomes hot again due to the particle production by the scalar field ϕ oscillating near the minimum of its effective potential $V(\phi)$. However, in most models the reheating temperature, T_R, is not very large. Therefore monopoles and domain walls do not appear again after inflation.

We should like to emphasize that for a realization of this scenario *there is no need to have a domain of initial size bigger than horizon H^{-1}, where the conditions necessary for inflation are satisfied.* It is quite sufficient that initially $\partial_\mu\phi\partial^\mu\phi \leq V(\phi) \sim M_P^4$ in a domain of a smallest possible size $l \sim M_P^{-1} \sim H^{-1}$. (Note that this size coincides with a typical initial size of a closed universe at the Planck time.) Since $\partial_\mu\phi\partial^\mu\phi \leq M_P^4, V(\phi) \leq M_P^4$ in any classical spacetime, the above-mentioned initial conditions are quite natural. For a more detailed discussion of initial conditions which are necessary for inflation (and in particular for a discussion of the often repeated erroneous statement that for a realization of chaotic inflation scenario one must have domains of a homogeneous scalar field of a size much bigger than H^{-1}) see ref. [7].

2.2 Scalar field fluctuations, perturbations of density and galaxy formation

According to quantum field theory, empty space is not entirely empty. It is filled with quantum fluctuations of all types of physical fields. These fluctuations can be regarded as waves of

physical fields with all possible wavelengths, moving in all possible directions. If the values of these fields, averaged over some macroscopically large time, vanish, then the space filled with these fields seems to us empty and can be called the vacuum.

In the exponentially expanding universe the vacuum structure is much more complicated. The wave-lengths of all vacuum fluctuations of the scalar field ϕ grow exponentially in the expanding universe. When the wavelength of any particular fluctuation becomes greater than H^{-1}, this fluctuation stops propagating, and its amplitude freezes at some nonzero value $\delta\phi(x)$ because of the large friction term $3H\dot{\phi}$ in the equation of motion of the field ϕ. The amplitude of this fluctuation then remains almost unchanged for a very long time, whereas its wavelength grows exponentially. Therefore, the appearance of such a frozen fluctuation is equivalent to the appearance of a classical field $\delta\phi(x)$ that does not vanish after averaging over macroscopic intervals of space and time.

Because the vacuum contains fluctuations of all wavelengths, inflation leads to the creation of more and more new perturbations of the classical field with wavelengths greater than H^{-1}. The average amplitude of such perturbations generated during a time interval H^{-1} (in which the universe expands by a factor of e) is given by

$$|\delta\phi(x)| \approx \frac{H}{2\pi}. \tag{12}$$

Perturbations of the field lead to adiabatic perturbations of density $\delta\rho \sim V'(\phi)\delta\phi$, which after inflation grow, and at the stage of the cold matter dominance acquire the amplitude [13], [14], [7]

$$\frac{\delta\rho}{\rho} = \frac{48}{5}\sqrt{\frac{2\pi}{3}}\frac{V_\phi^{3/2}}{M_P^3 V'(\phi)}, \tag{13}$$

where ϕ is the value of the classical field $\phi(t)$ (4), at which the fluctuation we consider has the wavelength $l \sim k^{-1} \sim H^{-1}(\phi)$ and becomes frozen in amplitude. In the theory of the massive scalar field with $V(\phi) = \frac{m^2}{2}\phi^2$

$$\frac{\delta\rho}{\rho} = \frac{24}{5}\sqrt{\frac{\pi}{3}}\frac{m}{M_P}(\frac{\phi}{M_P})^2. \tag{14}$$

Taking into account of (4), (5) and also of the expansion of the universe by about 10^{30} times after the end of inflation, one can obtain the following result for the density perturbations with the wavelength $l(cm)$ at the moment when these perturbations begin growing and the process of the galaxy formation starts:

$$\frac{\delta\rho}{\rho} \sim 0.8\frac{m}{M_P}\ln l(cm). \tag{15}$$

At a galaxy scale ($l \sim 10^{21} - 10^{22} cm$)

$$\frac{\delta\rho}{\rho} \sim 40\frac{m}{M_P}, \tag{16}$$

which gives a desirable amplitude $\frac{\delta\rho}{\rho} \sim 10^{-4} - 10^{-5}$ for $m \sim 2.10^{-7} - 2.10^{-6} M_p$. In what follows we will assume that $m \sim 10^{-6} M_P$.

3 Self-Reproducing Inflationary Universe

In our previous investigation we only considered local properties of the inflationary universe, which is quite sufficient for a description of the observable part of the universe of the present size $l \sim 10^{28}$ cm. Indeed, in accordance to (15) our universe remains relatively homogeneous on a scale

$$l \leq l^* \sim exp(\frac{M_P}{m})\ cm \sim 10^{5.10^5} cm. \tag{17}$$

The corresponding density perturbations were formed at the time, when the scalar field $\phi(t)$ was bigger than ϕ^*, where

$$\phi^* \sim \frac{M_P}{2}\sqrt{\frac{M_P}{m}} \sim 10^3 M_P, \tag{18}$$

see (14). (Note that $V(\phi^*) \sim \frac{m^2}{2}(\phi^*)^2 \sim m M_P^3 << M_P^4$). On a scale $l > l^*$ the universe becomes extremely inhomogeneous due to quantum fluctuations produced during inflation. We are coming to a paradoxical conclusion, that the global properties of the inflationary universe are determined not by classical but by quantum effects.

Let us try to understand the origin of such a behavior of the inflationary universe.

A very unusual feature of the inflationary universe is that processes separated by distances l greater than H^{-1} proceed independently of one another. This is so because during exponential expansion any two objects separated by more than H^{-1} are moving away from each other with a velocity v exceeding the speed of light. (This does not contradict special relativity because v is not the speed of any signal; it is just the rate at which the general expansion of the universe separates two distant points.) As a result, any observer in the inflationary universe can see only those processes occurring nearer than H^{-1}.

An important consequence of this general result is that the process of inflation in any spatial domain of radius H^{-1} occurs independently of any events outside it. Any two inflationary domains displaced by more than H^{-1} cannot collide or eat one another, or do each other any damage. Their expansion is due not to the annexation of the territory of their neighbors, but rather to the peaceful (and very rapid) growth in their own volume, as allowed by general relativity. In this sense any inflationary domain of initial size exceeding $2H^{-1}$ can be considered as a separate mini-universe, expanding independently of what occurs outside it.

To investigate the behavior of such a mini-universe, with an account taken of quantum fluctuations, let us consider an inflationary domain of initial size roughly H^{-1} containing a

sufficiently homogeneous field whose initial value ϕ greatly exceeds M_P. Eq.(4) tells us that during a typical time interval $\Delta t = H^{-1}$ the field inside this domain will be reduced by

$$\Delta\phi = \frac{M_P^2}{4\pi\phi}. \tag{19}$$

By comparison of (12) and (19) one can easily see that if ϕ is much less than $\phi^* \sim \frac{M_P}{2}\sqrt{\frac{M_P}{m}}$, the decrease of the field ϕ due to its classical motion is much larger than the amplitude of the quantum fluctuations $\delta\phi$ generated during the same time. But for large ϕ (up to the classical limit of $10^4 M_P$), $\delta\phi(x)$ will exceed $\Delta\phi$, i.e. the Brownian motion of the field ϕ becomes more rapid than its classical motion. Because the typical wavelength of the fluctuation field $\delta\phi(x)$ generated during this time is H^{-1}, the whole domain volume after Δt will effectively have become divided into e^3 separate domains (mini-universes) of diameter H^{-1}. In almost half of these domains the field ϕ grows by $|\delta\phi(x)| - \Delta\phi$, which is not very different from $|\delta\phi(x)|$ or $H/2\pi$, rather than decreases. During the next time interval $\Delta t = H^{-1}$ the field grows again in half of these mini-universes. It can be shown that the total physical volume occupied by a permanently growing field ϕ increases with time like $exp(3 - \ln 2)Ht$, and the total volume occupied by a field that does not decrease grows almost as fast as $\frac{1}{2}e^{3Ht}$.

Because the value of the Hubble constant $H(\phi)$ is proportional to ϕ, the main part of the physical volume of the universe is the result of the expansion of domains with nearly the maximal possible field value, M_P^2/m, for which $V(\phi)$ is close to M_P^4. There are also exponentially many domains with smaller values of ϕ. Those domains in which ϕ eventually becomes smaller than about $30M_P$ give rise to the mini-universes of *our* type. In such domains, ϕ eventually rolls down to the minimum of $V(\phi)$, and these mini-universes are subsequently describable by the usual Big Bang theory. However a considerable part of the physical volume of the entire universe remains forever in the inflationary phase [10].

Similar results are also valid for the old [16] and the new inflationary scenarios [17], in which some part of the volume of the universe can always remain in a state corresponding to a local extremum of $V(\phi)$ at $\phi = 0$. In our chaotic-inflation case, the results are even more surprising. Not only can the universe stay permanently on the top of a hill as in the old and new inflationary scenario; it can also climb perpetually up the wall toward the largest possible values of its potential energy density [10]-[11]. How can it be that the universe unceasingly produces inflationary mini-universes in energetically unfavorable states with large $V(\phi)$? What energy source supports such a process?

The answer is that the probability for a successful climb up the wall is very small indeed, but those domains in which ϕ jumps high enough are immediately rewarded by a huge growth of their volumes.

The energy source that supports inflation is the gravitational energy associated with $a(t)$, the scale factor of the universe. This gravitational energy is negative, so that the total energy of a closed universe, being the sum of the positive energy of matter and the negative

gravitational energy, is zero. Just this unbounded reservoir of gravitational energy makes possible the exponentially rapid growth of the total energy of matter during inflation. The negative gravitational energy seeks any opportunity to become more negative, that is, to make inflation a nonstop process. Just this possibility is realized in any inflationary domain with $\phi \geq \phi^*$.

Thus in our scenario the universe, in which there was initially at least one domain of a size on the order of H^{-1} filled with a sufficiently large and homogeneous field ϕ, unceasingly reproduces itself and becomes immortal. One mini-universe produces many others, and this process goes on without end (even though each particular mini-universe may eventually collapse later [8]).

But this means that it is vanishingly improbable that our mini-universe would have been the first in the sequence of mini-universes. Moreover, it no longer seems necessary to assume that there actually was some first mini-universe appearing from nothing or from an initial singularity at some moment $t = 0$ before which there was no space-time at all.

From general topological theorems about singularities in cosmology it does not actually follow that our universe was created *as a whole* at some moment before which the universe did not exist. The usual supposition that the whole universe appears from the unique Big Bang singularity at $t = 0$ is based on the implicit assumption that the universe *as a whole* is sufficiently homogeneous. Indeed, the observable part of our universe is very homogeneous. Observed density fluctuations are less than a part in a thousand and there has been no reason to expect that the universe is inhomogeneous on a larger scale beyond the 10^{10}-light-year horizon. In a homogeneous universe one can use the density $\rho(t)$ as a measure of time. In that case it can be shown that the universe appears *as a whole* from a singularity at $t = 0$. The initial density $\rho(0)$ is infinite, and it becomes possible to describe the whole universe in terms of classical space-time after the Planck time M_P^{-1} (about 10^{-43} seconds), when the energy density everywhere simultaneously becomes smaller than the Planck density M_P^4.

With the invention of the inflationary scenario the situation changes drastically. At present only inflation can explain why the observable part of the universe is so homogeneous, but from inflation it also follows that on a much larger scale the universe is extremely *in*homogeneous. In some parts of the universe the energy density ρ is now of the order of M_P^4, 125 orders of magnitude higher than the 10^{-29} or $10^{-30} g \cdot cm^{-3}$ we can see nearby. In such a scenario there is no reason to assume that the universe was initially homogeneous and that all its causally disconnected parts started their expansions simultaneously.

If the universe is infinitely large (like the Friedmann open or flat universe), then it cannot have had a single beginning; a simultaneous creation of infinitely many causally disconnected regions is totally improbable. Therefore the universe cannot be infinite *ab initio*, or it must exist eternally as a huge self-reproducing entity. Some of its parts appear at different times from singularities, or may die in a singular state. New parts are constantly being created from the space-time foam when $V(\phi)$ exceeds the Planck density, or they may revert to the

foamlike state again as a result of large fluctuations in ϕ. But the evolution of the universe as a whole has no end, and it may have had no beginning.

The model we have studied above was, of course, oversimplified. In realistic theories of elementary particles there exist many different types of scalar fields ϕ_i. The potential energy $V(\phi_i)$ often has many different local minima, in which the universe may live for an extremely long time, much greater than the 10^{10} years of our observable domain. For example, in the supersymmetric $SU(5)$ theory, $V(\phi_i)$ has several different minima of almost equal depth. Because the laws governing the interactions of elementary particles at the low energies at which we do experiments depend on the values of the classical fields ϕ_i, each of these minima corresponds to a different low-energy physics. In one of them the $SU(5)$ symmetry between all types of interactions remains unbroken - that is, the scalar fields ϕ_i remain equal to zero. In other minima various symmetry breaking patterns are realized, and in only one of these minima is the broken symmetry of the weak, strong and electromagnetic interactions that which we in fact observe.

During inflation there are large-scale fluctuations of all the fields ϕ_i. As a result, the inflationary universe becomes divided into an exponentially large number of inflationary mini-universes, with the scalar fields taking all possible values. As inflation ends in some mini-universes, these scalar fields roll down to all possible minima of $V(\phi_i)$. The universe becomes divided into many different exponentially large domains, realizing all possible types of symmetry breaking between the fundamental interactions. In some of these mini-universes the low-energy physics is quite different from our own. We cannot now see them because the size of our own domains is much greater than the size of its 10^{10}-light-year observable portion. We could not live in these domains because our kind of life requires our kind of low-energy physics.

It is very important that in the inflationary universe there is lots of room for all possible types of symmetry breaking and for all possible types of life. There is, therefore, no longer any need to require that in the true theory the minimum of $V(\phi_i)$ corresponding to our type of symmetry breaking be the only one or the deepest one. This new cosmopolitan viewpoint may greatly simplify the task of building realistic models of the elementary particles.

The change of the values of the scalar fields ϕ_i – that is to say, the change of the vacuum state – is the simplest kind of "mutation" that may occur during inflation. Much more interesting possibilities appear if one considers chaotic inflation in the higher-dimensional Kaluza-Klein theories. In those domains in which the energy density of the field ϕ grows to the Planck density, quantum fluctuations of the metric at a length scale of M_P^{-1} become of order unity. In such domains an inflationary d-dimensional universe can squeeze locally into a tube of smaller dimensionality $d-n$ (or vice versa). If this tube is also inflationary (in $d-n$ dimensions) and the initial length of the tube is greater than M_P^{-1} (which is quite probable near the Planck density), then its further expansion proceeds independently of its prehistory and of the fate of its mother universe. In an eternally existing universe such processes should

occur even if their probability is very small. In fact the probability of such processes is small only if $V(\phi)$ is far below M_P^4.

Thus the inflationary universe becomes divided into different mini-universes in which all possible types of compactification produce all sorts of dimensionalities [18]. By this argument we find ourselves inside a four-dimensional domain with our kind of low-energy physics not because other kinds of mini-universes are impossible or improbable, but simply because our kind of life cannot exist in other domains.

This may have important implications for the building of realistic Kaluza-Klein and superstring theories. For example, it is extremely complicated, if not impossible, to construct a theory in which only one type of compactification can occur, leading precisely to a four-dimensional inflationary universe with the low-energy particle physics of our experience. But from the point of view discussed here, there is no need to require that the results compactification and inflation have wrought in our realm be the only possible results, or the best. It is enough to find a theory in which such a compactification is possible. This problem is still difficult, but it is much easier than the one we have been trying to solve.

4 Chaotic Inflation versus Extended Inflation

4.1 Extended Inflation

The first versions of the inflationary universe scenario were based on the models where the process of inflation was determined by the evolution of just one scalar field ϕ. Even this simplest class of models considered in the previous sections leads to many unusual and unexpected properties of the universe, such as a non-trivial thermal history of the universe, the existence of a mechanism of formation of a scale-free (flat) spectrum of adiabatic density perturbations, the absence of the global end of the universe evolution etc.

However, in most of the realistic models of elementary particles there are many different scalar fields. Many interesting possibilities which may arise in theories with many scalar fields still remain unexplored. One of the most interesting models of that type suggested this year is the extended inflation scenario [6], which is essentially a realization of the old inflationary universe scenario by Guth [3] in the context of the Jordan-Brans-Dicke theory (JBD)[9] with the action of the following type:

$$S = \int d^4x\sqrt{-g}\,[\frac{f(\phi)R}{16\pi} - \frac{1}{2}\partial_\mu\phi\partial^\mu\phi - V(\phi) + L(\varphi)]. \qquad (20)$$

Here $\phi^2 = \frac{b}{2\pi}\Phi$, where Φ is the JBD field; φ is the inflaton scalar field. In the first papers on the extended inflation scenario it was assumed that the effective gravitational constant $G = M_p^{-2} = f^{-1}(\phi)$ is equal to $\frac{b}{2\pi\phi^2}$, with $b \gg 1$. It was assumed also that $V(\phi) = 0$ and that

the effective potential of the field φ has a deep minimum at $\varphi = 0$, as in the old inflationary universe scenario [6]. Then it was understood that a successful realization of this scenario is possible only for $1 \ll b < 25$, which is incompatible with the experimental constraints on this parameter in the JBD theory, $b > 500$ [19,20], and to cure this problem it was suggested to add to the theory a non-vanishing effective potential of the field ϕ [20]. Later it was argued that a much better scenario (hyperextended inflation) can be suggested if one takes $f(\phi) = M^2 + \xi\phi^2 - \alpha\phi^4/M^2$ [21] (see also [22]).

The reason why this theory may resolve the graceful exit problem is very simple. The moment when the phase transition from the false vacuum completes is determined by the condition $\epsilon(t) \equiv \Gamma/H^4(t) \geq \epsilon_{cr}$ where Γ is the number of bubbles nucleated per unit four-volume, $\epsilon_{cr} \approx \frac{3}{4\pi}$ [23]. At the first stages of inflation $H(t)$ is big, $\Gamma \ll H^4(t)$ and $\epsilon(t) \ll \epsilon_{cr}$. In the ordinary Einstein theory this relation holds forever, which is the origin of the graceful exit problem. But in the theory (20) inflation is not exponential. The Hubble constant $H(t)$ decreases in time due to the change of the field ϕ. At some moment $t = t_{cr}$ the value of $\epsilon(t)$ becomes smaller than ϵ_{cr} and inflation completes.

The discovery of the new class of inflationary models is certainly very important. Of course, those who wish to have just one preferable scenario may be disappointed by the appearance of new candidates, but in my opinion it is better to know all existing possibilities, which should give us a better chance to suggest a compete cosmological theory which would be consistent with the future theory of all fundamental interactions. In any case, since the chaotic inflation scenario is at present rather well understood [7], it is quite reasonable to study other, more complicated versions of inflationary cosmology.

In order to continue investigation of the new class of models one should first understand their relation to other models and theories suggested so far. Many relevant comments on this question are contained in different papers on extended inflation. However, some of these comments were strongly biased by the understandable desire to show the advantages of the new models. For example, it was claimed that chaotic inflation requires fine tuning of parameters and exotic quantum effects at the Planck density. It was claimed also that the modifications of the Einstein theory, which are necessary for the realization of the extended inflation scenario, naturally appear in virtually every realistic theory of elementary particles, including the superstring theory. Some authors believe that extended inflation provides the only way to produce exponentially big domain walls and strings, and practically everybody believes that this scenario provides the only way to solve the graceful exit problem of the old inflation.

In this section we will try to examine the validity of these statements. We will also discuss the problem of initial conditions for extended inflation and suggest a further extension of this scenario, which we call eternal extended inflation. Finally, we will suggest a possible solution of the graceful exit problem of old inflation which does not require any modifications of the Einstein gravity theory.

4.2 Chaotic Inflation and Extended Inflation

Let us first remember some facts about chaotic inflation [7].

1) In the simplest models of the chaotic inflation scenario with the power-law effective potential $V(\phi) \sim \frac{\lambda\phi^n}{nM_p^{n-4}}$ inflation occurs at $\phi \gtrsim nM_p/12$. This means that for small λ inflation may occur well outside the dangerous region of Planck densities, at $V(\phi) \ll M_p^4$.

2) In the models with the effective potential which looks like $V_o \exp(\frac{c\phi}{M_p})$ at $\phi > \phi_o$, $c \lesssim 5$, $\phi_o < M_p$, inflation occurs for all $\phi > \phi_o$. In this case one can have both $V(\phi) \ll M_p^4$ and $\phi \ll M_p$ during inflation (though the last condition is not necessary at all for the validity of the chaotic inflation scenario).

3) In our opinion, the most natural initial conditions for chaotic inflation should be imposed as close as possible to the hypersurface of the Planck density, for the simple reason that this is the *first* time when the *initial* conditions can be imposed on *classical* fields in a *classical* space-time. However, if one wishes, one can impose initial conditions at a density much smaller than M_p^4. It is most important that for small λ the crucial process of the self-reproduction of the inflationary universe [10,11] may occur at densities much smaller than the Planck density.

Thus, we believe that no exotic processes at the Planck density are necessary for the realization of the chaotic inflation scenario.

Now let us consider the issue of fine tuning. In order to do it we will give a simple example of a semi-realistic theory where chaotic inflation is possible [7]:

$$L = \frac{RM_p^2}{16\pi} + L_{GUT} - \frac{1}{2}\partial_\mu\varphi\partial^\mu\varphi + \frac{m^2}{2}\varphi^2 - \beta\varphi^2\phi^2. \qquad (21)$$

Here L_{GUT} is a Lagrangian of some basic grand unified theory, φ is some gauge singlet field with a mass $m \leq 10^{12} - 10^{13}GeV$ interacting with some scalar field (or fields) ϕ from the basic theory with a coupling constant $\beta \sim 10^{-6}$. For example, in the SU(5) theory the corresponding interaction can be either $-\beta\varphi^2 H_5^2$ or $-\beta\varphi^2 Tr\Phi^2$. Due to radiative corrections the effective potential $V(\varphi)$ at $\varphi^2 > m^2/\beta$ acquires a contribution $C\frac{\beta^2}{64\pi^2}\varphi^4(\ln\frac{\beta\varphi^2}{m^2} + O(1))$, where $C = O(1)$ is some constant which depends on the properties of the field ϕ in the SU(5) theory (whether it stands for H_5 or for Φ). This theory leads to inflation with all desirable properties including density perturbations $\frac{\delta\rho}{\rho} \sim 10^{-5}$. This model is similar to the Shafi-Vilenkin model [24], but is simpler and leads to a more efficient reheating of the universe [7]. This model is also much simpler than any version of extended inflation suggested so far.

Is there any fine tuning of parameters in this model ? In order to understand it let us represent the last two terms in (21) in the form

$$\left(\frac{1}{2}(c\beta M_p)^2 - \beta\phi^2\right)\varphi^2, \qquad (22)$$

where $c \leq O(1)$. The only feature of this model which can be considered unnatural is the presence of a small coupling constant $\beta \sim 10^{-6}$. The need for such a small parameter in the theory is related to the experimental fact that the anisotropy of the microwave background radiation $\frac{\delta T}{T}$ is "unnaturally" small, $\frac{\delta T}{T} \sim \frac{\delta \rho}{\rho} \sim 10^{-5}$. We are not sure that the existence of a small parameter in the theory which explains the existence of some other experimentally measured unnaturally small quantity should be considered as a fine tuning. For example, nobody considers as a fine tuning the presence of a small coupling constant $2 \cdot 10^{-6}$ of the interaction between the electron and the Higgs boson in the standard theory of weak and electromagnetic interactions, since this constant is responsible for the smallness of the electron mass. In any case, a similar small parameter $M_F/M_p < 10^{-5}$ is present for a similar reason in all models of extended inflation [20,25], and the authors of these models do not consider it as a fine tuning. On the other hand, if one is allowed to modify the Einstein theory and consider the Jordan-Brans-Dicke theory with the parameter $b \sim 10^3$ [6], one may consider as well the induced gravity theory with the Lagrangian $\xi\phi^2 R$ with $\xi \sim 10^3$ (or one may just add such a term to the Lagrangian (21)). In such a theory the coupling constant β should be of the order $50\xi 10^{-6} \sim 10^{-1}$, which does not look like a fine tuning at all [26]. In the chaotic inflation scenario based on supergravity one can get $\frac{\delta T}{T} \sim \frac{\delta \rho}{\rho} \sim 10^{-5}$ without introducing any dimensionless parameters smaller than 10^{-2} [27], and in the models based on the Kaluza-Klein theory one may avoid introducing any small parameters whatsoever [28].

Therefore the only real problem of the chaotic inflation scenario is not the fine tuning problem or the problem of exotic processes at the Planck density, but the question whether it is possible to realize it in the context of a completely realistic theory of elementary particles. Since the notion of a realistic theory of elementary particles nowadays changes every 5 years (GUTs, supergravity, superstrings...), one should know all possible versions of the inflationary universe scenario in order to be better prepared for the future changes of the particle theory. This, rather than the "defects" of chaotic inflation, should serve as a justification of the investigation of such relatively complicated theories as the extended inflation scenario.

The possibility to justify the modifications of the Einstein theory proposed in [6,20,21] in the context of realistic theories of elementary particles does not seem very easy. Whereas radiative corrections of the type of $\xi\phi^2 R ln\phi$ with some small coefficients proportional to coupling constants do naturally appear in many theories, neither the JBD theory with $b \gg 1$ nor the hyperextended inflation with $f(\phi) = M^2 + \xi\phi^2 - \alpha\phi^4/M^2$ arise as a natural consequence of "virtually every" realistic theory of elementary particles. In particular, the low energy limit of the superstring theory is not the JBD theory but the ordinary Einstein gravity. In principle, one can represent the superstring theory in a form similar to the JBD theory, but the corresponding coefficient b in this theory proves to be a small (and not adjustable) parameter. As a result, instead of inflation one typically has a regime in which the scale factor $a(t)$ linearly grows in time. (For a review of problems with inflation in the context of the superstring theory see [29] and references therein.)

Now let us investigate the problem of initial conditions in the extended inflation scenario. In our opinion, the original idea that in this scenario inflation starts after the high temperature symmetry restoration, does not work in a nice way for the same reason as in the original old inflation scenario and in the new inflation scenario; see the beginning of this paper and also refs. [7,30]. The best way to investigate this scenario which we see at present is to consider whether it is likely or not that at the very early stages of the evolution of the universe (i.e. near the Planck time) the inflaton field φ was occasionally in a state near the local minimum of $V(\varphi)$ in some part of the universe bigger than the horizon H^{-1}. This means that one should proceed exactly as in the chaotic inflation scenario.

A similar approach to the old and new inflation would not give us very encouraging results. The reason is that in all realistic models of new inflation, as well as in the old inflation scenario, the false vacuum energy is smaller than $O(10^{-10})M_p^4$. Therefore the field φ can be sufficiently homogeneous at a scale of the horizon at the moment when inflation may start, but only if at the Planck time it is homogeneous on a scale many orders of magnitude bigger than the Planck length, which seems unnatural [7].

There is no such problem in the chaotic inflation scenario since inflation may start directly at the Planck time. If one wishes to avoid uncertainties related to the processes at the Planck density, one may consider inflation starting with a density two, ten or one hundred times smaller than M_p^4, but there are no problems related to the absence of the possibility of starting inflation at the energy density bigger than $10^{-10}M_p^4$. Therefore in the chaotic inflation scenario inflation may start if the scalar field was originally sufficiently homogeneous on a scale just a few times bigger than the Planck length [7], [31].

Fortunately, some versions of the extended inflation scenario have a similar advantage ! Indeed, in this scenario the notion of the Planck density depends on the value of the field ϕ: $M_p^4(\phi) = f^2(\phi)$. Therefore inflation may start near the Planck density with the fields ϕ and φ related to each other as follows [36]:

$$V(\varphi) \sim f^2(\phi). \tag{23}$$

In this sense extended inflation, just like chaotic inflation, is free from the difficulties with the initial conditions which hampered a successful realization of the old and new inflation (see, however, below).

One can get an independent (though speculative) confirmation of this conclusion by an investigation of the quantum creation of the universe from "nothing" in the extended inflation scenario. According to [32]-[35], the probability of quantum creation of the inflationary universe filled with the field φ with $V(\varphi) \lesssim M_p^4$ is suppressed by the factor

$$P \sim \exp(-\frac{3M_p^4}{8V(\varphi)}). \tag{24}$$

In the extended inflation scenario this expression should be replaced by

$$P \sim \exp(-\frac{3f^2(\phi)}{8V(\varphi)}), \tag{25}$$

which implies that the process of quantum creation of the inflationary universe is not exponentially suppressed only if the relation (23) holds[3].

One should note, however, that in some versions of the extended inflation scenario inflation may occur only at $V(\varphi) \ll f^2(\phi)$, as in the standard old inflation scenario. For example, it can be easily shown that the condition $M_F^4 \sim f^2(\phi)$ is incompatible with inflation in the hyperextended inflation model suggested in [21] ($f(\phi) = M^2 + \xi\phi^2 - \alpha\phi^4/M^2$ with $M \gg M_F$, $\xi, \alpha = O(1)$). (Other difficulties with the hyperextended inflation with "natural" parameters ξ and α are discussed in [25].)

One more problem related to the initial conditions for extended inflation is connected with the volume of the phase space of all possible values of the fields ϕ and φ satisfying the condition (23). Eq. (23) typically has an infinitely big set of solutions and only a finite part of it leads to extended inflation. For example, if $V(\varphi)$ is a polynomial function of φ with a local minimum at $\varphi = 0$, then the extended inflation scenario is realized only for the initial values of φ corresponding to a finite vicinity of $\varphi = 0$, whereas for all other initial values of φ from $-\infty$ to $+\infty$ either there is no inflation or the chaotic inflation scenario is realized along the lines of ref. [36]. It seems therefore that even though there is no *exponential* suppression of the probability of initial conditions satisfying eq. (23), the set of those initial conditions which lead to a realization of extended inflation is vanishingly small as compared with the set of those initial conditions for which extended inflation does not occur.

A possible way to resolve this problem is to say that the probability of initial conditions with big $f^2(\phi)$ and $V(\varphi)$ for some reasons is extremely small. At the moment we do not see why this conjecture could be true in the simple models of extended inflation considered so far.

Another possible resolution is related to the process of permanent self-reproduction of inflationary domains which occurs in this scenario at a sufficiently large energy density $V(\varphi)$ [36].

4.3 Eternal Extended Inflation

Let us consider the original extended inflation model (20) with $b \gg 1$ and $V(\phi) = 0$ and let us study the stage of inflation with the field $\varphi = 0$ corresponding to the local minimum of $V(\varphi)$. As in ref. [6], we will denote $V(\varphi = 0) = M_F^4$.

[3]According to (25), quantum creation is not suppressed for $V(\varphi) > f^2(\phi)$ as well. However, in this case one cannot speak about creation of a *classical* space-time.

During inflation one can neglect $\frac{\ddot{\phi}}{\phi}$ as compared with $H \equiv \frac{\dot{a}}{a}$ and $\ddot{\phi}$ as compared with $3H\dot{\phi}$ and $\dot{\phi}^2$. In such a case equations for a and ϕ in the theory (20) with $V(\phi) = 0$ and $b \gg 1$ take a very simple form:

$$H = \frac{2}{\phi}\sqrt{\frac{b}{3}}M_F^2 \,, \tag{26}$$

$$3H\dot{\phi} = \frac{4}{\phi}M_F^4 \,. \tag{27}$$

From these equations one can easily see that during the typical time $\Delta t = H^{-1}$ the field ϕ grows by $\Delta\phi = \phi/b$, which leads to a gradual decrease of H. According to [23], inflation completes in the whole universe at the moment when $\frac{3H^4}{4\pi}$ becomes smaller than Γ, the number of bubbles nucleated per unit four-volume.

However, taking into account quantum fluctuations of the field ϕ, this conclusion is not entirely correct. According to [37], quantum fluctuations during inflation produce perturbations $\delta\phi$ of the classical scalar field ϕ with a wavelength bigger than H^{-1}. The average amplitude of perturbations generated during the time $\Delta t = H^{-1}$ is given by $|\delta\phi| = H/2\pi$. This is bigger than the classical growth $\Delta\phi = \phi/b$ of this field for

$$\phi < M_F \left(\frac{b^3}{3\pi^2}\right)^{1/4} \tag{28}$$

This result has important consequences.

It is well known that the process of inflation in any spatial domain of radius H^{-1} occurs independently of any events outside it ("no-hair theorem" for de Sitter space). In this sense any inflationary domain of initial size exceeding $2H^{-1}$ can be considered as a separate mini-universe, expanding independently of what occurs outside it.

To investigate the behavior of such a mini-universe, with quantum fluctuations taken into account, let us consider an inflationary domain of initial size $O(H^{-1})$ containing a sufficiently homogeneous field ϕ. During a typical time interval $\Delta t = H^{-1}$ the mean value of the field ϕ inside this domain will grow by $\Delta\phi = \phi/b$. However, if $\Delta\phi \ll |\delta\phi|$, the average growth of the field ϕ is not important. During the time $\Delta t = H^{-1}$ the domain grows e times and its volume grows e^3 times. Because the typical wavelength of perturbations $\delta\phi(x)$ generated during this time is H^{-1}, the whole domain effectively becomes divided into e^3 separate domains (mini-universes) of size $O(H^{-1})$. In almost half of these domains the field ϕ does not grow, but rather decreases by $|\delta\phi(x)| - \Delta\phi \sim H/2\pi$. This means that during this time the total volume of the universe occupied by the decreasing field ϕ grows approximately by $e^3/2 \sim 10$ times. A similar statement remains true for the next time interval $\Delta t = H^{-1}$, etc. This means that any inflationary domain of initial size bigger than $O(H^{-1})$, filled with the field $\phi < M_F \left(\frac{b^3}{3\pi^2}\right)^{1/4}$, permanently reproduces new and new inflationary domains of a similar type, and this process never completes (eternal extended inflation). The theory of this

effect is completely analogous to the theory of a similar effect in the eternal chaotic inflation scenario [10,11].

It is important that the process of permanent reproduction of inflationary domains occurs in a wide interval of values of the scalar field ϕ, corresponding to

$$\frac{3}{4b}M_p^4(\phi) < M_F^4 < M_p^4. \tag{29}$$

This means that in order to prove the existence of the regime of self-reproduction of the universe in the extended inflationary universe scenario with $b \gg 1$, just as in the chaotic inflation scenario, there is no need to study exotic quantum effects at the Planck density. The results obtained above mean that even though the fraction of initial conditions which lead to extended inflation seems to be vanishingly small, the total volume of the parts of the universe which experience extended inflation may be exponentially large.

Note, that the effects discussed above do not return us to the problem with the impossibility of completing the phase transition in the old inflation scenario. Indeed, in the eternal extended inflation scenario many domains with $\phi > M_F \left(\frac{b^3}{3\pi^2}\right)^{1/4}$ are produced as well. In such domains fluctuations of the field ϕ are small and the phase transition completes. This just means that when computing the size of the homogeneous part of the universe in the extended inflation scenario [6] one should use $\phi \sim M_F \left(\frac{b^3}{3\pi^2}\right)^{1/4}$ instead of the initial value $\phi \sim M_F \left(\frac{b}{2\pi}\right)^{1/2}$ corresponding to the Planck energy density. A similar result is valid for the chaotic inflation as well [7].

4.4 Solution of the Graceful Exit Problem Without Modifying the Einstein Gravity

As we have seen in the previous sections, the most interesting realizations of chaotic and extended inflation have many common features. One such feature is the possibility to produce exponentially big bubbles, strings and domain walls due to phase transitions which may occur during inflation. In the context of chaotic inflation this possibility was first suggested three years ago [15], and has now been revived again in the extended inflation scenario.

But is it possible to solve the graceful exit problem of the old inflation scenario with the help of chaotic inflation without considerable modifications of the Einstein gravity ? Or, to be more precise, is it possible to avoid the graceful exit problem if the inflaton field which drives the last stages of inflation in the Einstein gravity theory has a potential with a deep local minimum ? As we will show now, the answer to this question is positive.

The most straightforward way to do so is just to make a conformal transformation and to recast the JBD theory in the Einstein form with a complicated effective potential being a

product of $V(\varphi)$ and $\exp C\phi$ where C is some constant [38,25,39,40]. In such a formulation the extended inflation scenario is equivalent to a peculiar version of the chaotic inflation scenario where inflation is driven by two scalar fields simultaneously. (This is the deep reason why many results obtained in the context of the chaotic inflation scenario remain valid for extended inflation as well.) However, in the chaotic inflation scenario with two scalar fields a much more natural possibility does exist [12], related to the theory of phase transitions during inflation mentioned above [15].

Indeed, let us consider again the simplest version of the chaotic inflation scenario (21) with the Lagrangian L_{GUT} containing the effective potential $V(\phi)$ with a deep local minimum at $\phi = 0$, as in the old inflationary universe scenario,

$$V(\phi) = M_F^4 + \frac{\alpha}{2}M_F^2\phi^2 - \frac{\gamma}{3}M_F\phi^3 + \frac{\lambda}{4}\phi^4. \tag{30}$$

Then the total effective potential of the fields ϕ and φ in the theory (21) takes the following form:

$$V(\phi,\varphi) = M_F^4 + \frac{\alpha}{2}M_F^2\phi^2 - \frac{\gamma}{3}M_F\phi^3 + \frac{\lambda}{4}\phi^4 - \left(\frac{1}{2}(c\beta M_p)^2 - \beta\phi^2\right)\varphi^2 + C\frac{\beta^2}{64\pi^2}\varphi^4(\ln\frac{\beta\varphi^2}{m^2} + O(1)), \tag{31}$$

where $C, c = O(1)$.

As we have already mentioned, the theory (21) with $\beta \sim 10^{-6}$ leads to a natural realization of the chaotic inflation scenario even without taking into account $V(\phi)$ (30). Now let us consider the behavior of the fields ϕ and φ in the theory (21), (31).

According to our previous arguments, the most natural initial values of the fields ϕ and φ should satisfy the constraint $V(\phi,\varphi) \sim M_p^4$ (though, of course, one can easily take $V(\phi,\varphi)$ several times smaller). Then the field ϕ will roll down to the minimum of $V(\phi,\varphi)$ more rapidly than the field φ since the effective mass of the field ϕ is much bigger. Soon after that inflation will be driven mainly by the field φ. At this stage the effective mass squared of the field ϕ acquires a very big positive contribution,

$$M_{eff}^2(\phi) = \alpha M_F^2 + 2\beta\varphi^2. \tag{32}$$

Therefore at this stage of the evolution of the universe (at $\varphi \gg M_p$) the effective potential of the field ϕ has the only minimum at $\phi = 0$, the field ϕ rapidly rolls down to this minimum and stays there.

With a decrease of the field φ, its contribution to the vacuum energy density becomes smaller than M_F^4, and after that inflation is driven by the field ϕ, as in the old inflation scenario.

Let us take for definiteness $M_F \sim 10^{15}$ GeV, which is a natural GUT scale. Then the old inflation takes over at $\varphi < M_p$, i.e. at the very end of the preceding stage of chaotic

inflation. For smaller values of β old inflation starts earlier, i.e. at bigger φ. At this stage the field φ continues its slow rolling down to the minimum of its effective potential. (Recall that the massive scalar field in de Sitter space decreases as $\exp(-\frac{m^2 t}{3H})$ for $m < H$.) Therefore the effective mass squared $M^2_{eff}(\phi)$ of the field ϕ will change rather slowly, see eq. (32).

The rest of the story is quite obvious. The probability of bubble production Γ is extremely sensitive to the value of the effective mass of the field: it rapidly increases with the decrease of $M^2_{eff}(\phi)$. Thus, the parameter $\epsilon(t) \equiv \Gamma/H^4$ depends on time, though for a quite different reason than in the extended inflation scenario. In the extended inflation scenario the Hubble parameter H decreases in time. Here the decay rate Γ increases in time. In both cases the phase transition completes when/if $\epsilon(t)$ becomes sufficiently big. The theory of the phase transition crucially depends on the values and signs of the coupling constants. If the effective value of α ($\alpha_{eff} = M^2_{eff}/M^2_P$) in the process of decrease of the field φ always remains big and positive, then the action for tunneling is very big and the phase transition never completes. If the constant γ is big and α_{eff} gradually becomes very small, then the phase transition completes. If the constants γ and λ are small, then the phase transition completes only when α_{eff} becomes negative. In that case no big bubbles appear after the phase transition. One can easily check by the standard methods that with the values of parameters similar to those discussed above one can easily get density perturbations $\frac{\delta\rho}{\rho} \sim 10^{-5}$.

This means that one can actually suggest models in which the universe at the last stages of inflation is described by the old inflationary scenario, and that the graceful exit problem of this scenario can be solved without any modification of the Einstein gravity.

References

[1] E.B. Gliner, Sov. Phys. JETP **22** (1965) 378; Dokl. Akad. Nauk SSSR **192** (1970) 771;
E.B. Gliner and I.G. Dymnikova, Pis. Astron. Zh. **1** (1975) 7;
I.E. Gurevich, Astrophys. Space Sci. **38** (1975) 67.

[2] A.A. Starobinsky, JETP Lett. **30** (1979) 682; Phys. Lett. **91B** (1980) 99.

[3] A.H. Guth, Phys. Rev. **D23** (1981) 347.

[4] A.D. Linde, Phys. Lett. **108B** (1982); **114B** (1982) 431; **116B** (1982) 335, 340;
A. Albrecht and P.J. Steinhardt, Phys. Rev. Lett. **48** (1982) 1220.

[5] A.D. Linde, Phys. Lett. **129B** (1983) 177.

[6] D. La and P.J. Steinhardt, Phys. Rev. Lett. **62** (1989) 376.

[7] A.D. Linde, **Particle Physics and Inflationary Cosmology** (Harwood Academic Publishers, New York, 1990);
A.D. Linde, **Inflation and Quantum Cosmology** (Academic Press, Boston, 1990).

[8] A.D. Linde, Phys. Lett. **B227** (1989) 352.

[9] P. Jordan, Zeit. Phys. **157** (1959) 112;
C. Brans and C.H. Dicke, Phys. Rev. **124** (1961) 925.

[10] A.D. Linde, Phys. Lett. **175B** (1986) 395; Physica Scripta **T15** (1987) 169; Physics Today **40** (1987) 61.

[11] A.S. Goncharov, A.D. Linde and V.F. Mukhanov, Int. J. Mod. Phys. **A2** (1987) 561.

[12] A.D. Linde, CERN preprint TH. 5806 (1990).

[13] V.F. Mukhanov and G.V. Chibisov, JETP Lett. **33** (1981) 523.
S.W. Hawking, Phys. Lett. **115B** (1982) 339;
A.A. Starobinsky, Phys. Lett. **117B** (1982) 175;
A.H. Guth and S.-Y. Pi, Phys. Lett. **49** (1982) 1110;
J. Bardeen, P.J. Steinhardt and M. Turner, Phys. Rev. **D28** (1983) 679;
R. Brandenberger, Rev. Mod. Phys. **57** (1985) 1.

[14] V.F. Mukhanov, JETP Lett. **41** (1985) 493;
V.F. Mukhanov, L.A. Kofman and D.Yu. Pogosyan, Phys. Lett. **193B** (1987) 427.

[15] L.A. Kofman and A.D. Linde, Nucl. Phys. **B282** (1987) 555.

[16] J.R. Gott, Nature **295** (1982) 304;
K. Sato, H. Kodama, M. Sasaki and K. Maeda, Phys. Lett. **B108** (1982) 35.

[17] P.J. Steinhardt, in **The Very Early Universe**, G.W. Gibbons, S.W. Hawking, S. Siklos, eds., Cambridge U.P. Cambridge, England (1982), p. 251;
A.D. Linde, **Nonsingular Regenerating Inflationary Universe**, Cambridge University preprint (1982).
A. Vilenkin, Phys. Rev. **D27** (1983) 2848.

[18] A.D. Linde and M.I. Zelnikov, Phys. Lett. **B215** (1988) 59.

[19] E.J. Weinberg, Phys. Rev. **D40** (1989) 3950.

[20] D. La, P.J. Steinhardt and E.W. Bertschinger, Phys. Lett. **B 231** (1989) 231.

[21] P.J. Steinhardt and F.S. Acetta, Phys. Rev. Lett. **64** (1990) 2740.

[22] J. Garcia-Bellido and M. Quiros, CERN preprint TH.5674/90 (1990).

[23] D. La and P.J. Steinhardt, Phys. Lett. **B220** (1989) 375.

[24] Q. Shafi and A. Vilenkin, Phys. Rev. Lett. **52** (1984) 691.

[25] E.W. Kolb, D.S. Salopek and M.S. Turner, Fermilab preprint FNAL-PUB-90/116-A (1990)

[26] B.L. Spokoiny, Phys. Lett. **147B** (1984) 39;
D.S. Salopek, J.R. Bond and J.M. Bardeen, Phys. Rev. **40** (1989) 1953;
D.S. Salopek and J.R. Bond, CIAR preprint Print-89-0820 (1989);
R. Fakir and W.G. Unruh, Phys. Rev. **D41** (1990) 1783, 1792.

[27] A.S. Goncharov and A.D. Linde, Class. Quant. Grav. **1** (1984) L75.

[28] Q. Shafi and C. Wetterich, Phys. Lett. **152B** (1982) 51; C. Wetterich, Nucl. Phys. **B324** (1989) 141.

[29] K. Olive, Phys. Rep. **190** (1990) 307.

[30] M. Duncan and L. G. Jensen, Minnesota University preprint UMN-TH-830/90.

[31] A.D. Linde, Phys. Lett. **162B** (1985) 281;
D.S. Goldwirth and T. Piran, Phys. Rev. Lett. **64** (1990) 2852;
R. Brandenberger and J.H. Kung, Phys. Rev. **D42** (1990) 1008.

[32] A.D. Linde, JETP **60** (1984) 211; Lett. Nuovo Cim. **39** (1984) 401.

[33] Ya.B. Zeldovich and A.A. Starobinsky, Sov. Astron. Lett. **10** (1984) 135.

[34] V.A. Rubakov, Phys. Lett. **148B** (1984) 280.

[35] A. Vilenkin, Phys. Rev. **D30** (1984) 549.

[36] A.D. Linde, Phys. Lett. **B238** (1990) 160.

[37] A. Vilenkin and L. Ford, Phys. Rev. **D26** (1982) 1231;
A.D. Linde, Phys. Lett. **116B** (1982) 335;
A.A. Starobinsky, Phys. Lett.**117B** (1982) 175.

[38] S. Kalara, N. Kaloper and K. Olive, Nucl. Phys. **B341** (1989) 252.

[39] A.L. Berkin, K. Maeda and J. Yokoyama, Phys. Rev. Lett. **65** (1990) 141.

[40] B. Campbell, A. Linde and K. Olive, CERN preprint TH.5850/90 (1990).

Albert Tavkhelidze and Andrei Linde

THE SCALE OF THE UNIVERSE

G. Burbidge
Center for Astrophysics and Space Sciences
University of California, San Diego, U.S.A. 92093

ABSTRACT

A discussion is given first of the evidence that the universe is expanding, and then of the best determination of the value of the Hubble constant H_o. A comparison is made between the age of the universe assuming different cosmological models, and the age determination for the stars and the chemical elements. Recent work by Sandage and his associates using the surface brightness test for elliptical galaxies, has shown for the first time that the redshifts of normal galaxies are due to expansion. As far as H_o is concerned, we conclude that the best current value is 52 ± 2 km sec^{-1} Mpc^{-1} recently determined by Sandage.

I. INTRODUCTION

The standard big bang model requires the universe to have a finite age. However, our universe could have arisen as a bubble from a finite part of an infinite universe without beginning or end, or we may live in a genuine steady-state universe without beginning or end. While it appears to be highly unlikely now, we may live in a static universe. This was the common view prior to about 1920.

In any case, the only observational handles we can get on the scale of the universe come from the distance scale, through the determination of H_0, giving also a time scale $= H_0^{-1}$. All of the large scale properties of the universe then depend on the value of a multiplier m so that (provided that $\wedge = 0$) the age of the universe is mH_0^{-1}, where m can take a range of values < 1 in Friedmann cosmology; in a steady-state universe the average age of galaxies is mH_0^{-1} where $m = \frac{1}{3}$. Since an independent approach to the time scale can be obtained through studies of stellar evolution, or from radioactivity, we can always set a lower limit to mH_0^{-1}, since if τ_S is the timescale associated with stellar evolution, and τ_R is the time scale associated with radioactivity, $mH_0^{-1} \geq$ the greater of τ_S and τ_R.

In the extremely unlikely case of a static infinite universe, the appropriate local time scale would be given by one of the values of τ, and the corresponding length scale would be $c\tau$, since we would have no other.

From the observational point of view, the length-scale time-scale problem reduces to (a) understanding the nature of the redshift phenomenon, and (b) determining a

global value for the Hubble constant H_0. The time scales associated with stellar evolution and radioactive decay of the heavy elements will be discussed later.

Before we turn to the observations, it is worthwhile making a few remarks about the current atmosphere and attitudes existing among cosmologists and their bearing on what is known, as compared with what is believed.

Nearly everyone currently believes that we live in a universe of Friedmann type. For this there is some evidence. Nearly everyone here probably accepts inflation and believes that the cosmological constant is $\Lambda = 0$. Many believe that $\Omega = 1$. There is no observational evidence in support of these beliefs, but they lead to strong biases in the way the data are discussed, and even the way conferences are organized. For example, let us look at the beliefs as they relate to time scales. Only if you believe in the articles of faith above, must the age of the stars and elements, be less then or equal to $2/3H_\circ$.

As it happens, the time scale arguments can equally well be used to support the steady state cosmology (cf Arp et al.[1]), so beware of prejudice!

In the remainder of this lecture, I shall avoid polemics and concentrate on hard evidence. I turn first to the redshifts.

II. REDSHIFTS AND EXPANSION

Undoubtedly Hubble was the first astronomer to show conclusively that the redshifts of what we now know to be very local galaxies were proportional to the

distances which were then believed[2]. The strange thing about Hubble's result was that while a good redshift-distance relation was found, we know that the majority of the galaxies in his compilation based on redshifts mostly by Slipher are systems which we believe now do not take part in the general expansion. The compilation includes such galaxies as the Magellanic Clouds, M31 and M33 in the local group, M81 and M82 in the M81 group, M101, and others all of which are dominated by local gravitational forces. Not surprisingly when we looked at this analysis in modern times, Hewitt and I[3] putting in the modern distances for the galaxies in Hubble's 1929 list[2], did not get a clear-cut linear relation.

It is clear now that most of the galaxies in Hubble's list are not partaking of the general expansion, so the riddle remains, how did Hubble find one?

The answer appears to be that he relied to a considerable extent on four galaxies, his most distant ones - NGC 4382, NGC 4472, NGC 4649 and M87, all of which lie in the Virgo cluster. Also while his distances were wildly in error, since he was basing them on brightest "stars" and mean luminosities of galaxies, he showed that the linear relation that he derived predicted the correct velocity for NGC 7619, which had a redshift nearby four times as great as the faintest of his galaxies. The redshift of this galaxy was reported by Humason[4] in a paper immediately before Hubble's paper and Hubble had clearly communicated it to the National Academy. Also, Hubble was aware that his result would be interpreted in terms of what he called the de Sitter cosmology.

Given that there is a linear relation between distance and redshift z, if cz is interpreted as a velocity of expansion, Hubble's law can be re-interpreted as a relation between distance and expansion velocity, and it is this which gave rise to the idea that the universe was non-static. Solutions of Einstein's equation allowing expansion had been obtained by Friedmann and by Lemaitre. Hence it was easy to reach the conclusion that Hubble had discovered evidence for the expanding universe, a conclusion that practically all of us believes today.

However, what had been found was simply a linear relation between D and $z = (\lambda_o - \lambda_{lab})\lambda_{lab}$. It was immediately realized that this could also be interpreted in terms of the reduction of the energy of a photon as it travels through a uniform intergalactic medium. This became known as the tired light hypothesis[5,6].

It is difficult to know what position was taken by leaders in the field 60 years ago, but we could guess, judging by present day behavior that the majority, following enthusiastic leaders like Eddington, accepted the expanding universe hypothesis with the redshift due to expansion. Actually this is not the case. Hubble[7] at the time of his Silliman Lectures was still sceptical of this interpretation and Curtis[8] considered that the explanation of the redshifts was still a matter of taste.

Attempts at Mount Wilson by Humason and Hubble and at Lick by Mayall, in the 1930s and 40s to observe fainter and fainter galaxies were successful, though the observing times were very long. It was realized that rich clusters of galaxies were very good distance indicators (since one could use the brightest galaxies as

standard candles). In a landmark paper largely prepared by Sandage and based on observations mostly made by Humason and Mayall which was published in 1956[9] the redshift apparent magnitude diagram (the Hubble diagram) for more than 800 field galaxies was published, together with the Hubble diagram for clusters out to z = 0.2. The Hubble diagram using customary units has a slope of 5, and this was found to be quite precisely the case for the clusters and satisfactorily so for the field galaxies. We shall not discuss here the arguments made extensively in recent years by Segal (cf Segal[10]) to the effect that the redshift apparent magnitude relation has a quadratic dependence on z. We have discussed this elsewhere and are not completely convinced that for comparatively bright galaxies Segal is wrong. However the Hubble law for rich clusters appears to be good and unassailable. Moreover Sandage and Tammann[11] have found a good linear relation for bright galaxies.

The fact remained that the redshift had still not been shown to be due to expansion and not tired light. However, a powerful theoretical argument against the tired light hypothesis emerged, and remains. It is that any atomic process in which the photon loses energy will also scatter the radiation so that the effect of atomic interactions will be to broaden the image of a distant object. No trace of such an effect is found.

A real observational test of the nature of the redshift can be made by studying the surface brightness of standard objects as a function of z. If we are looking at true expansion, the surface brightness (SB) is proportional to $(1+z)^{-4}$, while for tired light or any other process in which only energy is lost, the surface brightness is

proportional to $(1+z)^{-1}$. These results go back to the work of Tolman[12,13] and of Hubble and Tolman[14]. Elliptical galaxies are the obvious systems to use for the test. Early work bearing on this problem was carried out by Geller and Peebles[15], and by Djorgovski and Spinrad[16]. Geller and Peebles discussed the change in diameter of first ranked galaxies with z, and the change of apparent magnitude within that diameter as z increases. The surface brightness is proportional to l/D^2 where l is the apparent luminosity. Both l and D are functions of q_o but the ratio is independent of q_o. Since no surface brightnesses were available Geller and Peebles discussed l and D as functions of z separately. Djorgovski and Spinrad studied D as a function of q_o and z attempting either to find q_o by comparison of observations with the family of theoretical $D(q_o z)$ curves, or look for the evolution of D with z.

Real progress on this fundamental problems has recently been made by Sandage and Perelmuter[17,18,19]. They began[17] by showing that the measurement of sizes and flux levels of elliptical galaxies at large $z(\sim 0.5)$ required to carry out the test was feasible with present-day ground based telescopes. They discussed operational methods of observing practical measures of metric radius and also showed that the effect of passive evolution of the galaxies (simply the changes due to the evolution of stars) is small compared to the effect being looked for. They then proceeded to determine the dispersion in the surface brightness after the data were reduced to a common absolute magnitude, thus taking out the variation of $< SB >$ with M_B.

To do this, they used ellipticals in nearby clusters - Virgo, Fornax and Coma, and field galaxies. It is known that the average surface brightness is strongly correlated

with M_B. Galaxies brighter than M_B = -20 have fainter average surface brightnesses as M_B increases.

This means that surface brightnesses over a range of M_B in distant clusters are required to reduce the data to "standard" conditions. Studies of the nearby sample show that the dispersion in the surface brightness distributions after reducing the data to M_B = -22 is only -0.5 magnitudes. At a redshift of 0.5, the $(1+z)^4$ factor amounts to $1.^m8$, showing that even at this redshift the uncertainty will be small[18].

In their third paper[19] Sandage and Perelmuter have applied the methods that they developed to the first ranked galaxies in 25 clusters with redshifts ranging from 0 to about 1. They used the photographic data obtained by Djorgovski and Spinrad[16]. After an elaborate reduction procedure they have shown first that there is selection bias in the data so that there is an increase in absolute luminosity of individual galaxies with increasing z (the Scott effect) and this gives a result which tends to mimic the result they are looking for. Having eliminated this, they have then searched for the expansion result (proportional to $(1+z)^{-4}$) in the data of Djorgovski and Spinrad and they appear to have found it.

Their results are shown in Fig 1 in which we see the correlation of the surface brightness with log(1+z). The solid line is the least squares regression that uses the surface brightness as the independent variable. The slope is $d< SB >d\log(1+z) = 8.9 \pm 2.5$. The dashed line is the slope of 10.0 expected for expansion. When values of q_o are specified, the slopes are 9.9, 10.8 and 11.5 (± 1.5)

for values of q_o of 0, 0.5 and 1.0 respectively. These are also shown in Fig 1.

I have spent considerable time on this investigation because I consider it of fundamental importance. For the first time, more than 60 years after Hubble's original paper, we have good evidence for genuine expansion.

This applies to the normal galaxies.

To discuss the other classes of object in the extragalactic universe, it is convenient to write the observed redshift z_o as a product of number of terms so that

$$(1 + z_o) = (1 + z_c)(1 + z_r)(1 + z_i)$$

Here z_c is the cosmological (expansion) redshift, z_r is the redshift component associated with random motion, and z_i is the redshift due to intrinsic properties. So far it has been assumed the $z_c \gg z_r$ and that $z_i \approx 0$. This is appropriate for normal galaxies, since it follows from the existence of the Hubble relation. Random motions range from $\sim$300 km sec^{-1}, to values $\sim$1000 km sec^{-1} when we are concerned with the motions of galaxies in a rich cluster. Since the Hubble relation is well established for normal galaxies from values of cz$\simeq$3000 km sec^{-1} out to values cz $\sim$ 200,000 km sec^{-1} it is clear that z_r/z_c is a decreasing ratio as z_c increases.

However, there is evidence that some redshift components are not due to expansion or random motion so that a finite and even dominant term z_i may play a role for some objects. There are several lines of evidence:

1. The periodicity at very small values $\triangle cz \simeq 72.5$ km sec^{-1} originally found by Tifft[20,21,22,23] in the differential motion of galaxies in clusters, then in binary galaxies, and in the redshift differences between galaxies in small groups. It is fashionable to ignore this work, but there is no good scientific reason for this. The results have been obtained many times, and other workers[24] have confirmed some of them. The work at least suggests that a small component of z in normal galaxies is of intrinsic origin.

   A good example of the phenomenon is shown in Fig 2 taken from Arp and Sulentic[25].

2. Luminous connections between galaxies with very different redshifts have been found by Arp[26] (and earlier references). Some of these are most convincing. We show in Fig 3, the most spectacular case from Arp[27]. Other cases are published by Arp[26]. Not all of them is convincing. Very little work in this area has been carried out except by Arp, but it should be remembered that it was Arp's discovery of such objects which led to his removal from the observing schedule (cf Arp[26], Burbidge[28]).

   This work, if taken at face value, suggests that an intrinsic redshift component of order $cz \sim 10^3$ km sec^{-1} can exist under some conditions in galaxies.

   However both this effect and the Tifft effect must be comparatively small, since if they were not we would not find a good Hubble relation, and this certainly exists.

3. The strongest evidence for intrinsic redshifts comes from objects whose line spectra do not arise in stars, and whose continuum energy is largely non-thermal in origin. These are the quasi-stellar objects, or quasars, and the objects clearly related to them, sometimes called active galactic nuclei, and powerful radio galaxies.

Soon after the QSOs were discovered some thirty years ago, it was clear that they did not behave like galaxies. The first test, a plot of redshifts against apparent magnitudes, gave practically a scatter diagram, and no indication of a good Hubble relation, though it was clear that one could exist if there were a very large scatter in intrinsic luminosities of these objects[29,30]. Interestingly enough, the most recent diagrams of this type plotted by Segal[31] show a good quadratic relation between m and z which supports Segal's chronometric cosmological model. They are shown in Fig. 4.

The rapid flux variability and changes of apparent size over timescales of years shows that the objects are exceedingly small, and that either highly relativistic bulk motion nearly pointing at us is implied, with values of $\gamma = (1\text{-}\beta^2)^{-\frac{1}{2}}$ which lie in the range ~2-10, or the objects are much closer than is implied by using their redshifts to obtain distances (i.e. assuming the correctness of Hubble's law). Despite the fact that such large values of γ require values of $\beta = v/c \simeq 0.99$ or greater, and that no one has shown how such motions can be generated, let alone maintained, this interpretation has been preferred, so that the study of "superluminal motions" is treated as a

serious topic. It is interesting to note in passing, particularly in view of the discussion later in III, that since γ depends directly on the values of H_o which is assumed, the radio astronomers generally use a "large" value of $H_o = 100$ km sec^{-1} Mpc^{-1}. This minimizes the value of γ they have to assume! The refusal to consider these effects evidence that the QSOs are comparatively close by with the redshifts largely intrinsic, is symptomatic of the sociological problem associated with the redshift discussion.

However it is the observational evidence of the association of QSOs with bright galaxies that provides the strongest case for large intrinsic redshift components. Starting in the late 1960s, Arp showed that there were many cases of QSOs with large redshifts lying near to bright galaxies with very small redshifts. The most famous case of NGC 4319 and Mk 205, originally discovered by Weedman[32] was shown to have an optical bridge extending the $\sim 40''$ between the QSO with $z = 0.07$ and NGC 4319 with $z = 0.003$ (cf Arp[33] and Sulentic and Arp[34]). While the existence of the bridge was denied, and continues to be denied by some, the evidence that it exists is unequivocal. However, the majority of the evidence for the physical association of QSOs with bright galaxies rests on statistical arguments. By now some 600 of the QSOs among about 5000 with measured redshifts ($z = 0.1$–4.7) are known to lie within $10'$ of galaxies[35] and the redshifts of all but a very small fraction of the pairs (about 30) are very different.

One of the earliest statistical analyses was of the association of QSOs in the 3C catalogue of radio sources with the bright galaxies in the Shapley-Ames catalogue. It was shown that 10% of them lay within 6′ of bright galaxies, and that this is a highly statistically significant result[36,37]. This result shows that the pairs are physically associated although the redshifts are very different. More recently it has been shown that there is a bridge of hydrogen joining the QSO and galaxy in one pair, 3C 232 and NGC 3067. Arp and others found many more remarkable cases of apparent associations, and in 1979 a further statistical analysis of these was made[38]. The conclusion again was that there were far more QSOs close to galaxies with very different redshifts than were expected by chance. The surface density on the sky of QSOs has been known for many years and it has never been revised. It is therefore a simple matter to ask how many objects are expected by accident and compare this to what has been found. The most recent analysis based on several hundred pairs[35] leads to no doubt of the reality of the effect. Up to now the data have mostly been ignored, usually on the grounds that Arp has not done his statistics properly or that the result is too radical to believe. Most recently, there has been a swing in favor of accepting the evidence on the grounds that it can be explained by gravitational microlensing by objects in the halos of the galaxies, but this effect while it can occur, can not at all explain the magnitude of the effect seen[39,40,41]. Thus we must accept that a large part of the redshifts of QSOs is intrinsic, or local to the objects.

This, of course, does not affect our conclusions about normal galaxies

discussed earlier. It does have very considerable repercussions on cosmology in the sense that we can no longer argue that there is any evidence for the evolution of QSOs in numbers of fluxes as a fraction of epoch. Moreover, if all of these objects with large redshifts are actually comparatively local, with $z_c \approx 0.1$, we can no longer say that we have any evidence from discrete objects about the universe beyond $z \simeq 1$.

There is one other issue which is very puzzling and may ultimately make us rethink the currently popular cosmology.

This is the existence of peaks and periodicity in the distribution of redshifts. This effect was first found in the spectra of QSOs and related objects and it has not gone away (cf Burbidge and Burbidge[42]; Burbidge[43]; Burbidge and O'Dell[44]; Karlsson[45,46,47]; Depaquit, Pecker and Vigier[48]; Fang and Sato[49]; Fang[50]; Burbidge and Hewitt[51]). Most recently similar evidence has has been found for faint galaxies[52]. It should also be remembered that the currently popular view that galaxies appear to be concentrated in thin sheets in space. (cf Geller and Huchra[53]) can equally well be interpreted as the presence of sharp redshift peaks and broad valleys. Here again serious attempts should be made to explain the observed phenomena rather than ignoring them hoping that they are not real.

In summary, I have tried, in this section, to bring out the fact that now, after more than 60 years, good evidence from normal galaxies has been developed which shows that the universe is expanding. There is also evidence that some objects – not

normal galaxies – have large redshifts which are intrinsic in origin. However, the existence of a good Hubble relation for normal galaxies means that their redshifts are cosmological in origin.

We now turn to the classical problem of the scale, i.e. the determination of the Hubble constant H_o.

III. THE DETERMINATION OF H_o

In 1936, Hubble[7] gave his best estimate of the Hubble constant as 550 km sec^{-1}. The value that Hubble and Humason had derived from 1929 onward was between about 500 and 550. Later it was shown that this value was grossly in error. It turned out that there were two classes of cepheid variables[54,55], and this led to a reduction of H_o by a factor of about 2.6 Thus, Humason, Mayall and Sandage[9] put $H_o = 180$ km $sec^{-1}Mpc^{-1}$. Later, Sandage[56] showed that what Hubble had taken as brightest stars in nearby galaxies were actually HII regions and he reduced H_o to 75 km $sec^{-1}Mpc^{-1}$. For the last 20 years there has been an extensive debate in the literature over a more exact value, and it has been customary for theoreticians to put $H_o = 100h$ km $sec^{-1}Mpc^{-1}$ where $\frac{1}{2} \leq h \leq 1$. This uncertainty involving a factor of 2 has been treated very seriously, and until the recent debacle by NASA it has often been stated that the uncertainty would only be reduced by observations made using the Hubble Space Telescope.

The distance scales inside our galaxy are firmly established, and as soon as we get outside the galaxy the method is to use objects which have some kind of standard

property – the absolute magnitude of the brightest stars in a galaxy, globular clusters, supernovae, etc.

While a great effort has been made to refine the details, it is possible to get a result which is close to the truth by using very simple methods, as the following example will show.

More than 30 years ago, Hoyle and I, in studying Baade's direct plates of the Hercules cluster of galaxies (cf Burbidge and Burbidge[57])realized that it might be possible to determine H_o by comparing the diameters of the many open spirals in the Hercules cluster with the diameter of local spirals such as our own galaxy, M31 and M33. We borrowed a ruler from a colleague in the Mount Wilson offices and measured the diameters directly from the plates. In the course of a Saturday afternoon, we derived a value of H_o of about 60 km sec^{-1}Mpc and wrote up a short note which we sent to the Astrophysical Journal on the following Monday. S. Chandrasekhar was the Editor at the time and he sent the paper to Allan Sandage to referee. Allan came to us very concerned that the publication of such a result using such a simple method would make the field which involved so many detailed steps and corrections look rather artificial. He was so persuasive (and he was, and is, a friend) that we withdrew the paper!

Returning to the modern determination of H_o, a detailed study of the literature and the arguments between the main protagonists, namely those who have maintained the position that H_o is close to 100 km sec^{-1} Mpc – de Vaucouleurs, Aaronson,

Mould, Tully, etc., and those who have argued that H_o is close to 50 km sec^{-1} Mpc^{-1}, particularly Sandage and Tammann, has led me clearly to the conclusion that a small value of H_o is the correct global value. In what follows, I shall describe the major steps that lead to this.

The first point to be made is that there is general agreement that out to about 10 Mpc the value of H_o is about 50. For distance $\leq$10Mpc the evidence comes from the use of cepheids with velocities corrected to the centroid of the local group[58,59]. Further out the same value of H_o applies[60,61] for the galaxies in the volume limited sample out to cz = 500 km sec^{-1} in the catalogue of Kraan-Korteweg and Tammann[62]. This sample, since it is volume limited, is totally free of Malmquist bias.

Argument has largely centered about the use of the Tully-Fisher relation[63] for galaxies beyond this distance. Kraan-Korteweg, Cameron and Tammann[64], Tammann[65] and Sandage[66] have argued that the relation is progressively displaced toward brighter absolute magnitudes as the redshift increases, and that this is due to Malmquist bias. Tully[67] does not accept that Malmquist bias is present and obtains values of $H_o \simeq 90$ which he believes is real. This effect, the apparent increase of H_o with distance is reminiscent of the early arguments based on a hierarchical universe originally proposed by Charlier and revived by de Vaucouleurs[68,69].

The consequences of such a model predicted by Haggerty and Wertz[70] were shown to be incompatible with the Hubble relation for cz as small as 1000 km/sec[71] and

as studies of galaxy group at higher redshifts (out to cz $\simeq$10000 km sec^{-1}) were made[72,73,74] no evidence was found that H_o varied systematically as a function of z.

It is this issue in modern times advocated by Tully[67] and in many papers denied by Sandage that has been the basis for supporting that there is a real uncertainty in the global value of H_o.

We now follow Sandage[75] in showing how this whole problem of the "local" velocity field can be got around.

The method is to use clusters and supernovae at distances far enough away so that the local velocity effects will be negligible. If $\triangle v/v$ less than 10% in individual clusters, this will lead to a much smaller error in H_o when averaged over the sky. Distances obtained using such distant objects can then be compared with the distance of the center of the Virgo cluster for which there are many indicators.

Sandage has used 17 clusters ranging from the larger Ursa Major cluster which has a redshift cz = 1270 km sec^{-1} to the Hercules cluster with cz = 11212 km sec^{-1}. The recession velocities adopted are corrected to the centroid of the Local Group, and also for a perturbation on us, due to the Virgo cluster amounting to an infall velocity of 220 km sec^{-1}.

Distance moduli for these clusters are obtained by several techniques. These include the Tully-Fisher method as discussed by Kraan-Korteweg et al.[64] nuclear magnitudes of the first 10 elliptical when available[76] D-σ distance indicators for

ellipticals[77] the surface brightness absolute magnitude relation for dwarf ellipticals[78], the absolute magnitudes of supernovae of Type 1a[79] and others.

The Hubble diagram for these clusters taken from Sandage[75] is shown in Fig 5. It is clearly a very tight relation.

It remains to discuss the determination of the distance to the core of the Virgo cluster. There are many methods now available. Sandage uses globular clusters, normal novae, supernovae of type Ia using both photometric and expansion parralux methods, the Tully-Fisher method, and the sizes of the Virgo spirals relation to M31 and our galaxy. The different moduli are shown in Table 1. The adopted modulus is 31.70 ± 0.09 or a distance of 21.9 ± 0.9 Mpc.

It remains to determine the velocity of the Virgo core freed of all perturbations. The equation of the line drawn through the points in Fig 5 is

$$logv = 0.2\triangle(m\text{–M}) + 3.072 \pm 0.008$$

so that when $\triangle(m\text{–M}) = 0$,

$$v_{Virgo} = 1180 \pm 22 \text{ km sec}^{-1}.$$

This is the value tied to clusters with a mean cz = 6000 km sec^{-1}.

A second method used by Sandage is to obtain a value of v_{Virgo} from the brightest cluster galaxies. He uses a method similar to that used for clusters just described.

Using the mean apparent magnitude of first ranked cluster galaxies at the distance of the Virgo cluster, and combining this with the value obtained using 96 first ranked cluster galaxies[80] he obtains a second value of

$$v_{Virgo} = 1107 \pm 55 \text{ km sec}_{-1}.$$

A third method is through the supernovae where a value of $M_B(\max) = -19.79 \pm 0.12$ for Type Ia SN is used. The result has lower weight but Sandage finds that using it

$$v_{Virgo}(\text{SN}) = 1037k \pm 45 \text{ km/sec}_{-1}$$

Averaging the three values with slightly different weighting give

$$< v_{Virgo} > = 1144 \pm 18 \text{ km sec}^{-1}$$

Now since $D_{Virgo} = 2.1.9 \pm 0.9$ Mpc, we find that $\underline{H_\circ = 52 \pm 2 \text{ km sec}^{-1} \text{ Mpc}^{-1}}$ or if we believe that further revision in D_{Virgo} is likely,

$$\underline{H_\circ = 52 \pm (21.0/D) \text{ km sec}^{-1} \text{ Mpc}^{-1}.}$$

Van den Bergh[81] has recently obtained a value for D of 20 ± 2 Mpc.

I believe that there can be little in error in this determination. Thus we should put $\underline{H_\circ^{-1} = 19.2 \, ^{+0.8}_{-0.7} \text{ years.}}$

I would like to believe that the work of Sandage just described lays to rest the idea that global values of $H_\circ$ as large as 90 or 100 are still feasible, but this may be

asking too much. In recent years, methods other than those used above have been attempted. With Sandage, I believe that they are not giving the right answer, but a few comments are in order.

Three methods of comparatively recent origin all suggest that the distance to the Virgo cluster is only about 15 Mpc and this has the effect of increasing the value of the Hubble constant by nearly 50%. The newer methods are the use of the sizes of giant HII regions and the correlation of their sizes with the velocity dispersion in them, – the $H\beta - \sigma$ correlation[82] the use of the bright end of the planetary nebula luminosity function as a standard candle[83], and the surface brightness fluctuation method of Tonry and Schneider[84] where one determines a mean absolute magnitude for a particular stellar content that gives rise to the observed surface brightness and normalizes to a fixed surface brightness.

The problem with the first of these, the $H\beta$-σ relation, is that the sample is flux limited and not volume limited, so that as Sandage has shown, the $H\beta$ power increases as z^2 for the galaxies used. Thus the Malmquist bias remains in the data.

In both the use of planetary nebulae, and the surface brightness of a particular star mix, the problem centers about the assumption that must be made that in each galaxy used there has been an identical history of stellar evolution, i.e. it must be tacitly assumed that the star formation history in all systems has been identical. This is very unlikely, and the only way to avoid such assumptions is to determine empirically, using galaxies with known distances, the true dispersion in the peak

luminosity of planetary nebulae, and the mean surface brightness $< M >$ respectively. Because this has not been done the uncertainties associated with these methods means that they should be given much lower weight, so I still feel confident that the value of the Hubble constant derived in the latest work by Sandage will stand up.

This completes our discussion of the determination of H_o. We turn next to the timescales which can be deduced from nucleosynthesis and stellar evolution.

IV. TIMESCALES FROM NUCLEOSYNTHESIS AND STELLAR EVOLUTION

There are several ways that these timescales can be determined. They all require that we determine the ages of the stars or/and, from the existence of radioactive isotopes and their daughter nuclei which are made in the stars, the ages of those elements.

A few general remarks are in order. Age dating is very strongly restricted to very small distances on the extragalactic scale, i.e. to our own galaxy and its immediate vicinity. Age dating from the transuranium isotopes restricts us to the solar system. We shall discuss possible extrapolations later.

We first discuss age dating using the Hertzsprung-Russell diagram for star clusters.

Globular Clusters:

To date the clusters, it is necessary to measure the absolute bolometric magnitude of the main-sequence turn-off. When this is done by fits of the main sequences of color magnitude diagrams to a fiducial main sequence, the ages of most clusters are the same to within about 20%. The mean age of the globular clusters turns out to be 19.1 ± 2.1Gy for a normal (solar system) 0/Fe ratio, and 15.5 ± 1.7 Gy if the 0/Fe ratio is about four times normal[85].

It is also possible to measure the turn off from the main sequence by calibrating the absolute magnitudes of the RR Lyrae stars as a function of the Fe/H ratio. This calibration can then be used in globular clusters in which relative photometry has been obtained reaching below the turnoff, thus setting the turn-off level. This leads to practically no spread in ages in the mean with a mean age of 14 Gy with $0/Fe = 4$[86].

These are the clusters that were formed early in the history of the galaxy according to the classical picture of Eggen, Lynden-Bell and Sandage[87] which remains a good first order model. According to this scheme, the disk formed later.

The Disk Stars

The oldest galactic cluster may be NGC 6791[88,89] with an age of 12.5 Gy. The ages of NGC 188 and M 67 have been in dispute for several years, with ages that range from 6-10 Gy (cf Demarque[90]. The ages are derived by the method described for globular clusters. The newest method of age determining of disk stars is the cooling

age of white dwarfs, and ages as low as 9 Gy are found by this technique. However, the range of ages based on the same observational evidence can vary between 5 and 13 Gy depending on the detailed physics of the cooling process[91,92].

What we can conclude from all of these attempts to determine ages from stellar evolutionary arguments for stars in our own galaxy is that they are still uncertain, probably by factors of order 2. There may be real differences of the order of several Gy between different star groups – e.g. the halo stars are probably on the average older than those in the disk.

All of the data suggest ages $<H_o^{-1}$. However, whether or not the ages of the oldest stars are no more than $\frac{2}{3}H_o^{-1}$ (the expectation of the idealists) is much less certain. It may well be that some globular clusters are older than this.

The Age of the Elements

Ever since it was established that the elements are made in the stars, estimates of the age of the heavy elements using the methods of nuclear cosmochronology have been made. The isotopes which were used are ^{232}Th, ^{235}U, and ^{238}U, and all of those parent nuclei are made in the r-process in supernovae. It is supposed that they are made steadily in supernovae until the material out of which the solar system formed was segregated 4.6 Gy ago. Since the first determinations by Burbidge et al.[93], the calculations have been revised several times and Fowler has done the most extensive work. In his recent studies[94] he has concluded that the age of the elements is $11.0 \pm 1.6(1\sigma)$Gy.

Ages of Galaxies in General

We have no unambiguous evidence of the ages of most galaxies. It has been generally assumed that spiral galaxies like our own, and ellipticals, have ages of the order of 10 Gy. These arguments come from the fact that the colors measuring the energy distributions from the main bodies of the galaxies suggest that the stellar populations are similar to those found in our galaxy and its nearby companions. Of course this does not rule out the possibility that systems much older than our own galaxy may exist.

Systems much younger in evolutionary terms may also be present. Now that a large number of galaxies have been observed in the far infrared by IRAS we know that there is a large population of what are often called starburst galaxies. These are systems which contain much interstellar matter in the form of dust and massive molecular clouds, in which extensive star formation is occurring. Much of the radiation is emitted in the far infrared (10μ–500μ) by dust heated by ultraviolet radiation from young stars. A closeby galaxy of this type is M82, only some 2.5 Mpc away from us. It is reasonable to suppose that in such galaxies there is an underlying population of older stars. However, there is a small fraction of the infrared galaxies which are exceedingly luminous ($L \simeq 10^{12} L_{\odot}$) which have highly irregular forms, and in which only weak optical emission lines can be detected. It is often argued that they are merging galaxies. However, I believe a strong case can be made for the proposal that they are very young (<0.1 Gy) galaxies[95]. If this is the case no old ($\geq$ 1 Gy) stars should be present, and their chemical composition

will be anomalous.

The existence of very young galaxies may also be indicated by the presence of dwarf galaxies, which appear to be no more than giant HII regions[96].

To summarize the discussion so far. Our galaxy has an age of ~14 Gy. It contains stellar components which have formed more recently than about 14 Gy ago. The evidence is compatible with the proposal that the oldest systems are no older than this, but the data do not rule out the existence of objects in the universe which are say 20 to 30 Gy old. Very young galaxies with ages < 1 Gy – the high luminosity IRAS systems are probably present.

Galaxies at Large Redshifts

Can we get any information about the timescale for the universe from observations at large redshifts? Obviously if we believe that we live in an evolving universe, observations of objects at large redshifts means that we are observing them when they were much younger. In recent years, there have been a number of studies of high redshift radio galaxies. These are in no sense normal galaxies. They all have very strong emission line spectra and they show extended emission. Some show evidence for faint Lyman α emission[97] and in at least two cases, 3C 326.1[98] and 3C 294[99] with z = 1.825, 1.786 respectively very large clouds of ionized gas detected from Lyα emission are found to lie adjacent to the "galaxies". We have no real idea of the stellar content of such objects but it is speculated by some that they are galaxies in the process of formation. At such redshifts, in the simplest Einstein–

deSitter cosmology, where the age of the universe is $2/3H_o^{-1}$, we must be seeing these objects only a few Gy after the beginning.

Little is really known about them and in my view the nature of their redshifts is unclear. Thus, while I feel duty bound to mention them, I do not think that they really tell us much about young galaxies.

Another approach using high redshift objects is through absorption in the spectra of QSOs. Absorption in the spectra of QSOs is common for QSOs with $z > 2$. It has been generally argued that most of the absorption is due to clouds randomly distributed along the light paths between us and the QSOs. If the data are interpreted in this way, there is considerably more absorbing material then was previously assumed to be present in the halos of galaxies, etc. Hydrogen clouds which are small enough so that only Lyα, Lyβ pairs are seen (the Lyα forest), and systems containing heavier elements, have been identified at many redshifts. In a few cases, Wolfe and his colleagues[100,101] have argued that some are likely to be protogalactic disks, and are thus evidence for galaxies forming at $z \geq 1$.

While this is very attractive work, we have described in Section II evidence which strongly suggests that the redshifts of QSOs are not of cosmological origin. If this is the case, all of the absorption must be intrinsic to the QSOs (i.e. due to ejected clouds) as is already believed for the broad absorption lines, and therefore it can have nothing to do with galaxy formation at large redshifts.

V. CONCLUSIONS

It is fashionable to argue that cosmology has come of age in the last decade and that with the advent of much new data we are convincing ourselves that the hot big bang represents the correct cosmological model.

However, only a few quantities can really be measured and only some of these have been measured. I have concentrated on two of them here. The proof that the redshifts of normal galaxies are due to expansion is, to my mind, quite fundamental whether or not it has tacitly assumed to be so for 60 years.

The determination of H_o and q_o has proved the greatest challenge to the observers. It has been known for many years that the determination of q_o from the shape of the Hubble relation at fairly large redshifts is made almost impossible because of the uncertainties in the evolutionary corrections, a lack of properly chosen clusters, both bright and faint, to measure, and the difficulty of measuring redshifts of normal galaxies accurately. The formal value still differs by 2 in the recent analyses[102]. The use of radio galaxies by Spinrad and Djorgovski[103] suggests a small value for q_o, but again there is considerable uncertainty.

If $\Lambda = 0$, we can obtain q_o by measuring the mass energy density in the universe, and as is well known this leads to a value of $q_o \approx 0.03$ for visible matter and a value of $q_o \approx 0.1$-0.3 if we make allowance for dark matter which we derive by assuring that the galaxies are stable, and that the virial can be used to derive the masses of groups and clusters of galaxies. However, there is no direct observational evidence

in favor of the so-called closure density corresponding to $q_o = \frac{1}{2}$.

I have devoted much of the paper to a study of the determination of H_o and conclude with Sandage that $H_o = 52$ km sec^{-1}Mpc^{-1} i.e. $H_o^{-1} = 19.2$ Gy and the age of the favored Einstein-de Sitter model $= 2/3\ H_o^{-1} = 12.8$ Gy.

What do these results alone tell us about the cosmological model? From Section IV taking into account the uncertainties it can be concluded that the oldest objects in our Galaxy may have ages $\leq 2/3 H_o^{-1}$.

At the same time we cannot rule out the possibility that some globular clusters have ages greater than $2/3H_o^{-1}$. The existence of even older galaxies clearly cannot be ruled out also. On the other end of the time scale, there are clearly galaxies which are very young in evolutionary terms, both luminous IRAS galaxies and the galaxies which largely consist of O and B stars and ionized gas. Such galaxies may have ages (since star formation began) $\ll 1$ Gy.

Now in the steady state cosmology the average age of the matter around us equals $H_o^{-1}/3$ or about 6.5 Gy. Thus, there is nothing in the age determinations discussed in Section IV which argues against the steady state, and the discovery of young galaxies is evidence in its favor. The counter argument is, of course, that the existence of galaxies young in evolutionary terms does not mean that they only condensed very recently. They could be protogalaxies which condensed in a hot big bang universe and have only recently begun to form stars.

Of course, in this discussion, I have omitted what is normally considered to be the strongest observational evidence in favor of the hot big bang, and against the steady state cosmology, namely, the extremely smooth and isotropic black body radiation whose discovery we are celebrating here.

In my view, the major weakness in this argument remains the problem of reconciling the extreme smoothness of this radiation in contrast to the lumpiness of the visible matter. It may ultimately have to be conceded that these two components were never coupled together. In this case, the radiation field may have been generated by the galaxies, from star light, with its black body nature arising from absorption and re-emission by dust grains in the form of iron "needles"[104,105]. Under these conditions, it is possible to explain all of the observational properties of the universe in terms of a modified steady state universe[1].

ACKNOWLEDGEMENTS

Except for a brief digression in the last section, I have tried to discuss the scale of the universe from a purely observational standpoint. I have drawn heavily on the work and conclusions of my good friend, Allan Sandage, who has probably contributed more than anyone else to solutions to the problems I have described here.

I also wish to thank Del Hewitt for her help. My research at the University of California, San Diego is supported in part by NASA grant No. NAGW 1737.

REFERENCES

1. Arp, H.C., Burbidge, G., Hoyle, F., Narlikar, J.V., and Wickramasinghe, N.C. 1990, Nature, **346**, 807.
2. Hubble, E. 1929, Proc. Nat. Acad. Sci., **15**, 168.
3. Burbidge, G. 1981, Ann. N.Y. Acad. of Sci., **375**, 123.
4. Humason, M.L. 1929, Proc. Nat. Acad. Sci., **15**, 167.
5. Zwicky, F. 1929, Phys. Rev., **15**, 773.
6. Zwicky, F. 1929, Phys. Rev., **33**, 1077.
7. Hubble, E. 1936, *The Realm of the Nebulae,* (Yale University Press).
8. Curtis, H.D. 1933, Handbuch der Physik, Vol. **II**, Part 1, p. 891.
9. Humason, M.L., Mayall, N.U., and Sandage, A.R. 1956, A.J., **61**, 97.
10. Segal, I. 1980, M.N.R.A.S., **192**, 755.
11. Sandage, A.R. and Tammann, G.A. 1974, Ap.J., **190**, 525.
12. Tolman, R.C. 1930, Proc. Nat. Acad. Sci., **16**, 511.
13. Tolman, R.C. 1934, *Relativity, Thermodynamics & Cosmology,* (Clarendon Press; Oxford).
14. Hubble, E. and Toman, R.C. 1935, Ap.J., **82**, 302.
15. Geller, M. and Peebles, P.J.E. 1972, Ap.J., **174**, 1.
16. Djorgovski, S. and Spinrad, H. 1981, Ap.J., **251**, 417.
17. Sandage, A. and Perelmuter, J.-M. 1990, Ap.J., **350**, 481.
18. Sandagè, A. and Perelmuter, J.-M. 1990, Ap.J., in press.
19. Sandage, A. and Perelmuter, J.-M. 1990, Ap.J., in press.
20. Tifft, W.G. 1976, Ap.J., **206**, 38.
21. Tifft, W.G. 1980, Ap.J., **236**, 70.
22. Tifft, W.G. 1982, Ap.J. Suppl., **50**, 319.
23. Tifft, W.G. 1982, Ap.J., **257**, 442.
24. Guthrie, B.N.G. and Napier, W.M. 1990, M.N.R.A.S., **243**, 431.
25. Arp, H.C. and Sulentic, J. 1985, Ap.J., **291**, 88.

26. Arp, H.C. 1987, *Quasars, Redshifts and Controversies,* (Berkeley: Interstellar Media).

27. Arp, H.C. 1971, Ap. Letters, **7**, 221.

28. Burbidge, G. 1988, Sky & Telescope, **75**, 38.

29. Bahcall, J.N. and Hills, R.E. 1973, Ap.J., **179**, 699.

30. Burbidge, G. and O'Dell, S.L. 1973, Ap.J., **183**, 759.

31. Segal, I. 1990, private communication.

32. Weedman, D.W. 1970, Ap.J. (Letters), **161**, L113.

33. Arp, H.C. 1971, Ap. Letters, **9**, 1.

34. Sulentic, J.W. and Arp, H.C. 1987, Ap.J., **319**, 687.

35. Burbidge, G., Hewitt, A., Narlikar, J.V., Das Gupta, P. 1990, Ap.J. Suppl., November

36. Burbidge, E.M., Burbidge, G.R., Solomon, P., and Strittmatter, P.A. Ap.J., **170**, 233.

37. Kippenhahn, R. and De Vries, H.L. 1974, Astr. Space Sci., **26**, 131.

38. Burbidge, G. 1979, Nature, **282**, 451.

39. Linder, E.V. and Schneider, P. 1988, Astr. Ap., **204**, L8.

40. Narajan, R. 1989, Ap.J. (Letters), **339**, L53.

41. Arp, H.C. 1990, Astr. Ap., **229**, 93.

42. Burbidge, G. and Burbidge, E.M. 1969, Nature, **222**, 735.

43. Burbidge, G. 1968, Ap.J. (Letters), **154**, L41.

44. Burbidge, G. and O'Dell, S.L. 1972, Ap.J., **178**, 583.

45. Karlsson, K.G. 1971, Astr. Ap., **13**, 333.

46. Karlsson, K.G. 1977, Astr. Ap., **58**, 237.

47. Karlsson, K.G. 1990, Astr. Ap., in press.

48. Depaquit, S., Pecker, J.C. and Vigier, J.-P. 1985, Astron. Nach., **306**, 7.

49. Fang, L.-Z. and Sato, H. 1983, Acta. Astronomica Sinica, **24**, 410.

50. Fang, L.-Z. 1990, preprint.

51. Burbidge, G. and Hewitt, A. 1990, Ap.J. (Letters), **359**, L33.

52. Broadhurst, T.J., Ellis, R.S., Koo, D.C. and Szalay, A. 1990, Nature, **1343**, 726.

53. Geller, M. and Huchra, J. 1989, Science, **246**, 897.

54. Baade, W. 1952, Trans. I.A.U., **8**, 397.

55. Thackeray, A.D. and Wesselink, A.J. 1953, Nature, **171**, 693.

56. Sandage, A.R. 1958, Ap.J., **127**, 513.

57. Burbidge, G. and Burbidge, E.M. 1959, Ap.J., **130**, 629.

58. Sandage, A.R. 1986, Ap.J., **307**, 1.

59. Sandage, A.R. 1987, Ap.J., **317**, 557.

60. Richter, O.-G. and Huchtmeier, W.K. 1984, Astr. Ap., **132**, 253.

61. Huchtmeier, W.K. and Richter, O.-G. 1986, Astr. Ap. Suppl., **63**, 323.

62. Kraan-Korteweg, R.C. and Tammann, G.A. 1979, Astr. Nach., **300**, 181.

63. Tully, R.B. and Fisher, J.R. 1977, Astr. Ap., **54**, 661.

64. Kraan-Korteweg, R.C., Cameron, L.M. and Tammann, G.A. 1988, Ap.J., **331**, 620.

65. Tammann, G.A. 1988, *Extragalactic Distance Scale,* ed. S. van den Bergh and C. Pritchet, ASP Conf. Series No. 4 (Brigham Young University Press: Provo) p. 282.

66. Sandage, A.R. 1988, Ap.J., **331**, 605.

67. Tully, R.B. 1988, Nature, **334**, 209.

68. de Vaucouleurs, G. 1970, Science, **167**, 1203.

69. de Vaucouleurs, G. 1971, Pub. A.S.P., **83**, 113.

70. Haggerty, M.J. and Wertz, J.R. 1971, M.N.R.A.S., **155**, 495.

71. Sandage, A.R., Tammann, G.A., and Hardy, E. 1972, Ap.J., **172**, 253.

72. Sandage, A.R. and Tammann, G.A. 1975, Ap.J., **198**, 313.

73. Sandage, A.R. 1975, Ap.J., **202**, 563.

74. Tammann, G.A. 1987, Observational Cosmology, I.A.U. Symp. No. 124, ed. A. Hewitt, G. Burbidge, and L.-Z. Fang (Dordrecht: Reidel) p. 151.

75. Sandage, A.R. 1990, Ap.J., in press.

76. Weedman, D.W. 1976, Ap.J., **203**, 6.

77. Faber, S., Wegner, G., Burstein, D., Davies, R., Dressler, A., Lynden-Bell, D. and Terlevich, R. 1989, Ap.J. Suppl., **69**, 763.

78. Ferguson, H.C. and Sandage, A. 1988, A.J., **96**, 1599.

79. Leibundgunt, B. and Tammann, G.A. 1990, Astr. Ap., in press.

80. Sandage, A.R. and Hardy, E. 1973, Ap.J., **183**, 743.

81. van den Bergh, S. 1989, Astr. Ap. Rev., **1**, 111.

82. Melnick, J., Terlevich, R., and Moles, M. 1988, M.N.R.A.S., **253**, 297.

83. Jacoby, G.H. 1989, Ap.J., **339**, 39.

84. Tonry, J.L. and Schneider,D. 1988, A.J., **96**, 807.

85. Sandage, A.R. 1990, J. Roy. Astron. Soc. Canada, **84**, 70.

86. Sandage, A.R. and Cacciari, C. 1990, Ap.J., **350**, 645.

87. Eggen, O.J., Lynden-Bell, D. and Sandage, A.R. 1962, Ap.J., **136**, 748.

88. Janes, K. 1988, Calibration of Stellar Ages, Van Vleck Obs. contr. No. 7, ed. A.G.D. Phillip, (L. Davis Press, Schenectady, N.Y.) p. 59.

89. Kaluzny, J. 1989, Acta Astronomica, in press.

90. Demarque,P. 1990, J.R. Astron. Soc. Canada, **84**, No. 2.

91. Winget, D.E. and van Horn, H.M. 1987, Second Conf. on Blue Stars, ed. A.G.D. Phillip, D. Hayes, and J. Liebert (L. Davis Press: Schenectady, N.Y.) p. 363.

92. Mazzitelli, I. and d'Antona, F. 1987, Second Conf. on Blue Stars, ed. A.G.D. Phillip, D. Hayes, and J. Liebert (L. Davis Press: Schenectady, N.Y.) p. 635.

93. Burbidge, E.M., Burbidge, G.R., Fowler, W.A. and Hoyle, F. 1957, Rev. Mod. Phys., **29**, 547.

94. Fowler, W.A. 1987, Quart. J.R.A.S., **28**, 87.

95. Burbidge, G. 1986, Pub. A.S.P., **98**, 1252.

96. Sargent, W.L.W. and Searle, L. 1970, Ap.J. (Letters), **162**, L155.

97. Spinrad, H., Filippenko, A.V., Wyckoff, S., Stocke, J.T., Wagner, R. Lawrie, D.G. 1985, Ap.J. (Letters), **299**, L7.

98. McCarthy, P.J., van Breugel, W., Spinrad, H. and Djorgovski, S. 1987, Ap.J. (Letters), **321**, L29.

99. McCarthy, P.J., Spinrad, H., van Breugel, W., Liebert, J., Dickinson, M., Djorgovski, S. and Eisenhardt, P. 1990, preprint.

100. Wolfe, A.M., Turnshek, D.A., Smith, H.E. and Cohen, R. 1986, Ap.J. Suppl., **61**, 249.

101. Wolfe, A.M. 1990, private communication.

102. Gunn, J.C., Hoessel, J. and Oke, J.B. 1986, Astr. J., **306**, 30.

103. Spinrad, H. and Djorgovski, G. 1987, Observational Cosmology, I.A.U. Symp. No. 124, Ed. A. Hewitt, G. Burbidge and L.-Z. Fang (Dr. Reidel: Dordrecht), p. 129.

104. Hoyle, F., Wickramasinghe, N.C. 1988, Astrophys. Sp. Sci., **147**, 245.

105. Hoyle, F., Wickramasinghe, N.C. and Burbidge, G. 1990, 29th Liege International Astrophysical Colloquium, EAS SP, in press.

106. Hewitt, A. and Burbidge, G. 1987, Ap.J. Suppl., **63**, 1.

107. Hewitt, A. and Burbidge, G. 1989, Ap.J. Suppl., **69**, 1.

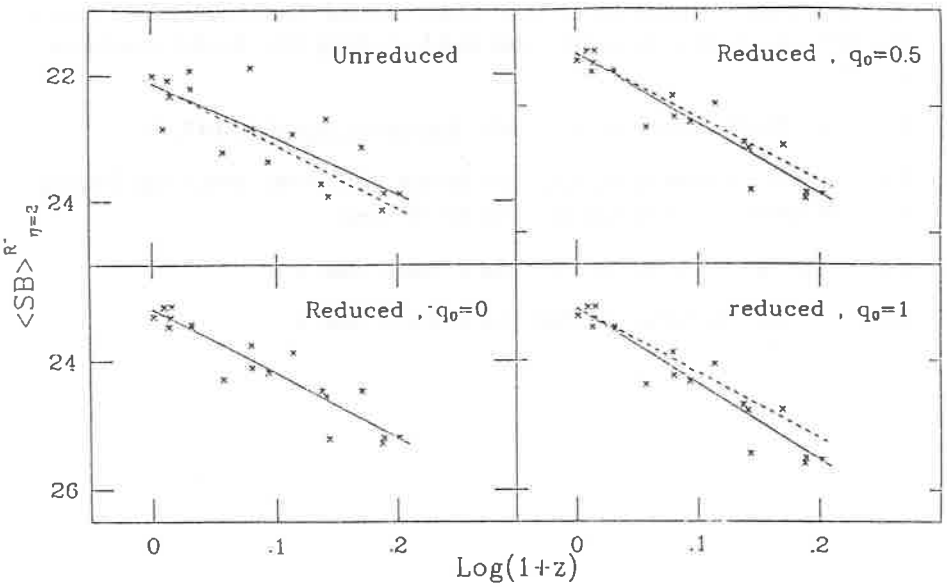

Fig 1. Plot surface brightness <SB> in apparent magnitude units per square arc second against log(1+z) for elliptical galaxies from Sandage and Perelmuter[19]. The dotted line has the slope of 10 expected for the case of expansion, i.e. $<SB> \propto (1+z)^{-4}$.

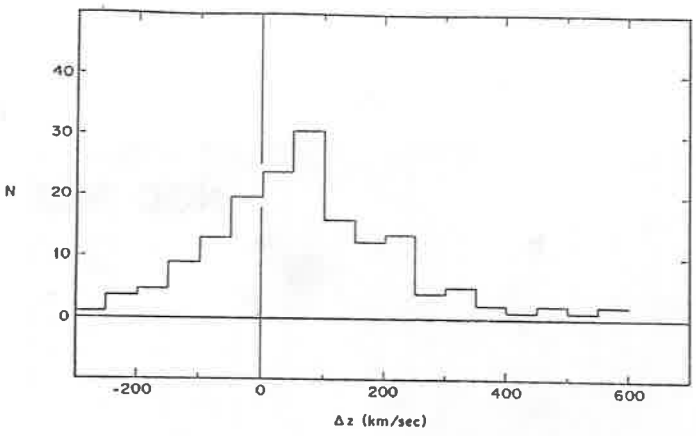

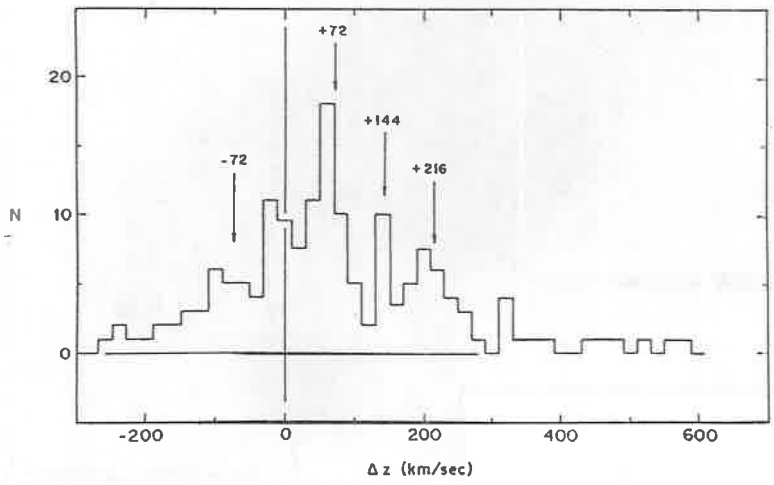

Fig 2. Top figure shows a plot of all values of $\Delta\nu = z/c$ for all accurate measures of velocity differences $\Delta\nu$ between the dominant galaxy in a group and the satellite galaxies. Since for such a large number of systems there should be as many with $+\Delta\nu$ as $-\Delta\nu$, the peak of the curve should be at zero velocity. It can be seen that it is clearly displaced about 80 km sec^{-1} to the red. This may be the effect of a small intrinsic redshift component.

In the bottom figure a subset of the same data is plotted using a smaller bin size. The peaks at multiples of 72.5 km sec^{-1} originally found by Tifft[20] in other data are marked.

Both figures are taken from Arp Sulentic[25].

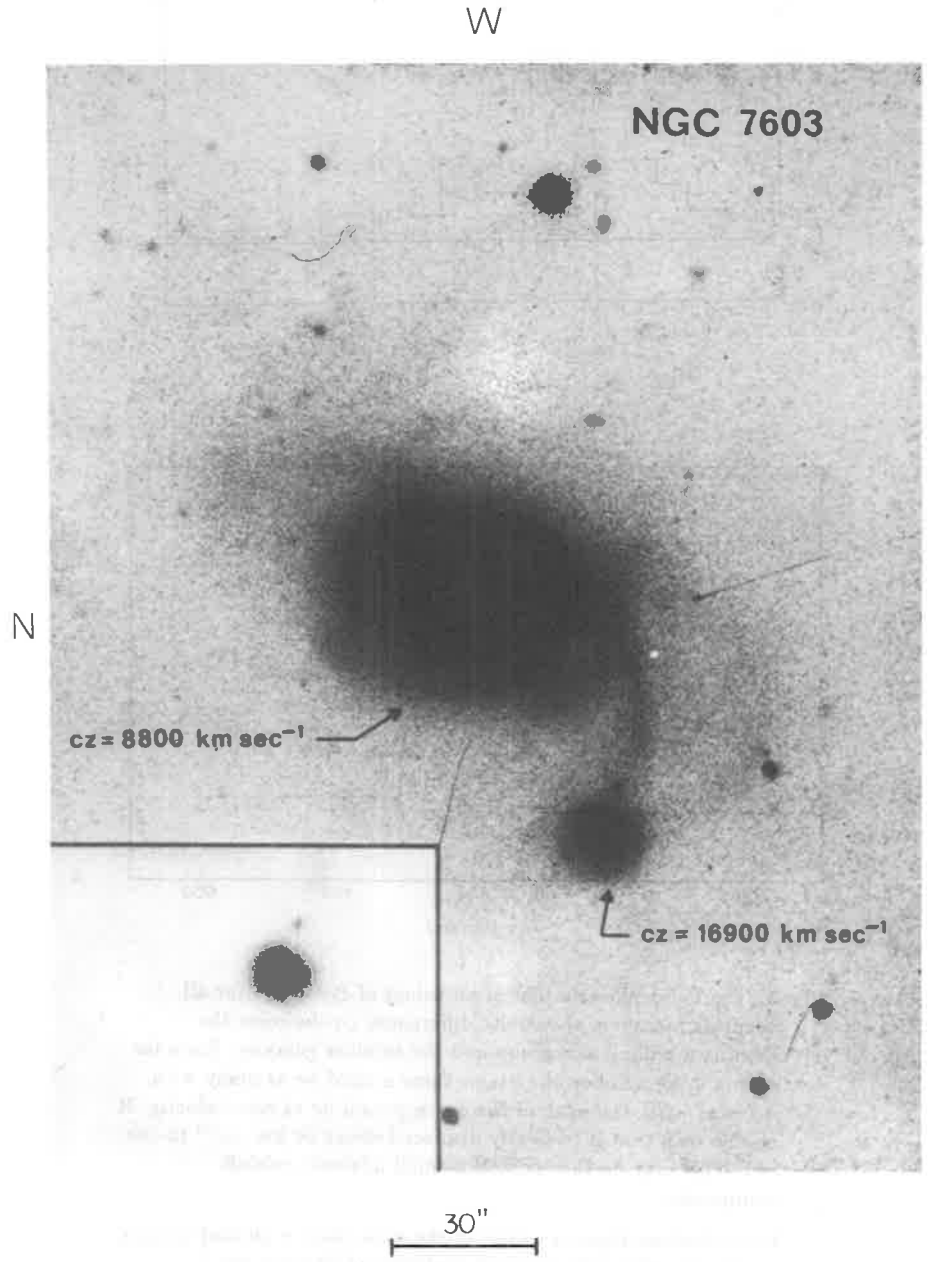

Fig 3. This picture is reproduced from a plate by Arp. The redshifts of the two galaxies have been added to the original figure[33].

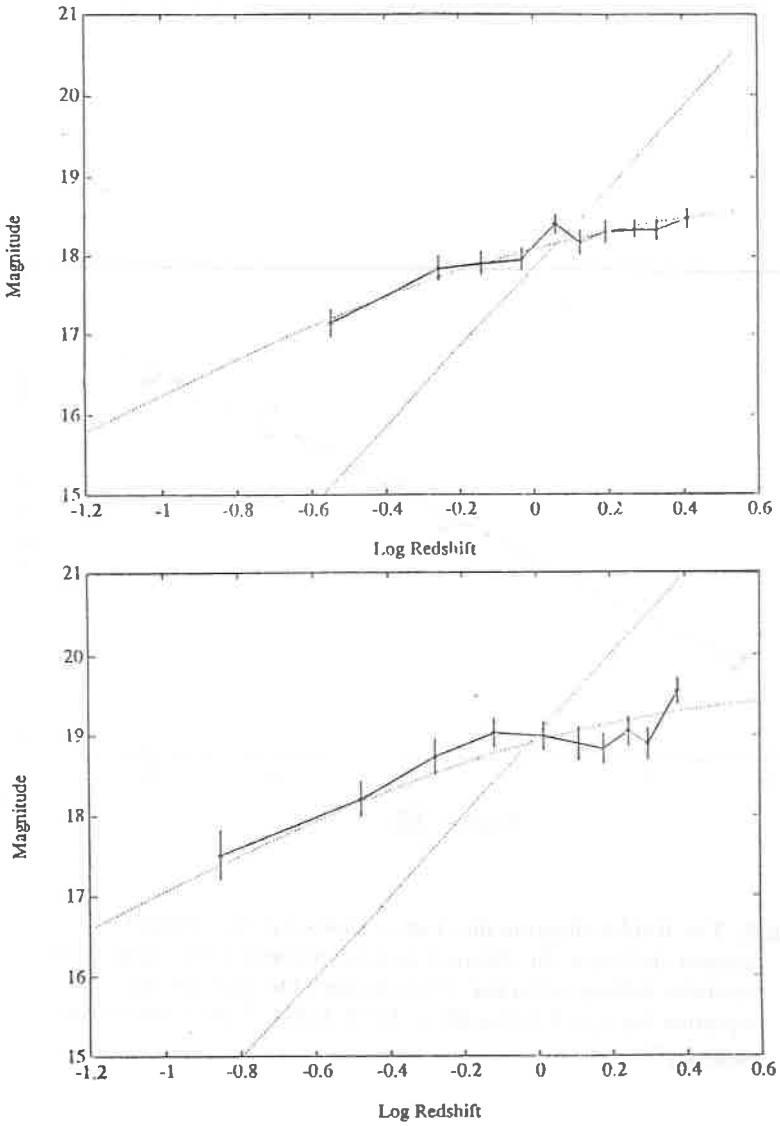

Fig 4. The redshift-apparent magnitude relation for two samples of quasi-stellar objects, about 500 radio-selected QSOs, (upper figure) and about 400 optically selected QSOs (lower figure). They are taken from Segal[31], who has used the catalogues of Hewitt and Burbidge[106,107]. The dotted straight line at approximately 45° is the Hubble relation or normal galaxies with a slope of 5. The curved dotted line is the quadratic relation obtained from the chronometric cosmology where m = 2.5log[z/(1 +z)]+ constant.

In each case the constants have been fitted from the data. The error bars are the standard deviation of the N/10 measurements in each of the 10 bins.

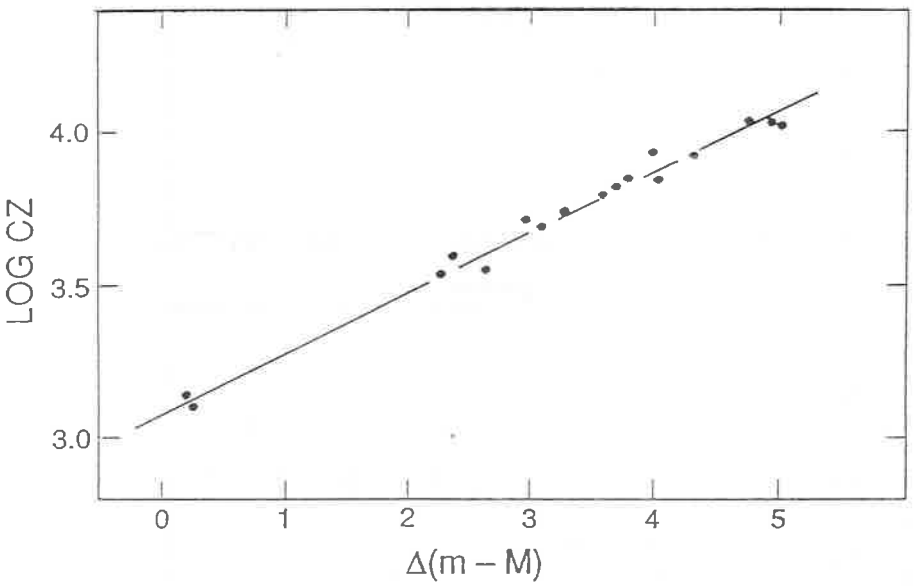

Fig 5. The Hubble diagram for clusters plotted as the redshift against the log of the distance ratio (expressed as the magnitude modulus difference) to the Virgo cluster. The line has the equation $\log \nu = 0.2\Delta(m\text{-}M) + 3.072 \pm 0.008$. This is taken from Sandage[75].

Cosmic Backgrounds

Jim and Alison Peebles

MEASURING THE CMR SPECTRUM BEFORE AND AFTER COBE

David Wilkinson

Physics Department, P.O. Box 708
Princeton University
Princeton, NJ 08544 USA

ABSTRACT

For 25 years most measurements of the spectrum of the cosmic microwave radiation have been made from the ground or from balloons, one wavelength at a time. Early this year two space-based experiments[1-2] dramatically changed the field by obtaining precise results, fitting a 2.735 K blackbody curve to 1% accuracy over a wavelength range from 1 cm to 0.5 mm. Earlier work suffered from several sources of systematic error, only recently managing to achieve 1% accuracy.[3] The keys to high accuracy direct measurements of the CMR are to (1) run the instrument close to thermal equilibrium with the incoming radiation and (2) avoid foreground sources (atmosphere, Galaxy, ground radiation...) if possible. This talk examines the shortcomings of ground-based and balloon-based CMR experiments to see how the COBE[1] and the UBC rocket[2] experiments managed to make such a huge improvement. Future ground-based work will focus on long wavelengths ($\lambda > 20$ cm) where antenna size is a problem for balloon-based and space experiments, and where Galactic emission is a more important source of error than atmospheric emission.

INTRODUCTION

The 25th anniversary of the discovery of the Cosmic Microwave Radiation (CMR) was most appropriately celebrated by two very precise measurements of the spectrum, both announced at conferences in January, 1990. In the proceedings of this conference Ed Cheng and Mark Halpern show the results of the Cosmic Background Explorer (COBE) satellite and the University of British Columbia rocket experiments. The data show superb fits to blackbody curves, as predicted by the standard Big Bang cosmological model. Limited by instrument size, the experiments measure shortward of $\lambda = 1$ cm; Galactic dust emission competes with the CMR for $\lambda < 0.5$ mm. Between these wavelengths the spectrum of the sky is Planckian to within the current accuracy of the data, about 1%.

Since Penzias and Wilson[4] discovered the CMR, there have been dozens of direct measurements of the absolute intensity of the radiation at wavelengths between 50 cm and 0.3 mm.[5-9] Why then were the COBE and the UBC rocket results such a dramatic improvement over years of work from the ground and from balloons? The next three sections of this paper answer this question and show how the early work illuminated the systematic errors arising in the instruments and from foreground sources. Understanding those errors was essential in the design of COBE's Far Infrared Spectrometer (FIRAS) and the UBC rocket package. That basic understanding was developed by 1975. It has taken 15 years to develop the technology, build and test the instruments, and achieve successful space flight. In the fifth section I will discuss briefly measurements at long wavelenghths, $\lambda > 20$ cm. Distortions of the Rayleigh-Jeans part of the CMR spectrum can arise from inverse Compton scattering (Sunyaev-Zeldovich effect) and from bremsstrahlung radiation by early warm plasma.[10-11] The unknown thermal history of the Universe is being probed. Subtracting the Galactic synchrotron emission, rising as $T \propto \lambda^{2.8}$, provides the main challenge for long wavelength measurements.

GROUND-BASED MEASUREMENTS

Spectral measurements of the CMR separate chronologically into two groups, before and after 1975. (There was a hiatus of spectrum experiments from 1970 to 1980 when many experimenters were working on anisotropy.) Comparing the results from the two groups indicates that the ground-based measurements were accurate and systematic effects were properly evaluated. Averaging the early results[8] gives $T_{CMR} = 2.72 \pm 0.08$ K ($\chi^2 = 7.0$ for 13 degrees of freedom); the second group[5] gives $T_{CMR} = 2.66 \pm 0.04$ K ($\chi^2 = 5.1/7$). So, the temperature obtained by ground-based experiments was stable over time, and accuracy improved. The work in the second group was due to a U.S./Italian collaboration working at White Mountain, California; accuracy of the early bunch was dominated by Princeton results obtained from the same site in 1967.[6] Both averaged results agree within errors with the best new temperature measurement, 2.735 $\pm$0.017 K.[2]

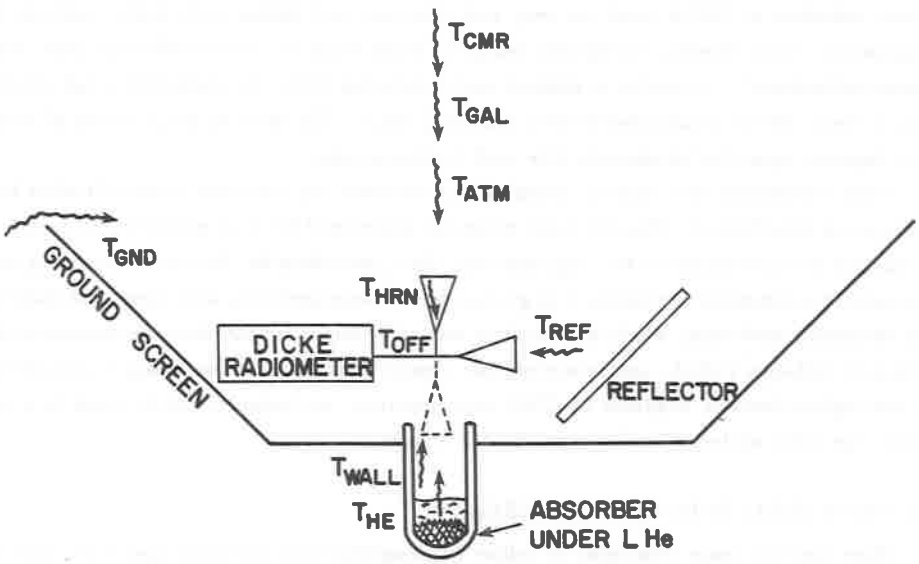

Fig. 1. Sources of extraneous signal for typical ground-based experiment. The vertical antenna measures the sky or the cold load. The reflector can be moved to change zenith angle and measure the atmospheric emission.

TABLE 1.

Contributions to three ground-based measurements of the CMR temperature, showing signal and error contributions.

	$\lambda = 49$ cm (ref. 12)	$\lambda = 6.3$ cm (ref. 13)	$\lambda = 3.3$ mm (ref. 14)
Sky (antenna T)	13.6±0.4	3.76±0.01	14.82±0.02
Cold Load	5.7±0.2	3.68±0.01	2.09±0.04
Galaxy	6.7±0.7	0.04±0.03	—
Atmosphere	2.0±0.1	1.00±0.06	13.63±0.09
Horn or Refl.	0.4±0.2	—	0.18±0.05
Ground	0.8±0.4	0.02±0.01	0±0.02
CMR (physical T)	3.7±1.2 K	2.70±0.07 K	2.60±0.09 K

Figure 1 illustrates the main sources of error in ground-based experiments. At long wavelengths ($\lambda > 20$ cm) Galactic emission competes with the CMR signal; atmospheric emission is a problem at all wavelengths, but generally gets worse at short wavelengths; ground radiation at 300 K must be very well shielded; and signal from warm instrument components – horn antenna, waveguide, reflector, warm walls of the cold reference load, and internal reflections[3] – must be evaluated and subtracted from the measured total power. Each of these effects contributes error in the final result. The relative contribution of each effect depends upon the wavelength, site, and technique used.

Table 1 illustrates this point by breaking out the error contributions from each effect for three typical experiments. The dominant errors are underlined for each measurement. Galactic emission is unavoidable at very long (and very short) wavelengths. Errors in measuring the atmospheric component are intrinsic in ground-based measurements, and they arise mainly from variability with time, which is difficult to reduce by improvements in instrumentation or technique; balloons, rockets, and spacecraft are clearly indicated. As the means to get above the atmosphere became available to CMR experimenters, we began to think about how to address the other systematic effects sketched in Figure 1.

THE NEAR-IDEAL SPECTRUM EXPERIMENT

There are two main principles to follow in designing high accuracy spectrum experiments: 1) avoid competing external radiation sources – Galaxy, atmosphere, and ground – 2) minimize the effects of instrument imperfections by cooling (the front end, at least) to the temperature of the CMR radiation. The basic ideas are sketched in Figure 2. Galactic emission is minimized by choosing a wavelengthrange between 3 cm and 0.3 mm; fortunately most of the CMR energy is in the Galactic window. Atmospheric emission is avoided by getting into space or to balloon altitudes which have clear atmospheric windows between absorption lines. Balloon altitudes suffice for wavelengths between strong oxygen and ozone lines. Ground radiation can be reduced to a few mK by using low-sidelobe antennas and well-designed ground screens.

The advantage of operating the reference absorber and the radiometer at T_{CMR} is illustrated by the simplified radiation transfer equation

$$T_{DET} = T_{CMR}(1 - \alpha) + T_o\alpha \ , \ (\alpha << 1) \ , \tag{1}$$

where α is the absorption coefficient of the walls of the horn and waveguide leading to the detector. T_o is the temperature of the walls, T_{DET} is the temperature of the radiation at the detector. Notice that if $T_o = T_{CMR}$, the absorption and radiation terms cancel and $T_{DET} = T_{CMR}$. Similarly, the effect of a small reflection from the reference absorber is compensated by reduced emission if the temperature of the radiation coming out of the horn equals the absorber temperature. Having the instrument in approximate thermal equilibrium with the incoming radiation greatly reduces the systematic effects and errors due to instrument imperfections.

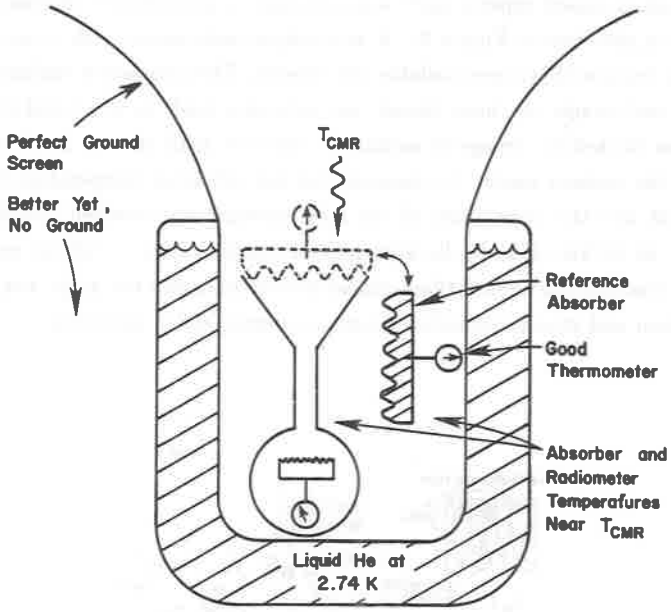

Fig. 2. The near-ideal CMR spectrum experiment. Balloon experiments have approximated the ideal; COBE/FIRAS and the UBC rocket experiments have nearly achieved it.

BALLOON-BASED MEASUREMENTS

Early in the 1970's groups at Berkeley[15], M.I.T.[16] and Queen Mary College[17] began flying cryogenic bolometers in balloons, attempting to measure the CMR flux at wavelengths near and shortward of the predicted blackbody peak, $\lambda < 3$ mm. Balloons were used to avoid strong atmospheric emission at short wavelengths (see Table 1). Bolometers were used because heterodyne radiometers were very insensitive at mm wavelengths; furthermore, since liquid He was needed to cool the reference load, it could be used to cool the detector and spectrometer as well. Michelson interferometers and bandpass filters were used to select wavelength. These were difficult experiments, and success came slowly as illustrated by the series of experiments that followed at Berkeley.[18] Each new experiment improved, in part, by finding and correcting systematic errors in the preceding experiments. Meanwhile, John Mather was applying what he learned in the first Berkeley experiment to design the FIRAS instrument aboard COBE which produced the definitive CMR spectrum discussed by Ed Cheng at this conference. The balloon instruments were naturally close to thermal equilibrium because they were cooled to reduce emission. However, Bernstein[18] has recently found that a spectral distortion seen by Woody and Richards was likely due to emission from a warm apodizing flare at the top of the cooled horn antenna – a vivid example of the advantages of instrument and radiation in thermal equilibrium.

Another balloon-based experiment[3] was designed to approximate thermal equilibrium. The apparatus is sketched in Figure 3. A heterodyne radiometer with room temperature mixers was used because they were available and reliable. The correlation radiometer* allowed a passive front-end (magic tee, horn throat, and reference load) to be cooled to 2.7 K while mixer noise was blocked by cryogenic isolators. The cold load (shown in place) faces cold radiation from the isolator loads. To measure the sky radiation temperature the cold load was moved aside and the upper part of the horn antenna was lowered to couple with its throat section. At 26 km altitude the atmospheric emission at $\lambda = 1.2$ cm was a few mK. The apparatus was tilted to avoid balloon emission overhead, and the angle was varied to set bounds on balloon and ground radiation entering antenna/shield sidelobes.

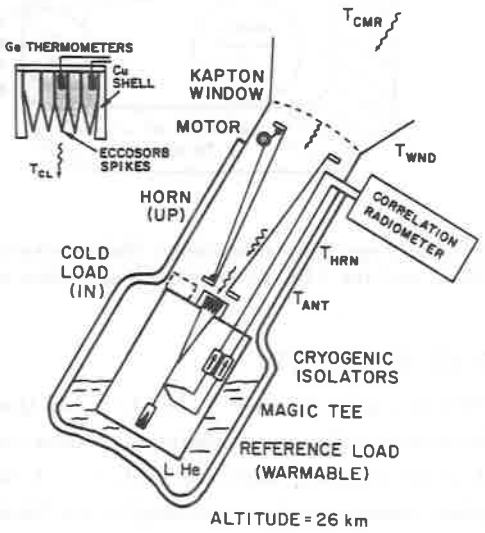

Fig. 3. A balloon experiment operated near thermal equilibrium. A blowup of the cold load is shown; in flight its temperature varied around 2.7 K and was measured to ± 5 mK accuracy. Radiometer noise per observation was ± 3 mK.

Unlike COBE or the UBC rocket package, this instrument was still in air, so a transition needed to be made from cryogenic temperature to the ambient air temperature, about - 50° C. The top of the horn antenna was relatively warm, and horn emission added 50 mK ± 12 mK to the sky signal. Also, we chose to leave a window in place to keep air away from the cold surfaces; it added 35 mK ± 12 mK to the radiometer signal. These two effects, due to

* This idea was worked out with R. Weiss over Mexican food and XX in Palo Alto after a tedious committee meeting of some sort.

our two out-of-equilibrium components accounted for most of the final error of ± 25 mK. Accurate balloon-based measurements of this sort are possible at wavelengths from 10 cm to 1 cm – a range not yet covered by space experiments. At longer wavelengths the antenna and the cold load would become ungainly, and at $\lambda > 20$ cm Galactic emission becomes the main problem anyway.

PROSPECTS FOR LONG WAVELENGTH MEASUREMENTS

At wavelengths longer than 21 cm the pioneering work of Howell and Shakeshaft[12] still stands out. Using (very large) scaled horn antennas they measured the absolute sky temperature at wavelengths of 49 cm and 74 cm; the Galactic contributions alone were 6.7 K and 20.6 K, respectively. Since the two beams were the same size, they assumed that the Galactic component scaled like $\lambda^{2.8}$ and used their two sky temperatures to calculate the Galactic signal and the CMR temperature, assumed to be the same at both wavelengths. They obtained $T_{CMR} = 3.7 \pm 1.2$ K. To look for a distortion in the CMR spectrum using this method, a third frequency is needed. An attractive feature of this method is that Galactic maps made with large telescopes are not used, except to estimate the spectral index. The zero levels of these maps are known to be uncertain and to vary with declination due to the ground radiation pickup inherent to dish antennas.

Sironi and his collaborators have started a program to measure the CMR spectrum at long wavelengths. With a large unshielded antenna in the Alpe Gera, Italy, they obtained $T_{CMR} = 3.0 \pm 1.2$ K at $\lambda = 50$ cm.[19] At this conference Sironi reports a new measurement from the Antartica giving a preliminary result of $T_{CMR} = 3.0 \pm 0.9$ K at $\lambda = 36$ cm.

At Princeton we have begun a series of measurements using scaled antennas from $\lambda = 21$ cm to $\lambda = 50$ cm.[20] Galactic emission will be evaluated using λ dependence over small and large ranges. Atmospheric emission will be measured by varying zenith angle. Wall emission is minimized by operating the radiometer front-end and the cold load in thermal equilibrium with incoming radiation, in this case CMR + Galaxy + atmosphere. Observations will be carried out at the Green Bank Observatory in West Virginia to minimize interference.

CONCLUSION

Measurements of the CMR spectrum over the past 25 years taught us two things: 1) the spectrum is essentially blackbody (with some possible distortions) and 2) how to make better measurements. The basic lessons still apply to accurate measurements needed at $\lambda > 1$ cm. Balloon-based measurements can achieve better than 1% accuracy at $\lambda < 10$ cm. At longer wavelengths, ground-based measurements make more sense, but better techniques are needed to measure the Galactic and atmospheric emissions and to reduce wall emission.

With the spectacular success of COBE/FIRAS and the UBC rocket experiment, the search for distortions at $\lambda > 1$ cm has intensified. Considerable progress can be made by applying what we already know.

Work on the CMR at Princeton is supported by the National Science Founation and the National Aeronautics and Space Administration. I thank Suzanne Staggs for reading and commenting on this manuscript.

REFERENCES

1) Mather, J., et al. 1990, *Ap. J. Lett.*, **354**, L37. Cheng, E., these proceedings.
2) Gush, H. P., Halpern, M., and Wishnow, E. 1990, *Phys. Rev. Lett*, **65**, 537. Halpern, M. these proceedings.
3) Johnson, D. G. and Wilkinson, D. 1987, *Ap. J. Lett.*, **313**, L1.
4) Wilson, R. W., these proceedings.
5) Smoot, G., et al. 1988, *Ap. J.*, **331**, 653 and papers cited in Table 1.
6) Wilkinson, D. 1967, *Phys. Rev. Lett.*, **19**, 1195. Stokes, R., et al. 1967, *Phys. Rev. Lett.*, **19**, 1199. Boynton, P., et al. 1968, *Phys. Rev. Lett.*, **21**, 462.
7) Weiss, R. 1980, *Rev. Astr. Astrophy.*, **18**, 489.
8) Peebles, P. J. E. 1971, *Physical Cosmology* (Princeton: Princeton University Press), p. 134.
9) Wilkinson, D., Proceedings of "Particle Astrophysics" Conference, E. Norman, ed. (World-wide Publ. 1990).
10) Sunyaev, R. A. and Zel'dovich, Ya. B. 1970, *Ap. Space Sci.*, **7**, 20.
11) Danese, L. and De Zotti, G. 1977, *Riv. Nuovo Cimento*, **7**, 277.
12) Howell, T. F. and Shakeshaft, J. R. 1967, *Nature*, **216**, 753.
13) Mandolesi, N., et al. 1986, *Ap. J.*, **310**, 561.
14) Bersanelli, M., et al. 1989, *Ap. J.*, **339**, 632.
15) Mather, J. C. 1974, Ph.D. Thesis, Berkeley.
16) Muehlner, D. and Weiss 1973, *Phys. Rev. Lett.*, **30**, 757.
17) Robson, E. I., et al. 1974, *Nature*, **251**, 591.
18) Woody, D. P. and Richards, P. L. 1981, *Ap. J.*, **248**, 18. Peterson, J. B., Richards, P. L., and Timusk, T. 1987, *Phys. Rev. Lett.*, **55**, 332. Bernstein, G. M., Fisher, M. L., Richards, P. L., Peterson, J. B., and Timusk, T. 1990, *Ap. J.*, **362**, 107.
19) Sironi, G., et al. 1990, *Ap. J.*, **357**, 301.
20) Staggs, S. and Wilkinson, D., "After the First Three Minutes" Conference Proceedings, C. Bennett, ed., College Park, MD.

FIRST RESULTS OF THE COBE SATELLITE MEASUREMENT OF THE ANISOTROPY OF THE COSMIC MICROWAVE BACKGROUND RADIATION

G. F. Smoot[1], C. L. Bennett[2], A. Kogut[3], J. Aymon[1], C. Backus[4], G. De Amici[1], K. G. Galuk[4], P. D. Jackson[4], P. Keegstra[4], L. A. Rokke[4], L. Tenorio[1], S. Torres[4], S. Gulkis[5], M. G. Hauser[2], M. Janssen[5], J. C. Mather[2], R. Weiss[6], D. T. Wilkinson[7], E. L.Wright[8], N. W. Boggess[2], E. S. Cheng[2], T. Kelsall[2], P. Lubin[9], S. T. Meyer[6], S. H. Moseley[2], T. L. Murdock[10], R. A. Shafer[2], and R. F. Silverberg[2]

[1]Lawrence Berkeley Laboratory and Space Sciences Laboratory, University of California, Berkeley, [2]Laboratory for Astronomy and Solar Physics, NASA, Goddard Space Flight Center, [3]National Research Council, NASA/GSFC, [4]ST Systems Inc., [5]NASA Jet Propulsion Laboratory, Pasadena, [6]Massachusetts Institute of Technology, [7]Princeton University, [8]University of California, Los Angeles, [9]University of California, Santa Barbara, [10]General Research Corporation

ABSTRACT

We review the concept and operation of the Differential Microwave Radiometers (DMR) instrument aboard NASA's Cosmic Background Explorer (COBE) satellite. The sky is found to be remarkably uniform in the millimeter to centimeter wavelength range. There is the previously known first order dipole anisotropy at the level of one part in a thousand and no evidence in the entire sky for signal other than galactic emission at a level of one part in ten thousand. At this level of sensitivity systematic errors are a critical concern. We discuss the ongoing experiment with emphasis on the software identification and subtraction of potential systematic effects. We present preliminary results obtained from the first six months of DMR data and discuss implications for cosmology.

INTRODUCTION

The cosmic microwave background (CMB) is the most accessible relic from the era over which the universe has evolved from a relatively structureless plasma to the highly-ordered state observed today. In standard models of cosmology, CMB photons have travelled unhindered from the surface of last scattering in the early universe to the present era; as such, the CMB maps the large scale structure of space-time in the early universe. Despite a quarter-century of effort, no intrinsic anisotropy in the CMB has been detected.

The Differential Microwave Radiometers (DMR) instrument aboard NASA's Cosmic Background Explorer (COBE)* satellite is intended to provide precise maps of the microwave sky on large angular scales, limited only by instrument sensitivity and integration time. It consists of six differential microwave radiometers, two independent radiometers at each of three frequencies: 31.5, 53, and 90 GHz (wavelengths 9.5, 5.7, and 3.3 mm). These frequencies encompass a window in which the CMB dominates foreground galactic emission by at least a factor of roughly 1000. The multiple frequencies allow subtraction of galactic emission using its spectral signature, yielding maps of the CMB and thus the distribution of matter and energy in the early universe. Each radiometer measures the difference in microwave power between two regions of the sky separated by 60°. The combined motions of spacecraft spin (75 s period), orbit (103 minute period), and orbital precession (~1 degree per day) allow each sky position to be compared to all others through a massively redundant set of all possible difference measurements spaced 60° apart.

---

* The National Aeronautics and Space Administration/Goddard Space Flight Center is responsible for the design, development, and operation of the Cosmic Background Explorer. GSFC is also responsible for the software development through to the final processing of the space data. The COBE program is supported by the Astrophysics division of NASA's Office of Space Science and Applications.

A software analysis system receives data telemetered from the satellite, determines the instrument calibration, and inverts the difference measurements to map the microwave sky in each channel. Although the experiment has been designed to minimize or avoid sources of systematic uncertainty, both the instrument and the software can potentially introduce systematic effects correlated with antenna pointing, which would create or mask features in the final sky maps. In the following sections we discuss the ability of the DMR to distinguish systematic artifacts from cosmological signals, present preliminary results from the first six months of operation, and discuss some implications of these results for cosmology.

INSTRUMENT DESCRIPTION AND OPERATION

Each radiometer consists of a superheterodyne receiver switched at 100 Hz between two identical corrugated horn antennas. The antennas, designed for low sidelobes and compact size, have a main lobe well described by a Gaussian profile with 7° FWHM and are pointed 60° apart, 30° to either side of the spacecraft spin axis /1/. The two channels at 31.5 GHz share a single antenna pair with an orthomode transducer splitting the input into opposite circular polarizations. A single local oscillator provides a common reference signal to independent mixer-preamp assemblies for the two channels at each frequency. The signals in each channel undergo further amplification, detection, synchronous demodulation, and 0.5 s integration before being digitized and stored in an on-board recorder. Both channels share a common enclosure and thermal regulation system. The 53 and 90 GHz radiometers are similar but have two antenna pairs at each frequency, each with identical linear polarization response. A detailed description of the DMR instrument may be found in Smoot *et al.* /2/.

Small imbalances between the two arms of each radiometer generate an instrumental baseline even when the two antennas receive identical amounts of power from the sky. Changes in the radiometer (e.g., amplifier temperature or local oscillator frequency drifts) can modulate this instrumental signature. In addition, the on-board digitization stores the output voltage as a 12-bit positive integer, mapping ±4 K instrument signal to the range [0,4095] and in effect adding a constant of 2048 digital units (du) to the instrument baseline. As an example consider the differential signal from the 53B channel for a six-month period following launch. It showed a rapid rise immediately after launch reflects the expected cooling of components to orbital conditions. The baseline then stabilized in the orbital environment and remains constant thereafter within 6 mK over six months. As the spacecraft rotates, the antennas interchange position on the sky every 38 seconds. This interchange enables ust to distinguish celestial anisotropies, which change sign upon instrument rotation, from instrument imbalances, which do not. The switching at spin, orbital, and longer periods provides a powerful tool to separate sky signals from instrumental effects.

Solid-state noise sources provide in-flight calibration by injecting broad-band microwave power into the front end of each radiometer at regular intervals (every two hours). All radiometers are calibrated simultaneously. There are two noise sources for each frequency; each noise source is coupled to both channels. One noise source injects broad-band microwave power into the positive arm and the other to the negative arm. Fired sequentially, they provide an approximate square-wave reference pulse (Figure 1). Details of pulse shape are unimportant provided the pulses are repeatable and receive identical analysis during ground tests and in orbit.

Laboratory tests prior to launch determined the power emitted by each noise source by comparing the noise source signal to the signal produced by covering the antenna apertures with targets of known, dissimilar temperatures (approximately 300 K and 77 K). A series of such tests at different noise diode temperatures established the thermal dependence of the noise source power; the effect is generally negligible. The noise sources provide a transfer standard of ground tests to flight conditions provided the noise sources remain stable in orbit. By comparing a single noise source observed in both channels to both noise sources observed in a single channel, changes in radiometer calibration can be distinguished from changes in noise source performance.

Figure 3 shows the noise source square-wave amplitudes and corresponding derived calibration factor for the 53B channel for six months following launch. The noise source square-wave amplitude is the product of the microwave power and the radiometer calibration; the rapid drift immediately after launch reflects the expected large temperature changes as components stabilized to flight conditions.

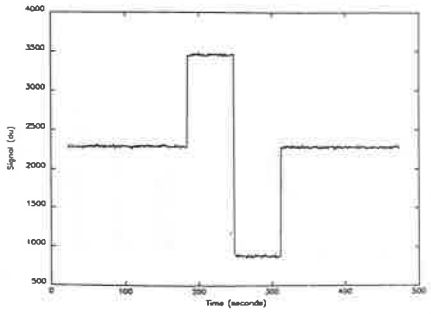

Figure 1. Uncalibrated differential temperature from the 53B radiometer during a noise source calibration sequence.

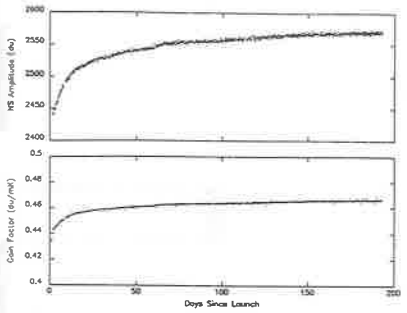

Figure 3. Noise source signal amplitude and derived calibration factor for the 53B radiometer for six months following launch.

Figure 4. Uncalibrated differential temperature from the 53B radiometer The spacecraft spin allows the two antennas alternately to view the Moon, while the orbital motion sweeps the antenna beam pattern over the Moon.

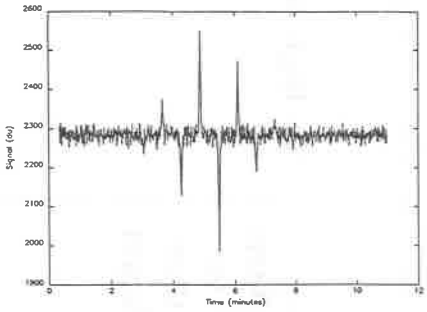

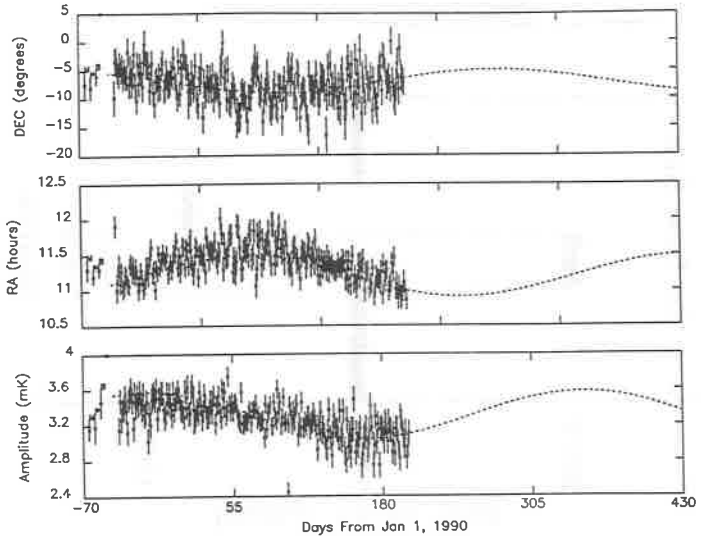

Figure 5. Amplitude and direction of the dipole anisotropy observed by the 53B radiometer each day for six months following launch. Systematic effects and galactic emission have not been removed from the data prior to fitting a dipole anisotropy.

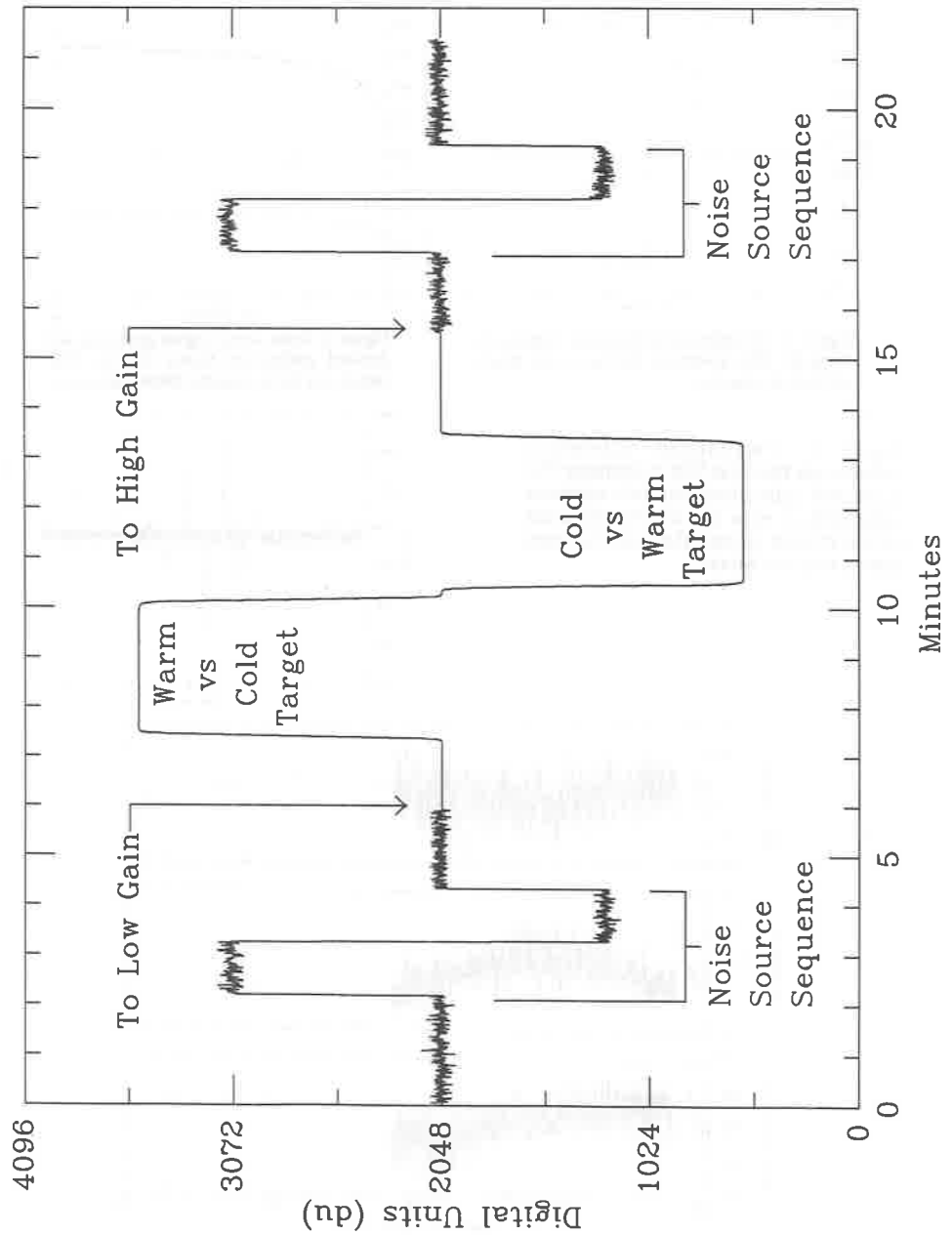

Figure 2. Noise source signal amplitude and absolute warm/cold target calibration signal for the 53B radiometer from calibration in ground cold vacuum test chamber.

Several celestial sources provide an independent determination of the calibration factor. The DMR observes the Moon for a fraction of an orbit two weeks of every month. Figure 4 shows the output of the 53B channel during a ten-minute observation of the Moon. The lunar signal is the product of the antenna beam pattern, radiometer calibration, and lunar microwave emission. Given knowledge of the antenna pointing, beam pattern, and a model of lunar emission, the calibration factor can be deduced. This method is limited primarily by knowledge of the lunar emission, but serves as a useful check on the absolute calibration of the DMR instrument. The Moon also serves as a precise check on any changes in noise source performance. The lunar signal at constant phase provides a stable external source to which the relative internal noise source performance may be referred.

The Earth's motion about the solar system barycenter provides a second independent determination of the calibration factor. The ~30 km s^{-1} motion produces a Doppler-shift dipole of known magnitude (~0.3 mK) and direction. Figure 5 shows the effect through the first six months of data. The modulation in amplitude and direction is apparent, but at low signal to noise. Given sufficient observing time (approximately one year), this method may produce the most accurate determination of the absolute calibration of the DMR instrument. The DMR calibration will be discussed more fully in a forthcoming paper /3/.

COBE was launched on November 18, 1989 into a 900-km circular, near-polar orbit (inclination 99°). The Earth's gravitational quadrupole moment precesses the orbit to follow the terminator, allowing the instruments to point away from the Earth and perpendicular to the Sun to avoid both solar and terrestrial radiation. Throughout most of the year, the satellite orbit provides an exceptionally stable environment. During the two months surrounding summer solstice, the satellite is unable to shield from the Earth and Sun simultaneously, and the Earth limb becomes visible over the shielding surrounding the instrument aperture plane as the satellite passes over the North Pole. During the same period, the satellite enters the Earth's shadow as the orbit crosses over the South Pole. The resultant eclipse modulates both the spacecraft temperatures (removing the heat input from the Sun) and bus voltages (running on batteries while solar panels are inoperative).

DATA REDUCTION AND ANALYSIS

Description of Data Processing

Data from the COBE satellite are digitized and stored in an on-board tape recorder before being telemetered daily to a ground station. A pre-processor strips the DMR data from the telemetry stream and writes a raw data archive. A second processor merges the raw DMR data with spacecraft attitude and orbit information and checks the quality of the data, flagging data known or suspected to be unusable. Data of questionable telemetry quality are flagged, as are data without accompanying attitude information or spurious data written with the instrument science telemetry disabled. This accounts for less than 1% of the data. The processor flags spikes and transients in the data, discarding all points that lie more than five times the RMS scatter from the daily mean (< 0.1% of the data). There are no known celestial sources other than the Moon that would exceed this limit. Finally, the processor flags the data for the presence in the main beam of various celestial sources (e.g., the Moon) which could contaminate the data. The results presented below discard all data with the Moon closer than 25° to an antenna. The merged, flagged data are then written to a second time-ordered archive.

A calibration program uses the estimated noise source emitted power and the in-flight square-wave calibration signal to determine the radiometer calibration factor. The noise sources provide calibration pulses every two hours; the calibration program interpolates smoothly between calibrations and writes the result to the time-ordered archive. The mean baseline, smoothed over a 4-hour period, is also written to archive. To preserve data integrity and allow for future refinements in baseline and calibration estimation, the time-ordered archive carries the baseline and calibration factor separately and does not explicitly correct and overwrite the raw data. A sky map program then subtracts the baseline, calibrates each datum, and corrects the differential signal to the solar system barycenter. The results presented below contain no other corrections. A sparse matrix algorithm varies the temperatures of 6144 map pixels independently to provide a least-squares fit to the data. The pixel size is approximately 3°, smaller than the 7° DMR beam; consequently, there is some correlation

between neighboring pixels for sources in the sky. Further details of the data processing algorithms may be found in Torres *et al.* /4/.

Limits on Potential Systematics

The sky maps produced by the sparse matrix algorithm may in principle contain contamination from local sources or artifacts from the data reduction process itself. Effects which are systematically correlated with antenna pointing or orbital period will appear preferentially in certain pixels and will not average down as the instrument accumulates more data. The data reduction process must distinguish cosmological signals from a variety of potential systematic effects. These can be categorized into several broad classes.

The most obvious source of non-cosmological signals is the presence in the sky of foreground microwave sources. These include thermal emission from the COBE spacecraft itself, from the Earth, Moon, and Sun, and from other celestial objects. Non-thermal radio-frequency interference (RFI) must also be considered, both from ground stations and from geosynchronous satellites. Although the DMR instrument is largely shielded from such sources, their residual or intermittent effect must be considered. A second class of potential systematics is the effect of the changing orbital environment on the instrument. Various instrument components have slightly different performance with changes in temperature, voltage, and local magnetic field, each of which can be modulated by the COBE orbit. Longer-term drifts can also affect the data. Finally, the data reduction process itself may introduce or mask features in the data. The DMR data are differential; the sparse matrix algorithm is subject to concerns of both coverage (closure) and solution stability. Other features of the data reduction process, particularly the calibration and baseline subtraction, are also a source of potential artifacts. All potential sources of systematic error must be identified and their effects measured or limited before maps with reliable uncertainties can be produced.

A variety of techniques exist to identify potential systematics and place limits on their effects. For the case of known celestial sources or geosynchronous RFI, the mapping program can produce a sky map in appropriate object-centered coordinates. The contribution of the source at a given distance from beam center can be read directly from the maps to the noise limit. Spike detection and direct inspection of the data during satellite telemetry transmission limit the effects of asynchronous or intermittent RFI. Limits to the effect of diffracted terrestrial radiation can be obtained by subtracting sky maps produced near summer solstice (with the Earth limb above the shielding) from maps of similar sky coverage and integration time, obtained when the Earth is below the shield. The degree to which the subtracted maps differ from Gaussian noise provides an estimate of the effect of the differential terrestrial signal. Based on this analysis, the combined limit for local foreground contribution to the six-month maps is $\Delta T < 0.15$ mK (95% confidence level).

Systematics associated with environmental effects (e.g., instrument magnetic, thermal, and voltage susceptibilities) typically are modulated at orbital or longer periods. Although these susceptibilities have been measured prior to launch, we desire a direct comparison of the effect in orbit with that measured on the ground. The sparse matrix mapping program has the capability for simultaneous least-squares fitting to both the pixels and specified models for systematics. Over a six month period, the orbital inclination and precession combine to decouple orbit-related effects from large-scale structure on the sky. Magnetic effects appear in the maps primarily as power in low-order spherical harmonics. A least-squares fit to six months of data yields a limit to magnetic artifacts of $\Delta T < 0.17$ mK.

A least-squares analysis is ideal for magnetic susceptibility as the spacecraft sweeps through the Earth's known field each orbit. It is of only limited use for thermal or voltage susceptibilities, since the normal orbital variation in these signals is below the digitization limit of the temperature and voltage sensors. For these effects, the sharp increase in variation during seasonal eclipses over the South Pole provide a useful upper limit and a potential means of estimating the effects. The baseline shows no obvious evidence of additional power at the orbital period during the eclipse season. We conclude that orbital thermal and voltage variations during eclipses perturb the output by $\Delta T < 0.12$ mK during seasonal eclipses, and are < 0.01 mK during the rest of the year when stability improves a factor of ten or more.

The extent to which the data reduction process itself may introduce artifacts in the sky maps is not readily susceptible to analytic solution. Examples include the stability of the sparse matrix solution in the presence of noise and signals that do not sum to zero over a closed pixel path (e.g., drifts). Instead, we use Monte Carlo simulations to test the solution stability and its ability to correctly identify various initial random patterns on the sky. We conclude that the sparse matrix algorithm is robust and capable of recovering the input sky map with uncertainties consistent with the Gaussian instrument noise per pixel.

A further concern is the interaction of baseline and gain estimation on different time scales than downstream processing. We currently estimate the gain and baseline daily, while processing many days at a time through the sparse matrix routine. Signals systematically correlated with pointing and orbit may be able to propagate through the software if the effects are present daily but at too low a signal-to-noise ratio to be removed in the baseline or gain estimation. The effects may not average to zero as additional data accumulated and could eventually produce artifacts in the sky maps. To estimate the propagation of such effects, we run the entire software system using simulated data containing known signals at low S/N, and compare the resultant maps to maps produced with inputs identical but for the signal under investigation.

Table 1 summarizes current limits to potential systematics. The results in many cases are limited by sky coverage, signal to noise, and available analysis software. We anticipate increasingly tighter limits to potential systematics as coverage, integration time, and software improve.

TABLE 1 95% C.L. Upper Limits to Potential Systematic Effects

Foreground Emission	Peak Magnitude	Magnitude in Maps
COBE shield and dewar	<0.04 mK	<0.002 mK
Earth	<0.3 mK	<0.07
Moon (>25 degrees)	<0.04 mK	<0.02
Sun	<0.03 mK	<0.02
Planets	<0.26 mK	<0.26 a
Galaxy	<0.3 mK	<0.13 b
Extragalactic	<0.02 mK	<0.01
Orbit Environment	**Peak Magnitude**	**Magnitude in Maps**
Magnetic	<0.3 mK/G	<0.17
Thermal	<20 mK/K	<0.01
Voltage	<20 mK/V	<0.01
Cross-talk	<2 mK	<0.0001
Software Artifacts	**Peak Magnitude**	**Magnitude in Maps**
Solution Stability	$<10^{-6}$	<0.0001
Baseline Residuals	<2 mK	<0.03
Calibration Residuals	<2 %	<0.06
Absolute Calibration	<5 %	<0.17 c
Antenna Pointing	<1°	<0.03
Total Systematics		<0.24 mK

a Effect limited to one pixel
b Excluding data within 10° of galactic plane
c Dipole term only

RESULTS

Figure 7 shows preliminary maps of the microwave sky for each of the six DMR channels. The independent maps at each frequency enable celestial signals to be distinguished from noise or spurious features: a celestial source will appear at identical amplitude in both maps. The three frequencies allow separation of cosmological signals from local (galactic) foregrounds based on spectral signatures. The maps have been corrected to solar-system barycenter and do not include data taken with an antenna closer than 25° to the Moon; no other systematic corrections have been made. All six maps clearly show the dipole anisotropy and galactic emission. The dipole appears at similar amplitudes in all maps while galactic emission decreases sharply at higher frequencies, in accord with the expected spectral behavior.

An observer moving with velocity $\beta = v/c$ relative to an isotropic radiation field of temperature T_0 observes a Doppler-shifted temperature

$$T = T_0 \frac{(1 - \beta^2)^{1/2}}{1 - \beta\cos(\theta)} = T_0 [\, 1 + \beta\cos(\theta) + \frac{1}{2}\beta^2 \cos(2\theta) + O(\beta^3) \,] \qquad (1)$$

The first term is the monopole CMB temperature without a Doppler shift. The second term, proportional to β, is a dipole distribution, varying as the cosine of the angle between the velocity and the direction of observation. The term proportional to β^2 is a quadrupole, varying with cosine of twice the angle with amplitude reduced by 1/2 β from the dipole amplitude. The DMR maps clearly show a dipole distribution consistent with a Doppler-shifted thermal spectrum, implying a velocity for the solar system barycenter of β=0.00123 ± 0.00003 (68% CL), or v = 370±10 km s^{-1} toward (l,b) = (264°±2,49°±2°), where we assume a value T_0=2.735 K. The solar system velocity with respect to the local standard of rest is estimated at 20 km s^{-1} toward (57°,23°), while galactic rotation moves the the local standard of rest at 220 km s^{-1} toward (90°,0°) /5,6/. The DMR results thus imply a peculiar velocity for the Galaxy of v_g = 550 ± 10 km s^{-1} in the direction (266° ± 2°, 30° ± 2°). This is in rough agreement with independent determinations of the velocity of the local group, v_{lg} = 507 ± 10 km s^{-1} toward (264 °± 2°, 31° ± 2°) /7/.

Figure 8 shows the DMR maps with this dipole removed from the data. The only large-scale feature remaining is galactic emission, confined to the plane of the galaxy. This emission is present at roughly the level expected before flight and is consistent with emission from electrons (synchrotron and HII) and dust within the galaxy. The ratio of the dipole anisotropy (the largest cosmological feature in the maps) to the Galactic foreground reaches maximum in the frequency range 60-90 GHz. There is no evidence of any other emission features.

We have made a series of spherical harmonic fits to the data, excluding data within several ranges of galactic latitude. The only large-scale anisotropy detected to date is the dipole. Quadrupole and higher-order terms are limited to amplitude $\Delta T/T < 10^{-4}$. Similarly, a search for Gaussian or non-Gaussian fluctuations on the sky showed no features to limit $\Delta T/T < 10^{-4}$. The results are insensitive to the precise cut in galactic latitude and are consistent with the expected Gaussian instrument noise. The reported uncertainties are 95% confidence level unless otherwise stated, and include the effects of systematics as listed in Table 1.

DISCUSSION

The DMR limits to CMB anisotropies provide significant new limits to the dynamics and physical processes in the early universe. The dipole anisotropy provides a precise measure of the Earth's peculiar velocity with respect to the co-moving frame. Limits to higher-order anisotropies limit global shear and vorticity in the early universe. If the universe were rotating (in violation of Mach's Principle), the resultant metric causes null geodesics to spiral; in a flat universe the resultant anisotropy is dominated by a quadrupole term /8,9/. The limit $\Delta T/T < 10^{-4}$ for quadrupole and higher spherical harmonics limits the rotation rate of universe to $\Omega < 3 \times 10^{-24}$ s^{-1}, or less than one ten-thousandth of a turn in the last ten billion years.

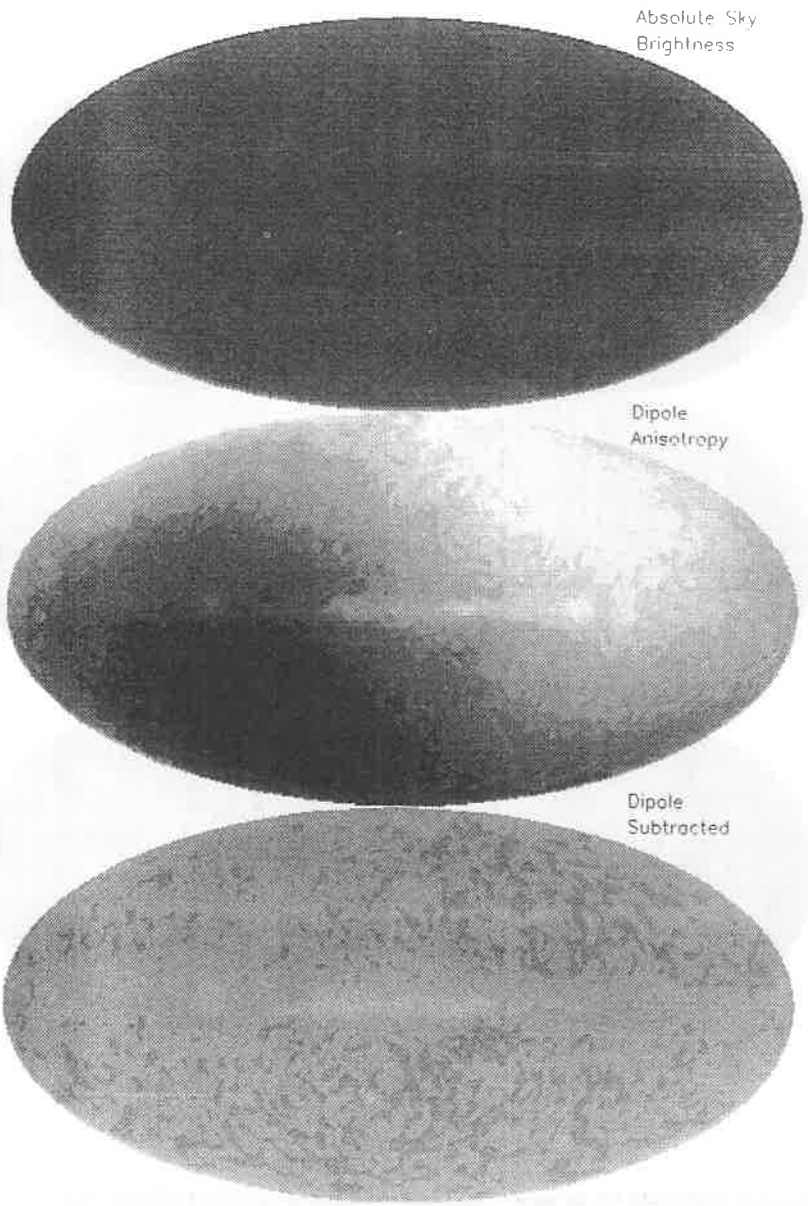

Figure 6 *COBE* DMR full sky maps of the temperature of the sky at 53 GHz (6mm wavelength). The maps are in galactic coordinates and have been corrected to solar system barycenter.

6.A Absolute Sky Brightness on a scale from 0 to 3.6 K

6.B Relative sky brightness with mean removed and scale to about -4 to +4 mK. The dipole anisotropy (0.1%) and galactic plane are clearly visible.

6C. Relative sky brightness with monpole and dipole removed. The galactic plane is only significant visible signal. The other structure evident is consistent with instrument observing noise.

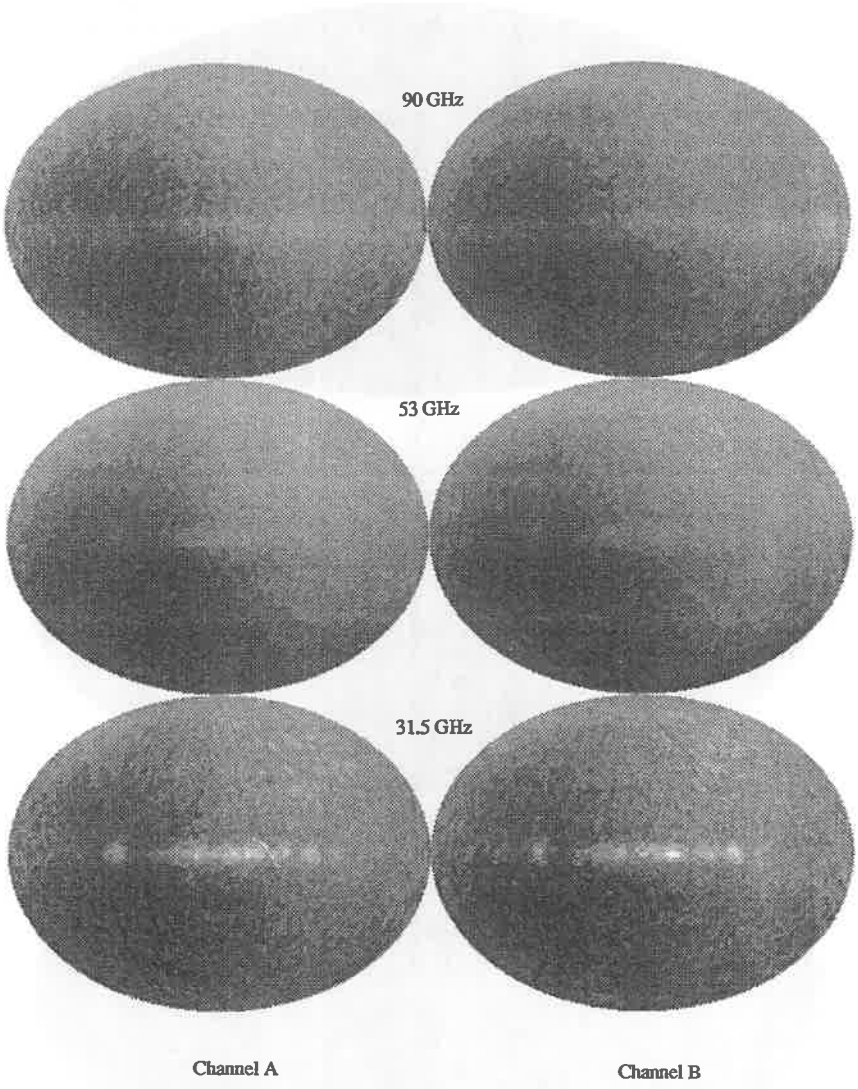

Figure 7. COBE DMR full sky maps of the relative temperature of the sky at frequencies 31.5, 53.0, and 90.0 GHz. The maps are in galactic coordinates and have been corrected to solar system barycenter. The maps show variations in received power and are insensitive to the mean temperature of about 2.735 K.

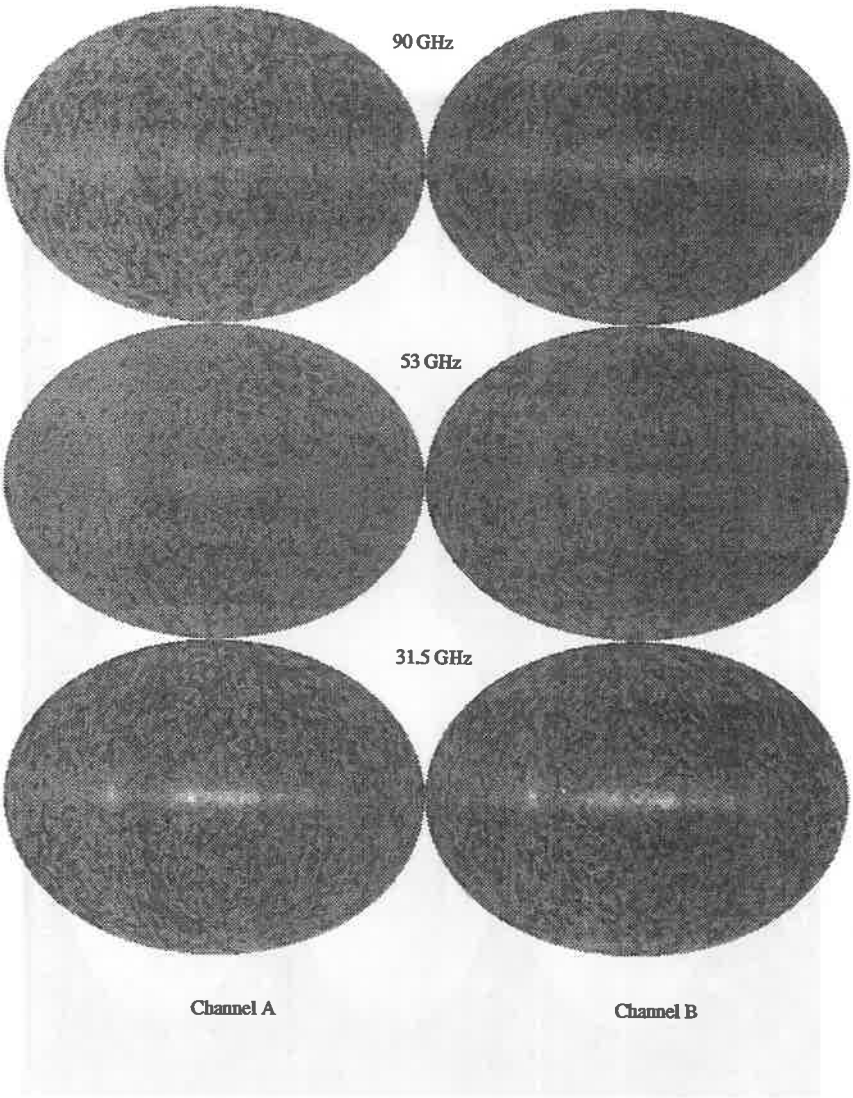

Figure 8. COBE DMR full sky maps at frequencies 31.5, 53.0, and 90.0 GHz. A dipole anisotropy corresponding to a motion of 370 km/s through a 2.735 K blackbody has been subtracted from the maps shown in Figure 7.

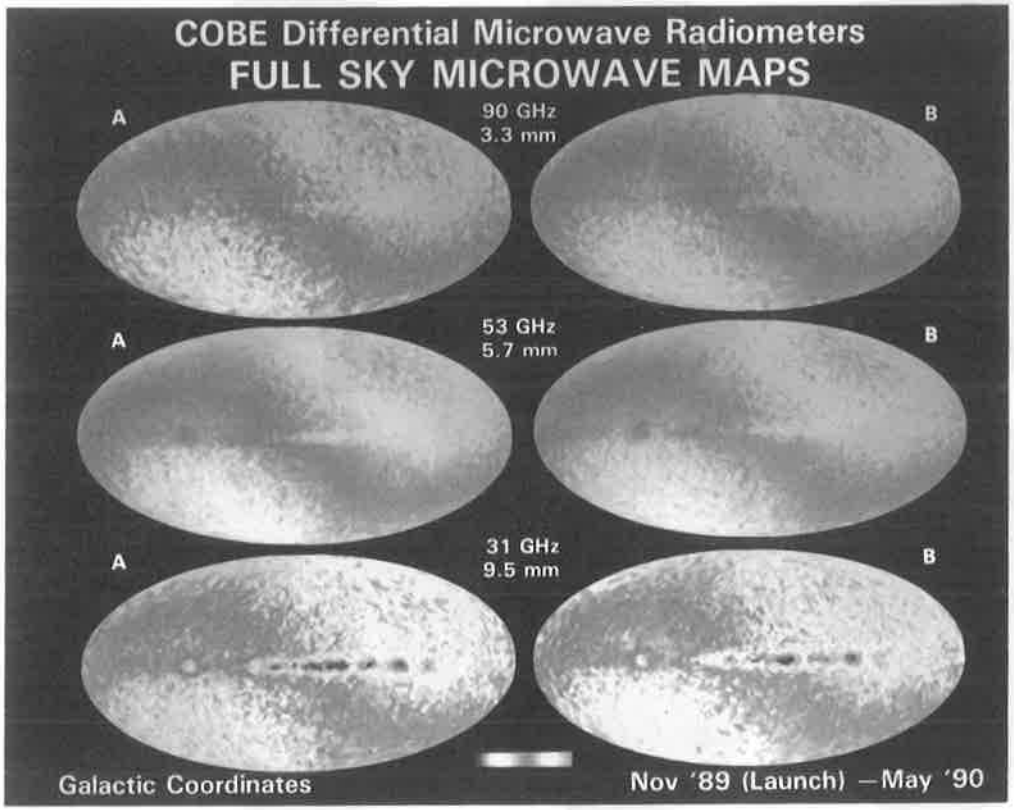

Figure 7. COBE DMR full sky maps of the relative temperature of the sky at frequencies 31.5, 53.0, and 90.0 GHz. The maps are in galactic coordinates and have been corrected to solar system barycenter. The maps show variations in received power and are insensitive to the mean temperature of about 2.735 K.

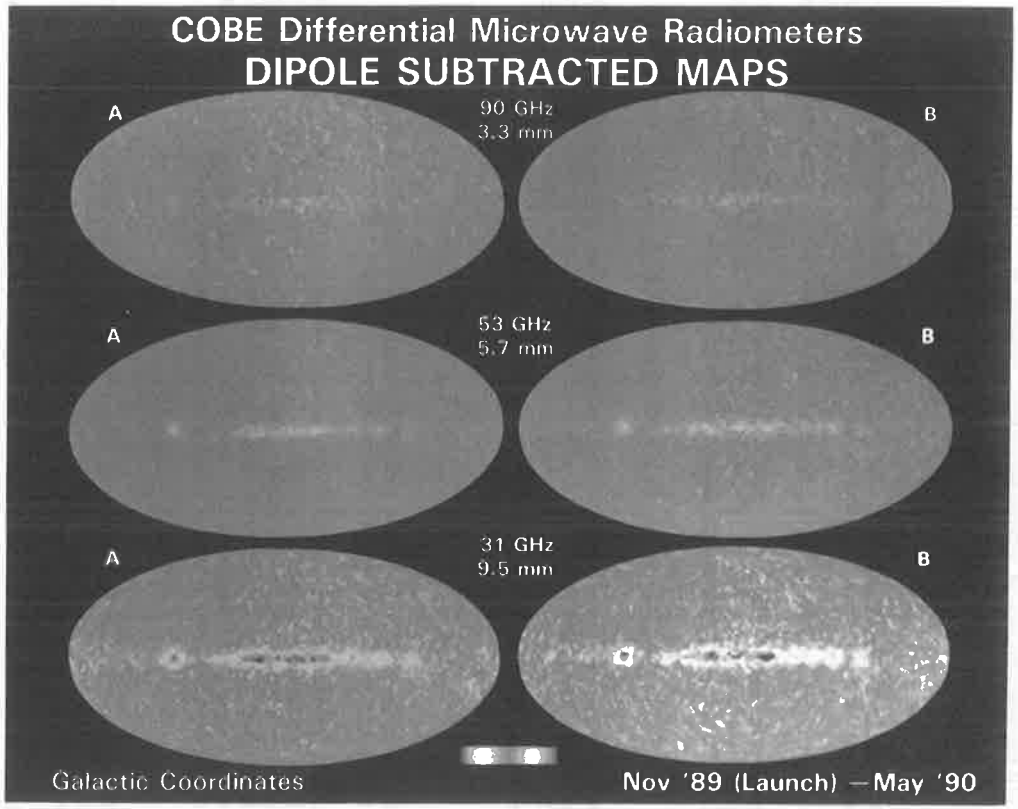

Figure 8. COBE DMR full sky maps at frequencies 31.5, 53.0, and 90.0 GHz. A dipole anisotropy corresponding to a motion of 370 km/s through a 2.735 K blackbody has been subtracted from the maps shown in Figure 7.

If the expansion of the universe were not uniform, the expansion anisotropy would lead to a temperature anisotropy in the CMB of similar magnitude. The large-scale isotropy of the DMR results indicate that the Hubble expansion is uniform to one part in 10^4. This provides additional evidence for hot big bang models of cosmology, and indicates that the currently observed expansion of the universe can be traced back at least to the radiation-dominated era.

Inhomogeneities in the density in the early universe also lead to temperature anisotropies in the CMB as the CMB photons climb out of varying gravitational potential wells /10,11/

$$\Delta T/T \sim \frac{1}{2} \frac{\delta \rho}{\rho} \left(\frac{H_0 L}{c}\right)^2 \qquad (2)$$

The DMR results imply that the universe at the surface of last scattering was isotropic and homogeneous to the 10^{-4} level. The results have implications for structures beyond the present Hubble radius: on large scales the universe is isotropic and homogeneous. The large scale geometry of the universe is thus well-described by a Robertson-Walker metric with only local perturbations.

One such potential local perturbation is gravitational radiation. Long-wavelength gravitational waves propagating though this region of the universe distort the metric and produce a quadrupole distortion in the CMB. For a single plane wave the resultant CMB anisotropy is

$$\Delta T/T \sim \frac{1}{2} (A_r - A_e) (1 - \cos(\theta)) \cos(2\phi) \qquad (3)$$

where A_r and A_e are the proper strains at the emitter and receiver, respectively /12/. The DMR is sensitive primarily to gravitational waves with scale sizes > 7° at the surface of last scattering, or ~200 Mpc today. The limits $\Delta T/T < 10^{-4}$ for quadrupole and higher spherical harmonics limit the energy density of single plane waves or a chaotic superposition to

$$\Omega_{GW} < 4 \times 10^{-3} \left(\frac{\lambda_{GW}}{10 \text{ Mpc}}\right)^{-2} h^{-2} \qquad (4)$$

where Ω_{GW} is the energy density of the radiation relative to the critical density, λ_{GW} is the wavelength at the current epoch, and h is the Hubble constant in units 100 km s^{-1} Mpc^{-1}.

Cosmic strings provide another mechanism for local perturbations in the metric. They are nearly one-dimensional topological defects predicted by many particle physics gauge theories and are characterized by a large mass per unit length, μ /13/. The large mass and relativistic velocity produce CMB anisotropies through the relativistic boost and the Sachs-Wolfe effect (gravitational lensing alone does not produce anisotropy in an isotropic background). Many authors have calculated the anisotropy produced by various configurations of cosmic strings , with typical values /14,15/

$$\Delta T/T \sim 8\pi\beta\gamma \frac{G\mu}{c^2} \qquad (5)$$

The DMR experiment limits the existence of large-scale cosmic strings to $G\mu/c^2 < 10^{-4}$. There is no evidence for higher-order topological defects such as domain walls. The large scale geometry of the universe appears to be uniform and without defects.

The observed isotropy of the universe on large angular scales presents a major problem for cosmology. At the surface of last scattering the horizon size was ~100 kpc (~2°). Regions separated by more than 2° were not in causal contact; consequently, DMR measures some 10^4 causally disconnected regions of the sky. Standard models of cosmology fail to explain why these regions are observed to have the same temperature to order unity, much less the 10^{-4} isotropy implied by the DMR observations. Inflationary scenarios provide one solution. In these models, the universe undergoes a spontaneous phase transition ~10^{-32} seconds after the Big Bang, causing a period of exponential growth in which the scale size increases by 30 to 40 orders of magnitude. The entire

observed universe would then originate from a small pre-inflationary volume in causal contact with itself, eliminating the problem. In the simplest inflationary models, the pre-inflationary matter and radiation fields are diluted to zero along with any pre-existing anisotropies. The process of inflation, however, generates scale-free anisotropies with a Harrison- Zel'dovich spectrum which result in small but detectable CMB anisotropies in the present universe /16,17/. Although current DMR limits are an order of magnitude above the predicted spectrum, we anticipate achieving sufficient sensitivity over the planned mission to test the predictions of inflationary models.

A second major problem in cosmology is the growth of structure in the universe. The largest structures in the current universe (walls and voids) are observed to have density fluctuations $\delta\rho/\rho$ of order unity on scale sizes ~50 Mpc. Structures of this size are at the horizon scale at the surface of last scattering; consequently, the primordial density fluctuations are small and most of the growth is in the linear regime. The assumption of linear growth requires peculiar velocities ~ 0.01c in order to move the matter the required 10^8 light years of co-moving distance in the ~10^{10} years estimated to have elapsed since the surface of last scattering, an order of magnitude greater than the peculiar velocity inferred from dipole anisotropy. To explain the observed structure without violating limits on CMB anisotropy, and to generate the critical density required by inflationary models, many astrophysicists have turned to cosmological models in which most of the matter in the universe (> 90%) is composed of weakly interacting massive particles (WIMPs). The dynamical properties of this "dark matter" allow it to clump faster than the baryonic matter, which later falls into the WIMP gravitational potential wells to form the structures observed today. The gravitational potential and motion of these particles produce CMB anisotropy whose amplitude depends on the angular scale size. For scale size ~ 10° most reasonable models predict $\Delta T/T \sim 1\text{—}3 \times 10^{-5}$, depending on the average density of the universe /18/. Although current observations do not provide significant limits to these models, we anticipate that the DMR will provide a stringent test of such models as it continues to accumulate data.

CONCLUSIONS

Six months after launch, the instrument is working well and continues to collect data. The results are currently limited by instrument noise and upper limits to potential sources of systematic error. The current data show the expected dipole anisotropy, consistent with a Doppler-shifted thermal spectrum. Galactic emission is present at levels close to those expected prior to launch, and is largely confined to the plane of the galaxy. There is no evidence for any other large-scale feature in the maps. The DMR results limit CMB anisotropies on all angular scales >7° to $\Delta T/T < 10^{-4}$. The results are consistent with a universe described by a Robertson-Walker metric and show no evidence of anisotropic expansion, rotation, or localized defects (strings). As sky coverage improves and the instrument noise per field of view decreases, we anticipate improved calibration, better estimates of potential systematics, and increasingly sensitive limits to potential CMB anisotropies. In principle, the DMR is capable of testing predictions of both inflationary and dark-matter cosmological models.

REFERENCES

1. Toral, M.A., *et al.*, *IEEE Transactions on Antennas and Propagation*, **37**, 171 (1989).
2. Smoot, G.F., *et al.*, *Ap. J.*, **360**, 685 (1990).
3. Bennett, C.L., *et al.*, in preparation.
4. Torres, S., *et al.*, *Data Analysis in Astronomy*, ed. Di Gesu *et al.*, Plenum Press (1990).
5. Kerr, F.J., and Lyndon-Bell, D., *MNRAS*, **221**, 1023 (1990).
6. Fich, M., Blitz, L., and Stark, A., *Ap. J.*, **342**, 272 (1989).
7. Yahil, A., Tamman, A., and Sandage, A., *Ap. J.*, **217**, 903 (1977).
8. Collins, C.B., and Hawking, S.W., *MNRAS*, **162**, 307 (1973).
9. Barrow, J.D., Juskiewicz, R., and Sonoda, D.H., *MNRAS*, **213**, 917 (1985).
10. Sachs, R.K., and Wolfe, A.M., *Ap. J.*, **147**, 73 (1967).
11. Grischuk, L.P., and Zel'dovich, Ya. B., *Sov. Astron.*, **22**, 125 (1978).
12. Burke, W.L., *Ap. J.*, **196**, 329 (1975).
13. Vilenkin, A., *Physics Reports*, **121**, 263 (1985).
14. Stebbins, A., *Ap. J.*, **327**, 584 (1988).
15. Stebbins, A., *et al.*, *Ap. J.*, **322**, 1 (1987).
16. Gorski, K., *Ap. J. Lett.* (submitted 1990).
17. Abbott, L.F., and Wise, M.B., *Ap. J. Lett.*, **282**, L47 (1984).
18. Bond, J.R. and Efstathiou, G, *Ap. J. Lett.*, **285**, L45 (1984).

George Smoot

STATUS OF THE *COBE*

Edward S. Cheng
NASA/Goddard Space Flight Center
Laboratory for Astronomy and Solar Physics
Infrared Astrophysics Branch, Code 685.0
Greenbelt, MD 20771

Bennett, C. B., Boggess, N. W., Hauser, M. G., Mather, J. C., Dwek, E., Gulkis, S., Janssen, M., Kelsall, T. K., Lubin, P. M., Meyer, S. S., Moseley, S. H., Jr., Murdock, T. L., Shafer, R. A., Silverberg, R. F., Smoot, G. F., Weiss, R., Wilkinson, D. T. and Wright, E. L.

ABSTRACT

The Cosmic Background Explorer *(COBE)*, NASA's first satellite dedicated to cosmology, was launched on November 18, 1989. With two noted exceptions, the observatory and all three instruments are operating flawlessly. Based on preliminary analyses using software designed primarily to monitor instrument performance, the data appear to be of excellent quality and the prelaunch expectations for the ultimate sensitivities of the instruments have been confirmed.

After this conference, on September 21, 1990, the cryogen was depleted, ending over 10 months of liquid Helium operations. The main focus of the project is now shifting from operations to data analysis. A detailed understanding of the systematic errors of the instruments is crucial to the ultimate usefulness of the data sets for cosmology. Several of these problems are described.

Introduction

The Cosmic Background Explorer (*COBE*) contains three instruments, the Diffuse Infrared Background Experiment *(DIRBE)*, Differential Microwave Radiometer *(DMR)* and Far InfraRed Absolute Spectrophotometer *(FIRAS)*. These instruments provide over four decades of spectral coverage (1 cm to 1μ), at moderate spatial resolution (7° for *DMR* and *FIRAS*, and 0.7° for *DIRBE*).

The goal of the mission is to achieve background limited sensitivities for studying the Cosmic Microwave Background Radiation (CMBR) spectrum and anisotropies, and the Cosmic Infrared Background (CIB) which is the postulated diffuse light from primeval objects. At the completion of its mission, *COBE* will have produced a set of all-sky maps corrected for instrumental and spacecraft effects, analyzed data products based on these maps, and tools for further analysis.

It is essential that all sources of possible data contamination from the instruments, the spacecraft and the local spacecraft environment are identified and understood before scientific interpretation and modeling. Careful instrument design, a stable high-orbit environment, and a long lifetime allowing for careful systematic checks all contribute to this effort. The ability to control and understand the systematic errors is a crucial difference between the *COBE* and previous attempts at similar studies. Several potential error sources are highlighted in the instrument sections below.

The major scientific problems facing all the *COBE* instruments is the need to remove foreground sources in order to reveal the cosmological signals. For the *DMR*, the major foreground source is galactic

synchrotron and bremsstrahlung radiation in the 31 GHz and 53 GHz channels and interstellar dust emission in the 90 GHz channel. For *FIRAS*, it is emission from interstellar dust. For *DIRBE*, interstellar dust emission, interplanetary dust emission and interplanetary dust scattering (Zodiacal light) all come into play. The spectral coverage of the *COBE* and the per pixel sensitivities for one year of observation for each of the instruments are shown in Figure 1, together with some models of the expected foreground sources of radiation.

The Spacecraft

The *COBE* spacecraft (see Figure 2) is in a 99° inclination, 885 km circular (polar) orbit with a 6 PM ascending node. With this orientation, the spin axis of the spacecraft is always pointing away from the Earth and Sun, and the orbital period is roughly 102.8 minutes. The spacecraft rotates at 0.82 revolutions per minute to modulate the *DIRBE* and *DMR* beams (the *FIRAS* beam is aligned with the spin axis and is unaffected by the rotation).

The entire instrument package is surrounded by a reflective radiation shield which successfully deployed immediately after launch. This shield prevents direct radiation from the Earth or Sun from reaching the top of the spacecraft and scattering into the instrument apertures, and also guards against RF interference from the spacecraft transmitters or terrestrial sources.

With the two exceptions noted below, the spacecraft has been operating flawlessly, providing the necessary power, communications and attitude control for the three instruments.

During the first two weeks of operation, one of the gyroscopes failed,

necessitating a reconfiguration of the attitude control system. This restored the pointing accuracy of the spacecraft, which has since been within specifications.

There is also evidence for small transient glints from the Sun reflecting off parts of the radiation shield. The source of these has yet to be unequivocally identified, but could be due to either a stray piece of thermal blanket material, or an unexpected orientation of one of the successfully deployed *DMR* horn covers. The danger of significant direct emission into the beams of any of the instruments is small, given the small solid angle of the glint and the small sidelobe and stray light sensitivity of the beams. However, this is one of the many effects which must be further evaluated to preserve the integrity of the data sets.

On September 21, 1990, the liquid Helium cryogen was depleted. The *FIRAS* instrument has been completely shut down, and the long-wavelength bands of the *DIRBE* are disabled because of the elevated cryostat temperature. The *DMR* continues to function normally since it operates outside the cryostat. The four short-wavelength bands of the *DIRBE* are also expected to operate indefinitely, as long as the cryostat stays below the predicted equilibrium temperature of approximately 70 K.

The Instruments

Only the cryogenic instruments (*DIRBE* and *FIRAS*) are discussed below. The *DMR* is covered in a separate contribution to the proceedings.

The instrument descriptions have been published elsewhere[1,2] and will not be repeated. We focus on several interesting effects which can cause potential systematic errors in the data.

DIRBE

All but two of the *DIRBE* detectors are all operating at noise levels which are better than expectations. The two long-wavelength bands at 250μ and 150μ, which use silicon bolometer detectors, were known before launch to have slightly higher noise than predicted. The flight performance is roughly a factor of 3 and 10 less sensitivity, respectively.

Since the *DIRBE* measures absolute flux, it is necessary for the cryogenic chopper to switch the detector signals between the sky and an internal cold reference (at ≈ 2 K). Any variation or excess emission in the cold reference state could produce an offset which mimics a sky signal. Ground testing revealed that the cryogenic detector preamplifiers, which are shielded but operate internally at ≈ 80 K, may be visible to the detectors and thus become the source of a small extraneous signal. This effect was recognized and has been fully characterized in-flight.

To achieve the goal of 1% photometry, it is necessary to linearize the output of the *DIRBE* detectors. Depending on the spectral band and signal level, up to 10% corrections are required. The linearity of all the bands have been characterized by using the two independent internal reference sources in the instrument. The measurement is made by selecting predefined settings for the two sources, and observing these settings individually and then together. These corrections will be incorporated in the software under development.

The challenge in the *DIRBE* data is to remove the local astrophysical foreground to reveal any infrared emission from primeval objects. As is evident in Figure 1, this would require intensive modeling of the foregrounds which are substantially brighter than the cosmological signals.

The eventual success of this effort will, in large, rely on the large spectral coverage of the *COBE*, coupled with *DIRBE* beam being 30° from the spin axis of the spacecraft. This allows for simultaneous viewing (over an orbit) of almost half of the sky and in particular, permits sampling of the same part of the sky at a range of solar elongations (roughly 64° to 124°).

FIRAS

The major unexpected event for the *FIRAS* was the (on-orbit) discovery of the mirror transport mechanism electronics sensitivity to trapped proton flux in the South Atlantic Anomaly (SAA). This mechanism provided the linear scanning motion which produces the interferogram. The problem has been traced to proton sensitivity in the photodetector which read the cryogenic linear grating marks and which thus is an integral part of the servo feedback loop. The failure mode was disruptive, with the linear carriage being driven to its end-of-travel, dissipating excessive heat within the cryostat until an independent supervisory circuit reversed the motion. It was not possible to fix this problem directly, but turning off the mirror mechanism during SAA crossings dramatically reduced the number of incidents. The remainder of the occurrences were infrequent, and caused only minor changes in the instrument temperature. However, at the level of sensitivity we expect to achieve, the data with elevated temperatures must be either excised or corrected in the software.

The difference between the *FIRAS* and all preceding instruments used for measuring the CMBR spectrum is the existence of an on-board external calibrator. This calibrator could be commanded into the horn,

allowing for a substitution experiment where the sky emission is replaced by a synthetic blackbody. While the spectrum of the external calibrator can be shown to be a blackbody to the required precision (emissivity greater than 0.999), there is a discrepancy among the three thermometers used to measure its absolute temperature. This discrepancy is as large as 6 mK at 2.7 K and close to 1 K at 25 K. Consequently, the calibration of the high frequency ($\ll 0.5$ mm) data, which requires the warmer external calibrator temperatures in order to generate sufficient flux at high frequencies, is somewhat confused. These discrepancies have been observed directly in the flight data, as well as being inferred from modeling of the photometric calibration runs where we allowed the temperatures of the external calibrator to be free parameters. Work is under way to understand the source of these discrepancies and to minimize their effect on the calibrations.

The *FIRAS* calibration procedure is described further in the calibration poster contribution to this conference. A summary is included elsewhere in these proceedings.

The ultimate accuracy of the *FIRAS* will be limited by our knowledge of the spectrum of the external calibrator when it is being observed, instrument stability, detector linearity, and the amount of time we have devoted to the calibration. The analyses to date have provided extremely encouraging results for these limiting factors, and confirm our ultimate ability to reach an accuracy of 10^{-9} Watts/meter^2/steradian or better for each 7° field of view and 5% spectral resolution element.

Preliminary Results

The significant preliminary results from the *COBE* as of this conference

have been reported previously[2,3]. In short, the quantitative results are the spectrum of the CMBR (*FIRAS*) and the infrared spectrum of the sky at the South Ecliptic Pole (*DIRBE*). In addition, there is a striking qualitative map from the *DIRBE* which is shown in Figure 3.

The difficulty in producing these results arises mainly from the need to understand the error sources in the actual flight environment coupled with the immaturity of the software which has been designed to help in these analyses. Given this situation, the only quantitative statements which can be made are those that can be independently verified by either instrument design or by referencing to known astronomical fluxes.

For example, the *FIRAS* CMBR spectrum was produced relatively early in the mission. The reason that this was possible is that the external calibrator spectrum matched the sky spectrum extremely well. We arrived at this conclusion by observing the sky and then the external calibrator, and adjusting the external calibrator temperature until there was very little difference (in the output of the instrument) between these two cases. Changing the external calibrator temperature by a small amount after achieving this state allows for deriving a calibration for the noise level. The full accuracy of the instrument is not yet realized because of calibration uncertainties, and incomplete knowledge of the emission from the instrument itself. Understanding both these effects requires a more complete model of the instrument which takes into account data measuring the calibration at high signal-to-noise ratios, and which probes the emission of the instrument structures. The final processing software takes these effects into account and is presently being tested and completed.

The Future

With the bulk of the raw data already collected, the emphasis for the *COBE* team is shifting towards data processing and analysis. The software which was designed to produce the final data products must be completed and tested before reliable sky maps can be made. In addition, proper characterization, analysis and removal of the systematic error sources needs to be done using the flight data. The amount of work is somewhat instrument dependent, but is expected to occupy the next several years.

DMR and warm *DIRBE* operation has been approved by NASA for a second year (until at least December 1991). A third year of operation has been requested and is being considered by NASA. The operational demands are expected to be minimal during this phase, and the new data collected will not seriously affect the analysis effort for the data acquired during the first year of operation.

Acknowledgements

It is a pleasure to acknowledge the vital contributions of the many people who have made this challenging mission not only possible, but enjoyable as well.

The National Aeronautics and Space Administration/Goddard Space Flight Center (NASA/GSFC) is responsible for the design, development, and operation of the *Cosmic Background Explorer (COBE)*. GSFC is also responsible for the development of the analysis software and for the production of the mission data sets. The *COBE* program is supported by the Astrophysics Division of NASA's Office of Space Science and Applications.

References

1) Gulkis, S., Lubin, P. L., Meyer, S. S. and Silverberg, R. F. 1990. *Scientific American* **262**:1, p. 132.

2) Mather, J. C., Hauser, M. G., Bennett, C. B., Boggess, N. W., Cheng, E. S., Eplee, R. E., Freudenreich, H. T., Gulkis, S., Isaacman, R. B., Janssen, M., Kelsall, T. K., Lisse, C. M., Meyer, S. S., Moseley, S. H., Jr., Murdock, T. L., Shafer, R. A., Silverberg, R. F., Smoot, G. F., Spiesman, W. J., Toller, G. N., Weiland, J. L., Wilkinson, D. T. and Wright, E. L. March 1990. *IAU* Proceedings.

3) Mather, J. C., Cheng, E. S., Eplee, R. E., Isaacman, R. B., Meyer, S. S., Shafer, R. A., Weiss, R., Wright, E. L., Bennett, C. B., Boggess, N. W., Dwek, E., Gulkis, S., Hauser, M. G., Janssen, M., Kelsall, T. K., Lubin, P. M., Moseley, S. H., Jr., Murdock, T. L., Silverberg, R. F., Smoot, G. F. and Wilkinson, D. T. 1990. *Ap. J. Lett.* **354**:L37.

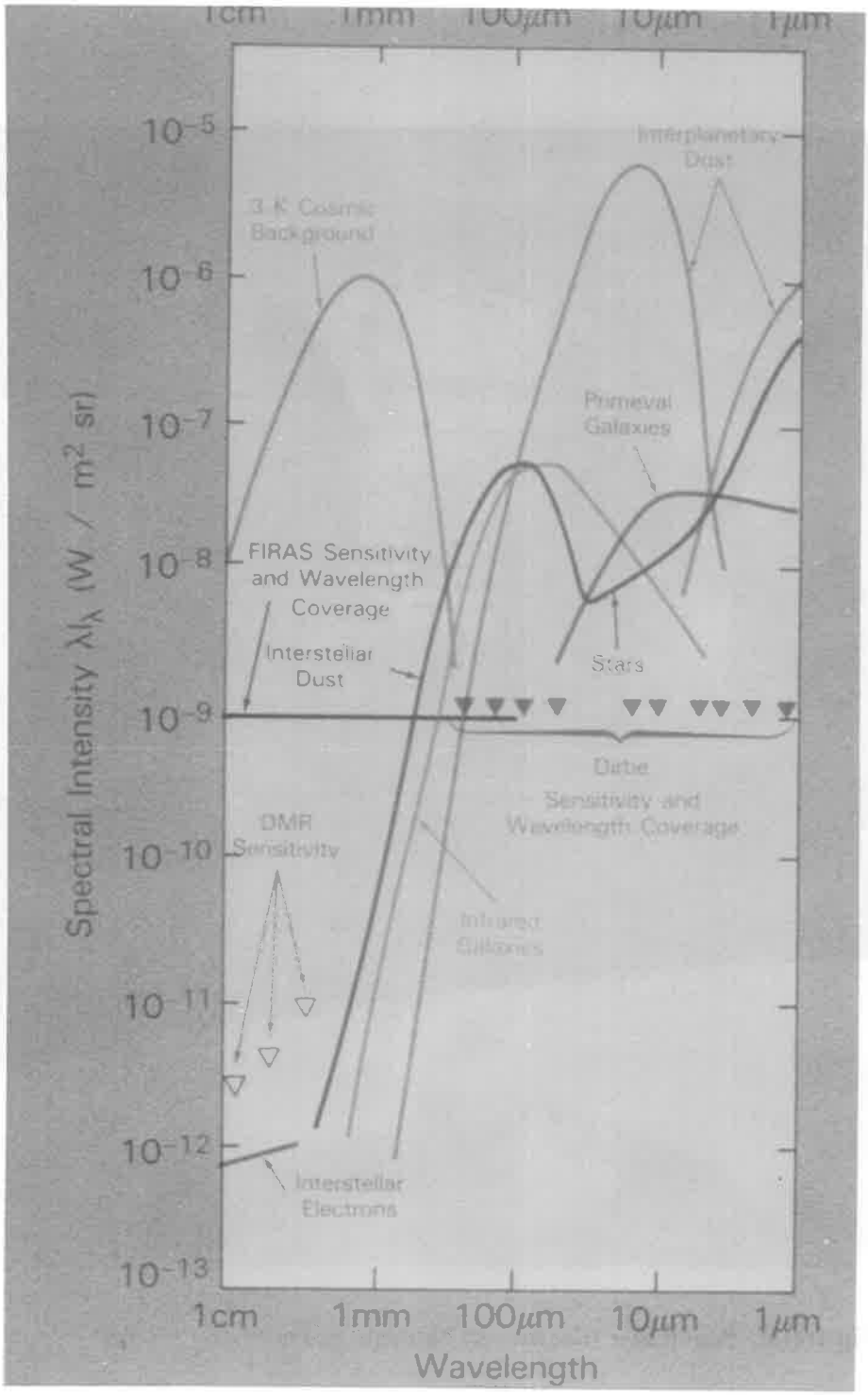

Figure 1. The sky spectrum as seen by *COBE*.

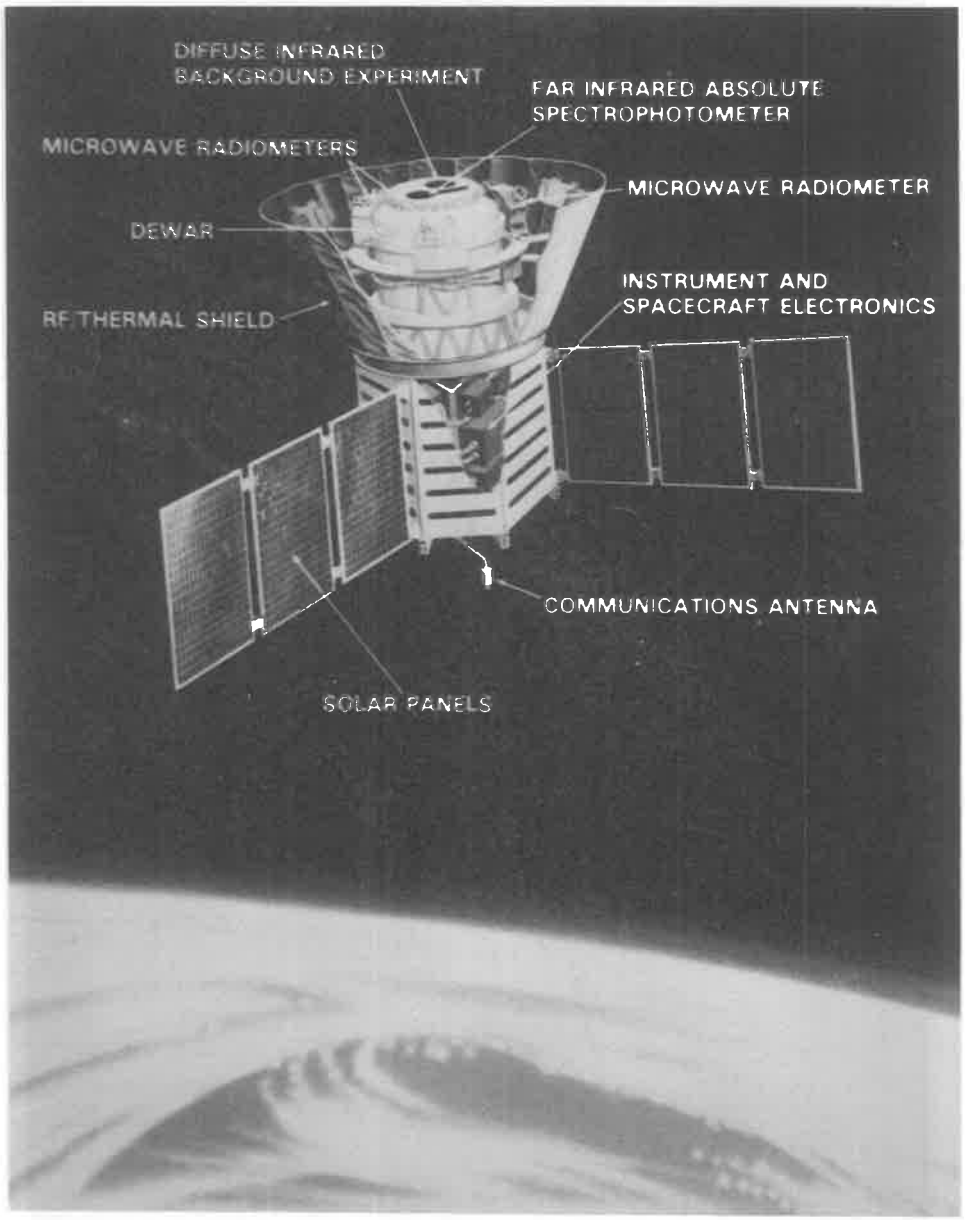

Figure 2. Schematic diagram of external parts of the *COBE*.

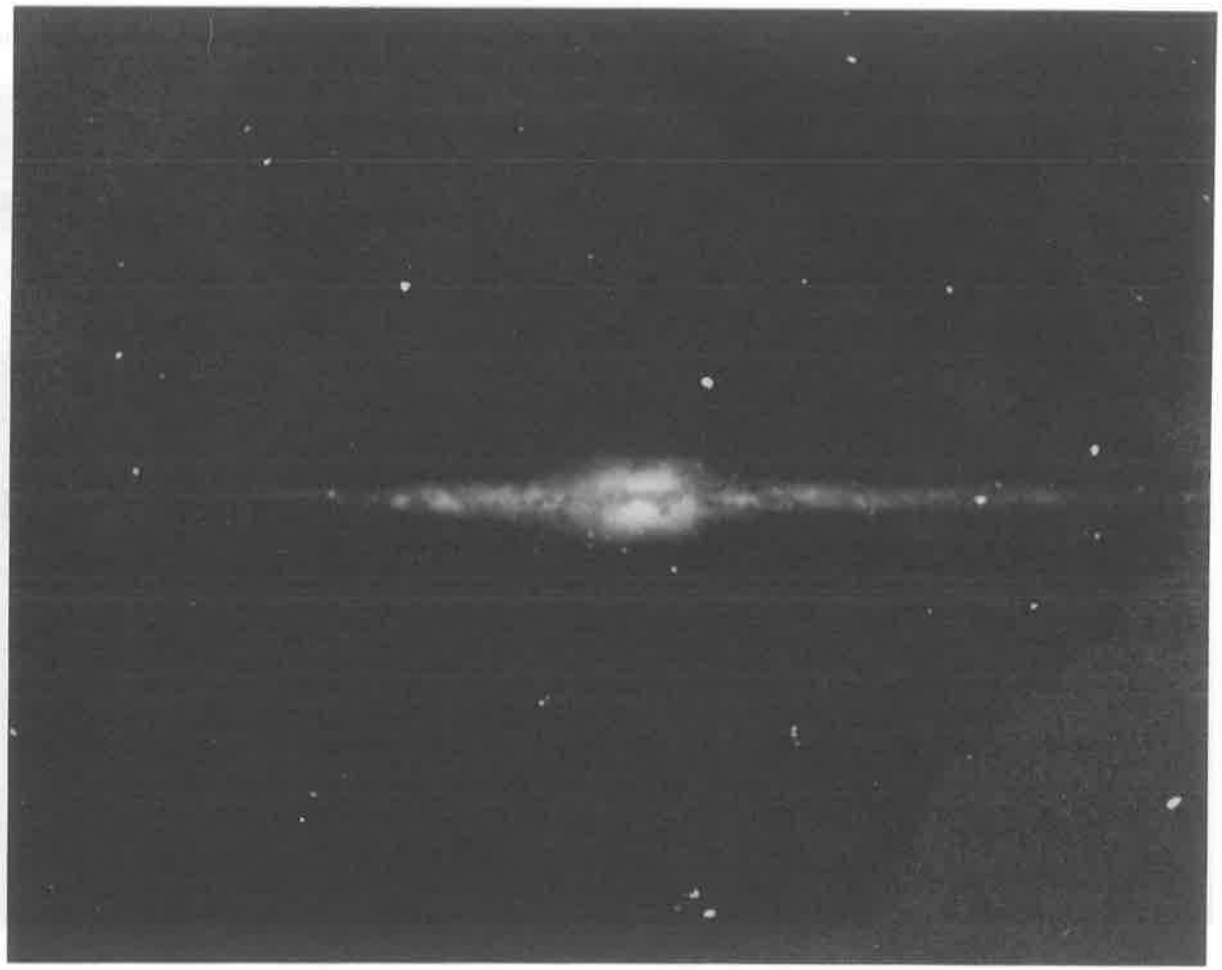

Figure 3. The galactic plane at J, K and L bands as seen by the *DIRBE* and represented by blue, green and red colors, respectively.

Alain Blanchard, Dominique Leglu and Lawrence Krauss

LARGE SCALE ANISOTROPY OF THE COSMIC MICROWAVE BACKGROUND

Nicola Vittorio ◇ *& Roberto Scaramella* ‖

◇ *Dipartimento di Fisica, Università dell'Aquila, Italy.*

‖ *Osservatorio Astronomico di Roma, Monteporzio, Italy.*

Abstract

We discuss two aspects related to the large scale CMB temperature distribution: i) the statistical distribution of various observables over the ensemble of cosmic observers; ii) the statistics of the CMB temperature fluctuations over the single observable microwave sky. The first point must be taken into account in order to properly compare theoretical predictions with the observations. The second point is important in order to optimize observational strategies and for discriminating between competing scenarios. We consider here both flat, cold dark matter models and open, pure baryonic universes.

1 Introduction

In the framework of gravitational instability theories, mainly two scenarios have been considered in the last years for describing the formation and evolution of large scale structure in the universe. These are the flat, biased cold dark matter (CDM) and an open, baryonic dark matter (BDM) models. The CDM model (*e.g.* Blumenthal *et al.* 1984) has most of its theoretical appeal in being uniquely determined in the framework of the inflationary scenario, which *a priori* predicts a flat universe, as well as the statistics (Gaussian), the spectrum (scale–invariant) and the nature (iso–entropic) of the fluctuations of the density field (see

Blau and Guth 1987 for a review). The BDM scenario (Peebles, 1987) is more phenomenological and less defined from first principle considerations. It has several parameters to be fixed *a posteriori*, *e.g.* the ionization history of the universe, the primordial spectral index, and the density parameter. Here the large scale structure forms from the gravitational amplification of initially isocurvature matter density fluctuations. So, while CDM has its own success in explaining small and intermediate scale structures and provides a self–consistent scenario from the Planck era to the present time, BDM seems to meet observational evidence for a low density parameter, for large values of the Hubble constant ($H_0 \gtrsim 80\,\mathrm{km\,s^{-1}}/Mpc$), and for coherent large scale flows (*e.g.* Gunn, 1989).

In a CDM scenario, CMB anisotropies on large angular scales are expected because of gravitational potential fluctuations on the last scattering surface (Sachs and Wolfe, 1967). As in flat universes potential fluctuations are constant in time, the amplitude of CMB anisotropies is independent of the location of the last scattering surface and, then, of the thermal history of the universe. An obvious disadvantage arises, however, in comparing theory with observations. Due to the long range nature of the gravitational interactions and to the assumed scale– invariant power spectrum, our own microwave sky does not consitute a fair sample for the large scale CMB anisotropy: temperature fluctuations in different patches of the sky are not necessarely statistically independent, and the CMB temperature autocorrelation function (acf) can remain significantly different from zero even for large angular separations. Then, an angular average over all the sky does not coincide with an ensemble average, and this may constitute a handicap for directly comparing observational upper limits to ensemble averaged theoretical predictions. In a BDM scenario there are not large scale potential fluctuations on the last scattering surface: matter density inhomogeneities are strongly damped on scales larger than the matter radiation Jeans length at decoupling. On large angular scales, unaffected by any possible smearing due to an early reionization of the intergalactic medium, one should see CMB temperature fluctuations due to the primordial entropy inhomogeneities, which have been gradually transferred in radiation energy density fluctuations, because of the constant curvature constraint. It turns out that the CMB pattern in this case has a much steeper correlation function. Then, an angular ergodicity holds to a very good approximation, *i.e.* an angular average over a single microwave sky practically coincides with an ensemble average.

In both CDM and BDM scenarios, we expect CMB temperature fluctuations to be Gaussian distributed over the ensemble: in fact, the ensemble statistics is the same both for primordial density and for CMB temperature fluctuations, because the latter are related to the former by a linear operator which does not alter the statistical properties over the ensemble. On the other hand, as we can observe CMB temperature fluctuations only on our own last scattering surface, it is important to quantify the statistics of the CMB fluctuations

on the celestial sphere, *a priori* different from the ensemble statistics if an angular ergodicity does not hold (Sazhin 1985). Knowing the statistics of the CMB temperature fluctuation on our own microwave sky is crucial, for example for optimizing observational strategies, or for discriminating among competing scenarios (Coles and Barrow 1987, Coles 1988, Gott *et al.* 1990). In fact, non Gaussian (hereafter non–G for shortness) CMB fluctuations are expected in the string (Bouchet, this volume) or texture (Turok and Spergel 1990) scenarios, and possibly also in some particular inflationary models (see Matarrese *et al.* 1990, Kofman *et al.* 1990, and references therein).

Here we want to discuss the theoretical predictions for the large scale CMB anisotropy in both CDM and BDM scenarios and the upper limits we can set on ensemble averaged observables. We want also to discuss the statistical properties of the CMB pattern of a single observable microwave sky.

2 Theoretical background

The CMB temperature fluctuation field is naturally expanded in spherical harmonics: $\Delta(\vec{x},\hat{\gamma}) = \sum_{\ell=2}^{\infty}\sum_{m=-\ell}^{m=+\ell} a_\ell^m(\vec{x})Y_\ell^m(\hat{\gamma})$. Here $\vec{x}$ is the observer position, $\hat{\gamma}$ an angular direction around $\vec{x}$, and we neglect the dipole anisotropy dominated by our present peculiar velocity relative to the comoving frame.

The large scale pattern of the CMB temperature distribution in our own sky (e.g. $\vec{x}=0$) is then uniquely determined by the set of coefficients $\{a_\ell^m(0)\}$. Another observer, in $\vec{x}=\vec{x}_1$, would possibly detect a different CMB pattern, described by another set of coefficients $\{a_\ell^m(\vec{x}_1)\}$. In the framework of the gravitational instability scenarios, each coefficient $a_\ell^m(\vec{x})$ is assumed to be a stochastic variable of the position $\vec{x}$, to obey to a Gaussian distribution function with zero mean, $\langle a_\ell^m(\vec{x})\rangle = 0$, and with a rotationally invariant variance $\langle |a_\ell^m(\vec{x})|^2\rangle \equiv \Sigma_\ell^2$, independent of the index m. Here the symbol $\langle\rangle$ indicates an ensemble average, or, equivalently, an average over all the possible observer positions. In the most general case, however, correlations are expected between different multipoles measured by close observers also when one considers ensemble averages. This spatial coherence is lost inversely with ℓ for sufficiently distant observers, i.e. when $|\vec{x}-\vec{x}'| \gg r_0/\ell$ with $r_0 = 2c/H_0$. Indeed for two generic observers, separated by $\vec{s}=\vec{x}-\vec{x}'$, one finds that $\left\langle a_\ell^m(\vec{x})a_{\ell'}^{m'}(\vec{x}')\right\rangle_V = \mathcal{D}(\ell,\ell',m,m',\vec{s})$, where $\mathcal{D}$ is a quite complicated function (Scaramella and Vittorio 1991). This expression can be greatly simplified by angular averaging over all the possible $\vec{s}$ directions. In this way we obtain $\int d\Omega_s \mathcal{D}(\ell,\ell',m,m',\vec{s}) = 4\pi\Sigma_\ell^2\delta_{\ell\ell'}\delta^{mm'}\mathcal{R}_\ell(s/r_0)$, where $\mathcal{R}_\ell(s/r_0) \propto \int_0^\infty dx\; x^{n-2}\, j_0(sx/r_0)\,[j_l(x)]^2$ and j_q is the spherical Bessel function of order q. It is easy to show that the first zero of $\mathcal{R}$ occurs at separations which decrease with increasing ℓ.

The observable acf of the CMB temperature fluctuation field is (Scaramella and Vittorio

1989, 1990):

$$C(\vec{x},\alpha,\sigma_B) = \left\langle \Delta(\vec{x},\hat{\gamma}_1)\Delta(\vec{x},\hat{\gamma}_2) \right\rangle_{sky} \tag{1a}$$

$$= \frac{1}{4\pi}\sum_{l=2}^{\infty} Q_l^2(\vec{x})\, P_l(cos\,\alpha)\, \exp\left\{ -\left[\left(\ell+\frac{1}{2}\right)\sigma_B\right]^2 \right\} \tag{1b}$$

The symbol $\langle\ \rangle_{sky}$ in Eq.(1a) indicates an angular average on the single observable sky, over all the possible line sight pairs an angle $\alpha \equiv \cos^{-1}(\hat{\gamma}_1\cdot\hat{\gamma}_2)$ away. We are *not* averaging over all the possible observer positions. For simplicity, however, we will drop henceforth the explicit dependence of the CMB observable acf and of the coefficients $\{a_\ell^m\}$ on $\vec{x}$. Then, $C(0,\sigma_B)$ defines the variance of the CMB temperature fluctuations as measured by an observer in $\vec{x}$. We model the antenna beam with a Gaussian of dispersion σ_B. Observing the sky with an antenna of finite resolution implies applying a low–pass filter, which exponentially attenuates high order harmonics. In Eq.(1b) $Q_\ell^2 = \sum_{m=-\ell}^{\ell} |a_\ell^m|^2$. The quantity Q_2 defines the magnitude of the CMB quadrupole anisotropy (the quadrupolar pattern is obviously insensitive to any antenna beam smearing on angular scales of few degrees). The observable CMB temperature acf is then uniquely determined by a set of coefficients $\{Q_\ell^2\}$, each distributed as a Chi-squared with $2\ell+1$ degrees of freedom, with expected values and variances given by (Abbott and Wise 1984, Bond and Efstathiou 1987):

$$\langle Q_\ell^2(\vec{x})\rangle = (2\ell+1)\,\Sigma_\ell^2; \qquad Var[Q_\ell^2(\vec{x})] = 2(2\ell+1)\,\Sigma_\ell^4\,.$$

Because of the mutual independence of different Q_ℓ^2's it is straightforward to obtain mean and variance for the observable acf (Bond and Efstathiou, 1987; Scaramella and Vittorio, 1990)

$$\langle C(\alpha,\sigma_B)\rangle = \frac{1}{4\pi}\sum_{l=2}^{\infty} \langle Q_l^2\rangle\, P_l(cos\,\alpha)\, \exp\left\{ -\left[\left(\ell+\frac{1}{2}\right)\sigma\right]^2 \right\} \tag{2a}$$

$$Var[C(\alpha,\sigma_B)] = \frac{1}{16\pi^2}\sum_{l=2}^{\infty} Var[Q_l^2]\, P_\ell^2(cos\,\alpha)\, \exp\left\{ -2\left[\left(\ell+\frac{1}{2}\right)\sigma\right]^2 \right\} \tag{2b}$$

We want to stress that the observable quantity is that given in Eq.(1), while theoreticians usually quote the expression in Eq.(2a).

The variance of the CMB temperature fluctuations measured by a single subtraction (ss) or double subtraction (ds) experiment, operating with an antenna beam size σ_B and a beam-switching angle α, are given by:

$$\Delta_{ss}^2(\alpha,\sigma_B) = 2[C(0,\sigma_B) - C(\alpha,\sigma_B)] \tag{3a}$$

$$\Delta_{ds}^2(\alpha,\sigma_B) = \frac{3}{2}C(0,\sigma_B) - 2C(\alpha,\sigma_B) + \frac{1}{2}C(2\alpha,\sigma_B). \tag{3b}$$

In CDM, large scale CMB anisotropy are determined by the Sachs and Wolfe (1967) effect, according to the following expression (Peebles, 1982):

$$\Delta(\vec{x},\hat{\gamma}) \;=\; -\frac{2}{r_o^2}\int_0^\infty \frac{d^3k}{8\pi^3}\,\frac{\delta_{\vec{k}}}{|\vec{k}|^2}\,\exp\left\{i\,\vec{k}\cdot[\vec{x}+r_0\hat{\gamma}]\right\}\;,$$

After a spherical harmonic expansion, it can be shown (Peebles, 1982) that for a scale–invariant power spectrum, appropriate for CDM fluctuations, $\Sigma_\ell^2 \propto [2\ell(\ell+1)]^{-1}$.

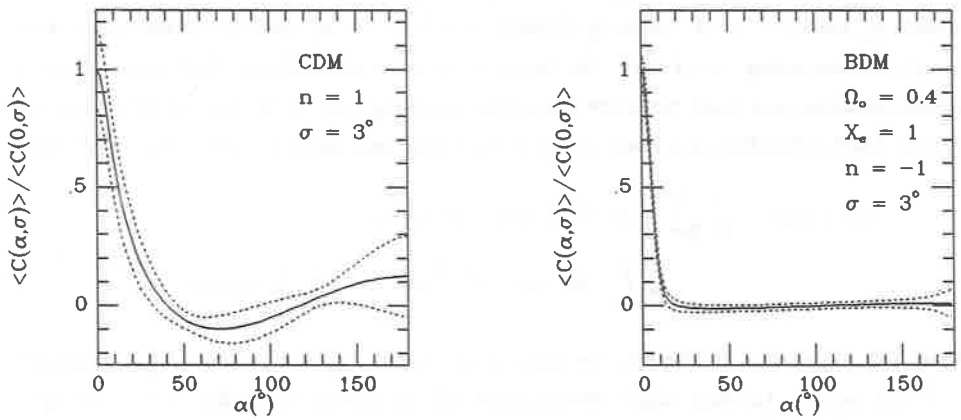

Figure 1 *Ensemble averaged acf normalized at zero lag (solid line), with the* ± 1 *dispersion band (dotted lines).*

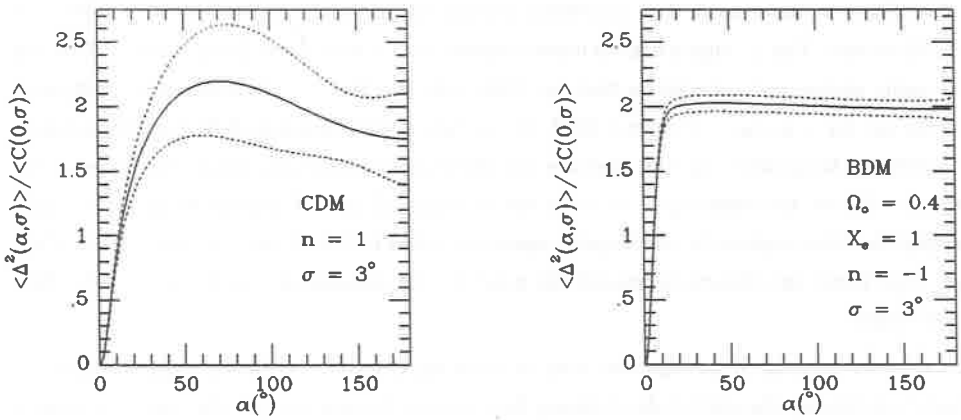

Figure 2 *Ensemble averaged* $\Delta^2_{s,s}$ *normalized to the acf at zero lag (solid line), with the* ± 1 *dispersion band (dotted lines).*

For BDM, the situation is just a bit more complicated, because in principle one should take into account the curvature of the universe when propagates the CMB radiation brightness from last scattering up to the present. The expression for the unsmoothed mean acf becomes

(Górski and Silk 1990):

$$\langle C(\alpha)\rangle = \frac{1}{16}\int d\tilde{k}\ \tilde{k}^2 P_{rad}(\tilde{k})\frac{sin(\tilde{k}y)}{\tilde{k}sinh(y)} \tag{4}$$

where $\tilde{k}$ is a wavenumber in units of the curvature radius $r_C = c/H_0\sqrt{1-\Omega_0}$, and y is the spatial distance between two points on the last scattering surface, separated by an angle α. The radiation power spectrum can be approximated in the region of interested as: $P_{rad} \sim (8/15)^2 A k^n exp(-k^2 r_{LS}^2 \sigma_J^2)$, where $\sigma_J \approx \sqrt{1.5}/k_J r_{LS}$ is the angle subtended on the last scattering surface (*i.e.* at comoving distance r_{LS} from us) by the matter–radiation Jeans length at decoupling, $\approx 2\pi/k_J$. The factor 8/15 takes into account both initial entropy inhomogeneities and small curvature fluctuations growing later in this models (Kodama and Sazaki, 1986; Efstathiou and Bond, 1987) In the small angle approximation, Eq.(4) becomes:

$$\langle C(\alpha,\sigma_B)\rangle = \frac{4}{25}\frac{A}{2\pi^2}\int k^{(n+2)}dk\ \exp\left[-k^2 r_{LS}^2\sigma_J^2\right]\times$$
$$\frac{1}{2}\int_{-1}^{+1} d\mu\ \exp\left[-k^2 r_{LS}^2\sigma_B^2(1-\mu)^2\right] J_0(k r_{LS}\alpha\sqrt{1-\mu^2})$$

From this expression and Eq.(3), one can evaluate both $\langle\Delta_{ss}^2(\alpha,\sigma_B)\rangle$ and $\langle\Delta_{ds}^2(\alpha,\sigma_B)\rangle$, for $\alpha \lesssim$ few degrees. For large angles we evaluated $\langle Q_\ell^2\rangle$ by directly expanding $\langle C(\alpha)\rangle$ in Legendre polynomials (*c.f.* Górski and Silk 1990). Then, through Eq.(2a) and Eq.(3a) we evaluate $\langle C(\alpha,\sigma_B)\rangle$ and $\langle\Delta_{ss}^2(\alpha,\sigma_B)\rangle$, respectively.

In Fig.1 we show mean and dispersion around the mean of the CMB acf for CDM and BDM models. The ± 1 sigma band is more extended for CDM than for BDM models. This can be easily understood considering that for CDM only the first ($\lesssim 15$) harmonics contributes to the acf for, *e.g.* $\sigma_B \sim 3^\circ$ as in COBE: $\langle C(\alpha,\sigma_B)\rangle$ is then dominated by few, Chi-squared distributed harmonics. On the contrary, for BDM many more harmonics contribute to the sum ($\sim$ 80 for the same $\sigma_B = 3^\circ$) and the variance of the acf around its mean becomes negligible. This implies that an angular ergodicity holds for BDM but not for CDM. In Fig.2 we show mean and dispersion around the mean for the differential (single subtracted) CMB anisotropy.

In order to predict the expected level of CMB anisotropy on different angular scales, we have to normalize the amplitude of density fluctuations. We impose that the *rms* mass density fluctuations, averaged over an 8 h^{-1}Mpc sphere, is unity. We adopt the same normalization for both CDM and BDM models, and theoretical predictions for CMB anisotropies are shown in Table 1. A biasing parameter, b, is usually introduced to reconcile the dynamical determinations of the density parameter with the flatness of the CDM models (see, Dekel and Rees, 1987, for a review). The theoretical predictions of flat CDM models have then to be reduced by a factor b^{-1}, with $b \approx 1.5$.

Table 1

CDM	Ω_0	Ω_b	n	$\langle\Delta^2_{ss}(6^o,3^o)\rangle^{1/2}$	$\langle\Delta^2_{ss}(60^o,3^o)\rangle^{1/2}$	$\langle Q^2_2\rangle^{1/2}$
	1.0	0.03	1	$6.0\cdot10^{-6}$	$1.4\cdot10^{-5}$	$1.5\cdot10^{-5}$
	1.0	0.10	1	$6.7\cdot10^{-6}$	$1.6\cdot10^{-5}$	$1.6\cdot10^{-5}$
	1.0	0.20	1	$7.9\cdot10^{-6}$	$1.8\cdot10^{-5}$	$1.9\cdot10^{-5}$
BDM	Ω_0	x_e	n	$\langle\Delta^2_{ss}(6^o,3^o)\rangle^{1/2}$	$\langle\Delta^2_{ss}(60^o,3^o)\rangle^{1/2}$	$\langle Q^2_2\rangle^{1/2}$
	0.1	1.0	0	$1.2\cdot10^{-5}$	$1.5\cdot10^{-5}$	$4.5\cdot10^{-6}$
	0.1	0.1	-1	$3.5\cdot10^{-5}$	$4.6\cdot10^{-5}$	$1.5\cdot10^{-5}$
	0.1	0.1	0	$3.8\cdot10^{-6}$	$4.8\cdot10^{-6}$	$1.4\cdot10^{-6}$
	0.4	1.0	0	$1.4\cdot10^{-5}$	$1.8\cdot10^{-5}$	$5.4\cdot10^{-6}$
	0.4	0.1	-1	$2.7\cdot10^{-5}$	$3.5\cdot10^{-5}$	$1.3\cdot10^{-5}$
	0.4	0.1	0	$4.5\cdot10^{-6}$	$5.7\cdot10^{-6}$	$1.7\cdot10^{-6}$

CMB expected anisotropies in flat CDM models, as a function of the baryon density parameter Ω_b. Density fluctuations are adiabatic, scale–invariant ($n = 1$) and normalized to the galaxy clustering on small scales (i.e. $b = 1$). These predictions have to be reduced by a factor b^{-1} if light does not traces mass. CMB anisotropies in open BDM models, either fully ionized ($x_e = 1$) or partially ionized ($x_e = 0.1$), with primordial spectral indeces $n = -1$ and $n = 0$, respectively.

3 CMB sky statistics

In this section we briefly discuss how can happen that the CMB temperature fluctuations when observed in a single microwave sky with a large antenna beam, may not be Gaussian distributed, even if the primordial matter density fluctuations constitute a random Gaussian field. This effect is due to a dominance of low order multipoles of the CMB anisotropy pattern and is then relevant for models with adiabatic fluctuations, as CDM.

The asimmetry and the peakdness (or flatness) relative to the Normal distribution is usually quantified in terms of the adimensional parameters of skewness, $\mathcal{S}$, and kurtosis, $\mathcal{K}$:

$$\mathcal{S} \equiv \frac{[C^{(3)}(\mathbf{0},\vec{x})]}{[C(0,\vec{x})]^{3/2}} \quad ; \quad \mathcal{K} \equiv \frac{[C^{(4)}(\mathbf{0},\vec{x})]}{[C(0,\vec{x})]^2} - 3 \ ,$$

Here $C^{(3)}(\mathbf{0},\vec{x})$ and $C^{(4)}(\mathbf{0},\vec{x})$ are the third and fourth central moment of the temperature fluctuations of the CMB sky observed form position $\vec{x}$, and $\mathbf{0}$ is a shorthand to denote that both $C^{(3)}$ and $C^{(4)}$ are evaluated at zero lag. A positive (negative) value of $\mathcal{S}$ implies a

deficit (excess) of very hot pixels in the sky. A positive (negative) value of $\mathcal{K}$ implies that the distribution is more (less) peaked than a Gaussian. Note that $\mathcal{S}$ and $\mathcal{K}$ are independent of any normalization of the primordial density fluctuations.

We Monte Carlo simulated 5,000 different skies with a $\sigma = 3.0^\circ$ resolution and 4584 ($3^\circ \times 3^\circ$) sky pixels.

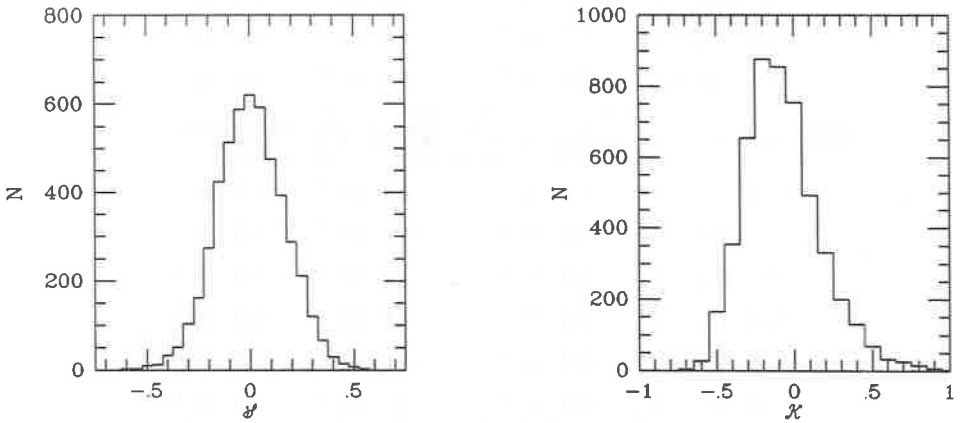

Figure 3 *Distribution function of the skewness (left panel), and kurtosis (right panel) for the scale–invariant case.*

In the scale–invariant case, appropriate for the CDM model, $\langle \mathcal{S} \rangle_V$ vanishes, while $\langle \mathcal{K} \rangle_V$ although very small, is still significantly different from zero and negative. Non vanishing values of $\mathcal{S}$ and/or $\mathcal{K}$ are quite likely for a given observer, implying a non–G CMB temperature pattern on the sky (*c.f.* Fig.3). The rms values of $\mathcal{S}$ and $\mathcal{K}$ are a not negligible 0.2 and 0.3 respectively, while 95% of the observers will measure $|\mathcal{S}| < 0.36$, and/or $|\mathcal{K}| < 0.48$. The rms values of skewness and kurtosis are much larger than the rms values obtained by sampling a real Gaussian field over the celestial sphere. In fact, we performed a Kolmogorov–Smirnov test on the CMB temperature distribution of *each* microwave sky, simulated assuming scale–invariant, Gaussian distributed (over the ensemble) density fluctuations. We evaluated the probability of accepting the null hypothesis, $\mathcal{H}_0$, that the numerically derived pdf for the sky pixel temperature fluctuation is drawn from a Normal distribution. The cumulative distribution of such probability from a sample of 5,000 cosmic observers shows that 29% (46%) of the simulations are consistent with $\mathcal{H}_0$, with probability less than 1% (5%). In other words, in $\sim$ 30% of the cases the temperature fluctuation distribution in a single CMB sky is not Gaussian at least at the 99% confidence level. So, while for a given direction (*i.e.* a given $\hat{\gamma}$) $\Delta(\vec{x}, \hat{\gamma})$ is Normally distributed over the ensemble of cosmic observers (*i.e.* different $\vec{x}$), for a given observer (*i.e.* a given $\vec{x}$) $\Delta(\vec{x}, \hat{\gamma})$ may not be Normally distributed over the ensemble of sky pixels (*i.e.* different $\hat{\gamma}$).

4 Comparison with observations

The existence of an intrinsic dispersion around the mean values of $C(\alpha, \sigma_B)$ and $\Delta_{ss}(\alpha, \sigma_B)$ requires some carefulness in comparing theory and observations. From Fig.1, it is clear that, at least for CDM, it is not enough to compare ensemble averaged quantities with the observational upper limits. A single CMB sky may be characterized by local values quite different from the ensemble averaged ones. An unambigous approach consists in perfórming Monte Carlo simulations of the microwave sky, in order to determine the probability distribution function (pdf) for different observables. We do not need simulations for the quadrupole anisotropy: as already mentioned, Q_2^2 has a Chi-squared distribution with five degrees of freedom. We show our numerically derived pdf's for $C(10^\circ, 2^\circ.9)$ and $C(20^\circ, 2^\circ.4)$ in Fig.4, and for $\Delta^2(6^\circ, 2^\circ.2)$ and $\Delta^2(60^\circ, 3^\circ)$ in Fig.5, each normalized to its expected value for CDM models. Note that these distributions can be very non–G over the ensemble of comic observers.

For each of these observables we have observational upper limits. The Berkeley (Lubin *et al.* 1983) and the Princeton (Fixsen *et al.* 1983) groups set an upper limit at the 90% confidence level on the amplitude of the quadrupole component: $Q_2 < 2.2 \cdot 10^{-4}$. The Princeton group also published an upper limit on the CMB temperature acf: $C(\alpha, 2^\circ.9) < 1.4 \cdot 10^{-9}$, for $10^\circ < \alpha < 180^\circ$, at the 90 % confidence level. More recently, the RELIC satellite borne experiment (Strukov *et al.* 1990) posed an upper limit at the 95% confidence level on the quadrupole anisotropy: $Q_2 < 1.1 \cdot 10^{-4}$. Preliminary results of COBE set, for the moment, an upper limit at a similar level (Smoot, private comunication). The RELIC experiment posed also upper limits to the CMB temperature acf: $C(20^\circ, 2^\circ.4) < 5.5 \cdot 10^{-10}$, but the limits are even tighter at larger angular scales. The Florence group (Melchiorri *et al.* 1981) obtained $\Delta_{ss}(6^\circ, 2^\circ.2) < 5.4 \cdot 10^{-5}$, at the 95% confidence level.

In order to constrain the ensemble averaged quantities, easily predicted from the theory, we proceed as follows. Let us consider as an example the CMB quadrupole anisotropy and let us identify the ϵ left tail of its distribution, by imposing that only a fraction ϵ of the cosmic observers would obtain an upper limit smaller than the observed one, $Q_2^{(UL)}$. Such a tail is obviously bounded between 0 and $\gamma_\epsilon = Q_2^{(UL)}/\langle Q_2^2 \rangle^{\frac{1}{2}}$. Then

$$\langle Q_2^2 \rangle^{\frac{1}{2}} \leq \gamma_\epsilon^{-1} \cdot Q_2^{(UL)}$$

As $\gamma_\epsilon < 1$, the more conservative upper limit on $\langle Q_2^2 \rangle^{\frac{1}{2}}$ is weaker than that obtained by directly limiting $\langle Q_2^2 \rangle^{\frac{1}{2}}$ with $Q_2^{(UL)}$. For example, at the 99% confidence level (*i.e.* $\epsilon = 0.01$) the upper limit on the magnitude of the expected quadrupole is almost a factor of three greater than the observational upper limit.

On the other hand, the quoted upper limits have a confidence level by themselves, which should also be taken in account. A more realistic approach consists in considering the joint

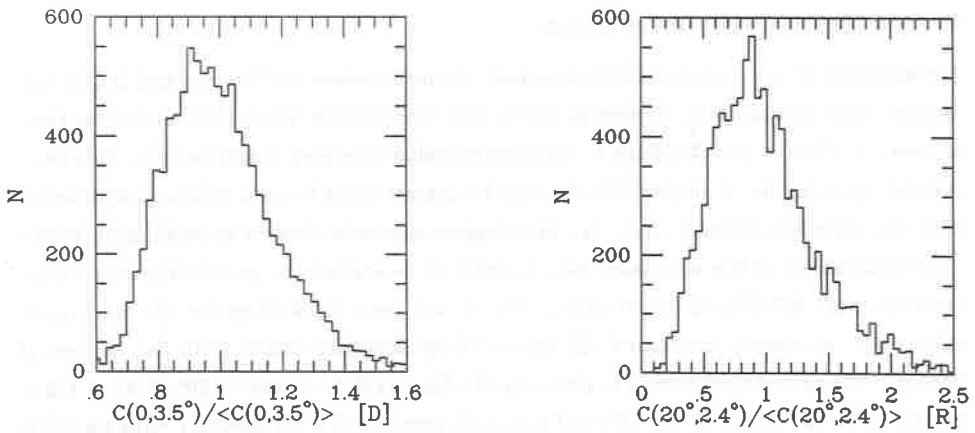

Figure 4 *Distribution function of the acf, normalized to the ensemble averaged value. We use* $\sigma_B = 3°.5$ *(left panel) and* $\sigma_B = 2°.4$ *(right panel) as for the RELIC satellite.*

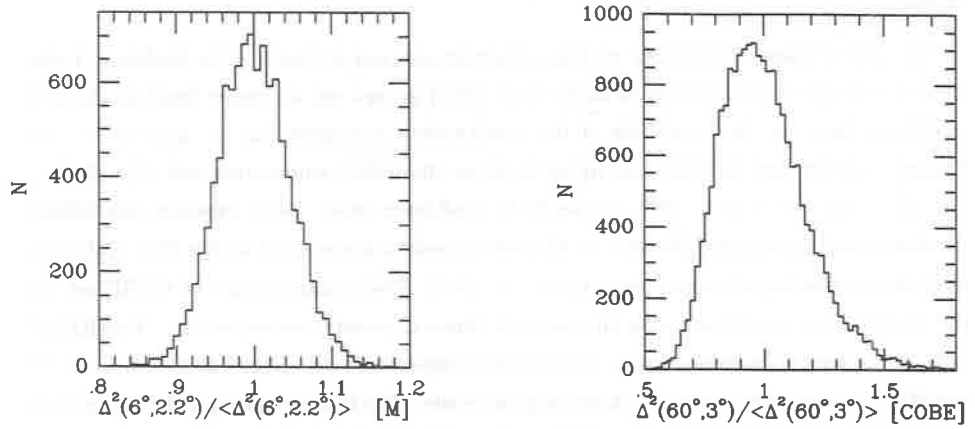

Figure 5 *Distribution function of* $\Delta^2_{\bullet\bullet}$*, normalized to the ensemble averaged value, for the Melchiorri et al. (left panel), and COBE (right panel) experiments.*

probability, P_T, of having $Q_2^{(UL)}$ from the experiments and $\langle Q_2^2 \rangle^{1/2} < \gamma_\epsilon^{-1} Q_2^{(UL)}$ from the theory. The total confidence level, $1 - \epsilon_T$, is given by the product of the confidence level of the observational upper limit times $(1 - \epsilon)$, where ϵ has been defined above. Strictly speaking, this procedure is not unique: the same total confidence level, can be reached by different combinations. This degeneracy is however limited by the requirement that the total confidence level is 95% and by the fact that from an operational point of view we can not safely reduce ϵ below the value of 0.01: for a much smaller value, Poissonian sampling can contaminate the tail of our numerically derived pdf's. We then convert published upper limits, quoted to their own confidence level, to new limits at the 99% confidence level. The limits on the expected values of different observables are obtained with $\epsilon = 4\%$. This analysis provides upper limits, at 95% total confidence level, directly on the ensemble averaged quantities.

Table 2

Observable	Experimental limit y_{lim}		Ensemble average
y	quoted	adopted (99%)	upper limit (95%)
Q_2 [BPG]	$2.6 \cdot 10^{-4}$ (90%)	$4.1 \cdot 10^{-4}$	$1.0 \cdot 10^{-3}$
Q_2 [R]	$1.1 \cdot 10^{-4}$ (95%)	$1.4 \cdot 10^{-4}$	$3.2 \cdot 10^{-4}$
$C(10°, 2°.9)$	$1.4 \cdot 10^{-9}$ (90%)	$2.2 \cdot 10^{-9}$	$3.5 \cdot 10^{-9}$
$C(20°, 2°.4)$	$6.9 \cdot 10^{-10}$ (95%)	$9.1 \cdot 10^{-10}$	$2.4 \cdot 10^{-9}$
$\Delta^M_{ss}(6°, 2°.2)$	$5.5 \cdot 10^{-5}$ (95%)	$5.8 \cdot 10^{-5}$	$6.0 \cdot 10^{-5}$

These upper bounds are given in Table 2.

The Monte Carlo simulations have been performed using scale invariant density fluctuations. The upper limits we obtain on the ensemble averaged quantities apply to any scenario, with scale–invariant, adiabatic fluctuations, as in CDM. In BDM models with $-1 \lesssim n \lesssim 0$, only the quadrupole keeps its broad distribution (a χ^2 with 5 degrees of freedom). The pdf's for the other observables tend to be Gaussian distributed around the expected values, with a negligible dispersion ($\lesssim 3\%$). So, for BDM models we are entitled to constrain, *e.g.* $\langle C(\alpha, \sigma_B) \rangle$, or $\langle \Delta^2_{ss}(\alpha, \sigma_B) \rangle^{1/2}$ directly with the observational bounds.

5 Conclusions

We have reviewed few aspects of the CMB anisotropy on large angular scales. We have used as a guide line two alternative scenarios for the formation and evolution of the large scale structure of the universe: the CDM and the BDM models.

These two scenarios are characterized by a very different amount of large scale power. As far as density fluctuations are concerned, a BDM universe is more inhomogeneous than a CDM model: this is due either to the primordial spectrum ($-1 \lesssim n \lesssim 0$, flatter than the CDM scale– invariant one) and to the prominent feature in the BDM power spectrum at the matter–radiation Jeans length at decoupling. The situation reverses for the large scale CMB anisotopy. Low order harmonics determine most of the microwave sky pattern in the CDM model. On the contrary, in a BDM scenario such a pattern is determined by high order harmonics and the antenna beam size critically defines the coherence angle of the CMB temperature fluctuation field. This is clearly shown in Fig.1: patches of the sky separated by more than σ_B are still correlated in CDM, while are practically uncorrelated in BDM.

In Sect.3 we discussed how such a dominance of low order mutipoles in CDM models determines a certain degree of non-G in the distribution of temperature fluctuations in the

observable CMB sky. From our analysis it follows that in order to reject at the 95% confidence level the standard assumption (i.e., that primordial density fluctuations are a scale–invariant random Gaussian field) it will be sufficient to measure $|\mathcal{S}| > 0.36$ and/or $|\mathcal{K}| > 0.48$. These numbers will also be useful benchmarks for future studies of anisotropies induced by non–G random density fields. We stress, however, that these are strictly theoretical bounds for a given value of the beam amplitude and for a given sampling rate (i.e. splitting in 4 pixels, as it was done by Lubin *et al.* 1985, a 7° FWHM beam). Indeed, for practical relevance to experiments crucial factors are the sky sampling and the presence of experimental noise. The latter in fact will obviously water down any diffuse intrinsic non–G temperature distribution of the CMB sky, to an extent inversely proportional to the S/N ratio. In this respect, the numbers we quoted are almost upper bounds, that can be reached only when S/N$\gg 1$ and for the actual number of sky pixels we used.

The dominance of low order mulipoles in the CDM scenario also implies that the observables characterizing the large scale CMB anisotropy [*i.e.* Q_2^2, $C(\alpha, \sigma_B)$, etc.] have a quite large spread around their expected values. It is important to take this effect into account in order to properly constrain with observations ensemble averaged quantities, easily predicted from the theory. Up to now, we are unable to constrain the rms (over the ensemble) quadrupole anisotropy to better than $3 \cdot 10^{-4}$. This upper bounds applies to the CMB quadrupole anisotropy of both CDM and BDM models, as the Q_2^2 distribution is indipendent of the considered scenario. On the contrary, the other BDM observables [as $\langle \Delta_{ss}^2(\alpha, \sigma_B) \rangle^{1/2}$ and $C(\alpha, \sigma_B)$] can be directly constrained by the observational upper limits, as the theoretical dispersion around the mean values is for any practical purpose negligible.

A comparison between the theoretical predictions of Table 1 and the observational upper limits on the ensemble averaged quantities shows that even the unbiased CDM model is still far from being constrained from the available large angular scale anisotropy measurements. If COBE will be able to reach a sensitivity of $\approx 2 \cdot 10^{-6}$ on the quadrupole determination, which is not unrealistic after two or three years of operation, the CDM scenario should start to be directly testable, even with a bias $b \lesssim 2$. In BDM scenarios, the expected quadrupole anisotropy depends quite strongly on the parameter choice, namely the ionization fraction x_e and the primordial spectral index.

Taking into account the theoretical distribution of $\Delta_{ss}^2(60°, 3°)$ around its mean value, we can conclude that a biased flat CDM model (with $\Omega_b \lesssim 0.1$) will be ruled out at the 95% confidence level if COBE will be able to set an upper limit $\Delta_{ss}^{(COBE)}(60°, 3°) \simeq b^{-1} 1.2 \cdot 10^{-5}$ at the 99% confidence level. On the contrary, in order to rule out all the BDM models considered here it would be necessary an upper limit $\Delta_{ss}^{(COBE)}(60°, 3°) \simeq 4 \cdot 10^{-6}$ at the 99% confidence level. But even $\Delta_{ss}^{(COBE)}(60°, 3°) \sim 10^{-5}$ would be still constraining at least for some of the BDM models.

Acknowledgements: We are indebted with J.Peebles for having made available to us his calculations on BDM density fluctuation power spectra.

References

Abbott and Wise, 1984, *Ap. J. (Lett.)* **282**, L47.

Blau, S.K., and Guth, A.H., 1987, *"300 Years of Gravitation,"*, S.W. Hawking and W. Israel (eds.), (Cambridge U. Press, Cambridge).

Blumenthal, G., Faber, S., Primack, J., and Rees, M. 1984: *Nature*, **301**, 584

Bond, J.R. and Efstathiou, G., 1987, *M.N.R.a.S.* **226**, 655.

Coles, P., and Barrow, J.D., 1987, *M.N.R.a.S.* **228**, 407.

Coles, P., 1988, *M.N.R.a.S.* **234**, 509.

Dekel, A., and Rees, M. J. 1987: *Nature*, **326**,455

Efstathiou, G., and Bond, J.R. 1987, *M.N.R.a.S.* **227**, 33P.

Fixen, D.J., Cheng, E.S., and Wilkinson, D.T., 1983, *Phys. Rev. Lett.* **44**, 1563.

Górski, K., and Silk, J., 1989 *Ap. J. (Lett.)* **346**, LL1.

Gott, J.R., Park, C., Juszkiewicz, R., Bies, W.E., Bennet, D.P., Bouchet, F.R., and Stebbins, A., 1990, *Ap. J.* **352**, 1.

Gunn, J.E., 1989: In 'The Extra-Galactic Distance Scale', A.S.P. Conference series, eds C. Pritchet and S. van den Bergh.

Kodama, H, Sazaki, M., 1986 *Internat. J. Mod. Phys.*, **A1**, 265

Kofman, L., Blumenthal, G. , Hodges, H., and Primack, J. 1990; In *"Large Scale Structures and Peculiar Motions in the Universe,"*, Rio de Janeiro, Brasil, Latham D.W. and da Costa L.N. (eds.), ASP Conference Series, in press.

Lubin, P., Epstein, G., Smoot, G., 1983, *Phys. Rev. Lett.* **50**, 616.

Lubin, P., Villela, T., Epstein, G., and Smoot, G., 1985, *Ap. J. (Lett.)* **298**, L1.

Matarrese, S., Lucchin, F., and Ortolan, A. 1990; In *"Large Scale Structures and Peculiar Motions in the Universe,"*, Rio de Janeiro, Brasil, Latham D.W. and da Costa L.N. (eds.), ASP Conference Series, in press.

Melchiorri, F., Melchiorri, B.O., Ceccarelli, C., and Pietranera, L., 1981, *Ap. J. (Lett.)* **250**, L1.

Peebles, P.J.E., 1982, *Ap. J. (Lett.)* **263**, L1.

Peebles, P.J.E. 1987: *Nature*, **327**, 210

Sachs, R.K., and Wolfe, M.A., 1967, *Ap. J.* **147**, 73.

Sazhin, M.V., 1985, *M.N.R.a.S.* **216**, 25p.

Scaramella, R., and Vittorio, N., 1988, *Ap. J. (Lett.)* **331**, L53.

Scaramella, R., and Vittorio, N., 1990, *Ap. J.* **353**, 372.

Scaramella, R., and Vittorio, N., 1991, *Ap. J. (Lett.) in press*, L .

Strukov, I.A., 1989, talk given at *"The Cosmic Microwave Background: 25 years later,"*, l'Aquila, Mandolesi, R., and Vittorio, N. (eds.), in press.

Turok, N. and Spergel, D., 1990, preprint.

David Wilkinson, Bruce Partridge and Douglas Morrison

FLUCTUATIONS IN THE COSMIC MICROWAVE BACKGROUND: THE FIRST MEASUREMENTS (AND MOTIVATION), AND RECENT RESULTS

R. B. Partridge
Haverford College
Haverford, PA 19041

Abstract

Why did we begin searches for anisotropies in the cosmic microwave background radiation? What techniques were introduced into the field by these early experiments? What was the impact of these first results? What is the present status of searches for fluctuations on various angular scales?

These are among the questions addressed in this talk.

For virtually the entire 25 year history of the cosmic microwave background, fluctuations in its intensity have been searched for by observational astronomers. In this paper, I want to look back over the past quarter century to see what we have learned so far, and what the scientific motivations have been for searches for fluctuations in the angular distribution of the cosmic microwave background radiation (CBR). Note the plural "motivations"; over the years the reasons advanced for searches for CBR anisotropy have changed, and they may well change again in the future.

I. The Early Years (1965-1970)

To begin at the very beginning, Penzias and Wilson (1965) showed that their "excess noise"--the 3 K CBR--was substantially isotropic. Indeed, its very isotropy made it difficult to identify. On the other hand, an isotropic signal was just what was expected if the Big Bang explanation of the CBR by Dicke and his colleagues (1965) was correct. Thus the first motivation of searches for anisotropy was to test the Big Bang origin of the 3 K radiation. We must remember that it took the astronomical community a few years to accept the notion of a hot Big Bang: the years 1965-1970 saw the appearance of a number of non-cosmological models for the signal seen by Penzias and Wilson and soon confirmed by Roll and Wilkinson (1966). We turn to these models first, then to the early observational results used to test them.

a.) Tests of Non-cosmological Models

As late as 1967, I can remember being asked how we could be sure the CBR was not solar, interplanetary or Galactic in origin. After all, the energy density in starlight in our Galaxy is of the same order of magnitude as a 3 K blackbody radiation field. To test such theories, we needed to show not just that the radiation was isotropic,

but that no strong correlation was seen with the Galactic plane, the plane of the ecliptic and so on. This test (as well as attempts to confirm the blackbody spectrum of the radiation) was very much in the minds of the Princeton group when I joined it as a postdoc in 1965. Dave Wilkinson and I set out to improve the sensitivity of Penzias and Wilson's (1965) isotropy limit by roughly two orders of magnitude, and thus to make this crucial test of the large-scale isotropy of the radiation more secure.

In the meantime, another class of non-cosmological models for the CBR emerged which could reproduce the large-scale isotropy also expected in the Hot Big Bang model: the suggestion that the summed emission from all galaxies (or all radio sources) in the Universe was responsible for the CBR (Layzer, 1968; Wolfe and Burbidge, 1969). From the outset, I believe such theories had trouble explaining the thermal spectrum of the CBR, but there was another test as well: the small-scale isotropy of the radiation. If discrete sources produce the CBR, we expect some shot-noise, random fluctuations in its intensity from place to place in the sky (Hazard and Salpter, 1969; Smith and Partridge, 1970). The smaller the solid angle of the sky surveyed, the larger the relative amplitude of such fluctuations would be.

I wish I could say that we observers were motivated from the beginning by the realization that the CBR provides a unique way of studying the large-scale structure in the Universe. In the late 1960's, however, we were more concerned with simply establishing the validity of the Hot Big Bang model.

b.) Sources of Anisotropy in the Hot Big Bang Model

While we were setting up and/or writing up experiments to measure or set limits on $\Delta T/T_o$, our theory colleagues were exploring various processes which could introduce anisotropies in a *cosmological* CBR. Among the crucial papers were ones by Sachs and Wolfe (1967), Thorne (1967), Novikov (1968) Peebles and Wilkinson (1968), Silk (1968), Ozernoi and Chernin (1968), and Hawking (1969). These explored ways in which anisotropic expansion, the motion of the solar system, and velocity or density perturbations could induce temperature fluctuations on various angular scales. In these crucial papers, it turned out, lay the *real* reason to probe the angular distribution of the CBR.

c.) Early Observational Limits

The first sensitive experiment designed to search for temperature fluctuations in the CBR produced results by late 1966 (Partridge and Wilkinson, 1967). The improvement in sensitivity was achieved in large part by making *differential* measurements of the sky; our scheme for doing so is shown in fig. 1. The horn antenna we employed was the one designed by Roll and Wilkinson for their 3 cm spectral measurement, hence it had a fairly broad beam, ~10° at the half-power points. Our observational technique allowed us to scan a circle in the sky at $\delta = -8°$ each day. Stacking many days' runs allowed us to beat down atmospheric and instrument noise. Even though our observations were made through the murky atmosphere of New Jersey, we were able to set limits of $\leq 2\times10^{-3}$ on $\Delta T/T_o$. The major limitation on our accuracy was emission from the Earth's atmosphere, a problem still plaguing isotropy measurements to this day.

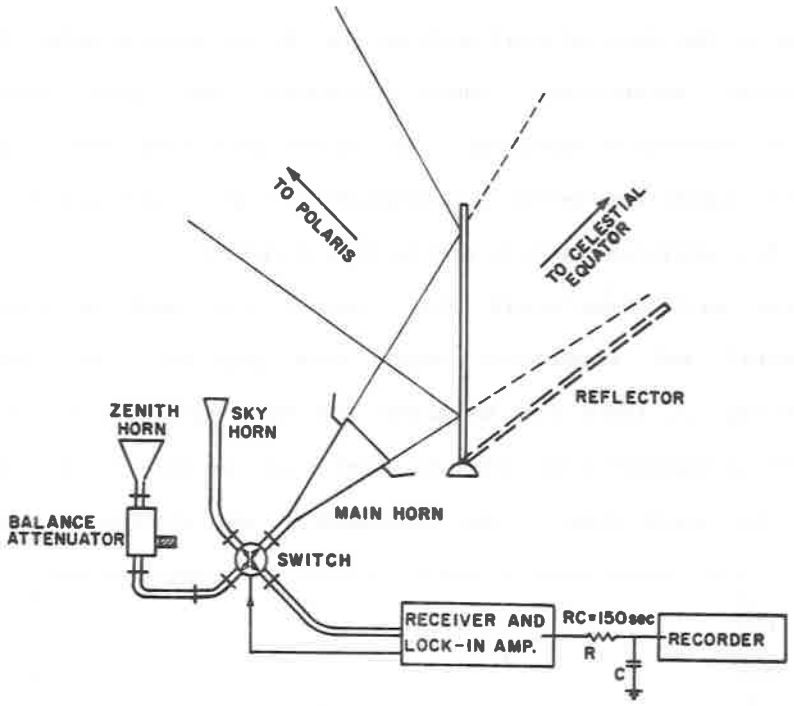

1.) Equipment used by Partridge and Wilkinson (1967) for the first isotropy measurement. With the reflector up, as shown, the instrument viewed a fixed region of the sky near the North Celestial Pole; this served as a reference. With the reflector down, the instrument scanned a circle at $\delta = -8°$ as the Earth rotated. Anisotropy in the CBR along that circle would have shown up as a time-varying signal. The zenith and sky horns provided convenient means of balancing the radiometer.

Shortly after our 1967 paper appeared, Conklin and Bracewell (1967a, 1967b) presented the results of the first search for CBR fluctuations using a conventional radio astronomical antenna as opposed to specially designed equipment. The sensitivity was roughly comparable to ours, but the angular scales probed were much smaller, as expected since their aperture was ~100 times larger than our small horn antenna.

These very early results already established a fundamental division in the observational work on the CBR--between programs based on existing, conventional, radio telescopes, and those employing specially constructed equipment. The former have been used to probe arcminute scales and below; all measurements on larger scales like degrees have employed smaller, specialized equipment.

These early experiments also revealed the need to separate instrumental and atmospheric noise from possible CBR signals. Consider fig. 2, taken from Wilkinson and Partridge (1967): is the variation we measured from point to point real, or merely the kind of scatter one would expect from instrumental and atmospheric noise?

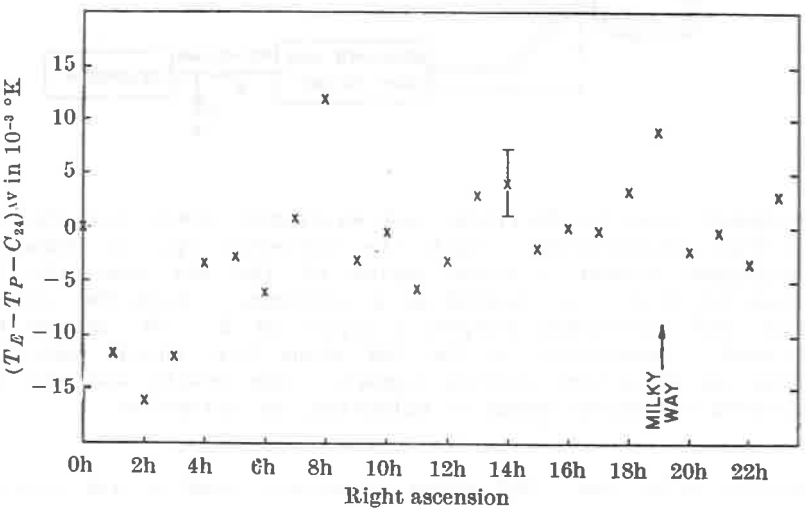

2.) Temperature differences, corrected for the dipole amplitude C_{24}. A typical one-sigma error bar is shown.

Our estimates of the 1σ noise for each point are shown by the error bars. Qualitatively, there is no evidence for real sky variation substantially in excess of the instrumental noise, but one would like a *quantitative* estimate. Conklin and Bracewell (1967a) attempted to correct for instrumental and atmospheric noise by assuming that it

scaled exactly as $t^{-1/2}$. By plotting their observed scatter as a function of integrating time, t, and extrapolating to $t^{-1/2} = 0$, they obtained an estimate of the residual sky variance. There is no guarantee at all, however, that atmospheric noise or even instrument noise decreases as $t^{-1/2}$. In the late 1960's, a less model-dependent means of separating instrument noise from a possible point-to-point variation on the sky was developed, largely by John Deeter, then a graduate student at the University of Washington (see Boynton and Partridge, 1973). It is based on a likelihood ratio test, and turns out to depend very sensitively on a reliable estimate of the amplitude of the instrumental noise. These questions, too, are still with us (see, e.g., Lasenby and Davies, 1983; Readhead et al., 1989; Boughn et al., 1990a).

Finally, the Earth's atmosphere again. Atmospheric noise clearly dominated the error budget of our Princeton experiment, where the beam switch angle was 98°. On the other hand, it is not clear whether atmospheric or instrumental effects played the major role in the experiments of Conklin and Bracewell (1967a, b) where the angular scales were much smaller. These conclusions highlight a second bifurcation within the field: searches for small-scale fluctuations could be done from the Earth's surface; searches on larger angular scales could not. Indeed, there were only three further attempts to measure the large-scale isotropy from the ground. Together with Jerry Beery, Dave Wilkinson and I tried to reduce atmospheric problems by going to a hot, dry site. We selected the sunniest spot in the U.S.--Yuma, Arizona. The U.S. Army evidently had done the same research; they had selected Yuma as a place to test equipment and munitions in a desert environment. We shared a small fenced-off area

with a pile of nerve-gas shells, left out in the sun to see when they'd start to leak. Not every radio astronomy installation needs to be equipped with gas masks! In the end, however, it was once again the atmosphere and not the nerve gas (or the rattlesnakes, Gila monsters or scorpions) which killed off that experiment, which never really got published (but see my 1969 review). Boughn, Fram and I (1971) had a stab at short wavelength measurements (λ = 9 mm), again from the ground, in this case a less exotic locale, Princeton, New Jersey.

Conklin, meanwhile, had a better idea--to reduce atmospheric problems by going to high altitude. His experiment (Conklin, 1969) was free enough from atmospheric problems to provide tentative evidence for the existence of a dipole anisotropy, soon to be confirmed by more accurate observations. By 1970, we had given up on using the ground for such measurements, and moved to balloons or high-flying aircraft (e.g., Henry, 1971; Smoot et al., 1977; Corey, 1978); COBE is the culmination of that development.

In experiments with smaller beam switch angles, the atmospheric contribution could be more accurately subtracted; hence such experiments could remain on the ground. Since most work on scales $\lesssim 1^\circ$ made use of conventional, large, radio telescopes, we had little choice anyway! In the late 1960's and early 1970's several radio telescopes were pushed to their sensitivity limits to search for fluctuations in the CBR on ~1′ to ~1° scales. Observations at $\lambda \sim 3$ mm were made by Epstein (1967), Penzias, Schraml and Wilson (1969) and Boynton and Partridge (1973). By the early 1970's, we knew that the CBR was strikingly isotropic on arcminute as well as degree

scales: $\Delta T/T_0 \leq 2\times10^{-3}$. As Boynton and I pointed out, that degree of isotropy was inconsistent with a discrete-source origin of the CBR.

d.) Evolution of Experimental Techniques

These early programs saw the introduction of many experimental techniques still in use today. Consider, for instance, large-scale measurements of the CBR. The earliest large-scale measurements relied on the rotation of Earth to scan the sky. (Hence the early names "24 hour" and "12 hour" for T_1 and T_2.) Then Henry (1971) introduced the idea of rotating the apparatus around the local vertical instead. This allowed a quicker scan to be made, reducing the effect of receiver gain variations, and could produce a survey of a large area of the sky as the direction of the local vertical swept across the sky. All subsequent searches for the dipole and quadrupole components have used that trick. Henry also introduced a symmetrical arrangement of two horn antennas (fig. 3), again the standard configuration used in later experiments up to and including COBE (one exception is the experiment of Fabbri et al. (1980) where the beam is switched by a mirror, as in our old Princeton work; another is the work of Boughn et al. [1990b]).

To search for small-scale anisotropies, differential measurements of small patches of the sky separated by a small angle θ_S are possible. Rapid beam switching with θ_S typically a few to 10 arcmin is available at conventional radio telescopes. In most cases, this is achieved by wobbling the secondary mirror or by switching between two feed horns on either side of the optical axis (fig. 4). To further control systematic errors, one can nod the telescope as well to perform what radio astronomers call "on-off" observations--see

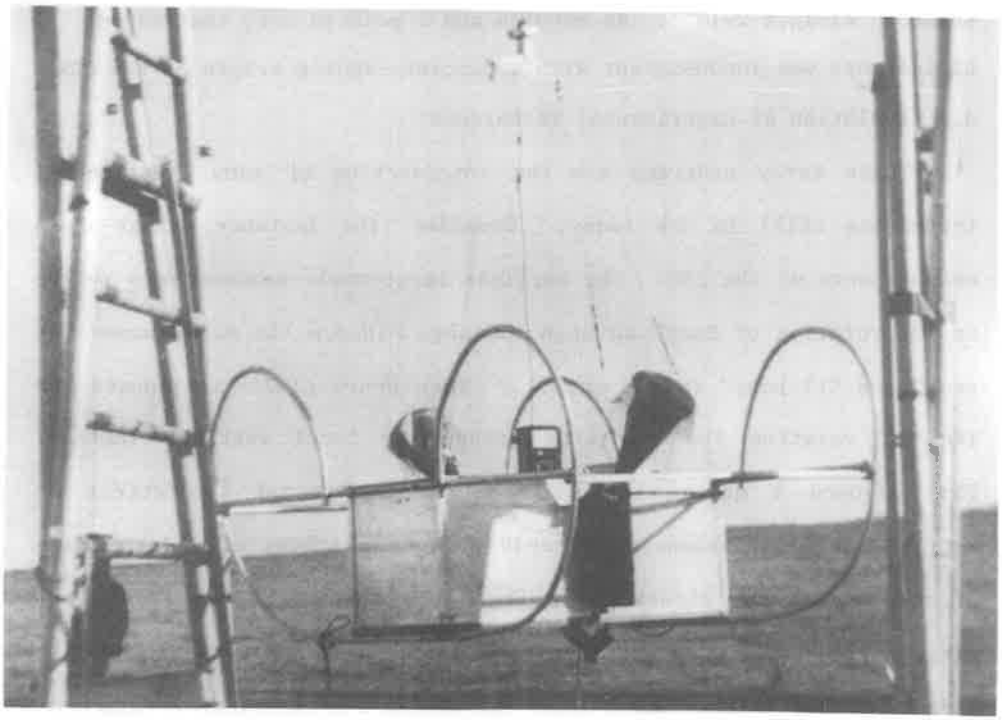

3.) Henry's (1971) balloon-borne apparatus on the test stand: note the two horns, symmetrically placed with respect to the zenith. Temperature differences between the inputs from the two horns were measured.

fig. 4b. This technique, which produces the characteristic beam pattern shown in fig. 5, was first used in CBR studies by Epstein (1967); it is now standard. Most radio astronomers use beam switch angles roughly twice the width of the beam itself, $\theta_{\frac{1}{2}}$. Hence we are often stuck with $\theta_S \approx 2\theta_{\frac{1}{2}}$ even though such a small beam throw is not ideal for probing the correlation function of CBR fluctuations. Specially designed equipment can of course use larger values of $\theta_S/\theta_{\frac{1}{2}}$.

In a related effort to minimize systematic errors, some of us used drift scans--an observing mode in which the telescope is kept fixed while a small region of the sky drifts through the beam. After 5-10 min or so, the telescope can then be moved to the West to allow the same region to drift through the beam again. When combined with on-off observing (e.g., Boynton and Partridge, 1973), this technique

offers the advantage of canceling out to first order differential side-lobe pickup. Variants of this technique are still in use (e.g., Davies et al., 1987).

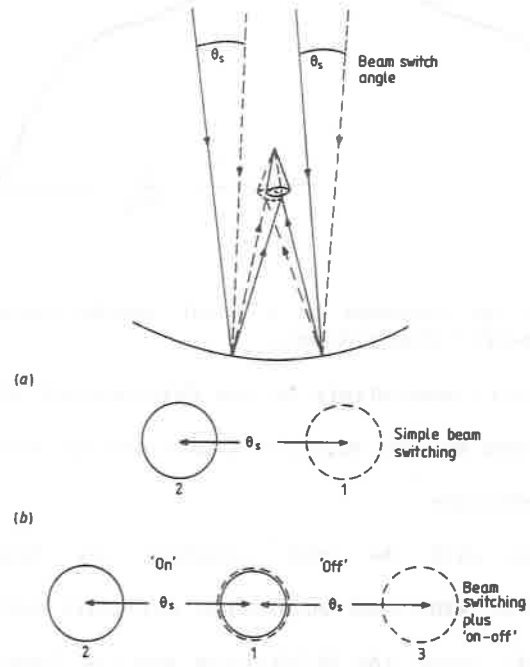

4.) Beam switching--(a) shows how the beam switching can be accomplished by changing the position of the receiver at the prime focus of a telescope. In (b), the resulting placement of the beam(s) is shown for simple beam switching and for "on-off" observations. The signal in the latter case is $2T_1-(T_2+T_3)$.

II. Subsequent Developments and New Directions (~1970-1985)

After the initial burst of activity described above, efforts to find and measure anisotropies in the CBR slowed a bit: much of the cream had been skimmed. On the other hand, the 70's saw the emergence of several new research groups with an interest in the CBR. I think of the MIT group under Ray Weiss, the two Berkeley groups (under Paul Richards and later George Smoot), the Soviet group (Stankevich, Pariiskii and their colleagues) and groups in Italy and Britain. These groups brought fresh ideas as well as fresh energy to the field.

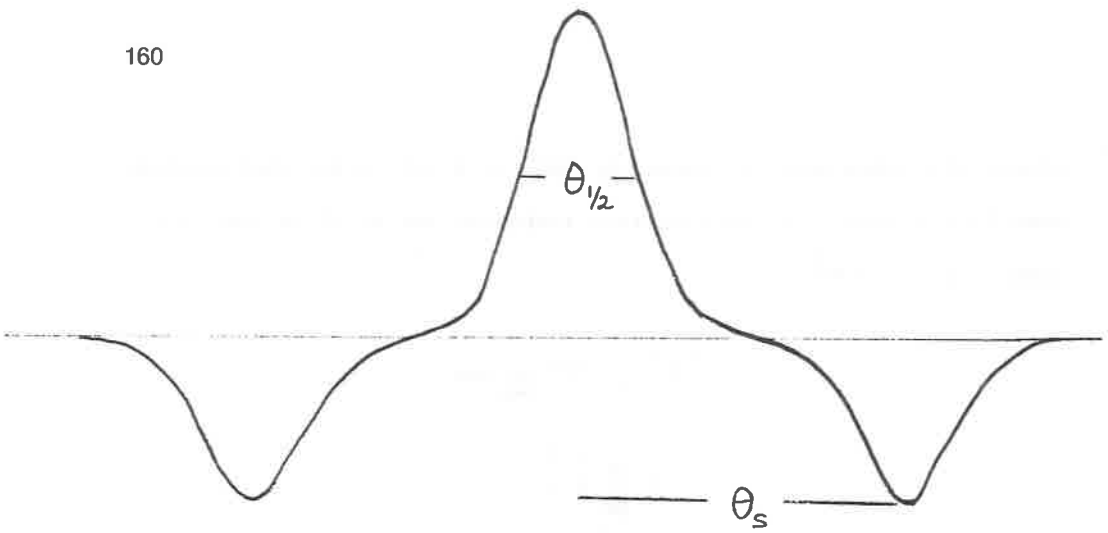

5.) Beam pattern, or response to a point source moved through the beam, for "on-off" observations.

In this paper, I will concentrate on new developments in searches for CBR fluctuations (see my 1991 book for a more general survey).

a.) Bolometric Detectors

Let me begin with the most important new development, the introduction of very wide-band bolometric detectors into CBR studies (by Weiss, Richards, Gush, the Melchiorris and the Queen Mary College group; see, for instance, Muehlner and Weiss, 1973 and 1976; Robson, 1976; Woody and Richards, 1979; Melchiorri et al., 1981; and Gush, 1981). Even the crude devices available a decade ago offered sensitivity equal to or better than superheterodyne receivers (expressed in $K/\sqrt{t}$). As heterodyne receivers have improved, so have bolometers, and the latter remain the best choice for $\lambda \lesssim 3$ mm thanks to their large band width.

The Melchiorris and their colleagues were the first to use sensitive bolometers to search for anisotropies. As so often happens, a new technique produced a noticeable improvement in sensitivity but also introduced new problems. One was the need to convert measured

values of intensity fluctuations at high frequency and in a broad frequency band to values of ΔT expressed in *thermodynamic* temperature. To make this correction (which can be large at $\lambda \sim 1$ mm), the exact shape of the instrumental bandpass as well as the CBR temperature must be known. A more vexing problem encountered in these bolometric measurements at $\lambda \sim 1$ mm was emission from warm dust in our Galaxy (Melchiorri et al. 1981). As we know from IRAS observations, that dust is patchy, particularly at high galactic latitudes. Its millimeter wave emission spectrum is not well characterized (COBE will soon change that); nor is its spatial frequency spectrum.

b.) Interferometry

I believe Goldstein, Marscher and Rood (1976) were the first to note that radio interferometry could be used to set limits on sky fluctuations. Bob Rood, a then student Buddy Martin and I set out in 1978 to use an interferometer to search for arcsecond scale CBR fluctuations (Martin et al., 1980). A year or so later, the VLA arrived, allowing an improvement of nearly two orders of magnitude in sensitivity (Knoke et al., 1984; Fomalont et al, 1984). I have written elsewhere about the various advantages of interferometry over searches with a single dish (Partridge, 1988a, b); here let me remind you of just two. First, smaller angular scales can be probed (in principle down to 10^{-3} arcsec or below). Second, interferometry produces a two-dimensional map of the sky. Let us look at each in a bit more detail.

Canonical CBR fluctuations are imprinted at the epoch of recombination at $z \sim 1000$ (e.g., Bond and Efstathiou, 1984; Vittorio and Silk, 1984). The thickness of the last scattering surface

($\Delta z \sim 100$) wipes out fluctuations on scales $\lesssim 5'-10'$. On the other hand, CBR fluctuations produced by other mechanisms, such as hydrodynamic shocks (Ostriker and Vishniac, 1986) or by cosmic strings (Kaiser and Stebbins, 1984) may have more power at smaller scales. Thus probing scales $\lesssim 1'$ can be used to test such models. The finer resolution also permits one to locate, and then exclude, discrete radio sources.

If we know the statistical properties of the CBR fluctuations in advance (e.g., random phase Gaussian fluctuations), a few samples of the sky suffice to set limits on their amplitude (see Readhead et al., 1989). Different models, however, produce quite different statistics; cosmic strings, for instance, cause distinctly non-Gaussian fluctuations as Kaiser and Stebbins (1984) and Bouchet et al. (1988) among others have shown. *Maps* of the microwave sky provide the best way to see and study the differences in the statistical properties of the CBR, and these maps must have adequate resolution to detect the sharp discontinuities imprinted on the CBR by strings. VLA maps of the CBR in principle offer these advantages. For instance, a typical VLA map contains $\sim$ 1000 independent map elements; the most sensitive filled-aperture results in print are for twelve (Uson and Wilkinson, 1984) or seven (Readhead et al., 1989) independent sky points.

Until very recently (see below), the drawback to interferometric studies has been sensitivity. The minimum detectable temperature for a filled aperture telescope operated for t sec. with a bandwidth $\Delta\nu$ is

$$\Delta T \equiv T_{rms} = \frac{2\ T_{sys}}{\sqrt{\Delta\nu t}} \quad . \quad . \quad . \quad . \quad . \quad . \quad . \quad . \quad . \quad (1)$$

where T_{sys} is the system noise temperature.* The corresponding figure for an interferometer is

$$\Delta T = \frac{T_{sys}}{\sqrt{\Delta\nu t}\,\sqrt{n(n-1)}} \left(\frac{\Omega_p}{\Omega_s} \right)^{\frac{1}{2}} \quad \ldots\ldots\ldots \quad (2)$$

where n is the number of elements of the array, so n(n - 1) is the number of correlators. The ratio (Ω_p/Ω_s) is the solid angle of the beam of the individual telescopes of the array divided by the synthesized beam solid angle. As noted above, $\Omega_p/\Omega_s \sim 1000$ for the VLA in its most compact configuration, and n = 27. Thus the VLA is in principle roughly as sensitive as a filled-aperture instrument with the same T_{sys}--or at least it would be if the integrating times and bandwidth were the same. To date, *all* the CBR studies made at the VLA add up only to 1-2 weeks of integrating time, and $\Delta\nu$ is limited to 100 MHz, so published limits are currently ~3 times less sensitive than the best filled-aperture results.

It is also worth noting parenthetically that a closer packed array would lower Ω_p/Ω_s without changing any of the other factors in eqn. 2. Some years ago, the group at the Mullard Radio Astronomy Lab were pushing just such an idea--the Very *Small* Array!

c.) Polarization

A variety of mechanisms may produce linearly polarized fluctuations in the CBR both on a large scale and on arcminute scales (see Basko and Polnarev, 1980; Negroponte and Silk, 1980; Tolman, 1985; and Bond and Efstathiou, 1987). Searches for large-scale polarization were initiated in the late '70's (Caderni et al., 1978; Nanos, 1979; Lubin and Smoot, 1979). The best current limits are

*The factor 2 takes account of beam-switching.

those of Lubin et al. (1983); they are comparable to the present limits on the quadrupole anisotropy of the total intensity. Each antenna of the VLA is equipped with a receiver for right circular polarization and one for left circular polarization. In addition, since phase is recorded, all four Stokes parameters can be measured. As a consequence, the VLA has been used for polarization studies of the CBR (on scales $\leq 1'$).

III. The Current Situation (~1985-present)

As we all know, there is no unambiguous evidence for anisotropy in the CBR on any angular scale except the dipole moment introduced by the motion of the Earth. Hence we are left considering a variety of upper limits at all smaller scales.

a.) The Dipole Moment

Thanks to recent balloon-borne (e.g., Boughn et al., 1990b); rocket-borne (Halpern et al., 1988) and satellite experiments (Strukov et al., 1987; COBE) we now know the amplitude of the dipole moment in the CBR to an accuracy of a few percent (see Table 1). The agreement between results obtained by different groups and at different wavelengths is heartening. From Table 1, I derive $T_1 = 3.3 \pm 0.1$ mK for the dipole moment (expressed in thermodynamic temperature), with a maximum at $\alpha = 11^h.2 \pm 0^h.1$, $\delta = -7° \pm 1°$. The velocity of the Earth and Sun derived from these CBR measurements is far more precise than our knowledge of the solar motion in the Galaxy. Nevertheless, we can calculate roughly the velocity of the Milky Way and/or the local group. This value of ~600 Km/sec is surprisingly large, and has been a crucial datum for theorists considering models for large-scale structure (e.g., N. Vittorio, this symposium).

Table 1 *Results (expressed in thermodynamic temperature) of recent measurements of the large-scale distribution of the CBR.*

Group	Berkeley	MIT/UBC	Moscow	Princeton	Princeton
Reference	Lubin et al (1985)	Halpern et al (1988)	Strukov et al (1987) Klypin et al (1987)	Fixsen et al (1983)	Boughn et al (1990)
Wavelength, mm	3	~ 1.7	8	12	15
Vehicle	balloon	balloon	satellite	balloon	balloon
Detector	heterodyne	bolometric	heterodyne	heterodyne	maser ampl.
Dipole amplitude, T_1, mK	3.4 ± 0.2	3.4 ± 0.4	3.16 ± 0.12	3.1 ± 0.2	3.36 ± 0.10†
Direction of solar motion, R.A. and Dec.	$11^h.2 \pm 0^h.1$ $-6° \pm 1.5°$	$12^h.1 \pm 0^h.24$ $-23° \pm 5°$	$11^h.3 \pm 0^h.16$ $-7.5° \pm 2.5°$	$11^h.2 \pm 0^h.05$ $-8° \pm 0.7°$	$11^h.0 \pm 0^h.1$ $-6° \pm 1.5°$
Limit on quadrupole moment, T_2, mK	0.4*	n.a.	≤ 0.08**	≤ 0.19	0.07

†Includes estimated systematic error.

*Calculated from Table I of Lubin et al by the present author, by taking the quadrature sum of the measured coefficients $Q_1 \ldots Q_5$.

**Taking the more conservative, model-independent upper limit.

Within a few months, the final results from COBE should be available. Despite the now rather old-fashioned design of the Differential Microwave Radiometers (DMR), they should produce measurements of the CBR dipole at least as precise as the earlier work, and less susceptible to systematic errors (hence giving more accurate coordinates for the maximum of the dipole). At the moment, all I can say is that the DMR results are in good agreement with the entries of Table 1.

b.) Quadrupole and Other Low-Order Moments

COBE should also provide our most accurate and error-free upper limits on the quadrupole and other low-order moments in the angular distribution of the CBR. We already have some sharp constraints on the quadrupole moment (e.g., Klypin et al., 1987): $T_2/T_0 \leq 2\text{-}3\times10^{-5}$. As has been noted frequently, the small amplitude of T_2 compared to the dipole moment sets strong limits on possible anisotropic cosmological models.

COBE's DMR antennas have beam widths of ~7°; thus all scales >7° will be probed. Since COBE will map the sky at many wavelengths, Galactic emission can be better controlled, so we should end up with more precise and less error-prone upper limits on $\Delta T/T_0$ over the range of angular scales 7°-90°. My guess is that COBE will improve the best current limits ($\Delta T/T_0 \leq 5\times10^{-5}$; Klypin et al., 1987) by roughly a factor of 2-3 to a few times 10^{-5}.

c.) Degree Scales

As noted above, most conventional radio telescopes have angular resolution of arcminutes. To probe the 1/2°-10° range has required the construction of special equipment. A variety of approaches have

been tried (e.g., Melchiorri et al., 1981; Lasenby and Davies, 1983; Mandolesi et al., 1986; Page et al., 1990; and Davies et al., 1987).

The last mentioned is the most interesting. In that paper, a positive detection at a level corresponding to $\Delta T/T = 3.5 \times 10^{-5}$ is reported; the wavelength of observation is 3 cm, and both the beam size and the beam switch angle are ~8°. It is not yet entirely clear that the signal seen by Davies and his colleagues is in fact produced by fluctuations in the CBR. Patchy Galactic emission may contribute some or all of the flux they measure.

I've made a crude attempt to scale high-latitude Galactic emission from lower frequency maps to ν ~ 10 GHz (fig. 6). The extrapolation to 10 GHz should be viewed with suspicion, but the figure does give us grounds to suspect the Galaxy. I gather that the

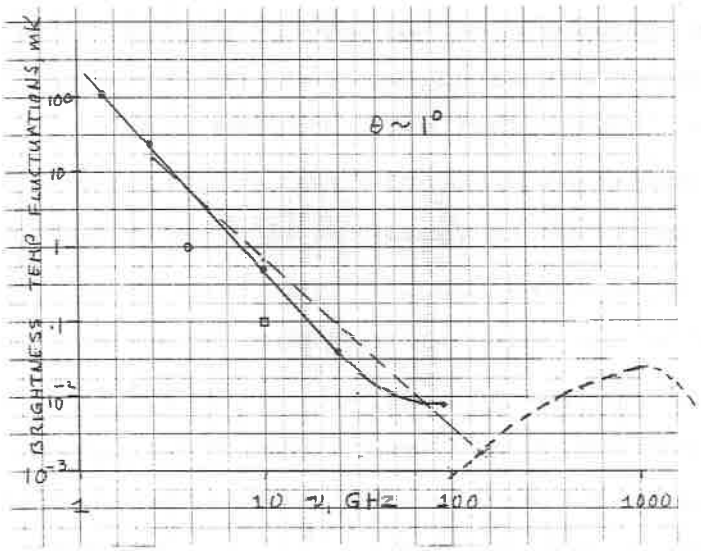

6.) My very rough estimates of the maximum level of fluctuations expected from Galactic emission alone (on scales of ~1°) near the Galactic pole. Solid line, synchrotron and bremsstrahlung; dashed line, fluctuations in spectral index alone; short dashes, thermal dust emission. The square is the measurement of Davies et al. (1987).

Jodrell-Canary Islands group is currently checking this possibility by observing at both lower and higher frequencies.

It is also worth mentioning that very interesting new results on degree scales should soon be emerging from Lubin's group at Santa Barbara. Preliminary results reported last year give $\Delta T/T \lesssim 3\times10^{-5}$ at 95% confidence level on a scale of 1°; the observations were made at λ = 3 mm, where Galactic emission should be close to a minimum. These results are discussed by Vittorio here. Likewise, Timbie and Wilkinson (1990) have built a novel two-element interferometer to probe degree scales. Their current level of sensitivity is $\Delta T/T_0 \leq 1.1\times10^{-4}$.

d.) Scales of 10 arcsec-1 arcmin

With one interesting exception (Kreysa and Chini's [1989] work at λ = 1 mm discussed below), all sensitive limits on $\Delta T/T$ on scales $\lesssim$1′ have been set with a single instrument, the 27-telescope Very Large Array. Table 2 shows results published to date. It is worth noting an apparent qualitative discrepancy between our results at λ = 6 cm (Martin and Partridge 1988) and those of Fomalont et al. (1988) at the same wavelength; they report upper limits, we report a "detection" of sky variance at a slightly higher level than their upper limit. I've used quotation marks around "detection" because it is likely that some of our "signal" results from a combination of an instrumental effect and the presence of weak radio sources (discussed in more detail in Partridge, 1988b).

The effect of discrete radio sources can be reduced by working at shorter wavelengths (roughly, $\Delta T \sim \lambda^{2.7}$). Hence both groups working at the VLA have used higher frequency receivers to probe the CBR. Work at λ = 2 cm (Hogan and Partridge, 1989) turned out not to be

Reference	λ, cm	Pol.	Angular Scale	Limits on on ΔT/T, ×10⁴
Martin & Partridge (1988)	6	I	18"–80"	1.7±0.5
"	"	I	36"–160"	1.3±0.2
Fomalont et al (1989)	"	I	12"	< 8.5
"	"	I	18"	< 1.2
"	"	I	30"	< 0.8
"	"	I	60"	< 0.6
Partridge et al (1988)	"	Q	60"–160"	< 0.4
"		U	"	< 0.5
"		V	"	< 0.6
Hogan & Partridge (1989)	2	I	5".3–48"	< 6.3
"	2	I	10"–48"	< 3.2
"	2	I	18"–50"	< 1.6
Partridge et al. (1991)	3.6	I	~10"	< 2.0
Tentative results	3.6	I	40"–60"	< 0.2

Table 2. VLA limits on CBR fluctuations. See text for discussion of the 3.6 cm work.

really conclusive; on 18" scales, $\Delta T/T_0 \leq 1.6\times10^{-4}$. We have now joined forces with Fomalont to use the newly available, low-noise, 3.6 cm receivers to make the most sensitive CBR search yet at sub-arcminute scales. Here, I can only describe the observations briefly and report preliminary results.

We observed two different regions of the sky, both previously mapped in detail at 6 cm. Small patches of the sky, free of "bright" ($S_6 > 1$ mJy) 6 cm sources, were selected for study at 3.6 cm. The angular resolution of the VLA at 3.6 cm was 9"-10"; we used 2" cells to construct maps of each patch of the sky covering an area ~ 3x the size of the primary beam of the individual elements of the array. The rms noise in these maps is very low, 3.3-3.4 μJy per synthesized beam in the best of the two cases. We also have constructed maps at lower resolutions, 18", 30" and 60". At 60", the rms noise has increased to 6-7 μJy (because fewer telescopes contribute to the low spatial frequency signal).

If we were simply to ascribe *all* the noise in our map to CBR fluctuations, we would find $\Delta T/T_0 \sim 2\times10^{-4}$ and $\sim 2\times10^{-5}$ on 10" and 60" scales. Most of the noise, however, is clearly instrumental (as we can show by a variety of means; see Knoke et al., 1984; Martin and Partridge, 1988). Correcting for instrumental noise will reduce the values of $\Delta T/T_0$ given above by at least a factor of 3, if our experience at 6 cm is any guide. Thus we expect to be able to reach sensitivities corresponding to $\Delta T \leq 7\times10^{-5}$ and $\leq 8\times10^{-6}$ at 10" and 60", respectively, even *before* correction for discrete sources. Note that our sensitivity increases with angular scale up to one arcminute

and may be better than the best filled-aperture measurements at $\theta \sim 1'$.

The one non-interferometric observation to probe scales below 1′ is the work of Kreysa and Chini (1989); high resolution was obtained by using a high frequency. More important, the detector used was based on a bolometer--a wave of the future.

IV. The Future

Let me close by sharing a few thoughts about the future of the field.

On all scales $\gtrsim 7°$, COBE is likely to set the standard, in part because it avoids atmospheric emission, but mainly because its multiwavelength observations will make correction for Galactic emission much easier.

At the opposite end of the spectrum of angular scales, the VLA has been pushed about as far as it can be--we are up against the limitations of bandwidth and integrating time. Interferometric observations at much higher frequency (and much larger bandwidth) offer a promising new approach. Given the number of telescopes in millimeter arrays now available, they are not yet competitive.

I do expect to see rapid progress--pushing to $\Delta T/T_0 \sim 10^{-5}$ or below--on scales of 0.5°-3° or so. New groups (Santa Barbara, Chicago); new technology (small scale interferometers [Timbie and Wilkinson, 1990], bolometric and other high sensitivity detectors [Lubin, 1990; Page et al. 1990; Melchiorri here]); and even new sites (the South Pole and balloon-borne platforms) will all contribute. Observations on these scales will provide particularly useful tests of conventional models of structure formation (see Bond and Efstathiou, 1987).

Let me end with a word of caution or even pessimism. On scales of a few minutes to degrees, a fundamental limit on our ability to detect CBR fluctuations may be set not by the atmosphere or even the Galaxy, but by the foreground maze of radio sources (Franceschini et al., 1989). Hints of that problem have cropped up already in the work of Readhead et al. (1989). We need to study the number counts, redshift distribution, high frequency spectra, and clustering properties of radio sources more carefully. This is rather old-fashioned, pedestrian, radio astronomy--but it may be crucial to the next generation of isotropy experiments as well as to even more visionary projects like LDR, SIRTF and so on. Il ne faut pas vendre le peau de l'ours avant de l'avoir tué.

References

Basko, M. M., and Polnarev, A. G. 1980, *Mon. Not. Roy. Astr. Soc.*, 191, 207.

Bond, J. R. and Efstathiou, G. 1984, *Ap. J. (Letters)*, 285, L45.

Bond, J. R., and Efstathiou, G. 1987, *Mon. Not. Roy. Astr. Soc.*, 226, 655.

Bouchet, F. R., Bennett, D. P., and Stebbins, A. 1988, *Nature*, 335, 410.

Boughn, S. P., Fram, D. M., Partridge, R. B. 1971, *Ap. J.*, 165, 439.

Boughn, S. P., Uson, J. M., and Cottingham, D. A. 1990a, in preparation.

Boughn, S. P., Cheng, E. S., Cottingham, D. A., and Fixsen, D. J., 1990b, submitted to *Ap. J.*

Boynton, P. E., and Partridge, R. B. 1973, *Ap. J.*, 181, 243.

Caderni, N., Fabbri, R., Melchiorri, B., Melchiorri, F. and Natale, V. 1978, *Phys. Rev.* D17, 1908.

Conklin, E. K. 1969, *Nature*, 222, 971.

Conklin, E. K., and Bracewell, R. N. 1967a, *Phys. Rev. Letters*, 18, 614.

_____ 1967b, *Nature*, 216, 777.

Corey, B. E. 1978, thesis, Princeton University.

Davies, R. D., Lasenby, A. N., Watson, R. A., Daintree, E. J., Hopkins, J., Beckman, J., Sanchez-Almeida, J., and Rebolo, R., 1987, *Nature*, 326, 462.

Dicke, R. H., Peebles, P. J. E., Roll, P. G., and Wilkinson, D. T., 1965, *Ap. J.*, 142, 414.

Epstein, E. E. 1967, *Ap. J. (Letters)*, 148, L157.

Fabbri, R., Guidi, I., Melchiorri, F. and Natale, V. 1980, *Phys. Rev. Letters*, 44, 1563.

Fomalont, E. B., Kellermann, K. I., and Wall, J. V. 1984, *Ap. J. (Letters)*, 277, L23.

Fomalont, E. B., Kellermann, K. I., Anderson, M. C., Weistrop, D., Wall, J. V., Windhorst, R. A., and Kristian, J. A. 1988, *A. J.*, 96, 1187.

Franceschini, A., Toffolatti, L., Danese, L., and De Zotti, G. 1989, *Ap. J.*, 344, 35.

Goldstein, Jr., S. J., Marscher, A. P., and Rood, R. T. 1976, *Ap. J.*, 210, 321.

Gush, H. P. 1981, *Phys. Rev. Lett.*, 47, 795.

Hawking, S. W. 1969, *Mon. Not. Roy. Astr. Soc.*, 142, 129.

Hazard, C., and Salpeter, E. E. 1969, *Ap. J. (Letters)*, 157, L87.

Henry, P. S. 1971, *Nature*, 231, 561.

Hogan, C. J., and Partridge, R. B. 1989, *Ap. J. (Letters)*, 341, L29.

Kaiser, N. and Stebbins, A. 1984, *Nature*, 310, 391.

Klypin, A. A., Sazhin, M. V., Strukov, I. A., and Skulachev, D. P. 1987, *Soviet Astron. Letters*, 13, 104.

Knoke, J. E., Partridge, R. B., Ratner, M. I., and Shapiro, I. I. 1984, *Ap. J.*, 284, 479.

Kreysa, E., and Chini, R. 1989, in *Third ESO-CERN Symposium*.

Lasenby, A. N., and Davies, R. D. 1983, *Mon. Not. Roy. Astr. Soc.*, 203, 1137.

Layzer, D. 1968, *Astrophys. Letters*, 1, 99.

Lubin, P. M. 1990, in *The Cosmic Microwave Background: 25 Years Later*, ed. N. Mandolesi and N. Vittorio, Kluwer Publ. Co., Dordrecht, Netherlands.

Lubin, P., Melese, P. and Smoot, G. 1983, *Ap. J. (Letters)*, 273, L51.

Lubin, P. M. and Smoot, G. F. 1979, *Phys. Rev. Letters*, 42, 129.

Mandolesi, N. et al 1986, *Nature*, 319, 751.

Martin, H. M., and Partridge, R. B. 1988, *Ap. J.* 324, 794.

Martin, H. M., Partridge, R. B., and Rood, R. T. 1980. *Ap. J. (Letters)*, 240, L79.

Melchiorri, F., Melchiorri, B., Ceccarelli, C., and Pietranera, L., 1981, *Ap. J. (Letters)*, 250, L1 .

Muehlner, D. J., and Weiss, R. 1973, *Phys. Rev. Letters*, 30, 757.

Muehlner, D., and Weiss, R. 1976 in *Infrared and Submillimeter Astronomy*, G. Fazio, ed., D. Reidel Publ. Co., Dordrecht, Netherlands.

Nanos, G. P. 1979, *Ap. J.*, 232, 341.

Negroponte, J., and Silk, J. 1980, *Phys. Rev. Letters*, 44, 1433.

Novikov, I. D. 1968, *Sov. Astron. J.*, 12, 427.

Ostriker, J. P. and Vishniac, E. T. 1986, *Ap. J. (Letters)*, 306, L51.

Ozernoi, L. M. and Chernin, A. D. 1968, *Soviet Astron. Journal*, 12, 901.

Page, L. A., Cheng, E. S., and Meyer, S. S. 1990, *Ap. J. (Letters)*, 355, L1.

Partridge, R. B. 1969, *American Scientist*, 57, 37.

Partridge, R. B. 1988a, *Reports on Progress in Physics*, 51, 647.

Partridge, R. B. 1988b, in *Third ESO/CERN Symposium, Astronomy, Cosmology and Fundamental Physics*, eds. Caffo et al, Kluwer Academic Publishers, Dordrecht, Netherlands.

Partridge, R. B. 1991, *3 K: The Cosmic Microwave Background Radiation*, in preparation for Cambridge University Press.

Partridge, R. B. and Wilkinson, D. T. 1967, *Phys. Rev. (Letters)*, 18, 557.

Peebles, P. J. E., and Wilkinson, D. T. 1968, *Phys. Rev.*, 174, 2168.

Penzias, A. A., Schraml, J., and Wilson, R. W. 1969, *Ap. J. (Letters)*, 157, L49.

Penzias, A. A. and Wilson, R. W. 1965, *Ap. J.*, 142, 419.

Readhead, A. C. S., Lawrence, C. R., Myers, S. T., Sargent, W. L. W. Hardebeck, H. E., and Moffet, A. T. 1989, *Ap. J.*, 346, 566.

Robson, E. I. 1976, in *Far Infrared Astronomy*, ed. M. Rowan-Robinson, Pergamon Press, Oxford.

Roll, P. G., and Wilkinson, D. T. 1966, *Phys. Rev. Letters*, 16, 405.

Sachs, R. K., and Wolfe, A. M. 1967, *Ap. J.*, 147, 73.

Silk, J., 1968, *Ap. J.*, 151, 459.

Smith, M. G., and Partridge, R. B. 1970, *Ap. J.*, 159, 737.

Smoot, G. F., Gorenstein, M. V., and Muller, R. A. 1977, *Phys. Rev. Letters*, 39, 898.

Strukov, I. A., Skulachev, D. P., Boyarskii, M. N., and Tkachev, A. N. 1987, *Soviet Astron. Letters*, 13, 65.

Timbie, P. T., and Wilkinson, D. T. 1990, *Ap. J.*, 353, 140.

Thorne, K. S. 1967, *Ap. J.*, 148, 51.

Tolman, B. W. 1985, *Ap. J.*, 290, 1.

Uson, J. M., and Wilkinson, D. T. 1984, *Ap. J.*, 283, 471.

Vittorio, N., and Silk, J. 1984, *Ap. J. (Letters)*, 285, L39.

Wilkinson, D. T. and Partridge, R. B. 1967, *Nature*, 215, 719.

Wolfe, A. M., and Burbidge, G. R. 1969, *Ap. J.*, 156, 345.

Woody, D. P., and Richards, P. L. 1979, *Phys. Rev. Lett.*, 42, 925.

MEASUREMENT OF THE SUNYAEV-ZEL'DOVICH EFFECT

Mark Birkinshaw
Department of Astronomy, Harvard University

ABSTRACT

Many attempts have been made to measure the Sunyaev-Zel'dovich effect, but reliable detections exist for only a few clusters of galaxies. In each case, the observable signal, at about -0.5 mK, is rather smaller than was first predicted.

The angular extent of the Sunyaev-Zel'dovich effect has been measured for the three best-observed clusters. This structural information can be compared with X-ray data on the clusters and information on the distribution and velocities of the cluster galaxies: the results can be used to investigate the properties of the X-ray emitting intracluster gas and to estimate the value of the Hubble constant.

Further improvements in the observations should result in the detection and mapping of a number of clusters over the next few years, and the Sunyaev-Zel'dovich effect should become a more useful probe of the intracluster medium as a result.

CLUSTERS AND THE MICROWAVE BACKGROUND RADIATION

Interesting information about clusters of galaxies and the Universe can be obtained from structures in the microwave background radiation (MWBG) caused by clusters. Fortunately, these structures should be among the easiest to detect, because we know where to search for them (towards prominent optical and X-ray clusters of galaxies), and because they are relatively intense (compared to cosmological effects).

Two main classes of MWBG anisotropy introduced by clusters of galaxies have been discussed — structures of gravitational origin, and structures introduced by scattering. Into the first class fall three effects which are caused by distortions of the Hubble flow near clusters of galaxies.

(1) Gravitational lensing by a cluster of galaxies moving across the line of sight causes a fractional intensity change

$$\frac{\Delta I}{I} \approx -\Delta\theta \, \frac{v_{\rm perp}}{c} \tag{1}$$

where $\Delta\theta(b)$ is the angle by which light rays with impact parameter b are deflected by the cluster, and $v_{\rm perp}$ is the cluster's velocity across the line of sight (Birkinshaw 1989). $\Delta\theta \lesssim 1$ arcmin and the peculiar velocity, $v_{\rm pec} \lesssim 1000\ {\rm km\,s^{-1}}$ for a typical cluster, so that $\Delta I/I < 10^{-6}$. The angular structure of ΔI reflects the scale of the cluster gravitational potential and indicates the direction of the cluster's proper motion.

(2) If a cluster of galaxies is gravitationally bound, then it does not participate in a local Hubble expansion, and light that crosses the cluster is redshifted differently than light that bypasses the cluster. The MWBG towards the cluster therefore displays an intensity change

$$\frac{\Delta I}{I} \approx -\frac{\phi}{c^2} \cdot \frac{H_0 R}{c} \tag{2}$$

where $\phi(b)$ is some measure of the Newtonian gravitational potential of the cluster at impact parameter b, and R is the cluster's size (Dyer 1976; Nottale 1984). For typical clusters ϕ/c^2 ($\approx \Delta\theta$) and $H_0 R/c$ are both of order 10^{-4}, so that $\Delta I/I < 10^{-7}$.

(3) The cluster might also be detached from the Hubble flow more dramatically, if it is collapsing (or expanding). If the collapse speed is $v_{\rm coll}$, the centre of the cluster will display a MWBG anisotropy of order

$$\frac{\Delta I}{I} \approx -\frac{\phi}{c^2} \cdot \frac{v_{\rm coll}}{c} \tag{3}$$

(Nottale 1984). If $v_{\rm coll} \lesssim 100\ {\rm km\,s^{-1}}$, so that clusters do not collapse on a Hubble time, $\Delta I/I \lesssim 10^{-7}$.

The effects of scattering on the MWBG have been discussed by Sunyaev & Zel'dovich (1972; 1980b). Several anisotropies are introduced by inverse-Compton interactions between electrons of the hot, X-ray emitting, intracluster medium and photons of the microwave background radiation.

(1) The first is an effect of order

$$\frac{\Delta I}{I} \approx -2\tau_e \frac{kT_e}{m_e c^2} \tag{4}$$

which is caused by the asymmetric distribution of frequency shifts imparted to photons by inverse-Compton scatterings in an electron gas of optical depth τ_e and temperature T_e. In a high-luminosity X-ray cluster the central optical depth may be as high as 10^{-2}, and the electron temperature is typically 7 keV. The central anisotropy introduced by the scattering is therefore $\Delta I/I \approx -3 \times 10^{-4}$, corresponding to a brightness temperature change $\Delta T_{\rm RJ} \approx -0.8$ mK in the Rayleigh-Jeans part of the spectrum.

(2) A second Sunyaev-Zel'dovich effect is caused if the cluster of galaxies (or gas associated with a galaxy in the cluster; Rephaeli 1990) is moving relative to the Hubble flow. If the cluster as a whole has a line-of-sight peculiar velocity $v_{\rm los}$, an effect

$$\frac{\Delta I}{I} \approx -\tau_e \frac{v_{\rm los}}{c} \tag{5}$$

is produced. If $v_{\rm los} < 10^3$ km s^{-1}, then $\Delta I/I < 3 \times 10^{-5}$, smaller by a factor $\approx 0.9(v_{\rm los}/10^3\ {\rm km\,s^{-1}})({\rm T_e/keV})^{-1}$ than the pure-scattering Sunyaev-Zel'dovich effect.

It is clear that the gravitational anisotropies are generally less intense than the structures produced by scattering: in what follows, only the Sunyaev-Zel'dovich (SZ) effects will be considered. Other effects from scattering are also possible: for example, small amounts of polarization are introduced into the MWBG by transverse motions of clusters of galaxies (see the reviews by Sunyaev & Zel'dovich 1980a and Rephaeli 1990).

If the intracluster medium in a cluster of galaxies is approximately isothermal, then observations at a single frequency cannot distinguish the scattering and velocity SZ effects, since the angular structure of the effects is the same (that of the electron optical depth, $\tau_{\rm e}$). If we adopt an isothermal β-model for the intracluster medium (as is commonly used to describe the X-ray structures of clusters of galaxies; Cavaliere & Fusco-Femiano 1976; 1978), the angular structure of the electron optical depth (and the SZ effects) is

$$\tau_{\rm e}(\theta) = \tau_{\rm e0}(1 + \theta^2/\theta_{\rm cx}^2)^{\frac{1}{2}-\frac{3}{2}\beta} \tag{6}$$

where $\tau_{\rm e0}$ is the optical depth through the cluster centre and $\theta_{\rm cx}$ is the angular core radius of the cluster. The parameter β describes the partition of energy between gas and galaxies in the cluster. β usually lies in the range $0.5 - 1.0$, as determined from X-ray images and spectra of clusters: for such values of β, the SZ effect of a cluster is two or three times more extended than its X-ray surface brightness.

The two SZ effects can, in principle, be separated by their different spectra. The brightness temperature change produced by the velocity effect is independent of frequency, while the spectrum of the pure scattering effect has an unusual spectral shape, being most negative at zero frequency, passing through zero at 219 GHz (if the temperature of the MWBG is $T_{\rm R} = 2.74$ K; Mather *et al.* 1990), and appearing as a positive effect at higher

frequencies, with a maximum at 311 GHz. At present, no direct spectral measurement of the SZ effects from any cluster of galaxies has been made, and so it is normally assumed that $v_{\rm los} < 10^3$ km s^{-1}, so that the velocity effect is much smaller than the pure scattering effect.

A detected SZ effect can be put to several uses. First, it provides information on the properties of a cluster atmosphere. $\Delta T_{\rm RJ}$ is proportional to the line-of-sight integral of the electron pressure whereas the X-ray surface brightness is approximately proportional to the line-of-sight integral of $n_{\rm e}^2 T_{\rm e}^{1/2}$, so that a comparison of the angular structures of the two effects should provide information on the distributions of electron temperature and electron concentration in the cluster gas. This allows a test of the isothermality of the gas that is independent of the X-ray spectrum, which is useful because the X-ray data are biased to high-density regions by the $n_{\rm e}^2$ factor, whereas the SZ data are more sensitive to lower-density regions, where the path lengths are longer.

If the velocity effect could be detected, then it would measure the peculiar velocities of clusters of galaxies in the distant Universe. On such large scales, the gravitational dynamics should be linear, so that the spectrum of fluctuations that condensed into present-day objects should be sampled directly.

The SZ effect can also be used as a cosmological probe. Most obviously, since the effect arises from the propagation of the MWBG through a distant cluster of galaxies, the observation of the effect from a cluster at redshift $z_{\rm c}$ proves that the background radiation originates at redshifts greater than $z_{\rm c}$. However, more attention has focussed on the use of the SZ effect in the determination of the value of the Hubble constant (Gunn 1978; Silk & White 1978; Birkinshaw 1979; Cavaliere *et al.* 1979). In its simplest form, the central SZ effect of a cluster

$$\Delta T_{\rm RJ}(0) \propto n_{\rm e}(0)\, T_{\rm e}(0)\, D_{\rm A}\, \theta_{\rm cx} \tag{7}$$

(if $v_{\rm los} = 0$) and the total X-ray flux density

$$S_{\rm X} \propto n_{\rm e}(0)^2\, \frac{(D_{\rm A}\theta_{\rm cx})^3}{D_{\rm L}^2}\, \Lambda(T_{\rm e}(0)) \tag{8}$$

are compared. $D_{\rm A}$ and $D_{\rm L}$ are the angular diameter and luminosity distances of the cluster, $\Lambda(T_{\rm e})$ is the cooling function of the gas, and the constants of proportionality encode the structure of the gas. If the central electron concentration, $n_{\rm e}(0)$, is eliminated then

$$\frac{D_{\rm L}^2}{D_{\rm A}} \propto \frac{\Delta T_{\rm RJ}(0)^2}{S_{\rm X}}\, \theta_{\rm cx}\, f(T_{\rm e}(0)) \tag{9}$$

where all the quantities on the right hand side of this equation can be measured. $f(T_{\rm e})$ is a known function of the electron temperature, which can be measured from the X-ray spectrum. Thus $D_{\rm L}^2/D_{\rm A}$, and the value of the Hubble constant, can be determined when the constant of proportionality in this relation has been found.

Table 1. Observations of the Sunyaev-Zel'dovich effect

Reference	frequency (GHz)	beamsize (arcmin)	beamthrow (arcmin)	Notes
Parijskij 1972	7.5	1.3 × 40	—	1B, DS, RA
Rudnick 1978	15.0	2.2	17.4	2B, DS, RA
Perrenod & Lada 1979	31.4	3.5	8	2B, PS1, RA
Schallwich 1979	10.7	1.2	8.2	2B, DS, RA
Lake & Partridge 1980	31.4	3.6	9	1B, PS1, RA
Birkinshaw *et al.* 1981	10.6	4.5	15	2B, PS1, RA
Andernach *at al.* 1983	10.7	1.2	3.2, 8.2	3B, DS, RA
Lasenby & Davies 1983	5.0	8 × 10	30	2B, PS1, RA
Meyer *et al.* 1983	90 – 300	5.0	5.0	1B, PS2, BO
Birkinshaw & Gull 1984	10.7	3.3	14.4	2B, PS1, RA
ditto	20.3	1.8	7.2	2B, PS1, RA
Birkinshaw *et al.* 1984	20.3	1.8	7.2	2B, PS1, RA
Uson 1985	19.5	1.8	8.0	2B, PS2, RA
Andernach *at al.* 1986	10.7	1.2	3.2, 8.2	3B, DS, RA
Radford *et al.* 1986	89.6	1.3	4.0	1B, DS, RA
ditto	89.6	1.2	4.2	1B, PS1, RA
ditto	105	1.7	19	1B, PS1, RA
Chase *et al.* 1987	261	1.9	3.0	1B, PS2, BO
Partridge *et al.* 1987	4.9	0.3 – 1.4	—	IN(4 arcmin)
Uson 1987	19.5	1.8	8.0	2B, PS2, RA
Birkinshaw 1990	20.3	1.8	7.2	2B, PS1, RA

Notes:
- nB — detector system providing n beams
- BO — bolometer detector
- DS — drift or driven scans
- PS1 — position switching by fixed azimuth, elevation offsets
- PS2 — position switching to fixed α, δ
- IN($\theta_{\rm max}$) — interferometer, sensitive to scales $< \theta_{\rm max}$
- RA — radiometer

Finally, the integrated SZ effects of clusters produce a background of confusing signals in the MWBG on arcminute angular scales. This background may be difficult to distinguish from the fluctuations arising from processes near recombination (Rephaeli 1981). The integrated effect will also appear as a small inverse-Compton distortion of the spectrum of the MWBG.

OBSERVATIONS OF THE SUNYAEV-ZEL'DOVICH EFFECT

Many attempts to measure the Sunyaev-Zel'dovich effect have been made since 1972 (see Table 1, which collects the final or latest reports of each group's measurements), but no new observations have been published since the review of Birkinshaw (1990). Readers are referred to that paper for a description of the methods that have been used to search for the effect and the limitations that these methods impose.

Although an SZ signal ≈ -0.5 mK should be easy to detect in a few hours of observation, it is clear that the earliest measurements reported in the papers of Table 1 suffered from the presence of unsuspected systematic errors — from spillover signals, confusion with radio sources, errors in the gain of the telescope, non-gaussian statistics

Table 2. Well-observed clusters: measurements with $\Delta T_{\rm RJ}$ error < 0.5 mK

Cluster	$\theta_{\rm cx}$ (arcmin)	$\Delta T_{\rm RJ}$ (mK)	Reference	$\Delta T(0)$ (mK)
0016+16	1.0	-0.72 ± 0.18	Birkinshaw & Gull 1984	-1.83 ± 0.46
		-0.37 ± 0.16	Birkinshaw & Gull 1984	-0.71 ± 0.31
		-0.64 ± 0.08	Birkinshaw *et al.* 1984	-1.10 ± 0.34
		-0.48 ± 0.12	Uson 1987	-0.78 ± 0.20
		-0.44 ± 0.10	Birkinshaw 1990	-0.75 ± 0.17
Abell 576	7.9	-1.26 ± 0.27	Lake & Partridge 1980	-3.35 ± 0.72
		-1.12 ± 0.17	Birkinshaw *et al.* 1981	-1.92 ± 0.29
		$+1.10 \pm 0.44$	Lasenby & Davies 1983	$+1.82 \pm 0.73$
		-0.14 ± 0.29	Birkinshaw & Gull 1984	-0.37 ± 0.77
Abell 665	2.0	-0.53 ± 0.22	Birkinshaw *et al.* 1981	-1.02 ± 0.42
		$+0.03 \pm 0.25$	Birkinshaw & Gull 1984	$+0.05 \pm 0.45$
		-0.55 ± 0.13	Birkinshaw & Gull 1984	-1.01 ± 0.24
		-0.34 ± 0.05	Birkinshaw *et al.* 1984	-0.50 ± 0.07
		-0.37 ± 0.14	Uson 1987	-0.51 ± 0.19
		-0.30 ± 0.10	Birkinshaw 1990	-0.44 ± 0.15
Abell 2125	1.6	$+0.77 \pm 0.44$	Lake & Partridge 1980	$+1.65 \pm 0.94$
		-0.39 ± 0.22	Birkinshaw *et al.* 1981	-0.73 ± 0.41
		-0.31 ± 0.39	Birkinshaw & Gull 1984	-0.60 ± 0.76
Abell 2218	2.1	-1.04 ± 0.48	Perrenod & Lada 1979	-2.00 ± 0.92
		-1.22 ± 0.25	Schallwich 1979	-1.58 ± 0.32
		$+0.71 \pm 0.38$	Lake & Partridge 1980	$+1.36 \pm 0.73$
		-1.05 ± 0.21	Birkinshaw *et al.* 1981	-1.97 ± 0.39
		-0.38 ± 0.19	Birkinshaw & Gull 1984	-0.74 ± 0.37
		-0.31 ± 0.13	Birkinshaw & Gull 1984	-0.57 ± 0.24
		-0.34 ± 0.05	Birkinshaw *et al.* 1984	-0.50 ± 0.07
		-0.29 ± 0.24	Uson 1985	-0.40 ± 0.33
		$+0.16 \pm 0.43$	Radford *et al.* 1986	$+0.40 \pm 1.08$
		$+0.41 \pm 0.32$	Radford *et al.* 1986	$+0.89 \pm 0.69$
		-0.35 ± 0.09	Birkinshaw 1990	-0.51 ± 0.13

for the sky noise, etc. In consequence, the early results generally disagree with more recent work, and were unable to detect effects at the -0.5 mK level reliably. An expurgated view of the current observational situation is given in Table 2, where the best results (those with errors < 0.5 mK) are collected. Only clusters with more than three measurements with small errors are represented in Table 2: it is a reflection on the state of the art that all the measurements in the Table were made using the technique of single-dish radiometry. The other techniques that have been attempted (using bolometers at mm-wavelengths, and using interferometers) have not yet achieved the same sensitivity as the 'traditional' approach.

The results for any particular cluster in Table 2 cannot be compared directly because they arise from observations at slightly different positions, made with telescopes with different beam-widths and beam-throws, at different frequencies, and in different observing modes. A rough correction for this has been made by assuming that the angular structure of the SZ effect in each cluster, $\Delta T_{\rm RJ}(\theta)$, follows equation (6) with $\beta = 0.8$ and a value of $\theta_{\rm cx}$ appropriate to the redshift of the cluster, assuming $r_{\rm cx} \equiv D_{\rm A}\theta_{\rm cx} = 500$ kpc. The measured $\Delta T_{\rm RJ}$ has then been deconvolved, assuming that the observations were made at

Table 3. Minimum χ^2 estimates for $\Delta T(0)$

Cluster	Overall $\Delta T(0)$ (mK)	χ^2	$N_{\rm df}$	$P(>)$
0016+16	-0.85 ± 0.11	5.8	4	0.22
Abell 576	-1.53 ± 0.24	31.5	3	< 0.01
Abell 665	-0.52 ± 0.06	7.6	5	0.18
Abell 2125	-0.40 ± 0.34	5.5	2	0.07
Abell 2218	-0.56 ± 0.06	39.2	10	< 0.01

the cluster centre, to calculate the central SZ effect at zero frequency, $\Delta T(0)$.

Note the poor agreement of the $\Delta T(0)$ results in Table 2. The minimum-χ^2 estimate of $\Delta T(0)$ for each cluster based on these measurements is given in Table 3: it can be seen that the values of χ^2 are large (and the probabilities of obtaining larger values of χ^2 by chance, $P(>)$, are small) in most cases. Although part of the problem is the over-simple model that has been used for the deconvolution, it is likely that much of the discordance comes from residual systematic errors at the level of the random errors. This is particularly evident for Abell 576 and Abell 2218.

Based on Table 3, there are only three clusters, 0016+16, Abell 665, and Abell 2218, for which there is reasonable evidence for the detection of the SZ effect — and in one of those cases (Abell 2218), the data are appreciably discordant (removing the three measurements that make the largest contributions to χ^2 changes $\Delta T(0)$ only slightly, to -0.50 ± 0.06 mK, with $\chi^2 = 8.0$ and 7 degrees of freedom). Three is not a large number of detections to show for 18 years of work — it is to be hoped that improved techniques will make it possible to observe a large sample of clusters in a uniform way, rather than the *ad hoc* collection of clusters that have become popular. In the absence of such a sample, it is not possible to make strong statistical statements about the range of SZ effects displayed by clusters of galaxies, or the overall effect that clusters of galaxies have on the MWBG.

RESULTS OF OBSERVATIONS AT 20.3 GHZ FROM OVRO

Over the past 11 years, the 40-m telescope at the Owens Valley Radio Observatory (OVRO) has been used to search for the SZ effect and other structures in the MWBG. Since 1982 the telescope has been equipped with a tunable K-band maser operating with a bandwidth of 350 MHz about a centre frequency $\approx$ 20.3 GHz. The receiver package illuminates the dish to provide two 1.8-arcmin primary beams separated by 7.2 arcmin on the sky. The gains in these beams are almost equal, and the system noise temperature is about 40 K. After about 100 hours of test data taken during 1982, approximately 4500 hours of useful data have been taken with this system.

Observations at OVRO are made using beam-switching and position-switching in azimuth (see Fig. 1), which results in the point under study being compared with points on surrounding reference arcs. Each position-switching cycle lasts about 75 sec, made up of 10 sec with the 'main' beam on source, then 2×10 sec with the 'reference' beam on source,

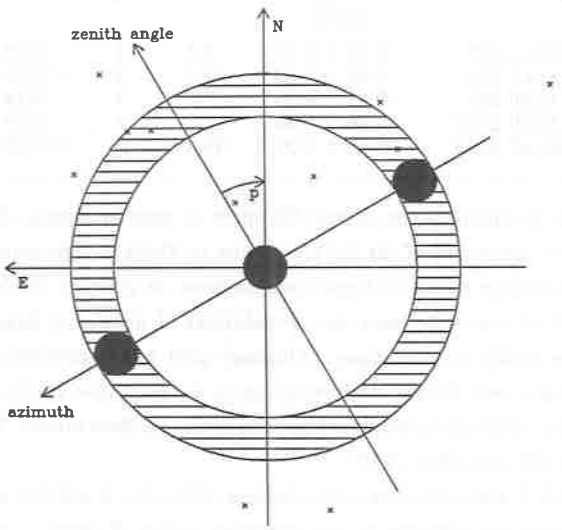

Figure 1. The observing strategy using the OVRO 40-m telescope and position-switching in azimuth, demonstrated for observations of a point 7 arcmin south of the nominal centre of Abell 665. The locations of radio sources (from Moffet & Birkinshaw 1989) near Abell 665 are marked with crosses. As the sky rotates relative to the azimuth/elevation coordinate system, the telescope is switched so that it spends time $\tau/4$ with the main beam on source (and the reference beam off source to the west), then $\tau/2$ with the reference beam on source (and the main beam off source to the east), then $\tau/4$ with the main beam on source again, so that the off-source points rotate about the on-source point. After an observation of many τ-cycles ($\tau = 40$ sec for most observations) the net signal is the difference between the brightness on the source and on the reference arcs. Note that this mode of observing tends to modulate the signals contributed by radio sources lying near the reference arcs according to the parallactic angle, p.

and a final 10 sec with the 'main' beam on source again. The remainder of the time is spent moving and steadying the telescope. During each 'on' or 'off' segment of the cycle, the difference between the brightnesses in the two beams is recorded, and the mean brightness difference between the central point and the reference points is stored at the end of each cycle. Although this method of observing is efficient at subtracting atmospheric (and many systematic) signals, the overall system noise temperature is significantly increased in poor weather.

The sizes of the primary beams and the beam separation also restrict the choice of clusters that can be observed efficiently. Small clusters fill only a small fraction of the primary beams, and large clusters show little change on brightness over the beam separation: in either case the net signal in a beam-switched experiment is small. Adopting

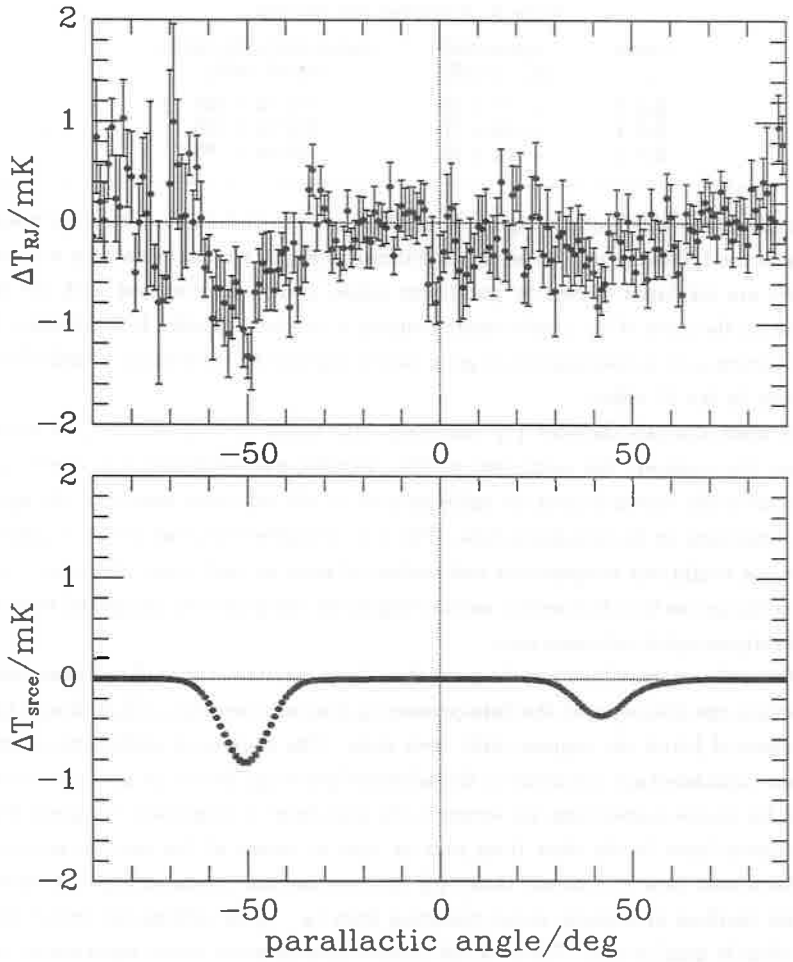

Figure 2. The upper panel shows the SZ data taken at a point 7 arcmin from the nominal centre of Abell 665 binned by parallactic angle. Significant structure can be seen near parallactic angles $-50°$ and $+45°$ (note that since the beams occupy an angle of about 15° on the reference arcs, only groups of about 15 points are independent samples of the sky although all points contain independent data). The lower panel shows the predicted scan, based on the multi-frequency VLA survey of Abell 665 by Moffet & Birkinshaw (1989). The locations and brightnesses of the two main sources agree well with the values found directly from the SZ data.

the same β-model for clusters that was used earlier ($\beta = 0.8$, $r_{cx} = 500$ kpc), it is found that the OVRO 40-m telescope is most efficient (detecting more than 60 per cent of the central SZ effect of a cluster) at redshifts between about 0.1 and 0.5. Good efficiency is achieved for clusters at redshifts greater than about 0.05.

Table 4. Reference sky results

name	measured ΔT_{RJ} (μK)	maximum systematic signal (μK)
Ref 1	$+ 58 \pm 42$	-117 to $+194$
Ref 3	$+115 \pm 77$	-249 to $+195$
Ref 5	$+ 44 \pm 43$	-188 to $+ 83$

An advantage of this observing method is that sources in the reference arcs produce an identifiable modulated signal. An example is shown in Fig. 2, where the data for a point near Abell 665 are displayed binned by parallactic angle, and then compared with the signals predicted on the basis of an interferometric survey of the field (Moffet & Birkinshaw 1989). For full accuracy, it is necessary that good source surveys be conducted in each field that is observed in the SZ effect.

The data analysis includes (1) removing data taken in bad weather, or when the telescope, the receiver, the computer, or the operator had problems; (2) rejecting data that are seriously contaminated by radio sources in the reference arcs; and (3) applying source corrections to the remaining data. The (much smaller) data-set is then combined to estimate the brightness temperature and statistical error at each point observed, but note that step (2) means that the results are not brightness temperatures compared with points on uniformly-sampled reference arcs.

Systematic errors, which may be present in these results because of problems with the observations, the telescope, or the data-processing, can only be estimated, although control observations of blank sky regions limit their sizes. The sources of systematic error that have been considered are (a) errors in the telescope pointing; (b) errors in the radio source list used for source corrections; (c) errors in the zero level of brightness temperature; and (d) the discordance in the data from year to year in excess of the random errors. The results tabulated here incorporate factor (d) into the random errors, and specify maximum ranges for residual systematic errors resulting from (a – c) by adding the errors directly (rather than in quadrature). The strictest control on systematic errors *must* always be the comparison of results from independent measurements by different observers using varied techniques on several telescopes.

Consider first the results for three regions of blank sky, observed as controls on the experiment (Table 4). It is clear that the results are close to zero (they all lie within the maximum systematic error range), and that there is no large negative offset in the measurements (a 'fake' SZ effect caused by systematic errors). The maximum possible systematic errors on these results are large because only short radio source surveys have been done in these fields. These reference regions lie far from any target cluster, and constitute distant controls on the performance of the system. Closer controls on the systematic errors are also important, since systematic errors due to spillover may be sensitively dependent on the sampling in azimuth and elevation.

A number of clusters of galaxies have been observed at OVRO: the results at their

Table 5. Cluster centre results

name	measured $\Delta T_{\rm RJ}$ (μK)	maximum systematic signal (μK)
0016+16	-407 ± 70	-31 to $+137$
Abell 401	-222 ± 97	-195 to $+229$
0302+17	-376 ± 116	-317 to $+475$
Abell 586	-694 ± 236	-447 to $+475$
Abell 665	-292 ± 32	-119 to $+50$
Abell 669	$+78 \pm 194$	-253 to $+121$
Abell 1413	-183 ± 95	-168 to $+238$
Abell 1704	-215 ± 61	-244 to $+364$
1358+62	-119 ± 101	-395 to $+134$
1512+36	-558 ± 158	-519 to $+301$
1558+41	-13 ± 141	-256 to $+228$
1559+41	-159 ± 224	-454 to $+236$
1602+432	-36 ± 65	-277 to $+230$
1602+434	$+54 \pm 126$	-279 to $+230$
Abell 2218	-385 ± 37	-106 to $+35$
Abell 2397	-132 ± 69	-278 to $+227$

nominal centres are collected in Table 5 (which supercedes the measurements reported in Birkinshaw 1990) and illustrated in Fig. 3. Detections of the SZ effect at the 3σ level have been achieved in clusters 0016+16, 0302+17, Abell 665, Abell 1704, 1512+36, and Abell 2218 if only the random errors are considered. However, the systematic error limits are large for clusters where extensive radio source surveys have not been performed, so that it is only for 0016+16, Abell 665, and Abell 2218 that detections are claimed on the basis of these data. These three detections are consistent with other recent observations of these clusters (see Table 2) — in particular, Uson's (1985, 1987) observations with the NRAO 130-ft telescope (with similar operating characteristics to the OVRO 40-m telescope, but a different observing strategy) are in good agreement with the results in Table 5.

Although these cluster centre results are of interest, the main emphasis of the observations at OVRO has been the measurement of the angular structure of the SZ effect. Measurements were made on NS lines through the nominal centres of 0016+16, Abell 665 and Abell 2218, with results as displayed in Figure 4. For each of the clusters there is a significant dip in the temperature of the microwave background radiation towards the cluster centre. For Abell 665, this dip is offset ≈ 2 arcmin from the cluster centre — a similar offset in the X-ray emission was found independently, after the SZ offset was discovered. The close coincidences between the centres of the X-ray structures and the SZ profiles constitutes strong evidence for the reality of the SZ effect.

IMPLICATIONS OF THESE RESULTS

The microwave background radiation

From Table 5 it appears that not all clusters of galaxies display SZ effects $\Delta T(0) < -1$ mK, but it seems likely that many rich clusters should display SZ effects at a level $\Delta T(0) \approx -0.5$ mK. The integrated effect from clusters should then produce an SZ confusion level

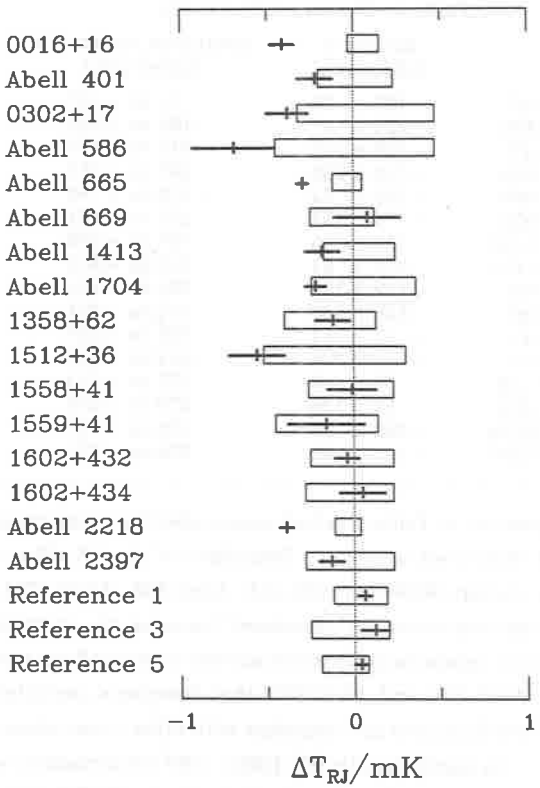

Figure 3. The results for the reference sky observations (Table 2) and the cluster centres (Table 3) presented graphically. The boxes indicate the maximum ranges of systematic errors that may be present in the data, and the crosses represent the measured brightness temperatures with their $\pm 1\sigma$ errors. A detection of the SZ effect is claimed when a cross lies significantly below the systematic error box.

$\approx 30\ \mu$K on arcminute angular scales (Rephaeli 1981). This SZ confusion may complicate the search for arcminute-scale primordial anisotropies in the background radiation, and the integrated SZ effect of clusters will appear in spectral observations of the background radiation at a level $y \approx 10^{-5}$.

Non-cosmological models for the origin of the MWBG can also be limited by these data. The detection of an SZ effect towards 0016+16, which lies at redshift 0.54, proves that a large fraction of the microwave background radiation originates at greater redshifts.

The intracluster medium

The results for the clusters in Table 2 may be studied in terms of the intracluster medium, with the assistance of X-ray data from the *Einstein*, *EXOSAT*, and *Ginga* satellites. In most cases, however, the fractional errors in the SZ data are large, and they contribute

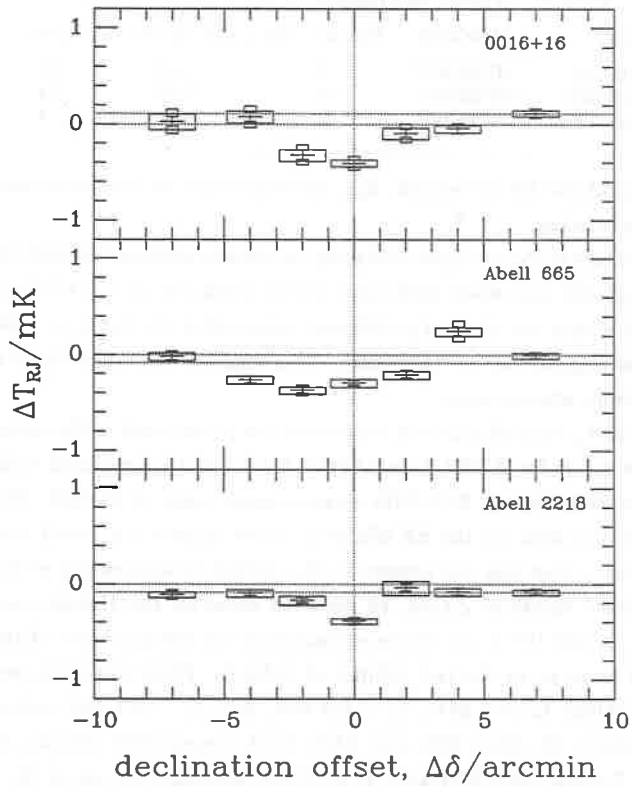

Figure 4. The scan results for 0016+16, Abell 665, and Abell 2218. The declination offsets of each point are measured with respect to a nominal centre for the cluster, and the cross with error bars represents the scan result with $\pm 1\sigma$ errors. The box around each point indicates the *maximum* estimated additive systematic error, and the small boxes at the ends of the error bars indicate the increase in the error suggested by the year-to-year discordance in the data. The horizontal dotted lines indicate the systematic error on the overall zero level. The point 4 arcminutes north of the nominal centre of Abell 665 is contaminated by a variable radio source, which renders the data here strongly discordant. Note that the centre of the SZ effect in Abell 665 lies about 2 arcmin south of the nominal cluster centre: a similar offset is seen in the X-ray image of the cluster.

little that is new. This is not the case for the three scanned clusters of Fig. 4, where the structural information as well as the central SZ decrement may be used to constrain models of the cluster atmospheres. As an example, the data of Fig. 4 have been fitted to isothermal β-models (6), assuming $\beta = 0.8$, and allowing the location of the centre of the gas distribution and the value of θ_{cx} to vary (the data are not sufficiently precise for β and θ_{cx} to be estimated independently). The results from this fit are given in Table 6, which reports the fitted declination of the centre of the gas distribution, $\delta(1950)$, the full-width

Table 6. Derived parameters for the scanned clusters

cluster	$\delta(1950.0)$	θ_{SZ}/arcmin	$\Delta T(0)$/mK	T_e/keV
0016+16	16°08′45″	2	−1.09	10
Abell 665	66°02′15″	8	−0.67	12
Abell 2218	66°18′00″	2	−0.78	8

at half maximum of the SZ decrement, θ_{SZ}, and the depth of the decrement, $\Delta T(0)$, for each of the three clusters.

The fitted values of θ_{SZ} in Table 6 display no simple relationship with the redshift of the cluster. Abell 665 and Abell 2218 have similar redshifts ($z \approx 0.18$) but the angular sizes of their SZ effects are distinctly different, while 0016+16 (at $z = 0.54$) has an SZ effect of a similar angular size to Abell 2218. This suggests that these three clusters have intrinsically different atmospheres.

If the value of θ_{cx} is fixed for these clusters at the values used in the deconvolutions of Table 2, the new values for $\Delta T(0)$ deduced from the scans are consistent with the average values calculated *excluding all 20.3-GHz measurements made at OVRO*. Thus it appears that the more recent data on the SZ effects in these clusters (at least) are achieving a degree of consistency that was not present in the earliest measurements of the SZ effect.

Using the fitted values of $\Delta T(0)$, an assumed value for the Hubble constant ($H_0 = 50\ \mathrm{km\,s^{-1}\,Mpc^{-1}}$), and the X-ray fluxes, estimates of the temperatures of the cluster gas can be obtained as given in the last column of Table 6. These are consistent within the errors with the values $T_e > 6$ keV, $T_e = 9.5$ keV, and $T_e = 6.7$ keV deduced from the X-ray data for 0016+16, Abell 665, and Abell 2218, respectively (White, Silk & Henry 1981; Hughes & Tanaka 1990; McHardy *et al.* 1990), although the use of the fluxes rather than the X-ray images introduces large errors into the method. The consistency of these results suggests that the velocity SZ effect is not significant for these clusters — but since this corresponds to their peculiar velocities only being less than about $5 \times 10^3\ \mathrm{km\,s^{-1}}$, this is not particularly informative.

The accuracy of the SZ effect data must be improved if further information on the properties of the cluster gas is to be obtained. This will be difficult, because the remaining major sources of error are systematic. A good strategy would be to image the clusters using a small interferometer (e.g. Saunders 1988). A first experiment might attempt to produce maps of the clusters with similar quality to the *Einstein* X-ray images. This requires a sensitivity $\approx 30\ \mu$K in a 20-arcsec diameter synthesized beam, which could be achieved at cm-wavelengths by long observations with an array of small antennas.

The Hubble constant

The value of the Hubble constant can be deduced by comparing the SZ and X-ray data for the best-studied clusters. A detailed discussion of this process for Abell 665 is given by Birkinshaw *et al.* (1990) who find a value of the Hubble constant near $55\ \mathrm{km\,s^{-1}\,Mpc^{-1}}$ with a formal statistical error of about $\pm 15\ \mathrm{km\,s^{-1}\,Mpc^{-1}}$. Values of H_0 as large as

100 $\mathrm{km\,s^{-1}\,Mpc^{-1}}$ are permitted only if the SZ and X-ray data contain the maximum estimated systematic errors.

The accuracy of this method is limited by the assumptions involved in determining the constant of proportionality in equation (9), although a major contribution to the error arises from the error in ΔT_{RJ}. The problem is that while the X-ray data are sensitive to the highest-density, central, gas in the cluster, the SZ data are sensitive to the low-density, outer, gas. The constant of proportionality in equation (8) relates the properties of the gas in these regions through a simple model (equation 6), but there is no reason to suppose that such a simple model is an adequate representation of the global properties of the cluster atmosphere. A degree of confidence in the use of equation (6) to describe the gas is gained when several clusters are studied if the results are consistent with one another. McHardy *et al.* (1990) suggest a value of H_0 close to 30 $\mathrm{km\,s^{-1}\,Mpc^{-1}}$ based on Abell 2218, and only a limit $H_0 > 30$ $\mathrm{km\,s^{-1}\,Mpc^{-1}}$ can be found from the data for 0016+16 until a good X-ray spectrum of the cluster becomes available. Thus there is no inconsistency in the result for H_0 at present (although the value that is implied is rather low), but the method has not yet been subjected to a critical test.

ACKNOWLEDGEMENTS

This material is based upon work that has been partially supported by the National Science Foundation under Grant numbers AST-8815131 and AST-9005038. The Government has certain rights in this material.

REFERENCES

Andernach, H., Schallwich, D., Sholomitski, G.B. & Wielebinski, R., 1983. *Astr. Astrophys.*, **124**, 326.

Andernach, H., Schlickeiser, R., Sholomitski, G.B. & Wielebinski, R., 1986. *Astr. Astrophys.*, **169**, 78.

Birkinshaw, M., 1979. *Mon. Not. R. astr. Soc.*, **187**, 847.

Birkinshaw, M., 1989. In *Gravitational Lenses*, 59; eds Moran, J., Hewitt, J. & Lo, K.Y.; Springer-Verlag, Berlin.

Birkinshaw, M., 1990. In *The Cosmic Microwave Background: 25 Years Later*, 77; eds Mandolesi, N. & Vittorio, N.; Kluwer, Dordrecht.

Birkinshaw, M. & Gull, S.F., 1984. *Mon. Not. R. astr. Soc.*, **206**, 359.

Birkinshaw, M., Gull, S.F. & Hardebeck, H., 1984. *Nature*, **309**, 34.

Birkinshaw, M., Gull, S.F. & Northover, K.J.E., 1981. *Mon. Not. R. astr. Soc.*, **197**, 571.

Birkinshaw, M., Hughes, J.P & Arnaud, K.A., 1990. In preparation.

Cavaliere, A., Danese, L. & De Zotti, G., 1979. *Astr. Astrophys.*, **75**, 322.

Cavaliere, A. & Fusco-Femiano, R., 1976. *Astr. Astrophys.*, **49**, 137.

Cavaliere, A. & Fusco-Femiano, R., 1978. *Astr. Astrophys.*, **70**, 667.

Chase, S.T., Joseph, R.D., Robertson, N.A. & Ade, P.A.R., 1987. *Mon. Not. R. astr. Soc.*, **225**, 171.

Dyer, C.C., 1976. *Mon. Not. R. astr. Soc.*, **175**, 429.

Gunn, J.E., 1978. In *Observational Cosmology*, 1; eds Maeder, A., Martinet, L. & Tammann, G.; Geneva Obs., Sauverny, Switzerland.

Hughes, J.P. & Tanaka, Y., 1990. In preparation.

Lake, G. & Partridge, R.B., 1980. *Astrophys. J.*, **237**, 378.

Lasenby, A.N. & Davies, R.D., 1983. *Mon. Not. R. astr. Soc.*, **203**, 1137.

Mather, J.C., Cheng, E.S., Eplee, R.E.Jr., Isaacman, R.B., Meyer, S.S., Shafer, R.A., Weiss, R., Wright, E.L., Bennett, C.L., Boggess, N.W., Dwek, E., Gulkis, S., Hauser, M.G., Janssen, M., Kelsall, T., Lubin, P.M., Moseley, S.H.Jr., Murdock, T.L., Silverberg, R.F., Smoot, G.F. & Wilkinson, D.T., 1990. *Astrophys. J.*, **354**, L37.

McHardy, I.M., Stewart, G.C., Edge, A.C., Cooke, B.A., Yamashita, K. & Hatsukade, I., 1990. *Mon. Not. R. astr. Soc.*, **242**, 215.

Meyer, S.S., Jeffries, A.D. & Weiss, R., 1983. *Astrophys. J.*, **271**, L1.

Moffet, A.T. & Birkinshaw, M., 1989. *Astr. J.*, **98**, 1148.

Nottale, L., 1984. *Mon. Not. R. astr. Soc.*, **206**, 713.

Parijskij, Yu.N., 1972. *Astr. Zhurn.*, **49**, 1322.

Partridge, R.B., Perley, R.A., Mandolesi, N. & Delpino, F., 1987. *Astrophys. J.*, **317**, 112.

Perrenod, S.C. & Lada, C.J., 1979. *Astrophys. J.*, **234**, L173.

Radford, S.J.E., Boynton, P.E., Ulich, B.L., Partridge, R.B., Schommer, R.A., Stark, A.A., Wilson, R.W. & Murray, S.S., 1986. *Astrophys. J.*, **300**, 159.

Rephaeli, Y., 1981. *Astrophys. J.*, **245**, 351.

Rephaeli, Y., 1990. In *The Cosmic Microwave Background: 25 Years Later*, 67; eds Mandolesi, N. & Vittorio, N.; Kluwer, Dordrecht.

Rudnick, L., 1978. *Astrophys. J.*, **223**, 37.

Saunders, R.D.E., 1988. In *The Post-Recombination Universe*, 187; eds. Kaiser, N. & Lasenby, A.N.; Kluwer, Dordrecht.

Schallwich, D., 1979. Poster presented at IAU Symposium **97**, *Extragalactic Radio Sources*, Albuquerque, New Mexico.

Silk, J.I. & White, S.D.M., 1978. *Astrophys. J.*, **226**, L103.

Sunyaev, R.A. & Zel'dovich Ya.B., 1972. *Comm. Astrophys. Sp. Phys.*, **4**, 173.

Sunyaev, R.A. & Zel'dovich Ya.B., 1980a. *Ann. Rep. Astr. Astrophys.*, **18**, 537.

Sunyaev, R.A. & Zel'dovich Ya.B., 1980b. *Mon. Not. R. astr. Soc.*, **190**, 413.

Uson, J., 1985. *Observational and Theoretical Aspects of Relativistic Astrophysics and Cosmology*, 269; eds Sanz, J.L. & Goicoechea, L.J.; World Scientific Publ. Co.

Uson, J., 1987. NRAO GreenBank Workshop **16**, 255; eds O'Dea, C. & Uson, J.; NRAO GreenBank, WV.

White, S.D.M., Silk, J.I. & Henry, J.P., 1981. *Astrophys. J.*, **251**, L65.

THE HIGH–ENERGY COSMIC BACKGROUND RADIATIONS

Xavier Barcons
Departamento de Física Moderna, Universidad de Cantabria, 39005 Santander, Spain

ABSTRACT

Our current level of observational knowledge and understanding of the X–ray and γ–ray cosmic background radiations is reviewed. The contribution of known sources to the background is discussed and some models for the 'residual' background are summarized. Especial emphasis is made on the isotropy of the background on both large and small angular scales and on its importance in the study of the structure of the Universe at the 'galaxy formation' epoch. Future prospects concerning space projects are discussed.

1. INTRODUCTION

Besides being the confirmation of the Big Bang theory, the Microwave Background Radiation (MBR) is so relevant in modern Cosmology because it provides a picture of the epoch $z \sim 10^3$ just when matter and radiation decoupled and gravitating structures began to grow. The X–Ray Background (XRB) and the γ–Ray Background (GRB) can only arise after the Universe has undergone some nonlinear evolution and therefore provide us with an integrated picture of more recent epochs ($z \lesssim 10$). As it will be argued here, some details of the link between an extremely uniform Universe at $z \sim 10^3$ and an extremely lumpy one at $z \sim 0$ can be learned by studying the XRB and the GRB.

The XRB was actually discovered in 1962[1] during a rocket flight which also found the first extra–solar X–ray source (Sco X–1). The spectrum of the XRB (see Fig. 1) is now well determined in the 3–300 keV band from the HEAO–1 A2 and A4 experiments[2,3], where its remarkable isotropy at high galactic latitudes reflects an extragalactic origin. In the 2–10 keV band, a good fit to the XRB spectrum is provided by a power law with energy spectral index $\alpha \sim 0.4$. At energies below 3 keV, only upper limits to the extragalactic intensity are known, since the galactic contribution becomes important even at high galactic latitude[4] and actually, below 0.3 keV the observed XRB is though to arise in a local bubble ~ 100 pc accross. The best available data on the GRB spectrum still comes from the HEAO–1 A4 experiment[3] in the 0.1–10 MeV band and form SAS–2[6] at energies 30–100 MeV. The spectrum shows an excess at ~ 1 MeV (the MeV bump) and a very steep slope above ~ 30 MeV. The extragalactic origin of most of this radiation was first demonstrated back in the 70's with the use of a double–Compton telescope[7]. Since most of the energy in the high–energy backgrounds is concentrated below the spectral break at ~ 30 keV and there is significantly more and better data available in this band, most of our discussion will refer to it.

The first explanation for the origin of the extragalactic XRB was given by Hoyle[8] in terms of thermal bremsstrahlung of a hot intergalactic medium within the steady–state cosmology. This model was soon rejected[9], but later re–adapted to the standard Big Bang cosmology[10,11]. Aside the requirement of a high baryonic density Universe ($\Omega_b \sim 0.25$) and a rather high energy budget, this model predicted spectral distortions in the submillimeter region of the MBR[12], whose existence has been ruled out by COBE[13].

The remaining generic model is that the XRB and the GRB arise as the integrated emission from extragalactic sources. It was soon realized[14] that if all QSO had the same X–ray to optical luminosity ratio as 3C273, these objects would saturate the XRB. Actually, extragalactic objects, and especially clusters of galaxies and AGN are strong X–ray emitters

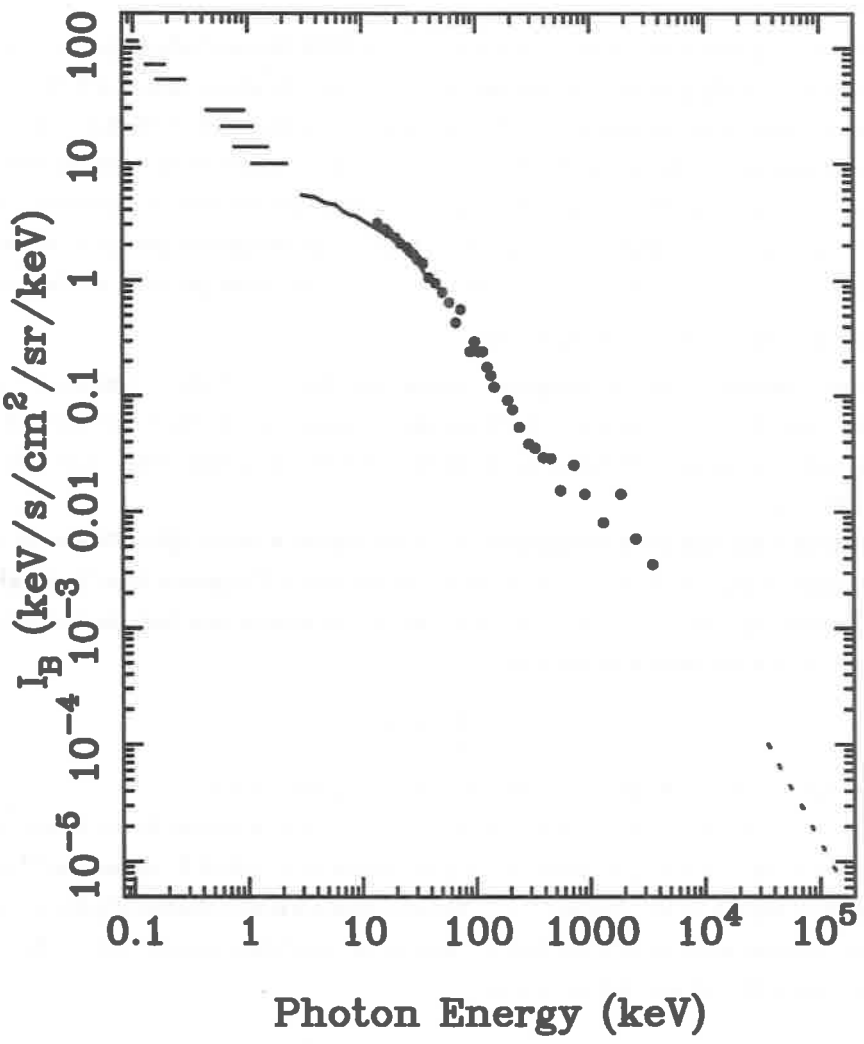

Figure 1. The spectrum of the cosmic high–energy background radiations (see text for details). Upper limits below 3 keV are from the Wisconsin group[5], the solid line from HEAO–1 A2[2], dots from HEAO–1 A4[3] and the dotted curve from SAS–2[6].

(AGN being also γ–ray emitters), but what fraction they contribute to the high–energy backgrounds is very strongly dependent on the faint end of their luminosity functions and their evolution, and therefore unkown. These points are discussed in Section 2, while Section 3 summarizes some of the physical models for the (yet undiscovered) sources of most of the XRB.

Section 4 presents the large–scale features of the XRB. Section 5 shows how to analyze fluctuations in integrated backgrounds and how they relate to source counts and their clustering on scales below the beamsize, with special emphasis to the XRB. In Section 6 measurements of angular correlations in the intensity of the XRB are presented and their importance towards the understanding of the large–scale structure of the Universe is highlighted. Section 7 summarizes our current knowledge of the high energy background radiations and some prospects for the future (in connection with X–ray and γ–ray space projects) are discussed.

2. EXTRAGALACTIC FOREGROUNDS

Most extragalactic sources, ranging from 'normal' galaxies[15] to clusters of galaxies[16] and AGN[17] emit X–rays. In addition, AGN are also supposed (and in some cases seen) to be γ–ray emitters, whose contribution to the GRB could be substantial (Refs. 18,19, but see Refs. 20, 21).

The flux distribution of extragalactic sources is described by the $N(>S)$ relation, i.e., the number of sources (here per square degree) which have a flux greater than S in a given band. Note that $N(>0)$ is the total surface density of sources and that the background intensity, in the corresponding band can be written as

$$I_B = \int S\, n(S)\, dS \tag{1}$$

where $n(S) = -dN(>S)/dS$ is the differential source counts function.

Some flux–limited samples of extragalactic sources exist in several X–ray bands. The HEAO–1 A2 all–sky survey provided a complete sample of 2–10 keV X–ray sources[22] with fluxes $S(2-10) > 3.1\times10^{-11}$ erg cm^{-2} s^{-1}. These sources are mostly clusters of galaxies (with typical temperatures $\sim$ 6 keV) and Seyferts (with energy spectral index $\alpha(2-10) \sim 0.6-0.8$). Source counts fit well a euclidean relation

$$N(>S) = 3.4 \times 10^{-19}\, S(2-10)^{-1.5}\ \mathrm{deg}^{-2} \tag{2}$$

At smaller energies (1–3 keV), the *Einstein Observatory* provided several surveys at different flux limits: the Medium Sensitivity Survey[23], its extension[24,25] and the Deep Survey[26] and its revision[27]. The sources in the Medium Sensitivity Surveys are mostly clusters of galaxies (with typical temperatures $<$ 6 keV) and and different types of AGN[25].

The Deep Survey shows that the faintest sources at its limiting sensitivity ($S(1-3) > 2.6 \times 10^{-14}$ erg cm^{-2} s^{-1}) are mostly QSO[28] whose spectra have energy spectral index $\alpha(0.3-3) \gtrsim 1$, except for the radio–loud QSOs which have flatter X–ray spectra[29,30]in this band. All of the *Einstein Observatory* surveys are consistent with

$$N(>S) = 1.4 \times 10^{-19}\, S(0.3-3)^{-1.5}\ \mathrm{deg}^{-2} \qquad (3)$$

Comparison of (3) and (2), taking into account that $S(2-10) \approx S(0.3-3)$ for $\alpha \sim 0.7$, shows that ~ 3 times less sources are detected by the *Einstein Observatory* than expected, assuming that (2) can be extrapolated down to the Medium Sensitivity Survey flux (see Section 5). Several facts might contribute to this discrepancy: AGN could be absorbed at low energies[31] and high–luminosity low surface brightness clusters could be missed in the *Einstein* surveys.

In any case, the contribution of known X–ray sources is small: even the Deep Survey (which already detected $\sim$ 19 sources deg^{-2}) only accounts for $\sim$ 25 per cent of the 1–3 keV XRB, assuming that the extragalactic background flux in this band is given by an extrapolation of the XRB above 3 keV with a $\alpha = 0.4$ power law spectrum (see however Refs. 4,32). The origin of the *residual* background is one of the most striking and still open cosmological problems, since the brightest sources have a spectrum much steeper than the XRB below $\sim$ 30 keV and the residual XRB is much flatter than the spectrum of any known extragalactic X–ray source.

As fas as the GRB is concerned, the situation is even more controversial, since the most reliable information about the $N(>S)$ relation in that band comes from extrapolations of the X–ray source counts. It must also be mentioned that it is difficult to reconcile a high fraction of both the XRB and the GRB being produced by AGN, because the break at 30 keV shown by the background spectrum is not exhibited by any of the few AGN with known spectrum at this energy. It then appears that the foreground created by known high–energy extragalactic sources leaves a residual spectrum for the XRB and the GRB whose shape does not seem to fit with any known type of source.

3. MODELS FOR THE ORIGIN OF THE HIGH–ENERGY BACKGROUNDS

As already mentioned, the absence of distortion in the spectrum of the MBR rules out the possibility that a hot uniform intergalactic medium ($T_{IGM} \gtrsim 10^8$ K, $\Omega_{IGM} \sim 0.25$) produces the 3–100 keV XRB. Pressure confinement of this gas might provide an explanation for the MeV bump[12] but would produce more distortion in the MBR spectrum[33]. Independently of the clumping mechanism, upper limits on the Compton distortion y–parameter in the MBR and the absence of anisotropies on $\sim$arcmin scales, restrict the regions containing this gas to $\lesssim 1$ Mpc[34], which leads again to a discrete source model for the background.

A phenomenological model for the spectrum of 'universal' AGNs, whose integrated emission would give rise to the high–energy background, has been recently studied[35]. The steep spectrum invariably shown by all known extragalactic X–ray sources at energies $< 3\,\mathrm{keV}$ is a real problem for such models since the total (galactic plus extragalactic) background intensity at $\sim 0.25\,\mathrm{keV}$ can be easily violated[36]. It has also been argued that the radio properties of QSOs are only due to differences in the orientation of the thick accretion torus, in which case most low–luminosity AGN could be hidden, but providing enough flux for the background even with a right spectral shape[37].

As an alternative to these models, spectral evolution might also be able to explain the shape of the residual background (see Ref. 38 for a discussion) Precursor AGN have been often considered[39,40,41,42] and still remain a good possibility. The XRB would in this case come from early epochs $z \gtrsim 2$.

The break at $\sim 30\,\mathrm{keV}$ in the XRB spectrum is still a major problem. Since galactic X–ray binaries seem to have a hard spectrum with a cutoff at $\sim 10 - 40\,\mathrm{keV}$, low metallicity massive star–forming galaxies (where these objects would be more abundant) have been proposed as candidates for the XRB[43]. These objects would be well correlated with the IRAS starburst galaxies and in this case the XRB would arise at $z \lesssim 1$.

Other models have also been proposed. The $\sim 30\,\mathrm{keV}$ break could just be a redshifted $\sim 511\,\mathrm{keV}$ break in AGN where electron–positron pairs are important[44,45]. Such models require that these sources produce the background in a very narrow redshift range, because otherwise the spectral agreement disappears. However, a more recent model, in which X–rays in AGN are reflected by a thick accretion torus, produce a natural break at 10–50 keV[46]. In that model the XRB could come from everywhere at $z \lesssim 5$.

The origin of the GRB has some problems too. First, the mean energy spectral index for AGN connecting the X–ray and γ–ray bands cannot be too steep in order to have some flux in the GRB[19,20]. The MeV bump is anyway difficult to reproduce in this framework[20], and a steepening of the typical AGN spectrum is required at $\gtrsim 30$ MeV by the GRB.

4. LARGE–SCALE ISOTROPY

At X–ray energies, the galaxy dominates the large–scale features in the sky[47,48,49]. In the 2–10 keV band (where we have the most reliable results), the galactic contribution is only important at $|\, b \,| < 20^{\circ}$ and can be removed. A second large–scale anisotropy is expected in the X–ray sky due to the motion of the local group with respect to the isotropic background frame. This is known as the Compton–Getting effect which has the form

$$\left(\frac{\Delta I_B}{I_B}\right)_{CG}(\epsilon,\theta) = \frac{v}{c}\left(3 - \frac{d\ln I_B(\epsilon)}{d\epsilon}\right)\cos\theta \qquad (4)$$

where $I(\epsilon)$ is the background intensity at energy ϵ and v is the peculiar velocity of the local group ($\sim 360\,\mathrm{km\,s^{-1}}$ from the dipole anisotropy of the MBR). The Compton–Getting effect is therefore expected to have an intensity ~ 0.5 per cent at X–ray wavelenghts. A major difference with the MBR dipole anisotropy is comes into play here since in the X–ray band fluctuations due to source confusion noise are grater than the expected dipole anisotropy on any scale $\lesssim 90^o$ and the detection of this systematic effect is more difficult.

Only upper limits were found to this 24–hr anisotropy in the Ariel–V data[47], allowing $v \lesssim 500\,\mathrm{km\,s^{-1}}$ in the 2–18 keV band at 90 per cent confidence. The A2 all sky survey detected (at 95 per cent significance) a dipole signal in the 2–10 keV band, with a velocity $v = 475 \pm 165\,\mathrm{km\,s^{-1}}$ consistent with a Compton–Getting contribution only[49]. The XRB dipole vector could only be detected with a big error circle encompassing the MBR dipole vector. Although its direction is also consistent with the direction of the supergalactic plane, the energy dependence of the dipole amplitude does not agree with a local origin of the XRB[50].

Back to the first attempts to detect large scale structures in the X–ray sky, the Ariel–V data also showed a 2σ 12–hr effect, roughly aligned with the motion of the local group[47] which (if not due to the galaxy) could be showing the enhanced X–ray emission from the 'Great Attractor' which is causing our peculiar velocity. The large uncertainty in the amplitude of the XRB dipole allows this extra contribution to the Compton–Getting effect. In fact, the dipole of the distribution of the HEAO–1 A2 X–ray sources[22] is roughly aligned with the MBR vector and saturates at $z \sim 0.017$. It is quite possible then that the XRB dipole contains both the velocity effect and the direct effect (due to overproduction of X–rays in the direction of the dipole). Detailed cosmological consequences are discussed in Ref. 52.

5. SMALL–SCALE FLUCTUATIONS AND SOURCE COUNTS

Spatial fluctuations in integrated backgrunds are, unlike the ones in the MBR, dominated by source confusion. This means that fluctuations are actually detected but they can be associated to beam–to–beam variations in the number of sources that make up the background and that are not bright enough to be detected as such at the corresponding angular resolution. Clustering of these sources would result in a decrease in the effective number of sources (now clusters of sources) per beam and would therefore increase fluctuations. The distribution of fluctuations for a given beamsize can therefore be used to infer some properties ($N(>S)$, clustering, etc.) of the underlying source populations.

5.1 The $P(D)$ curve

One invariable feature of the distribution of fluctuations (the $P(D)$ curve, where D is the deflection or deviation from the mean) in the high–energy backgrounds is their non–gaussianity.

Although second moments of this distribution have been sometimes used to measure fluctuations, these are usually dominated by the brightest sources below the detection threshold. It is then much more appropriate to use the whole $P(D)$ distribution.

The relation of fluctuations to source counts in integrated backgrounds has been known for many years[53,54] and it is a very common tool in radio astronomy (see, e.g., Ref 55). Bright sources only appear in the tail of the $P(D)$ distribution, while the most abundant faintest ones only produce increasingly small gaussian noise (central limit theorem). It then happens that the shape of the $P(D)$ curve is dominated by those sources for which there is about ~ 1 source per beam. This corresponds to much fainter levels than usual source detection thresholds, which means that analyses of the $P(D)$ curve can be used to test the $N(>S)$ curve to very faint levels without actually 'detecting' the sources.

Let $G(\vec{n}-\vec{n}')$ be the beam response function, i.e., the ratio between observed and incident flux of a source located in the direction $\vec{n}'$ when the detector points towards $\vec{n}$. The beam response function is normalized in such a way that the effective solid angle (in deg^2) for flux collection is $\Omega_{eff} = \int d\Omega_{\vec{n}'}\, G(\vec{n}-\vec{n}')$. Let us assume that the background is created by a source population with flux distribution given by $n(S)$ point sources per unit flux and square degree, which are uniformly distributed in the sky (i.e., no angular clustering on the beamwidht scale). The expected fluctuations are distributed like [48,54]

$$P(D) = \int d\omega\, \mathrm{e}^{-i\omega(D+\langle I_B\rangle)} \exp\Big(\int d\Omega_{\vec{n}'} \int dS\, n(s)[\mathrm{e}^{i\omega SG(\vec{n}-\vec{n}')} - 1]\Big) \qquad (5)$$

If the number of counts per beam is small, this might need a convolution with Poisson counting noise.

Now, if sources are clustered, the observed $P(D)$ curve would be broader. This possibility is parametrised by convolving eq. (5) with a gaussian of variance σ, which is called the excess variance. The final $P(D)$ curve is then fitted to the data via χ^2 minimisation or likelihood analysis. This allows to find best fit parameters for the source counts $n(S)$ down to the flux level S where $N(>S)/\Omega_{eff} \sim 1$. Since, invariably, no excess variance is found, upper limits on $\frac{\sigma}{\langle I_B\rangle}$ can be used to constrain clustering in the Universe.

5.2 Results in the 2–12 keV band

Early work on *Uhuru* data in the 2–6 keV band showed that the above technique is, under some circumstances, more powerful than standard source counting algorithms in order to determine source counts[56]. Later, with the use of the HEAO–1 A2 database, it was shown[48,49] that eq. (2) could be extrapolated down to $S(2-10) \sim 2\times 10^{-12}\,\mathrm{erg\,cm^{-2}\,s^{-1}}$ and that excess fluctuations on 25 deg^2 beams could not exceed ~ 2 per cent. This upper limit was subsequently used[33,57,58] to find the maximum contribution of clustered X–ray sources to

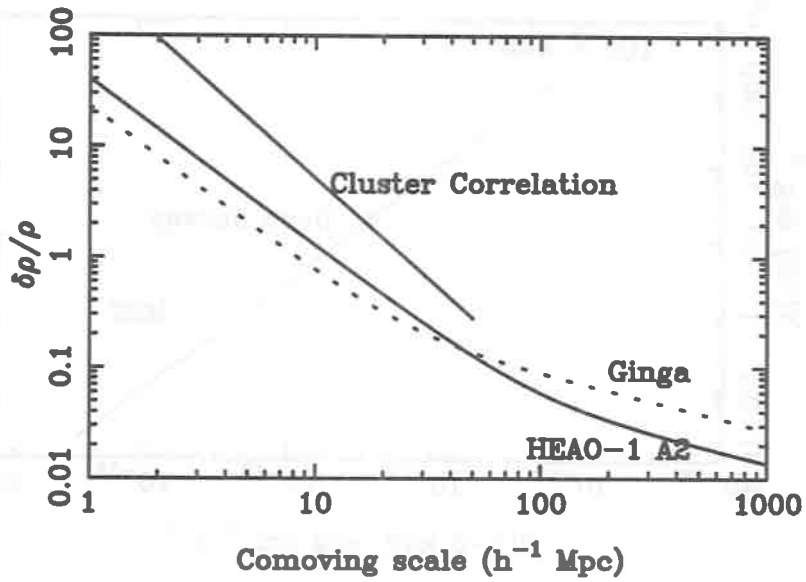

Figure 2. Upper limits to the density fluctuations in the Universe assuming that X–rays trace mass and that the XRB comes from $z = 2 \pm 0.5$, using bounds on excess fluctuations in the XRB. The upper limit from the cluster–cluster correlation function is shown for comparison.

the XRB and to constrain the large–scale lumpiness of the Universe (see below). In particular it was shown that significant clustering of X–ray sources on scales $\gtrsim 10\,h^{-1}$ Mpc is forbidden by the isotropy of the XRB.

Recent work on *Ginga* LAC data in the 4–12 keV band with a $\sim 1^o \times 2^o$ beam has confirmed that source counts, as given in eq. (2), can be extrapolated down to $S(2-10) \sim 10^{-12}\,\mathrm{erg\,cm^{-2}\,s^{-1}}$ (see Refs. 31,59). This confirms the discrepancy between source counts in this band and the Medium Sensitivity Surveys (eq. 3) if the energy spectral index is $\alpha \gtrsim 0.7$. Also, excess fluctuations in this band are seen to be less than 4 per cent on that scale[59].

In order to show the cosmological importance of upper limits on excess fluctuations, let us assume that the XRB comes from a $\Delta z \sim 1$ bin around $z \sim 2$, and that X–ray sources trace mass. With a gaussian model for the beam profile and a gaussian correlation function, a very simple expression can be found for the inhomogeneities $\frac{\delta\rho}{\rho}$ on any scale[33]. Bounds on $\frac{\delta\rho}{\rho}$ are shown in Fig. 2 both for the HEAO–1 A2 and the *Ginga* upper limits on excess fluctuations. The cluster–cluster correlation function is also shown for comparison. It is clear from Fig. 2 that the sources that give rise to the XRB are more smoothly distributed than clusters. Another important conclusion is that at the intermediate redshifts we are considering ($z \sim 2$) and assuming again that X–rays trace mass, the Universe is linear ($\frac{\delta\rho}{\rho} < 1$) on comoving

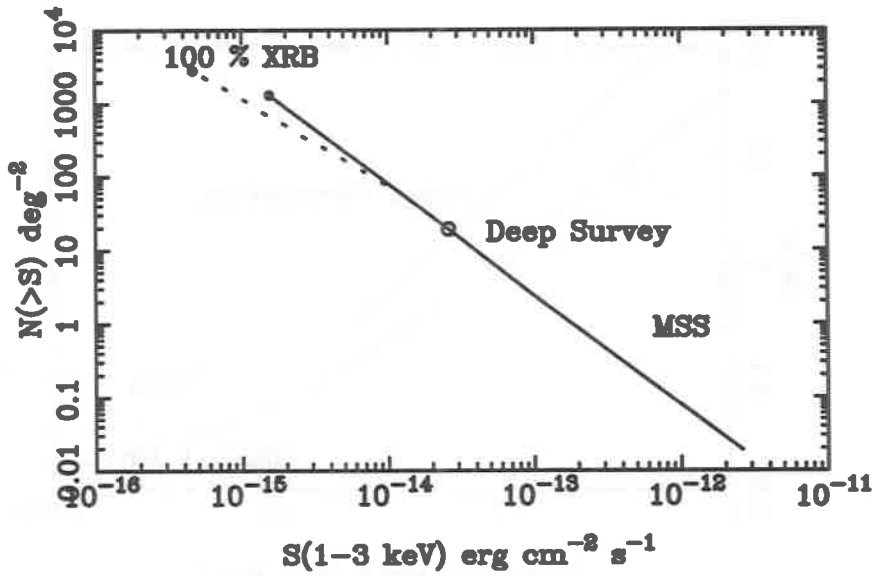

Figure 3. The $N(>S)$ curve in the 1–3 keV band. The XRB level is drawn by assuming an extrapolation from higher energies with an energy spectral index $\alpha = 0.4$. The dotted line represents the extrapolation of the Euclidean law and the dashed line a broken power law with slope -1.2 below $S(1-3) = 1.3 \times 10^{-14}\,\mathrm{erg\,cm^{-2}\,s^{-1}}$.

scales $\gtrsim 10\,\mathrm{h}^{-1}$ Mpc and that we have a direct proof of the smoothness of the Universe on comoving scales $\gtrsim 100\,\mathrm{h}^{-1}$ Mpc.

5.3 Source counts in the 1–3 keV band

The *Einstein Observatory* IPC provided an up to now unique tool to study XRB fluctuations on ~arcmin scales below 3 keV. A few high-galactic latitude deep exposures were used by Hamilton & Helfand[60] to test source counts below the Deep Survey limit. Using Monte Carlo simulations against which they compared the second moment of the $P(D)$ distribution, they concluded that the $N(>S)$ curve cannot be extrapolated down to the flux level where the (extrapolated) 1–3 keV XRB would be saturated, but that these source counts must flatten soon below the Deep Survey limit. Their best fit gives a total surface density of $\sim$ 5000 sources deg^{-2} which is actually a lower limit since sources could be clustered. A subsequent analysis[61] confirmed the presence of a break at $S(1-3) \sim 1.3\times10^{-14}\,\mathrm{erg\,cm^{-2}\,s^{-1}}$ but it was argued that the extent of the Point–Spread–Function in the IPC did not allow to determine the slope of the source counts below that break. In that case, a conservative lower limit of $\sim$ 1500 sources deg^{-2} was found.

So far, these are the most controversial results, since $\sim$ 5000 sources deg^{-2} outnumbers

the surface density of AGN by a huge number, unless once upon a time all galaxies emitted X–rays like AGN. The situation is illustrated in Fig 3.

6. THE SMALL–SCALE CORRELATION FUNCTION OF THE BACKGROUND

A statistic which is particularly sensitive to the clustering and extension of the underlying extragalactic sources is the small–scale autocorrelation function (ACF) of the corresponding background. If $I_B(\vec{n})$ is the background intensity received from a direction given by the unit vector $\vec{n}$ in a given energy band and for a specific beam profile, the ACF is defined as

$$W(\theta) = \frac{\langle [I_B(\vec{n}) - \langle I_B \rangle][I_B(\vec{n}') - \langle I_B \rangle] \rangle}{\langle I_B \rangle^2} \qquad (6)$$

where $\cos\theta = \vec{n}.\vec{n}'$ and the average is taken over all the available pairs of pointings. It is clear that some positive non–cosmic signal in eq. (6) is expected on scales below the beamwidth, so care has to be taken in properly deconvolving this effect.

The background ACF is an integrated measure of the source correlation function convolved with the beam plus some contribution if the angular size of the sources is $\lesssim \theta$. Explicit expressions in terms of source correlation functions, surface brightness profile, luminosity functions and several evolution parameters are given in Refs. 23,62,63. Since up to now all measured ACFs on any angular scale and on any energy band are compatible with zero, upper limits can be used to constrain the clustering amplitude of the sources.

With the HEAO–1 A2 database[64], the ACF of the 2–10 keV XRB at ~ 3 deg was shown to be less than $\sim 4 \times 10^{-4}$ with similar limits on larger angular separations[64]. Some cosmological implications concerning the cluster and AGN correlation functions were drawn[63]. More recent work with a set of pointed exposures with the *Ginga* LAC has shown that in the 4–12 keV band $W(2^o) < 10^{-4}$ which poses stronger limits on clustering amplitudes[65]. In particular, a correlation length $r_0 < 20\,h^{-1}$ Mpc for typical X–ray clusters seems to be a firm limit (consistent with bright X–ray cluster clustering[66]), and it is also concluded that no population of objects with clustering properties similar to those of QSO[67] can produce more than ~ 50 per cent of the 4–12 keV XRB.

On ~arcmin scales, and with the use of a few deep *Einstein Observatory* IPC fields, a signal below 5 arcmin was found, although it is very likely that it is instrumental in origin (overlapping beams)[63]. A 95 per cent confidence upper limit $W(5\,\text{arcmin}) < 0.09$ was found, although it is currently being revised and could be substantially reduced. This corresponds to scales ~ 1 Mpc at a typical redshift ~ 1, which makes these results very interesting for the study of the structure of the Universe on scales of clusters of galaxies.

Table 1. Present and future high–energy observatories

0.1	1.0	10	10^2	10^3	10^4	(keV)
		GINGA (Feb 87)				
	ROSAT (Jun 90)					
				GRANAT (Dec 89)		
				GRO (90 ?)		
	ASTRO D (Mar 93)					
	AXAF (95 ?)					
	XMM (98 ?)					

7. OUTLOOK

Twenty-eight years after the discovery of the high–energy cosmic background radiation, there is no compelling model for its origin. Discrete sources seem to be the only reliable possibility. Although some models for the physics of these sources do exist, we will have to await for more powerful X–ray telescopes to test them.

The isotropy of the high–energy background radiations poses relevant constraints on the large–scale structure of the Universe at the 'galaxy formation' epoch. It might happen that with the new generation of X–ray and γ–ray instruments in space, these backgrounds provide the most direct and stringent constraints on galaxy formation theories.

Table 1 shows the different X–ray and γ ray observatories that are already operating or that will be launched in the foreseeable future. Of especial interest is the ASTRO–D mission which will have a resolution of about $\sim$ 2 arcmin and that with the use of the techniques outlined in Section 5 could be able to almost resolve the XRB (i.e., to test source counts down to almost the saturation level of the XRB)[68]. AXAF and XMM (with resolutions of $\sim$0.5 arcsec and $\sim$ 30 arcsec respectively) would certainly be able to do it, and also to isolate a high fraction of these sources. At γ–ay energies the SIGMA telescope on board of the GRANAT observatory, and the GRO will surely result in a substantial improvement of our knowledge of the sources of the extragalactic GRB and their distribution. Therefore the next decade is going to be crucial towards our understanding of the high–energy background radiations and with a little bit of luck the 1990's might see how an explanation is found for the *first* background radiation discovered.

ACKNOWLEDGEMENTS

I thank Andy Fabian for making possible our collaboration in this field. Partial financial support for this work was provided by the CICYT and the Comisión Mixta Caja Cantabria / Universidad de Cantabria.

REFERENCES

1) Giacconi, R., Gursky, H., Paolini, F. & Rossi, B., *Phys. Rev. Lett.*, **9**, 439 (1962)
2) Marshall, F.E. *et al.*, *Astrophys. J.*, **235**, 4 (1980)
3) Gruber, D.E., Rthschild, R.E., Matteson, J.L. & Kinzer, R.L., *MPE Rep.*, **184**, 129 (1984)
4) Wu, X., Hamilton, T., Helfand, D.J. & Wang, Q., Preprint (1990)
5) McCammon, D. & Sanders, W.T., *Ann. Rev. Astr. Astrophys.*, **28**, 657 (1990)
6) Fichtel, C.E., Simpson, G.A. & Thompson, D.J., *Astrophys. J.*, **222**, 833 (1978)
7) Schönfelder, V. & Lichti, G., *Astrophys. J.*, **191**, L1 (1974)
8) Hoyle, F., *Astrophys. J.*, **137**, 993 (1963)
9) Gould, R.J. & Burbidge, G.R., *Astrophys. J.*, **138**, 969 (1963)
10) Cowsik, R. & Kobetich, E.J., *Astrophys. J.*, **177**, 585 (1972)
11) Barcons, X., *Astrophys. J.*, **313**, 547 (1987)
12) Guilbert, P.W. & Fabian, A.C., *Mon. Not. R. astr. Soc.*, **220**, 439 (1986)
13) Mather, J.C. *et al.*, *Astrophys. J.*, **354**, L437 (1990)
14) Setti, G. & Woltjer, L., *Astr. Astrophys.*, **76**, L1 (1979)
15) Fabbiano, G., *Ann. Rev. Astr. Astrophys.*, **27** (1989)
16) Sarazin, C.L., *Rev. Mod. Phys.*, **58**, 1
17) *23rd ESLAB Symposium, Two Topics on X-ray Astronomy: 2. AGN and the X-ray background.* ESA SP-296, Vol. 2 (1989)
18) Bignami, G.F., Fichtel, C.E., Hartman, R.C. & Thompson, D.J., *Astrophys. J.*, **232**, 649 (1979)
19) Mereghetti, S., *Astrophys. J.*, **354**, 58 (1990)
20) Gao, Y.–T., Cline, D.B. & Stecker, F.W., *Astrophys. J.*, **357**, L1 (1990)
21) Cline, D.B. & Gao, Y.–T., *Astrophys. J.*, **348**, 33 (1990)
22) Piccinotti, G. *et al.*, *Astrophys. J.*, **253**, 485 (1982)
23) Gioia, I.M. *et al.*, *Astrophys. J.*, **283**, 495 (1984)
24) Gioia, I.M. *et al.*, *Astrophys. J. Suppl.*, **72**, 567 (1990)
25) Stocke, J. *et al.*, Preprint (1990)
26) Giacconi, R. *et al.*, *Astrophys. J.*, **234**, L1 (1979)
27) Primini, F.A. *et al.*, Preprint (1990)
28) Griffths, G.E. *et al.*, *Astrophys. J.*, **283**, 495 (1983)
29) Wilkes, B.J. & Elvis, M., *Astrophys. J.*, **323**, 243 (1987)
30) Canizares, C.R. & White, J.L., *Astrophys. J.*, **339**, 27 (1989)
31) Warwick, R.S. & Stewart, G.C., Ref. 17, p. 727
32) Garmire, G. & Nousek, J., *Bull. Am. Astr. Soc.*, **12**, 853 (1981)
33) Barcons, X. & Fabian, A.C., *Mon. Not. R. astr. Soc.*, **230**, 189 (1988)
34) Barcons, X., Fabian, A.C. & Rees, M.J., Preprint (1990)
35) Scheartz, D.A. & Tucker, W.H., *Astrophys. J.*, **332**, 157
36) Fabian, A.C., Canizares, C.R. & Barcons, X., *Mon. Not. R. astr. Soc.*, **239**, 15P (1989)
37) Setti, G. & Woltjer, L., Ref. 17, p. 811

38) Fabian, A.C., In: *The Post–Recombination Universe*, Ed. N. Kaiser & A.N. Lasenby, Kluwer, p. 51 (1988)
39) Leiter, D. & Boldt, E., *Astrophys. J.*, **260**, 1 (1982)
40) Boldt, E. & Leiter, D., *Astrophys. J.*, **276**, 427 (1984)
41) Boldt, E. & Leiter, D., *Astrophys. J.*, **322**, L1 (1987)
42) Giacconi, R. & Zamorani, G., *Astrophys. J.*, **313**, 20 (1987)
43) Griffiths, R.E. & Padovani, P., Ref. 17, p. 743
44) Zdziarski, A., *Mon. Not. R. astr. Soc.*, **233**, 739 (1988)
45) Fabian, A.C., Done, C. & Ghisellini, G., *Mon. Not. R. astr. Soc.*, **232**, 21P (1988)
46) Fabian, A.C., George, I.M., Miyoshi, S. & Rees, M.J., *Mon. Not. R. astr. Soc.*, **242**, 14P (1990)
47) Warwick, R.S., Pye, J.P. & Fabian, A.C., *Mon. Not. R. astr. Soc.*, **190**, 243 (1980)
48) Shafer, R.A., Ph. D. Thesis, University of Maryland (1983)
49) Shafer, R.A. & Fabian, A.C., In:*Early Evolution of the Universe and its present Structure*, Ed. G.O. Abell & G. Chincarini, Reidel, p. 333 (1983)
50) Boldt, E., *Phys. Rep*, **146**, 215 (1987)
51) Jahoda, K. & Mushotzky, R.F., *Astrophys. J.*, **346**, 638 (1989)
52) Goicoechea, L.J. & Martín–Mirones, J.M., *Mon. Not. R. astr. Soc.*, **244**, 493 (1990)
53) Scheuer, P.A.G., *Proc. Cambridge Phil. Soc.*, **53**, 764 (1957)
54) Scheuer, P.A.G., *Mon. Not. R. astr. Soc.*, **167**, 419 (1974)
55) Wall, J.V., Scheuer, P.A.G., Pauliny–Toth, I.I.K. & Witzel, A., *Mon. Not. R. astr. Soc.*, **198**, 221 (1982)
56) Fabian, A.C., *Mon. Not. R. astr. Soc.*, **172**, 149 (1975)
57) Mészáros, A. & Mészáros, P., *Astrophys. J.*, **327**, 25 (1988)
58) Bayoly, Z., Mészáros, A. & Mészáros, P., *Astrophys. J.*, **335**, 54 (1988)
59) Butcher, J.A., *et al.*, In preparation (1990)
60) Hamilton, H.H. & Helfand, D.J., *Astrophys. J.*, **318**, 93 (1987)
61) Barcons, X. & Fabian, A.C., *Mon. Not. R. astr. Soc.*, **243**, 366 (1990)
62) Barcons, X. & Fabian, A.C., *Mon. Not. R. astr. Soc.*, **237**, 119 (1989)
63) De Zotti, G., *et al.*, *Astrophys. J.*, **351**, 22 (1990)
64) Persic, M. *et al.*, *Astrophys. J.*, **336**, L47 (1989)
65) Carrera, F.J., *et al.*, *Mon. Not. R. astr. Soc.*, submitted (1990)
66) Lahav, O., Edge, A.C., Fabian, A.C. & Putney, A., *Mon. Not. R. astr. Soc.*, **238**, 881 (1989)
67) Shanks, T., Fong, R., Boyle, B.J. & Peterson, B.A., *Mon. Not. R. astr. Soc.*, **227**, 339 (1987)
68) Barcons, X. & Fabian, A.C., *Adv. Space Res.*, in the press (1990)

Matter Contents of the Universe

David Schramm, Eunice and David Wilkinson

PROBING CREATION WITH BIG BANG NUCLEOSYNTHESIS

David N. Schramm
The University of Chicago,
5640 S. Ellis Avenue, Chicago, IL 60637
and
NASA/Fermilab Astrophysics Center,
Fermi National Accelerator Laboratory
Box 500, Batavia, IL 60510-0500

ABSTRACT

Big bang nucleosynthesis is the complementary cosmological test to the microwave background. This paper focuses on big bang nucleosynthesis and, in particular, the recent LEP (and SLC) results on the number of neutrinos are discussed as a positive laboratory test of the standard cosmology scenario. Discussion is also presented on the improved light element observational data as well as the improved neutron lifetime data. Alternate nucleosynthesis scenarios of decaying matter or of quark-hadron induced inhomogeneities are also discussed. It is shown that when these scenarios are made to fit the observed abundances accurately, the resulting conclusions on the baryonic density relative to the critical density, Ω_b, remain approximately the same as in the standard homogeneous case, thus, adding to the robustness of the standard model conclusion that $\Omega_b \sim 0.06$. This latter point is the driving force behind the need for non-baryonic dark matter (assuming $\Omega_{total} = 1$) and the need for dark baryonic matter, since $\Omega_{visible} < \Omega_b$. Recent accelerator constraints on non-baryonic matter are discussed, showing that any massive cold dark matter candidate must now have a mass $M_x \gtrsim 20GeV$ and an interaction weaker than the Z^0 coupling to a neutrino. It is also noted that recent hints regarding the solar neutrino experiments coupled with the see-saw model for ν-masses may imply that the ν_τ is a good hot dark matter candidate .

INTRODUCTION

It is appropriate that a meeting on the microwave background also discuss big bang nucleosynthesis (BBN) since, together, these form the principle modern tests of the standard hot big bang model of the Universe. Furthermore, these two tests have been symbiotically related since the early work of George Gamow and his associates. Furthermore, just as the new COBE[1] results have given renewed confidence in the $3K$ background argument, the LEP collider (along with the SLC) and the light element abundance measurements have given us renewed confidence in the BBN arguments. As a physicist it is worth noting that the microwave background probes events at temperatures $\sim 10^4 K$ and times of $\sim 10^5$ years, that is, the overlap of atomic physics with cosmology, whereas the light element abundances probe the Universe at temperatures $\sim 10^{10} K$ and times of ~ 1 sec. Thus, it is the nucleosynthesis results that played the most significant role in leading to the particle-cosmology merger that has taken place this past decade. Together, these two areas cover the blending of most of modern physics with cosmology and have led to the development of the field of physical cosmology as distinct from astronomical or mathematical cosmology which dominated cosmological studies 25 years ago.

Since the popular press sometimes presents misleading headlines implying *doubts* about the big bang, it is important to note here that the real concerns referred to in these articles are really in regard to observations related to models of galaxy and structure formation. The basic hot big bang model itself is in fantastic shape with high accuracy confirmations from COBE and, as we will discuss, nucleosynthesis. However, there is admittedly no fully developed model for galaxy and structure formation that fits all of the observations. (But, of course, there is also no fully developed first principles model for star formation either.) That we might not really know exactly how to make galaxies and large-scale structure in no way casts doubt on the hot, dense early universe which we call the big bang. (We also have trouble predicting earthquakes and tornadoes, but that hasn't meant that we throw out the concept of a sperical Earth.)

Before going into the specific argument as to the relationship of BBN to LEP and the current standing of the abundance arguments as well as alternative models, let us review the history of BBN. This will draw heavily on other recent conference proceedings[2]

HISTORY OF BIG BANG NUCLEOSYNTHESIS

It should be noted that there is a symbiotic connection between BBN and the $3K$ background dating back to Gamow and his associates Alpher and Herman. The initial BBN calculations of Gamow and his associates[3] assumed pure neutrons as an initial condition and thus were not particularly accurate, but their inaccuracies had little effect on the group's predictions for a background radiation.

Once Hayashi recognized in 1950 the role of neutron-proton equilibration, the framework for BBN calculations themselves has not varied significantly. The work of Alpher, Follin and Herman[4] and Taylor and Hoyle[5], preceeding the discovery of the 3K background, and Peebles[6] and Wagoner, Fowler and Hoyle,[7] immediately following the discovery, and the more recent work of our group of collaborators[8,9,10,11,12] all do essentially the same basic calculation, the results of which are shown in Figure 1. As far as the calculation itself goes, solving the reaction network is relatively simple by the standards of explosive nucleosynthesis calculations in supernovae (c.f. the 1965 calculation of Truran *et al.*),[13] with the changes over the last 25 years being mainly in terms of more recent nuclear reaction rates as input, not as any great calculational insight (although the current Kawano/Walker code[11,12] is somewhat streamlined relative to the earlier Wagoner code[7].) With the possible exception of ^7Li yields, the reaction rate changes over the past 25 years have not had any major affect.[9,11,12,13,14] The one key improved input is a better neutron lifetime determination, a point to which we will also return shortly.

With the exception of the effects of elementary particle assumptions to which we will also return, the real excitement for BBN over the last 25 years has not really been in redoing the basic calculation. Instead, the true action is focused on understanding the evolution of the light element abundances and using that information to make powerful conclusions. In particular, in the 1960's, the main focus was on ^4He which is very insensitive to the baryon density. The agreement between BBN predictions and observations helped support the basic big bang model but gave no significant information at that time with regard to density. In fact, in the mid-1960's, the other light isotopes (which are, in principle, capable of giving density information) were generally assumed to have been made during the T-Tauri phase of stellar evolution,[15] and so, were not then taken to have cosmological significance. It

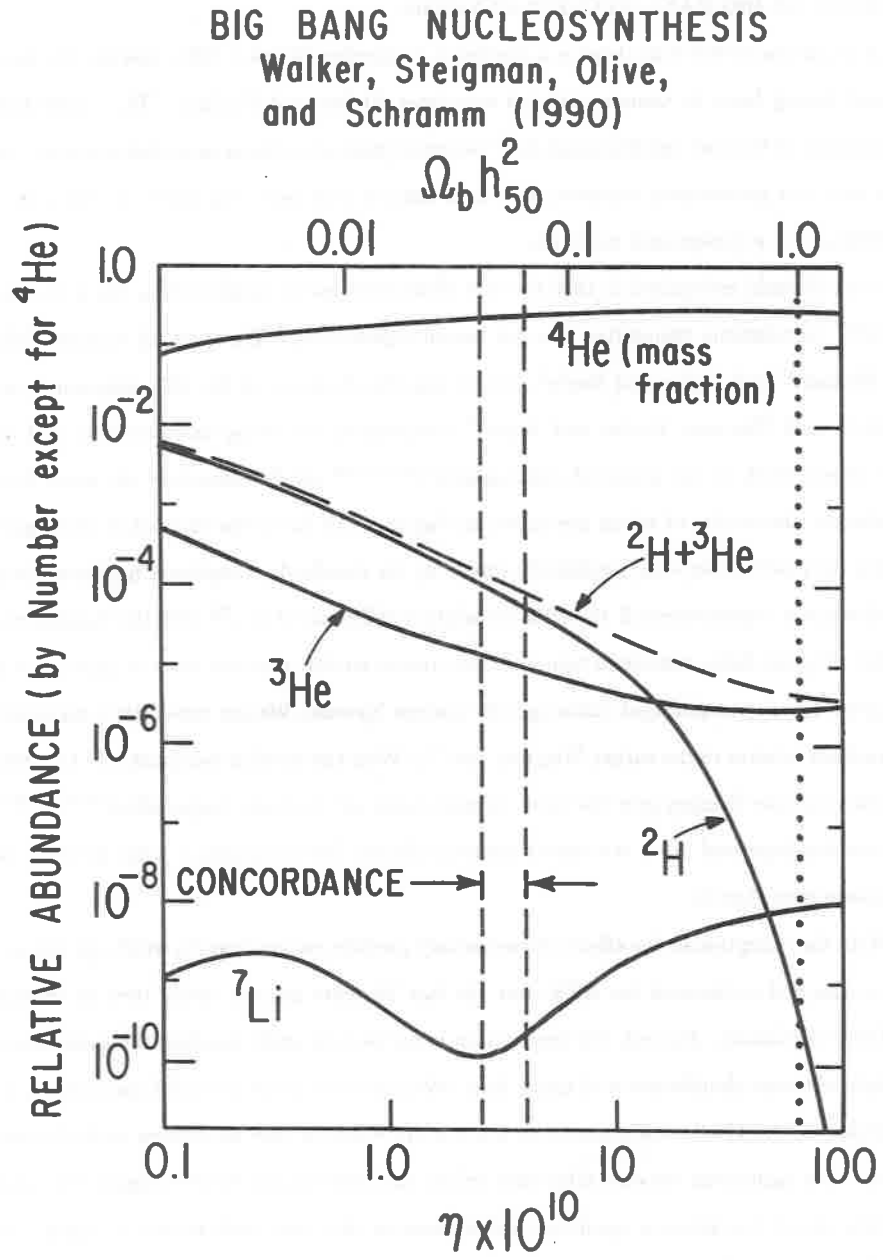

Figure 1. BBN abundances versus the baryon to photon ratio, η, or equivalently the fraction of the critical density, Ω_b.

was during the 1970's that BBN fully developed as a tool for probing the Universe. This possibility was in part stimulated by Ryter *et al.*[16] who showed that the T-Tauri mechanism for light element synthesis failed. Furthermore, ^2H abundance determinations[17,18] improved significantly with solar wind measurements and the interstellar work from the Copernicus satellite. Reeves, Audouze, Fowler and Schramm[19] argued for cosmological ^2H and were able to place a constraint on the baryon density excluding a universe closed with baryons. Subsequently, the ^2H arguments were cemented when Epstein, Lattimer and Schramm[20] proved that no realistic astrophysical process other than the big bang could produce significant ^2H. It was also interesting that the baryon density implied by BBN was in good agreement with the density implied by the dark galactic halos.[21]

By the late 1970's, a complimentary argument to ^2H had also developed using ^3He. In particular, it was argued[22] that, unlike ^2H, ^3He was made in stars; thus, its abundance would increase with time. Since ^3He like ^2H monotonically decreased with cosmological baryon density, this argument could be used to place a lower limit on the baryon density[23] using ^3He measurements from solar wind[17] or interstellar determinations.[24] Since the bulk of the ^2H was converted in stars to ^3He, the constraint was shown to be quite restrictive.[9] Support for this point[25] also comes from the observation of ^3He in horizontal branch stars which, as processed stars still having ^3He on their surface, indicates the survivability of ^3He.

It was interesting that the lower boundary from ^3He and the upper boundary from ^2H yielded the requirement that ^7Li be near its minimum of $^7Li/H \sim 10^{-10}$, which was verified by the Pop II Li measurements of Spite and Spite,[26] hence, yielding the situation emphasized by Yang *et al.*[9] that the light element abundances are consistent over nine orders of magnitude with BBN, but only if the cosmological baryon density is constrained to be around 6% of the critical value. It is worth noting that ^7Li alone gives both an upper and a lower limit to Ω_b. However, while its derived upper limit is more than competitive with the ^2H limit, the ^7Li lower limit is not nearly as restictive as the $^2H +^3 He$ limit. Claims that big bang nucleosynthesis can yield Ω_b lower than 0.01 must necessarily neglect the $^3He +^2 H$ limit.

The other development of the 70's for BBN was the explicit calculation of Steigman, Schramm and Gunn,[27] showing that the number of neutrino generations, N_ν, had to be small to avoid overproduction of ^4He. This will subsequently be referred to as the SSG

limit.(Earlier work had noted a dependency of the ^4He abundance on assumptions about the fraction of the cosmological stress-energy in exotic particles,[28,5] but had not actually made an explicit calculation probing the quantity of interest to particle physicists, N_ν.) To put this in perspective, one should remember that the mid-1970's also saw the discovery of charm, bottom and tau, so that it almost seemed as if each new detector produced new particle discoveries, and yet, cosmology was arguing against this "conventional" wisdom. Over the years the SSG limit on N_ν improved with ^4He abundance measurements, neutron lifetime measurements and with limits on the lower bound to the baryon density; hovering at $N_\nu \lesssim 4$ for most of the 1980's and dropping to slightly lower than 4[29,30,10] just before LEP and SLC turned on.

BIG BANG NUCLEOSYNTHESIS: Ω_b and N_ν

The power of Big Bang Nucleosynthesis comes from the fact that essentially all of the physics input is well determined in the terrestrial laboratory. The appropriate temperature regimes, 0.1 to $1MeV$, are well explored in nuclear physics labs. Thus, what nuclei do under such conditions is not a matter of guesswork, but is precisely known. In fact, it is known for these temperatures far better than it is for the centers of stars like our sun. The center of the sun is only a little over $1keV$, thus, below the energy where nuclear reaction rates yield significant results in laboratory experiments, and only the long times and higher densities available in stars enable anything to take place.

To calculate what happens in the big bang, all one has to do is follow what a gas of baryons with density ρ_b does as the universe expands and cools. As far as nuclear reactions are concerned, the only relevant region is from a little above $1MeV$ ($\sim 10^{10}K$) down to a little below $100keV$ ($\sim 10^9K$). At higher temperatures, no complex nuclei other than free single neutrons and protons can exist, and the ratio of neutrons to protons, n/p, is just determined by

$$n/p = e^{-Q/T},$$

where $Q = (m_n - m_p)c^2 \sim 1.3MeV$.

Equilibrium applies because the weak interaction rates are much faster than the expansion

of the universe at temperatures much above $10^{10}K$. At temperatures much below $10^{9}K$, the electrostatic repulsion of nuclei prevents nuclear reactions from proceeding as fast as the cosmological expansion separates the particles.

Because of the equilibrium existing for temperatures much above $10^{10}K$, we don't have to worry about what went on in the universe at higher temperatures. Thus, we can start our calculation at $10MeV$ and not worry about speculative physics like the theory of everything (T.O.E.), or grand unifying theories (GUTs), as long as a gas of neutrons and protons exists in thermal equilibriuim by the time the universe has cooled to $\sim 10MeV$.

After the weak interaction drops out of equilibrium, a little above $10^{10}K$, the ratio of neutrons to protons changes more slowly due to free neutrons decaying to protons, and similar transformations of neutrons to protons via interactions with the ambient leptons. By the time the universe reaches $10^{9}K$ $(0.1MeV)$, the ratio is slightly below $1/7$. For temperatures above $10^{9}K$, no significant abundance of complex nuclei can exist due to the continued existence of gammas with greater than MeV energies. Note that the high photon to baryon ratio in the universe ($\sim 10^{10}$) enables significant population of the MeV high energy Boltzman tail until $T \lesssim 0.1\ MeV$.

Once the temperature drops to about $10^{9}K$, nuclei can exist in statistical equilibrium through reactions such as $n + p \leftrightarrow^{2} H + \gamma$ and ${}^{2}H + p \leftrightarrow^{3} He + \gamma$ and ${}^{2}H + n \leftrightarrow^{3} H + \gamma$, which in turn react to yield ${}^{4}He$. Since ${}^{4}He$ is the most tightly bound nucleus in the region, the flow of reactions converts almost all the neutrons that exist at $10^{9}K$ into ${}^{4}He$. The flow essentially stops there because there are no stable nuclei at either mass-5 or mass-8. Since the baryon density at big bang nucleosynthesis is relatively low (much less than $1g/cm^{3}$) and the time-scale short ($t \lesssim 10^{2}sec$), only reactions involving two-particle collisions occur. It can be seen that combining the most abundant nuclei, protons and ${}^{4}He$ via two body interactions always leads to unstable mass-5. Even when one combines ${}^{4}He$ with rarer nuclei like ${}^{3}H$ or ${}^{3}He$, we still get only to mass-7, which, when hit by a proton, the most abundant nucleus around, yields mass-8. (A loophole around the mass-8 gap can be found if $n/p > 1$, so that excess neutrons exist, but for the standard case $n/p < 1$). Eventually, ${}^{3}H$ radioactively decays to ${}^{3}He$, and any mass-7 made radioactively decays to ${}^{7}Li$. Thus, big bang nucleosynthesis makes ${}^{4}He$ with traces of ${}^{2}H$, ${}^{3}He$, and ${}^{7}Li$. (Also, all the protons left over that did not

capture neutrons remain as hydrogen.) For standard homogeneous BBN, all other chemical elements are made later in stars and in related processes. (Stars jump the mass-5 and -8 instability by having gravity compress the matter to sufficient densities and have much longer times available so that three-body collisions can occur.) With the possible exception of ^7Li,[9,10,11,12,14] the results are rather insensitive to the detailed nuclear reaction rates. This insensitivity was discussed in reference 9 and most recently using a Monte Carlo study by Krauss and Romanelli[14] An n/p ratio of $\sim 1/7$ yields a ^4He primordial mass fraction,

$$Y_p = \frac{2n/p}{n/p+1} \approx \frac{1}{4}$$

The only parameter we can easily vary in such calculations is the density that corresponds to a given temperature. From the thermodynamics of an expanding universe we know that $\rho_b \propto T^3$; thus, we can relate the baryon density at $10^{10}K$ to the baryon density today, when the temperature is about $3K$. The problem is that we don't know today's ρ_b, so the calculation is carried out for a range in ρ_b. Another aspect of the density is that the cosmological expansion rate depends on the total mass-energy density associated with a given temperature. For cosmological temperatures much above 10^4K, the energy density of radiation exceeds the mass-energy density of the baryon gas. Thus, during big bang nucleosynthesis, we need the radiation density as well as the baryon density. The baryon density determines the density of the nuclei and thus their interaction rates, and the radiation density controls the expansion rate of the universe at those times. The density of radiation is just proportional to the number of types of radiation. Thus, the density of radiation is not a free parameter if we know how many types of relativistic particles exist when big bang nucleosynthesis occurred.

Assuming that the allowed relativistic particles at $1MeV$ are photons, e, μ, and τ neutrinos (and their antiparticles) and electrons (and positrons), Figure 1 shows the BBN yields for a range in present ρ_b, going from less than that observed in galaxies to greater than that allowed by the observed large-scale dynamics of the universe. The ^4He yield is almost independent of the baryon density, with a very slight rise in the density due to the ability of nuclei to hold together at slightly higher temperatures and at higher densities, thus enabling nucleosynthesis to start slightly earlier, when the baryon to photon ratio is higher. No matter

what assumptions one makes about the baryon density, it is clear that ^4He is predicted by big bang nucleosynthesis to be around 1/4 of the mass of the universe.

THE SSG LIMIT – COSMOLOGICAL NEUTRINO COUNTING

Let us now look at the connection to N_ν. Remember that the yield of ^4He is very sensitive to the n/p ratio. The more types of relativistic particles, the greater the energy density at a given temperature, and thus, a faster cosmological expansion. A faster expansion yields the weak-interaction rates being exceeded by the cosmological expansion rate at an earlier, higher temperature; thus, the weak interaction drops out of equilibrium sooner, yielding a higher n/p ratio. It also yields less time between dropping out of equilibrium and nucleosynthesis at 10^9K, which gives less time for neutrons to change into protons, thus also increasing the n/p ratio. A higher n/p ratio yields more ^4He. As we will see in the next section, quark-hadron induced variations[31] in the standard model also yield higher ^4He for higher values of Ω_b. Thus, such variants still support the constraint on the number of relativistic species.[32]

In the standard calculation we allowed for photons, electrons, and the three known neutrino species (and their antiparticles). However, following SSG and doing the calculation (see Figure 2) for additional species of neutrinos, we can see when ^4He yields exceed observational limits while still yielding a density consistent with the ρ_b bounds from ^2H, ^3He, and now ^7Li. (The new ^7Li value gives approximately the same constraint on ρ_b as the others, thus strengthening the conclusion.) The bound on ^4He comes from observations of helium in many different objects in the universe. However, since ^4He is not only produced in the big bang but in stars as well, it is important to estimate what part of the helium in some astronomical object is primordial—from the big bang—and what part is due to stellar production after the big bang. The pioneering work of the Peimberts[33] showing that ^4He varies with oxygen has now been supplemented by examination of how ^4He varies with nitrogen and carbon. The observations have also been systematically reexamined by Pagel[34]. The conclusions of Pagel[34], Steigman *et al.*[35] and Walker *et al.*[11] all agree that the ^4He mass fraction, Y_p, extrapolated to zero heavy elements, whether using N, O, or C, is $Y_p \sim 0.23$ with an upper bound allowing for possible systematics of 0.24.

The other major uncertainty in the ^4He production used to be the neutron lifetime.

However, the new world average of $\tau_n = 890 \pm 4s (\tau_{1/2} = 10.3\ min)$ is dominated by the dramatic results of Mampe *et al.*[36] using a neutron bottle. This new result is quite consistent with a new counting measurement of Byrne *et al.*[37] and within the errors of the previous world average of $896 \pm 10s$ and is also consistent with the precise C_A/C_V measurements from PERKEO[38] and others. Thus, the old ranges of $10.4 \pm 0.2\ min$, used for the half-life in calculations,[39,9] seem to have converged towards the lower side. The convergence means that, instead of the previous broad bands for each neutrino flavour, we obtain relatively narrow bands (see Figure 2). Note that $N_\nu = 4$ is excluded. In fact, the SSG limit is now$N_\nu < 3.4$.[10,11]

The recent verification of this cosmological standard model prediction by LEP, $N_\nu = 2.98 \pm 0.06$, from the average of ALEPH, DELPHI, L3 and OPAL[40] collaborations as well as the SLC[40] results, thus, experimentally confirms our confidence in BBN. (However, we should also remember that LEP and cosmology are sensitive to different things.[41] Cosmology counts all relativistic degrees of freedom for $m_x \lesssim 10MeV$, with LEP and SLC counting particles coupling to the Z^0 with $m_x \lesssim 45GeV$.

While ν_e and ν_μ are obviously counted equally in both situations, a curious loophole exists for ν_τ since the current experimental limit $m_{\nu_\tau} < 35MeV$ could allow it not to contribute as a full neutrino in the cosmology argument[42]. Proposed experiments which push the m_{ν_τ} limit down to less than a few MeV should eliminate this loophole. It might also be noted that if we assume m_{ν_τ} is light so that cosmologically $N_\nu = 3$, we can turn the argument around and use LEP to predict the primordial helium abundance ($\sim 24\%$), or even use limits on ^4He to give an upper limit on Ω_b (also $\lesssim 0.10$). Thus, LEP strengthens the argument that we need non-baryonic dark matter if $\Omega = 1$. In fact, note also that with $N_\nu = 3$, if Y_p is ever proven to be less than ~ 0.235, standard BBN is in difficulty. Similar difficulties occur if Li/H is ever found below $\sim 10^{-10}$. In other words, BBN is a falsifiable theory.

ALTERNATIVE PROPOSALS

As noted above, BBN yields all agree with observations using only one freely adjustable parameter, ρ_b. Thus, BBN can make strong statements regarding ρ_b if the observed light element abundances cannot be fit with any alternative theory. Before exploring the implications

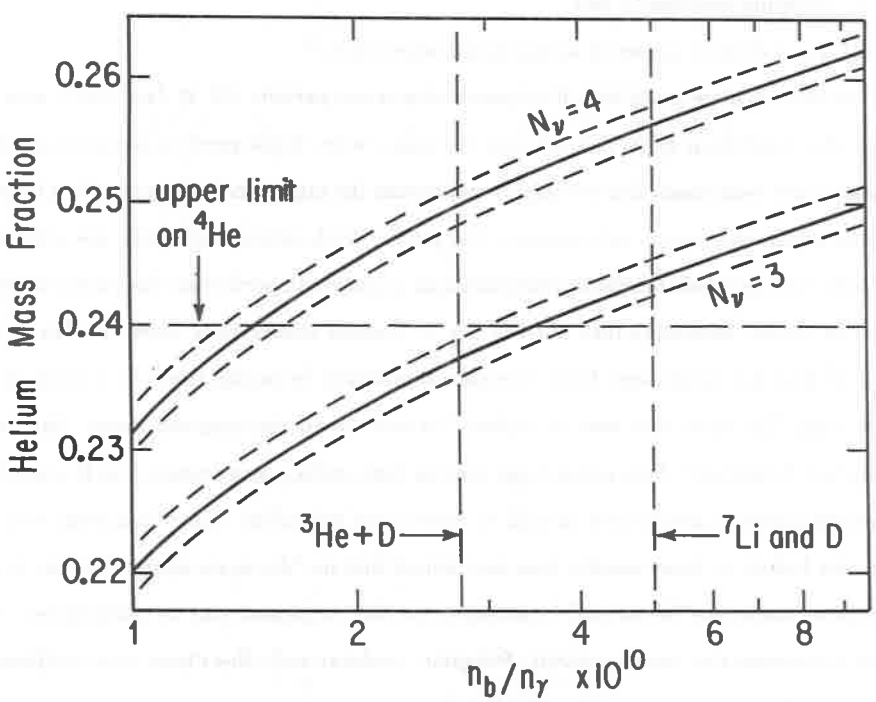

Figure 2. The SSG argument with recent parameter constraints showing the BBN helium mass fraction versus η for $N_\nu = 3$ and 4. Note that 4 is excluded.

for ρ_b, let us examine alternative proposals which have arisen to try to escape the power of the homogeneous BBN conclusions.

The two alternatives that have recently received interest are:

(1) Decaying particles;[43] and

(2) Quark-hadron transition inspired inhomogeneities.[31]

The first of these notes that if a species of massive particle ($M \gtrsim few\ GeV$) were to decay after traditional BBN, it could redo nucleosynthesis. While previous decaying particle proposals had been made, the new idea[43] emphasizes the importance of the resulting hadron cascade which, they argue, will dominate the yields. While interesting results are obtained, problems with detailed abundance determinations do result. In particular, this class of models seems to predict inevitably that $^6Li/^7Li >> 1$, whereas observations show $^7Li/^6Li \gtrsim 10$. While at first this might seem fatal, it is almost avoidable by noting that ^6Li is much more fragile than ^7Li; thus, it is easy to deplete ^6Li and obtain the observed ratios. However, Brown and Schramm[44] have pointed out that for high surface temperature Pop II stars, the convective zones do not go deep enough to destroy any primordial ^6Li. Pilachowski *et al.*[45] have now looked at those specific stars and indeed find no ^6Li, again seeing $^7Li/^6Li > 10$. Therefore, unless the Brown and Schramm convection argument can be surmounted, ^6Li seems to contrain this model seriously. Steigman, Audouze and others have noted additional problems with this model for ^3He and ^2H ratios.

Let us now look at the quark-hadron inspired inhomogeniety models.[31] While inhomogeneity models had been looked at previously (c.f. ref. 9) and were found to make little difference, the quark-hadron inspired models had the added ingredient of variations in n/p ratios.

The initial claim by Applegate *et al.*, followed by a similar argument from Alcock *et al.*, that $\Omega_b \sim 1$ might be possible, created tremendous interest. Their argument was that if the quark-hadron transition was a first-order phase transition (as some preliminary lattice gauge calculations implied), then it was possible that large inhomogeneities could develop at $T \gtrsim 100MeV$. The preferential diffusion of neutrons versus protons out of the high density regions could lead to big bang nucleosynthesis occurring under conditions with both density inhomogeneities and variable neutron/proton ratios. In the first round of calculations, it

was claimed that such conditions might allow $\Omega_b \sim 1$, while fitting the observed primordial abundances of ^4He,^2H,^3He with an overproduction of ^7Li. Since ^7Li is the most recent of the cosmological abundance constraints and has a different observed abundace in Pop I stars versus the traditionally more primitive Pop II stars,[26] some argued that perhaps some special depletion process might be going on to reduce the excess ^7Li. Reeves and Audouze each argued against such processes and tried to turn the argument around and use lithium abundances to constrain the quark-hadron transition.

At first it appeared that if the lithium constraint could be surmounted, then the constraints of standard big bang nucleosynthesis might disintegrate. (Although Audouze, Reeves and Schramm emphasized that the number of parameters needed to fit the light elements was somewhat larger for these non-standard models, nonetheless, a non-trivial loophole appeared to be forming.) To further stimulate the flow through the loophole, Mullaney and Fowler showed that, in addition to looking at the diffusion of neutrons out of high density regions, one must also look at the subsequent effect of excess neutrons diffusing back into the high density regions as the nucleosynthesis goes to completion in the low density regions. (The initial calculations treated the two regions separately.) Mullaney and Fowler argued that for certain phase transition parameter values (e.g. nucleation site separations $\sim 10m$ at the time of the transition), this back diffusion could destroy much of the excess lithium. Recent work by Banerjee and Chitre (private communication) suggests that more accurate treatment of the diffusion calculation could reduce the interesting separation distance by several orders of magnitude.

However, Kurki-Suonio, Matzner, Olive and Schramm,[32] the Tokyo group,[46] and the Livermore group[47] have recently argued that in their detailed diffusion models, the back diffusion not only effects ^7Li, but also the other light nuclei as well. They find that for $\Omega_b \sim 1$, ^4He is also overproduced (although it does go to a minimum for similar parameter values as does the lithium). One can understand why these models might tend to overproduce ^4He and ^7Li by remembering that in standard homogeneous big bang nucleosynthesis, high baryon densities lead to excesses in these nuclei. As back diffusion evens out the effects of the initial fluctuation, the averaged result should approach the homogeneous value. Furthermore, it can be argued that any narrow range of parameters, such as those which yield relatively low

lithium and helium, are unrealistic since in most realisitic phase transitions there are distributions of parameter values (distribution of nucleation sites, separations, density fluctuations, etc.). Therefore, narrow minima are washed out which would bring the ^7Li and ^4He values back up to their excesive levels for all parameter values with $\Omega \sim 1$. Furthermore, Adams and Freese[48] have argued that the boundary betwen the two phases may be fractal-like rather than smooth. The large surface area of a fractal-like boundary would allow more interaction between the regions and minimize exotic effects.

Figure 3 shows the results of Kurki-Suonio *et al.*[32] for varying spacing l with the constraints from the different light element abundances. Notice that the Li and even the ^4He constraint do not allow $\Omega_b \sim 1$. (The ^4He abundance constraint used in Kurki-Suonio *et al.* was a generous $Y_p \lesssim 0.25$; for the preferred $Y_p \lesssim 0.24$, the ^4He bound is about as tight as the Pop II Li constraint.) Note also that with the Pop II ^7Li constraint, the results for Ω_b are quite similar to the standard model with a slight excess in Ω_b possible if l is tuned to ~ 10.

Furthermore, initially it looked like quark-hadron inspired models might enable leakage[49] beyond mass-7, thus enabling ^9Be, ^{14}N, or maybe even r-process elements to become probes as whether or not the universe had such a transition (even if $\Omega_b \sim 1$). However, Tarasawa and Sato[46] have shown that when full multizone calculations of the type used by Kurki-Suonio *et al.* are utilized, then no significant leakage occurs.

One possible signature that remains for a first order quark-hadron transition is a slightly larger allowed range for Y_p that is concordant with $N_\nu = 3$ and with the other light element abundances. In particular, if ^4He were ever shown to be definitively $\lesssim 0.23$, it might be evidence for such a quark-hadron induced behavior since the standard homogenous case cannot accomodate such values. Of course, excessively low values for Y_p would still be unallowable.

One can conclude from the failure of the attempts to circumvent the standard BBN results that the results are amazingly robust. Even when many new free parameters are added, as in the quark-hadron case, the bottom line, when one requires concordance with the light element abundances, is essentially the same as the standard result. In other words, $\Omega_b \sim 0.06$ (although with fine-tuning the upper bound might be relaxed a bit to ~ 0.2 rather than 0.1).

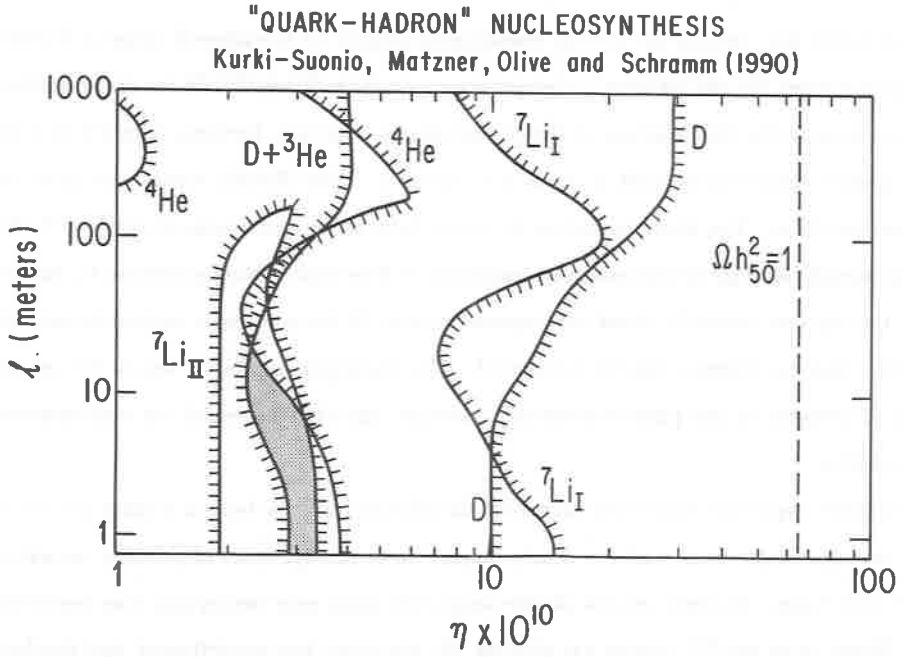

Figure 3. This shows the constraints on η of the various observed abundances in a first-order quark-hadron phase transition with nucleation sites separated by a distance l with density contrast $R \lesssim 10^3$. The Pop II lithium abundance used here is from the compilation of data given by Walker *et al.*[11] and is slightly more restrictive on η than that used in Figure 2 or used in the original Kurki-Suonio *et al.*[32] calculation from which this figure is derived. It should be noted that work by the Tokyo[46] group and by the Livermore group[47] confirms the conclusions on restricting Ω_b to values similar to the standard result even when $R \to \infty$.

LIMITS ON Ω_b AND DARK MATTER REQUIREMENTS

The narrow range in baryon density for which concordance occurs is very interesting. Let us convert it into units of the critical cosmological density for the allowed range of Hubble expansion rates. For the big bang nucleosynthesis constraints,[9,10,11,12,29,30] the dimensionless baryon density, Ω_b, that fraction of the critical density that is in baryons, is less than 0.11 and greater than 0.02 for $0.04 \lesssim h_0 \lesssim 0.7$, where h_0 is the Hubble constant in units of $100 km/sec/Mpc$. The lower bound on h_0 comes from direct observational limits and the upper bound from age of the universe constraints.[49] Note that the constraint on Ω_b means that the universe *cannot be closed with baryonic matter.* If the universe is truly at its critical density, then nonbaryonic matter is required. This argument has led to one of the major areas of research at the particle-cosmology interface, namely, the search for non-baryonic dark matter.

Another important conclusion regarding the allowed range in baryon density is that it is in very good agreement with the density implied from the dynamics of galaxies, *including their dark halos.* An early version of this argument, using only deuterium, was described over fifteen years ago.[21] As time has gone on, the argument has strengthened, and the fact remains that galaxy dynamics and nucleosynthesis agree at about 6% of the critical density. Thus, if the universe is indeed at its critical density, as many of us believe, it requires most matter not to be associated with galaxies and their halos, as well as to be nonbaryonic.

Let us put the nucleosynthetic arguments in context. The arguments requiring some sort of dark matter fall into two separate and quite distinct areas. First are the arguments using Newtonian mechanics applied to various astronomical systems that show that there is more matter present than the amount that is shining. These arguments are summarized in the first part of Table 1. It should be noted that these arguments reliably demonstrate that galactic halos seem to have a mass ~ 10 times the visible mass.

Note however that big bang nucleosynthesis requires that the bulk of the baryons in the universe are dark since $\Omega_{vis} << \Omega_b$. Thus, the dark halos could in principle be baryonic.[21] Recently arguments on very large scales[51] (bigger than cluster of galaxies) hint that Ω on those scales is indeed greater than Ω_b, thus forcing us to need non-baryonic matter. However, until these arguments are confirmed, we must look to the inflation paradigm.

TABLE I

"OBSERVED" DENSITIES

$$\left[\Omega \equiv \rho/\rho_c \text{ where } \rho_c = 2 \cdot 10^{-29} h_0^2 \text{g/cm}^3 \text{and } h_o \equiv \frac{\text{Ho}}{100 \text{ km/sec/mpc}}\right]$$

Newtonian Mechanics (cf. Faber and Gallagher[70])	
Visible	$\Omega \sim 0.007$ (factor of 2 accuracy)
Binaries Small groups Extended flat relation curves	$\Omega \sim 0.07$ (factor of 2 accuracy)
Clusters Gravitational lenses	$\Omega \sim 0.1$ to 0.3
Big Bang Nucleosynthesis (with $t_u \gtrsim 10^{10}$yrs.) (c.f. Walker *et al.*[11] and ref. therein)	$\Omega_b = 0.065 \pm 0.04$
Preliminary Large Scale Studies	
IRAS red shift study and peculiar velocities (Ref. [51])	$\Omega \gtrsim 0.3$
Density redshift counts (Loh and Spillar[71])	$\Omega \sim 1 \pm 0.6$
Inflation Paradigm (Guth[52])	$\Omega = 1$

This is the argument that the only long-lived natural value for Ω is unity, and that inflation[52] or something like it provided the early universe with the mechanism to achieve that value and thereby solve the flatness and smoothness problems. Thus, our need for exotica is dependent on inflation and big bang nucleosythesis and not on the existence of dark galatic halos. This point is frequently forgotten, not only by some members of the popular press but occasionally by active workers in the field.

Some baryonic dark matter must exist since from the $^2H +^3 He$ argument we know that the lower bound from big bang nucleosynthesis is greater than the upper limits on the amount of visible matter in the universe. However, we do not know what form this baryonic dark matter is in. It could be either in condensed objects in the halo, such as brown dwarfs and jupiters (objects with $\lesssim 0.08 M_\odot$ so they are not bright shining stars), or in black holes (which at the time of nucleosynthesis would have been baryons). Or, if the baryonic dark matter is not in the halo, it could be in hot intergalactic gas, hot enough not to show absorption lines in the Gunn-Peterson test, but not so hot as to be seen in the x-rays. Evidence for some hot gas is found in clusters of galaxies. However, the amount of gas in clusters would not be enough to make up the entire missing baryonic matter. Another possible hiding place for the dark baryons would be failed galaxies, large clumps of baryons that condense gravitationally but did not produce stars. Such clumps are predicted in galaxy formation scenarios that include large amounts of biasing where only some fraction of the clumps shine.

Hegyi and Olive[53] have argued that dark baryonic halos are unlikely. However, they do allow for the loopholes mentioned above of low mass objects or of massive black holes. It is worth noting that, as Schramm[2] points out, these loopholes are not that unlikely. Furthermore, recent observational evidence,[54], seems to show disk formation is relatively late, occurring at red shifts $z \lesssim 1$. Thus, the first several billion years of a galaxy's life may have been spent prior to the formation of the disk. In fact, if the first large objects to form are less than galactic mass, as many scenarios imply, then mergers are necessary for eventual galaxy size objects. Mergers stimulate star formation while putting early objects into halos rather than disks. Mathews and Schramm[55] have recently developed a galactic evolution model which does just that and gives a reasonable scenario for chemical evolution. (This scenario also provides a natural explanation for the number-versus-redshift relation of low

luminosity galaxies found by Cowie.[56] Thus, while making halos out of exotic material may be more exciting, it is certainly not impossible for the halos to be in the form of dark baryons. One application of William of Ockham's famous razor would be to have us not invoke exotic matter until we are forced to do so.

Non-baryonic matter can be divided following Bond and Szalay[57] into two major categories for cosmological purposes: hot dark matter (HDM) and cold dark matter (CDM). Hot dark matter is matter that is relativistic until just before the epoch of galaxy formation, the best example being low mass neutrinos with $m_\nu \sim 25eV$. (Remember $\Omega_\nu \sim \frac{m_\nu(eV)}{100h_0^2}$).

Cold dark matter is matter that is moving slowly at the epoch of galaxy formation. Because it is moving slowly, it can clump on very small scales, whereas HDM tends to have more difficulty in being confined on small scales. Examples of CDM could be massive neutrino-like particles with masses, M_x, greater than several GeV or the lightest supersymmetric particle which is presumed to be stable and might also have masses of several GeV. Following Michael Turner, all such weakly interacting massive particles are called "WIMPS." Axions, while very light, would also be moving very slowly[58] and, thus, would clump on small scales. Or, one could also go to non-elementary particle candidates, such as planetary mass blackholes or quark nuggets of strange quark matter, possibly produced at the quark-hadron transition.[59] Another possibility would be any sort of massive toplogical remnant left over from some early phase transition. Note that CDM would clump in halos, thus requiring the dark baryonic matter to be out between galaxies, whereas HDM would allow baryonic halos.

When thinking about dark matter candidates, one should remember the basic work of Zeldovich,[60] resurrected by Lee and Weinberg[61] and others,[62] which showed for a weakly interacting particle that one can obtain closure densities, either if the particle is very light, $\sim 25eV$, or if the particle is very massive, $\sim 3GeV$. This occurs because, if the particle is much lighter than the decoupling temperature, then its number density is the number density of photons (to within spin factors and small corrections), and so the mass density is in direct proportion to the particle mass, since the number density is fixed. However, if the mass of the particle is much greater than the decoupling temperature, then annihilations will deplete the particle number since, as the temperature of the expanding universe drops below

the rest mass of the particle, Boltzmann suppression prohibits production while the number is depleted via annihilations until the annihilation reacton freezes out. For normal weakly interacting particles, decoupling occurs at a temperature of $\sim 1MeV$, so higher mass particles are depleted. It should also be noted that the curve of density versus particle mass turns over again (see Figure 4) once the mass of the WIMP exceeds the mass of the coupling boson[63,64,65] so that the annihilation cross section varies as $\frac{1}{M_z^2}$, independent of the mass of the coupling boson. In this latter case, $\Omega = 1$ can be obtained for $M_x \sim 1TeV \sim (3K \times M_{Planck})^{1/2}$, where $3K$ and M_{Planck} are the only energy scales left in the calculation (see Figure 4). A loophole to this argument occurs if there is a matter-antimatter assymmetry as in the case of baryons. However, such particles would have to be Dirac particles and we will see that they are still severely constrained.

A few years ago the preferred candidate particle was probably a few GeV mass WIMP. However, LEP's lack of discovery of any new particle coupling to the Z° with $M_x \lesssim 45GeV$, coupled with underground experiments[66] clearly eliminates that candidate[67,68]. Constraints for particles not fully coupled to the Z^0 were discussed by Ellis, Nanopoulos, Roskowski and Schramm[68] and are updated and presented in Figures 5a and 5b. (The inclusion of the Kamiokande II results as well as the newer LEP limits yields an important update over the results of Ellis *et al.*[68] since it closes the loophole for Dirac particles near $12GeV$.) Note also that the generic constraints of Figure 5 also apply to other hypothetical particles since CDF and UA2 do not see any squarks, sleptons, Wś or Zś up to masses significantly greater than M_{Z^0}. Thus, whatever the coupling boson is, it must be greater than M_{Z^0} which means the effective value for $\sin^2 \phi_Z$ is < 1.

Furthermore, as Krauss[67] has emphasized, scaler particles such as sneutrinos interact like Dirac neutrinos so that the Kamiokande II and ionization experimental limits[66] also apply. Since asymmetric candidates are all Dirac particles, the restricted part of Figure 5b constrains asymmetric candidates where $\Omega = 1$ is no longer required to follow the locus shown. Thus, it seems that whether the particle is matter-antimatter symmetric or not, it is required to have an interaction weaker than weak and/or have a mass greater than about $20GeV$. Future dark matter searches should thus focus on more massive and more weakly interacting particles.

Also, as Dimopoulos[63] has emphasized, the next appealing crossing of $\Omega = 1$ (see Figure

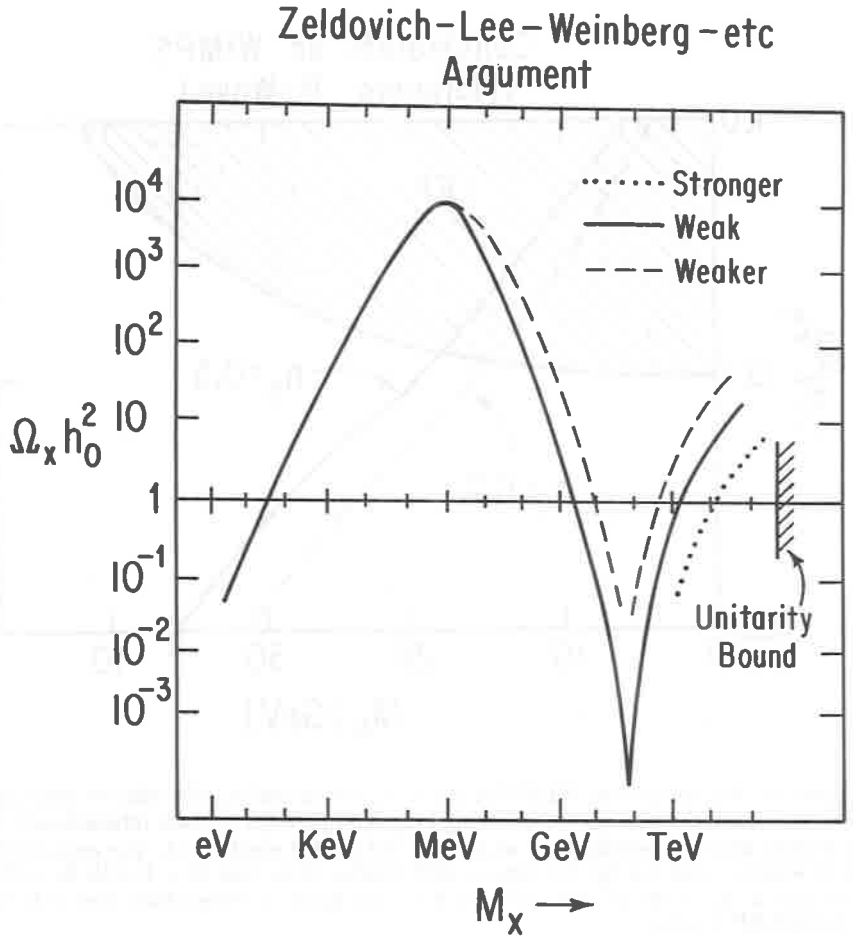

Figure 4. $\Omega_x h_0^2$ versus M_x for weakly interacting particles showing three crossings of $\Omega h_0^2 = 1$. Note also how the curve shifts at high M_x for interactions weaker or stronger than normal weak interaction (where normal weak is that of neutrino coupling through Z^0). Extreme strong couplings reach a unitarity limit at $M_x \sim 340 TeV$.

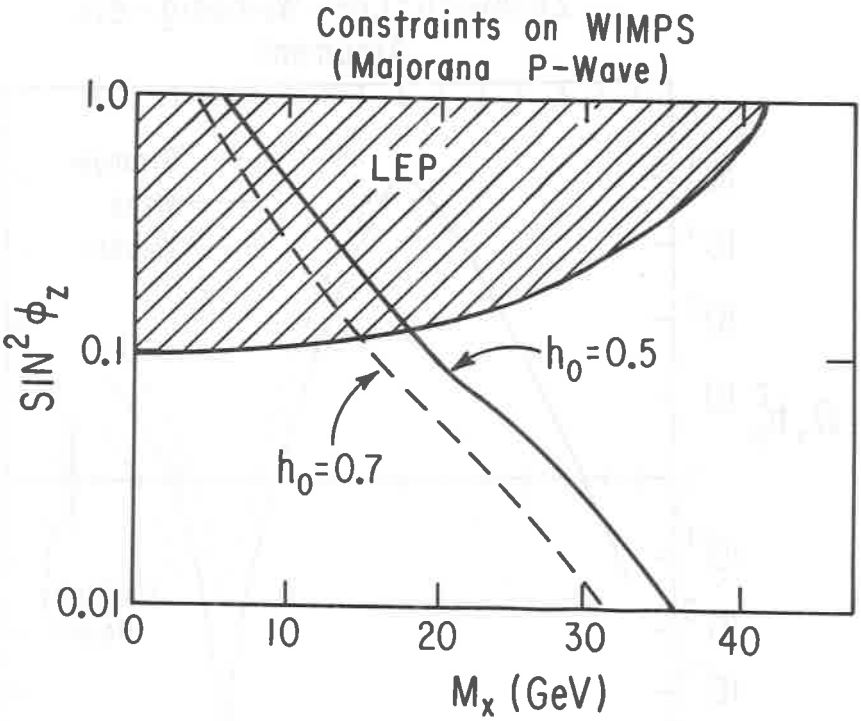

Figure 5a. Constraints on WIMPS of mass M_z versus $\sin^2\phi_z$, the relative coupling to the Z^0. The constraints are shown assuming Majorana particles (p-wave interactions). The diagonal lines show the combinations of M_z and $\sin^2\phi_z$ that yield $\Omega = 1$. The cross-hatched region is what is ruled out by the current LEP results. Note that $\Omega = 1$ with $h_0 = 0.5$ is possible only if $M_z \gtrsim 20GeV$ and $\sin^2\phi_z < 0.1$. This figure is revised from that of Ref.[68] using latest LEP results.

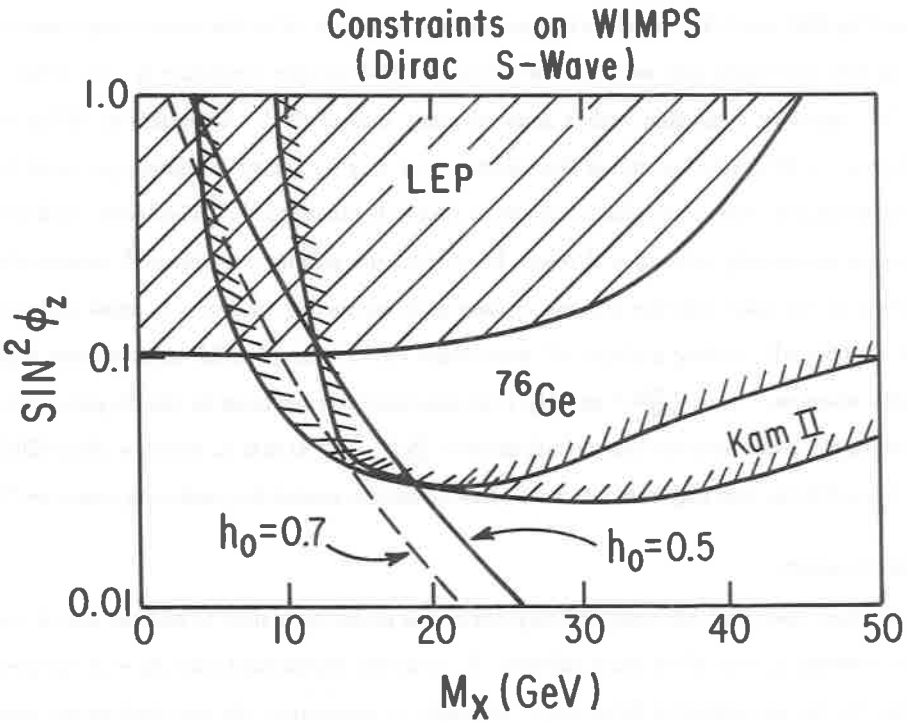

Figure 5b. This is the same as 5a but for Dirac particles (s-wave interactions). The ^{76}Ge region is that ruled out by the Caldwell *et al.* double-β decay style experiments. This figure is revised from that of Ref.[68] using latest LEP results and using new Kamiokande limits which closed a possible loophole near $M_x \sim 10GeV$. The current results require $M_x \gtrsim 20GeV$ and $\sin^2 \phi_z \lesssim 0.03$ for matter-antimatter symmetric particles and also exclude the entire cross hatched region for asymmetric particle candidates.

4) is $\gtrsim 1TeV$ (but, in any case, $\lesssim 340TeV$ from the unitarity bound[65]), which can be probed by SSC and LHC as well as by underground detectors. After the correct experimental constraints are taken into account, the favoured CDM particle candidate is now either a $10^{-5}eV$ axion or a gaugino with a mass of many tens of GeV. Of course an HDM ν_τ with $m_{\nu_\tau} \sim 20 \pm 10eV$ is still a fine candidate as long as galaxy formation proceeds by some mechanism other than adiabatic gaussian matter fluctuations.[69,72] This latter candidate becomes particularly attractive if recent hints from the gallium experiment[73] require the solution to the solar neutrino problem to have neutrino mixing with $\nu_e - \nu_\mu$ mass scales of 0.01 to 0.001 eV, making multiple eV mass scales for ν_τ quite plausible from see-saw type models where $m_{\nu_\tau} \sim m_{\nu_\mu}(\frac{M_{f_3}}{M_{f_2}})^2$ and M_{f_i} is an associated fermion mass for the ith generation. For example, if one uses the heavy quark masses $(\frac{M_t}{M_c})^2 \sim 10^4$ so that ν_τ becomes ideal HDM. Such possibilities also may help late-time phase transition models for producing structure.[72]

CONCLUSION

We have seen that big bang nucleosynthesis has grown with time to become one of our most powerful probes of the early universe. Its resultant requirement that $N_\nu \sim 3$ has been verified in the experimental laboratory. Attempts to circumvent the standard model have ended up yielding the same conclusions, thus adding to the robustness of the result. The conclusion that $\Omega_b \sim 0.06$ is the principle argument behind non-baryonic dark matter, but the other edge of the argument is that it also requires a significant amount of baryonic dark matter. Both of these predictions will be the focus of much observational and experimental research over the coming years. Considering the success of the previous predictions of big bang nucleosynthesis, devoting a major effort to looking for dark matter, both baryonic and non-baryonic, should not be in vain.

ACKNOWLEDGMENTS

I would like to thank my recent collaborators John Ellis, Savas Dimopoulos, Gary Steigman, Keith Olive, Michael Turner, Rocky Kolb and Terry Walker for many useful discussions. I would also like to acknowledge useful communications with Denys Wilkinson, Walter Mampe, Jim Byrne and Stuart Friedman on the neutron lifetime and with Bernard Pagel and Jay Gallagher on helium abundances. This work was supported in part by NSF Grant

AST 88-22595 and by NASA Grant # NAGW-1321 at the University of Chicago, and by the DoE and NASA Grant # NAGW-1340 at the NASA/Fermilab Astrophysics Center.

REFERENCES

1. J. Mather *et al.*, COBE preprint, Goddard Space Flight Center *Astrophys. J.*, in press (1990).
2. D. Schramm, *Proc. of the 1990 Rencontre de Physique at La Thuile, March 1990*, ed. M. Greco, in press (1990).

   D. Schramm, *Proc. 1990 Nobel Symposium, Gräftvållen, Sweden*, in press (1990).

   D. Schramm, *Proc. of the Moriond Astrophysics Meeting on Particle Astrophysics at Les Arcs, Savoie, France, March 1990*, ed. T. Piran, in press (1990).
3. R.A. Alpher, H. Bethe and G. Gamow, *Phys. Rev.* **73** (1948) 803.
4. R.A. Alpher, J.W. Follin and R.C. Herman, *Phys. Rev.* **92** (1953) 1347.
5. R. Taylor and F. Hoyle, *Nature* **203** (1964) 1108.
6. P.J.E. Peebles, *Phys. Rev. Lett.* **16** (1966) 410.
7. P. Wagoner, W.A. Fowler and F. Hoyle, *Astrophys. J.* **148** (1967) 3.
8. D.N. Schramm and R.V. Wagoner, *Ann. Rev. of Nuc. Sci.* **27** (1977) 37.

   K. Olive, D.N. Schramm, G. Steigman, M. Turner and J. Yang, *Astrophys. J.* **246** (1981) 557;

   A. Boesgaard and G. Steigman, *Ann. Rev. of Astron. and Astrophys.* **23** (1985) 319.
9. J. Yang, M. Turner, G. Steigman, D.N. Schramm and K. Olive, *Astrophys. J.* **281** (1984) 493.
10. K. Olive, D.N. Schramm, G. Steigman and T. Walker, *Phys. Lett B.* **236** (1990) 454.
11. T. Walker, G. Steigman, D. Schramm, H.-S. Kang and K. Olive, *Astrophys. J.*, submitted (1990).
12. L. Kawano, D.N. Schramm and G. Steigman, *Astrophys. J.* **327** (1988) 750.
13. J.W. Truran, A.G. Cameron and A. Gilbert, *Canadian Journal of Physics* **44** (1966) 563.
14. L. Krauss and P. Romanelli, Yale University preprint and *Ap.J.*, in press (1990).
15. W. Fowler, J. Greenstein and F. Hoyle *Geophys. J.R.A.S.* **6**, 6 (1962).
16. C. Ryter, H. Reeves, E. Gradstajn and J. Audouze, *Astron. and Astrophys.* **8** (1970) 389.
17. J. Geiss and H. Reeves, *Astron. and Astrophys.* **18** (1971) 126;

    D. Black, *Nature* **234** (1971) 148.
18. J. Rogerson and D. York, *Astrophys. J.* **186** (1973) L95.
19. H. Reeves, J. Audouze, W.A. Fowler and D.N. Schramm, *Astrophys. J.* **179** (1973) 909.
20. R. Epstein, J. Lattimer and D.N. Schramm, *Nature* **263** (1976) 198.
21. J. R. Gott, III, J. Gunn, D.N. Schramm and B.M. Tinsley, *Astrophys. J.* **194** (1974) 543.
22. R.T. Rood, G. Steigman and B.M. Tinsley, *Astrophys. J.* **207** (1976) L57.
23. J. Yang, D.N. Schramm, G. Steigman and R.T. Rood, *Astrophys. J.* **227** (1979) 697.
24. T. Wilson, R.T. Rood and T. Bania, *Proc. of the ESO Workshop on Primordial Healing*, ed. P. Shaver and D. Knuth (Garching: European Southern Observatory, 1983).

25. M.R. Hartoog, *Ap.J.* **231** (1979) 161.
    J. Ostriker and D.N. Schramm, FNAL/Princeton preprint (1990).
26. J. Spite and F. Spite, *Astron. and Astrophys.* **115** (1982) 357;
    R. Rebolo, P. Molaro and J. Beckman, *Astron. and Astrophys.* **192** (1988) 192;
    L. Hobbs and C. Pilachowski, *Astrophys. J.* **326** (1988) L23.
27. G. Steigman, D.N. Schramm and J. Gunn, *Phys. Lett.* **66B** (1977) 202.
28. V.F. Schvartzman, *JETP Letters* **9** (1969) 184;
    P.J.E. Peebles, *Physical Cosmology* (Princeton University Press, 1971).
29. D.N. Schramm and L. Kawano, *Nuc. Inst. and Methods* **A 284** (1989) 84.
30. B. Pagel, *Proc. of 1989 Rencontre de Moriond*
31. R. Scherrer, J. Applegate and C. Hogan, *Phys. Rev. D 35* (1987) 1151;
    C. Alcock, G. Fuller and G. Mathews, *Astrophys. J.* **320** (1987) 439;
    W.A. Fowler and R. Malaney, *Astrophys. J.* **333** (1988) 14.
32. H. Kurki-Suonio, R. Matzner, K. Olive and D.N. Schramm, *Astrophys. J.* **353** (1990) 406;
33. M. Peimbert and S. Torres-Peimbert, *Astrophys. J.* **193** (1974) 327.
34. B. Pagel, *ESO/CERN Proc.* (1990).
35. G. Steigman, D.N. Schramm and J. Gallagher, *Comments on Astrophys.* **14** (1989) 97.
36. W. Mampe, P. Ageron, C. Bates, J.M. Pendlebury and A. Steyerl, *Phys. Rev. Lett.* **63** (1989) 593.
37. J. Byrne, *et al. Phys. Lett. B*, submitted (1990).
38. H. Abele, M. Arnould, H.A. Borel, J. Dohner, D. Dubbers, S. Freedman, J. Last and I. Reichert, *Proc. Grenoble Workshop on Slow Neutrons* (1989).
39. G. Steigman, K. Olive, D.N. Schramm and M. Turner, *Phys. Lett. B* **176** (1986) 33.
40. ALEPH, DELPHI, L3, OPAL and MARK II collaboration papers in *Proc. of the Int. High Energy Conference, Singapore* (1990).
41. D.N. Schramm and G. Steigman, *Phys. Lett. B* **141** (1984) 337.
42. E. Kolb and R. Scherrer, *Phys. Rev. D* **25** (1982) 1481;
    A. Chakravorty, E. Kolb and D.N. Schramm, in progress (1990).
43. S. Dimopoulos, R. Esmailzadeh, L. Hall and G. Starkman, *Astrophys. J.* **330** (1988) 545.
44. L. Brown and D.N. Schramm, *Ap.J.* **329** (1988) L103.
45. C. Pilachowski, L. Hobbs and D. De Young, *Ap.J. Lett.* 345 (1989) L39.
46. H. Reeves, K. Sato and M. Tarasawa, U. of Tokyo preprint (1989).
    N. Tarasawa and K. Sato, U. of Tokyo preprint (1990).
47. C. Alcock, G. Fuller, G. Mathews, and B. Meyer, Livermore preprint (1990).
48. F. Adams and K. Freese, MIT preprint (1990)
49. L. Kawano, W. Fowler and R. Malaney, Caltech-Kellogg preprint (1990).
    J. Applegate, Columbia University preprint (1989).
50. K. Freese and D.N. Schramm, *Nucl. Phys.* **B233** (1984) 167.

51. M. Strauss, M. Davis and A. Yahil, U.C. Berkeley preprint (1989);
N. Kaiser and A. Stebbins, CITA preprint (1990);
E. Bertschinger, A. Dekel, and A Yahil, *Proc. Blois Symposium on the Microwave Background* (1990);
M. Rowan-Robinson and A. Yahil, *Proc. Rencontres de Moriond* (1989).
52. A. Guth, *Phys. Rev. D* **23** (1981) 347; see also K. Olive, *Physics Reports* **190** (1990) 309-403 or A. Lindei, *Particle Physics and Inflationary Cosmology* (NY: Harwood, 1990).
53. D. Hegyi and K. Olive, *Astrophys. J.* **303** (1986) 56.
54. J. Gunn, Talk at ITP Santa Barbara (1988);
D. York, Talk at University of Chicago (1988).
55. G. Mathews and D.N. Schramm, *Astrophys. J.*, submitted (1990).
56. L. Cowie, *Proc. IUPAP Conference on Primordial Nucleosynthesis and Evolution of Early Universe, Tokyo, September 1990*, in press (1990).
57. R. Bond and A. Szalay, *Proc. Texas Relativistic Astrophysical Symposium, Austin, Texas* (1982).
58. M. Turner, F. Wilczek and A. Zee, *Phys. Lett. B* **125** (1983) 35; **125** (1983) 519.
59. M. Crawford and D.N. Schramm, *Nature* **298** (1982) 538.
E. Witten, *Phys. Rev. D* **30** (1984) 272.
See also C. Alcock and A. Olinto, *Ann. Rev. Nuc. Part. Phys.* **38** (1988) 161.
60. Ya. Zeldovich, *Adv. Astron. and Astrophys.* **3** (1965) 241.
61. B. Lee and S. Weinberg, *Phys. Rev. Lett.* **39** (1977) 165.
62. H-Y. Chiu, *Phys. Rev. Lett.* **17** (1966) 712.
C.P. Hut, *Phys. Lett. B* **69** (1977) 85;
K. Sato and H. Koyayashi, *Prog. Theor. Phys.* **58** (1977) 1775.
63. S. Dimopoulos, R. Esmailzadeh, L. Hall and N. Tetradis, *Nucl. Phys. B*, submitted (1990).
64. D. Brahm and L. Hall, *Phys. Rev. D* **41** (1990) 1067.
65. K. Griest, M. Kamionkowski and M. Turner, FNAL preprint (1990).
K. Olive and M. Srednicki, *Phys. Lett. B* **230** (1989) 78.
66. D. Caldwell, *et al., Proc. La Thuile*, ed. M. Greco (1990); see also Kamiokande II Collaboration, Proc. IUPAP Sumposium on Primodial Nucleosynthesis and Evolution of Early Universe, Tokyo, September 1990, in press (1990).
67. L. Krauss, *Phys. Rev. Lett.*, in press (1990);
K. Griest and J. Silk, U.C. Berkeley preprint (1990).
68. J. Ellis, D. Nanopoulos, L. Roskowski and D.N. Schramm, *Phys. Lett. B*, in press (1990).
69. D. N. Schramm, *Proc. 1988 Berkeley Workshop on Particle Astrophysics*, ed, E. Norman (World Scientific, 1989).
70. S.M. Faber and J.S. Gallagher *Ann. Rev. Astron. and Astrophys.* **17**, 135 (1979).
71. E. Loh and E. Spillar, *Astrophys. J.* **329** (1988) 24.
72. C. Hill, D. Schramm and J. Fry, *Comments Nucl. Part. Phys.* **19** (1989) 25.
D. Schramm, *Proc. IUPAP Symposium on Primordial Nucleosynthesis and Evolution of Early Universe, Tokyo, September 1990*, in press (1990).
73. SAGE collaboration *Proc. Int. High Energy Physics Meeting, Singapore, August 1990*, in press (1990).

DETECTION OF DARK MATTER

Michel SPIRO
DPhPE/SEPh, CEN Saclay, 91191 Gif-sur-Yvette Cedex, France

ABSTRACT

This short review discusses the principles of dark matter detection and summarizes the main experimental results obtained up to now. Prospects and new ideas are presented.

INTRODUCTION

The estimate of the value of Ω, the ratio of the mean energy density in the universe to the critical energy density, is one of the main issue in modern cosmology. We can measure the components of Ω in various ways:

- from luminous matter (stars), Ω_{lum}
- from the dynamical behaviour of stars in spiral galaxies (galactic halos), Ω_{halo}
- from primordial nucleosynthesis (baryons), Ω_{bar}. We know from observations that the contributions from dust or gas to Ω are negligible. The estimates for the values of Ω_{lum}, Ω_{halo} and Ω_{bar} are shown in fig.1 and compared to the magic value $\Omega = 1$ which is the preferred value for aesthetical and theoretical reasons (to avoid fine tuning in initial conditions, and to agree with inflation theories). From all these values, one can draw two main conclusions:

1) All these estimates are below 1. However, the value $\Omega = 1$ is not at all excluded. The allowed range for the total contribution to Ω is $0.001 < \Omega_{tot} < 2$ where the lower limit comes from visible matter and the upper limit comes from the minimum estimate of the age of the universe combined with the measured expansion rate. To reach $\Omega = 1$, it seems unavoidable to invoke intergalactic non baryonic dark matter, such as:

WIMPs (Weakly Interacting Massive Particles: heavy neutrinos ν_h, or lightest supersymmetric particle LSP...)

or Light Neutrinos such as 30 to 100 eV ν_e or ν_μ or ν_τ (a light LSP could also be in principle possible).

2) The comparison of the allowed range for Ω_{lum}, Ω_{halo} and Ω_{bar} suggests that the halos of spiral galaxies, like our own galaxy, could be partly or totally made of MACHOs (Massive Astrophysical Compact Halo Objects) which is almost the only possibility left for baryonic dark matter: these MACHOs could be either aborted stars (brown dwarves, planet like objects), or star remnants (white dwarves, neutron stars, black holes) [1].

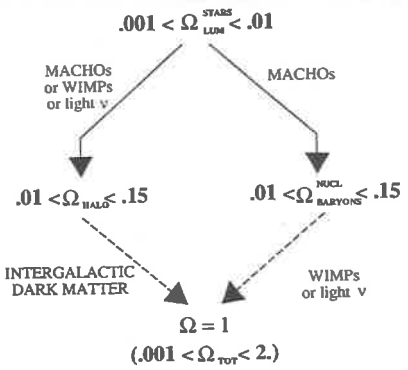

Fig.1 - Present status of Ω determinations

LEP + $p\bar{p}$ COLLIDER CONSTRAINTS ON WIMPS CANDIDATES WITH $\Omega_{WIMP} = 1$

Heavy Dirac or Majorana Neutrino ν_h

The LEP results on the Z^0 width, combined with the upper limits on the ν_e, ν_μ and ν_τ masses (10 eV, 250 keV and 35 MeV) excludes the possibility of any Dirac or Majorana neutrino in the mass range 35 MeV to 40 GeV. In particular, this excludes (fig.2) the 3 to 7 GeV range, which would naturally give $\Omega_{\nu h} = 1$ from the relic density which can be reliably estimated for heavy neutrinos in standard cosmology.

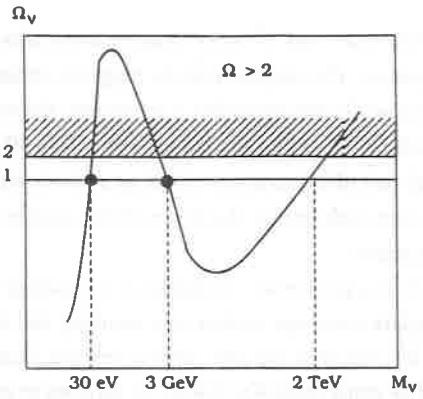

Fig.2 - Ω_ν as a function of the Dirac ν mass

Lightest Supersymmetric Particle (LSP)

1) Boson

An illustrative candidate of that type is the sneutrino $\tilde{\nu}$. The contribution of a $\tilde{\nu}$ to the width of the Z^0 is half that of a standard neutrino. Again, from the LEP results one can exclude a $\tilde{\nu}$ with mass < 35 GeV at the 3σ level.

2) Fermion

The LSP could naturally be in that case the neutralino χ, a linear combination of the photino, the zino and the two higgsinos which are necessary in the minimal supersymmetric theory.

- Again, the residual cosmological density of neutralinos having survived annihilation can be reliably estimated. The decoupling time is determined by their low-energy annihilation cross section which depends mostly on the neutralino mass and the lightest scalar-fermion mass (fig. 3). From CDF ($p\bar{p}$ experiment), we know already that the sfermion masses are > 100 GeV. Demanding $\Omega_\chi = 1$, this implies that 15 GeV < $M\chi$ < 1 TeV.

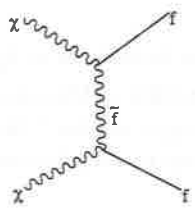

Fig. 3 - Annihilation diagram for neutralinos

- What do we learn from LEP? The Z^0 is not coupled to photino-photino, nor to Zino-Zino but does couple to two higgsinos. This implies that the higgsino masses are higher than 40 GeV although there are some loopholes in the derivation. Furthermore, the wino mass is greater than 40 GeV (again from LEP), which favours also a Zino mass greater than 40 GeV in any natural model. In summary LEP cuts already part of the parameter phase space for neutralinos below 30 GeV. This is bad news for direct detection experiments. As the neutralino masses get higher and higher, the rate of WIMPs scattering decreases.

- Furthermore, neutralinos can interact on quarks at low energy via two types of diagram, fig. 4 : the first one with squark exchange implies spin coupling and consequently no coherence factor, the second one via Z^0 exchange induces some coherence factor. Of course, this second diagram would be preferred by experimentalists due to the increase of the rate of elastic scattering. However, the chances that this process takes place are further reduced by LEP for < 30 GeV neutralinos.

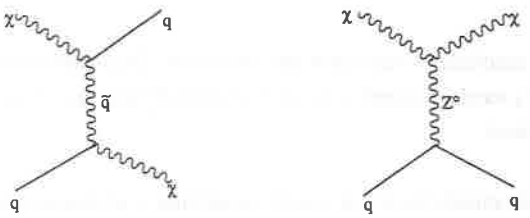

Fig. 4 - Elastic scattering diagrams for neutralinos

IS OUR GALACTIC HALO MADE OF MACHO's or WIMPs?

To answer this question, the idea [2] is to survey for several months, at 10% accuracy or better, the luminosity of a large number of stars in the Large Magellanic Cloud (LMC), see fig. 5, and search for stars that undergo a characteristic brightening due to a MACHO passing near the line

of sight and producing a gravitational microlensing event: when a spatially-small massive object (a deflector D which is the MACHO) happens to lie near enough to the line of sight between a light source (a star S from the LMC) and an observer O, then the observer collects more light from the star than he would in the absence of this deflector.

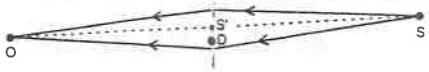

Fig. 5 - Microlensing of a LMC star (S) by a MACHO (D)

Of course, the observer, deflector and source stars are all moving (with typical galactocentric velocities of 200 km/s), so that the brightening of the star is time-dependent. The important characteristics of this light curve are its symmetry, unicity (the brightening occurs only once) and its achromaticity (the brightening is identical whatever the filter used by the observer).

The probability that a star undergoes a brightening due to microlensing with an amplification larger than 1.34 is simply the probability that the line OS crosses the zone of gravitational influence of area πR_0^2 associated to a deflector where $R_0^2=4GMd/c^2$ (M mass of the deflector) is the Einstein ring. For various values of deflector mass (MACHO masses), we give in table 1 the mean values of the excitation time (above 1.34 amplification) and the mean number of microlensing events expected for a survey of 10^6 stars in the LMC monitored during 10^7 seconds (4 months) [3].

Two groups , one in the US (Livermore, Berkeley), one in France (Saclay, Orsay, Paris, Marseille) are setting up experiments based on these principles. The experiments will be located in Chile and maybe also in Australia. This survey will be of interest for both particle physics and astrophysics. If MACHOs are indeed found, this will give a strong indication that non-baryonic dark matter is not clustered around galaxies, meaning that present searches for WIMPs are likely to be ineffective. On the other hand, if such compact objects are not found, then there would be an added incentive for all kind of WIMPs searches.

Table 1 : Microlensing events characteristics

Deflector Mass ($M_\odot$)	Mean R_0 (km)	Mean μlensing time	Nb of μlensing events
> 10	$> 3\ 10^9$	$>$ 1 year	0.5
1	$1\ 10^9$	3 mths	1.0
10^{-2}	$1\ 10^8$	9 days	5
10^{-4}	$1\ 10^7$	1 day	50
10^{-6}	$1\ 10^6$	2 hrs	500
10^{-8}	$1\ 10^5$	12 mins	5000

DIRECT DETECTION

The hypothesis that dark matter particles are gravitationally trapped in the galaxy leads to the conclusion that, like stars, they should have a local Maxwell velocity distribution with a mean spread of 250 km/s. Then, the mean kinetic energy E_r received by a nucleus of mass M_n (in units of GeV) in an elastic collision with a dark matter particle of mass M_X is:

$$E_r = 2 \text{ keV } M_n M_X^2/(M_X+M_n)^2$$

The energy distribution is roughly exponential [4]. The expected event rate for elastic scattering on a given nucleus, assuming that 0.4 GeV/cm^3 is the local density of the halo (needed to account for the flat rotation curve of stars) depends only on the mass and interaction cross section.

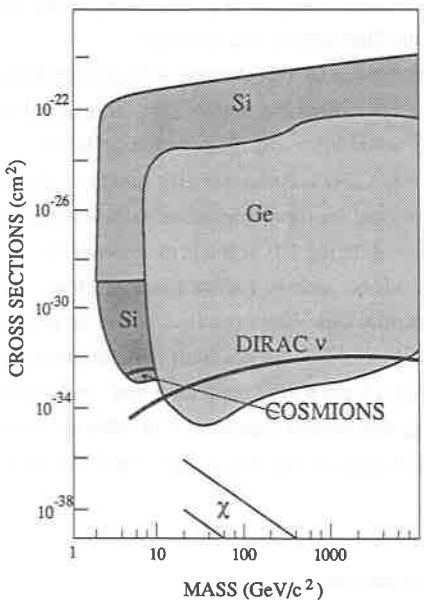

Fig. 6 - Exclusion zones for dark matter particles

Semiconductor Germanium and Silicon detectors have already set limits on cross sections and masses of dark matter particle [5]. Fig. 6 shows the exclusion plot for the mass and interaction cross sections of WIMPs obtained by these experiments.

Dirac neutrinos with masses from 11 GeV to 3 TeV are excluded. This closes almost completely the remaining allowed window by cosmology (fig. 2).

Cosmions are particles which were invented to solve both the dark matter problem and the solar neutrino problem [6]. If they exist, their masses (4 to 10 GeV/c^2) and cross sections on hydrogen (few picobarns) are well predicted. A special silicon experiment [7] excludes nearly all of the mass range possible for cosmions with coherent nuclear interactions (fig. 7) [8].

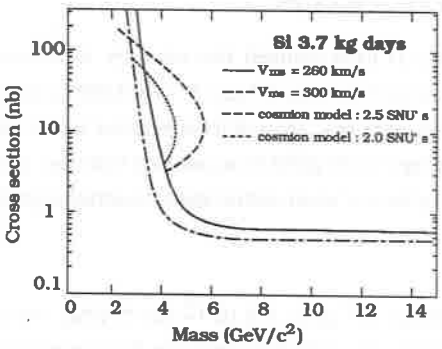

Fig.7 - Exclusion plots for the silicon experiment [7]. Also shown are the expected curves where should lie the Cosmions with coherent scattering for a resulting neutrino flux of 2 and 2.5 SNU's [8].

These conclusions depend crucially on the knowledge of the response of the detector to nuclear recoils in the keV range; fig.8 shows the relative ionisation (silicon nucleus/electron) as a function of the kinetic energy. These data have been obtained by using pulsed neutron beams [9]. They agree reasonably well with the predictions of a statistical model by Linhard et al. (LSS theory [10]).

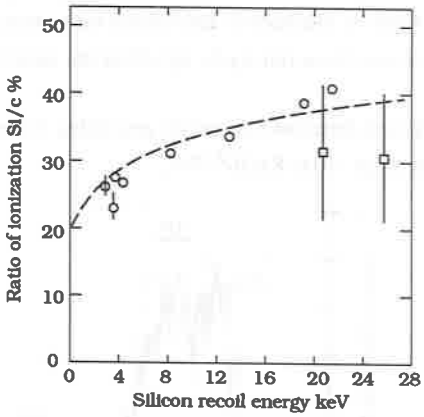

Fig.8 - Ratio between the observed energy (equivalent electron energy) and the calculated recoil energy as a function of the Silicon recoil energy.

Finally neutralinos (fig.6) are presently out of reach (rates 2 to 3 order of magnitudes below the radioactivity background) from these conventional techniques. The recent success in measuring both the ionisation and heat from a silicon bolometer looks promissing as a mean to reject background.

SEARCH FOR CHARGED DARK MATTER (CHAMPS)

A. de Rujula, S. Glashow and U. Sarid [11] have claimed that contrary to a common prejudice, dark matter halos could be made of charged particles C^+ and C^- (CHAMPS), provided that the mass of these particles is in the range 10 to 1000 TeV. Most of these particles should appear in form of superheavyhydrogen (C^+e^-) whose energy levels differ from ordinary hydrogen only by 1/2000 (relative difference in reduced mass) and in form of small neutral atoms (neutrachamps C^-p).

Search for C^+e^-.

The predicted terrestrial abundance for the past 10^7 years is $2\ 10^{-12}$ (10 TeV/M). Note that below 10^4 TeV these particles should be constantly mixed by the currents in the ocean [12]. An experiment [13] designed to search for superheavy isotopes of hydrogen started in Paris two years ago. This search is based on the centrifugation mostly of sea water (efficient above 10 TeV), followed by atomic spectroscopy. It is then sensitive to masses of 10^4 TeV to 10^8 TeV. The laser spectroscopy is based on the 1S to 3S excitation. The first results (fig. 9) were reported early this year [14]. With the recent improvements in the data analysis (combined runs) the experiment provides now a limit at 90% confidence level for the relative abundance in sea-water of superheavy hydrogen (10 to 10^4 TeV) compared to ordinary hydrogen of 10^{-14}.These results supplement those obtained by P. Smith et al.[15] from natural water by electrolysis and density measurement ($< 10^{-15}$) which are relevant however only if the evaporation-rain cycle would be the same for superheavy water as for light water.

A reported balloon experiment [16] using track etch detectors rule out the possibility that our halo is made of charged massive particles in the mass range 350 to $8.6\ 10^4$ TeV.

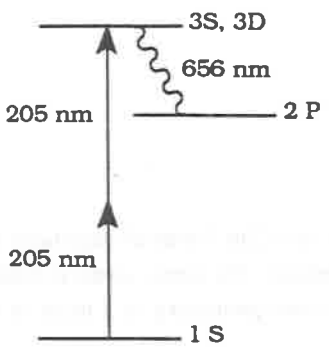

Fig. 9a - Two photon excitation scheme

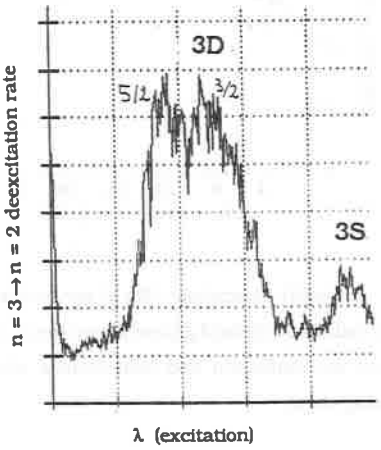

Fig. 9b - Excitation curve in the deuterium region

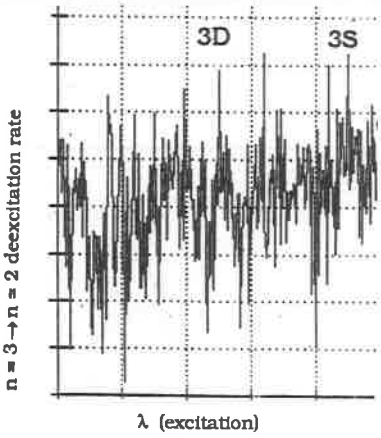

Fig. 9c - Excitation curve in the region where the presence of superheavy hydrogen is expected

Neutrachamps

The same previous experiment can also rule out masses of neutral C^-p composites between 100 and 4.10^4 TeV provided that they charge exchange with C or O nuclei with a cross section having a value in the interval 30mb to 30b. However recent calculations favour much higher cross sections (few thousand barns) [17].

THE CASE FOR LIGHT NEUTRINOS AND DETECTORS FOR THE COSMIC NEUTRINO BACKGROUND

Although they are not favoured by theories dealing with small scale structure formation (galaxy formation), 30 to 100 eV neutrinos are quite appealing to explain the nature of our halo [18].

The ν_e is now excluded due to the severe upper limit on the mass (10 eV)[19]. However the ν_μ and ν_τ are perfectly viable candidates. Even the limits on their masses coming from SN1987A [20] are not stringent enough.

Various theoretical proposals [21] were made in the past for the detection of the cosmic neutrinos. One involved effects on the endpoint of the Curie plot in tritium decay, another involved coherent effects of mechanical pressure of massless or massive particle, and other ones spin precession effects on polarized electrons and induced currents in superconductors. All these effects are extremely small and out of reach by present techniques.

Another method was recently presented [21]. It assumes a large magnetic moment for the ν_e as suggested by the observed (?) anticorrelation between the sunspot cycle and the solar neutrino flux. It is based on the bremsstrahlung in the coherent scattering of the neutrinos off free electrons in the detector material (1kton of highly conducting metal at 10 mK).

Since all this looks a little bit like science fiction, we can add another fascinating possibility. If our galactic halo is made of light neutrinos there should be a sharp resonant absorption line in the

spectrum of ultrahigh energy intergalactic neutrinos reaching the earth (fig. 10). The detection of such a narrow line would be a proof of the neutrino halo. Its position would provide for the neutrino mass: $2 M_\nu E_\nu = (M_{Z0})^2$.

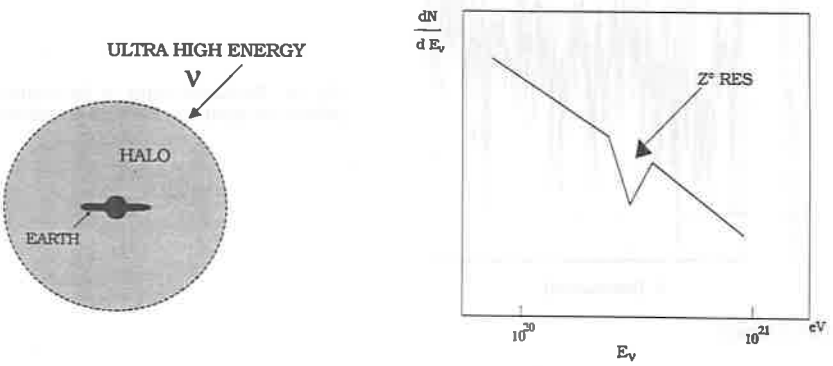

Fig.10 - ν resonant absorption by our galactic halo.

Obviously the direct (laboratory or next supernova) or indirect (oscillations) measurements of the ν_μ and ν_τ masses are of crucial importance in the context of the dark matter problem.

CONCLUSIONS

Where has all the matter gone? We are still desperately searching for the dark matter.

ACKNOWLEDGEMENTS

I thank J. Rich for many helpful discussions, R. Dosbioz and H. de Lignieres for the drawings, O. Lebey for editing the manuscript.

REFERENCES

1. B. Carr, The Quest For The Cosmological Constant, Moriond 1990, Editions Frontières.

2. B. Paczynski, Ap. J. **304** (1986) 1.

3. A. Milsztajn, Proceedings of the Rencontres de Moriond 1990, edited by O. Fackler and J. Tran Thanh Van, Publisher Editions Frontieres, p. 481.
M. Moniez, Orsay preprint, LAL 90-20, 1990 (Moriond Astrophysics, Les Arcs 1990).

4. J. Rich, in Dark Matter (Moriond 1988), edited by J. Audouze (Editions Frontières), p. 43.
J. R. Primack, B. Sadoulet and D. Seckel, Ann. Rev. Nucl. Part. Sci., **38** (1988) 751.
P.F. Smith and J.D. Lewin, Phys. Reports, **187** (1990), 203.

5. S. P. Ahlen et al., Phys. Lett. **B195** (1987) 603.
D. O. Caldwell et al., Phys. Rev. Lett. **61** (1988) 520.
J. Rich, R. Rocchia and M. Spiro, Phys. Lett. **B194** (1987) 173.

6. J. Faulkner and R.L. Gilliland, Ap. J. **299** (1985) 994.
D. N. Spergel and W.H. Press, Ap. J. **294** (1985) 663.
W. H. Press and D. N. Spergel, Ap. J. **296** (1985) 679.
R. L. Gilliland et al., Ap. J. **306** (1986) 7038.

7. D. O. Caldwell et al., Phys. Rev. Lett. **65** (1990) 1305.

8. J. Kaplan, F. Martin de Volanay, C. Tao and S. Turck-Chièze, to appear in Ap. J.

9. G. Gerbier et al., Phys. Rev. **D42** (1990) 3211.

10. J. Lindhard et al., Mat. Fys. Medd. Dan. Vid. Selsk. **33** n° 10 (1963).

11. A. De Rujula, S. Glashow and U. Sarid, Nucl. Phys. **B333** (1990) 173.

12. W. S. Broecker and T. H. Peng, Tracers in the sea, Eldigio Press, 1982.

13. B. Pichard et al., Phys. Lett. **B193** (1987) 383.

14. M. Spiro, Proceedings of the Rencontres de Moriond 1990, edited by O. Fackler and J. Tran Thanh Van Publisher Editions Frontieres, p. 489.

15. P. Smith et al., Nucl. Phys. **B206** (1982) 333.
T. K Hemmick et al., Phys. Rev. **D41** (1990) 2074.

16. S. W. Barwick et al., Phys. Rev. Lett. **64** (1990) 2859.

17. J. L. Basdevant, private communication.

18. R. Cowsik and J. Mc Clelland, Phys. Rev. Lett. **29** (1972) 669.
J. L. Basdevant, Preprint IAP- July 1984.

19. J. Wilkerson, to be published in the Proc. of Neutrino '90 (Geneva 10-15 June 1990).

20. J. A. Grifols and E. Masso, Phys. Lett. **242** (1990) 77.
G. Raffelt and D. Seckel, Phys. Rev. Lett. **60** (1988) 1793.
K. J. F. Gaemers et al. Phys. Rev. **D40** (1989) 309.

21. A. Loeb and G.D. Starkman, preprint IASSNS-AST90/10 submitted to Phys. Rev. Lett. References therein.

Alain Bouquet, Marc Lachièze-Rey and Fang Lizhi

GRAVITATIONAL LENSING

Laurent Nottale

CNRS. DAEC.
Observatoire de Paris-Meudon. F-92195 Meudon Cedex. France

Abstract.

This meeting is an opportunity to take stock of more than 70 years of theoretical and now observational work on gravitational lensing. We recall the early history of the field, considering lensing not only from the view point of mirages (i.e. image multiplication), but of any effect which the inhomogeneous universe implies on the propagation of light. Then we particularly consider: gravitational redshift effects, the ability of lensing at explaining discrepant reshift QSO-galaxy associations, microlensing by compact objects and finally some cosmological applications of lensing.

1. Early History of Lensing.

I take occasion of the partly historical character of the present meeting, which commemorates the discovery of the Microwave Background Radiation, to remind some historical stones in the field of another great consequence of Einstein's theory, i.e. gravitational lensing. In the present contribution, the expression "gravitational lensing" will be accepted in an extended sense, meaning any effect of gravitation on light. We will attempt at being as complete as possible up to the mid sixties, after which the burst of the subject prevents from being able to account exhaustively for it in the present frame.

The possibility of an effect of gravitation on light was first considered by Newton himself, who conjectured, in the frame of his particle theory for light, that such particles may be deviated by masses: "*Do not bodies act upon light at a distance and by their action bend its rays; and is not this action strongest at the least distance?*".[1] Soldner in 1804 calculated the expected deviation and found the now well known Newtonian result $\alpha=2GM/c^2r$.[2,3]

However the triumph of the wave theory of light during the XIXth century certainly prevented from taking this result seriously, before the problem of the interaction of matter (and gravitation) with light comes at the center of Einstein preoccupations in physics. As early as 1907, in the paper in which he first introduced the equivalence principle, he wrote: "*We will therefore assume the complete physical equivalence of a gravitational field and of a corresponding acceleration of the reference system [...] The clock at a point P for an observer anywhere in space runs* $(1+\phi/c^2)$ *times faster than the clock at the coordinate origin [...] It follows that light rays are curved by the gravitational field...*".[4]

In 1911, Einstein wrote a paper entitled "*On the influence of gravitation on the propagation of light*", in which he considered both the effects of gravitational redshift and of light deviation.[5] While he obtained yet the correct general relativistic result for the now so-called Einstein redshift, his light deviation result was still the Newtonian one. This is because the redshift effect is a purely temporal effect, which implies only the g_{oo} term of the metrics, itself being related to the scalar Newtonian potential, while the deviation effect implies also the spatial component g_{rr}, i.e. the tensorial instead of scalar character of the gravitational field. Finally the complete bending effect $\alpha=4GM/c^2r$, i.e. 1.75 arcsec at the solar limb, was predicted by Einstein as a direct consequence of the full general theory of relativity.[6]

Strictly speaking, the first observation of a gravitational lensing effect is the displacement of stars near the sun during the 1919 solar eclipse as observed by Eddington.[7] The question of light bending by the sun is a domain by se which is most of the time related to classical tests of general relativity, so that it will not be considered any more here (a review of its present status may be found e.g. in Ref.8 and references therein; see also Ref. 3).

The credit of first recognizing the potential action of a mass as a gravitational mirage (i.e. image multiplier) should certainly be given to Eddington (1920):[9] "*If two independent stars are seen in the same line of vision within about 1", one being at a great distance behind the other,* [...] *it would seem that we ought to see the more distant star not only by the direct way, which would be practically undisturbed, but also by a ray passing round the other side of the nearer star and bent by*

it to the necessary extent." The first occurence of the term "gravitational lens" seems to be due to Lodge (1919) who used it, but in order to dismiss it, writing:[10] "*It would be impermissible to say that the solar gravitational field acts as a lens, for it has no focal length*". The idea became at that time spreading widely enough that E. B. Frost, among others, outlined in 1923 a program for the search of such lens effects among stars.[11] Chwolson realized in 1924 that in case of perfect alignment of two stars, the image of the background one would become a ring centred on the foreground one.[12]

The subject burst again during the years 1936-37, after R.W. Mandl, a Czech electrical engineer, wrote to Einstein to draw his attention about the gravitational lens phenomenon.[13] Einstein then made some calculations[14] from which he rediscovered the ring configuration independently from Chwolson and concluded that any chance to observe the phenomenon was extremely small. Several subsequent papers were then published on the subject.[11,15-20]

Among all the works on the subject, Zwicky's contribution stands out as a particularly pioneering and far reaching one. The idea of gravitational lensing was relayed to him from Mandl by V.K. Zworykin. Zwicky realized that, if indeed lensing between stars may be very difficult to detect, this may not be the case with galaxies. The interesting point is that he was able to reach this conclusion precisely because he had just a few years ago discovered dark matter in clusters of galaxies, and so could use in his calculation galaxy masses of several 10^{11} solar masses, far larger than those assumed by others. We quote from his two 1937 papers: "*The problem in question, however , takes on a radically different aspect, if, instead of in terms of stars we think in terms of extragalactic nebulae. Provided that our present estimates of the masses of cluster nebulae are correct, the probability that nebulae which act as gravitational lenses will be found <u>becomes practically a certainty</u>*". "*The discovery of images of nebulae which are formed through the gravitational fields of nearby nebulae would* [...] *furnish an additional test for the general theory of relativity* [...] *enable us to see nebulae at distances greater than those ordinarily reached by even the greatest telescopes* [...] *throw very welcome new light on a number of cosmological problems* [...] *provide the most direct determination of nebular masses.*" Zwicky both made a definite prediction about the future discovery of lensing, (while most authors, even in the recent years, considered it as of purely mathematical interest), and understood that it was expected to become a unique and irreplaceable tool in cosmology, which is now the case. It will be seen hereafter how most of the program outlined hereabove is now undergoing achievement. Zwicky also proposed neutron stars as interesting objects for lensing,[20] and this is indeed now a subject of increasing interest.

The subject apparently fell again in a latency period until the beginning of the sixties.[21-26] New ideas of applications of lensing were then suggested in the years 1964-65, such as variability through microlensing by Liebes,[27] time delays and their use for the determination of cosmological parameters H_o and q_o by Refsdal[28], and the influence of lensing on the quasar phenomenon by Barnothy.[29] But at the same date the question was renewed from a completely different point of view, which may be called the "cosmological approach" to lensing.

2. The Cosmological Approach.

Indeed Zeldovich in 1963,[30,31] and independently Feynman in 1964,[32] were the first to investigate the possible changes brought to the magnitude-redshift and diameter-redshift relations due to the clumpy distribution of matter in the Universe, as compared to the totally uniform one which was assumed in the derivation of the Mattig relation.[33] This interrogation led to a whole field of research[34-41] most of the time based on the use of the optical scalar equations as written by Sachs in 1961,[42] which describes in a fully relativistic way the propagation of a light beam at the approximation of geometric optics. In this approach this propagation depends on two terms, a "matter" term (expressed in terms of the Ricci tensor, or equivalently directly in terms of the energy-momentum tensor) and a "shear" term, which depends on the Weyl tensor. In a direct interpretation the matter term describes the mass which is present into the light beam while the shear term accounts for external masses. But as will be seen hereafter, this interpretation finally evolved into a more interesting one.

The question first asked and then particularly studied by Dyer and Roeder,[43-45] was whether the actual emptiness of light beams applying on most observed distant sources (in the case where all the matter was distributed into clumps) disabled the Mattig relation. These studies allowed to realize clearly, by demonstrating that for such beams passing far from any clump the diameter-redshift relation did not show a minimum any more, that a Universe of non vanishing density plays the role of a lens as a whole. The problem was clarified by Weinberg's remark that, provided one may define for any source Robertson-Walker coordinates (which is equivalent to the neglect of redshift effects, see Ref.46) conservation of energy implies that the Mattig relation should remain valid in the mean.[47] In fact the amplification due to the shear effect of any mass exterior to a light beam compensates in the average the attenuation due to its emptiness. The question now still not fully solved is that of a detailed energy balance accounting for all levels of the hierarchy of structures present in the Universe.

The Optical Scalar Equation approach has the advantage over the pseudo-Newtonian one of being able to take naturally the background universe into account.[46]

Progress was accomplished in parallel on the "classical" lens problem. Of particular importance was the linearized Einstein theory of transparent lens by Bourassa and Kantowski[48] on which a large number of subsequent studies and models have been based.

3. Gravitational Mirages.

The subject entered in its modern era after the discovery in 1979 by Walsh, Carswell and Weymann of the first case of gravitational mirage, the double QSO 0957+561.[49] The case of the QSO pair 1635+267 (3.8" separation) is also instructive from the historical point of view: Two years before, in 1977, Sramek and Weedman had discovered it in an objective prism survey, but the low resolution of the spectra yielded redshifts of 1.94 and 1.99.[50] One must wait 1984 for their spectra to be recognized as identical, with redshifts 1.961 ± 0.003.[51] The number of QSO/galaxy lenses is now of the order of ten or more (see Ref. 52). They are expected to remain a rare

phenomemon, because of the low volume density of QSOs; it is only the advantage given to them by the high intrinsic luminosity and surface brightness of QSOs and their associated large redshifts which accounts for them having been observed at first.

But clearly statistical arguments indicate that one expects a far larger number of galaxy/galaxy lenses. However the extension of galaxies, implying superposition of lens and images, combined with the difficulty of observing high redshift galaxies, partly because of the $(1+z)^{-4}$ decrease of surface brightness with redshift, prevented up to now to achieve such an expectation. The first case of galaxy/galaxy lens, as observed by Le Fèvre et al.[53], is an example of these difficulties: images of mag>23 separated by less than 2 arcsec, two redshift systems (lens + source) superimposed int the same spectra. The research of lenses among distant galaxies and radiogalaxies is now a living field[54] and comes in completion to the continuing search among QSOs. Such searchs are now led into the form of coordinated programs: a 3 years ESO key-program (p.i.: J. Surdej) is presently running on that subject.[55]

A second burst of activity in the field of gravitational lensing followed the discovery by Fort et al.[56-58] and Lynds and Petrosian[59] of the images of distant galaxies distorted into giant arcs by the lensing effect of clusters of galaxies as a whole. The importance of clusters of galaxies as potential lenses had been stressed many years ago by some authors. Karoji and Nottale[60] had presented observational evidence in 1976 that the rich clusters of galaxies were able to perturb significantly the Hubble diagram of background galaxies. This was confirmed by subsequent studies.[61] Nottale and Hammer[62] have remarked that the richest clusters in the sky, if situated at $z \geq 0.2$, should reach their critical density. At the same date, Turner, Ostriker and Gott[63] have considered in a basic paper the effects of clusters, have insisted on the amplification bias and have predicted image separation of some ten arc seconds. The number of clusters behind which arcs have been found is now larger than 10.[64]

4. Gravitational Redshifts and the 3K Radiation.

There exists two different spectral shift effects. The first one is the generalization of the Einstein effect, (i.e. a consequence of a difference in gravitational potential between source and observer): in its application to the cosmological domain, one should account for the fact that extragalactic objects are embedded in a cosmological background of non zero density. One expects a center-edge effect for a cluster of galaxies of mass M, external radius R and core radius r_0:[46,65]

$$\delta z \approx \frac{G}{c^2} \frac{M}{R} [1/2 + \ln(R/r_0)]$$

Though expectedly small for most clusters, such an effect could eventually become observable for the richest of them, particularly those with a strongly peaked density profile in their central regions. For example, a cluster of 3 Mpc radius, 5.10^{15} $M_\odot$ total mass and 30 kpc internal cut-off radius would show a redshift difference between its central region and its limb of $\delta z \approx 5m/r \approx 100$ km/s, once translated in terms of radial velocity.

The redshift and time delay resulting from the crossing of a cluster by the light coming from a background source constitute a fainter effect, harder to set theoretically. It was first studied by

Rees and Sciama[66] in the frame of the vacuole model. However their calculation was only approximate, in that they did not explicitely work out the matching of metrics throughout the boundaries. This was done by Dyer[67], who get a result exactly twice the Rees and Sciama value. However Dyer's conclusion remained that this gravitational redshift was inobservable, since masses larger than 10^{19} $M_\odot$ would be needed. This conclusion was revised by a generalization of this calculation, made in terms of immediately observable quantities, to clusters in a phase of fast contraction[68]. In this case the temperature decrement may reach:

$$\delta T/T = -4\sqrt{2}\ (m/r_i)^{3/2}$$

where $m=GM/c^2$. Values of $\delta T/T$ larger than 10^{-5} can be obtained for clusters whose total mass would be greater than 10^{16} $M_\odot$. The problem of the setting of the effect in the frame of more realistic density profiles and velocity fields remains open. If, as is the case for the generalized Einstein redshift (see hereabove), such an account increases the theoretical expectation, this would increase also the possibility that the gravitational effect is indeed at work in the direction of the richest clusters of the Universe.

5. Lensing and the Anomalous Redshift Controversy.

One of the main argument of the supporters of the possible existence of large non cosmological redshifts consists in the apparent association on the sky of objects with very different redshifts. The argument may take its full weight only when it is accompanied by strong statistical evidence, which is the case, to my knowledge, for two samples corresponding to complete searches, discrepant quintets of galaxies[69] and Arp's complete sample in 0.174 square deg. of QSO-companion galaxy associations.[70] Gravitational lensing, by its ability to make correlations between foreground lensing matter and background objects, is clearly the best candidate standard theory to account for such observations, as recognized by Canizares.[71]

The suggestion that gravitational lensing effects may explain some of the discordant redshift galaxy-galaxy associations was made by Hammer and Nottale.[72] They studied the particular case of quintets of galaxies, for which statistical analyses on complete samples had previously been reported by Rose[73] and Nottale and Moles.[69] The hypothesis that a quartet acts as a lens on a background galaxy, applied in particular to VV172, allows to determine the quartet mass, and one finds precisely the dynamical mass obtained from its velocity dispersion.

Concerning QSO-galaxy associations, the hope to explain them by microlensing of stars or compact objects from the foreground galaxy halo was finally deceived, mainly because of the proximity of the galaxies.[74-77] However it was demonstrated by Nottale[46] that lensing by the combined effects of groups and distant clusters is likely to be the cause of the excess. Let us summarize the argument.

In a total area of 0.174 deg^2 made of annular regions around 27 companions of large nearby galaxies, Arp found a total number of 15 QSOs of apparent magnitude <20, while at most ≈2 were predicted if one admits a surface density $\sigma(<20)\approx 10$ QSO/deg^2. The probability of such a result is

less than 10^{-8}. However a case by case analysis of the data reveals that: *one object (M=-17.5) is not a QSO;*3 objects should rather be referred to as nuclei of Seyfert galaxies (M≈-21, to be compared to the remaining sample M<-25.5);*2 objects lie farther than the completion limit; *1 object exceeds the magnitude limit m<20. Thus only 8 QSOs are left, which still yield a significant effect with probability less than 10^{-3}.

Let us now consider the foreground matter distribution. Arp's method consists in searching around "galaxy-companion" pairs. But most of them are of different redshifts, and in fact result themselves from projection effects of local supercluster groups (z<0.001) upon background groups or clusters (z≈0.025).

But the main point is that *the distribution of the observed QSOs with respect to distant clusters is not at random*: Indeed, half of the sample falls behind Zwicky clusters, while distant clusters are very powerful amplifiers[62,63], as definitively demonstrated by the discovery of gravitational arcs.

So the excess density may be explained by the combined effect of :

**Amplification by halo stars or compact objects from companion galaxies*: at z≈0.025, one finds that 0.5-1.5 additional QSOs may be explained in this way, confirming once again the non ability of microlensing at making the whole effect.

**Lensing by matter term of halos + group + nearby clusters*. The surface density change is the result of two conflicting effects: increase due to luminosity magnification, decrease of the accessible volume by light beam convergence. For a source population whose integrated number density goes in terms of apparent magnitude as $\log(\sigma_o)=k.m$, this results in a final effect:

$$\sigma/\sigma_o = Amp^{2.5\,k-1}$$

For QSOs with m<20, one has k=0.8, so that $\sigma/\sigma_o=Amp$. So one finally gets for an isothermal sphere, in terms of velocity dispersion and apparent angle:

$$\sigma/\sigma_o = 1 + 4\pi\frac{\sigma_v^2}{c^2}\theta^{-1}$$

For a galaxy, with σ_v≈300 km/s, one gets $\sigma/\sigma_o\approx 1+0.05/\theta_{arcmin}$; for a group, with σ_v≈300 km/s, one gets $\sigma/\sigma_o\approx 1+0.2/\theta$ and for a typical cluster, $\sigma/\sigma_o\approx 1+0.5/\theta$. The final effect on the whole sample may be estimated to ≈1.3 additional QSOs.

**Lensing by distant clusters*: This is the dominant effect, due to their large redshifts (we recall that lensing effects increase very rapidly in terms of the deflector redshift up to z≈0.7).[46,62] Their magnification effect may be estimated to be ≈x2 to x3, yielding $\sigma/\sigma_o\approx 2.6$-3.9, and finally ≈4.5-6.8 additional QSOs.

The combined effect yields to an estimated number of 6.5 *to* 10 *QSOs, which compares fairly well to the observed number of* 8. So Arp's observations would have been the result of selection effect through the amplification bias. There are regions of the sky where, due to statistical fluctuations (or to the actual existence of very large scale structures) the surface density of distant

clusters of galaxies is larger than the average. These regions are expected to also yield an increased density of QSOs due to the lensing effect. The problem is that Arp's complete sample has been defined from an extension of a region where an excess density of QSOs had been already found by chance. This analysis is confirmed by the fact that the density of Zwicky clusters in Arp's fields is found to be ≈2.5 times that of the average catalog (see ref. 46 for additional information).

Another effect of QSO-galaxy associations has been recently found by Webster et al.[78]: 11 galaxies were found close to QSOs instead of an expected number of 2.6. One may conjecture that this effect may be explained by the same ingredients: lensing by cluster + selection effect due to amplification bias.

6. Microlensing.

Microlensing, i.e. lensing by stars or compact objects is a subject of increasing interest. While it was at first dismissed with respect to lensing by galaxies because of the separation of possible images (some 10^{-6} arcsec) too small to be observable, it has been later realized that it could be detected through variability and spectral change and so could yield several interesting physical informations on source and deflector. Microlensing, a subject now more and more studied from the theoretical and model approach (see e.g. the review by Schneider[79] or references) has been considered from the observational point of view into three different configurations:

*Effect of compact objects in halos of foreground galaxies: it has been shown by Nottale[80] that the whole behaviour of the OVV 0846+51W1, (4 magnitude burst over a time scale of ≈ 1 month, QSO spectrum turning to BLLac at brightest, variation of optical spectral index with luminosity, situation 12" south of a z=0.072 galaxy)[81] may be readily explained by the lensing differential action of a compact object of Jupiter mass ($\approx 10^{-3}$ $M_\odot$) which would be part of a 10^{12} $M_\odot$ halo, on the central regions of a QSO. It was independently suggested by Ostriker and Vietri[82] that BLLacs may be the result of lensing of AGNs combined with confusion between lens and source.

*Microlensing of individual images from mirages: this has been now observed in at least two cases, the double QSO 0957+56 and the "Einstein cross".[83,84]

*Search for variability of stars in the Large Magellanic Cloud due to possible compact objects in our Galaxy halo: see the specific communications on this subject in the present meeting.[85]

7. Applications of lensing.

To conclude this contribution, let us briefly consider how the applications of lensing to the measurement of masses and of cosmological parameters, (and thus to the problem of dark matter), and to the search of very distant objects, has now turned into an unescapable method in observational cosmology. Refsdal's suggestion[28] has known a beginning of achievement with the first measurement of the time delay between the images of the double QSO by Vanderriest et al.[86] and Schild.[87] But a significant improvement in the value of H_o from this data should wait either an increased knowledge of the velocity field in the galaxy and lens deflectors and of additional foreground objects, or the measurement of other time delays allowing to use the statistical method.

Maybe the domain for which lensing is now bringing the most useful informations is that of the search for dark matter. This includes mass determinations from modeling of individual mirage configurations, as well as statistical attempts (which are however complicated by the amplification bias). Up to now it has resulted into a confirmation of most dynamical estimates of masses, thus yielding an Ω_0 value not larger than ≈ 0.1. But a very large scale flat component of dark matter can not be excluded yet, even if lensing methods are also expected to be able to test for this case in the future.[88] Finally one may recall the ability which large arcs are given us, thanks to their clear morphological signature, to observe very distant possible primeval galaxies up to redshifts larger than 10 behind the richest clusters with $z<1$.[89]

References

1. Newton, I., 1704, *Optics*, Query 1, 2nd ed.
2. Soldner, J.G. von, 1804, *Berliner Astr. Jahrb.*, p.161
3. Zirker, J., 1985, *Mercury*, July-August 1985, p.98
4. Einstein, A., 1907, *Jahrbuch für Radioakt. und Elektronik* **4**, 411
5. Einstein, 1911, *Ann. Phys. Leipzig* **35**, 898
6. Einstein, 1916, *Annalen der Phys.* **49**, 769
7. Dyson, F.W., Eddington, A.S., Davidson, C.R., 1920, *Phil Trans. Roy. Soc.* **220A**, 291; *Mem. Roy. Astron. Soc.* **62**, 291
8. Will, C.M., 1989, in *"Tests of fundamental laws in physics"*, XXIVth Moriond conference, eds. O. Fackler and J. Tran Thanh Van, p.3, (Frontières)
9. Eddington, A.S., 1920, *Space, Time and Gravitation* (Cambridge University Press), p.134
10. Lodge, O.J., 1919, *Nature* **104**, 354
11. Zwicky, F., 1937, *Phys. Rev. Lett.* **51**, 679
12. Chwolson, O., 1924, *Astr. Nachrichten* **221**, 329
13. Mandl, R.W., 1936, Letter to Einstein, May 3
14. Einstein, A., 1936, *Science* **84**, 506
15. Zwicky, F., 1937, *Phys. Rev. Lett.* **51**, 290
16. Russell, H.N., 1937, *Sci. Am.* **156**, 76
17. Link, F., 1937, *Bull. Astron.* **10**, 73
18. Tikhov, A.G., 1937, *Izv. Gl. Astron. Obs. v Pulkove* **16**, 1
19. Tikhov, A.G., 1938, *Dokl. An. SSSR* **16**, n°4
20. Zwicky, F., 1941, *Phys. Rev. Lett.* **59**, 221
21. Zwicky, F., 1957, *Morphological Astronomy* (Springer-Verlag), p. 215
22. Darwin, C., 1959, *Proc. Roy. Soc.* (London) **A249**, 180
23. Mikhailov, A.A., 1959, *M.N.R.A.S.* **119**, 593
24. Idlis, G.M., and Gridneva, S.A., 1960, *Izv. Astrofiz. Inst. Acad. Nauk. Kaz.* SSR **9**, 78
25. Klimov, Yu G., 1963, *Dokl. Akad. Nauk. SSSR* **148**, 789
26. Metzner, A.W.K., 1963, *J. Math. Phys.* **4**, 1194
27. Liebes, S., 1964, *Phys. Rev.* **B133**, 835
28. Refsdal,S., 1964, *M.N.R.A.S.* **128**, 295, 307
29. Barnothy, J.M., 1965, *Astron. J.* **70**, 666
30. Zeldovich, Ya. B., 1964, *Soviet Astronomy - AJ* **8**, 13
31. Zeldovich, Ya. B., 1965, *Advances in A. and A.*, ed. Z. Kopal (NY: Acad. Press), p. 360
32. Feynman, R., 1964, Cal. Tech. Colloquium (unpublished)
33. Mattig, W., 1958, *Astron. Narichten*, **284**, 109
34. Dashevskii, V.M., Zeldovich, Ya.B., 1965, *Soviet Astr.-AJ* **8**, 854
35. Dashevskii, V.M., Slysh, V.I., 1966, *Soviet Astr.-AJ* **9**, 671
36. Bertotti, B., 1966, *Proc. Roy. Soc. London* **A269**, 195
37. Gunn, J., 1967, *Astrophys. J.* **147**, 61
38. Gunn, J., 1967, *Astrophys. J.* **150**, 737
39. Petrosian, V., Salpeter, E.E., 1968, *Astrophys. J.* **151**, 411

40. Kantowski, R., 1969, *Astrophys. J.* **155**, 89
41. Refsdal, S., 1970, *Astrophys. J.* **159**, 357
42. Sachs, R.K., 1961, *Proc. Roy. Soc. London* **A264**, 309
43. Dyer, C.C., Roeder, R.C., 1972, *Astrophys. J. Lett.* **174**, L115
44. Dyer, C.C., Roeder, R.C., 1973, *Astrophys. J. Lett.* **180**, L31
45. Dyer, C.C., Roeder, R.C., 1974, *Astrophys. J.* **189**, 167
46. Nottale, L., 1988, *Ann. Phys. Fr* **13**, 223
47. Weinberg, S., 1976, *Astrophys. J. Lett.* **208**, L1
48. Bourassa, R.R., Kantowski, R., 1975, *Astrophys. J.* **205**, 674
49. Walsh, D., Carswell, R.F., Weymann, R.J., 1979, *Nature* **279**, 381
50. Sramek, R.A., Weedman, D.W., 1978, *Astrophys. J.* **221**,468
51. Djorgovski, S., Spinrad, H., 1984, *Astrophys. J.* **282**, L1
52. Surdej, J., 1990, in "*Gravitational lensing*", Toulouse workshop, Y. Mellier, B. Fort & G. Soucail eds. (Springer-Verlag), p.57
53. Le Fèvre, O., Hammer, F., Nottale, L., Mathez, G., 1987, *Nature* **326**, 268
54. Le Fèvre, O., Hammer, F., 1990, in "*Gravitational lensing*", Toulouse workshop, Y. Mellier, B. Fort & G. Soucail eds. (Springer-Verlag), p.93
55. Surdej, J., et al., 1989, *The Messenger* **55**,8
56. Soucail, G., Fort, B., Mellier, Y., Picat, J.P., 1987, *Astron. Astrophys.* **172**, L14
57. Soucail, G., Mellier,Y., Fort, B., Hammer, F., Mathez, G., 1987, *A.& A.* **184**, L7
58. Soucail, G., Mellier,Y., Fort, B., Mathez, G., Cailloux, M., 1988, *A.& A.* , **191**, L19
59. Lynds, R., Petrosian, V., 1989, *Astrophys. J.* **336**, 1
60. Karoji, H., Nottale, L., 1976, *Nature*, **259**, 31
61. Hammer, F., Nottale, L., 1986, *Astron. Astrophys.*, **167**, 1
62. Nottale, L., Hammer, F., 1984, *Astron. Astrophys.*, **141**, 144
63. Turner, E.L., Ostriker, J.P., Gott III, J.R., 1984, *Astrophys. J.* **284**, 1
64. Fort, B., 1990, in "*Gravitational lensing*", Toulouse workshop, Y. Mellier, B. Fort & G. Soucail eds. (Springer-Verlag), p. 221
65. Nottale, L., 1990, in "*Gravitational lensing*", Toulouse workshop, Y. Mellier, B. Fort & G. Soucail eds. (Springer-Verlag), p. 29
66. Rees, M., Sciama, D., 1968, *Nature* **217**, 511
67. Dyer, C.C., 1976, *Mon. Not. R. Astron. Soc.* **175**, 429
68. Nottale, L., 1984, *Mon. Not. R. Astron. Soc.* **206**, 713
69. Nottale, L., Moles, M., 1978, *Astron. Astrophys.*, **66**, 355
70. Arp, H., 1982, *Astrophys. J. Lett.*, **263**, L9
71. Canizares,C.R., 1981, *Nature*, **291**, 620
72. Hammer, F., Nottale, L., 1986, *Astron. Astrophys.*, **155**, 420
73. Rose, J.A., *Astrophys. J.*, 1977, **211**, 311
74. Vietri, M., Ostriker, J.P., 1983, *Astrophys. J.*, **267**, 488
75. Zuiderwijk, E.J., 1985, *Mon. Not. Roy. Astr. Soc.*, **215**, 639
76. Peacock,J.A., 1986, *Mon. Not. Roy. Astr. Soc.*, **223**, 113
77. Linder, E.V., Scneider, P., 1988, *Astron. Astrophys.* **204**, L8
78. Webster, R.L., Hewett, P.C., Harding, M.E., Wegner, G.A., 1988, *Nature* **336**, 358
79. Schneider, P., 1990, in "*Gravitational lensing*", Toulouse workshop, Y. Mellier, B. Fort & G. Soucail eds. (Springer-Verlag), p. 175
80. Nottale, L., 1986, *Astron. Astrophys.*, **157**, 383
81. Arp, H., Sargent, W.L.W., Willis, A.G., Oosterbaan, C.E., 1979, *Astrophys. J.*, **230**, 68
82. Ostriker, J.P., Vietri, M., 1985, *Nature*, **318**, 446
83. Vanderriest, C., 1990, in "*Gravitational lensing*", Toulouse workshop, Y. Mellier, B. Fort & G. Soucail eds. (Springer-Verlag), p. 210
84. Irwin, M.J., Webster, R.L., Hewett, P.C., Corrigan, R.T., Jedrzejewski, R.I., 1989, *Astron. J.* **98**,
85. Spiro, M., 1990, this volume
86. Vanderriest, C., et al., 1989, *Astron. Astrophys.* **215**, 1
87. Schild, R., 1990, in "*Gravitational lensing*", Toulouse workshop, Y. Mellier, B. Fort & G. Soucail eds. (Springer-Verlag), p. 102
88. Nottale, L., 1990, in "The early universe and cosmic structures", 10th Moriond Astrophysics meeting, eds. Blanchard and Tran T. Van (Frontières)
89. Nottale, L., 1988, in "Dark Matter", 8th Moriond Astrophysics meeting, eds. Audouze and Tran T. Van (Frontières), p. 339.

Galaxies : Properties and distributions

Traditional vietnamese music performance :
From left : Professor Trân Van Khê, Bach Yên, Trân Quang Hai and Trân Thi Thuy Ngoc.

THE SPACE DISTRIBUTION OF DWARF AND LOW-SURFACE-BRIGHTNESS GALAXIES AND BIASED GALAXY FORMATION THEORIES

Trinh X. Thuan
Astronomy Department, University of Virginia
P. O. Box 3818, University Station
Charlottesville, VA 22903 USA

and

Jean-Michel Alimi
Laboratoire d'Astrophysique Extragalactique et de Cosmologie
Observatoire de Paris, Meudon, F-92195 Cedex, France

ABSTRACT

A 21-cm redshift survey of all 1845 northern galaxies ($\delta \geq -2°30'$), classified as dwarf or magellanic irregular by Nilson in the Uppsala General Catalogue, has been completed. The HI detection rate is ~84%, giving a total sample of 1557 galaxies with 21-cm redshifts.

The data was subdivided into volume-limited subsamples for two-point correlation analysis. We found that there is not a large difference between the clustering properties of dwarf, LSB and bright galaxies, confirming the visual impression given by redshift-space maps which show that dwarf and LSB galaxies follow very closely the structures delineated by bright galaxies and do not fill in the voids seen in the bright galaxy distribution. There is a suggestion that HI-rich dwarf-LSB galaxies are slightly less clustered than bright galaxies outside clusters, the ratio of the amplitudes of the bright/dwarf-LSB correlation functions being ~1.2, at a pair separation of 1 h^{-1} Mpc. Our results rule out a certain class of biased galaxy formation theories which predict a uniform spatial distribution of dwarf-LSB galaxies. If the bias parameter b_B for bright galaxies is in the range $1.0 \lesssim b_B \lesssim 2.0$, then the bias parameter b_D for dwarf-LSB galaxies is between 1.0 and 1.6. At the lower end of the range of possible b_B values, the dwarf-LSB population is unbiased. The pairwise peculiar velocity of HI-rich dwarf-LSB galaxies is ~460 $\pm$ 50 km s^{-1}, similar to that of bright galaxies outside clusters, indicating that both types of galaxies participate in the same gravitational potential.

INTRODUCTION

During the last decade, extensive redshift surveys of thousands of galaxies have revealed an extraordinary cosmic landscape where galaxies trace out large-scale structures in the shape of flattened pancakes or filaments reaching dimensions of up to ~50 Mpc. These large-scale structures delineate large voids, with diameters as large as ~65 Mpc, which appear to be completely empty of bright galaxies. These voids have been variously described as 'bubble-like structures'[1] or as part of a large interconnecting hole network resembling that of a sponge.[2]

However, there was a serious caveat to the previously described observations. They all suffer from selection effects which discriminate strongly against dwarf and low-surface-brightness (LSB) galaxies. Dwarf galaxies are so faint that they are missed by magnitude-limited redshift surveys, such as the Center for Astrophysics (CfA) survey[3] which included only galaxies brighter than $m_B = 14.5$. Within the redshift range of the CfA survey, more than 90% of the dwarf and LSB galaxies are fainter than 14.5 mag and are omitted. Dwarf galaxies are also small, so they are missed by diameter-limited surveys such as that of Fisher and Tully[4] whose lower diameter limit of 2 arc minutes is too large to include the majority of the dwarf galaxies. The ~200 dwarf galaxies in their sample probe only a relatively nearby volume of space.

Thus the question arises whether, by studying only the large-scale distribution of matter as traced by bright galaxies, we are not having a 'biased' view of the Universe. In fact, currently popular theories of biased galaxy formation[5] propose that luminous galaxies form only in regions of very high density contrast, and thus are tracers of the light, but not of the mass distribution on very large scales. The latter is better traced by dwarf galaxies which should be present everywhere,

including the voids. Inflationary cosmologies, which demand that the mass density parameter Ω be equal to 1, also require that severe biasing exists in order to be consistent with the observations that Ω (luminous matter) ~0.01 and Ω (luminous + dark baryonic matter) ~0.1.

In order to test observationally those theories of biased galaxy formation, it was essential to obtain redshifts for a reasonably complete sample of dwarf and LSB galaxies, with well-understood selection effects, and with a sky coverage and depth comparable to that of, for example, the CfA survey of bright galaxies. Then it may be possible to compare statistically the spatial distribution of bright and faint galaxies.

In addition to being important for large-scale structure problems, the study of a complete sample of field dwarf and LSB galaxies will also be crucial for tying down the faint end of the galaxian luminosity function. Knowledge of the latter can help to understand some outstanding astrophysical puzzles. One problem concerns the numerous quasar absorption lines seen blueward of the Lyman α line. Dwarf irregular galaxies have extended HI halos (~2 to 5 times the optical radius) and if they are numerous enough can provide a significant cross section to explain some of the quasar absorption lines.[6] Another problem concerns the presence of neutral hydrogen in some elliptical galaxies. Accretion of gas-rich dwarfs has been invoked[7] and knowledge of the HI-rich dwarf luminosity function would set contraints on such an accretion rate. Further, the number of dwarf galaxies around larger galaxies can, in principle, be used to set constraints on the size of massive halos around spiral galaxies and the rate of spiraling of dwarf galaxies into large galaxies due to dynamical friction.[8]

In the next section, we describe the Virginia 21-cm redshift survey of dwarf and LSB galaxies, and discuss some general properties of the

survey. In the following section, we use the two-point correlation function as a statistical measure of large-scale clustering to compare the space distribution of dwarf-LSB galaxies to that of bright galaxies. In the last section, we use our correlation function results to put constraints on biased galaxy formation theories.

The 21-cm redshift survey of dwarf and low-surface-brightness galaxies

We use the Uppsala General Catalogue of Galaxies (UGC)[9] as a starting point for assembling a complete sample of dwarf and LSB galaxies. In the UGC, Nilson[9] catalogued all northern galaxies ($\delta \geq -2°30'$) visible on the Palomar Sky Survey prints with a blue diameter larger than 1'. The UGC does not discriminate against LSB galaxies and hence is close to a volume-limited catalog. Moreover, its lower diameter limit of 1' includes almost an order of magnitude more dwarf and LSB galaxies than the Fisher and Tully[4] catalog. Our sample consists of all galaxies classified by Nilson to have an extreme late-type = a Hubble type of Dwarf, Dwarf irregular, Dwarf spiral, Irr, Sc-Irr or S-Irr; a de Vaucouleurs type of Sd-dm, Sdm, Sm or Im; or in the absence of these classifications, a van den Bergh luminosity class of IV-V or V. The objects thus selected are generally characterized by 1) a low surface brightness and 2) little or no central concentration of light on the red prints. These morphological criteria gave a list of 1845 dwarf and LSB galaxies, or 14% of the total of 12,940 UGC galaxies.

How complete is the dwarf-LSB galaxy sample thus assembled? Thuan and Seitzer[10] studied the completeness of the UGC as a function of limiting angular diameter by using the $\langle V/V_M \rangle$ test and found that the UGC was fairly complete for dwarf-LSB galaxies: $\langle V/V_M \rangle = 0.453$ for all dwarf-LSB galaxies larger than 1 arcminute, as compared to a value of 0.50 for a complete sample uniformly distributed in Euclidian space. Examination of

deeper plates obtained as part of the second Palomar Sky Survey[11] (plate limit ~26 mag arcsec^{-2} in B) confirms that conclusion: the incompleteness for our UGC sample is at most ~14%.

The next step was to obtain redshifts for the dwarf-LSB galaxy sample. The very low surface brightness of our sample galaxies makes their redshift measurements by optical means extremely difficult. For example, the mean surface brightness of the dwarf and LSB galaxies in the CfA slice[1] is 24.51 $\pm$ 0.76 mag arcsec^{-2}, only 0.8 mag arcsec^{-2} brighter than the lowest surface brightness level which can be seen on the Palomar Sky Survey prints.[12] Fortunately, dwarf and LSB galaxies usually contain significant amount (~10^8 $M_\odot$) of neutral hydrogen[13], which makes them relatively easy to detect (in typically 5 minutes on source) with the largest existing radio-telescopes. The 21 cm redshift observations began in 1977 and the last run was completed in 1986. The observations were carried out with the 300 m Arecibo telescope for galaxies in the declination zone $0 \leq \delta \leq 36°$ and with the 100 m Green Bank telescope (before its demise) for galaxies in other declination zones. All galaxies were searched in velocity in the range -400 to 6500 km s^{-1}, with an effective velocity resolution, after Hanning smoothing, of ~16 km s^{-1}. When time permitted, the search range was extended up to 12,000 km s^{-1} with the more powerful Arecibo telescope. More details on the observational techniques and the HI data can be found in Schneider et al.[14]. The HI detection rate is ~84%, giving a total sample of 1557 galaxies with 21 cm redshifts.

Our sample was originally intended as a survey of dwarf galaxies alone. However, based on their redshifts, many of the galaxies in our sample prove actually to be more distant and more luminous than their morphological classification initially suggested. The typical diameter of

a dwarf irregular galaxy being ~5.7 kpc[15], its angular size would be $\geq 1'$, the diameter limit of the Nilson catalog, only if its velocity is $\leq$ 1480 km s^{-1}. Our sample thus contains at least two galaxy subpopulations: bonafide small low luminosity dwarf galaxies (those with $v \lesssim$ 1480 km s^{-1}) and large, higher luminosity LSB galaxies (those with $v >$ 1480 km s^{-1}). The two populations cannot be distinguished by UGC data alone: the mean surface brightness, major axis size, axis ratio and apparent magnitude are nearly identical for both populations. The HI data is more discriminating. The dwarfs have smaller HI line widths (110 vs. 182 km s^{-1} for the mean HI width at half of maximum intensity) and larger HI fluxes (by a factor of 1.5). In the following, we shall consider, whenever possible, these two populations separately.

For the statistical studies described here, we further restrict the total sample to a galactic latitude $|b| \geq 40°$ to eliminate effects of galactic absorption, to $\delta \geq 0°$ because of the reduced sensitivity of the Arecibo telescope at negative declinations, and to $v \leq$ 10000 km s^{-1} because of the large incompleteness at large velocities, giving a total of 860 dwarf-LSB galaxies. The statistical dwarf-LSB sample covers 2.24 Sr of sky, and has a mean redshift of 2500 km s^{-1}. In the same region of the sky, there are 2154 CfA galaxies, with a mean redshift of 3650 km s^{-1}. Figures 1a and 1b show the right ascension versus galactocentric velocity maps for both the dwarf-LSB and CfA galaxy samples in the sky region defined above. Figure 2 shows the dwarf-LSB data (open circles) superposed on the bright galaxy data (crosses) in several selected declination zones. The data in other declination zones are given in Thuan et al.[16].

Examination of figures 1 and 2 confirms the conclusion already obtained by several groups, comparing the detailed spatial distribution of dwarf-

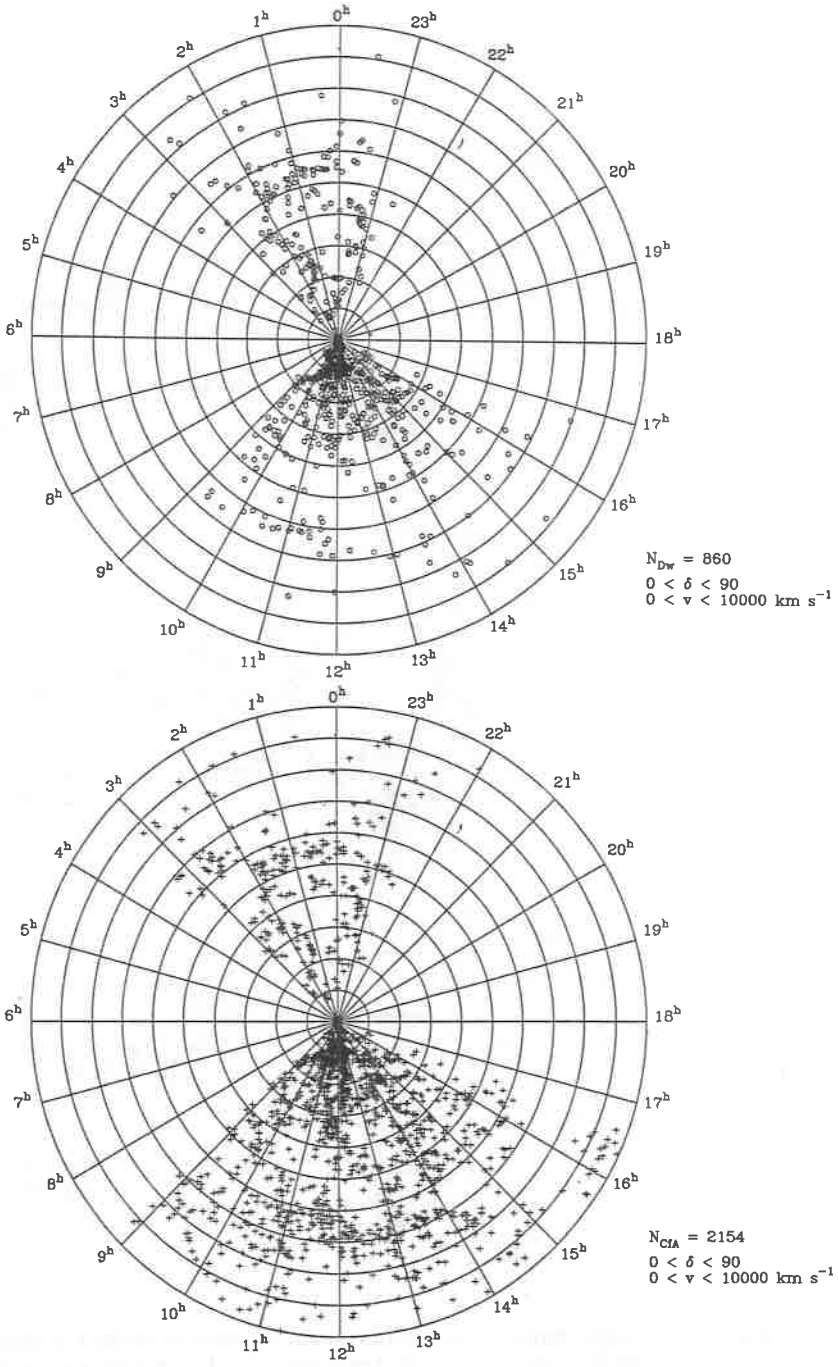

Figure 1. Right-ascension versus galactocentric velocity map for : a) the dwarf-LSB statistical sample ($a \geq 1'$, $\delta \geq 0°$, $|b| \geq 40°$); b) the CfA sample[3] ($m_B \leq 14.5$, $\delta \geq 0°$, $|b| \geq 40°$). The interval between circles is 1,000 km s^{-1}.

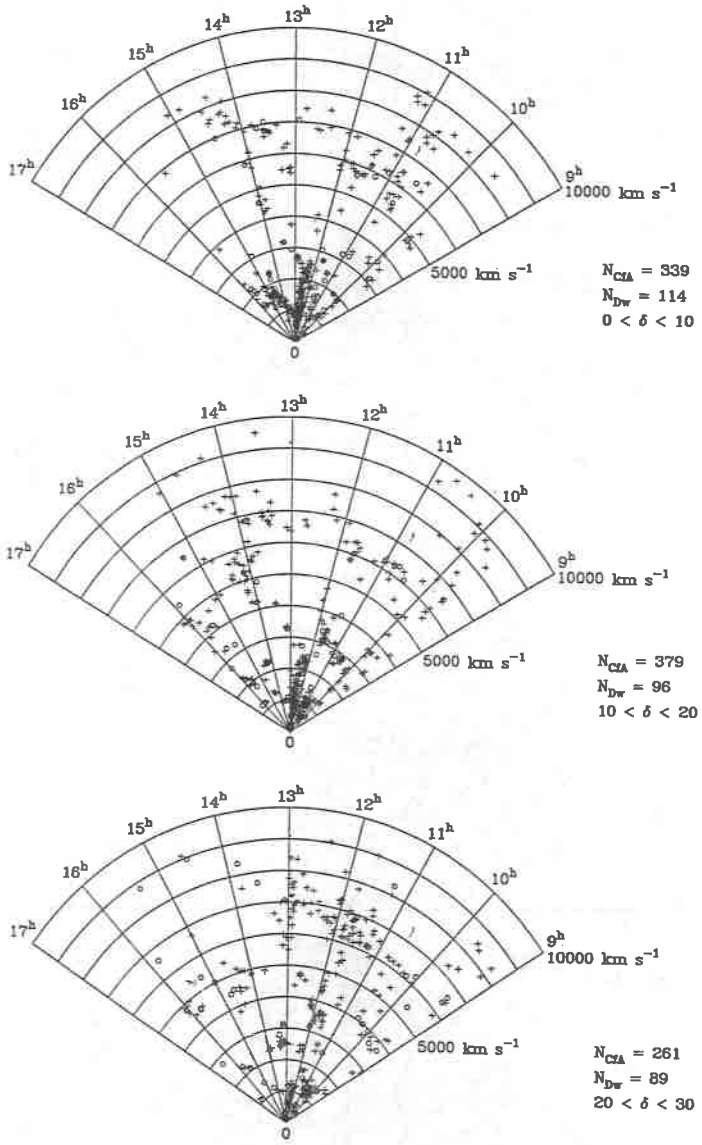

Figure 2. **Right-ascension versus galactocentric velocity maps for dwarf-LSB (open circles) and CfA (crosses) galaxies, in several declination ranges.**

LSB galaxies with that of bright galaxies in selected small regions of the sky[12),17)]: dwarf and LSB galaxies follow very closely the structures delineated by the bright galaxies and do not fill in the voids seen in the bright galaxy distribution. For example, the hole behind the Virgo cluster at ($12^h.5$, +12°, 5000 km s^{-1}) (figure 2b) and that near the Coma cluster at ($14^h.5$, +30°, 7000 km s^{-1}) (figure 2c) seen in the bright galaxy distribution are also devoid of dwarf and LSB galaxies. The dwarf and LSB distributions show structures which are not appreciably wider than the high surface brightness distribution. For example, in the Virgo cluster region ($12^h \lesssim \alpha \lesssim 13^h$, $0 \lesssim \delta \lesssim 20°$, $0 \lesssim v \lesssim 2500$ km s^{-1}) (figure 2a), the dwarf galaxies are just as narrowly confined to the bright galaxy structures as the bright galaxies themselves. The close agreement between the dwarf-LSB and bright galaxy distributions rules out a certain class of biased galaxy formation theories which predict explicitly that dwarfs should be present everywhere, including the voids.[5)] The similarity in the space distribution of dwarf-LSB and bright galaxies can also be inferred from the similarity in the redshift distributions of the two galaxy samples (figure 3). Both distributions show a prominent peak at $v \sim 1000$ km s^{-1}, mainly due to galaxies in the Virgo and Ursa Major clusters. A smaller peak is present at $v \sim 5000$ km s^{-1} caused by galaxies in the Perseus-Pisces supercluster. It is not more prominent because the Perseus-Pisces structure is close to the galactic plane and our constraint of $b < -40°$ eliminates a large number of galaxies in that region.

Two-point correlation and cross-correlation functions

We now quantify the visual impression given by figures 1 and 2 by computing the most widely used statistical measure of large-scale clustering, the two-point correlation, for the dwarf-LSB sample and

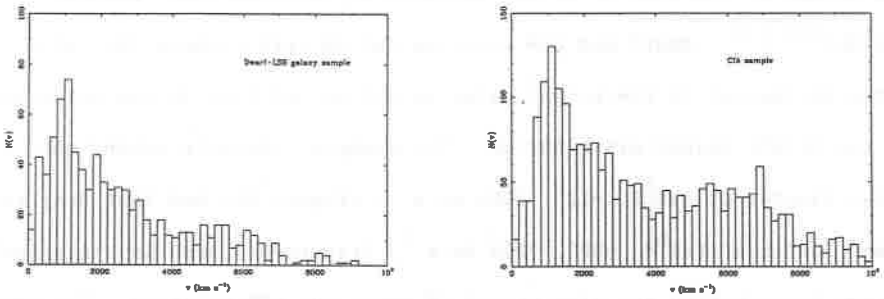

Figure 3. Redshift distribution (galactocentric velocities) of a) the dwarf-LSB statistical sample; b) the CfA sample in the same space volume.

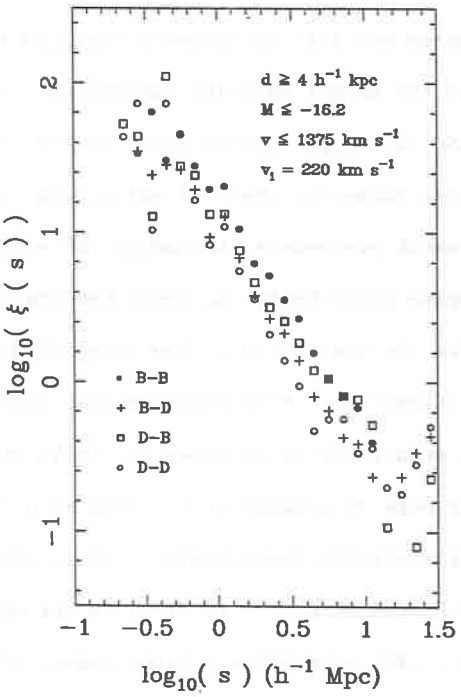

Figure 4. The auto-correlation functions in redshift space for dwarf-LSB (open circles) and bright CfA (filled circles) galaxies in the D1 sample. The cross-correlation functions calculated by counting dwarf galaxies around bright galaxies (crosses) and bright galaxies around dwarf galaxies (open squares) are also shown.

comparing it to that of the CfA sample. The results of this and the following sections are discussed in greater detail in Thuan et al[16].

We extract from the statistical sample, four volume-limited complete samples, two for dwarf galaxies and two for LSB galaxies. These are convenient for the calculation of correlation functions, because each galaxy carries exactly the same weight. Since the typical diameter of a dwarf galaxy is ~6 Kpc[15], we define two dwarf samples: D1, which contains all dwarfs with a linear diameter $d \geq 4$ Kpc (because all UGC galaxies have an angular diameter greater than 1 arcminute, this gives an upper velocity limit $v \leq 1375$ km s^{-1}), and D2 with $d \geq 8$ Kpc and $v \leq 2750$ km s^{-1}. In the same manner, we define two volume-limited LSB samples, LSB1 with $d \geq 11.58$ Kpc and $v \leq 3981$ km s^{-1}, and LSB2 with $d \geq 16$ Kpc and $v \leq 5500$ km s^{-1}.

a) The redshift correlation function

We first compute the auto-correlation functions in redshift space for each of the four complete dwarf-LSB samples. Peculiar motions are neglected for now, although we do take into account the Virgocentric infall motion, adopting a non linear flow model[18] and a Virgocentric infall velocity of 220 km s^{-1}. The results are fitted to a power law of the form: $\xi(s) = (s/s_o)^{-\gamma}$. We then compare these results with those for the auto-correlation functions computed for bright CfA galaxies in exactly the same volumes. We found that while the slopes of the auto-correlation functions for dwarf-LSB galaxies are nearly the same as that for bright galaxies[19] ($\gamma \sim 1.7$), the correlation lengths s_o are systematically smaller (by 5 to 45%) for dwarf-LSB galaxies as compared to those for bright galaxies. At a pair separation of $1h^{-1}$ Mpc, the auto-correlation amplitude in redshift space is ~1.0 to 2.1 times greater for bright than for dwarf-LSB galaxies. Figure 4 shows the redshift

auto-correlation functions for dwarf-LSB (open circles) and bright CfA galaxies (filled circles). It is evident that the open circles lie systematically below the filled circles.

b) The space correlation function

We have neglected until now peculiar velocity effects. In order to assess their influence, we need to compute the two-dimensional correlation function $\xi(r_p, \pi)$, where r_p and π are the separations perpendicular and parallel to the line of sight, as defined by Davis and Peebles[19]. Figure 5 shows, as an example, the function $\xi(r_p, \pi)$ for the D2 sample. Only the quadrant with positive π and r_p is shown since the quadrant with negative π and positive r_p can be derived by mirror symmetry. The contours $\xi(r_p, \pi) = 1$, 2 and 4 are shown, and they are clearly elongated in the π direction, showing convincingly that dwarf-LSB galaxies possess significant peculiar velocities which distort the redshift maps as compared to the true spatial distribution maps. We can use $\xi(r_p, \pi)$ to compute the rms pairwise peculiar velocity σ in the dwarf-LSB sample, following the formalism developed by Peebles[20]. We find that, independently of the dwarf-LSB volume-limited subsample considered, the pairwise peculiar velocity of dwarf and LSB galaxies is σ (dwarf/LSB) $\sim 460 \pm 50$ km s^{-1}. We have also calculated σ for the CfA bright galaxies in the same volume-limited samples, and the result is also σ (CfA) $\sim 460 \pm 50$ km s^{-1}. The similarity of σ indicates that dwarf-LSB and bright galaxies participate in the same gravitational potential.

We now compute the space correlation function, for each of the volume-limited subsamples, following the precepts of Davis and Peebles[19], and again fit the results to a power law of the form: $\xi(r) = (r/r_o)^{-\gamma}$. Comparison of the results of the space correlation analysis for dwarf-LSB galaxies with those for bright galaxies support the conclusions obtained

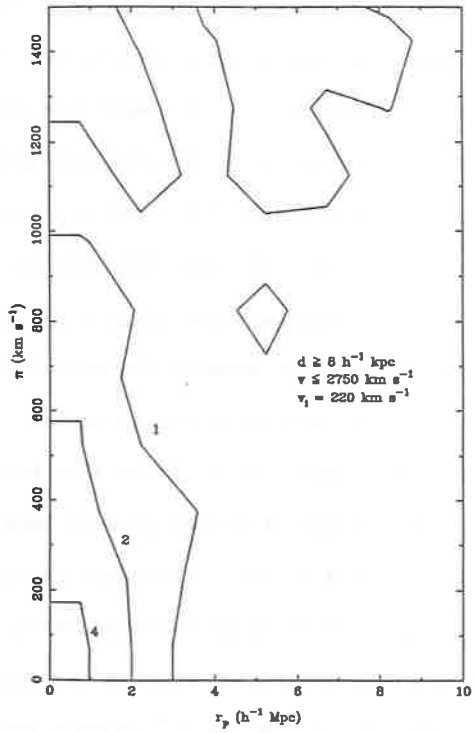

Figure 5. The two-point correlation function for dwarf galaxies in the D2 sample as a function of separations r_p and π perpendicular and parallel to the line of sight, calculated with a Virgocentric infall velocity of 220 km s^{-1}. The solid lines are contours of constant $\xi(r_p, \pi)$ and are labeled by its value.

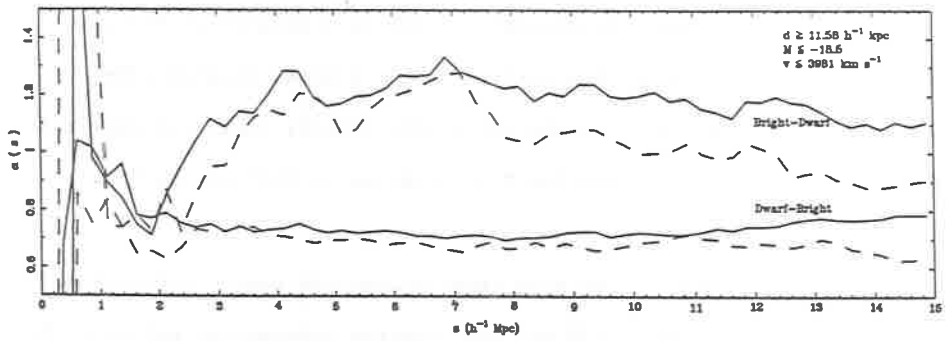

Figure 6. The cross-correlation coefficients α for the LSB1 sample as a function of pair separation s, with Virgocentric infall correction (v_i = 220 km s^{-1}) (solid lines) and without (dashed lines). We have calculated these coefficients both by counting dwarf galaxies around bright galaxies (the lines labeled bright-dwarf) and by counting bright galaxies around dwarf galaxies (the lines labeled dwarf-bright).

from the redshift correlation analysis: the correlation slopes are nearly the same for dwarf-LSB and bright galaxies ($\gamma \sim 1.7$), but the correlation length is ~33% smaller for the dwarf-LSB galaxies than for the bright CfA galaxies. The ratio of the correlation amplitudes (bright/dwarf-LSB) at a separation of 1 h^{-1} Mpc are respectively 2.7, 2.5, 1.9 and 2.1 for the D1, D2, LSB1 and LSB2 samples.

c) The correlation function for galaxies outside clusters

Can this difference in amplitude between the correlation functions of dwarf-LSB and bright galaxies be attributed to the well-known morphology-density relation shown by Binggeli et al[17] to also hold for dwarf galaxies? Since our 21-cm redshift survey is only sensitive to gas-rich dwarf irregular galaxies, it misses all the dwarf ellipticals which are found almost exclusively in dense cluster environments. For example, the Coma cluster region which is clearly visible in the distribution of the CfA galaxies at RA ~12h and v ~ 7000 km s^{-1} is much less prominent in the distribution of dwarf-LSB galaxies (figure 2c). The fraction of dwarf irregulars relative to the total dwarf population (dwarf irregulars + dwarf ellipticals) is a function of the density of the local environment: it is $\gtrsim$ 95% in the field, decreases to $\leq$ 68% in a cluster of medium density like Virgo and becomes nearly zero in a dense cluster like Coma.[16] The absence of clusters could artificially lower the amplitude of the dwarf auto-correlation function relative to that of the CfA galaxies.

To test this hypothesis, we have recalculated the space correlation function for all the dwarf-LSB and CfA complete subsamples, but with the exclusion of all galaxies in clusters. Galaxies in the Virgo, A400, A779, A1367 and Coma clusters were removed. The dwarf-LSB galaxies in our sample are not in rich Coma-like clusters, and excluding clusters

does not make any difference. Some of our HI-rich dwarfs are found in the Virgo cluster, so removing them does decrease the correlation length for the D1 sample, from 4.3 to 3.6 Mpc. By contrast, the changes in the correlation lengths of the auto-correlation functions of the bright CfA galaxies are evident in all 4 samples, decreasing, as expected, from ~6 Mpc to ~4.5 Mpc. There is now much less of a difference between the auto-correlation functions of dwarf-LSB and bright galaxies, although there is still a small hint that dwarf-LSB galaxies are slightly less clustered than bright galaxies. At a separation of 1 h^{-1} Mpc, the ratio of the amplitudes of the bright to dwarf-LSB autocorrelation functions are respectively 1.2, 1.3, 1.2 and 1.6 for the D1, D2, LSB1 and LSB2 samples.

Our results concerning the relative clustering of dwarf-LSB and bright galaxies support the conclusions of Thuan et al.[12], Eder et al.[17], Bothun et al.[21] and Binggeli et al.[17]: there is no large difference between dwarf-LSB and bright galaxies outside of clusters. While the data does suggest that HI-rich dwarf-LSB galaxies are slightly less clustered than bright galaxies in the field, the ratio of the bright/dwarf-LSB correlation amplitudes is ~1.2, not 2[22] nor 5[23].

d) The cross-correlation function

We now discuss another way for comparing the spatial distribution of the two galaxy populations: the cross-correlation functions in redshift space between dwarf-LSB and bright galaxies. We have computed the cross-correlation functions for all four volume-limited subsamples. The slope is again ~1.7, while the correlation length is intermediate between the dwarf-LSB and bright galaxy redshift auto-correlation lengths, being ~5 h^{-1} Mpc for all subsamples. The cross-correlation function for the D1 sample is shown in figure 4, computed in two ways: by counting the

number of dwarfs around bright galaxies (ξ_{BD}, crosses) and then by counting the number of bright galaxies around dwarfs (ξ_{DB}, open squares). Within the errors, both methods give the same results, which is a check that the normalization of the correlation function was done correctly.

To examine differences between various galaxy populations, without being too sensitive to the uncertainties on the amplitude of the individual correlation functions caused by normalization and sampling problems, it is useful to examine the ratios[24)]

$$\alpha_{DB}(s) = \frac{\int_o^s \xi_{DB}(s)\, s^2 ds}{\int_o^s \xi_{BB}(s)\, s^2 ds}$$

and

$$\alpha_{BD}(s) = \frac{\int_o^s \xi_{BD}(s)\, s^2\, ds}{\int_o^s \xi_{DD}(s)\, s^2 ds}$$

where D stands for dwarfs and B for bright galaxies.

The run of $\alpha_{DB}(s)$ and $\alpha_{BD}(s)$ as a function of pair separation s for the LSB1 sample is given, as an example, in figure 6, both with Virgocentric correction (solid line) and without (dashed line). The coefficients α_{DB} and α_{BD} are both nearly constant for $s \gtrsim 2\ h^{-1}$ Mpc, with $\alpha_{DB} \sim 0.8 \pm 0.1$ and $\alpha_{BD} \sim 1.2 \pm 0.1$, independent of Virgocentric correction and sub-sample.

Constraints on biased galaxy formation models

According to the linear biasing model, the density contrast of galaxies is related to the density contrast of the underlying matter by the bias parameter b:

$$\left(\frac{\delta\rho}{\rho}\right)_{gal} = b \left(\frac{\delta\rho}{\rho}\right)_{matter}$$

The cross-correlation functions ξ_{BD} and ξ_{DB} and the auto-correlation functions ξ_{BB} and ξ_{DD} can be written as:

$$\xi_{BD} = \xi_{DB} = b_B b_D \xi_{\rho\rho}$$
$$\xi_{BB} = b_B^2 \xi_{\rho\rho}$$

$$\xi_{DD} = b_D^2 \xi_{\rho\rho}$$

where b_B and b_D are respectively the bias parameters for bright and dwarf/LSB galaxies, and $\xi_{\rho\rho}$ is the auto-correlation function of the underlying mass distribution.

The above equations give:

$$\alpha_{DB} = \frac{b_D}{b_B} \sim 0.8 \pm 0.1$$

$$\alpha_{BD} = \frac{b_B}{b_D} \sim 1.2 \pm 0.1$$

In the above biasing model, α_{DB} should be the inverse of α_{BD}, a condition which is satisfied by the data. The fact that α_{DB} and α_{BD} are not equal to 1 confirm our results that dwarf-LSB galaxies are slightly less clustered than bright galaxies. We now attempt to put constraints on the bias parameter b_D for dwarf-LSB galaxies, from the range of acceptable b_B values. Numerical simulations of large-scale structures in the biased cold dark matter, $\Omega = 1$ model by Davis et al.[25] give $b_B = 2.5$. More recent simulations[26] have lowered that value to $b_B \sim 2.0$. Studies of luminosity segregation in the CfA catalog[27] give $1.0 \lesssim b_B \lesssim 1.5$. Thus, with $1.0 \lesssim b_B \lesssim 2.0$, we would have $1.0 \lesssim b_D \lesssim 1.6$. If b_B is at the low end of the range of possible values, the dwarf-LSB population would be unbiased.

Acknowledgements

We thank Dr. Tran Thanh Van and his staff for holding a cosmology conference in such as marvelous setting. It is singularly appropriate to discuss the origin and evolution of the Universe in a place so rich in history. The research of TXT has been supported by Air Force Office of

Scientific Research grant 89-0467 and National Science Foundation grant IN 89-15623. JMA is grateful for the support of a NSF-CNRS grant.

References

1) de Lapparent, V., Geller, M. J. and Huchra, J. P. 1986, Ap. J. (Letters), 302, L1.
2) Gott, J. R. et al. 1989, Ap. J., 340, 625.
3) Huchra, J., Davis, M., Latham, D. and Tonry, J. 1983, Ap. J. Suppl., 52, 89.
4) Fisher, J. R. and Tully, R. B. 1981, Ap. J. Suppl., 47, 139.
5) Dekel, A. and Silk, J. 1986, Ap. J., 303, 39.
6) York, D. G., Dopita, M., Green, R., and Bechtold, J. 1986, Ap. J., 311, 610.
7) Silk, J. and Norman, C. 1979, Ap. J., 234, 86.
8) Hausman, M. A. and Ostriker, J. R. 1978, Ap. J., 224, 320.
9) Nilson, P. 1973, Uppsala Astr. Obs. Ann., Vol. 6.
10) Thuan, T. X. and Seitzer, P. O. 1979, Ap. J., 231, 680.
11) Schombert, J. M. and Bothun, G. D. 1988, Ap. J., 95, 1389.
12) Thuan, T. X., Gott, J. R., and Schneider, S. E. 1987, Ap. J. (Letters), 315, L93.
13) Thuan, T. X. and Seitzer, P. O. 1979, Ap. J., 231, 327.
14) Schneider, S. E., Thuan, T. X., Magri, C. and Wadiak, E. J. 1990, Ap. J. Suppl., 72, 245.
15) Thuan, T. X. 1985, Ap. J., 299, 881.
16) Thuan, T. X., Alimi, J. M., Gott, J. R. and Schneider, S. E. 1991, Ap. J., March 20.
17) Thuan, T. X. 1988, in Dark Matter, eds. J. Audouze and J. Tran Thanh van, Editions Frontieres, Paris, p. 161; Eder, J. A., Schombert, J. M., Dekel, A. and Oemler, A. 1989, Ap. J., 340, 29; Binggeli, B., Tarenghi, M. and Sandage, A. 1990, Astr. Ap., 228, 42.
18) Schechter, P. 1980, A.J., 85, 801; Kraan-Korteweg, R. C. 1986, Astr. Ap. Suppl., 66, 255.
19) Davis, M. and Peebles, P. J. E. 1983, Ap. J., 267, 465; Blanchard, A. and Alimi, J. M. 1988, Astr. Ap., 203, L1.
20) Peebles, P. J. E. 1980, The Large-Scale Structure of the Universe (Princeton: Princeton University Press).
21) Bothun, G. D., Beers, T. C., Mould, J. R. and Huchra, J. P. 1986, Ap. J., 308, 510.
22) Salzer, J. J., Hanson, M. M. and Gavazzi, G. 1990, Ap. J., 353, 39.
23) Santiago, B. X. and da Costa, L. N. 1990, Ap. J., 362, 286.
24) Alimi, J. M., Valls-Gabaud, D. and Blanchard, A. 1988, Astr. Ap., 206, L11.
25) Davis, M., Efstathiou, G., Frenk, C. S. and White, S. D. M. 1985, Ap. J., 292, 371.
26) Gelb, J. M. and Bertschinger, E. 1989, B.A.A.S., 21, 1172; Park, C. P. 1990, M.N.R.A.S., 242, 59p.
27) Valls-Gabaud, D., Alimi, J. M. and Blanchard, A. 1989, Nature, 341, 215.

REDSHIFT SURVEYS

Margaret J. Geller and J.P. Huchra

Harvard-Smithsonian Center for Astrophysics

I. INTRODUCTION

Between 1976 and 1990, the number of galaxies with measured redshifts has risen steeply from 2,700 to more than 40,000. A field once data poor is becoming data rich. The new data are changing our perception of large-scale structure in the universe.

The largest project nearing completion — the Center for Astrophysics (CfA) redshift survey (Section II)— indicates that bright galaxies are distributed on thin surfaces — two-dimensional structures— which surround (or nearly surround) vast voids. Recent completion of a southern hemisphere survey (da Costa *et al.* 1988) gives some support to this picture. The narrow peaks in the deep surveys by Broadhurst *et al.* (1990) may be the intersection of the probes with structures similar to the "Great Wall" seen in the CFA survey (Section III) (Geller and Huchra 1989) and to the sheet in the Perseus-Pisces region. The message of all surveys is now clear: large structures are a *common* feature of all surveys big enough to contain them.

We take $H_o = 100h$ km $s^{-1}Mpc^{-1}$ with $h = 1$ unless otherwise specified.

II. THE LARGE-SCALE GALAXY DISTRIBUTION

Over the last few years each new approach to mapping out the distribution of individual galaxies has uncovered unexpectedly large structures. Surveys like the one of the Boötes (KOSS 1987) region are an efficient method of finding large voids. Surveys like the CfA redshift survey extension (Geller and Huchra 1989) which are complete over a region of large angular scale are less efficient for

identifying individual large structures, but they are necessary for quantitative characterization of the distribution of galaxies over a range of scales.

The goal of the Center for Astrophysics redshift survey extension is to measure redshifts for all galaxies in a merge of the Zwicky *et al.* (1961-1968) and Nilson (1973) catalogs which have $m_{B(0)} \leq 15.5$ and $| b_{II} | \geq 40$ °. There will be about 15,500 galaxies in the complete survey; more than 11,500 of these already have measured redshifts. The survey is now very nearly complete in 5 slices of the northern Galactic Hemisphere (a "slice" is a 6°-wide strip at constant declination) as well as 5 slice in the southern Galactic hemisphere. The northern strips cover the right ascension range $8^h \leq \alpha \leq 17^h$ and the declination ranges $20.5° \leq \delta < 44.5°$ and $8.5° \leq \delta < 14.5°$ (see Geller and Huchra 1989).

In the southern Galactic hemisphere a 30° -wide region (5 "slices") covering $6° \leq \delta > 36°$ with $0^h \leq \alpha \leq 4^h$ and $20^h \leq \alpha \leq 24^h$ is complete. More than 75% of the redshifts were measured with the 1.5-meter telescope and the MMT at Mt. Hopkins. The mean external error in the redshift measurements is ~35 km s^{-1} .

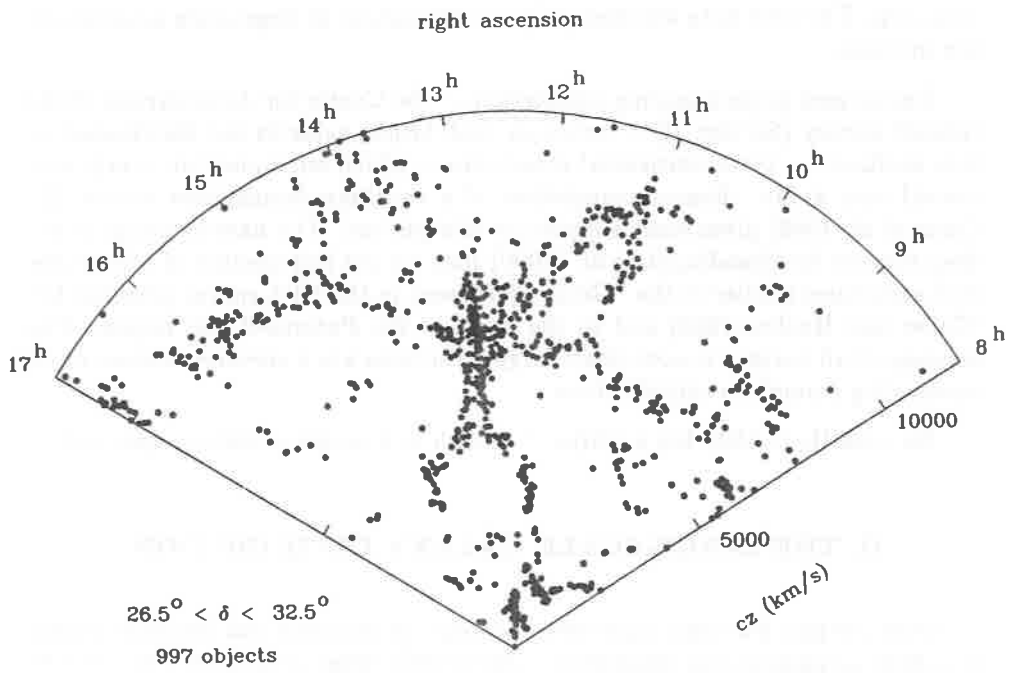

Figure 1: Observed velocity versus right ascension for the survey strip

centered at $\delta = 29.5°$. The strip is 6° in declination. Only the galaxies with velocities $\leq$ 15,000 km s^{-1} are shown.

Figure 1 is a plot of the observed velocity versus right ascension for the first strip centered at 29.5° (de Lapparent, Geller, and Huchra 1986): the strip is 6° wide in declination. The plot includes only the 1067 galaxies with redshifts $\leq$ 15,000 km s^{-1}. A galaxy of characteristic luminosity, M^*, is at roughly 9,000 km s^{-1} in this survey. Nearly every galaxy in this slice lies in an extended thin structure. The boundaries of the low density regions are remarkably sharp. The only pronounced velocity finger in this slice is the Coma cluster at $\sim 13^h$; however, many groups of galaxies are embedded in the structures (Ramella, Geller, and Huchra 1989).

Several of the voids are surrounded by thin structures in which the inter-galaxy separation is small compared with the radius of the empty region. The density of the survey is clearly important for definition of the structure. The largest low density region in this survey is located between 13^h20^m and 17^h with $4000 \lesssim cz \lesssim 9000$ km s^{-1} . The diameter of the void is $\sim$ 5000 km s^{-1} or 50 Mpc in the absence of large-scale flows. This void is comparable with the void in Boötes but is much more densely surveyed. The galaxy number density contrast for this void is $\delta\rho/\rho \simeq -0.8$, again comparable with the estimates for the Boötes void. Recent infra-red Tully-Fisher distances (Bothun *et al.* 1991) indicate that the diameter of the void is the same in physical space as in redshift space.

The first slice alone demonstrates that the thin structures in the distribution of galaxies are cuts through two-dimensional sheets, *not* one-dimensional filaments. A total of four complete slices covering the declination ranges $26.5° \leq \delta < 44.5°$ and $8.5° \leq \delta < 14.5°$ support the *qualitative* picture suggested by the first slice. Figure 2 shows a 3-D representation of these four slices. The most pronounced structure in this slice — the band of galaxies running across the entire right ascension range at velocities between 7500 km s^{-1} and 10,000 km s^{-1} — is the "Great Wall". About half of the galaxies in the survey are in this feature.

The apparent extension of the "Great Wall" in both right ascension and declination is limited only by the extent of the survey; we do not yet know the full extent of the structure. The equivalent spatial extent in these two dimensions is $\sim 60h^{-1}$ Mpc $\times$ 170 h^{-1} Mpc. The typical thickness of these sheets (approximately along the redshift direction) is $\lesssim 5h^{-1}$ Mpc FWHM. The density contrast between this wall and the mean for the survey is $\Delta\rho/\rho \simeq 5$. If we take $\Omega \simeq 0.2$, the mass in this observed portion of the Great Wall is $\sim 2 \times 10^{16} M_\odot$.

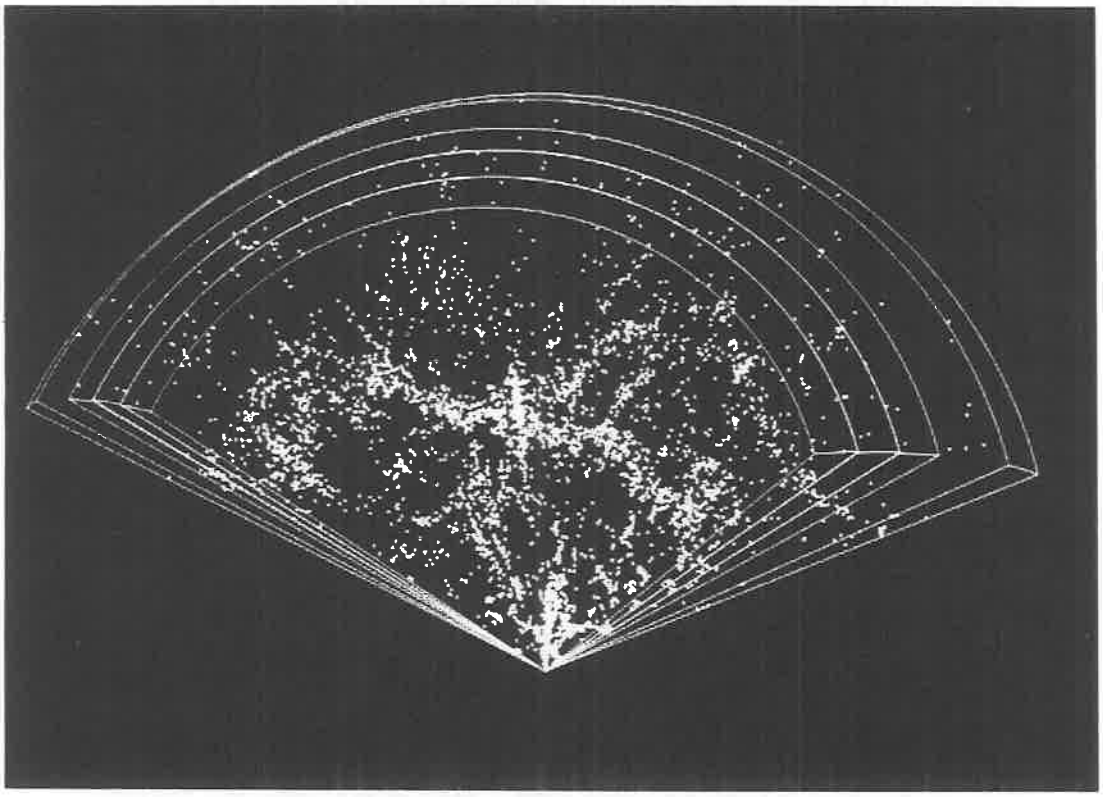

Figure 2: Projection of a three-dimensional display of four complete slices of the redshift survey. These slices cross the northe Galactic pole. The large feature running nearly horizontally throughout the survey is the "Great Wall".

The CfA survey is also complete in a portion of the region covered by the Arecibo surveys. Individual structures appear to be smaller in this region than in the North; however, the general character is similar. The similarity of the structure revealed by these surveys underscores the insensitivity of large-scale structure to the properties of individual galaxies. Figure 3 shows the 30°-wide "slice" which spans the declination range $6° < \delta \leq 36°$ and the right ascension range $20^h \leq \alpha \leq 4^h$. Comparison of these plots with Figures 2a—c in Haynes and Giovanelli (1986) shows that the structure in the 21-cm surveys are the same as those in the magnitude limited optical survey. The sampling density in the optical survey is greater than in the 21-cm survey by Giovanelli and Haynes, and the effective depth of the optical survey to $m_{B(0)} \leq 15.5$ is somewhat greater than the depth of the 21-cm surveys.

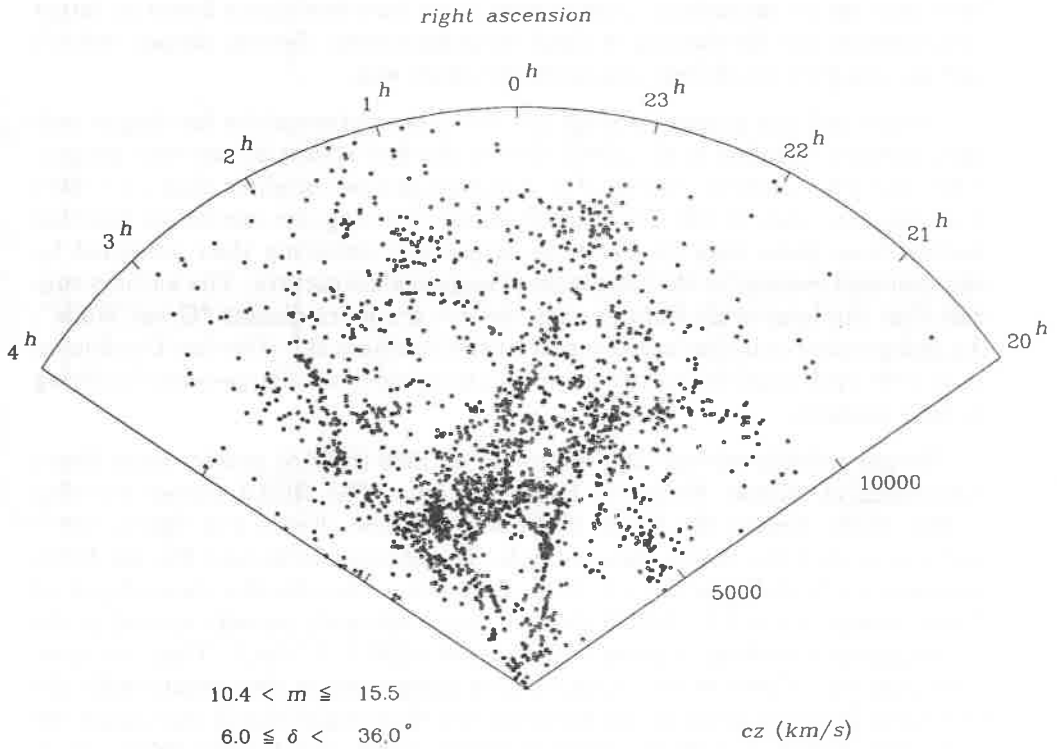

Figure 3: a). Observed velocity versus right ascension for the declination range $6° < \delta \leq 36°$ and right ascension range $20^h \leq \alpha \leq 4^h$.

An important message of both the optical and 21-cm surveys is that the largest inhomogeneities are comparable with the size of the sample. The Great Wall is a clear demonstration of this point. None of the existing redshift surveys

are thus large enough to be "fair".

The samples of the redshift survey in Figures 2 and 4 show that the scale of density fluctuations is comparable with the extent of these survey regions. Comparison of the redshift distributions for the three adjacent slices in the North and the 5 slices in the South provides a direct quantitative demonstration that these samples are not large enought to be "fair" (Vogeley, Geller and Huchra 1990). Each of these sampels covere $\sim$ 0.6 sr and includes $\sim$ 2500 galaxies. Vogeley *et al.* apply a two-tailed K-S test to the two velocity distributions: the probability that they are drawn from the same underlying distribution is 10^{-24}. N-body simulations must exhibit similar variations in the velocity distribution of comparably large independent samples.

The largest inhomogeneities we detect are the largest we *could* detect within the limits set by the extent of the survey — we have few direct limits on larger structures in the distribution of light-emitting matter. Several deeper redshift surveys designed to address this issue are under way.

Deeper reliable galaxy catalogs are an obvious prerequisite for deeper redshift surveys. Maddox *et al.* (1990) discuss the first results of one such project. They derived a uniform catalog of $\gtrsim 2$ million galaxies brighter than $b_J = 20.5$ from machine scans of 185 UK Schmidt plates. The angular correlation function derived from these data implies more large-scale clustering than predicted by the standard models for the formation of large-scale structure. The authors suggest that the large-scale features they observe are more distant "Great Walls". An independent machine-based survey of the Southern sky (Heydon-Dumbleton *et al.* 1990) will provide another important measurement of large-scale clustering in deep samples.

Deeper redshift surveys (Broadhurst *et al.* 1989 (BEKS) provide more direct indications of "Great Walls" at larger redshift. The BEKS survey contains a deep probe toward the North Galactic pole (Koo, Kron, and Szalay 1987) and one toward the South Galactic pole (Broadhurst, Ellis, and Shanks 1988) combines with shallower data in both directions. The effective mean depth of these surveys is $z \simeq 0.2$. BEKS observe appproximately equally spaced peaks in the galaxy distribution (with a spacing of $\sim$120 h^{-1} Mpc). They interpret these peaks as "Great Walls". Quantitative comparison of their results with the CfA redshift survey observations confirms that their suggestion is reasonable (de Lapparent, Geller, and Huchra 1991; Ramella, Geller, and Huchra 1991). All of these surveys confirm that large-scale inhomogeneities are a common feature of the galaxy distribution.

III. STATISTICS OF THE CfA REDSHIFT SURVEY

Lack of adequate statistical characterizations of the data makes comparison of different surveys difficult. Although the situation is improving rapidly, the limited extent of surveys compromises measures on scales much larger than

$10h^{-1}$ Mpc. Measuring high order properties of the distribution is an important challenge.

Most studies of galaxy clustering apply correlation function techniques (Peebles 1980 and references therein). However, calculation of the N-point correlation functions is only practical for small N. Statistics which depend upon the higher order moments of the galaxy distribution include measures of the topology of the distribution (Gott *et al.* 1989; Ryden *et al.* 1989), percolation statistics (Shandarin and Zeldovich), the void probability function (Fry *et al.* 1989; Ostriker and Strassler 1989; Vogeley *et al.* 1991), and the filling factor (de Lapparent, Geller, and Huchra 1991).

de Lapparent, Geller and Huchra (1991) show that galaxies fill $\lesssim 25 \pm 5\%$ of the volume of the CfA survey; the remaining $\gtrsim 75 \pm 5\%$ of the volume is devoid of bright galaxies ($M_{B(0)} \leq -18.0 + 5\log h$ at 5000 km s^{-1} ; $M_{B(0)} \leq -19.5 + 5\log h$ at 10,000 km s^{-1}). In other words, the voids occupy $\sim 75\%$ of the volume of the survey; the sheets fill $\sim 25\%$. By examining galaxy counts in cells de Lapparent, Geller, and Huchra (1991) and Ramella, Geller, and Huchra (1991) derive an average surface density for structures like the "Great Wall". The *average* surface number density is ~ 0.3 galaxy $h^2 \mathrm{Mpc}^{-2}$ with $M_{B(0)} \leq -18.2 + 5\log h$.

The deep probes of BEKS have an effective spatial extent of $\sim 5h^{-1}$ Mpc at $z \simeq 0.2$, comparable with the correlation length for individual galaxies. We can use the "Great Wall" in the CfA survey to study the way the BEKS probes would "detect" similar structures at redshifts ~ 0.2. About 50% of the time, these narrow probes detect the wall at a signal-to-noise $N_{struc}/N_{unif} \gtrsim 3 - 4$ where n_{struc} is the number of galaxies seen in the structure and N_{unif} is the numebr expected in the redshift interval (Δv=1500 km s^{-1})for a random distribution. Nearly all of the peaks in this great wall simulation contain samll groups of galaxies (Ramella, Geller, and Huchra 1991). Thus one might expect that the surface dansity of walls calculated from detection in the deep probes would be an overestimate and so might the size of voids.

IV. FOR THE FUTURE

Analyses of galaxy redshift surveys raise a number of important issues. The samples are probably not large enough to be representative; the largest well-defined structures are comparable with the extent of the surveys. It now appears that both shallow extended surveys and narrow deep probes uncover thin sheets like the "Great Wall".

A general description of large-scale structure also depends upon having surveys which are large enough to be representative. Deeper surveys extending over large angular scale are important for enabling the identification of structures larger than those which have already been observed; the largest structures provide one of the tightest constraints on models. At least two surveys are underway to meet this goal: one in the North (Geller *et al.* 1991) and one in the

South (KO ;S 1991). Both of these surveys reach to a limiting apparent magnitude $m_{B(0)} = 17.5$ and span $\sim 100^\circ$ across the sky. More ambitious projects are also plannes by several groups.

Further progress in mapping the large-scale structure of the universe requires reliable photometric catalogs. Even at the depth of the Zwicky catalog, there is no uniform survey of the sky. Systematic variations in the magnitudes from one region to another in a single catalog (not to mention variations from one catalog to another) almost surely compromise detailed analyses of the properties of the structures. The advent of large format CCD's has made fundamentally important digital surveys possible. An intermediate depth ($m \leq 20^{th}$ magnitude), multicolor survey should be the next major step in the study of large scale structure.

This work is supported in part by NASA Grant NAGW-201, by the Smithsonian Scholarly Srudies Program and by the Digital Equipment Corporation.

REFERENCES

Bothun,G.D., Beers,T.C., Mould,J., and Huchra,J.P. 1986, *Ap. J.* **308**, 510.

Bothun, G.D., Geller, M.J., Huchra, J.P., Kurtz, M.J., and Schild, R. 1991, in preparation.

Broadhurst, T.J., Ellis, R.S., Koo, D.C., and Szalay, A.S. 1990, *Nature*, submitted.

da Costa, L.N., Pellegrini, P.S., Sargent, W.L.W., Tonry, J., Davis, M., Meiksin, A., and Latham, D.W. 1988, *Ap.J.*, in press.

Davis, M. Efstathiou, G., Frenk, C. and White, S.D.M. 1985, *Ap.J.*, **292**, 371.

Fry, J.N., Giovanelli, R., Haynes, M.P., Melott, A.L., and Scherrer, R.J. 1989, *Ap.J.*, **340**, 11.

Geller, M.J. and Huchra, J.P. 1989 *Science*, **246**, 897.

Geller, M.J. *et al.* 1991, in preparation

Giovanelli, R., Haynes, M.P., and Chincarini, G. 1986, *Ap.J.*, **300**, 77.

Gott, J.R. III *et al.* 1989, *Ap.J.*, **340**, 625.

Haynes, M.P. and Giovanelli, R. 1986, *Ap. J. (Letters)*, **306**, L55.

Heydon-Dumbleton, N.H., Collins, C.A., and MacGillivray, H.T. 1990, *M.N.R.A.S.*, **238**, 379.

Huchra, J.P., Geller, M.J., de Lapparent, V., and Corwin, H. 1990, *Ap.J. Suppl.*, in press.

Kirshner, R.P., Oemler, A. Jr., Schechter, P.L., and Shectman, S.A. 1987, *Ap.J.*, **314**, 493.

Kirshner, R.P., Oemler, A. Jr., Schechter, P.L., and Shectman, S.A., in preparation.

Koo, D. Kron, R. and Szalay, A. 1986 in *13th Texas Symposium on Relativistic Astrophysics*, M. Ulmer, ed, (World Scientific: Singapore).

de Lapparent, V., Geller, M.J., and Huchra, J.P. 1986, *Ap.J. (Letters)*, **202**, L1.

de Lapparent, V., Geller, M.J., and Huchra, J.P. 1991, *Ap.J.*, in press.

Maddox, S.J., Efstathiou, G., Sutherland, W.J., and Lovejay, J., *M.N.R.A.S.*, **242**, 43p .

Nilson, P. 1973, *Uppsala General Catalogue of Galaxies, Uppsala Astr. Obs. Ann*, **6**.

Ostriker, J.P. and Strassler, M.J. 1989, *Ap.J.*, **338**, 579.

Ramella, M., Geller, M.J., and Huchra, J.P. 1989, *Ap.J.*, **344** 57.

Ryden, B.S. *et al.* 1989, *Ap.J.*, **340**, 647.

Shandarin, S.F., and Zeldovich, Ya. B. 1989, *Rev. Mod. Phys.*, **60**, 1.

Vogeley, M. J., geller, M.J., and Huchra, J.P. 1991, in preparation.

Zwicky, F.,Herzog, W., Wild, P, Karpowicz, M. and Kowal, C. 1961-1968, *Catalog of Galaxies and of Clusters of Galaxies*, (Pasadena: California Institute of Technology)

Margaret Keller and Avishai Dekel

PENCIL BEAM REDSHIFT SURVEYS AND LARGE-SCALE STRUCTURE

R. Fong, D. Hale-Sutton and T.Shanks
Department of Physics, University of Durham,
Durham DH1 3LE, England.

Abstract
We discuss here the use of deep pencil beam galaxy redshift surveys as a probe of the large-scale structure in the universe. We first show how these surveys complement the shallow large area redshift surveys and how they may be providing a 'fair sample' of the galaxy distribution. We also discuss the possibility that an observed large-scale regularity in a particular pencil beam direction may be a chance occurence due simply to the fact that galaxies cluster. We, finally, demonstrate the robustness of the estimates of the two-point galaxy correlation function that have been made using the presently available pencil beam surveys. In particular, the results show that, so far, there seems to be no need to invoke unexpectedly large power to be present on large scales in the clustering of galaxies.

1. Introduction

There are two general approaches to the considerations from galaxy catalogues of large-scale structure in the universe. In the 'morphological' or 'botanical' approach the distribution is examined visually for possible structures, such as 'filaments', 'sheets', and 'voids', and for the possible 'connectivity' of these 'detected' structures. Alternatively, the galaxy distribution is treated in an entirely objective statistical fashion and mean properties, i.e. various statistical measures, are estimated. If the catalogue is large enough to constitute a 'fair sample' (Peebles 1980), these measures then characterize the large-scale distribution of galaxies in the universe. The two approaches complement each other.

Scientifically, the estimation of statistical measures from fair samples, together with other observations, such as the observed constraints on the anisotropy of the microwave background, provide the quantitative evidence with which to test models for the distribution of galaxies and theories for the formation of large-scale structure. On the other hand, the visual appearance provides a means of interpreting quantitative results and can suggest new statistical tests for these visual structures. The crucial question is not of the existence of such structures, but as to what extent they are 'typical'. That is, can models with only a moderate amount of clustering, such as the hierarchical models of Soneira and Peebles (1978) or cold dark matter models (see, for example, Davis *et al.* 1985), also produce such visually impressive structures or is there really a need for unexpectedly large power on large scales? So, in the final analysis, it rests on the statistical estimates based on fair samples of the universe to provide the observational 'facts' of the distribution of galaxies, with the visually observed structures as illustrative of these 'facts'.

For this paper, we shall adopt both approaches, although in the statistical approach we shall restrict our discussions to the two-point correlation function (Peebles 1980), which has proved so useful in the analysis of galaxy distributions.

2. Pencil Beam and Large Area Redshift Surveys

The observational aspect of recent discussions of large-scale structure has been dominated by the visual observation of large 'voids', actually regions of under-densities, of up to $\sim 50 h^{-1}$Mpc in diameter, and of 'sheets' or 'walls' of galaxies, such as the so-called 'Great Wall' in the north, in large area redshift surveys (Huchra *et al.*, 1983, hereafter called CfA, de Lapparent, Geller and Huchra 1988, hereafter called CfA slice, and da Costa *et al.*, 1988, hereafter called SSRS). However, so far these surveys have been rather shallow, reaching to a depth of only $\sim 100 h^{-1}$Mpc, which is of similar order to the sizes of the claimed structures, raising then some uncertainty concerning the statistical results from these surveys. Deep pencil beam redshift surveys (Kirshner, Oemler and Schechter 1978, hereafter called KOS, Kirshner *et al.*, 1983, hereafter called KOSS, Peterson *et al.*, 1986, hereafter called D/AAT, Metcalfe *et al.*, 1989, hereafter called D/SAAO, and Broadhurst, Ellis and Shanks 1988, hereafter called BES) provide then an important complementary survey to these large area surveys. The pencil beams have, in general, been chosen to be in random directions in the sky and, if there are spatially large coherent structures, they would, furthermore, be probing an effective volume of space substantially larger than the actual volume within the pencil beams. Whatever the case may be, the hope is that they are deep enough and enough of them to provide a fair sample of the universe and, hence, that the resulting statistical analysis will provide good estimates of the global properties of the distribution of galaxies.

Visually, too, pencil beam redshift surveys have also led to claims of large-scale structures. The early pencil beam surveys of KOS and KOSS led to the introduction of the Boötes void; later more extensive surveys have shown that the entire region is not, in fact, completely devoid of galaxies, although it is still found to be significantly under-dense (see, e.g., Dey, Strauss and Huchra 1990). Similarly, D/AAT can also suggest the existence of 'voids', with some 'thin' structures cutting across the fields (Geller and Huchra 1988). The recently completed D/SAAO provides a similar impression, although being a 1-in-3 selected sample the structures are visually less clear. And, most recently, there has been the claim for possible regular structures ranging over a distance of $\sim 1600 h^{-1}$Mpc (Broadhurst *et al.*, 1990).

If we overlay the cone plots of KOS, D/AAT, D/SAAO and that of Parker *et al.* (1986) over

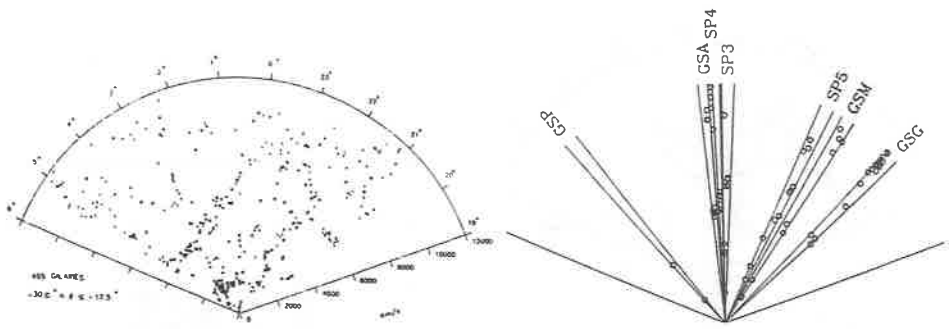

Fig. 1 The distribution of galaxies in the declination slice $-30.0° < \delta \leq -17.5°$: (a) Figure from da Costa *et al.* (1988), (b) galaxies within $120h^{-1}$Mpc in deep pencil beams drawn on the same scale as for (a). Fields SP3, SP4 and SP5 are from KOS, GSA is from D/AAT, and GSG, GSM and GSP are from the 1-in-3 sampled D/SAAO (Note that, in the case of GSP, only those galaxies that are strictly in this declination slice are shown).

the CfA slice and SSRS, we see that some of the structures seen in the pencil beam surveys are part of the more extended structures claimed to be present in the large area surveys (Geller and Huchra 1988). As an example, we present in Fig. 1 the SSRS slice with $-30.0° < \delta \leq -17.5°$ and the D/AAT, D/SAAO and KOS pencil beams in this slice, but truncated st the SSRS distance limit of $120h^{-1}$Mpc. In particular, the pencil beams are clearly sampling these visually observed structures and so statistical analyses carried out on them should provide a quantitative assessment of their significance.

3. Are there Large-Scale Regular Structures in the Universe?

The result of Broadhurst *et al.* (1990), hereafter referred to as BEKS, showing a 'regular' pattern with a characteristic scale of $128h^{-1}$Mpc and stretching over a range of $\sim 1600h^{-1}$Mpc from two almost oppositely aligned pencil beams was at the time unexpected and has been a stimulus for much theoretical work as to what models could admit such large structures (see, for example, the report by Trimble (1990) on the University of Kansas workshop in May 1990). Even though the singling out of two pencil beams hardly constituted a representative sampling of the universe, it seemed, for example, that such structures would be impossible to find in the distributions resulting from cold dark matter models.

Observationally, with the two nearest peaks in the number-redshift distribution being within $100h^{-1}$Mpc, it is worth examining them in the context of the large area surveys. Fig. 2a shows the two shallowest pencil beams used by BEKS as they sit in the corresponding declination slices from the CfA slice and SSRS. The peak in the north at $\sim 90h^{-1}$Mpc is part of the so-called 'Great Wall' and the peak in the south at $\sim 60h^{-1}$Mpc sits on another 'wall', sited at a large angle to the 'Great Wall' and at an acute angle to the line of sight. If such regularities are truly coherent structures and are a common occurence in the universe, an immediate consideration is to seek some simple geometric explanation. However, with the aforesaid observations, such an explanation seems to be out of the question.

This conclusion is further reinforced by a closer examination of the nearby distribution around these directions. For, just as visually striking is the presence from the large area surveys of other equivalently strong structures, such as the structure at $\sim 50h^{-1}$Mpc in the direction of the NP5 field of KOS and the structure in the south at $\sim 20h^{-1}$Mpc. For some of these, BEKS did note their presence in other available pencil beams, but they were not used as being at greater angles from the NGP-SGP line of sight than are NP5 and the GSA field of D/AAT. However, with so much structure present, extending the observing angle would not only enhance the clusters in the pencil beams used by BEKS, but the number-redshift distribution, N(z), would also become filled in and

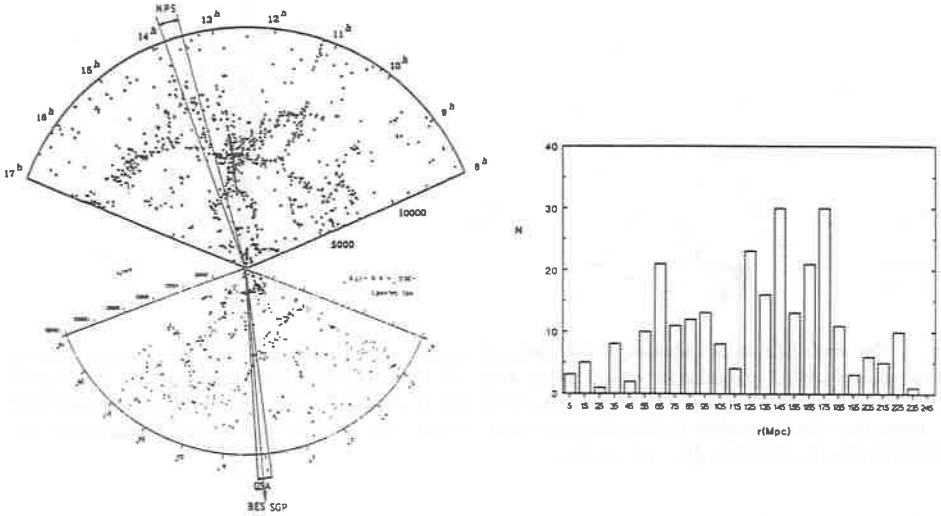

Fig. 2 (a) The two shallower pencil beam surveys used by BEKS as they lie in the declination slice of Fig. 1a and in the corresponding northern slice of the CfA slice. Also shown is the direction of the deep SGP pencil beam in BES. (b) The number-distance histogram for all the pencil beams from KOS, KOSS, D/SAAO and Parker *et al.* (1986) that lie within 14° of the SGP.

the regularity consequently weakened if not lost. This is very directly seen from the N(z) of the pencil beams from KOS, KOSS, D/SAAO and Parker *et al.* (1986) that are within 14° of the SGP, Fig. 2b. With the northern NP5 and deep SA57 fields used by BEKS lying at angles of 9° and 3.1°, respectively, with respect to the axis of the deep SGP field, 14° represents a reasonable extension of the observing angle in seeking some simple geometric picture for such a regularity.

The question is then raised as to whether the result may just be a statistical 'fluke'. So far, the result has been found for only one approximate direction and the solid angle covered by a deep field is only $\sim 10^{-4}$ ster., making the BEKS sample just one out of the possible 6×10^4 such samples from over the whole sky.

Models are being examined to obtain the frequency with which such regularities can occur. Exact periodicity is, indeed, difficult to obtain (Primack, private communication), but the observations do not exhibit very exact periodicity. For example, the observed peak in the south at $\sim 60 h^{-1}$Mpc is over $20 h^{-1}$Mpc from its 'predicted' BEKS position. Quantitatively, this is also reflected by there being only two outstanding 'spikes', corresponding to the fundamental and first harmonic of the regularity, in the power spectrum (Fig. 2 of EKS), with the second not much greater than the noise in the spectrum. Such approximate periodicities are now being shown to be obtainable in narrow pencil beam probes simply by chance from a wide range of clustering models (Stanhill *et al.* 1990), including cold dark matter models (Frenk 1990). In fact, in a poster paper Kaiser and Peacock (1990) show that even 'normal' Gaussian fluctations can produce such results. Simply, with clustering present the intersection of clusters with a narrow pencil beam can by chance produce an approximately periodic distribution over a relatively large range in distance, with such results expected to occur with a frequency of ~10%. Broadhurst *et al.* are now examining other directions in the sky and it will be interesting to have an estimate of this frequency.

However, for a useful measure, many lines of sight may need to be explored and the pencil beams each chosen to be in strict alignment for directly testing models for the distribution of galaxies. At present, there is one very deep line of sight with data from fields that are in an exact alignment and that is in the SGP direction. The GSA field of D/AAT and the deep SGP field from the AAT fibre optics survey of BES were included in BEKS. To these can be added the even deeper SGP field of the LDSS survey made at the AAT by Colless *et al.* (1990).

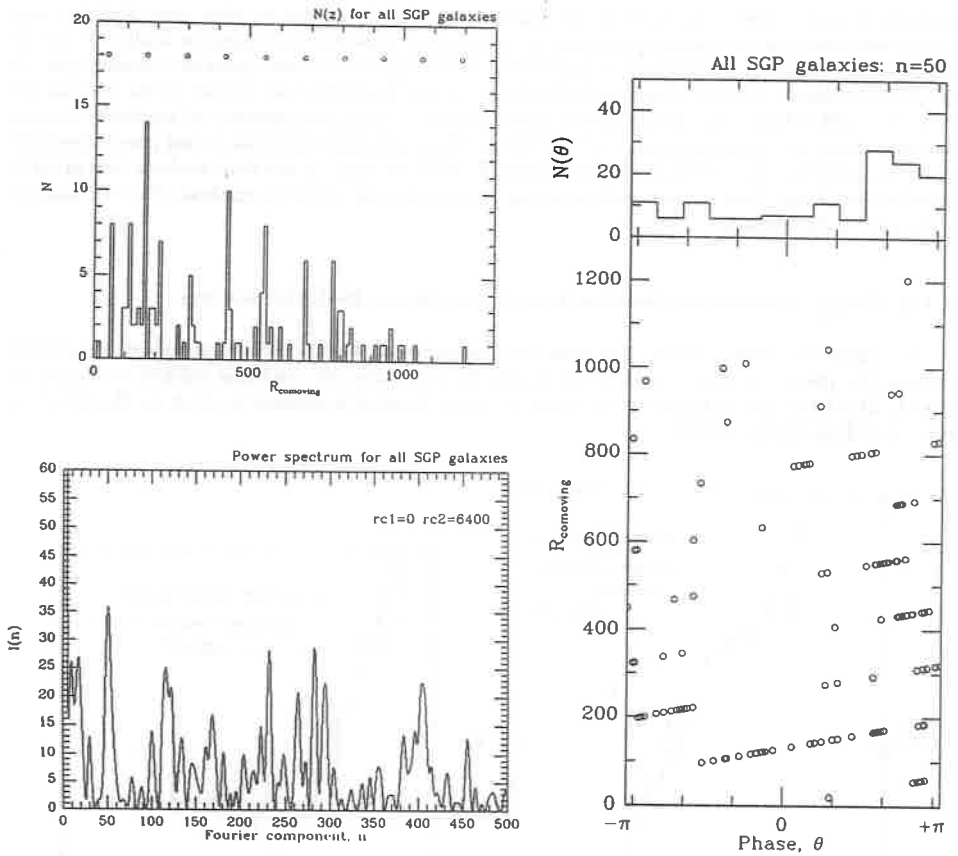

Fig. 3 (a) Histogram of the comoving distance of galaxies in the three redshift surveys centred on the SGP, with open circles at the positions in the BEKS regularity, (b) power spectrum of this distribution, (c) phase a galaxy has for the Fourier component with λ =128h^{-1}Mpc vs. comoving distance, with the histogram of phases in the upper box.

Fig. 3a presents $N(R_c)$, the number-distance distribution, for the three galaxy fields put together and Fig. 3b its power spectrum using an artificial baseline of L=6400h^{-1}Mpc to give Fourier components at $\lambda \sim 128h^{-1}$Mpc that are separated by $\Delta\lambda \sim 2.6h^{-1}$Mpc. R_c is the comoving distance of the galaxy in a $q_o = \frac{1}{2}$ Friedmann universe and the power spectrum is defined as in Webster (1976). We shall call

$$\theta = \frac{2\pi R_c}{\lambda} - 2\pi m$$

the phase for the nth Fourier component of a galaxy at R_c, where λ=L/n and m is an integer chosen such that $-\pi < \theta \leq \pi$. For small n and, hence, $\lambda \gg$ cluster sizes, galaxies in a cluster all have similar phases and for different n the power, I(n), will fluctuate about large values of $\gtrsim 2n_c$, where n_c is some average number of galaxies in a cluster. The manner of the fluctuations will depend on how clusters themselves cluster.

Although significant against a random hypothesis for the galaxy distribution, the 'spike' in the power spectrum at n≈50, corresponding to the BEKS periodicity of 128h^{-1}Mpc, is now comparable to other large amplitude Fourier components caused by the clustering in the data. This can further be seen from Fig. 3c showing many 'out-of-phase' galaxies; if the galaxy positions were exactly periodic, the points would in this plot all lie on a single vertical line at the 'phase' of the periodicity. More

generally, in power spectra analyses of the pencil beam redshift surveys in other lines of sight, large Fourier amplitudes were frequently obtained at a variety of wavelengths. Diagrams similar to that of Fig. 3c showed how the presence of even just one or two rich clusters can produce a strong spike in the power spectrum. Clearly, then, the rich clusters in the SA57 field are crucial to the prominence of the $\lambda = 128h^{-1}$Mpc spike in the BEKS power spectrum, with the presence of regularity coming essentially from the visual inspection of the $N(R_c)$. Thus, although the 'visual' and power spectrum results in particular lines of sight can be apparently very striking, in the final analysis any proof of the existence of any form of large-scale structure will require the objective analysis of a 'fair sample' of the galaxy distribution.

4. The Galaxy Correlation Function from Pencil Beam Redshift Surveys

The most succesful statistic has been and continues to be the two-point galaxy correlation function. We present in Figs. 4a and b our results for $\xi(s)$ using the combined redshift catalogues of D/AAT, D/SAAO and of Parker *et al.* (1986); a more detailed discussion is given in Shanks *et al.* (1989) and Hale-Sutton (1990).

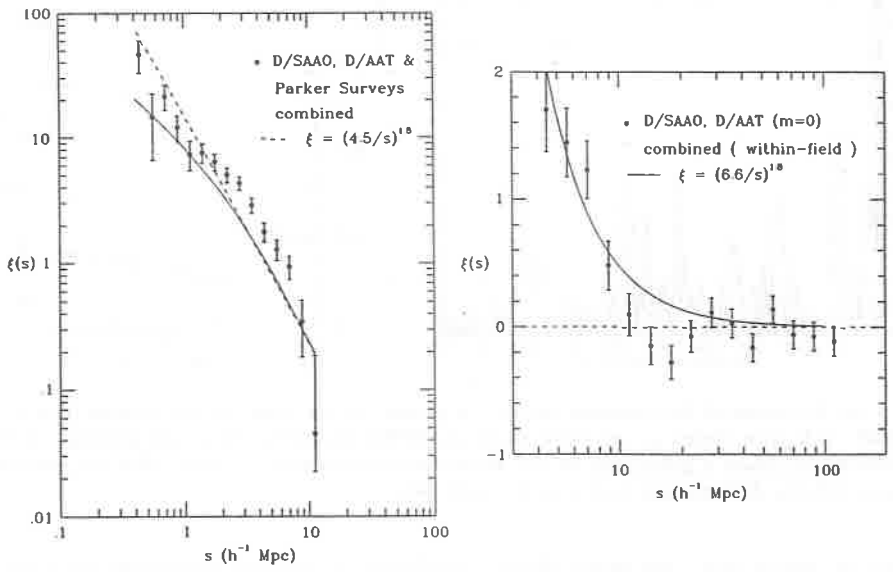

Fig. 4 Estimate of the two-point correlation function from the Durham pencil beam redshift surveys: (a) in a log-log plot, (b) in a linear-log plot.

It can be seen that our estimate of $\xi(s)$ is not just a pure power-law in s. A 'shoulder' is to be found at $\sim$1-2h^{-1}Mpc (Shanks *et al.* 1989), a feature that would naturally arise in hot dark matter models (Melott, private communication). However, as the coordinate s is obtained using the redshift, a feature of this form could be produced by peculiar velocities and infall. But reasonable models for these effects are not able to produce such a strong shoulder, providing support that this is a real detection of a large-scale structure; for peculiar motions to produce such a shoulder would require both $\Omega \approx 1$ and matter to be as strongly clustered as galaxies, which with present models and observations are incompatible requirements (Hale-Sutton 1990). On the other hand, such strong infall would have large-scale effects upon the galaxy maps in redshift space (Kaiser 1987). Either way, the presence of this shoulder in ξ has interesting physical consequences.

Fig. 4b also shows $\xi(s)$ as having a 'break' feature at s$\sim 7h^{-1}$Mpc at a fairly significant level;

for a review of early work on establishing such a feature see Peebles (1980). At larger scales, the errors in the estimate are so large that all that can be definitely said is that to within these errors the universe is isotropic and homogeneous at these large scales, i.e. $|\xi| \lesssim 0.1$ for $s \gtrsim 10h^{-1}$Mpc.

It may, however, be possible to improve on this estimate, since the errors could be optimised by weighting each galaxy by the factor

$$\frac{1}{1 + m\phi(z)}$$

where $\phi(z)$ is the selection function (Kirshner, Oemler and Schechter 1979, Davis and Peebles 1983, Kaiser 1986). Essentially, at large scales one is attempting to estimate the clustering of clusters. Then, a pair of clusters provides a single independent statistic to the pair counts from which ξ is estimated. Thus, if there are n_c galaxies in a cluster, the counting of pairs of galaxies produces $\frac{1}{2}n_c(n_c - 1)$ pairs in place of the single independent pair if only pairs of clusters were to be counted (see, also, the discussion in Sec. VI(d) of Peebles 1973). At very low redshifts, $\phi(z) = 1$ and $n_c = 1 + m$, where around a 'typical galaxy' there are m other galaxies in the same cluster. Hence, the weighting is inversely proportional to $1 + m\phi(z)$; this also satisfies the criterion that, as $\phi \to 0$, $n_c \to 1$. If only $\phi(z)$ is used, a high redshift cut-off is then needed (Davis and Peebles 1983), giving essentially the same weighting function.

The problem with this approach is in the determination of m, as ideally the clustering that we are actually trying to determine needs to be known beforehand. The value of m will also depend on the bin size used to estimate $\xi(s)$, for a small bin size will, in general, not completely enclose the 'clusters' involved at the scale of interest. Additionally, in our case, account needs to be taken of the cone shape of our pencil beams; it can be seen from Fig. 1 that clusters may well only be partially detected within the volume inside a pencil beam. Of course, if the interest is in using the results to test against a particular model, the model itself can be used to calculate m. Models can still be used to provide possible values for m for a simple observational estimate of ξ, but, if the actual clustering is not accurately enough reflected in the models, the errors in the estimate could even be made worse.

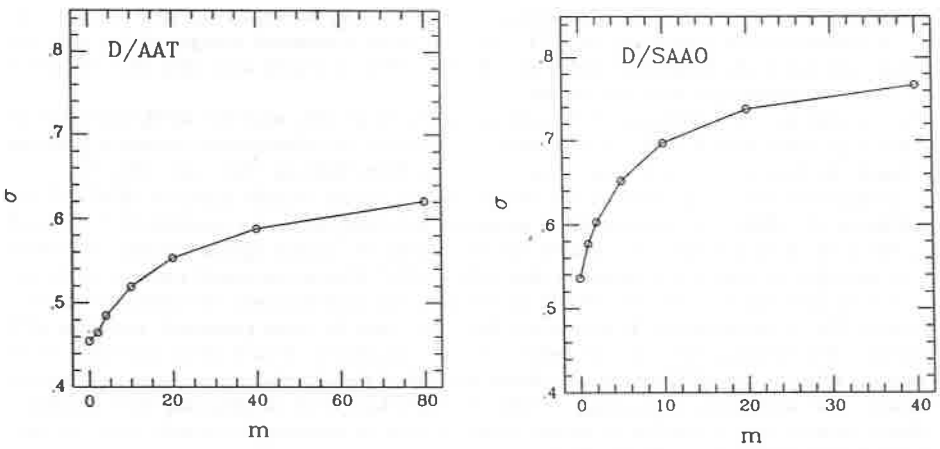

Fig. 5 The field-to-field errors in the estimate for $\xi(s)$ for $10h^{-1}\text{Mpc} \leq s \leq 100h^{-1}\text{Mpc}$ vs. the weighting parameter, m (see text), calculated such that $\phi(z) \to 1$ when $z \to 0$.

Thus, we have first found m empirically by simply investigating the change in the field-to-field errors in $\xi(s)$ with various trial values for m in the weighting function above. Fig. 5 shows, surprisingly, that the smallest errors are obtained using $m \approx 0$. To gain further insight into this result, we have used hierarchical simulations (Soneira and Peebles 1978) of our pencil beam survey. This rather conservative model gave a best value of $m \approx 4$. The result of using m=4 to estimate

ξ(s) from the observed data is shown in Fig. 6a; the general features of ξ(s) are still the same as in Fig. 4. However, if we use as high a value as 40 for m (Fig. 6b), any features in ξ(s) at s$\gtrsim$10h^{-1}Mpc become quite uncertain. But, a histogram of pair counts vs. distance based on the smooth fit to the number-redshift distribution, N(z), show that for m=40 the pairs are mainly coming from galaxies at ~200h^{-1}Mpc, making the estimate sensitive to the fit to the high redshift 'tail' of N(z).

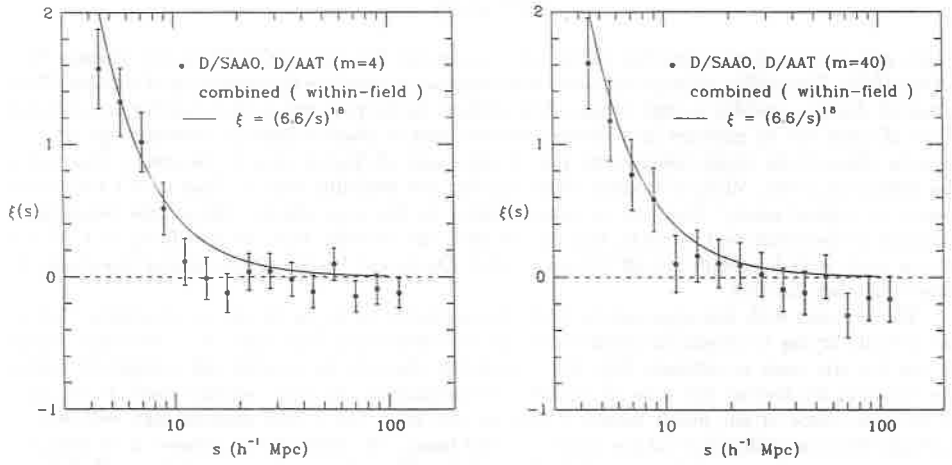

Fig. 6 Estimates of the correlation function using (a) m = 4 and (b) m = 40 in the weighting factor (see text).

What can clearly be said is that our estimates are remarkably stable, all agreeing to within the errors, in contrast to the results for the CfA slice, for which substantial changes of ξ(s) with the weighting were found (de Lapparent, Geller and Huchra 1988). It would seem then that the pencil beams survey is providing a good fair sample.

But, at present, our empirically 'best' estimate of ξ(s) is at odds with the APM/Oxford result (Maddox *et al.* 1990) and the ROE result (Collins, 1990) for the two-dimensional correlation function, $\omega(\theta)$, based on deep surveys over large areas of the Southern Galactic Cap, and with the recent result on large-scale clustering based on cell counts using an all sky redshift survey of IRAS galaxies (Efstathiou *et al.*, 1990). The latter result is somewhat surprising when one considers that, at small scales, the ξ for IRAS galaxies has a smaller amplitude than for normal optical galaxies. To obtain then the value for the variance of counts in their cells of 40h^{-1}Mpc in size would require ξ to be not only not scale invariant, but also to actually exceed the usual smooth power-law extrapolation from the form of ξ(s) at small scales! It is possible that there may be some systematic problems with the analysis. For example, the cells are assumed to be independent of each other and there could be problems with the use of Maximum Likelihood methods if the distribution is not exactly known; for instance, the assumption of Gaussian statistics by Efstathiou *et al.* in obtaining their Maximum Likelihood estimate of ξ if applied to simple counts in cells to estimate the density does not give the usual Poisson result of $\rho = \sum_i N_i / \sum_i V_i$.

With the large area two-dimensional surveys from the measurement of Schmidt photographic plates using the fast measuring machines, APM and COSMOS, $\omega(\theta)$ is small, $\lesssim$0.03, at the angular scales which, for these deep surveys, correspond to length scales of 10-20h^{-1}Mpc. There is then a need to ascertain more directly any possible systematic effects there may be in such a catalogue. For example, it would be well worth while to make extensive CCD calibrations of the catalogues. For example, CCD zero-points so far available show large differences (with an rms difference of $0\overset{m}{.}12$) with those from plate overlaps that have been used to set the zero-points of the Schmidt fields in the APM catalogue (see Fig. 23 in Maddox, Efstathiou and Sutherland, 1990), although this need not imply that the actual rms errors over the catalogue are of this order.

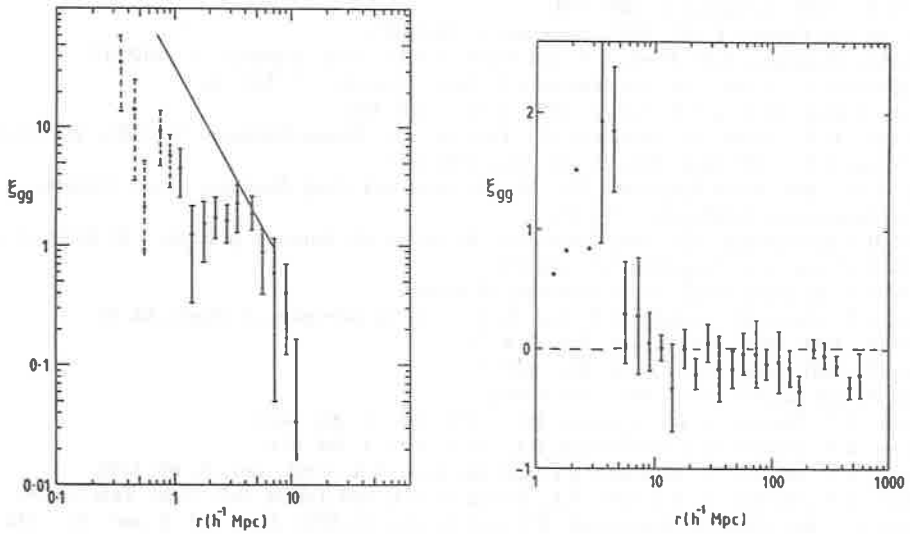

Fig. 7 Estimate of the two-point correlation function from the deep pencil beam redshift survey of BES: (a) in a log-log plot, (b) in a linear-log plot.

In conclusion, we see that ξ(s) is already showing some interesting structure and there could well be further structure on scales $>10h^{-1}$Mpc with such low power that, if they are there, the signal would not be statistically significant with respect to the present errors in the estimates for ξ(s) (see Shanks *et al.* 1989 for a further discussion). Thus, it is important to make more accurate estimates of ξ(s) from deep enough redshift surveys over a much larger volume of space. At present, the 'best' estimate from the pencil beam redshift surveys seem robust and this seems to be confirmed by the ξ(s) shown in Fig. 7 using all five of the deep pencil beams of BES, as well as by the lack of any 'fairly strong' structure at scales $>10h^{-1}$Mpc in the ξ(s) from the Durham QSO catalogue (Shanks *et al.*, 1988). Even more interestingly, the new Las Campanas Deep Redshift Survey, probing twice the depth of D/AAT and D/SAAO and the largest volume of space so far, is providing added corroboration of our results with a ξ(s) that shows similar large-scale features, with, in particular, a 'break' that is also at $\sim 10h^{-1}$Mpc (Kirshner *et al.* 1990). Thus, it seems that, in so far as the pencil beams are probing the visually observed large-scale structures seen in the shallower large area redshift surveys (Sec. 2), these results are showing that there may not be any need for unexpectedly large power to be present on large scales in order to have such visually striking structures.

Acknowledgements

It is a pleasure to acknowledge useful discussions with Carlos Frenk, Adrian Melott, Nigel Metcalfe, Joel Primack, Ian Smail and Nial Tanvir and to thank Matthew Colless for providing a computer file of the LDSS catalogue.

References

Boyle, B.J., Fong, R., Shanks, T. and Peterson, B.A., 1990. *Mon. Not. R. astr. Soc.*, **243**, 1.

Broadhurst, T.J., Ellis, R.S. and Shanks, T., 1988. *Mon. Not. R. astr. Soc.*, **235**, 827.

Broadhurst, T.J., Ellis, R.S., Koo, D.C. and Szalay, A.S., 1990. *Nature*, **343**, 726.

Colless, M., Ellis, R.S., Taylor, K. and Hook, R.N., 1990. *Mon. Not. R. astr. Soc.*, **244**, 408.

Collins, C.A., 1990. This volume.

da Costa, L.N., Pellegrini, P.S., Sargent, W.L.W., Tonry, J., Davis, M., Meiksin, A. and Latham, D.W., 1988. *Astrophys. J.*, **327**, 544.

Davis, M. and Peebles, P.J.E., 1983. *Astrophys. J.*, **267**, 465.

Davis, M., Efstathiou, G.P., Frenk, C.S. and White, S.D.M., 1985. *Astrophys. J.*, **292**, 371.

de Lapparent, V., Geller, M.J. and Huchra, J.P., 1988. *Astrophys. J.*, **332**, 44.

Dey, A., Strauss, M.A. and Huchra, J., 1990. *Astr. J.*, **99**, 463.

Efstathiou, G.P., Kaiser, N., Saunders, W., Lawrence, A., Rowan-Robinson, M., Ellis, R.S. and Frenk, C.S., 1990. *Mon. Not. R. astr. Soc.*, **247**, 10P.

Frenk, C.S., 1990. *Nobel Symposium No. 79: The Birth and Early Evolution of our Universe*, ed B. Skagerstam, Graftavallen, Sweden.

Geller, M.J. and Huchra, J.P., 1988. *Large-Scale Motions in the Universe*, p. 3, eds V.C. Rubin and G.V. Coyne, S.J., Princeton University Press.

Hale-Sutton, D., 1990. *Ph.D. thesis*, University of Durham.

Huchra, J.P., Davis, M., Latham, D.W. and Tonry, J., 1983. *Astrophys. J. Suppl.*, **52**, 89.

Kaiser, N., 1986. *Mon. Not. R. astr. Soc.*, **219**, 785.

Kaiser, N., 1987. *Mon. Not. R. astr. Soc.*, **227**, 1.

Kaiser, N. and Peacock, J.A., 1990. This volume.

Kirshner, R.P., Oemler, A. and Schechter, P.L., 1978. *Astr. J.*, **83**, 1549.

Kirshner, R.P., Oemler, A. and Schechter, P.L., 1979. *Astr. J.*, **84**, 951.

Kirshner, R.P., Oemler, A., Schechter, P.L. and Shectman, S.A., 1983. *Astr. J.*, **88**, 1285.

Kirshner, R.P., Oemler, A., Schechter, P.L., Shectman, S.A. and Tucker, D.L., 1990. This volume.

Maddox, S.J., Efstathiou, G., Sutherland, W.J. and Loveday, J., 1990. *Mon. Not. R. astr. Soc.*, **242**, 43P.

Maddox, S.J., Efstathiou, G. and Sutherland, W.J., 1990. *Mon. Not. R. astr. Soc.*, **246**, 433.

Metcalfe, N., Fong, R., Shanks, T. and Kilkenny, D., 1989. *Mon. Not. R. astr. Soc.*, **236**, 207.

Parker, Q.A., MacGillivray, H.T., Hill, P.W. and Dodd, R.J., 1986. *Mon. Not. R. astr. Soc.*, **220**, 901.

Peebles, P.J.E., 1973. *Astrophys. J.*, **185**, 413.

Peebles, P.J.E., 1980. *Large-Scale Structure in the Universe*, Princeton University Press.

Peterson. B.A., Ellis, R.S., Efstathiou, G., Shanks, T., Bean, A.J., Fong, R., and Zen-Long, Z., 1986. *Mon. Not. R. astr. Soc.*, **221**, 233.

Shanks, T., Hale-Sutton, D., Fong, R. and Metcalfe, N., 1989. *Mon. Not. R. astr. Soc.*, **237**, 589.

Shanks, T., Boyle, B.J. and Peterson, B.A., 1988. *Proceedings of a Workshop on Optical Surveys for Quasars*, p. 244, eds P.S. Osmer *et al.*, Astr. Soc. of the Pac., San Francisco.

Soneira, R.M. and Peebles, P.J.E., 1978. *Astr. J.*, **83**, 845.

Stanhill, D., Dekel, A., Blumenthal, G.R. and Primack, J.R., 1990. *Astrophys. J.*, submitted.

Trimble, V., 1990. *Nature*, **345**, 665.

Webster, A., 1976. *Mon. Not. R. astr. Soc.*, **175**, 61.

A NEW METHOD OF ANALYSING DEEP REDSHIFT SURVEYS

Olga Buryak and Andrei Doroshkevich
Keldysh Institute of Applied Mathematics
Academy of Sciences USSR
125047 Moscow, USSR
Marek Demianski
Institute for Theoretical Physics
University of Warsaw
Warsaw, Poland
International Center for Relativistic Astrophysics -ICRA
Dipartimento di Fisica, Universita di Roma
Roma, Italy

ABSTRACT

We present a new method of analysis of deep galactic surveys. The main result is the estimation of the mean distance between noncorrelated complexes of galaxies along a line of sight. We show that the mean size of voids is a function of the richness of complexes. A possible explanation of the apparent regularity in distribution of galaxies on a scale of 13 000km/s is discussed.

INTRODUCTION

At present a lot of attention is concentrated on studying empty regions (voids) in 3-dimensional catalogs (Oort, 1983, Fry 1988). Statistics of voids is however quite poor and there are problems with obtaining quantitative characteristics of a single void which is usially an element of a complicated multiconnected structure. It is also quite difficult to find a relation between parameters of voids and characteristics of the initial spectrum. Therefore, as a rule, conclusions of such analysis are rather vague.

In this report we propose a new method of analysis of deep galactic surveys which allows one to get reasonably reliable information on the structure of the Universe on a scale of 20 -25 h^{-1} Mps and larger. We briefly discuss a theoretical basis of this method. Its possibilities are illustrated on presently available observational material. We obtain an estimate of the typical size of voids. These questions are discussed in more detail by Buryak, Demianski, Doroshkevich, 1991.

THEORY

As it is known (White, 1979; Fry 1985; Otto et al., 1986) the probability of not finding any galaxy in a volume V is given by

$$P_o(V)=\exp[-f(V)], \qquad (1)$$

where the function f(V) is expressed in terms of many-point correlation functions $\xi(x_1, x_2, \ldots, x_k)$ by

$$f(V)=\rho_o V - \sum_{k=2}^{\infty} \frac{(-1)^k}{k!} \rho_o^k \int_V d^3x_1 d^3x_2 \ldots d^3x_k \xi_k(x_1, x_2, \ldots, x_k) \qquad (2)$$

where ρ_o is a mean density of galaxies.

Analysing the distribution of points in deep galactic surveys it is convenient to treat the problem as one-dimensional and to characterize the position of a galaxy by using only the distance along the line of sight ignoring the angular distribution.

In this case instead of (1) and (2), the probability of appearance of a void of diameter $l \geq x$ is given by

$$W_o = \exp[-n(x)] \qquad (3)$$

where

$$n(x) = x/l_o - \sum_{k=2}^{\infty} \frac{(-1)^k}{k!} l_o^k \int_o^x dy_1 dy_2 \ldots dy_k t_k(y_1, y_2, \ldots, y_k) \qquad (4)$$

where l_o is a quantity which has to be determined and which characterizes the distance between non-correlated points (complexes of galaxies formed by intersection of the observational cone with real filaments, walls, or superclusters) and t_k is the k-th order onedimensional correlation function of complexes of galaxies. Relation (3) is equivalent to (1) when V is chosen to be a truncated cone of aperture θ. In such a case (1) integrated over angular variables reduces to (3).

When one uses cluster analysis to study distribution of galaxies in deep surveys (Doroshkevich and Klypin, 1987) it is useful to introduce three functions which depend on the radius of clusterization R, namely, the mean diameter of voids separating clusters $\lambda(R)$, multiplicity of clusters k(R), and the mean size of a cluster or, what is more convenient, a filling factor p(R) which is defined as a fraction of the depth of the survey occupied by clusters. With the help (3) it is not difficult to obtain relations

$$\lambda(R)=\int_R^\infty x\eta'(x)e^{-\eta(x)}dx = Re^{-\eta(x)} + \int_R^\infty e^{-\eta(x)}dx$$

$$p(R)=\lambda_o^{-1}\int_o^\infty e^{-\eta(x)}dx$$

$$\lambda_o=\int_o^\infty e^{-\eta(x)}dx \qquad (5)$$

$$k(R)=W_o^{-1}(R)=\exp \eta(R)$$

Instead of the function $\lambda(R)$ it is more useful to introduce a function $l(R)$ which is identical to a mean distance between particles when they are non-correlated

$$l(R)=e^{\eta(R)}\lambda(R)-R = e^{\eta(R)}\int_R^\infty e^{-\eta(x)}dx = \lambda_o(1-p)/W_o(R) \qquad (6)$$

Of course, when $t_k=0$, $\eta(r)=R/l_o$, and we obtain

$$p(R) = 1-e^{-R/l_o}$$

$$l(R) = \lambda_o = l_o \qquad (7)$$

Let us also note that if for $R > R_1$ all functions t_k are close to zero and

$$\eta(R) = R/l_o + \text{const} \qquad (8)$$

then also $l(R) = l_o$.

The quantity l_o characterizes mean diameter of empty regions along a random straight line. l_o depends on the initial spectrum of perturbations and on the process of formation of galaxies.

To estimate the statistical representability of a survey it is convenient to determine λ_o from the relation (6) which does not depend on the shape of $t_k(x)$ and $\eta(x)$. Deviation of λ_o from a constant value characterizes the representability of the survey.

ANALYSIS OF OBSERVATIONAL DATA

At present there are three deep galactic surveys which can

be analysed by the method presented above. There are six plates of the size 3 square degrees each (KOSS survey) which contain 281 radial velocities of galaxies up to $16^m.5$ (Kirshner et al., 1983) and five plates of the size 13 square degrees each of the Anglo-Australian survey (DARS survey) containing 342 radial velocities of galaxies up to 17^m (Peterson et al., 1986). The survey containing all 623 galaxies of the KOSS and DARS are denoted by SUM. There is also the Anglo - Australian survey (DAFS) consisting of five plates of diameter 20 arcmin each (Broadhurst et al., 1988) containing 188 redshifts of galaxies with $20^m.5 < b < 21^m.5$.

RESULTS

For samples KOSS, DARS and SUM the function $\lambda(R)$ has a characteristic plateau in the region $0.15 \leq p \leq 0.5$ (or $700km/s \leq R \leq 1300km/s$) what shows that the full 1D distribution of complexes is uncorrelated and allows one, for each sample, to determine l_o (see Fig 1). Using the criterion λ_o = const to assess the stastistical significance of our results we see that for all samples statistical errors are large in the region $p > 0.7$ only. In Fig 2 we present the dependence $\lambda_o(p)$ for the survey SUM. It is apparent that the function $\lambda_o(p)$ is almost constant for $0.15 < p < 0.7$ and strongly fluctuates outside this region. For all surveys the value $p = 0.7$ roughly corresponds to $R \simeq l_o$. This seems to indicate that effects mentioned above are mainly connected with strong decrease of number of clusters for $R \geq l_o$ (the influence of the percolation effect). Therefore, to get sensible results in the region $p > 0.7$ it is nessesary to

substantially increase the observational data.

It is interesting that there exists a systematic difference in the value of l_o for samples of the KOSS ($l_o \approx$ 2350km/s) and DARS ($l_o \approx$ 1380km/s) surveys which, probably, is caused by differences in angular sizes between the KOSS and DARS surveys. The dependence of l_o on the size of the plate is very closely connected with the problem of completeness of the survey. Theoretical analysis of this problem is complicated but we have a possibility of empirically estimating such an influence, for example, for the DARS survey.

The DARS plates cover a region of an angular diameter $\theta \approx 4.2$ degree and it is possible to repeat the analysis for subsumples enclosed in a narrower cone. In this way we find an approximate relation

$$l_o(\theta) = d \sqrt{1+r_o/\langle r\theta \rangle} \qquad (9)$$

where r_o = 700km/s, d = 1150km/s and $\langle r\theta \rangle$ denotes the averaged typical diameter of the observational cone. Relation (9) depends only on the real geometrical characteristics of the survey and it only weakly depends on the depth of the survey.

For the KOSS survey θ = 1.6 degree and according to (9) l_o = 1730 km/s instead of a culculated value 2350km/s. Therefore we see that the difference between KOSS and DARS surveys is partly connected with the difference of the angular size of the surveys.

It is very important to compare KOSS and DARS surveys with the survey of the faint galaxies DAFS. Results of our analysis is presented in Fig. 3 which show l(p) and λ(p). Typical parameters characterising this survey are l_o =

2610km/s for distances in the range 400km/s < R < 4000km/s. According to (9) we obtain l_o = (2100 - 2200)km/s, which is reasonably close to the above value. We see that results of the KOSS, DARS and DAFS surveys are in good agreement and they confirm the existence of noncorrelated distribution of complexes with a typical density l_o^{-1}.

CONCLUSION

The main result of our analysis of deep galactic surveys is the estimation of the mean distance between noncorrelated complexes of galaxies along the line of sight

$$l = l_o \simeq (1300 - 1600)\text{km/s} \qquad (10)$$

Because the value of l_o depends on the angular size of the survey it is impossible to obtain a more precise estimate of l_o without analysing the completness of the sample. The fact that l_o depends on the average diameter of the sample $\langle r\theta \rangle$ explains why the value of l_o is different for different surveys.

Analysis of angular dependence of our results shows that they strongly depend on the small scale clustering galaxies which is described by their correlation function. Let us also note that the number of galaxies in the DARS survey is approximately proportional to θ (but not θ^2 as in the homogeneous case) and the function f(V) in (1) has the form

$$\begin{aligned} f(V) &= F(D, m_o, \theta) + R/l(\theta) \\ &= \tfrac{1}{2} \ln(\theta/11') + R/l_o(\theta) \\ N_{gal} &= (384 \pm 50)\ (\theta/120') \\ 120' &\geq \theta \geq 20' \end{aligned} \qquad (11)$$

where D is the depth, θ its angular size and m_o is the

limiting apparent luminosity of the survey.

As it was mentioned before (Doroshkevich and Klypin, 1987) with R $\simeq$ 800km/s only 25% of clusters contain more than four objects (but they contain 70% of all galaxies). At the same time 50% of clusters contain only one galaxy. This means that a majority of elements of the large scale structure are poor chains of galaxies and small groups of galaxies which contain few bright galaxies inside a plate of the survey.

This means also that the actual distances between rich clusters will be larger than l_o and will depend on richness (and luminosity) of the selected sample of objects. It is quite possible that this effect results in an excess correlation and apparent regularity in distribution of galaxies on a scale of $130h^{-1}$ Mps found recently by Broadhurst et al. 1990

We have analysed the SGP plates of the DAFS survey and we have obtained 8 complexes with a mean distance $\langle l \rangle$ = 12900km/s with the value of the filling factor p = 0.844 and $l_o = \langle l \rangle (1-p)$ = 2000km/s. In the framework of our approach the results of Broadhurst et al. 1990 analysis have a natural explanation and the apparent regularity in the galaxy distribution is attributed to position of high peaks (rich complexes) of the uncorrelated 1D distribution of complexes.

As it was mentioned earlier, perturbations of the total density of the Universe, including the dark matter, on a super - large scale are definitely small. However, at present the observational limits of fluctuations of temperature of microwave background radiation are applicable only to larger scales (Doroshkevich and Klypin, 1988)

$$l_{CMB} \leq 120h^{-1}(\sigma_o/0.1)^{-1/3}\text{Mpc} \qquad (12)$$

where l_{CMB} denotes a typical scale of non-homogeneities and σ_o their amplitude. Reliable information on the large scale structure on intermediate scales practically does not exist.

REFERENSES

Broadhurst,T.J., Ellis,R.S., Koo,D.C., and Szalay, A.S., 1990, Nature, 343, 726

Broadhurst,T.J., Ellis,R.S., and Shanks,T., 1988, Mont.Not.R.astr. Soc., 235, 827

Buryak,O.E., Demianski,M., Doroshkevich,A.G., 1991, Astrophys.J., in press.

Doroshkevich,A.G., and Klypin,A.A., 1987, Sov. Astron., 64, 1137

Doroshkevich,A.G., and Klypin,A.A., 1988, Mont.Not.R.astr.Soc., 235, 865

Fry,J.N., 1985, Astrophys.J., 289, 10

Fry,J.N., 1988, Publ. Astr. Soc. Pacific, 100, 1336

Kirshner,R.P., Oemler,A.J., Schecter,P.L., and Schectman,A.S., 1983, Astron.J., 88, 1285

Oort,J.,H., 1983, Ann. Rev. Astron. Astrophys. 21, 373

Otto,S., Politzer,H.D., Prescill,J., and Wise,M.B., 1986, Astrophys.J., 304, 62

Peterson,B.A., Ellis,R.S., Efstathiou,G., 1986, Mont.Not.R.astr.Soc., 221, 233

White,S.D.M., 1979, Mont.Not.R.astr.Soc., 186, 145

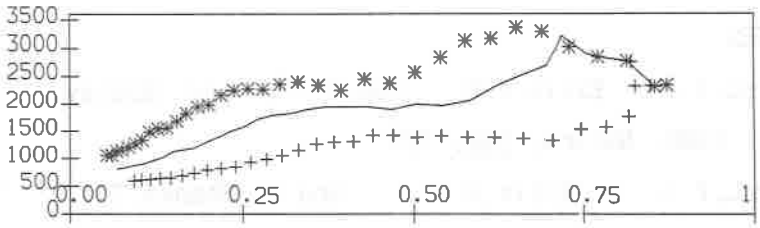

fig.1 function l(p) for samples
dars(+), koss(*) and sum(solid line)

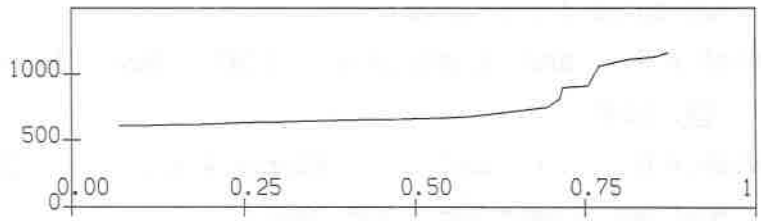

fig.2 function λ(p) for the sample sum

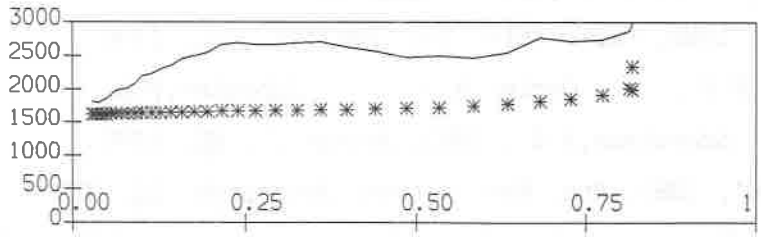

fig.3 functions l(p) and λ(p)(*)
for the sample darf

RECONSTRUCTION METHODS IN COSMOLOGY

Avishai Dekel
Racah Institute of Physics, The Hebrew University of Jerusalem

ABSTRACT

I describe several reconstruction methods for bringing the observed peculiar velocities to common grounds with theoretical predictions. I focus on new developments in the *POTENT* procedure which recovers the three dimensional velocity field by applying the requirement of potential flow. These include a new method for determining the mass-density field in the quasilinear regime and the improvement of signal over noise when the data set is extended. I also suggest an alternative procedure – *OMNIPOTENT*. Possible flaws in the general procedure are discussed, including tests of the basic ansatz of potential flow. I then describe only one of the many applications of the reconstructed dynamical fields – the microwave background anisotropies – and only briefly summarize other comparisons with theory.

I. INTRODUCTION

Since the discovery of the Cosmic Microwave Background (CMB), which we are celebrating here, cosmology has become a phenomenological science with the main effort directed at confronting theory with observation. For a quantitative comparison, one must bring each observation to a common ground with the corresponding theoretical prediction, which sometimes requires "reconstruction" of a certain quantity that is not directly observable. The picture is summarized schematically in the following figure.

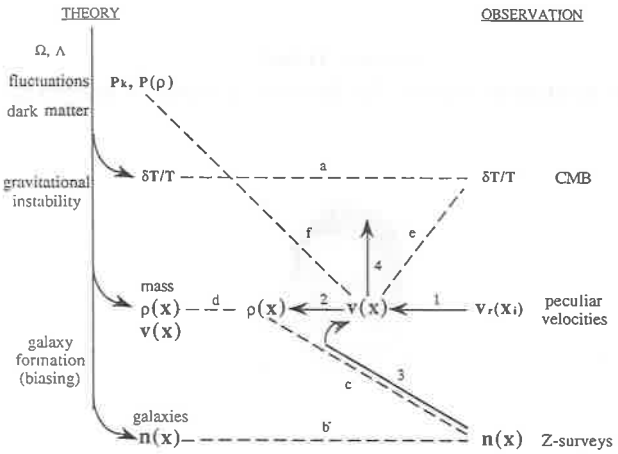

Figure 1 : Reconstruction from observations and confrontation with theory

A theoretical model for the formation of large-scale structure, within the "standard" framework, consists of the following five basic ingredients:

• The *cosmological model*; e.g. a homogeneous Robertson-Walker universe with an Inflation phase. This model is characterized by the parameters Ω and Λ, which affect the rate of cosmic evolution and the characteristic scale of structure – the horizon when the universe turns matter dominated.

• The *initial fluctuations*; their probability distribution $P(\rho)$ (Gaussian or not), their power spectrum P_k (scale-invariant or not) and the way they are distributed among the different component of energy density (adiabatic versus isocurvature).

• The nature of the dominant *dark matter* (DM), which filters the fluctuation power spectrum in a characteristic way during the plasma era. The DM could be baryonic or nonbaryonic, "hot" or "cold" (CDM) – depending on when it became non-relativistic.

• The way the fluctuations evolve under *gravitational instability*; The linear evolution yields a prediction for $\delta T/T$ fluctuations in the CMB. Further nonlinear evolution, using simulations or approximate methods, predicts the statistical properties of the *dynamical* fields today: the fluctuations in the *mass* density $\rho(\vec{x})$ and the associated peculiar velocity $\vec{v}(\vec{x})$.

• The process of *galaxy formation*, or a "biasing" scheme, which determines where galaxies form given the dynamical fields, and yields the properties of the galaxy number density field $n(\vec{x})$. The relation between the galaxy and mass distributions is commonly described by

a linear biasing factor, $\delta n/n = b\ \delta\rho/\rho$. This is the most uncertain component among the model ingredients.

The relevant observations, until a few years ago, primarily consisted of two kinds: upper limits on $\delta T/T$ on different angular scales[1)] and maps of galaxies on the sky and in redshift space[2)] form which a galaxy number density field $n(\vec{x})$ can be obtained by weighting each galaxy inversely with the selection function. While $\delta T/T$ is directly comparable to the observed upper limits[3)] (a), the galaxy distribution could be compared to the corresponding theoretical prediction (b) only after specific assumptions are made concerning biasing.

The new, very promising kind of data consists of *peculiar velocities* of galaxies. In principle, it is related to the predicted dynamical fields so its comparison with theory can bypass the complex issue of biasing. The only assumption to make is that the galaxies are honest traces of the large-scale velocity field. However, the raw data consists of only the radial components of the velocities along the lines of sight, $v_r(\vec{x}_i)$, and it is sparse and noisy, so *reconstruction* is needed before a comparison with theory is possible. Methods have been developed to reconstruct a smoothed, three-dimensional *velocity* field out of this data (1). The original method of this kind is *POTENT*[4,5,6)], which uses the potential nature of the flow predicted by gravity. I will comment below on new developments concerning *POTENT* (§§II-IV) and new methods (§V). In particular, given the velocity field one can reconstruct the underlying *mass-density* field, assuming a value for Ω (2). I will briefly discuss a new, simple technique to do that in the quasi-linear regime[7)] (§III). Also, I will address the question of where the potential analysis could go wrong, and discuss tests of the basic ansatz of potential flow (§VI).

The dynamical fields can also be reconstructed from a galaxy redshift survey (3), provided that it is fairly complete and uniform over the sky, such as the *IRAS* samples. One can first translate $\delta n/n$ into a mass-density field by assuming a certain biasing scheme, and then reconstruct the peculiar velocity field assuming Ω and a dynamical scheme (e.g. linear theory). This was discussed by others in this meeting[8)].

One can also attempt to operate a 'time machine' to trace the dynamical fields back into the linear regime (4); this is beyond the scope of this talk.

The ingredients of the theoretical models can now be tested and constrained by comparing the reconstructed dynamical fields against each other and against the theoretical predictions. I will discuss only one such application (e) – relating the velocity field to the CMB anisotropies (§VII). In the concluding section I will only briefly summarize the results of several other attempts of this sort (§VIII). These include the comparison (c) of the *IRAS* and *POTENT* reconstructed fields[9)], aiming at determining Ω and b, and a similar comparison with optical surveys. They also include a comparison of the reconstructed dynamical fields with the theoretical ones (d) via the fluctuation power spectrum on large scales and an attempt to address directly the statistical nature of the primordial fluctuations (f).

II. POTENT VELOCITY RECONSTRUCTION

Potential analysis has been used to reconstruct the three-dimensional velocity field from its observed radial components. The basic *POTENT* method developed by Bertschinger and

myself is described in the literature[4-7]. It has been tested using an idealized N-body simulation[4,7], and under nonuniform sparse sampling and measurement errors[5,6].

The raw data are distances r_i and redshifts z_i for a set of objects (galaxies or clusters) in directions $\hat{r}_i$. The basic sample[6,8], contains a total of 973 galaxies in 493 objects. The distances have been measured based on the Tully-Fisher relation for spirals and the $D_n - \sigma$ relation for ellipticals and SO's. The redshifts are corrected to the CMB frame and the corresponding radial peculiar velocities are $v_{ri} = cz_i - H_0 r_i$. (H_0 is set to unity so distances can be measured in km s^{-1}.)

Given the radial velocities of a sparse sample, *POTENT* first smooths and interpolates the data into a spherical grid using a tensor window function to produce a smoothed radial velocity field, $v_r(\vec{r})$. This is the most likely value of the velocity averaged over a local spherical Gaussian window of radius R_s centered on $\vec{r}$. In the current analysis we use $R_s = 1200$ km s^{-1}. The smoothing is done with a weighting scheme that mimics volume averaging in order to minimize the errors due to sampling gradients, and the effect of measurement errors is reduced by weighting inversely with the individual expected errors σ_i^2.

In order to obtain the tangential components of the velocity field $\vec{v}(\vec{r})$, we make the crucial assumption that the velocity field is derived from a scalar *potential*: $\vec{v}(\vec{r}) = -\vec{\nabla}\Phi(\vec{r})$, i.e., it has zero vorticity. According to gravitational instability theory in the linear regime, this velocity potential is proportional to the gravitational potential and the no-vorticity mode is the only growing mode. Based on Kelvin's circulation theorem, the flow remains vorticity free even in the quasi-linear regime, as long as orbit mixing does not occur. Finally, we have demonstrated that the flow remains a potential flow, to a good approximation, when regions of collapse and orbit mixing are properly smoothed over[4].

The velocity potential at each point on a spherical grid can therefore be calculated by integrating the radial velocity along radial rays,

$$\Phi(\vec{r}) = -\int_0^r v_r(r', \theta, \phi) dr' \ . \tag{1}$$

Differentiating this potential in the transverse directions then recovers the two missing components of the velocity. (In practice, we interpolate the potential into a cubic grid before differentiating to obtain the velocity field.)

III. POTENT MASS DENSITY RECONSTRUCTION

Given the smoothed velocity field $\vec{v}(\vec{r})$, we now wish to reconstruct the underlying mass-density fluctuation field, $\delta(\vec{r})$. Our method of doing that has been improved drastically since the original version of *POTENT*. In the linear regime the relation is simple: $\delta_d = -\vec{\nabla} \cdot \vec{v}/Hf(\Omega)$, where $f(\Omega) = \mathrm{d}(\ln\delta)/\mathrm{d}(\ln a)$ and a is the universal expansion factor. But our system is not linear, so we need a practical quasi-linear approximation. By testing several methods against N-body simulations we[7] found the best approximation to be the exact solution of the continuity equation under the assumption of Zel'dovich displacements of particles with a universal time dependence[10]. Despite the Lagrangian nature of the Zel'dovich approximation, this density can be expressed in terms of the partial derivatives of the *Eulerian* velocity field, which makes it very useful.

Let $\vec{q}$ be the initial (Lagrangian) comoving position of a particle. The Zel'dovich approximation assumes that the comoving position of that particle at time t (the Eulerian position) is

$$\vec{r}(\vec{q},t) = \vec{q} + D(t)\ \vec{\psi}(\vec{q})\ . \tag{2}$$

The approximation is in writing the displacement as a product of a spatial perturbation function, $\vec{\psi}(\vec{q})$, and a universal time-dependent function, $D(t)$. The comoving peculiar velocity is then

$$\vec{v}(\vec{q},t) = \dot{D}(t)\ \vec{\psi}(\vec{q}) = DHf(\Omega)\ \vec{\psi}(\vec{q})\ . \tag{3}$$

In the second equation we have used the fact that $D(t)$, in the Zel'dovich approximation, is the linear growth rate of density fluctuations, $\delta \propto D(t)$, so $\dot{D}/D = Hf(\Omega)$.

If the velocity field has been smoothed over the scale where collapse and orbit mixing had occurred, one can assume that there is a one-to-one correspondence between $\vec{r}$ and $\vec{q}$. This allows us to write the Zel'dovich displacement in *Eulerian* space,

$$\vec{q}(\vec{r}) = \vec{r} - D\ \vec{\psi}[\vec{q}(\vec{r})]\ . \tag{4}$$

The continuity equation, in the Zel'dovich language, can be written as $\rho_r(\vec{r})\ \mathrm{d}^3r = \rho_q \mathrm{d}^3q$, where ρ_r is the Eulerian density and ρ_q is the Lagrangian (mean) density. The density contrast is therefore

$$\delta_c(\vec{r}) = \left\| \frac{\partial \vec{q}}{\partial \vec{r}} \right\| - 1 = \left\| I - (Hf)^{-1} \frac{\partial \vec{v}}{\partial \vec{r}} \right\| - 1\ , \tag{5}$$

where the double vertical bars denote the Jacobian determinant and I is the unit matrix. Note that this is a non-linear expression but it still involves only the first partial derivatives.

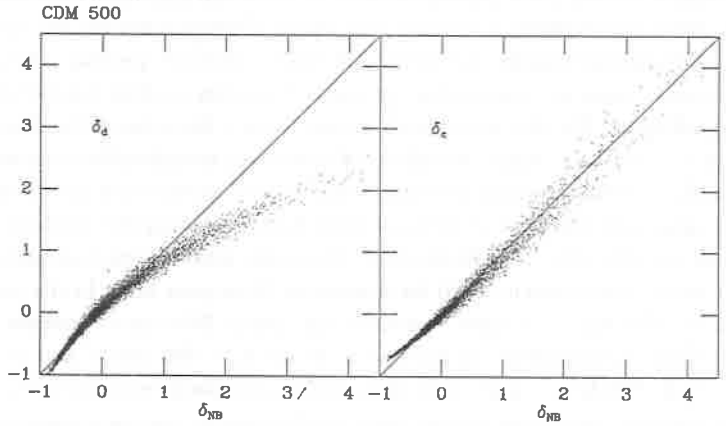

Figure 2 : The "linear" (left) and quasi-linear (right) approximations for the density contrast, derived from the velocity field, versus the true density in a CDM N-body simulation, Gaussian smoothed with radius 500 $\mathrm{km\,s^{-1}}$.

This approximation was tested against N-body simulations of CDM and Neutrino cosmologies with $\Omega = 1$, smoothed with a Gaussian of radius 500 $\mathrm{km\,s^{-1}}$ or 1000 $\mathrm{km\,s^{-1}}$.

Figure 2 shows the "linear" and the quasi-linear approximations derived from the velocity field versus the true density contrast in the CDM simulation with 500 $\mathrm{km\,s^{-1}}$ smoothing. The *rms* error of δ_c is less than 0.1 over the range $-0.8 \leq \delta \leq 4.5$. It thus provides a very useful tool for reconstructing the mass density field from the *POTENT* velocity field.

The tight relation between the true density and the linear approximation in the quasi-linear regime also suggests a method for the inverse problem of extracting the quasi-linear velocity from a given density field specified over a large region. This new inversion procedure can improve the prediction of the peculiar velocity field from galaxy redshift surveys such as the IRAS survey.

The inverse problem of extracting the velocity field from a given density field (e.g. from a redshift survey like *IRAS*) needs non-linear corrections as well. Even in the linear regime, it requires non-local integration of the relation $\delta_d \propto -\vec{\nabla} \cdot \vec{v}$. The tight correlation seen in the N-body simulations between the true and the "linear" densities that are derived from the true velocities suggests the following scheme for introducing non-linear corrections. Use an empirical fit based on the N-body simulations to translate the given density to an equivalent "linear" density, δ_d, and then integrate the linear relation for the velocity as usual. A useful empirical fit of this sort, good to an accuracy of about 0.1 in the range $-0.8 < \delta < 4.5$, is given by

$$\delta_d = \delta - 0.2\delta^2 + 0.025\delta^3 \ . \tag{6}$$

This method is now being used in the *POTENT–IRAS* comparison[11].

IV. POTENT ERROR ANALYSIS

What makes the *POTENT* output suitable for quantitative studies is the error analysis[5,6]. The largest source of error is the random distance errors of the individual data points, whose effect on the reconstructed fields is assessed using Monte Carlo simulations. We construct 100 artificial redshift-distance samples in which the distance (and hence peculiar velocity) of each object is scattered using an independent zero-mean Gaussian random number of standard deviation equalling σ_i. We also scatter each redshift with a Gaussian of standard deviation $\sigma_f = 150\ \mathrm{km\,s^{-1}}$ in order to mimic the effects of small-scale sampling fluctuations. For each artificial sample we reconstruct the potential, velocity and density fields and then construct maps of the mean and standard deviation of these fields (denoting the standard deviations σ_ϕ, σ_v and σ_δ respectively). The standard deviation provides our error estimate while the mean of the noise simulations is useful for diagnosing Malmquist bias. In the well-sampled regions [out to 3000 $\mathrm{km\,s^{-1}}$ in most directions and nearly 6000 $\mathrm{km\,s^{-1}}$ toward the Great Attractor at Hydra Centaurus (GA)] the rms errors are $\sigma_v < 250\ \mathrm{km\,s^{-1}}$ and $\sigma_\delta < 0.2$, but the errors exceed 1000 $\mathrm{km\,s^{-1}}$ and 1.0 respectively in some poorly sampled noisy regions.

Besides suffering from large measurement random errors, our reconstructed fields are subject to *biases*. In particular, a sampling gradient bias and the Malmquist bias cause some concern. We estimated the Malmquist bias in the velocity field, using N-body artificial data, to be less than 200 $\mathrm{km\,s^{-1}}$ nearly everywhere for the 1200 $\mathrm{km\,s^{-1}}$ window. This error is thus small compared to the random errors. The sampling gradient bias arises from the coupling of gradients in the true velocity field and the selection function. It is difficult to assess from

the data, but we showed, using Monte Carlo simulations of the N-body "data", that with our volume weighting scheme (weight of the contribution from each object $\propto R_4^3$, where R_4 is the distance from the object to the fourth nearest object), this bias is generally much smaller than the scatter due to distance errors. There are, however, a few very empty regions where sampling bias might be severe enough to generate coherent artificial flows having no physical reality. These include regions of low Galactic latitude (small supergalactic Y) and voids in the galaxy distribution away from the supergalactic plane. Being unable to quantify the sampling gradient biases in these regions at this stage, we can simply exclude very empty regions from any quantitative analysis, based on some criterion for "emptiness". For example, we exclude all grid points where the distance to the 4th nearest neighboring object, R_4, is greater than some value, R_4^{max}.

Thus, in any use of *POTENT* output, we can impose three inclusion criteria: $R < R^{max}$ for the spherical volume where reconstruction has been done, $R_4 < R_4^{max}$ for exclusion of too empty regions, and $\sigma_v < \sigma_v^{max}$ or $\sigma_\delta < \sigma_\delta^{max}$ for exclusion of too noisy regions.

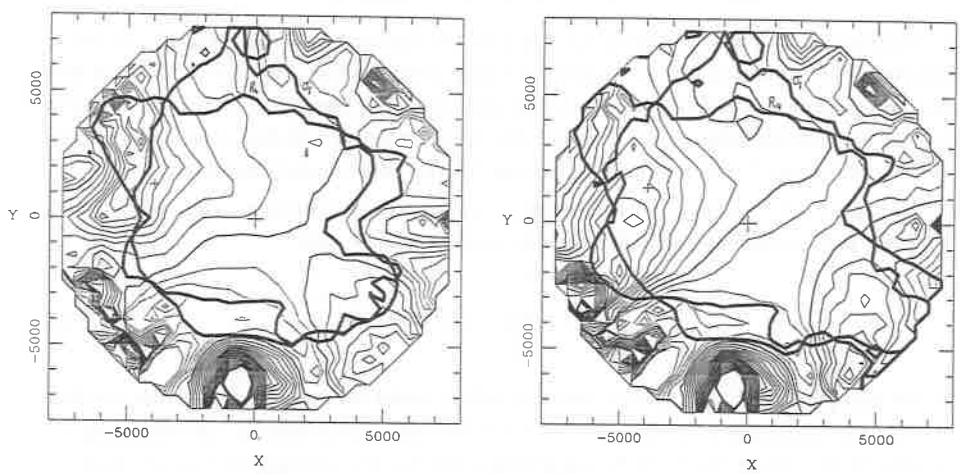

Figure 3 : Density contrast in the supergalactic plane. Left: from the original data input to *POTENT*. Right: based on a preliminary extended sample with 501 new galaxies in the GA and in the Pisces regions. The smoothing radius is 1200 km s^{-1}. Positive and negative contours are solid and dotted respectively, with the zero contour slightly heavier and contour spacing 0.1. The heavy contours mark errors: $\sigma_\delta = 0.4$ and $R_4 = 1500$.

The inclusion of more data in any given region can improve the signal to noise significantly. This is demonstrated in Figure 3. Shown is the "old" *POTENT* density map based on the original data[6] in comparison with a *POTENT* reconstruction of an extended data set. The new data is still preliminary. It includes 501 new spirals, partly grouped in 183 objects, both in the GA region (by A. Dressler and S. M. Faber) and in the Pisces region (by J. Willick), but it has not been carefully tested, matched and merged with the old data set yet. The point of showing this is to demonstrate the effect on the errors. The error contours move outwards. The density peak of the GA now shows up at a level of $\delta = 1.4 \pm 0.3$ and

it has moved slightly toward the galactic plane ($X = -4500$, $Y = 0$). The Pisces peak is at $\delta = 1.0 \pm 0.4$, but the still poorly-sampled Perseus region (near $X = 5000$, $Y = 0$) is dominated by noise: it carries large errors both in terms of σ_δ and R_4.

V. OMNIPOTENT – AN ALTERNATIVE TO POTENT

The constraint of no-vorticity can be applied to the data in several different ways. For example, one alternative to *POTENT*, termed *OMNIPOTENT*, is now being investigated by G. Blumenthal and myself. It promises to have three basic advantages over *POTENT*: the data is smoothed simultaneously with the derivation of the full velocity field and not as a preceeding step, the sampling-gradient bias is reduced, and the derivation of the density does not require numerical differentiation.

In order to evaluate the peculiar velocity and its spatial derivatives at a point $\vec{r}$, expand the i'th component of the velocity at any point $\vec{r}+\vec{x}$ at its neighborhood in terms of powers of x_j,

$$v_i(\vec{x}) = B_i + L_{ij}x_j + Q_{ijk}x_jx_k + C_{ijkl}x_jx_kx_l + \dots \ . \tag{7}$$

The requirement $\vec{\nabla} \times \vec{v} = 0$ simply means that the matrices L_{ij}, Q_{ijk} and C_{ijkl} are all *symmetric*. The expansion can be truncated at any order, making a model for the local flow with a finite number, p, of free parameters (the various matrix elements) to be determined by the data. The zero'th order model with only the first term, the bulk flow, has 3 parameters, the linear model has 9, the quadratic model has 24, the cubic model has 66, etc.

Given a set of N objects with measured radial peculiar velocities u_n at positions $\vec{r}_n$ $(n = 1, N)$, we determine these parameters by minimizing the sum

$$\chi^2 = \sum_{n=1}^{N} [u_n - \vec{v}(\vec{r}_n) \cdot \hat{r}_n]^2 W(\vec{r}_n, \vec{r}) \ , \tag{8}$$

provided that $pleq N$. W is a window function, which could be a spherical Gaussian window as in *POTENT*. Then, the desired velocity at $\vec{r}$ is $\vec{v}(\vec{r}) = \vec{B}$, and the density contrast, using the continuity density under the Zel'dovich approximation (eq. 5), is simply $\delta_c(\vec{r}) = \|I - L_{ij}\| - 1$.

The zero'th order scheme of this sort is somewhat analogous to the *POTENT* procedure, which first fits a local bulk flow in the neighborhood of each point. The linear term provides a straightforward density determination. A model of higher order allows more degrees of freedom and therefore more flexibility in the local fit. It eliminates several biases that *POTENT* suffers from, including the sampling-gradient bias that arises from the averaging of the velocities sampled inhomogeneously within the window. But there are also disadvantages that become severe when the model has too many parameters: a bias is introduced because the data has to be interpolated from a larger volume about each point and the small-scale noise in the data is picked up and may eventually dominate the fit. We find for the current data that the optimal model is either the quadratic or the cubic model. This method is being tested and applied to the data.

Another method for reconstructing the density field from the peculiar velocities have been suggested by Stebbins and Kaiser[12]. It is based on "maximum probability" estimation

of the density Fourier components. The method works nicely and it produces informative maps over an extended volume, but it is somewhat model-dependent. The basic limitation of this method is that the resultant density is modulated by the quality of the data: in regions of good data the density contrast is allowed be be high but where the data is poor the estimated density contrast is forced to be low. As a result, for example, the Virgo cluster turns out to be a higher peak than the GA. The resulting maps are therefore not uniform and it would not be straightforward to use them for a quantitative comparison with other data or theory.

VI. IMPOTENT – WHERE CAN WE GO WRONG?

• *Systematic Distance Errors.* Several authors have pointed out that the large-scale flow might be an artifact of a systematic zero-point variation in the galaxy scaling-laws that are used in the distance measurements[13]. Evidence is accumulating against this possibility[14]. In particular, it seems that any such systematic effect would require unnatural large-scale coherence across the sky that needs an explanation as much as the GA phenomena does.

A promising test for the reality of the velocity measurements can be provided by comparing the results from the Tully-Fisher and the $D_n - \sigma$ relations. Bertschinger showed in his talk to what extent the *POTENT* smoothed radial velocities, as deduced by the two different methods at the same points in space, agree with each other. We find that the velocity and density fields extracted by *POTENT* from the two orthogonal sets of data in the regions where the uncertainties in both are acceptable reveal the same main features including the GA, the big underdense region between us and Pisces, and the bulk flow. This similarity provides an encouraging confirmation for the reality of the velocity field.

• *Potential Flow.* The ansatz of potential flow is based on theoretical considerations. It is impossible to confirm its validity by observation independently of further assumptions because vorticity could always be hidden in the tangential velocities which we cannot observe. Given the radial components of any velocity field, with or without vorticity, *POTENT* would recover the one potential flow that corresponds to the given radial velocities. The resulting velocity and density maps could be very different from the true ones.

This is illustrated in the following amusing example. Consider a "true" velocity field that mimics a huge "galaxy" in the XY plane (centered, say, at $x = 3000$, $Y = 0$): a circular motion about an axis (normal to the XY plane) with a flat rotation curve (500 $\mathrm{km\,s^{-1}}$, say) extending all the way to infinity. Such a velocity field corresponds to a spherical distribution of mass about the center of rotation with an r^{-2} density fall off. Given the radial components of this field, *POTENT* recovers a monotonic potential gradient along the Y axis, perpendicular to the line of sight near the center of the "galaxy". The derived velocity and density maps are shown in Figure 4, with the latter revealing fictitious density maximum and minimum on the two sides of the true density peak (at about $X = 3000$, $Y = \pm 2000$).

We are in a process of applying *POTENT* to more general velocity fields with large-scale vorticity, e.g. as generated by explosions or by cosmic turbulence. But the above simple case already reveals a characteristic, detectable imprint of vorticity: that the mass distribution as recovered by *POTENT* does not follow the light distribution, under the *assumption* that

the light does trace the true mass distribution (e.g. the true "galaxy") via some monotonic biasing scheme. As described by Bertschinger here, we find that the *IRAS* and *POTENT* densities are monotonically correlated with each other (e.g. their density maxima at the GA almost coincide), so this result can serve as a reassuring test of the potential flow ansatz.

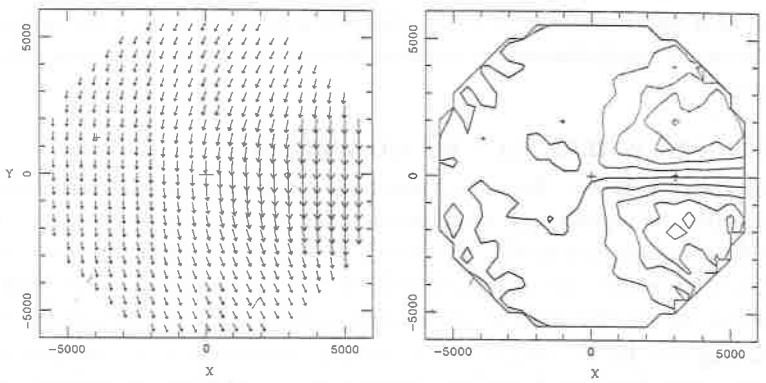

Figure 4 : The velocity (left) and density (right) fields reconstructed by *POTENT* from the line-of-sight velocities of a rotating "galaxy" with a flat rotation curve centered at $X = 3000$, $Y = 0$.

Another test of the potential flow ansatz is possible under the *assumption* of large-scale isotropy. If there is vorticity such that the velocity recovered by *POTENT* is not real, there is no reason for it to be isotropic. In fact, the *POTENT* procedure imposes a preferred direction at each point – the radial direction to the origin – so the radial and tangential velocities could violate the isotropy condition $\langle v_{tan}^2 \rangle = 2\langle v_{rad}^2 \rangle$. We have found that the *POTENT* velocity field inside 4000 km s^{-1} obeys this condition well within the 1σ error bars derived from the Monte Carlo simulations.

Also reassuring is the fact that main features in the velocity field recovered by *POTENT* are also recovered by the "maximum probability" method[12], which is not explicitly dependent on the ansatz of potential flow.

Finally, since vorticity does exist on small scales where collapse has occurred, it is important to formally confirm our hypothesis, so far based on N-body simulations[4], that the smoothed velocity field on sufficiently large scales is indeed vorticity-free to a satisfactory accuracy.

• *Sparse and Noisy Data.* In order to distinguish between signal and noise, it is crucial to estimate the uncertainties in the analysis. As discussed in §IV, we have confidence in our analysis of the uncertainties due to the distance measurement errors and discrete sampling (including Malmquist bias and shot-noise), but we do not have yet a satisfactory way of estimating the remaining biases due to sampling gradients, except of eliminating too-empty regions altogether. Nevertheless, we do have already a fairly good indication for where the results should be trusted and where they are dominated by errors, and every use of these results should take the local uncertainties into account. The errors are expected to

be reduced significantly when more data fills poorly sampled regions and penetrates deeper with improved distance measurement tools.

VII. CMB MAP OF OUR NEIGHBORHOOD

Fluctuations in the gravitational potential and in the velocity field cause fluctuations in the temperature of the CMB. We can therefore reconstruct maps of the CMB anisotropy $\Delta T/T$ as seen by a distant observer viewing our region of the universe as a patch on his last scattering surface. These maps[15], for the first time, are based on the measured gravitational potential and on the basics of gravitational instability rather than on a specific theoretical model.

In the linear approximation, applicable on large scales, the peculiar gravitational potential $\phi(\vec{r})$ is proportional to the velocity potential recovered by *POTENT*: $\phi(\vec{r}) \simeq (3/2)\Omega^{0.4}\Phi(\vec{r})$. The current data is sufficient to recover the potential out to $\lesssim 6000\ \mathrm{km\,s^{-1}}$ with a signal to noise ratio of nearly 10[6]. The local potential field is dominated by one huge potential well, the GA. The flow toward the GA is coherent over a scale of nearly $10000\ \mathrm{km\,s^{-1}}$, with a magnitude of $\sim 500\ \mathrm{km\,s^{-1}}$, and the corresponding maximum variation in ϕ is $\sim 8 \times 10^{-5}c^2$.

Gravitational potential fluctuations on the last-scattering surface cause CMB anisotropy via the Sachs-Wolfe and Doppler effects[16]. For a matter-dominated universe, the CMB brightness temperature fluctuation in direction $\vec{n}$ is

$$\frac{\Delta T}{T} = \frac{1}{3c^2}\left[\phi(\vec{x}_e) - \phi(\vec{x}_o)\right] - \frac{1}{c}\vec{n}\cdot(\vec{v}_e - \vec{v}_o)\ , \tag{9}$$

where $\vec{x}_o$ and $\vec{v}_o$ are the observer's comoving position and peculiar velocity and $\vec{x}_e$ and $\vec{v}_e$ are the comoving position on the last-scattering surface in the direction $\vec{n}$ and the effective peculiar velocity of the photon-baryon fluid there at decoupling. (The finite thickness of the last-scattering surface has been accounted for approximately by the *POTENT* smoothing of the potential with a Gaussian of radius $1200\ \mathrm{km\,s^{-1}}$, or 7'.) The first term, the Sachs-Wolfe gravitational redshift, is dominant on scales larger than 2° (for $\Omega = 1$) while the second, the Doppler contribution, is important on smaller scales. A comoving separation $|\Delta\vec{x}_e|$ on the last-scattering surface corresponds ($\Omega = 1$) to an angular separation $2\arcsin(|\Delta\vec{x}_e|/4c)$. The Sachs-Wolfe anisotropy is generic while the Doppler anisotropy, as well as the adiabatic contribution that we have neglected, depends on the amounts of baryonic and nonbaryonic matter and on the mode of perturbation (e.g., adiabatic or isocurvature).

For $\Omega = 1$, in the linear regime, the gravitational potential remains constant in time. We can therefore compute the Sachs-Wolfe contribution to the anisotropy in the radiation decoupled at $z_{dec} \simeq 1300$ directly from the potential field derived by *POTENT* today. The Doppler contribution may be estimated crudely by assuming that the photon-baryon fluid at decoupling has the same peculiar velocity field as the dark matter, i.e. smaller than the present velocities by a factor $(1 + z_{\mathrm{dec}})^{-1/2}$. Radiation last scattered locally would now be reaching a distant observer nearly at the edge of our horizon. Figure 5 shows maps of the relative brightness temperature fluctuations caused by the Sachs-Wolfe and Doppler effects for such an observer looking upon the local universe from the direction of the Supergalactic

north pole. The GA corresponds to the potential well just beyond the left edge of the map. (If $\Omega < 1$, the angular scale would decrease and the amplitude of $\Delta T/T$ would increase, with the model-dependent Doppler and adiabatic contributions dominating the Sachs-Wolfe anisotropy.)

Although Figure 5 shows the CMB anisotropy viewed by a distant observer in one small region of his last-scattering surface, the Copernican principle argues that we should see similar regions of anisotropy on our last scattering surface. The maximum Sachs-Wolfe anisotropy, caused by the GA, is about 1.7×10^{-5} on a scale of 1° (for $\Omega = 1$ and a 30 arcminute beam). The maximum Doppler contribution, 4.9×10^{-5}, is overestimated because the photon-baryon fluid typically oscillates with a smaller velocity than the dark matter. We are currently trying to estimate the Doppler contribution more accurately[18]. Anisotropy as large as that shown in Figure xxx would be seen only by a carefully placed observer with properly oriented beams directed right across the GA. The typical Sachs-Wolfe anisotropy on a 1° scale is $\sim 5 \times 10^{-6}$. Until accurate velocity measurements are made for galaxies beyond 6000 $\mathrm{km\,s^{-1}}$, we cannot estimate how frequently anisotropies as large as 2×10^{-5} should be seen, but, unless we live in a special place, anisotropies exceeding 10^{-5} should be fairly common.

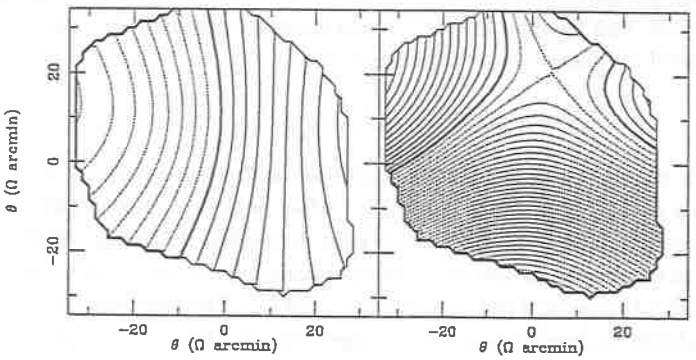

Figure 5 : Contour maps of $\Delta T/T$ for a distant observer who sees the last scattering of radiation occurring in the Supergalactic plane. Left: Sachs-Wolfe contribution. Right: an overestimate of the Doppler contribution. The contour spacing is $\Delta T/T = 10^{-6}$ with negative contours dotted and the zero contour (arbitrarily chosen) heavy. Regions with Sachs-Wolfe standard errors (arising from distance errors) greater than 2×10^{-6}, determined from Monte Carlo simulations, have been excluded. Each map has been convolved with a Gaussian beam of 30 arcmin FWHM (for $\Omega = 1$) to mimic the experiment of Lubin *et al.*[17], but no subtraction has been performed.

If $\Omega = 1$, the angular scale of the GA potential well is an excellent match to the two-beam subtraction experiment of Lubin *et al.*[5], with beams of 30' FWHM and a beam throw of 1°. Present anisotropy limits on this scale ($\Delta T/T \lesssim 3.5 \times 10^{-5}$, at 90% confidence[19]) are a factor of 2 or 3 above the Sachs-Wolfe anisotropies predicted here. These predictions, leaving aside the Doppler and adiabatic anisotropies, are minimal, unless the fluctuations were

smeared out by late reionization. If gravitational instability is responsible for the generation of large-scale peculiar motions, and if our neighborhood is not unique, the precursors of large-scale structure should soon be detected in CMB anisotropy experiments.

VIII. SUMMARY: COMPARISON WITH THEORY

I have tried to highlight in this talk several aspects of the *methods* for reconstructing the full dynamical fields from observations, focusing on recent developments in the POTENT analysis of peculiar velocities. The consistency of the results obtained separately from spirals and from Ellipticals and S0's, with independent distance estimators, indicates that the measured velocities are real. The agreement with the fields reconstructed by different methods[12], the monotonic correlation between fluctuations in the light and mass and the apparent isotropy of the reconstructed velocity field all support the basic ansatz of potential flow, which originated from theoretical argumentation based on gravitational instability.

Let me just briefly summarize the current results from the various ongoing comparisons of the reconstructed dynamical fields with theory.

• *Cosmography*[6]. Smoothed with a 1200 $\mathrm{km\,s^{-1}}$ Gaussian, the Great Attractor is an extended overdensity, centered near $X = -4500$, $Y = 0$ ($\pm 500\ \mathrm{km\,s^{-1}}$), with $\delta = 1.4 \pm 0.3$ at the peak. The Pisces peak is $\delta = 1.0 \pm 0.4$, but a large fraction of the Perseus-Pisces (PP) supercluster is still very poorly sampled. An extended, deep underdense region lies between the Local Group (LG) and PP.

bullet Power spectrum of mass-density fluctuations. The bulk flow in a top-hat sphere of radius 4000 $\mathrm{km\,s^{-1}}$ about us is[6] $V = 388 \pm 67\ \mathrm{km\,s^{-1}}$. This is fairly consistent with the prediction for CDM, $\langle V^2 \rangle^{1/2} = 287 b^{-1}\ \mathrm{km\,s^{-1}}$, even if the normalization is $b \simeq 2$. An analysis of the Mach number[20] of this flow, using the POTENT velocity field[21], gives $M = 1.2 \pm 0.2$. This is consistent at the 1σ level with the *rms* value predicted for CDM, indicating a general agreement of the shape of the power spectrum with CDM. A direct recovery of P_k from the POTENT output, by FFT of the potential field[22], reveals a detailed agreement with the power spectrum of CDM out to wavelength $\sim 100\ \mathrm{h^{-1}Mpc}$, where the logarithmic slope of P_k bends to $n \geq 0$. This is consistent with a Zel'dovich scale-invariant spectrum ($n = 1$) on larger scales, although we cannot explore such large scales yet in terms of the dynamical fields.

• *Probability distribution of fluctuations.* We find[23] that the one-point probability distribution function of the smoothed peculiar velocity field, $P_1(v)$, remains surprisingly constant even through nonlinear evolution. This constancy is exact under the Zel'dovich approximation, and is confirmed using N-body simulations. Thus, the velocity field observed today can provide a direct clue for the statistical nature of the initial fluctuations. We find that $P_1(v)$ of the observed (1D) velocities, as processed through POTENT or as predicted by the IRAS analysis, is indistinguishable from a normal distribution, suggesting that the initial fluctuations are Gaussian, and ruling out non-Gaussian models such as Cosmic Strings.

• *Galaxy formation and cosmological parameters.* The IRAS galaxy distribution, within $\sim 4000\ \mathrm{km\,s^{-1}}$ about the LG, is correlated with the mass fluctuations, both revealing the same main features in the GA, PP, and the void in between. A linear comparison yields

$b_I/\Omega^{0.6} = 1.0 \pm 0.2$[9,11], where b_I is the biasing factor for *IRAS* galaxies. A similar, but preliminary, comparison with optical data[24] yields $b_O/\Omega^{0.6} \simeq 2$. These are consistent with $\Omega = 1$ and typical b values of order unity or slightly higher, but it also allows $\Omega \simeq 0.1$, say, with severe "antibiasing": $b \simeq 0.5$. A recent attempt[11] to determine Ω and b independently, using the non-linear corrections (§III) in the comparison, seems to favor the standard option: $\Omega \simeq b \simeq 1$.

• *Microwave background and gravitational instability.* If our basic ideas concerning gravitational instability are valid, the GA indicates that $\delta T/T$ fluctuations on the order 10^{-5} should be detected (unless reionization has smeared out the fluctuations). This is still consistent with the observed upper limits, but the constraints are getting close.

My conclusion so far is that the observed velocities and the corresponding mass-density field are consistent with the "standard" model: a homogeneous universe with an Inflation phase, $\Omega = 1$ and $\Lambda = 0$, Gaussian, adiabatic initial fluctuations with a scale-invariant spectrum, cold dark matter with $\sim 10\%$ baryons and gravitational growth of fluctuations to the present structure. In this case, the indications[2,25] for an excess of power in the *galaxy* distribution on scales ≥ 40 h^{-1}Mpc must be accounted for by a non-trivial relation between galaxies and mass, where the biasing factor is both a function of scale and density. The alternative, of an $\Omega \sim 0.1$ baryonic universe[26], requires isocurvature fluctuations and reionization of $\delta T/T$ plus antibiasing.

ACKNOWLEDGEMENT

This talk describes work done in collaboration with Ed Bertschinger. The collaborators on various parts of the method are G. Blumenthal, S. Faber and A. Nusser. The main data is due to D. Burstein, A. Dressler, S. Faber and J. Willick. This research has been supported by US-Israel Binational Science Foundation grant 86-00190, and by Israeli Academy Basic Research grant 316/87.

REFERENCES

1. Smoot, G.F., this proceedings; Melchiori, F., this proceedings.
2. Maddox, J., this proceedings; Geller, M., this proceedings.
3. Partridge, B., this proceedings; Vittorio, N., this proceedings.
4. Bertschinger, E. and Dekel, A. 1989, *Astrophys. J. (Lett.)* **336**, L5.
5. Dekel, A., Bertschinger, E. and Faber, S.M. 1990, *Astrophys. J.* **364**, in press.
6. Bertschinger, E., Dekel, A., Faber, S.M., Dressler, A. and Burstein, D. 1990, *Astrophys. J.* **364**, in press.
7. Nusser, A., Dekel, A., Bertschinger, E. and Blumenthal, G.R., 1991, *Astrophys. J.* , in press.
8. Davis, M., this proceedings; Frenk, C.S., this proceedings.
9. Bertschinger, E., this proceedings.
10. Zel'dovich, Ya.B. 1970, *Astron. Astrophys.* **5**, 20.
11. Dekel, A., Bertschinger, E., Yahil, A., Strauss, M. and Davis, M. 1991, in preparation.
12. Stebbins, A. and Kaiser, N. 1990, preprint.
13. Djorgovski, S., de Carvalho, R. and Han, M.-S. 1989, in *The Extragalactic Distance*

Scale, ed. S. van den Bergh and C. J. Pritchet (Provo: Ast. Soc. Pac.), pp. 329.; Silk, J. 1989, *Astrophys. J. (Lett.)* **345**, L11.

14. Burstein, D. 1990, *Rep. Prog. Phys.*, in press.; Lucey, J.R. 1991, in *Observational Tests of Inflation*, ed. T. Shanks (Kluwer), in press.
15. Bertschinger, E., Gorski, K. and Dekel, A. 1990, *Nature* **345**, 507.
16. Sachs, R.K. and Wolfe, A.M. 1967, *Astrophys. J.* **147**, 73.
17. Lubin, P. *et al.* 1990, in *The Cosmic Microwave Background 25 Years Later*, eds. N. Mandolesi and N. Vittorio, in press.
18. Vittorio, N., Dekel, A. and Bertschinger, E. 1991, in preparation.
19. Vittorio, N. 1990, in *The Cosmic Microwave Background 25 Years Later*, eds. N. Mandolesi and N. Vittorio, in press.
20. Ostriker, J.P. and Suto, Y. 1990, *Astrophys. J.* **348**, 378.
21. Kolatt, T., Dekel, A., Hoffman, Y. and Bertschinger, E. 1991, in preparation.
22. Kolatt, T., Dekel, A. and Bertschinger, E. 1991, in preparation.
23. Kofman, L., Bertschinger, E., Gelb, J., Nusser, A. and Dekel, A. 1991, in preparation.
24. Bistoles, V., Dekel, A., Lahav, O., Tully, B. and Bertschinger, E. 1991, in preparation.
25. Maddox, S.J, Efstathiou, G., Sutherland, W.J. and Loveday, J. 1990, *M.N.R.A.S.* **242**, 43p.; Efstathiou, G., Kaiser, N., Saunders, W., Lawrence, A., Rowan-Robinson, M., Ellis, R.S. and Frenk, C.S. 1990, *M.N.R.A.S.* , in press; Bahcall, N. 1988, *Ann. Rev. Astr. Ap.* **26**,631; Fong, R., this proceedings.
26. Peebles, J.P.E., this proceedings; Blumenthal, G.R., Dekel, A. and Primack, J.R. 1988, *Astrophys. J.* **326**, 539.

Simon White and Marc Davis

$w(\theta)$ FROM THE EDINBURGH - DURHAM SOUTHERN GALAXY CATALOGUE

C.COLLINS[1]
R.NICHOL[2], S.LUMSDEN[3]
[1]*Royal Observatory, Blackford Hill, Edinburgh, EH9 3HJ, U.K.*
[2]*Department of Astronomy, Univ. of Edinburgh, EH9 3HJ, U.K.*
[3]*Astrophysics Group, ICSTM, London, U.K.*

Abstract

The two-point angular correlation function of galaxies is presented for the recently completed Edinburgh-Durham Southern Galaxy Catalogue. Despite many independent estimates, there has been little consensus reached as to the form of the two-point angular correlation function of galaxies on scales $\sim 10h^{-1}$Mpc. This galaxy survey consists of digitised COSMOS scans for 60 UK Schmidt fields centered at the SGP. Both star-galaxy classification errors and photometric errors in plate to plate matching, that could ruin a project of this kind, have been kept to a minimum. The catalogue is therefore ideally suited to probe the form of the correlation function on cosmologically interesting scales. We present our $w(\theta)$ results from the catalogue at 3 depths: $b_j = 17.5, 18.5, 19.5$. These correlation functions all indicate significant large-scale power out to beyond $10h^{-1}$Mpc with a break on scales $\simeq 20h^{-1}$Mpc. This is in conflict with the result obtained from the analysis of the Lick survey of galaxies[1)] and is consistent with the recently reported APM galaxy correlation function[2)].

Introduction

The two-point galaxy angular correlation function, $w(\theta)$, and its spatial equivalent, $\xi(r)$, are the two statistics which have been most commonly used to quantify the distribution of galaxies on large scales. The two-point correlation function measures the excess number of galaxies over that expected from a random distribution. The main advantage of this function as a measure of large-scale structure is that it provides a direct measure of the amplitude of density fluctuations on different scales, under the assumption that galaxies trace the mass. In this way the correlation function can provide a direct constraint on the amplitude of fluctuations in the early universe and the shape of the initial fluctuation spectrum[3,4]. Any putative feature in the correlation function may well reflect a particular preferred scale of galaxy clustering.

The most comprehensive investigation of $w(\theta)$ carried out on large scales has been the analysis of the Lick astrographic survey of galaxies[5]. This work[1] (hereafter GP) indicated the existence of a power-law form to the correlation function on angular scales $< 2.5°$ with a break feature at $\simeq \theta < 2.5°$, corresponding to a projected distance of $\simeq 9h^{-1}$Mpc. Despite the later confirmation of a power-law, and the establishment of the GP result as a "bench mark" for these kinds of studies, there remains considerable uncertainty as to the reality of the break feature. This is due to the effect of large systematic errors associated with the visual counting of galaxies and the lack of quality control in the Lick survey. This has caused some authors[6,7] to claim that the break observed in the correlation function may be the result of plate-to-plate variations in limiting magnitude.

The availability of fast photographic plate measuring machines, such as COSMOS and APM, has enabled large area galaxy catalogues to be constructed in an objective manner with quantifiable selection criteria[8]. In general, the results on $w(\theta)$ from digitised surveys confirm the existence of a break as first reported by GP. However, there is wide disagreement between authors with regard to the physical scale size of the break. Table 1 shows a compilation of break scale estimates (determined by the authors), using digitised galaxy catalogues. As this table indicates, estimates of the scale on which the correlation function deviates from a power-law vary by nearly an order

of magnitude. A close inspection of Table 1 reveals that there is a trend such that the larger area surveys tend to detect a break at larger spatial scales. This indicates that finite survey areas have been significant, at some level, in giving rise to systematically smaller break scales. However, the two largest surveys listed in Table 1[1,2] differ significantly in the amplitude of the break detected. It is this lack of consensus which has motivated this paper.

Table 1

Contiguous Area (deg^2)	Break Scale (h^{-1}Mpc)	Authors
14	3	Shanks *et al.* 1980[9]
22	3	Stevenson *et al.* 1985[10]
36	7	Hewitt *et al.* 1982[11]
100	7	Collins *et al.* 1988[12]
110	5	Stevenson *et al.* 1988[13]
500	9	Collins *et al.* 1988[14]
680	9	Maddox *et al.* 1988[15]
3500	9*	Groth & Peebles 1977[1]
4300	$\simeq$ 20*	Maddox *et al.* 1990[2]

* see Figure 6

The Catalogue

The Edinburgh-Durham Southern Galaxy Catalogue (hereafter EDSGC) consists of COSMOS data for 1.5 million galaxies, covering 60 Schmidt fields (an area of 0.5sr) centred at the SGP. Figure 1 shows the sky distribution of the 60 fields in the survey. The fully automated star-galaxy classification techniques we developed to construct the catalogue result in a 95% completeness to a limit of $b_j \sim 20.5$ and a residual stellar contamination of 10% brighter than this magnitude[8]. The photometric calibration of the survey has been motivated by the stringent limits in plate-plate errors which are necessary in order that spurious features in the correlation function are not introduced[6,7]. Over our 60 plate mosaic we have obtained accurate CCD galaxy calibration se-

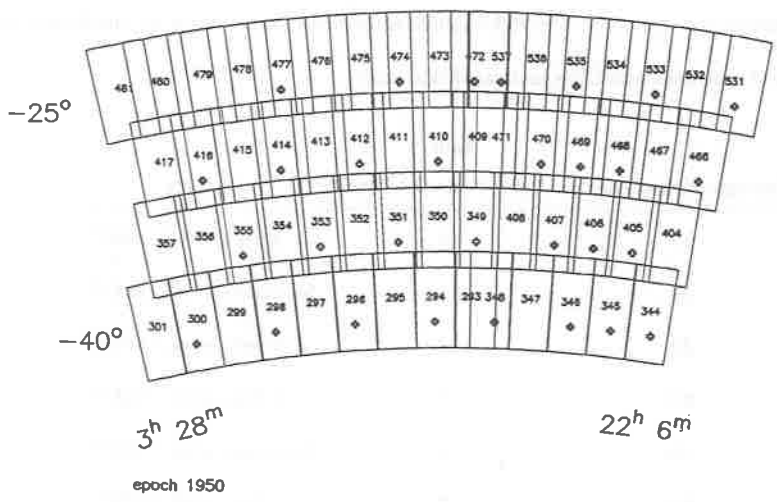

Figure 1: The UK Schmidt Survey Fields of the EDSGC

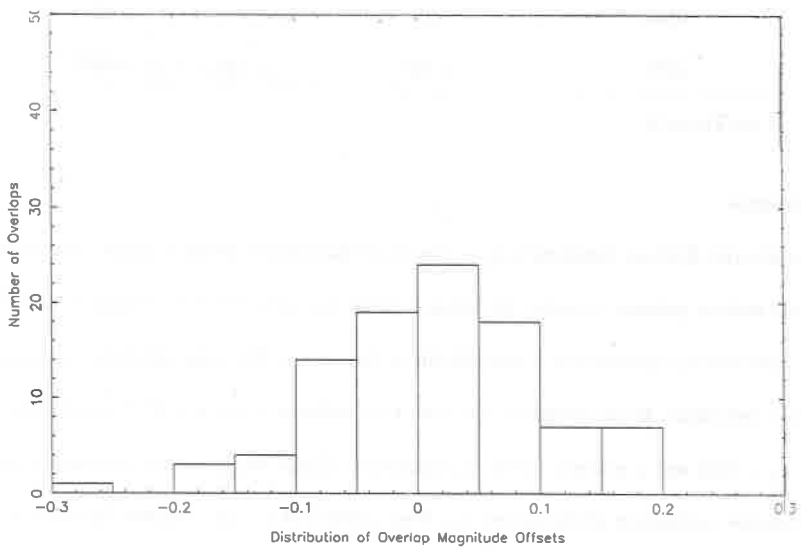

Figure 2: A Histogram of average magnitude offsets for galaxies in the overlap region of ajoining plates.

quences for 30 fields. For each of these fields we have obtained B and V CCD images of two loose clusters. Typically, this results in $10-15$ galaxies per field which enables the zero point of each field to be calculated to a magnitude uncertainty of 0.05. For each field without CCD sequences, the surrounding zero-pointed fields are used to determine the plate background magnitude. This procedure minimises the photometric uncertainties that would be introduced if the field overlaps were used to bootstrap calibrations across many fields. Figure 2 shows the resulting histogram of galaxy magnitude offsets for all overlaps in the survey. Each offset corresponds to the mean displacement of all galaxies (typically $1000-3000$) in the overlap region between adjoining fields. The best fit gaussian to this distribution gives a 1σ width of 0.08, implying a final calibration uncertainty on each plate of 0.05. The consistency between this result and the calibration uncertainty from the CCD sequences shows the stability of the calibration procedure and indicates that there is no significant systematic variation of the photometric zero point across the area of individual fields[16].

Estimating $w(\theta)$

A convenient definition for $w(\theta)$ can be found in terms of the probability of finding a galaxy. with areal number density N_g, in a solid angle element $\delta\Omega$, distance θ from a randomly chosen object;

$$\delta P = N_g[1 + w(\theta)]\delta\Omega. \quad (1)$$

It follows from this that an estimate of the correlation function on a scale θ for an ensemble of galaxies in a solid angle Ω is

$$1 + w(\theta) = 2n_{gg}/(N_g^2\Omega\,\langle\delta\Omega\rangle). \quad (2)$$

Here the number of discrete galaxy pairs is n_{gg} and $\langle\delta\Omega\rangle$ is the average solid angle subtended by object pairs at separation θ in the solid angle Ω. For our $w(\theta)$ estimates, $\langle\delta\Omega\rangle$ is calculated directly by Monte Carlo technique using a catalogue of random points, over an identical region of sky. If

the distribution of random points has a number density N_r then

$$1 + \mathrm{w}(\theta) = \frac{n_{gg}}{n_{gr}} \frac{2N_r}{N_g}, \tag{3}$$

where n_{gr} is the number of discrete galaxy-random pairs. The motivation for normalising to n_{gr}, as opposed to n_{rr}, is that this takes into account "edge effects" on the $\mathrm{w}(\theta)$ estimate resulting from clustering near the survey boundary[11].

As discussed previously with regard to Table 1, small area surveys systematically underestimate the correlation function. If the true form of the correlation function is $\mathrm{w}_t(\theta) = A\theta^{-\gamma}$, with no break on large scales, then

$$\int (\mathrm{w}_t(\theta) - B)\delta\Omega = 0, \tag{4}$$

where B is the amplitude of the integral constraint, which is given by

$$B = \frac{2A\theta^{-\gamma}}{2-\gamma}. \tag{5}$$

While negligible at $b_j < 19.5$ for an area the size of the EDSGC, the integral constraint is significant at brighter magnitudes.

Results

The $\mathrm{w}(\theta)$ for the full 60 plate mosaic was calculated, using Eqn. 3, at the magnitude limits $b_j = 17.5, 18.5, 19.5$. These results are shown in Figure 3. At 19.5 there are 231310 galaxies in the EDSGC and so in order to reduce the computation time at this depth, the data was first binned into cells of size $0.3° \times 0.3°$. A comparison between estimates using binned data and an all-pairs calculation, at a depth of $b_j = 18.5$, gave identical results.

A necessary, if not sufficient, condition that the estimates of $\mathrm{w}(\theta)$ must satisfy before features can be interpreted astrophysically is the scaling test. Our scaling procedure follows the standard methods[1,9]. At these moderate depths the details are relatively insensitive to the the scaling model used. In Figure 4 the correlation functions are shown scaled to the depth of the Lick survey of galaxies ($b_j = 18.6$) with integral constraints applied.

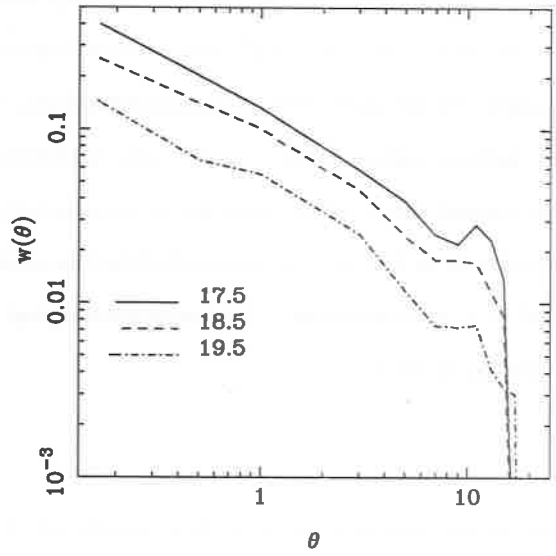

Figure 3: The w(θ) estimates at b_j =17.5,18.5,19.5

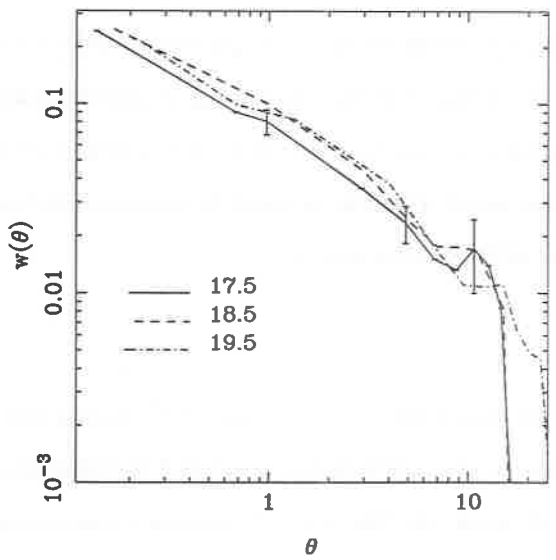

Figure 4: The w(θ) at b_j =17.5,18.5,19.5 with integral constraints applied and scaled to the Lick depth b_j=18.6

Figure 5 provides a comparison between the correlation function for interplate pairs (on different plates) and intraplate pairs (on the same plate). The two correlation functions were calculated at $b_j = 19.5$. The mean offset between the two correlation functions is 4×10^{-3} which translates into an RMS number density variation between plates of 6%. This compares favourably with the uncertainties between the plates based on magnitude differences in the overlap region between fields, and indicates that other systematics which could result in number density variations between plates are negligible. It is worth noting that for the Lick survey of galaxies, the interplate correlation function is larger by $\sim 15\%$ compared to the intraplate estimate. This demonstrates the high quality of the EDSGC compared to the Lick galaxy survey.

Discussion

The EDSGC correlation function along with that of the APM estimate and the GP result is shown in Figure 6. On small scales all the correlation functions agree. The most striking feature of these results is the extent to which both the EDSGC and APM correlation functions indicate more large-scale power. The EDSGC result shows evidence of a break on a scale corresponding to $20h^{-1}$Mpc. The scaling tests provide strong confirmation that the break is a real feature in the galaxy distribution. The significance of this result in terms of constraining models of galaxy formation is illustrated in Figure 6, where the $w(\theta)$ prediction from a CDM model is also given[3]. Clearly for $\Omega = 1$, the current models of CDM do not predict the necessary excess large-scale power evident in the EDSGC and APM correlation functions.

Summary

Previous estimates of the break position in the correlation function range from $3h^{-1}$Mpc to $20h^{-1}$Mpc. There is a direct trend apparent in these results such that larger area surveys give rise to larger estimates of the break scale. This is at least suggestive of large-scale power in $w(\theta)$. However, even the largest catalogues can differ in the amplitude of galaxy clustering when $w(\theta)$

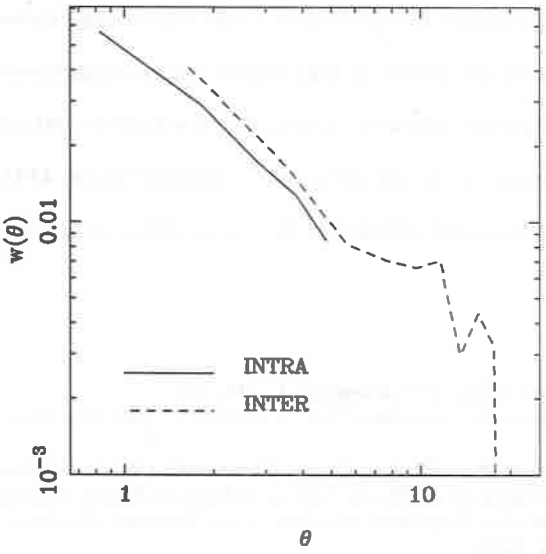

Figure 5: The w(θ) at b_j=19.5 for intraplate pairs and interplate pairs

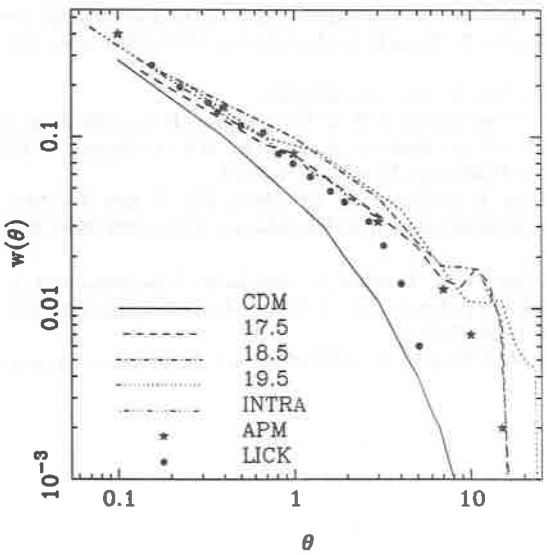

Figure 6: The scaled w(θ) shown in Fig.3 compared to the Lick w(θ) and APM w(θ). Also shown is the predicted w(θ) from standard biased CDM (b=2.5)

is small. The EDSGC has been constructed with optimised procedures in order to address these issues. The correlation function for our 60 plate mosaic is presented. Differences between the interplate and intraplate pairs indicate an RMS number density variation between plates of 6%, consistent with the magnitude calibration uncertainties. The EDSGC $w(\theta)$ indicates more large-scale power than is apparent in the Lick survey and is consistent with the APM result. At present these results cannot be adequately explained in the context of $\Omega = 1$ standard CDM theory.

References

[1] Groth, E.J. & Peebles, P.J.E., 1977.*Astrophys. J.*, **217**, 385.

[2] Maddox, S.J., Efstathiou, G., Sutherland, W.J. & Loveday, J., 1990.*Mon. Not. R. astr. Soc.*, **242**, 43p-47p.

[3] Bond, J.R. & Couchman, H., 1988.*Proc. Second Canadian Conference on General Relativity and Relativistic Astrophysics*, P.385, eds Coly, A. & Dyer, C., World Scientific, Singapore.

[4] Peebles, J.P.E., 1980.*The Large-Scale Structure of the Universe*, Princeton University Press, Princeton, New Jersey.

[5] Shane, C.D. & Wirtanen, C.A., 1967.*Publs. Lick Obs.*,**192**,209.

[6] Geller, M.J., de Lapparent, V. & Kurtz, M.J., 1984.*Astrophys. J.*, **287**, L55.

[7] de Lapparent, V., Kurtz, M.J. & Geller, M.J., 1986.*Astrophys. J.*, **304**, 585.

[8] Heydon-Dumbleton, N.H., Collins,C.A., & MacGillivray, H.T., 1989.*Mon. Not. R. astr. Soc.*, **238**, 379 - Paper II.

[9] Shanks, T., Fong, R., Ellis, R.S. & MacGillivray, H.T., 1980.*Mon. Not. R. astr. Soc.*,**192**, 209.

[10] Stevenson, P.R.F., Shanks. T., Fong, R. & MacGillivray, H.T., 1985.*Mon. Not. R. astr. Soc.*,**213**, 953.

[11] Hewitt, P., 1982.*Mon. Not. R. astr. Soc.*,**201**, 867.

[12] Collins, C.A., Heydon-Dumbleton, N.H. & MacGillivray, H.T., 1988.*Large Scale Structures of the Universe*,125-127, eds Audouze, J., Pelletan, M.C. & Szalay, A., IAU Symp. No. 130, Kluwer Academic Publishers, Dordrecht, Holland.

[13] Stevenson, P.R.F., Fong, R. & Shanks, T., 1988.*Mon. Not. R. astr. Soc.*,**234**, 801.

[14] Collins, C.A., Heydon-Dumbleton, N.H. & MacGillivray, H.T., 1988.*Mon. Not. R. astr. Soc.*,**236**, 7p-12p (Paper I).

[15] Maddox, S.J., Efstathiou, G. & Loveday, J., 1988.*Large Scale Structures of the Universe*,151-160, eds Audouze, J., Pelletan, M.C. & Szalay, A., IAU Symp. No. 130, Kluwer Academic Publishers, Dordrecht, Holland.

[16] Collins, C.A., Nichol, R. & Shanks, T., 1991.*Mon. Not. R. astr. Soc.*, in preparation.

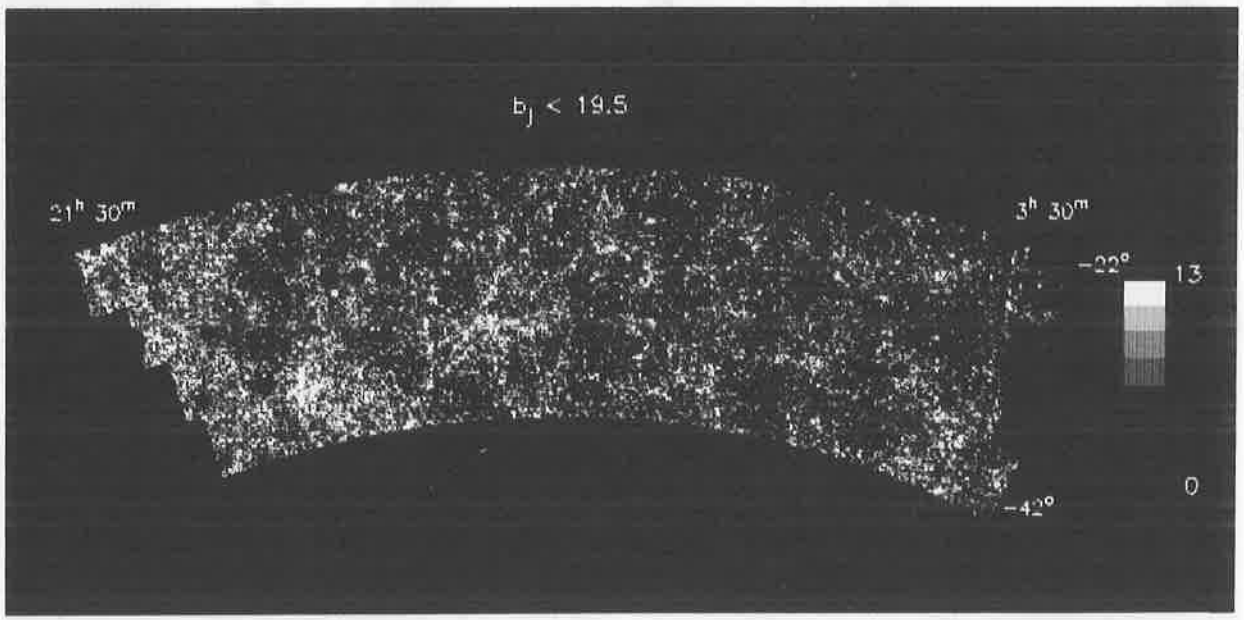

Figure 7: The EDSGC to a depth of $b_j = 19.5$ binned in 10 arcmin pixels

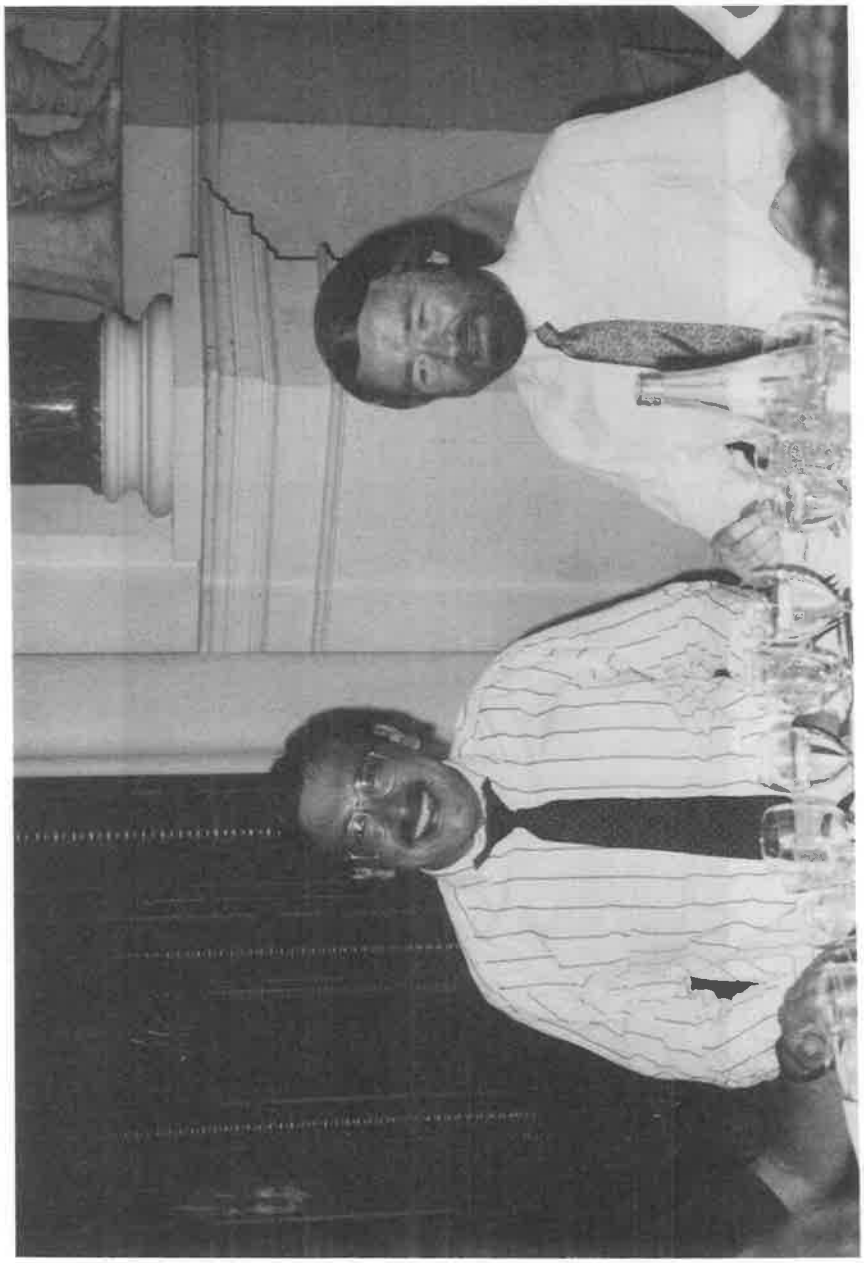

Carlos Frenk and Bernard Carr

OBSERVATIONAL CONSTRAINTS ON GALAXY FORMATION

J. A. Peacock

Royal Observatory, Blackford Hill, Edinburgh EH9 3HJ.

Abstract. This paper discusses some areas where recent work may be advancing, or at least enriching, our understanding of the process of galaxy formation. Four main themes are covered: (i) constraints on the assembly of mass via the abundance of high-z AGN; (ii) constraints on the epoch of star formation from observations of distant galaxies and and synthetic models for evolving galaxy spectra; (iii) searches for primaeval galaxies and their lack of success; (iv) evidence for or against bias in the formation of galaxies. Although no single piece of evidence is straightforward to interpret, there seems to be nothing which is badly inconsistent with a standard picture of hierarchical collapse, provided the degree of linear bias is small.

1 Introduction

Given that there have been many presentations at this meeting relating to large-scale structure, this review will attempt to concentrate on constraints on galaxy formation which derive from other areas of cosmology.

The problem with a discussion of galaxy formation is that there is no real agreement on the meaning of the term. It was clear at the 1988 Durham workshop (Frenk *et al.* 1989) that at least four distinct concepts are involved, and we shall discuss these in turn. They are (i) the assembly of mass, and constraints derived from the abundances of high-z objects; (ii) the formation of stars, and the ages of high-z objects; (iii) searches for primaeval galaxies and (iv) the question of bias, and whether there is any evidence for variations in galaxy properties with changing environment.

Mainly owing to the impressive work reported by Bertschinger at this meeting, $\Omega = 1$ will usually be assumed throughout. As usual, $h \equiv H_0/100\,\mathrm{kms}^{-1}\mathrm{Mpc}^{-1}$.

2 Mass functions and abundances

As has been discussed in a variety of recent papers, the mass function of collapsed objects as a function of epoch may be a powerful diagnostic of the process of galaxy formation (see *e.g.* Peacock 1990a for a review). Sadly, we are some way from possessing clean data on this question; the nearest we come at high redshift is the evolving luminosity function of active galaxies. For both radio-loud and radio-quiet AGN, it is a good approximation up to $z \simeq 2$ to describe the luminosity functions via Pure Luminosity Evolution: a conserved comoving density of objects with an evolving characteristic luminosity (L^*) which was a factor roughly 30 times larger at $z = 2$ than at the present (Boyle *et al.* 1987, 1988; Dunlop & Peacock 1990). The total comoving density is usually formally divergent at very low luminosities; restricting oneself to luminosities $L \gtrsim 0.1L^*$ gives characteristic densities of

$$\begin{aligned} &\rho \simeq 10^{-6}h^3\,\mathrm{Mpc}^{-3} \quad \text{radiogalaxies} \\ &\rho \simeq 10^{-5}h^3\,\mathrm{Mpc}^{-3} \quad \text{QSOs.} \end{aligned} \tag{1}$$

These are small figures, approximately 10^{-3} of the characteristic density ϕ^* for the relevant class of host galaxy (assuming QSOs to have spiral hosts, but that radio galaxies and quasars associate with elliptical galaxies only, something for which there is now a fair bit of evidence: Malkan 1984; Hutchings *et al.* 1989). Restricting oneself to the more luminous objects often studied at high redshift (*e.g.* 3CR galaxies) can reduce these abundances by two further powers of 10. It has often been stated on this basis that AGN pick out such a tiny fraction of the galaxy population as to tell us nothing useful about galaxy formation. To answer this point, it is instructive to recall that AGN host galaxies are indeed peculiar in the sense of being optically luminous, and therefore presumably massive (Smith *et al.* 1986). The total AGN densities involved are of the order of $\phi(L > 5L^*)$ for normal galaxies, and so it does seem reasonable to use high-z AGN as a probe of the general population of *massive* galaxies.

This line of argument was pursued in some detail in an important paper by Efstathiou & Rees (1988), who pointed out that even the observed small abundances of massive high-z galaxies may be too high for comfort in the context of hierarchical models such as CDM.

AGN MASSES What mass is to be assigned to a given AGN? For QSOs, Efstathiou & Rees made various arguments involving timescales to constrain the black hole mass, which give rather similar answers to the Eddington limit. One then has the question of what fraction of a galaxy's total mass can be in the form of a central engine. For luminous quasars ($M_B < -27.6$, $h = 0.5$), Efstathiou & Rees concluded

$$M_{\rm BH} \gtrsim 10^9 M_\odot \Rightarrow M_{\rm tot} \gtrsim 10^{12} M_\odot. \qquad (2)$$

The line of argument here is clearly less than completely watertight, but we can justify their number and strengthen their conclusions by looking at radio galaxies. Here, we know that the galaxies involved are of giant elliptical to cD luminosity. Low redshift examples such as M87 can have their total masses estimated, and answers in excess of $10^{12} M_\odot$ are obtained (*e.g.* White 1990). Since we are able to observe the galaxy light directly, without the nuclear contamination which exists for QSOs, we can be fairly confident that the *stellar* mass of radio galaxies has not altered by more than a factor ~ 2 between $z = 2$ and the present (Lilly & Longair 1984; Lilly 1989). Add to this the fact that galaxy stellar luminosity (and thus presumably mass) correlates hardly at all with radio power, and we can conclude that the total density of radio galaxies may be used as the comoving density of objects above the Efstathiou-Rees limit, raising their density by a factor ~ 10:

$$\rho(M \gtrsim 10^{12} M_\odot) \simeq 10^{-6} h^3 \,{\rm Mpc}^{-3}. \qquad (3)$$

THE MULTIPLICITY FUNCTION To interpret this observation requires a theory for the mass distribution function. For hierarchical models, where structure is built up by a succession of mergers, this exists in the form of the Press-Schechter method. This was originally introduced by Press & Schechter (1974), and has recently been the subject of considerable revived interest, in the course of which some of the obscurities concerning the functioning of the original method have been illuminated (Peacock & Heavens 1990; Peacock 1990a; Bond *et al.* 1991). This analysis tells us that, for a Universe with fluctuations with power spectrum $|\delta_k|^2 \propto k^n$, the characteristic mass of bound clumps grows as

$$M^*(z) \propto (1+z)^{-6/(n+3)}. \qquad (4)$$

On galaxy to cluster scales $-2 \lesssim n \lesssim -1$ empirically, as is also predicted by adiabatic CDM (which is why that theory is considered interesting). The form of the distribution about this characteristic value is usually described dimensionlessly in *multiplicity function* terms: the multiplicity function $M^2 f(M)/\rho_0$ (where $f(M)dM$ is the comoving density of objects in dM) gives the fraction of ρ_0 carried by objects in unit range of $\ln M$. This is illustrated for the CDM model in figure 1. The curves show not only the Press-Schechter multiplicity function

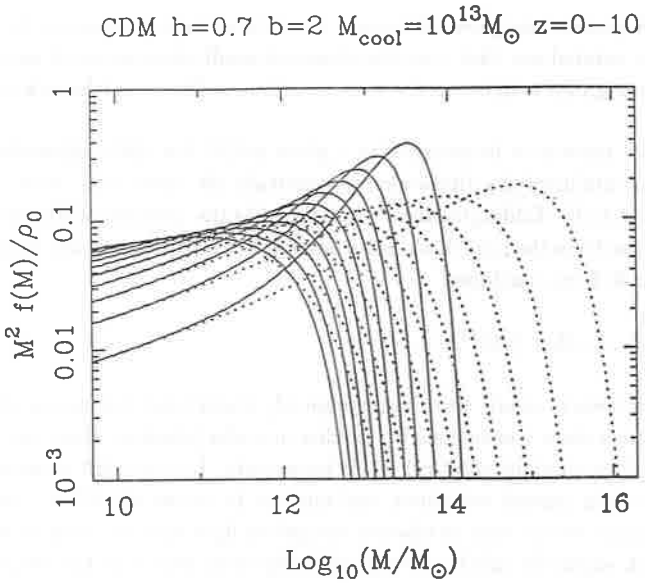

Figure 1. *The epoch dependence of the cooled mass function in CDM, according to the 'PS+cooling' model of Peacock & Heavens (1990) (dotted lines show the mass function without cooling). Note that, for $z \gtrsim 3$, the characteristic mass becomes $\lesssim M_*$ for radio galaxies (see main text).*

for collisionless haloes, but also a rough attempt to insert cooling criteria to obtain the galaxy mass function (Peacock & Heavens 1990).

OBSERVATIONS To order of magnitude, the multiplicity function should be compared with Mn/ρ_0, where n is the number density for a class of object. For radio galaxies, this product is $\sim 10^{-5}$; unsurprisingly, these rare objects are some way off closing the Universe. So long as M^* is larger than or of the order of the radio galaxy mass, the possible number of AGN sites is large enough to accommodate the observed population. However, for high enough redshift, M^* falls to the point where the number of massive objects falls exponentially. From figure 1, $M^2 f(M)/\rho_0$ for $M = 10^{12}\,M_\odot$ would appear to reach $10^{-5.5}$ only at $z \gtrsim 10$ (independent of cooling), but this is highly misleading. The Press-Schechter formalism deals in somewhat fictitious total masses, being normalised to assign every particle in the Universe to the halo of one or other collapsed object. On this basis, a constant M/L ratio would assign $10^{13.2}h^{-1}\,M_\odot$ to an L^* galaxy (Efstathiou *et al.* 1988); for objects of radio-galaxy luminosity, the appropriate figure is around $10^{14}\,M_\odot$. Of course, most of this mass is in 'no-man's land' between galaxies and so is hardly observable, but this is the figure which one must insert into the Press-Schechter machinery (this manipulation of unobservable masses can be avoided if one uses the formalism to predict velocity dispersions instead). The value of Mn/ρ_0 now becomes $10^{-3.5}$, and the higher value of mass now means that trouble will occur at rather lower redshift. For $b = 2.5$ CDM, Efstathiou & Rees concluded that an exponential fall in

AGN numbers would set in at $z \simeq 5$. At the time, this seemed marginally consistent with observation, but it also seemed possible that some of the assumptions might prove optimistic. With our increased number density, the critical redshift is reduced to $z \simeq 3$; does this conflict with data on high-z AGN?

Data at radio and optical wavelengths seem to suggest a deficit of AGN at $z \gtrsim 2$ (Osmer 1982; Peacock 1985; Warren *et al.* 1988; Schmidt *et al.* 1988; Dunlop & Peacock 1990), although the detailed behaviour may be rather complex. In the radio, one possible description is negative luminosity evolution, whereby the AGN L^* becomes fainter above $z \simeq 2$, but this appears not to be allowed by the QSO data. Here, the numbers of high-luminosity QSOs seem to hold up well out to $z = 4$, with a decline occurring only for objects of lower luminosity. Conclusions are limited by worries about sample completeness and sheer small-number statistics, and some of the details of the picture could change. Nevertheless, although the term 'redshift cutoff' is often used in this field, in fact the decline is rather gradual: perhaps only a factor 3 in comoving density between $z = 2$ and $z = 4$. There is certainly no evidence of the exponential decline predicted by the Efstathiou & Rees model.

There are two conclusions to be drawn. The first is that $b = 2.5$ CDM seems to be in serious trouble from the abundance of massive high-z AGN (and, indeed, from several other directions). However, models with a lower degree of bias would seem to be in no danger as yet. Second, even though almost any hierarchical model (not just CDM) would have difficulty in accounting for an unaltered abundance of objects of radio-galaxy mass at $z > 10$, this does not mean that we should never expect to see AGN at these redshifts. The characteristic mass does not evolve so rapidly ($M^*(z = 10)/M^*(z = 4) \simeq 0.1$ for CDM), and so objects of correspondingly lower mass could be relatively abundant at these redshifts (in fact, because $nM/\rho_0 \sim 1$ for objects near the peak of the multiplicity function, the comoving densities would rise in proportion by one or more orders of magnitude). Of course, the efficiency of black-hole formation at these redshifts is an open question, but radiation at the Eddington limit for proportionately smaller black holes could easily produce detectable numbers of AGN at $z > 10$.

3 The epoch of star formation

If galaxy formation concerns itself more with the formation of stars than the assembly of mass, then we face the challenge of dating objects to see when their stars form. One severe constraint of this form, which I shall not discuss, is of course the age of the globular clusters. Most recent interest, however, has concentrated on the galaxies at the highest redshifts – which are all radio loud ellipticals.

RADIO-GALAXY AGES From the first appearance of colour data on 3CR galaxies at $z \simeq 1$, it seemed likely that some of them should be rather old: the reddest galaxies were consistent with the spectrum of a redshifted present-day galaxy, with no active star formation (Lilly & Longair 1984). This was consistent with the observation by Hamilton (1985) of very red

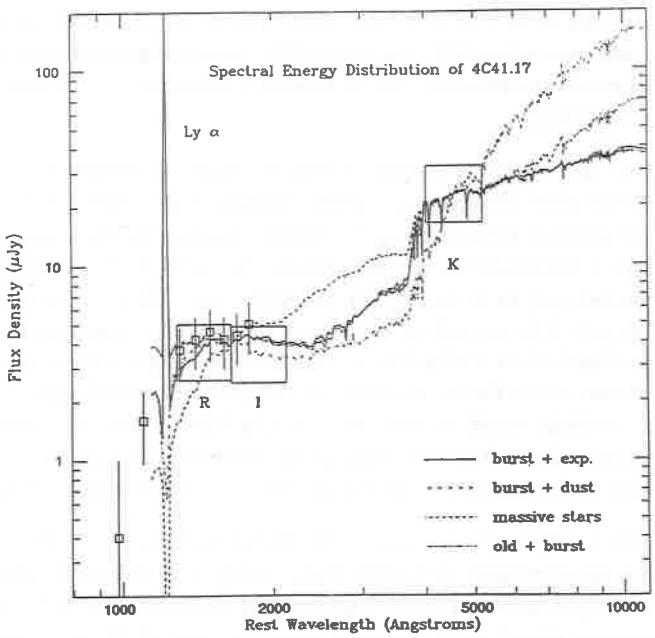

Figure 2. *The spectrum of 4C41.17 ($z = 3.8$) from Chambers et al. (1990), showing the characteristic flat-spectrum portion in the optical, with a strong rise to the infrared. It is this rise which forms an age indicator.*

optically-selected galaxies at somewhat lower redshifts, and argued for rather high formation redshifts in at least some cases.

This line of argument appeared to be confirmed by the discovery of 0902+34 (Lilly 1988). This was an object at $z = 3.4$ which still displayed a large jump in optical flux density between optical and infrared wavebands – a feature most plausibly interpreted as showing the presence of a well-developed giant branch. Using the evolutionary synthesis models by Bruzual (1983), Lilly deduced an age in excess of 1 Gyr, corresponding to a formation redshift in excess of 6 on even very conservative assumptions.

These apparently conclusive indications of high-z formation have been challenged recently by Chambers & Charlot (1990), who developed their own evolutionary code, and concluded that 0902+34 could have formed its stars in a short burst which is seen at an age < 0.3 Gyr. They reach similar conclusions for other high-z radio galaxies (the record holder, 4C41.17, is shown in figure 2); Chambers & Charlot argue that the high-z radio galaxies could have formed more-or-less at the redshifts we now observe them to have, and that there need be no general epoch of star formation at much higher redshift.

The reason for this difference in conclusion lies in radical differences between the stellar synthesis codes employed, which become greater as we move to redder objects. Figure 3 shows

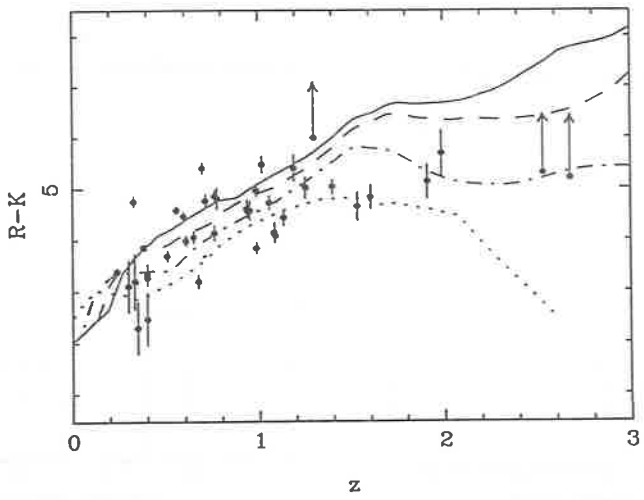

Figure 3. *The $R-K$ vs redshift diagram from Dunlop et al. (1989). The models shown correspond to $h = 1/2$, $\Omega = 0$, and formation redshifts of 3, 5, 10 and 20. Note that objects around $z = 1$ require in some cases models of age about 10 Gyr at that redshift (present age 20 Gyr) to explain the reddest colours).*

a colour-redshift plot for galaxies from the Parkes Selected Regions (PSR), which are a factor $\sim$ 20 less radio luminous than 3CR. Some of the reddest objects ($R - K \simeq 5$ at $z \simeq 1$; similarly inactive to *e.g.* 3C65) require model ages of around 10 Gyr according to the models of Guiderdoni & Rocca-Volmerange (1987, 1988); similar conclusions were reached using the Bruzual models by Windhorst *et al.* (1987). Chambers & Charlot nevertheless assert that 3C65 could have an age of only 1.7 Gyr. Their models are a modification of the Bruzual code, and the main difference lies in the treatment of post-main-sequence evolution, particularly the Asymptotic Giant Branch, with the result that they become very red much more rapidly. It seems particularly unsatisfactory that, a quarter century after Beatrice Tinsley made the first strides towards evolutionary synthesis of galaxy spectra, we can still be faced with an order of magnitude uncertainty in the age of some stellar populations. At present, the decision between the short and long time scales must be made according to other criteria.

THE ALIGNMENT EFFECT An argument in favour of the short timescales has been the so-called 'alignment effect' whereby the optical images of high-z galaxies were found to be elongated preferentially along the axis of any double radio source, often to the extent of being co-spatial with the radio lobes (McCarthy *et al.* 1987a,b; Chambers *et al.* 1987). One obvious interpretation of this is that the passage of the radio jets is causing star formation on a massive scale, implying that the properties of high-z radio galaxies are completely unrepresentative of normal galaxies (*e.g.* Rees 1989). Chambers *et al.* take the attitude that this process could lead to the radio source essentially constructing the galaxy over the period of the central activity. The fact that the lifetimes of radio outbursts are generally expected to be well less than 1 Gyr then ties in nicely with the low ages advocated by Chambers &

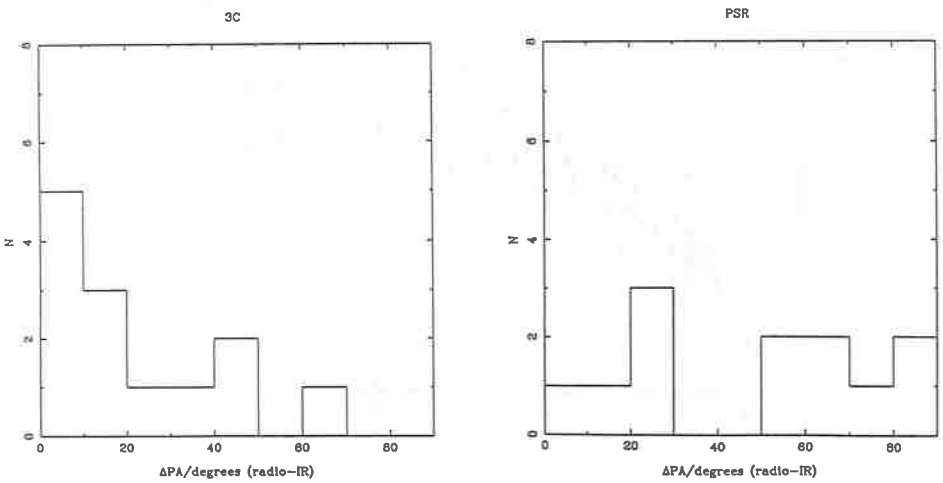

Figure 4. *Histograms of radio-IR alignment for complete subsamples in* $0.6 \lesssim z \lesssim 1.2$ *from the 3CR and PSR catalogues. Note the total lack of an alignment effect for the PSR objects.*

Charlot.

Alternatively, we should recall that optical images are dominated by the flat-spectrum contribution of active star formation, and that rather small numbers of massive stars can produce strong signals in this spectral window. In the infrared, conversely, one views the 'bump' produced by giant stars which may be expected to trace more robustly the underlying stellar population. Indeed, 3CR galaxies are somewhat less elongated in the infrared, but strong alignments are still found. Going to lower radio powers, however, produces a different result. For the PSR galaxies studied by Dunlop & Peacock (1991a,b) there is no alignment effect (see figure 4). This does suggest that any jet-induced star formation, while an important source of 'light pollution' for the most extreme 3CR sources, does make a relatively small contribution to the total infrared light of high-z radio galaxies. Hence, one is led to favour the models which give stellar ages in excess of 1 Gyr, so that the stars pre-date any radio activity.

There are other arguments in the same direction. One is the low scatter in the $K-z$ Hubble diagram, which has a dispersion of no more than 0.4 mag even at $z \simeq 2$ (Lilly 1989), making it implausible that the 3CR galaxies are still in the process of formation. Another is more of a theoretical prejudice.

Using the conditional multiplicity function results of Bond *et al.* (1991), we can derive the distribution of masses at some early epoch (with scale factor a_1) which merged to make an object at epoch a_0. For this calculation, we need to know the power spectrum in the form $\sigma^2(M)$, which is the variance in $\delta\rho/\rho$ at the *current* epoch, when filtered on the mass

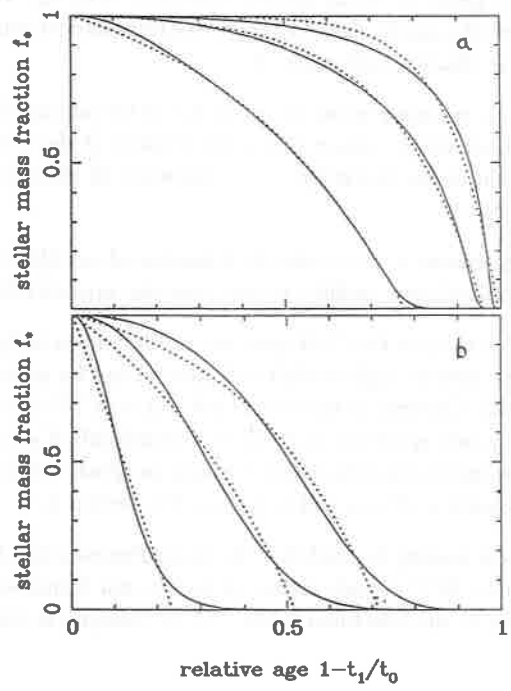

Figure 5. *Plots of the relative age distribution expected in high-z objects under two assumptions for star formation discussed in the text (a: model 1; b: model 2). The outer pair of solid lines give the 68% confidence limits for the age corresponding to a given stellar mass fraction; the central gives the median. The dashed lines are fits for an exponentially declining star-formation rate. This graph assumes the CDM power spectrum and $\nu = 3$, but is not very sensitive to these assumptions. In most cases it seems natural to have the majority of stars at least half as old as the Universe at the time of observation*

scale M. If we then define the following dimensionless variables describing the fluctuation amplitude at a_0 and the time and mass associated with the object at a_1: $\nu \equiv \delta_c/a_0\sigma_0$; $t \equiv a_1/a_0$; $\mu \equiv \sigma_0^2/\sigma_1^2$, then the integral mass distribution is

$$P(>\mu) = 1 - \mathrm{erf}\left[\frac{\nu(t^{-1}-1)}{\sqrt{2(\mu^{-1}-1)}}\right]. \tag{5}$$

We can therefore simply read off the integral mass distribution at a given epoch a_1. The mass defining a given cumulative probability, $\hat{\mu}$, is just

$$\hat{\mu} = \left[1 + c\nu^2(t^{-1}-1)^2\right]^{-1}, \tag{6}$$

where the coefficient c is 2.19 for the median, and $0.5 < c < 25$ defines the 68 per cent confidence band: loosely, the '$\pm 1\sigma$' limits on μ. Given a power spectrum, we can thus

construct the confidence limits on clump mass as a function of epoch. We shall consider two extreme possibilities for relating the mass history to the formation of stars. Consider just the epoch dependence of the characteristic mass $\bar{M}$.

Model 1 If we regard the merger process as mainly one of the adding of units of comparable mass, then it seems reasonable to expect that some fraction of the total mass is turned to stars at every generation of the hierarchy – *i.e.* whenever $\bar{M}$ changes by a factor 2. We therefore write $\delta M_* \propto \delta \ln \bar{M}$.

Model 2 The opposite extreme is to consider the formation of an object to proceed by adding small units to a large central mass (infall). In this case, one expects $\delta M_* \propto \delta \bar{M}$.

Implementing this method for CDM gives the results shown in figure 5, from which it seems likely that objects seen at high redshift will have an age for most of their stars which approaches the age of the Universe at that time ($10h^{-1}(1+z)^{-3/2}$ Gyr). This conclusion is not very dependent on power spectrum, and can be violated only if star-formation efficiency peaks late in the formation process (depending strongly on epoch or depth of potential well). This is related to the question of bias, and is discussed in section 5.

Finally, it is worth bearing in mind that the Gunn-Peterson test does require substantial energy input into the IGM at early times. If due to star formation, this requires that $\gtrsim 50\%$ of current metals be manufactured before $z = 4.7$ (Shapiro & Giroux 1989).

4 Protogalaxies and near-misses

As far as many observers are concerned, galaxy formation means the search for protogalaxies; a nice review of earlier surveys for these mythical beasts was given by Koo (1986). Again, the definition of these objects is not universally agreed upon. They are certainly galaxies in the process of forming the majority of their stars, but there is a divergence of opinion as to whether they need be located only at extreme redshifts, or whether they are forbidden to contain metals. If only star-formation rate matters, many of the radio galaxies discussed in the previous section have $L/\dot{L} \ll t(z)$ – *i.e.* could make all their stars in a time short by comparison with the local age of the universe. What about non-radio galaxies?

INFRARED PROTOGALAXIES The infrared is the obvious place to look for galaxies at $z \gtrsim 5$, because intervening Lyman-limit absorption will cause them to be invisible in optical bands. With the advent of 2D infrared detectors, surveys for these extremely red objects became practical, and quite a stir was therefore caused when Elston *et al.* (1988) announced the discovery of an object with an $R - K$ colour too red to be a normal galaxy. Spectroscopy by Lilly *et al.* 1988 showed this nevertheless to be an object at $z \simeq 0.3$, and at the time it seemed as though the colours of the candidate might have been in error. However, a survey at Edinburgh which has been carried out over the relatively large area of 1000 arcmin^2 confirms that objects of this extreme colour are quite common (figure 6). In fact, it is interesting to note that the colours of these galaxies are no redder than the least active radio galaxies

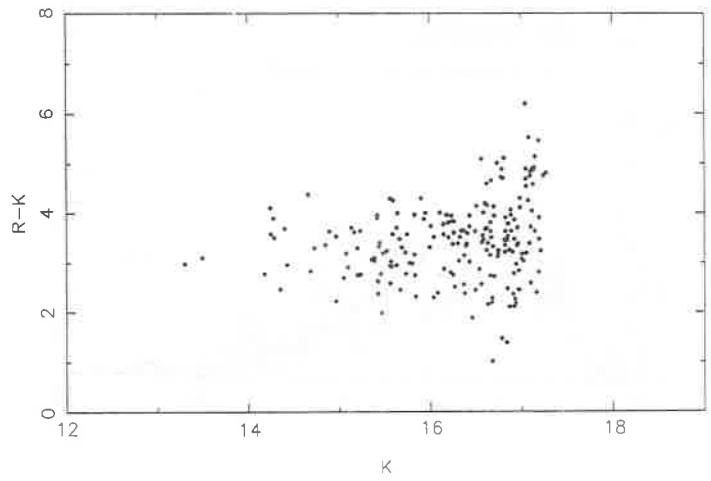

Figure 6. *An $R-K/K$ colour-magnitude plot for galaxies from the 2μm survey of Glazebrook et al. (1991). The population of very red objects at $K \simeq 17$, $R-K \simeq 5$ first detected by Elston et al. is extensive. There are no K-selected objects which cannot also be detected in the optical.*

discussed in the last section. Although we do not yet have spectra of these objects, it would be reasonable to expect them to lie at $z \simeq 0.5$; radio and infrared surveys would then agree with Hamilton's conclusion than very red galaxies are common (if not universal) at these redshifts. The extreme colours probably do not arise from dust (radio galaxy spectra show strong Lyα and flat rest-frame UV continua – see *e.g.* Lilly 1988 – and these would be very sensitive to dust), but may simply indicate a problem with synthetic spectral models; we have already encountered difficulties in making at least some models red enough to describe radio galaxies in a reasonable time scale.

BLUE GALAXIES If protogalaxies are not seen in the infrared, does this mean we are looking at too high redshifts? In 1988, it seemed that this was the case. For a decade or so, workers had become increasingly aware that counts of faint galaxies were higher than expected without evolution, and that the excess galaxies were rather blue in colour. Cowie *et al.* (1988) claimed that these blue galaxies were in effect protogalaxies undergoing their first starburst, and presented a model-independent argument to show that these objects must be responsible for the generation of a large fraction of present-day metals. Furthermore, one of these galaxies had a spectrum showing Lyα emission at $z = 3.4$ (Cowie & Lilly 1989); it seemed likely these were very close to being protogalaxies in some sense.

Things look rather different today, thanks mainly to the redshift surveys carried out at Durham (Broadhurst *et al.* 1988; Ellis 1990). The principal result of these surveys has been to establish that the blue galaxies lie at low redshifts: there is no tail of high-z luminous

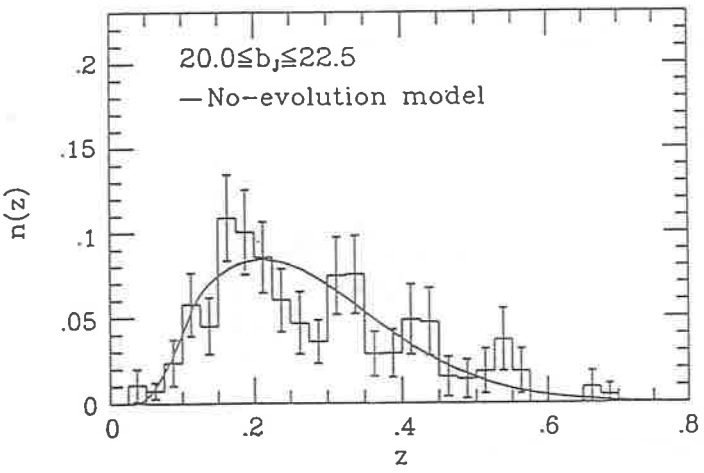

Figure 7. *The redshift distribution of faint blue-selected galaxies, from Ellis (1990). In shape (but not in amplitude) a no-evolution model fits perfectly. The excess of faint galaxies must therefore be caused not by luminosity evolution (brighter L^* at high redshift), but by a steepening of the faint end of the luminosity function at high redshift.*

starbursts (see figure 7). Subsequently, this has turned out to be true also of the fainter galaxies discussed by Cowie *et al.*; the $z = 3.4$ spectrum could not be confirmed (Lilly *et al.* 1990). The consequences are rather dramatic, in that major changes are taking place in the Universe at rather lower redshifts than previously imagined. In particular, the galaxy luminosity function itself must be changing shape. If we maintain the Schechter parameterisation, then the low-mass slope must be a function of redshift, and evolves very roughly as

$$\phi \propto L^{-\alpha(z)}\, e^{-L/L^*}\, dL; \qquad \alpha(z) \simeq 1 + 2z. \tag{7}$$

Such a representation is a misleading, since it implies that the evolution is universal, whereas the evolution seems to consist largely of a varying density of blue galaxies, predominately of sub-L^* luminosity. Nevertheless, emphasising that the luminosity function changes shape is important given that some workers have seen problems for $\Omega = 1$ models in the very high total numbers of galaxies seen down to faint limits (Koo 1989). This is clearly only going to be a difficulty if we cling to the invalid assumption that the faint-end slope of the luminosity function does not alter.

What is the interpretation of this evolution? Some workers have seen shape changes in $\phi(L)$ as indicative of merging – *i.e.* real changes in the mass distribution function of galaxies corresponding to destruction of low-mass galaxies (*e.g.* Rocca-Volmerange & Guiderdoni 1990), but examination of the infrared data makes this seem implausible. The poster by Glazebrook *et al.* (1991) demonstrates that the K-band counts are consistent with a no-evolution model; shape changes in $\phi(L)$ as radical as the above are strongly ruled out. Since the infrared waveband is arguably telling us rather more about the behaviour of the mass of

the galaxies than is the blue waveband, a picture of general merging seems unpromising. If the behaviour of blue galaxies does have a dynamical origin, we need to explain why these effects appear to be confined to galaxies of low mass.

Finally, despite the change in redshift, it may still be that the blue galaxies qualify to be regarded as protogalaxies in some sense. Cowie's argument from the extragalactic background light still applies: these objects make a large fraction of present-day metals. Their abundances are not primordial, but in hierarchical models such as CDM pregalactic enrichment from $\sim 10^6 M_\odot$ objects at $z \simeq 20$ is to be expected; these objects may be the closest that we are ever likely to get to protogalaxies. One last piece of evidence which is also in favour of substantial activity at low redshifts is the population of 'damped Lyα clouds'. Wolfe (1989) has argued that these systems represent galactic disks which have yet to form.

5 Bias

If $\Omega > 0.2$, then bias is an observed fact: cluster M/L ratios tell us that galaxies are over-represented in the cores of rich clusters by a factor 5 – 10 (if $\Omega = 1$). For about 5 years, the dominant ideas for explaining this observation have been based on exploiting our ignorance of the processes of star formation. Thus, the main models have been 'high-peak' bias (Bardeen *et al.* 1986) in which the earliest objects to collapse (mainly in protoclusters) propagate disruptive signals to prevent later brethren from forming, together with 'natural' bias (White *et al.* 1987; Kaiser 1988; Cole & Kaiser 1989) in which there is postulated some epoch dependence of the star-formation efficiency. Both of these schemes have the consequence that the properties of forming galaxies are modulated by density perturbations on all scales, so that there is some non-unity linear bias which applies even at very low density contrast:

$$\frac{\delta n}{n} = b\frac{\delta \rho}{\rho}. \tag{8}$$

Apart from the observation they were designed to explain (cluster M/L ratios or, equivalently, the cosmic virial theorem), what tests of these ideas do we have?

LARGE-SCALE STRUCTURE One prediction of high-peak bias was that dwarf galaxies should fill the voids (Dekel & Silk 1986), but this seems not to be observed. In fact, the trend revealed by large-scale redshift surveys appears more and more to be that galaxies of all types occupy the same 'skeleton' of voids, walls and filaments, with differences appearing only at rather high density contrast in the vicinity of clusters (see the presentations by Geller and by Thuan at this meeting).

As an example, figure 8 contrasts the luminosity-dependent clustering amplitude with predictions from the high-peak model (Valls-Gabaud *et al.* 1989). There appears to be no tendency for the effective bias parameter to vary with galaxy luminosity except at the very bright end, where one could well imagine that morphological segregation in clusters was playing a role. Now add to this the results from peculiar velocities (Kaiser & Lahav 1989;

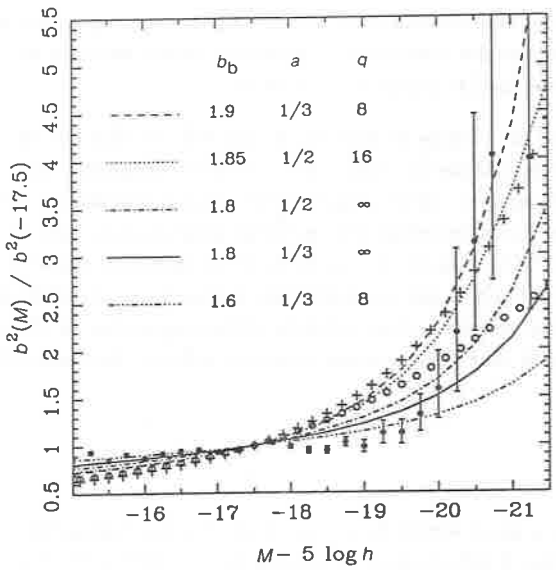

Figure 8. *The variation of relative bias with absolute magnitude (filled points plus error bars), taken from Valls-Gabaud et al. (1989). The various lines show versions of the high-peak biasing model, none of which can reproduce the lack of any trend in $b(M)$ fainter than $M \simeq -20$.*

Bertschinger's presentation at this meeting) which seem to argue for a value of b close to unity, rather than the traditional $b = 2.5$. The emerging picture is one in which light roughly traces mass on large scales; the voids appear empty because they are empty, not because of the assistance of linear biasing.

BIAS IN GALAXY PROPERTIES? Another way of phrasing the standard bias schemes is to say that they predict that the properties of galaxies will vary with environment. Kaiser (1988) raised the possibility that the peculiar velocities inferred from distance indicators such as Tully-Fisher could thus be corrupted by environment-dependent zero-point offsets, leading to 'phantom attractors'. In fact, such a possibility seems quite strongly constrained by a variety of arguments. First, and most simply, there is no correlation of elliptical galaxy distance-indicator residual with richness of environment (figure 9).

This is not so surprising in the case of the $D_n - \sigma$ relation, whose interpretation is really just that the centres of galaxies are dominated by stellar populations of roughly constant M/L, but the Faber-Jackson projection of the fundamental plane ought to be sensitive to modulating effects of cluster-scale waves (cluster galaxies of a given mass collapse earlier and therefore should show a higher velocity dispersion than field galaxies). In fact, the existence of a Faber-Jackson relation with only ~ 1 mag. scatter makes it difficult to see how 'natural' bias mechanisms can be operating: the dispersion in collapse times caused by cluster-scale power can easily lead to a much higher scatter in models with a high degree of bias (Peacock

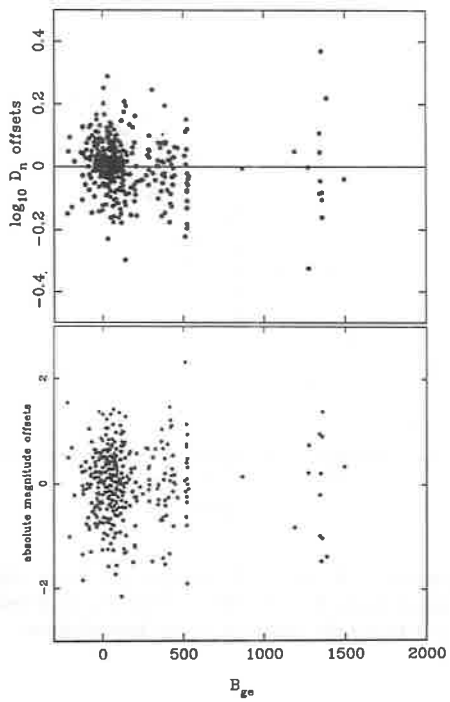

Figure 9. *Plots of offsets from the $D_n - \sigma$ and Faber-Jackson distance indicators, for the 'gang of 7' elliptical galaxies (from Nicholson 1990). The x axis is a measure of local galaxy density (see e.g. Prestage & Peacock 1988; the highest points correspond to Coma at Abell richness about 2). In neither case is there a significant correlation with environment.*

1990b). Further evidence that the peculiar velocity measurements are not spurious comes from the excellent agreement between velocities determined using $D_n - \sigma$ for ellipticals and Tully-Fisher for spirals (see Bertschinger's presentation at this meeting).

In short, the dynamical properties of galaxies show no hint of the spatial variations which would have been expected in models where bias is achieved by altering the amount of star formation in different environments.; galaxies in most locations in the universe seem remarkably homogeneous in all their properties. One final piece of evidence is shown in figure 10, which presents a colour-colour plot for Coma and Virgo elliptical galaxies. It had been suggested that there was an offset between these, perhaps indicating some difference in the formation processes in these clusters, but it now appears that this claim was erroneous. Faced with such uniformity, it does start to seem a little contrived to persist with the gross effects postulated by conventional biasing schemes. There is a very strong motivation for looking at mechanisms which achieve bias in clusters after galaxy formation. The so-called 'velocity bias' effect appears to be the most plausible contender at present (Carlberg & Couchman 1989; Carlberg *et al.* 1990; West & Richstone 1988).

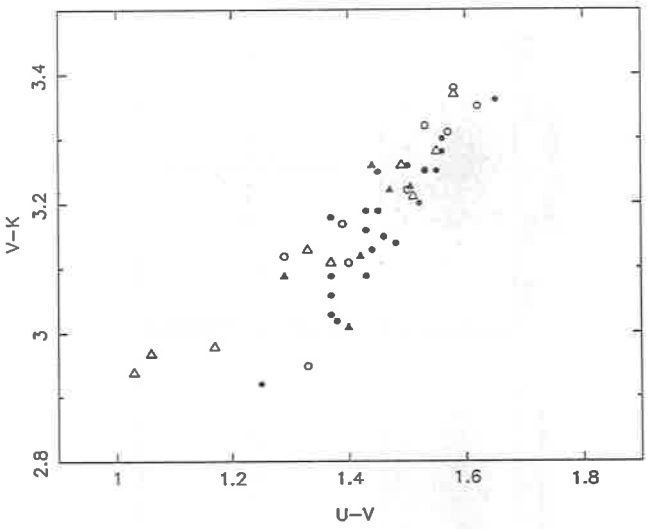

Figure 10. *The restframe $U-V$ vs $V-K$ plot for the Virgo (open symbols) and Coma (filled symbols) clusters (taken from Bower 1990). Contrary to previous claims, there is no evidence for any difference between the galaxies in the two clusters.*

6 Conclusions

This review has covered a rather diverse set of constraints on galaxy formation, and it would be too much to expect a single consistent picture to emerge from an area where great observational efforts are causing things to change on very short timescales. There are still some areas of controversy and uncertainty which need to be resolved, amongst which the most outstanding are:

(i) Can radio galaxies be rehabilitated as representatives of normal massive distant galaxies? If so, can we reduce the uncertainties in evolutionary synthesis models so that reliable ages can be determined?

(ii) Are searches for 'classical' protogalaxies worth persisting with, or should we accept that enriched objects such as radio galaxies, blue galaxies and Wolfe clouds are the nearest we will get in practice?

(iii) What triggers the blue galaxies, and why are they predominantly of low luminosity?

(iv) Is velocity bias really the explanation for cluster M/L ratios, and if so, what is the implication for our understanding of large-scale structure?

All of these are questions where we can expect considerable progress from new 'observations' (counting next-generation N-body experiments). For the present, the best we can say is that there seems to be nothing which is strongly inconsistent with a hierarchical picture

of galaxy formation in general, and CDM in particular, *provided* the degree of linear bias is low.

References

Bardeen, J.M., Bond, J.R., Kaiser, N. & Szalay, A.S., 1986. *Astrophys. J.*, **304**, 15. (BBKS)

Bond, J.R., Cole, S., Efstathiou, G. & Kaiser, N., 1991. *Astrophys. J.*, in press.

Bower, R.G., 1990. PhD thesis, University of Durham.

Boyle, B.J., Fong, R., Shanks, T. & Peterson, B.A., 1987. *Mon. Not. R. astr. Soc.*, **227**, 717.

Boyle, B.J., Shanks, T. & Peterson, B.A., 1988. *Mon. Not. R. astr. Soc.*, **235**, 935.

Broadhurst, T.J., Ellis, R.S. & Shanks, T., 1988. *Mon. Not. R. astr. Soc.*, **235**, 827.

Bruzual, G., 1983. *Astrophys. J.*, **273**, 105.

Carlberg, R.G. & Couchman, H.M.P., 1989. *Astrophys. J.*, **340**, 47.

Carlberg, R.G., Couchman, H.M.P. & Thomas, P.A., 1990. *Astrophys. J.*, **352**, L29.

Cowie, L.L., Lilly, S.J., Gardner, J.P. & McLean, I.S., 1988. *Astrophys. J.*, **332**, L29.

Cowie, L.L. & Lilly, S.J., 1989. *Astrophys. J.*, **336**, L41.

Chambers K.C. & Charlot, S., 1990. *Astrophys. J.*, **348**, L1.

Chambers, K.C., Miley, G.K. & van Breugel, W.J.M., 1987. *Nature*, **329**, 604.

Chambers, K.C., Miley, G. & van Breugel, W.J.M., 1990. *Astrophys. J.*, in press.

Cole, S. & Kaiser, N., 1989. *Mon. Not. R. astr. Soc.*, **237**, 1127.

Dekel, A. & Silk, J., 1986. *Astrophys. J.*, **303**, 39.

Dunlop, J.S., Guiderdoni, B., Rocca-Volmerange, B., Peacock, J.A. & Longair, M.S., 1989. *Mon. Not. R. astr. Soc.*, **240**, 257.

Dunlop, J.S. & Peacock, J.A., 1990. *Mon. Not. R. astr. Soc.*, **247**, 19.

Dunlop, J.S. & Peacock, J.A., 1991a. These proceedings.

Dunlop, J.S. & Peacock, J.A., 1991b. *Mon. Not. R. astr. Soc.*, in preparation.

Ellis, R.S., 1990. in *proc. Evolution of the Universe of Galaxies*, ed R.G. Kron, Astr. Soc. Pacif. Conf. Ser., **10**, 248.

Efstathiou, G. & Rees, M.J., 1988. *Mon. Not. R. astr. Soc.*, **230**, 5P.

Efstathiou, G., Ellis, R.S. & Peterson, B.A., 1988. *Mon. Not. R. astr. Soc.*, **232**, 431.

Elston, R., Rieke, G.H. & Rieke, M.J., 1988, *Astrophys. J.*, **331**, L77.

Frenk, C.S., Ellis, R.S., Shanks, T., Heavens, A.F. & Peacock, J.A., 1989. *The Epoch of Galaxy Formation* (Kluwer), NATO ASI **C264**.

Glazebrook, K., Peacock, J.A., Collins, C.A. & Miller, L., 1991. These proceedings.

Guiderdoni, B. & Rocca-Volmerange, B., 1987. *Astr. Astrophys.*, **186**, 1.

Guiderdoni, B. & Rocca-Volmerange, B., 1988. *Astr. Astrophys. Suppl.*, **74**, 185.

Hamilton, D., 1985. *Astrophys. J.*, **297**, 371.

Hutchings, J.B., Janson, T. & Neff, S.G., 1989. *Astrophys. J.*, **342**, 660.

Kaiser, N. & Lahav, O., 1989. *Mon. Not. R. astr. Soc.*, **237**, 129.

Kaiser, N., 1988. *Large-Scale Structures of the Universe*, proc. IAU symp. no. 130, eds J. Audouze, M.-C. Pelletan & A. Szalay (D. Reidel), p43.

Koo, D.C., 1986. in *Spectral evolution of galaxies*, eds C. Chiosi & A. Renzini (Reidel), p419.

Koo, D.C., 1989. in *The Epoch of Galaxy Formation*, eds Frenk, C.S., Ellis, R.S., Shanks, T., Heavens, A.F. & Peacock, J.A. (Kluwer), NATO ASI **C264**, 71.

Lilly, S.J. & Longair, M.S., 1984. *Mon. Not. R. astr. Soc.*, **211**, 833.

Lilly, S.J., 1988. *Astrophys. J.*, **333**, 161.

Lilly, S.J. *et al.* 1988. *Astrophys. J.*, **332**, L59.

Lilly, S.J., 1989. *Astrophys. J.*, **340**, 77.

Lilly, S.J., Cowie, L.L. & Gardner, J.P., 1991. *Astrophys. J. Suppl. Ser.*, in press.

McCarthy, P.J., *et al.*, 1987a. *Astrophys. J.*, **319**, L39.

McCarthy, P.J., *et al.*, 1987b. *Astrophys. J.*, **321**, L29.

Malkan, M.A., 1984. *Astrophys. J.*, **287**, 555.

Nicholson, D., 1990. *PhD thesis, University of Edinburgh.*

Osmer, P.S., 1982. *Astrophys. J.*, **253**, 28.

Peacock, J.A. & Heavens, A.F., 1990, *Mon. Not. R. astr. Soc.*, **243**, 133

Peacock, J.A., 1985. *Mon. Not. R. astr. Soc.*, **217**, 601.

Peacock, J.A., 1990a. in *The early universe and cosmic structures*, proc. 10^{th} Moriond Astrophysics meeting, Ed. A. Blanchard (Editions Frontières), in press.

Peacock, J.A., 1990b. *Mon. Not. R. astr. Soc.*, **243**, 517.

Press, W.H. & Schechter, P., 1974. *Astrophys. J.*, **187**, 425. (PS)

Prestage, R.M. & Peacock, J.A., 1988. *Mon. Not. R. astr. Soc.*, **230**, 131. (erratum: **236**, 959.)

Rees, M.J., 1989. *Mon. Not. R. astr. Soc.*, **239**, 1P.

Rocca-Volmerange, B. & Guiderdoni, B., 1990. *Mon. Not. R. astr. Soc.*, **247**, 166.

Schmidt, M., Schneider, D.P. & Gunn, J.E., 1988. in *Proceedings of a workshop on optical surveys for quasars*, eds Osmer, P.S., Porter, A.C., Green, R.F. & Foltz, C.B, A.S.P. conf. ser., **2**, 87.

Shapiro, P.R. & Giroux, M.L., 1989. in *The Epoch of Galaxy Formation*, eds Frenk, C.S., Ellis, R.S., Shanks, T., Heavens, A.F. & Peacock, J.A. (Kluwer), NATO ASI **C264**, 153.

Smith, E.P., Heckman, T.M., Bothun, G.D., Romanishin, W. & Balick, B., 1986. *Astrophys. J.*, **306**, 64.

Valls-Gabaud, D., Alimi, J.-M., & Blanchard, A., 1989. *Nature*, **341**, 215.

Warren, S.J., Hewett, P.C. & Osmer, P.S., 1988. in *Proceedings of a workshop on optical surveys for quasars*, eds Osmer, P.S., Porter, A.C., Green, R.F. & Foltz, C.B, A.S.P. conf. ser., **2**, 96.

West, M.J. & Richstone, D.O., 1988. *Astrophys. J.*, **335**, 532.

White, S.D.M., Davis, M., Efstathiou, G. & Frenk, C.S., 1987. *Nature*, **330**, 451.

White, S.D.M., 1990. in *Physics of the Early Universe*, proc 36^{th} Scottish Universities Summer School in Physics, eds Peacock, J.A., Heavens, A.F. & Davies, A.T. (Adam Hilger), p1.

Windhorst, R.A., Koo, D.C. & Spinrad, H., 1987. in *Galaxy distances and deviations from universal expansion*, eds. B.F Madore & R.B. Tully (Reidel), NATO ASI **C180**, 197.

Wolfe, A.M., 1989. in *The Epoch of Galaxy Formation*, eds Frenk, C.S., Ellis, R.S., Shanks, T., Heavens, A.F. & Peacock, J.A. (Kluwer), NATO ASI **C264**, 101.

NORMAL GALAXIES IN THE APM SURVEY

S.J.Maddox, W.J.Sutherland, G.Efstathiou,
Astrophysics,
Oxford, OX1 3RH
UK
J.Loveday and B.A.Peterson,
Mt. Stromlo and Siding Spring Observatories,
Australia

ABSTRACT

The APM Galaxy Survey is described and the steps in its construction are briefly summarised.

The number of galaxies counted in the survey as a function of magnitude increases much more steeply than expected from standard galaxy evolution models. This implies that the brightness of galaxies must have evolved very rapidly in the last $\sim$ 2Gyrs.

The angular two-point correlation function of galaxies in the survey is a power law at small angles, with a steeper fall to zero at large angles. Both the amplitude of the power law, and the angular scale at which the observations fall below the power law are smaller when measured for fainter galaxies in the survey. The variations in amplitude and break angle as a function of magnitude are consistent with that predicted by Limbers equation. The bend away from a power law is similar to that predicted in the standard CDM cosmogony, but occurs at a larger scale. Our measurements show more large-scale structure in the universe than predicted by standard CDM models.

Redshifts for a subsample of $\sim$ 2000 galaxies with $b_J < 17.0$ have been measured with the Mt. Stromlo 2.3 m telescope. This survey maps the 3D structure of the universe in a volume $\sim 10^6 h^{-3} Mpc^3$ and preliminary measurements of the clustering show large-scale power consistent with the angular measurements.

The observed large-scale power can be reproduced by a CDM model with $\Omega_{tot} = 0.2$, $h \approx 0.9$ and a non-zero cosmological constant which makes the universe geometrically flat.

THE APM GALAXY SURVEY

The APM Galaxy Survey contains 2 million galaxies brighter than $b_J = 20.5$ in an area of 1.5 steradians over the South Galactic Cap. It was constructed using the SERC Automatic Plate Measuring (APM) system in Cambridge (Kibblewhite *et al.* 1984) to digitise $5.8° \times 5.8°$ from each of 185 copies of UK Schmidt J survey plates. Full details of our analysis techniques, performance of the APM machine, and comparisons between copy plates and originals are presented elsewhere (Maddox 1988, Maddox *et al.* 1990a,b), and a brief summary is presented here.

The APM machine digitises photographic plates, detecting and analysing images in real time. For each UKST survey plate it measures the position, magnitude, second moments and surface brightness profile of $\sim 200,000$ objects. The plates in the fully analysed survey cover a contiguous area of 4300 square degrees, in the region $\delta < -17.5°$ and $b \lesssim |40|°$. We have recently extended the survey to cover a further 2100 square degrees of sky with $-17.5° < \delta < +2.5°$, but this area is not yet included in the analyses described below.

There are 10 million images brighter than $b_J = 20.5$ in the analysed area, of which only 2 million are galaxies. The image shape parameters are used to distinguish between galaxies, stars and merged objects (mostly stars). We have visually checked more than 4000 images on several UKST and AAT plates and find that the galaxy sample is 95% complete in the range $17 < b_J < 20.5$. We have estimated this incompleteness for each plate as a function of magnitude using a fit to the classifier histogram as in Figure 12 of Maddox *et al.* 1990a. Contamination from merged images is $< 6\%$ in the range $17 < b_J < 20$ but rises to 12% at $b_J = 20.5$ which is close to the magnitude limit for reliable image classification.

All galaxy candidates brighter than $b_J = 16.5$ have been checked by eye and assigned morphological types. This gives a sample of 17770 galaxies which is $> 95\%$ complete with essentially zero stellar contamination. We have also visually checked and classified a further 1 in 20 random sample of galaxies with $16.5 < b_J < 17$.

The photometry from each plate is first corrected for vignetting and emulsion sensitivity variations, and then adjusted relative to the other plates to produce a uniform survey (Maddox *et al.* 1990b). After correction, the typical magnitude error between 1° regions of each plate is 0.04 magnitudes, and the *rms* error in plate zero-points is 0.024 magnitudes. We have calibrated the corrected APM magnitudes using CCD magnitudes in two colours for 339 galaxies with $21 \gtrsim b_J \gtrsim 15$ (Maddox *et al.* 1990b,d and Loveday 1989) Since the APM magnitudes are not corrected for emulsion saturation, the calibration curve to give standard b_J as a function of corrected APM magnitude m_A is slightly non-linear. We use a quadratic fit to approximate the curve (Maddox *et al.* 1990d).

We have compared our magnitudes with the limited amount of published pho-

tometry for galaxies fainter than $b_J \sim 16$ in our survey area and find that our zero point is consistent with the mean of other work. The published magnitudes have only a small number of external calibrations and no consistency checks from plate overlaps, so we prefer to calibrate using only our own CCD data.

Several follow-up projects based on the survey are now underway. These include: the selection of uniform galaxy cluster catalogues (Sutherland *et al.* 1990a) and a redshift survey of clusters; the selection of compact groups of galaxies and a redshift survey to determine the fraction which are physically compact and interacting; the optical identification of IRAS sources (Sutherland *et al.* 1990b) and a redshift survey to find the ultraluminous IRAS galaxies; and the optical identification of Texas radio sources to find radio loud quasars and galaxies. In the rest of this article we describe 3 projects which concentrate on the distribution of normal galaxies in the survey.

GALAXY COUNTS

The study of galaxy number counts has been of primary interest for galaxy evolution since the deep 4-metre plate studies of Peterson *et al.* (1979) and Koo (1981) detected an excess in the number counts at $B \gtrsim 22$ relative to non-evolving models. However the measurement of galaxy counts at bright magnitudes has been plagued by substantial uncertainties from the fluctuations caused by galaxy clustering and limited photometric calibration. Since the APM survey is well calibrated and covers a large surface area it provides a reliable fair sample for galaxies as bright as $b_J = 16$. The number counts from our survey indicate evolution that is much more dramatic than previously thought.

After excluding regions of the survey near bright stars etc, we count the galaxy surface density in 0.1 magnitude bins. The thick line in Figure 1 shows the calibrated number counts after a small correction for the incompleteness of our galaxy selection (Maddox *et al.* 1990d). Note that we have plotted $\log N - 0.45(b_J - 16)$, so that the faint counts appear approximately flat. This plot is clearly preferable to a simple plot showing $\log N$, since this would span some 8 orders of magnitude, and make 50% discrepancies almost invisible.

In Figure 1 we have also shown the counts from several other studies. At bright magnitudes, $16 < b_J < 17$, we see that our counts are close to the mean of the other results, which show a large scatter. In contrast to other surveys, the errors on our counts are small enough to reliably establish the normalisation at such a bright magnitude. Between $17 < b_J < 19$ our counts are rather lower than the mean of the other results and fainter than $b_J = 19$ our counts agree well with the mean of other work, showing a slope $dN \propto 10^{0.45 b_J}$. The differences between our counts and previous measurements are consistent with sampling fluctuations and small zero-point uncertainties in previous work.

Also shown in Figure 1 is the no-evolution model of Ellis (1987), which we have

normalised 25% lower than in Ellis (1987) to match our count at $b_J \approx 17$. Our counts show a surprisingly large excess over the no-evolution model with 60% more galaxies at $b_J = 19$. Galaxies at this magnitude have a mean redshift of only $z \approx 0.1$ which corresponds to a look-back time of only 1.8 Gyr (assuming $h = 0.5, \Omega = 1$). The excess rises to 100% at $b_J = 20.5$.

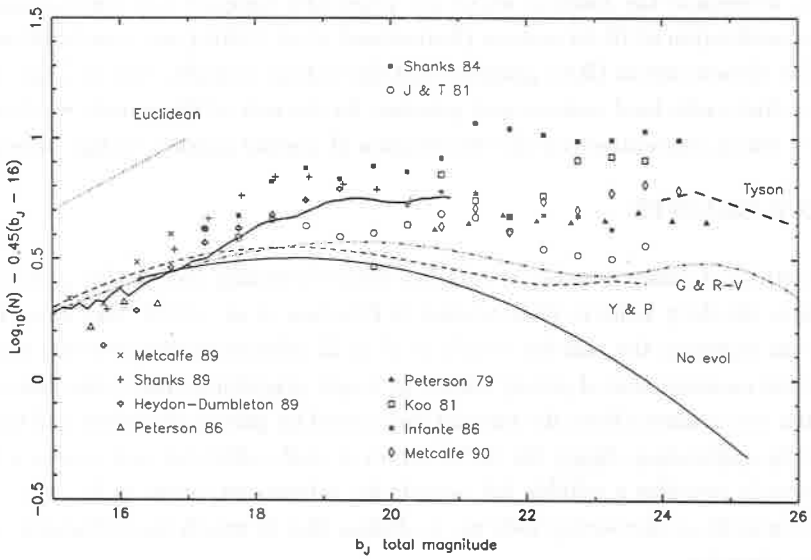

Figure 1. Differential galaxy counts per square degree per magnitude (i.e. count in 0.1 mag bins ×10, or count in 0.5 mag bins ×1.98). All counts have been multiplied by dex$[-0.45(b_J - 16)]$ to provide an expanded ordinate. The thick solid line shows our results. with linear and quadratic The various data points are as indicated on the Figure. The thin smooth line shows the no-evolution model of Ellis (1987), normalised to our counts at $b_J \approx 17$, and we also plot two evolution models (see text) from Yoshii & Peterson (1990) and Guiderdoni & Rocca-Volmerange (1990).

This result is so startling that we should explain why it has not been clearly detected before. The factor of 2 excess at $b_J = 20.5$ corresponds to 0.3 dex; the tendency in the past has been to normalise models at $b_J \sim 18$ (accounting for 0.12 dex) and to adopt the lower counts of Jarvis & Tyson (1981) and Peterson *et al.* (1979) at $b_J = 20.5$, accounting for another 0.1 dex. Thus it has been generally argued that the count excess at 20.5 is < 0.1 dex, consistent with mild-evolution models. The remaining discrepancies have been further obscured by plotting the counts with a highly compressed ordinate.

It is apparent from our counts that dramatic galaxy evolution is occurring at low redshift. However, the redshift surveys of Broadhurst *et al.* (1989; hereafter BES)

and Colless *et al.* (1990) show that the redshift distribution, $n(z)$, to $b_J = 22.5$ is very similar to the no-evolution prediction, despite the observed excess galaxy count compared to no-evolution models. BES showed that this is inconsistent with simple luminosity evolution models which match the number counts (e.g. Bruzual 1983), since these models predict a substantial high-redshift tail in $n(z)$ to $z > 0.5$ which is not observed. They suggest that the overall evolution of the galaxy luminosity function must look much more like pure density evolution than pure luminosity evolution. Using our lower counts at bright magnitudes makes the count excess a factor ≈ 3 at $b_J = 22.5$, and so the apparent inconsistency between the steep number counts and the non-evolving shape of the $n(z)$ is more extreme.

In Figure 1 we plot two theoretical models for faint number counts, both normalised to match our counts at $b_J \approx 17$: that from Yoshii & Peterson (1990) with $\Omega = 1, z_f = 10, x = 0.2$, and a model close to scenario C of Guiderdoni & Rocca-Volmerange (1990) with $\Omega = 0.2, z_f = 10$. Each of these models is based on Bruzual (1983) type luminosity evolution of a local mix of morphological types (see the original references for details), but with our normalisation they fail to match the counts at $b_J \gtrsim 19$ by a wide margin. This indicates that current models of galaxy evolution may require drastic revisions (see Rocca-Volmerange this volume).

ANGULAR CLUSTERING

The structure of the galaxy distribution on scales $\gtrsim 10\,h^{-1}$Mpc, can be related by linear perturbation theory to fluctuations in the early universe. If models in which perturbations are generated during an inflationary phase in the early universe are correct, then the fluctuations obey Gaussian statistics, and so *all* aspects of linear structure can be described by the two-point correlation function, $\xi_g(r)$. Thus, measurements of $\xi_g(r)$ on large scales are extremely powerful constraints on models of the early universe and, if the fluctuations are Gaussian, give a complete description of large-scale structure. From our two-dimensional catalogue we can infer $\xi_g(r)$ from measurements of the angular two-point correlation function $w(\theta)$.

We tested various methods of estimating $w(\theta)$ using Monte-Carlo simulations of clustered point distributions, and chose two estimators which are stable and unbiased, and also computationally efficient (Maddox *et al.* 1990c). Over the range of separations, $0.1° < \theta < 0.5°$, we used both estimators, and found no significant differences between the measurements. Residual contamination from uncorrelated merged images reduces the apparent clustering so we apply a correction factor for each magnitude range estimated from our visual classification checks. We apply further small corrections to account for residual errors in the uniformity of galaxy photometry and selection across the sky.

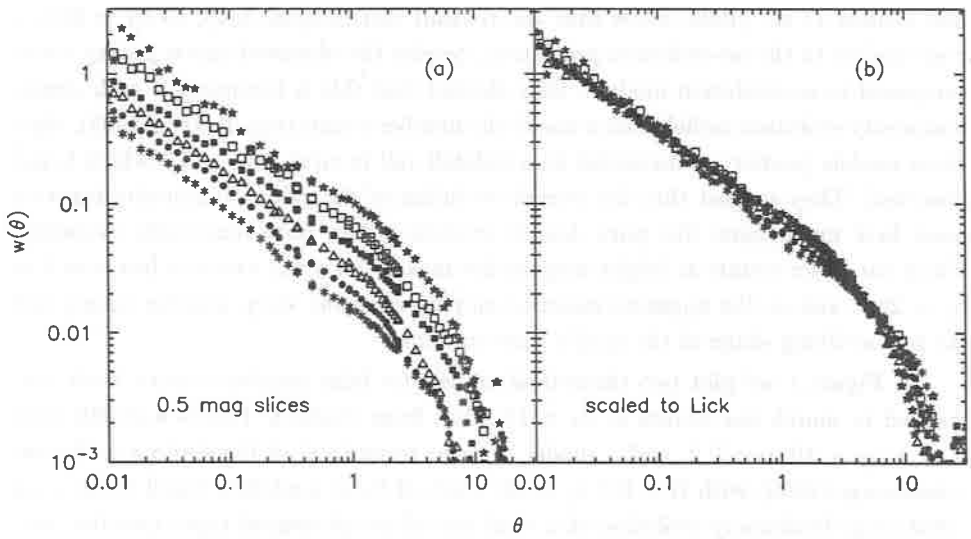

Figure 2. (a) The angular correlation function measurements from 6 magnitude slices of the APM Galaxy Survey. (b) The measurements after scaling to the depth of the Lick catalogue.

Figure 2a shows the resulting $w(\theta)$ measurements for each of six disjoint magnitude slices between $b_J = 17$ and 20.5. We have limited this analysis to the central 120 plates of our survey, which corresponds to $b \lesssim -50°$. At such high $|b|$ no significant errors are introduced by uncertainties in the correction for galactic absorption or increased contamination from merged stellar images at low galactic latitudes. For each slice $w(\theta)$ can be approximated by a power law at small angles. At larger angles the measurements gradually steepen away from power laws, eventually becoming indistinguishable from zero. The measurements for fainter slices have lower amplitudes, and the bend away from the power law occurs at smaller angles. We estimated the errors on our measurements by calculating $w(\theta)$ separately for four independent zones of the survey, and measuring the scatter between the areas. The *rms* for the faintest slice is $\sim 2 \times 10^{-3}$, showing that the bend below the power law is highly significant.

We have scaled our estimates of $w(\theta)$ to the depth of the Lick catalogue using the relativistic version of Limber's equation with $q_o = 0.5$ (Groth and Peebles 1977, hereafter GP77; Phillipps *et al.* 1978). We estimate the selection function for our survey using a parametric function which models the evolution of the galaxy luminosity function including the k-correction (Maddox *et al.* 1990c). We calculate the shifts in $\log(w)$ and $\log(\theta)$ using a two power law model for $\xi(r)$ and assuming that the clustering pattern is stable in proper coordinates. Figure 2b shows the curves from Figure 2a after scaling by the relevant factors. The agreement between these curves is excellent and the scatter is consistent with the errors expected from our plate matching procedure. This scaling test provides important evidence that our angular correlation

functions are measuring real clustering in the galaxy distribution rather than clustering induced by systematic errors.

Patchy obscuration could, in principle, contribute to $w(\theta)$. However, $w(\theta)$ for the faintest magnitude slice provides an upper limit on such an effect; even if the entire $w(\theta)$ for the faintest magnitude slice were caused by patchy obscuration, it would have little effect on $w(\theta)$ for the brightest three slices. It is therefore likely that patchy obscuration is unimportant.

On scales up to $\theta \approx 3°$ our results are in good agreement with $w(\theta)$ from the Lick survey (GP77) but on larger scales they disagree. On larger scales GP77 find that $w(\theta)$ breaks sharply from a power law on scales of $\gtrsim 3°$, whereas we find a more gentle decline. A detailed discussion of the comparison between our results and the Lick measurement is given by Maddox *et al.* (1990c), and we conclude that the discrepancy is probably caused by the filtering technique that GP77 used to remove spurious gradients in the Lick map. Though the difference is only marginally significant relative to the Lick error estimates, the extra power on large scales is very significant compared to our smaller errors.

The tests that we have applied to the APM Survey indicate that our angular correlation functions, including the excess signal over the Lick result, represent real galaxy clustering. However, the detection of small amplitude clustering on large scales is extremely sensitive to systematic errors, so these results clearly need to be confirmed by other data. The Mt. Stromlo/APM redshift survey described below provides such data and preliminary clustering measurements are consistent with the extra large-scale power seen in the faint angular data. Also, independent measurements of large-scale clustering from the random sampled redshift survey of IRAS galaxies (Lawrence *et al.* 1989) and the Edinburgh/Durham Southern Galaxy Catalogue (Collins *et al.* these proceedings) both support our detection of large-scale power in the galaxy distribution. Therefore we are confident that our measurements of $w(\theta)$ represent real large-scale power in the galaxy distribution.

This extra power on scales $20 - 40\,h^{-1}$Mpc is difficult to reconcile with the 'standard' $\Omega = 1$ biased Cold Dark Matter (CDM) model of Davis *et al.* (1985). The dotted curve in Figure 3 shows the predicted $w(\theta)$ based on $\xi(r)$ from the numerical simulations described by White *et al.* (1987), and it falls well below our data points. The thin solid line shows the linear theory calculation of $w(\theta)$ for a CDM model with $\Omega_0 = 0.2$, $h = 1$, and the dashed line shows a model with $\Omega_0 = 0.2$, $h = 0.75$ (Efstathiou *et al.* 1990a). These two curves bracket our results on angular scales $> 1°$ (corresponding to physical scales of $\gtrsim 5\,h^{-1}$Mpc) but fall below the observations on smaller scales, where $\xi(r)$ exceeds unity and linear perturbation theory is expected to fail.

To determine the shape of $\xi(r)$ in the non-linear regime, we have run N-body simulations of spatially flat low-density CDM universes (Efstathiou *et al.* 1990a)

The thick solid line in Figure 3 shows $w(\theta)$ computed from the N-body results for $\Omega = 0.2$, $h = 0.9$. This curve provides an excellent match to the APM results on large scales, but overshoots on small scales. Evidently, if this model is to match the observations, galaxies cannot be accurate tracers of the mass distribution on scales where the fluctuations are highly non-linear. We do not regard this as a particularly serious discrepancy because our models neglect physics that is likely to be important on small scales where $\xi(r) \gg 1$.

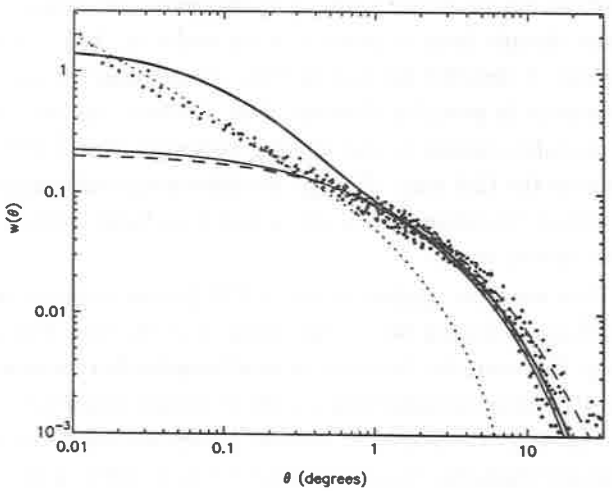

Figure 3. Comparison of the measured $w(\theta)$ with various cosmological models as described in the text.

The main conclusion to be drawn from this comparison is that a CDM model with $\Omega_0 h \sim 0.2$ can account for the large-scale clustering of galaxies seen in the APM Galaxy Survey. However this model fails to satisfy the observed constraints on microwave background anisotropies unless a significant cosmological constant, Λ, is included. If $\Lambda = 3(1 - \Omega)H_0^2$ then the predicted microwave anisotropies would be compatible with observations. Such a model has the additional attraction that the universe would be spatially flat, and so would also be consistent with the predictions of inflation (Efstathiou *et al.* 1990a).

THE MT. STROMLO/APM REDSHIFT SURVEY

Existing large redshift surveys such as the CfA survey (Huchra *et al.* 1983) and the Southern Sky Redshift Survey (SSRS) (da Costa *et al.* 1988) sample galaxies to a median depth of $\approx 6000 kms^{-1}$, but to study the distribution of galaxies on scales $\gtrsim$ 15 Mpc a volume of space $\gtrsim 10^6$ Mpc^3 must be sampled. We have nearly completed a large solid-angle galaxy redshift survey based on the visually checked galaxies brighter

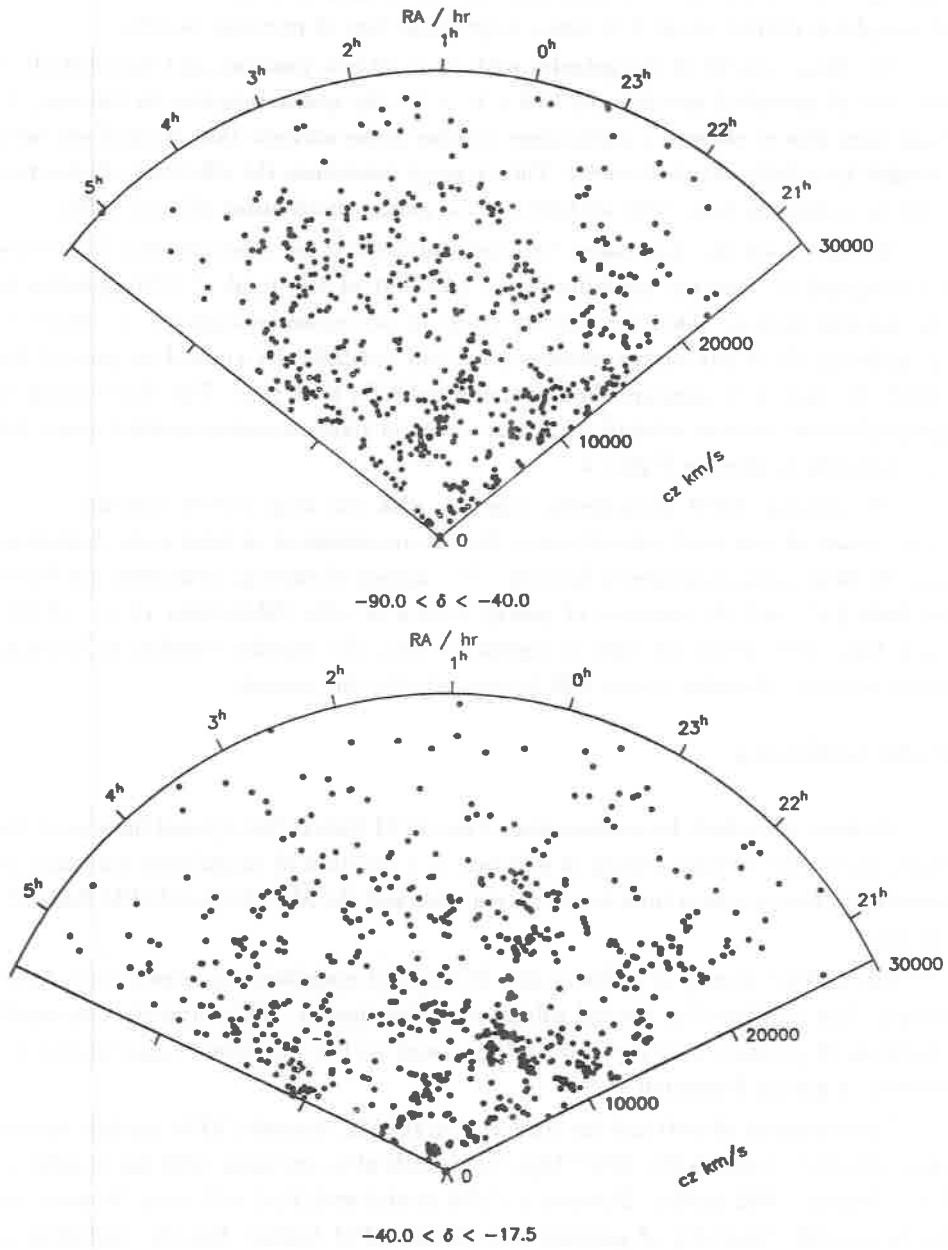

Figure 4. Redshift versus Right ascension cone plots of the Mt. Stromlo/APM Redshift Survey.

than $b_J = 17.$ in the APM Galaxy Survey. The median redshift is $12000 kms^{-1}$, and it samples a volume about four times larger than that of previous surveys.

We chose 1 in 20 of the galaxies with $b_J < 16.5$ at random, and included all of the 1 in 20 eyeballed sample with $16.5 < b_J < 17$. By sparse sampling in this way we have been able to observe a much larger volume of the universe than would have been possible for a fully sampled survey. This strategy maximises the efficiency of telescope time in estimating large-scale statistics of the galaxy distribution (Kaiser 1986).

We have used the Australian National University 2.3m telescope and dual-beam spectrograph to measure redshifts for $\sim$ 1400 out of the total of 1700 galaxies in the random sample. The *rms* velocity errors of our measurements are $\approx 35 kms^{-1}$. In addition, 63 of our survey galaxies have had redshifts determined as part of the SSRS. We intend to measure the remaining redshifts next year. The distribution of galaxies in our current redshift sample is shown in right-ascension–redshift space for two declination slices in Figure 4.

The reliable APM photometry, together with the large survey volume, $\sim 10^6$ Mpc^3, make this an ideal redshift survey for the measurement of large-scale clustering, and the field galaxy luminosity function. Preliminary clustering measurements based on both $\xi(r)$ and the variance of galaxy counts in cells (Efstathiou *et al.* 1990b) show large-scale structure that is consistent with the angular correlation function measurements. Detailed results will be presented in due course.

CONCLUSIONS

We have described the construction of the APM Galaxy Survey and three projects based on it: the surface density of galaxies as a function of magnitude; the angular correlation function as a function of magnitude; and the Mt. Stromlo/APM Redshift survey.

The surface density of galaxies as a function of magnitude increases much more steeply than predicted by normal galaxy evolution models. This suggests very rapid evolution of galaxies over the last $\sim$ 2Gyrs and so has important implications for theories of galaxy formation.

Measurements of $w(\theta)$ and the clustering in the Mt. Stromlo/APM redshift survey show structure on scales $20-40\,h^{-1}$Mpc that is difficult to reconcile with the 'standard' $\Omega = 1$ biased CDM model. However a CDM model with $\Omega_0 h \sim 0.2$ can account for the large-scale clustering of galaxies seen in the APM Galaxy Survey. Including a cosmological constant to give a flat geometry makes such a model compatible with the limits on anisotropies in the microwave background and also consistent with inflation.

References

Broadhurst, T.J., Ellis, R.S. and Shanks, T., 1989, *M.N.R.A.S.* , **235**, 827.

Bruzual, G., 1983. *Ap. J.***277**, 532.

Colless, M.M., Ellis, R.S., Taylor, K. & Hook, R.N., 1990. *M.N.R.A.S.* **244**, 408.

Collins, C., *et al.* 1990, *these proceedings.*

da Costa L.N., Pellegrini, P.S., Sargent, W.L.W., Tonry, J., Davis, M., Meiksen, A. and Latham, D.W., 1988, *Ap. J.*, **327**, 544.

Davis, M. and Huchra, J., 1982, *Ap. J.*, **245**, 437.

Davis, M.D., Efstathiou, G., Frenk, C.S. and White, S.D.M., 1985, *Astrophys. J.*, **292**, 371.

Efstathiou, G., Sutherland, W.J., and Maddox, S.J., 1990a, *Nature*, in press.

Efstathiou, G., Kaiser, N., Saunders, W., Rowan-Robinson, M., Lawrence, A., Ellis, R.S. & Frenk, C.S., 1990b, *M.N.R.A.S.* , , .

Ellis, R.S., 1987. In *"Observational Cosmology"*, Proceedings of IAU Symposium 124, eds. Hewitt *et al.* , Reidel.

Groth, E.J. and Peebles, P.J.E., 1977, (GP77), *Astrophys. J.* , **217**, 385.

Guiderdoni, B. & Rocca-Volmerange, B., 1990, *Astron. Astrophys.***227**, 362.

Heydon-Dumbleton, N., Collins, C.A. & McGillivray, H., 1989. *M.N.R.A.S.* **238**, 379.

Huchra, J.P., Davis, M., Latham, D. and Tonry, J., 1983, *Ap. J. Supp.*, **52**, 89.

Infante, L., Pritchet, C. & Quintana H., 1986, *Astron. J.***91**, 217.

Jarvis, J.F. and Tyson, J.A., 1981, *Astron. J.*, **86**, 476.

Kaiser, N., 1986, *M.N.R.A.S.* , **222**, 323.

Kibblewhite, E.J., Bridgeland, M.T., Bunclark, P., and Irwin, M.J., 1984, *Astronomical Microdensitometry Conference*, NASA Conf. Pub., **2317**, p277.

Koo, D.C., 1981, Ph.D., University of California, Berkley.

Lawrence, A., Rowan-Robinson, M., Crawford, J., Saunders, W., Ellis, R.S., Frenk, C.S., Parry, I., Efstathiou, G. and Kaiser, N., 1989, in preparation.

Loveday, J.L., 1989 *PhD. Thesis, Cambridge.*

Maddox, S.J., 1988, *PhD. Thesis, Cambridge.*

Maddox, S.J., Sutherland, W.J., Efstathiou, G., and Loveday J., 1990a, *M.N.R.A.S.* , **243**, 692.

Maddox, S.J., Sutherland, W.J., and Efstathiou, G., 1990b, *M.N.R.A.S.* , **246**, 433.

Maddox, S.J., Efstathiou, G., Sutherland, W.J., and Loveday J., 1990c, *M.N.R.A.S.* , **242**, 43P.

Maddox, S.J., Sutherland, W.J., and Efstathiou, G., Loveday, J., and Peterson, B.A., 1990d, *M.N.R.A.S.* , **247**, 1P.

Metcalfe, N., Fong, R., Shanks, T. & Kilkenny, D., 1989. *M.N.R.A.S.* **236**, 207.

Metcalfe, N., Shanks, T., Fong, R. & Jones, L.R., 1990, preprint.

Peterson, B.A., Kibblewhite, E.J., Bridgeland M., Hooley, T. and Horne, D., 1979, *Astrophys. J.*, **233**, L109.

Peterson, B.A., Ellis, R.S., Efstathiou, G., Shanks, T., Bean, A.J., Fong, R. & Zen-Long, Z., 1986. *M.N.R.A.S.* **221**, 233.

Tyson, J.A., 1988. *Astron. J.***96**, 1.

Rocca-Volmerange, B., *et al.* 1990, *these proceedings.*

Shanks, T., Stevenson, P.R.F., Fong, R. & McGillivray, H.T., 1984. *M.N.R.A.S.* **206**, 767.

Shanks, T., 1989. In *Proceedings of IAU Symposium 139*, ed. K. Mattila, Reidel.

Sutherland, W.J., Maddox, S.J., and Efstathiou, G., 1990, to appear in Astron. Soc. of the Pacific Conference series.

Sutherland, W.J., Maddox, S.J., McMahon, R.G., and Saunders, W., 1990, *M.N.R.A.S.* in press.

White, S.D.M., Frenk, C.S., Davis, M. and Efstathiou, G., 1987, *Astrophys. J*, **313**, 505.

Yoshii, Y., & Peterson, B.A., 1990, *Ap. J.*in press.

Vadim Kuzmin and Andrei Doroskevich

Future Prospects

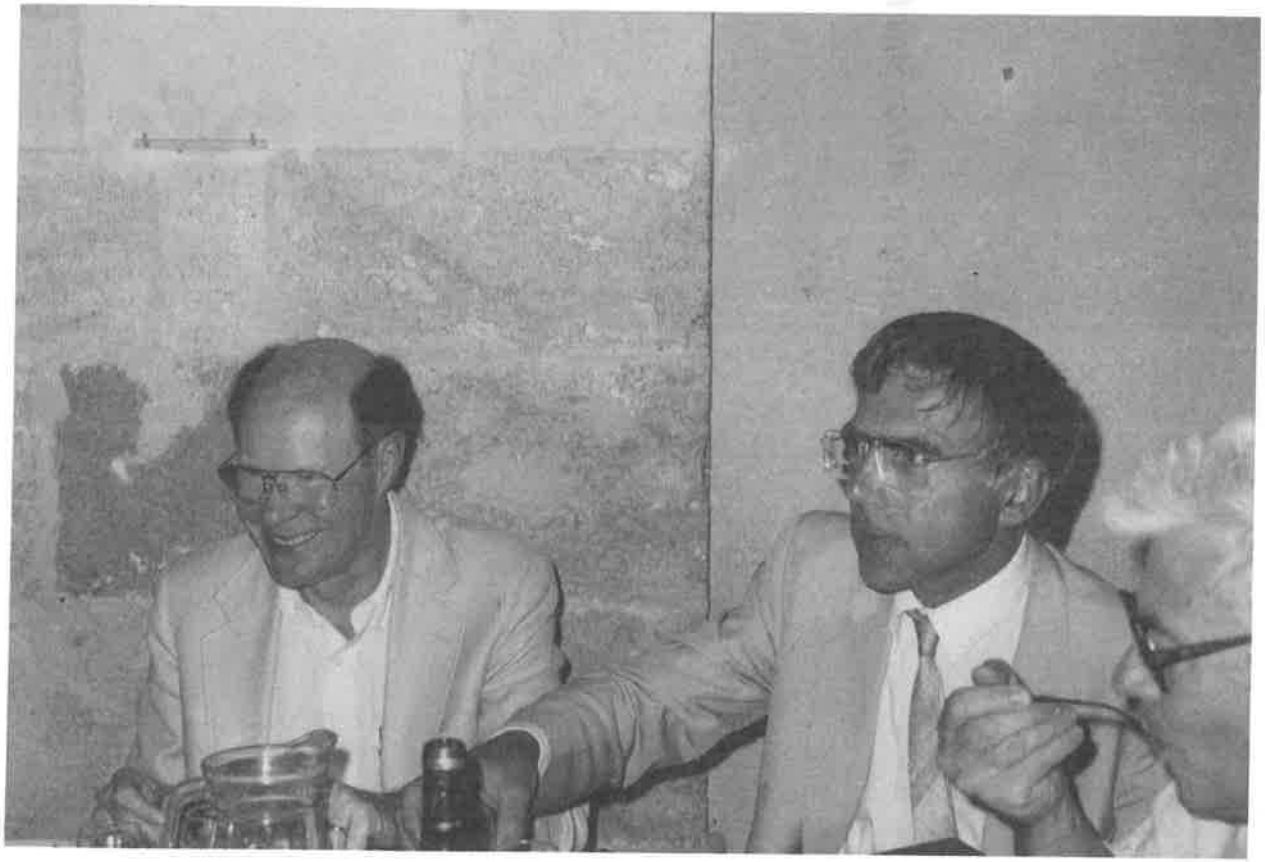

Robert Wilson and Pierre Léna

THE CURRENT STATE OF THE HUBBLE SPACE TELESCOPE

EDWARD J. GROTH
Joseph Henry Laboratories of Physics, Princeton University
Physics Department, Jadwin Hall, Princeton University, Princeton, NJ 08544 USA

ABSTRACT

The current state of the Hubble Space Telescope is described. There are two major problems: oscillation of the solar panels and spherical aberration in the optics. Aside from these two problems, the flight hardware is working well, better than expected in many cases. The problems are characterized and prospects for their resolution are discussed. The science impacts of the spherical aberration are outlined and some examples of recent science exposures are presented.

INTRODUCTION

The Hubble Space Telescope was launched in April, 1990. By late June, two major problems were apparent: oscillations of the solar arrays and spherical aberration in the telescope optics. In this paper, I briefly describe the oscillation problem, but focus mainly on the spherical aberration: its characterization, prospects for resolving the problem, the science impacts, and examples of science that can still be done with the HST.

The solar array oscillation has a ten second period and is produced by a thermal effect correlated with terminator crossings. The oscillation causes pointing jitter $\sim$ 100 milli-arcsec (smearing images) and can cause the fine guidance sensors to lose lock. At the time of the Blois conference, it was expected that the effects of the oscillations could be reduced to acceptable levels by the installation of a software filter in the pointing control system. Since the conference, the filter has been tried. It did, in fact, remove the 0.1 Hz oscillations but it interacted badly with the gyros causing them to switch to high rate mode which cannot be used for fine pointing. Also, it has been discovered that there is, and has been all along, a 0.6 Hz oscillation (probably excited by the 0.1 Hz oscillation) and this is the prime cause of losing lock. Despite these additional complications, optimism remains that the oscillation problem can be solved by software modifications in the pointing control system.

SPHERICAL ABERRATION

Figure 1 shows the first extreme out-of-focus star image obtained with the HST. With good optics, this would have been (modulo interference and diffraction effects) a uniformly illuminated image of the pupil: a disk with obscurations due to the secondary (the hole in the middle), the secondary spider (the cross), and the mirror support pads (three circular areas near the edge of the pupil). In fact, the surface brightness is much fainter near the outer edge than the inner edge. Since the image was obtained well inside the focus, the conclusion is that the light from the outer part of the pupil is not converging as fast as the light from the inner part; the outer edge of the wavefront is too flat.

The amount of spherical aberration can be "measured with a ruler." One measures the radii of the outer and inner edges of the pupil on the image of Figure 1 and on an image at another focus position. This is enough to determine the positions of paraxial and marginal focus which, in turn, are enough to determine the amount of spherical aberration.

In fact, considerably more analysis has been done to pin down the exact nature of the aberration. The image in Figure 1 can be satisfactorily reproduced (including the diffraction and interference effects) by a diffraction calculation which assumes spherical aberration, focus, and collimation errors. By comparing actual images at several different focus positions with such model calculations and by doing similar work with the off-axis faint object camera, one arrives at the following conclusions. The aberration is pure spherical: the shape of the primary mirror is in error by an r^4 term such that the mirror is too low at its outer edge (relative to the center) by about 2 microns. This amounts to a wavefront error $\sim$ 0.5 waves rms at visible wavelengths.

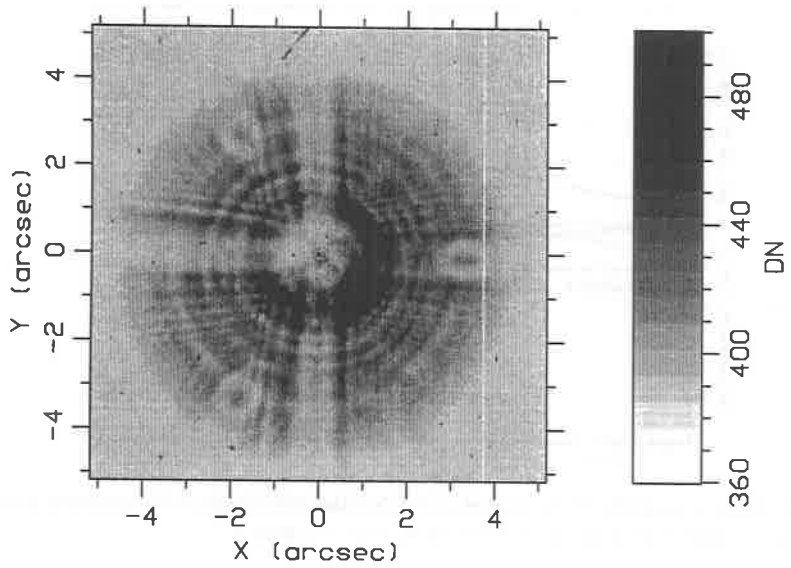

Figure 1. An extreme out-of-focus star image taken with the planetary camera (0.043 arcsec per pixel) through the 547 nm filter. In this and other images, the intensity scale is "Data Numbers," where 1 DN corresponds to about 7.5 detected photons.

Aberrations are often characterized with a set of orthonormal polynomials known as Zernike polynomials. Figure 2 shows the components of the spherical aberration Zernike: there is a fourth order term representing the figure error, a second order term from focus error, and a constant. The focus term minimizes the rms value of the polynomial and corresponds to the fact that one is free to adjust the focus to get the best images. It is this spherical Zernike polynomial whose rms is 0.5 waves even though the wavefront error of the r^4 term is about 8 waves from center to edge. The primary mirror is equipped with force actuators intended for removal of residual aberrations on orbit. They are located in two rings at the approximate positions of the nodes of the spherical Zernike; they were placed so that their use would not introduce any spherical aberration—thus they cannot be used to correct spherical aberration.

The current focus of the telescope has been set to maximize the light within an aperture of 0.1 arcsec radius. This focus is approximately half way between diffraction focus (which corresponds to the spherical Zernike in Figure 2) and paraxial focus. Here, wavefront error is approximately 1.4 waves rms at visible wavelengths. Figure 3 shows a typical star image at this focus setting. There is an approximately diffraction limited core surrounded by a low surface brightness halo which extends several arcseconds. Figure 4 shows the encircled energy curve for the star of Figure 3. The core (within radius 0.1 arcsec) contains only 12 to 15 percent of the light; at least 70 percent was expected. Burrows *et al.*[1] give additional details concerning the telescope optics.

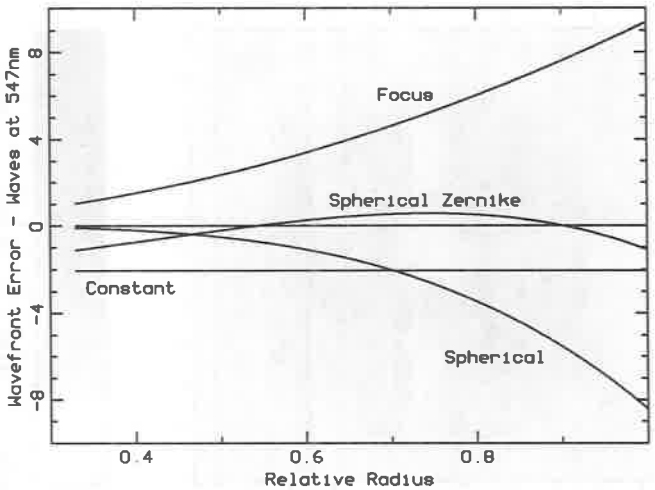

Figure 2. The components of the lowest order Zernike polynomial with spherical aberration include an r^4 spherical term, an r^2 focus term, and a constant.

PROSPECTS FOR RESOLUTION

It appears that the primary mirror has been manufactured "perfectly" but with the wrong conic constant—it is a slightly shallower hyperboloid than required. Analysis of records and manufacturing equipment has uncovered a spacing error in the null lens used to measure the figure of the primary mirror. The spacing error is consistent with the observed spherical aberration. Analysis of the historical data and the flight system is continuing in order to completely characterize the aberration.

Since the aberration appears to be a simple r^4 figure error, it is fairly straightforward to build correcting optics within an instrument. One needs to form an image of the pupil on an optical surface containing a compensating error.

The HST is planned as a fifteen year mission. It was realized that components would fail and instruments would become obsolete over this time period so the HST has been designed for on-orbit replacement of components and instruments. There are already three instruments in development: an improved wide field and planetary camera (WFPC II), an imaging spectrograph (STIS), and a near infrared camera and multi-object spectrograph (NICMOS). All of these can be modified to include correcting optics—in fact, the WFPC and NICMOS already have optical surfaces at or near a pupil image, and the figure of these surfaces can be modified to correct the aberration. The current plans are to install the WFPC II in 1993 and to accelerate the STIS so it can be installed with the NICMOS in 1996. In addition to these instrument modifications, other solutions are under study.

SCIENCE IMPACTS

The image structure shown in Figures 3 and 4 has several obvious impacts on the science observations that can be performed with the HST. For faint objects, all the signal-to-noise

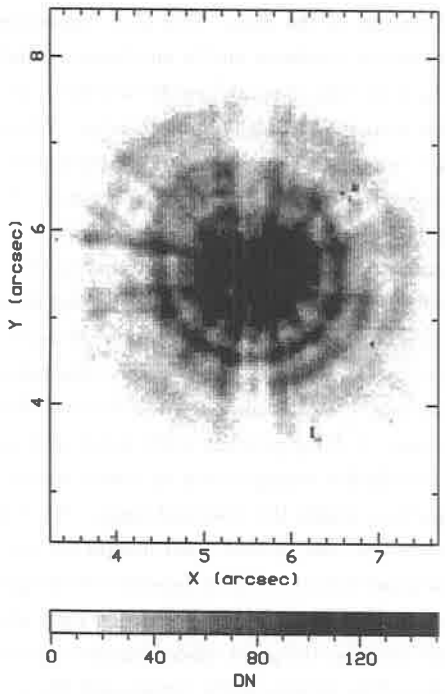

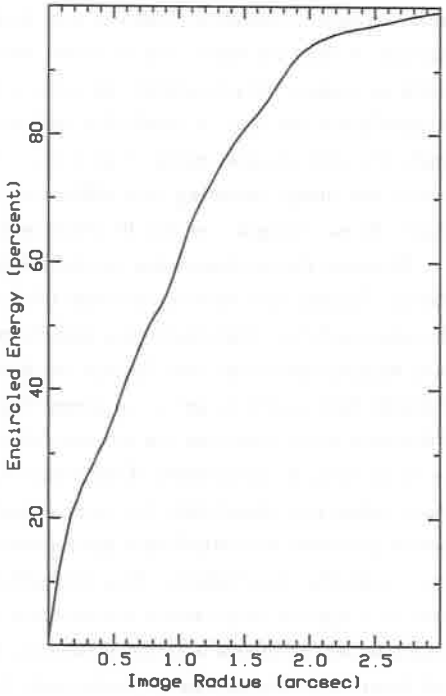

Figure 3 (left). A star image taken with the planetary camera (0.043 arcsec per pixel) and the 230 nm filter. This image was obtained as part of the fine focus run and is at the current best focus of the telescope. The stretch shows the halo at the expense of saturating the nearly diffraction limited core.

Figure 4 (right). The encircled energy function for the star in Figure 3.

is in the core which contains 1/6 to 1/5 the light that was expected. This means a decrease of about two magnitudes in limiting magnitude for a given exposure time. To maintain the expected signal-to-noise ratio the exposure time must be increased a factor of 5–6 for photon limited observations such as spectroscopy or faint object camera UV imaging, and it must be increased a prohibitive factor of 25–36 for background limited observations such as faint object imaging. These considerations apply to isolated stellar objects. In crowded fields, the overlapping halos of the brighter stars produce a sea of background light above which the fainter objects must be detected.

There has been much discussion of image processing, specifically deconvolution, as a technique to restore HST images and recover some of the science of HST. In extreme cases, these discussions take on a religious fervor with proponents of image processing seeming to argue that it can recover all HST capabilities and opponents seeming to say that it can do nothing. In fact, the truth is somewhere in between.

Deconvolution is basically a trade of brightness information for spatial information; it

cannot create information which is not already present in the data. The two magnitude decrease in limiting magnitude is determined by photon statistics and is an absolute limit which no amount of processing can overcome. To maintain adequate signal-to-noise ratio, deconvolution can only be applied to well exposed images with high signal-to-noise. When applied to such images, deconvolution can produce remarkable improvement in the appearance of the image, restoring near diffraction limited resolution to the bright portions of the image. As an example, see the 30 Doradus image in the next section.

However, deconvolution has several limitations. First, it perturbs the photometric information. Experiments have shown that when crowded field images are deconvolved and then photometered, the photometry has significantly larger errors than if the image is photometered without deconvolution. Second, while deconvolution may make faint stars in the halos of bright stars easier to see on an image display screen, it cannot improve the detectability of the faint stars since this is a photon statistics issue. A third problem with deconvolution has to do with the uniqueness of the result. One is basically trying to find an "input image" which, when convolved with the point spread function, yields the observed image. Such a convolution destroys spatial information and it is possible that several input images are consistent with the observations. This means that marginal features seen in deconvolved images must be subject to very careful scrutiny and must not be over-interpreted. Finally, there are some practical problems with deconvolution of HST images: the point spread function varies with location in the cameras, it varies with the color of the objects in the image, and there is some evidence that it is time dependent. Also, the wide field camera, the planetary camera, and the $f/48$ mode of the faint object camera are all undersampled at visible wavelengths.

For spectroscopy of an isolated object, one can maintain spectral resolution at the expense of an increase in exposure time by using a small aperture which admits only the core of the image. Alternatively, one can use a large aperture to get most of the light and then attempt to recover the spectral resolution by deconvolving the spectrum. Experiments show that to get an equivalent signal-to-noise in the deconvolved spectrum requires such a high signal-to-noise in the input spectrum that one does better by using the smaller aperture.

To summarize: observation types which are probably not possible with the HST in its current state include: high spatial resolution spectroscopy, large dynamic range crowded field photometry, and faint object detection. Observation types that probably can be done as well as expected (usually with an increase in exposure time) include: UV spectroscopy of isolated objects, UV imaging, and high resolution imaging of bright objects.

SAMPLE IMAGES

In late August, 1990, the HST program started a series of Science Assessment Observations (to assess HST's capabilities for science!) and Early Release Observations. The images in this section include some of the first images in these series.

Figure 5 is a portion of a wide field camera image (0.1 arcsec pixels, 368 nm filter) of the central object in the 30 Doradus nebula. Both the "raw" and deconvolved images are shown.

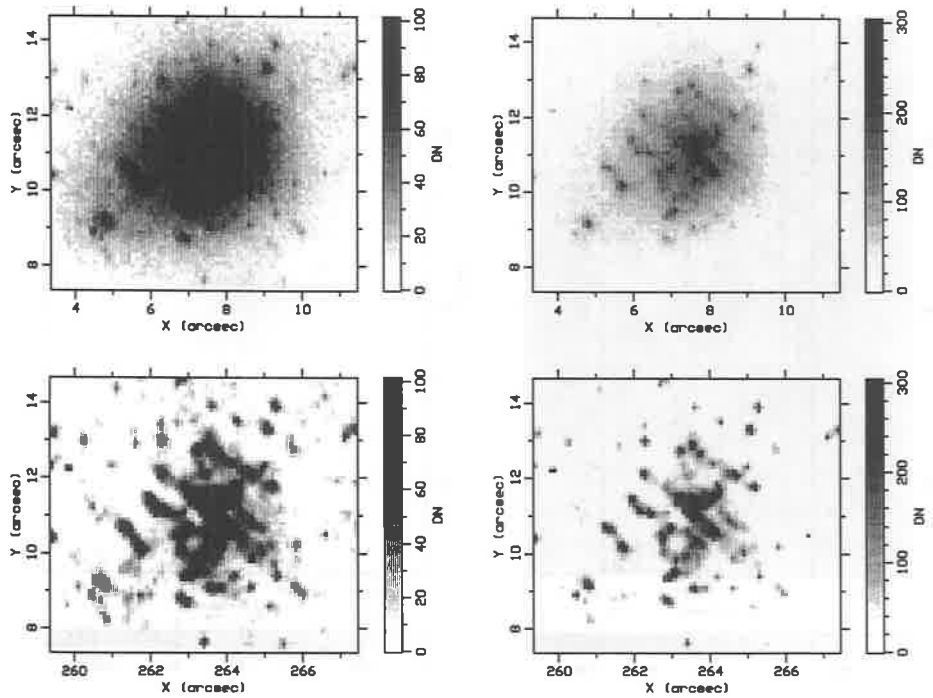

Figure 5. A wide field camera image of the central object, R136, of the 30 Doradus cluster. The 368 nm filter was used and the resolution is 0.1 arcsec per pixel. The top pair of images are "raw" images with different stretches, while the bottom pair are the results of applying the Lucy[2] deconvolution algorithm to the data in the top pair.

Deconvolution removes much of the halo light and allows many stars to be seen with one stretch. Either image resolves stars down to the pixel size and confirms ground based speckle work which had revealed eight objects within the central arc second. In addition, many more stars are detected. This image shows[3] that future work with the planetary camera (0.043 arcsec pixels) may be expected to provide a color-magnitude diagram, a luminosity function, and an initial mass function for the very center of this cluster.

Figure 6 shows the nucleus of the nearby S0 galaxy NGC 7457. This is a planetary camera image through the "wide V" (555 nm) filter and two stretches of the same data are shown in the figure. The light distribution follows a power law (exponent ~ -0.9) down to the limits of HST resolution—about 0.10 arcsec—which means that the nucleus is unresolved at a diameter of 7 pc.[4] This may be evidence that there is a compact object in the center of this apparently normal galaxy. In any case, the image gives a taste of what can be done with high resolution imaging of bright objects.

Figure 7 shows a wide field camera mosaic (all four CCDs have been put together) of the outer regions of the nearby galaxy NGC 925. This is a 900 second exposure with the wide V filter and is located about 2 arc minutes Northwest of the center of the galaxy.

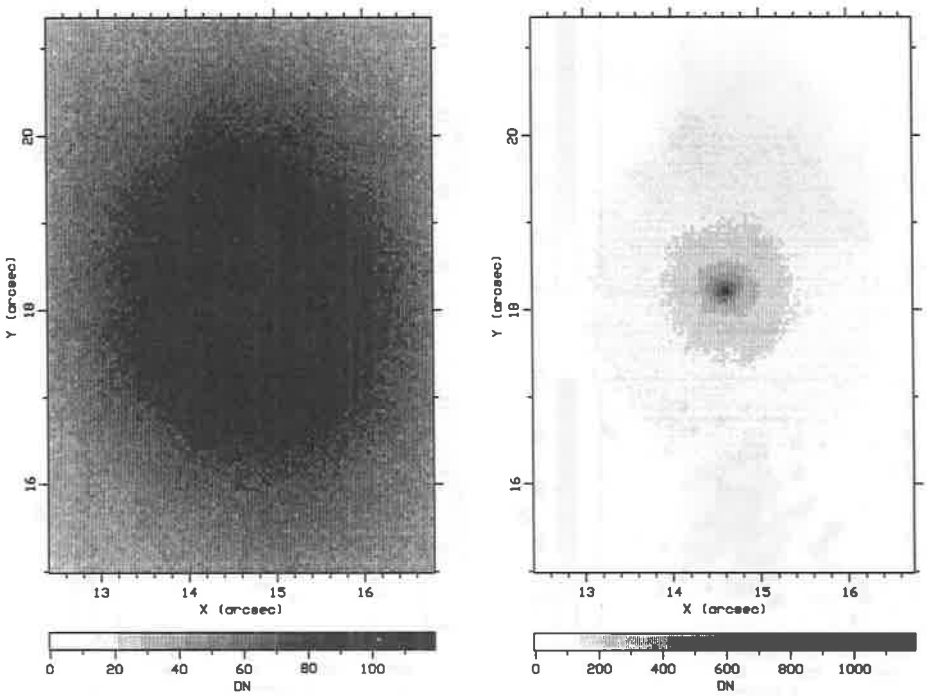

Figure 6. A planetary camera (0.043 arcsec per pixel) image of the S0 galaxy NGC 7457 through the 555 nm filter.

This is the "raw" image and the bright $\sim$ 5 arcsec blobs are the halos of single stars (or small groups of stars). A portion of the spiral arm in the lower left of Figure 7 is shown at full resolution (0.1 arcsec) in Figure 8. What appears to be nebulosity on ground-based photographs breaks up into stars and nebulosity in this image. At present, it's not known how much of the nebulosity in Figure 8 is true nebulosity and how much is simply due to the overlapping halos of stellar images. This image is one-half of an 1800 second exposure taken to assess the feasibility of measuring Cepheid variables in nearby galaxies. A preliminary analysis indicates that the limiting magnitude in the 1800 second image is about 24.5. At the distance of NGC 925, this is about two magnitudes short of being able to detect *and measure* a reasonable sample of the brightest Cepheids. With the same limiting magnitude for Virgo cluster galaxies, Cepheids are about three magnitudes out of reach.[5] It appears that the Cepheid program must be deferred until the WFPC II is installed.

CONCLUSION

For the near term, the HST is severely crippled by spherical aberration and much of the science planned for the HST must wait until the optics have been corrected. On the other hand, there is still much good science that can be done with the HST in its present condition, especially high resolution imaging of bright objects and UV spectroscopy. The challenge is

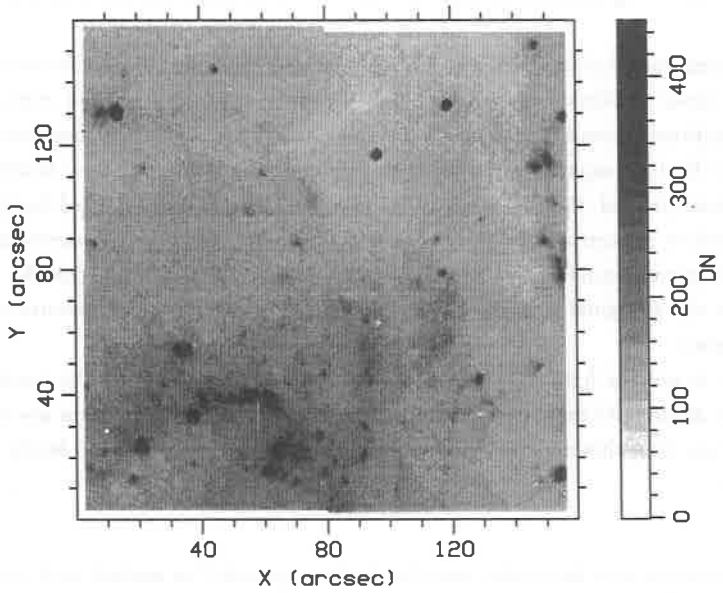

Figure 7. A mosaic of all four wide field camera CCDs from a 555 nm exposure of NGC 925. This image shows the full field of view of the wide field camera. The pixels have been averaged 6×6, so the resolution in this figure is only 0.6 arcsec.

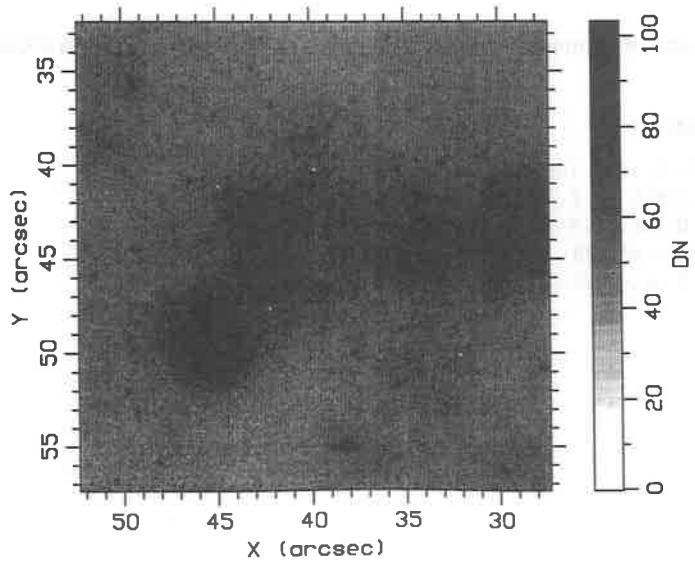

Figure 8. A full resolution (0.1 arcsec per pixel) portion of the spiral arm in the lower left of Figure 7.

to revise the observing program in order to make the best use of the HST until fixes are in place.

Those components of the HST which are not directly related to the spherical aberration or the solar array oscillation are working well; in many cases, better than expected. For example, the thermal condition is good, the solar arrays are delivering more output than specified, the battery capacity is larger than required, the spacecraft as a whole is using less power than planned, the communications margin is larger than expected (only two bits have so far had to be corrected by the error correcting code), and no components have failed over to a redundant component. All of this lends confidence that the HST can be fixed and achieve most of its original goals by the installation of replacement instruments containing corrective optics.

In order to put the fixes in place, both money and commitments will be required. The astronomical community must decide whether the goals of the HST program are still worth pursuing. If so, then this must be communicated to Congress and the top levels of NASA management.

It is impossible to acknowledge and thank all the people I've worked with on the HST program. However, I would like to give special thanks to the members of the WFPC team with whom I've worked most closely in putting together the materials for this talk: Jim Westphal (PI), Bill Baum, Bel Campbell, Shawn Ewald, Sandy Faber, Jeff Hester, Jon Holtzman, Deidre Hunter, Tod Lauer, Bob Light, Roger Lynds, Earl O'Neil, and Ed Shaya.

This research was supported in part by NASA through contract NAS5-29142.

REFERENCES

1) Burrows, C. J., *et al.* 1991, *Ap. J. (Letters)*, submitted.
2) Lucy, L. B. 1974. *A. J.*, **79**, 345.
3) Campbell, B., *et al.* 1991, *Ap. J. (Letters)*, submitted.
4) Lauer, T. R.,*et al.* 1991, *Ap. J. (Letters)*, submitted.
5) Holtzman, J. A., *et al.* 1991, *Ap. J. (Letters)*, submitted.

THE VERY LARGE EUROPEAN TELESCOPE

Pierre LENA

Université Paris VII et Observatoire de Paris
92195 Meudon Cedex, France

ABSTRACT

The European Very Large Telescope, approved in 1987, is now under construction. It will consist of four individual telescopes, 8-meter diameter each, located in the Chilean Andes, on Cerro Paranal, at an altitude of 2665 m. Individual telescopes are designed to maximize the image quality, using innovative techniques such as active or adaptive optics, flexible scheduling and seeing control, in order to approach or to reach the diffraction limit, especially at infrared wavelengths. The light collecting capability is enhanced in a mode where all four telescopes can combine incoherently their light, then providing the equivalent area of a 16-m diameter instrument. In a so-called coherent or interferometric mode, any number of telescopes can be combined to reach the angular resolution set by their separation.

We briefly review the instrumentation plan and the new capabilities brought by adaptive optics and interferometry.

OVERVIEW

The Very Large European Telescope (VLT), as described in its original proposal [1], consists of four 8-meter individual telescopes, devoted to optical astronomy, namely visible and infrared observations. Individual telescopes are equipped with an active primary mirror[2], made of ceramics (Zerodur), 17.5 cm thick, weighting 23 tons, open at f/1.8. The active control of the primary is achieved with push-pull actuators, controlled in real-time by a wavefront sensor using the light of a star in the field. All perturbations of frequencies below 1 Hz may be corrected. The concept of active optics is now fully demonstrated by the operation, since 1989, of the ESO New Technology Telescope (3.5 m) at La Silla[3]. The VLT specifications ask for a light concentration of 90% when the seeing is 0.4 arc sec FWHM. The current NTT operation led to a concentration of 80% within 0.15" in optical shop tests, and within 0.2" on site with the best seeing conditions[4].

Each telescope, placed on an altazimuth mount, will be equipped with two main Nasmyth foci, where field derotation is achieved on the instrument flange. In addition, each telescope feeds an individual Coudé focus and, from there, the light may be directed to two recombined foci : the incoherent recombined focus, where two or more telescopes can simultaneously feed a single instrument, increasing the collecting power up to an equivalent diameter of 16 meters; the coherent combined focus for the interferometric mode, to be described below. An additional Cassegrain focus will also be available.

The site of the VLT has been choosen in Decembre 1990 to be Cerro Paranal, a summit at 2665 meters high, located in Northern Chile, close to the Pacific coast, in a very dry and transparent climate (Fig.1). Compared to the existing ESO site at La Silla, the Paranal area[5] offers 40% more photometric nights, and an infrared transparency increased by 57%. A great attention is brought to the image quality of the VLT telescopes. Although the final dome concept is not yet choosen, aerodynamic studies are in progress to minimize the thermal interactions between the telescopes and the surroundings, and exploit at best the local conditions: systematic seeing surveys give an average seeing of the Paranal summit of 0.66".

The first 8-m telescope is expected to receive first light in 1996, and the other three telescopes will be phased with one new opening approximately every year. After the commissionning period of the instruments, the first telescope may therefore be open to the astronomical community before the end of 1996.

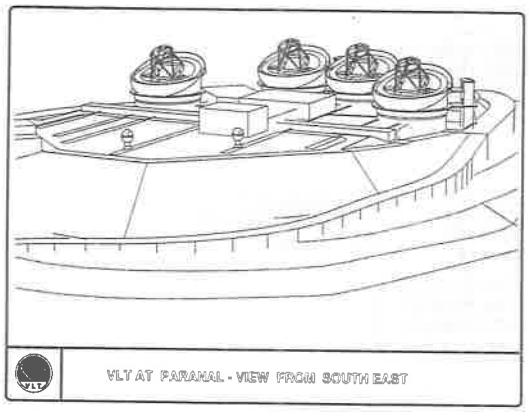

Figure 1. An overall artist view of the VLT on the summit of C.Paranal. The configuration of the telescopes in not definitive, neither their domes. In the background are the 8-meter telescopes and in the foreground the Interferometric Auxiliary Telescopes and their stations. Service buildings and aluminizing station are sketched and not shown at their definitive location.

THE INSTRUMENTATION

Figure 2 gives an overview of the instrumentation, respectively at visible (Fig.2a) and infrared (Fig.2b) wavelengths. Instruments are described in detail in the successive versions of the VLT Instrumentation Plan[6]. The construction plan of the instrumentation is staggered. The first generation includes a UV-Visible Focal Reducer Spectrograph, a UV-Visible Echelle Spectrograph, a High Angular Resolution Infrared Camera and a Medium Resolution Spectro-Imager. All these instruments should be ready by 1996, some of them beeing internally built at ESO, others being undertaken by consortia from various Institutes in Europe.

The second generation of instruments includes a Multi-fiber Area Spectrograph, a Visible Speckle Camera and a Mid-Infrared Imager Spectrograph, to be defined in 1991-1992. The equipment of the combined incoherent focus remains open. There is no question that the maximum sensitivity in the infrared can only be obtained by effectively adding the light of all four telescopes onto a single detector at the combined focus, which could be equipped with a High Resolution Echelle Spectrograph. At visible wavelengths, the progress of detectors may lead to alternate options : either the construction of a large High Resolution Spectrograph at the combined focus, or the electronic addition of signals coming from individual telescopes pointing the same object.

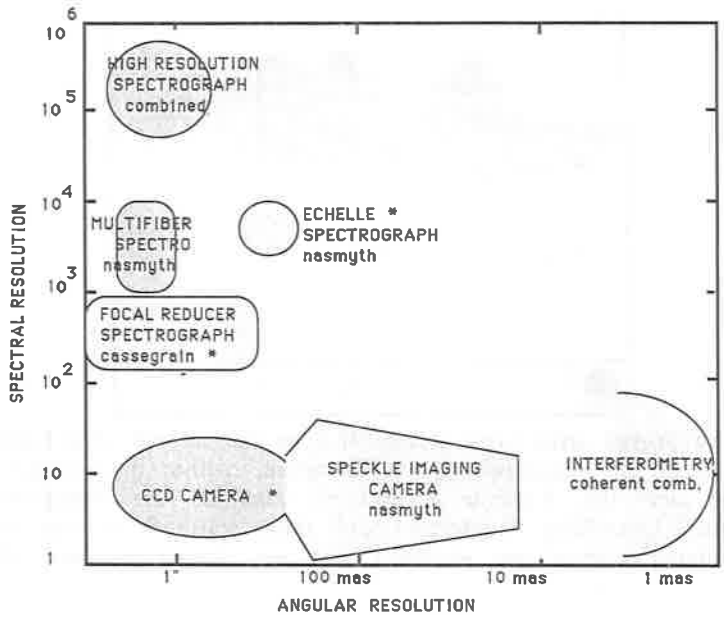

Figure 2a. The VLT Instrumentation Plan at Visible Wavelengths. The range of angular and spectral resolution of each foreseen instrument is indicated. The focus where the instrument will be placed is identified.

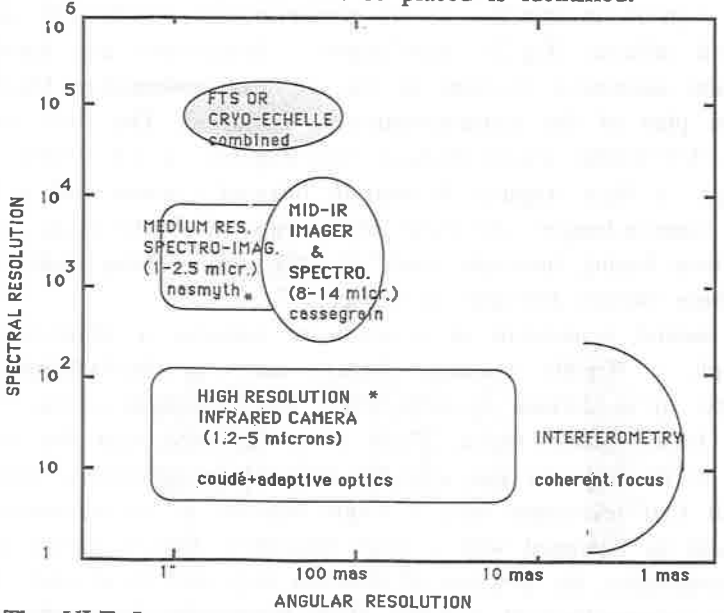

Fig.2b. The VLT Instrumentation Plan at Infrared Wavelengths. The angular and spectral resolution of each foreseen instrument is indicated. The focus where the instrument will be placed is identified.

ADAPTIVE OPTICS

Obtaining sharp images is considered as one of the main goals of the VLT to fully exploit its sensitivity to faint objects with good background discrimination. As stated above, the site seeing, the thermal and aerodynamic design of the enclosures, the performances of active optics on the primary are carefully scrutinized. As early as 1984, it was realized that the active correction, in real time, of the image distorsions induced by the atmospheric turbulence may considerably enhance the VLT performances, as compared with *a posteriori* methods of image sharpening known as shift-and-add, speckle interferometry, deconvolution, etc[7]. As the high frequency behavior (up to 1 kHz) of the atmospheric turbulence prevents corrections to be applied to the primary mirror, adaptive optics specifically refers to such corrections applied in real time by a flexible mirror on which is formed the image of the telescope entrance pupil. Satisfactory results (Fig.3) have been obtained on the ESO 3.6- meter telescope with a prototype adaptive optics system, which will lead to the final concept to be choosen for the VLT adaptive system.

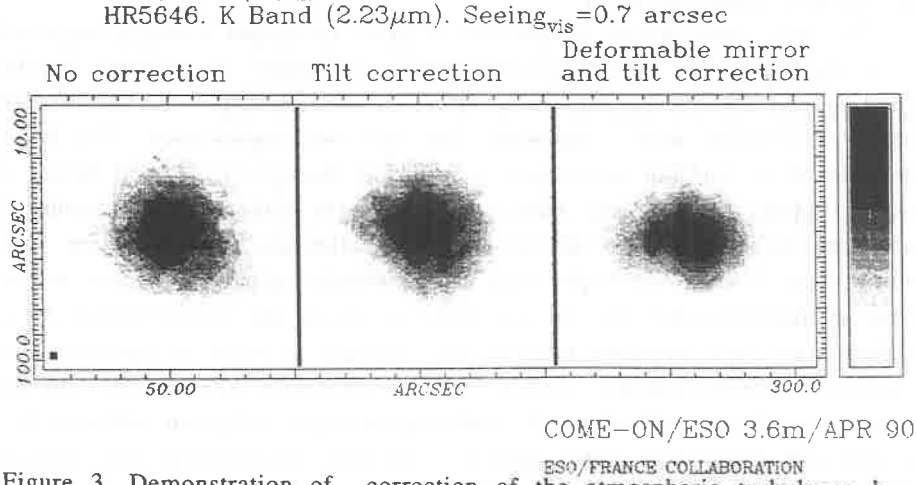

Figure 3. Demonstration of correction of the atmospheric turbulence by an adaptive optics system, mounted on the 3.6-meter ESO telescope at La Silla. Observations are made at 2.2 microns (K band) with an infrared camera. Left : long exposure image without correction and a 0.7" seeing. Center : low order correction of the atmosphere by supressing only image motion (tip-tilt correction). Right : adaptive correction, leading to a diffraction limited image[8].

Adaptive optics is expected to work best at infrared wavelengths (1-5 microns), where seeing limited images may be sharpened to the telescope

diffraction limit, i.e. to 25-125 milliarcsecond. Besides the intrinsic gain in angular resolution, additional gains in sensitivity are expected for unresolved or barely resolved objects, at wavelengths where the detector noise or the background noise dominate. In addition, background discrimination is improved for these objects. Spectrograph feed is an additional benefit of adaptive optics, since this technique allows to reduce the width of the slit in proportion of the energy concentration in the image. Finally, the adaptive corection partially restores the coherence of the incoming light, leading to significant sensitivity gains in interferometry.

Adaptive optics encounters certain limits. It requires a reference source. The availability of such source, its magnitude and distance to the object of interest in a particular astronomical field sets the maximum correction and image sharpening which can be obtained. This requirement may be alleviated in the long term if artificial reference stars, produced by laser echoes, become available.

THE INTERFEROMETRIC MODE

The array arrangement of the four 8-meter telescopes strongly suggested to be exploited for optical interferometry, in order to provide angular resolutions set by the maximum separation of the telescopes, i.e. up to 100 meters or slightly more, depending on the site capabilities. The beam extraction from the unit telescopes is achieved through the Coudé focus. A simple flipping mirror may then send the light either to the combined incoherent focus, described above, or to an alternate focus, where light coming from several telescopes may be coherently added. The most severe aspect of interferometry lies in the preservation of the signal phase. First, the light from each telescope must be put in phase as much as possible. This is achieved through adaptive optics on each telescope. Second, the internal metrology of the overall telescope configuration must be known within a few microns, and maintained stable against vibrations, wind effects, etc. through active controls. Third, the phase offsets due to Earth rotation and non-zenithal pointing must constantly be compensated for by optical delay lines with continuously variable delays. Fourth, the phase differences between two telescopes, induced by the atmosphere (piston effects), must either be accepted, which leads to a limit in sensitivity, or be monitored on a field reference star whenever possible. Each of these potential difficulties appears solvable or has already been solved on existing interferometers.

The VLT program includes[9] two additional telescopes, the Interferometric Auxiliary Telescopes, ca.2 meter in diameter, to be placed in the vicinity of the large 8 meters, to be moved on a set of fixed stations and

feeding also the common interferometric focus. These telescopes play several roles : they are available 100% of the time for interferometric use, including development of instrumentation, science programs, training and software development; they form a Sub Array which can be expanded by further addition of telescopes of the same class; they can be coupled to the 8 meters in a progressive manner, in order to fully qualify the high sensitivity obtained with the 8 meters. The overall ground configuration of the telescopes (8 meters and Auxiliaries) will be optimized to preserve the site seeing quality, and simultaneously to offer the best spatial frequency coverage (u-v coverage) in the interferometric configuration.

The interferometric focus will be equipped with beam combining optics at visible and infrared wavelengths, in order to measure the complex degree of coherence (visibility) of the light in each point of the u-v spatial frequency plane provided by the telescope arrangment and the exploration offered by the Earth rotation (aperture synthesis). It is expected that the Sub Array will begin its commissioning phase in 1996-1997, with a progressive coupling of one or more 8 meters in the year 2000.

The limiting sensitivities of the VLT Interferometric mode at infrared wavelengths are given in Table 1 in a most conservative approach. Progress in sensitivity are expected when adaptive optics and phase tracking are developing.

Table 1. The sensitivity of the VLT interferometric mode with 8-meter telescopes.

Seeing	H	K	L	M	N	Q
0.5"	11.2	12.3	10.4	8.6	7.6	5.4
	35	8	21	69	38	70
1.0"	8.9	10.1	8.5	6.7	5.8	4.5
	280	59	120	390	210	150

This Table gives the limiting magnitudes observable in the infrared with the array detectors expected in the coming years (read-out noise of 30 electrons). Values are given in magnitudes (upper line) or Janskys (lower line), and for two different seeing conditions. These numbers are conservative values, and will be improved with new methods of telescope cophasing.

CONCLUSION

The VLT concept is innovative in a number of aspects. First, it adopts the novel approach of active optics for its light-weight primary and a now mandatory approach of seeing optimization in its design and operation plan; second, its instrumentation plan incorporates the most sensitive detectors, integrated spectrographs and high resolution cameras; third, adaptive optics is included in the initial design to provide nearly diffraction-limited images whenever feasible; fourth, the array configuration is exploited in a coherent mode to achieve angular resolutions ranging from 1 to 10 milliarc sec, for a typical 100 meter baseline.

These overall capabilities should offer exceptional opportunities to extragalactic and cosmological research.

REFERENCES

1) Proposal for the construction of the 16-m Very Large Telescope, ESO, Garching, March 1987

2) Dierickx P., Enard D., Merkle F., Noethe F., Wilson R.N., 1990, S.P.I.E., **1271**, in press

3) Wilson R.N., Franza F., Noethe L., J.Mod.Optics, 1987, **34**, 485; ibid., 1987, **35**, 1427; ibid., 1989, **36**,1415, ibid., 1990, in press.

4) Tarenghi M., Wilson R.N., 1989, S.P.I.E., **1114**, 302

5) VLT Site Selection Working Group, Final Report, ESO/STC 110 Rev., 1990

6) VLT Instrumentation Plan, ESO-STC 105, 1990

7) *Diffraction Limited Imaging with Very Large Telescopes*, 1989, Alloin D., Mariotti J.-M., NATO ASI Series, Kluwer

8) Rousset G. *et al*, 1990, Astron.Astrophys. **230**, L29

9) The VLT Interferometer Implementation Plan, VLT Report 59b, ESO, Garching, Oct.1989

COSMOLOGY FROM SPACE : EUROPEAN PROJECTS

Marc Lachièze-Rey

S.Ap., CEN Saclay
91191 Gif sur Yvette cedex FRANCE

INTRODUCTION

Already in this conference, a significant proportion of the observational results presented or discussed come from spatial observations. Probably, a similar conference in ten years, for instance to celebrate the 35th anniversary of the CMB discovery, would involve an even higher proportion. I will shortly present which kind of results may be expected from space observations ; and what are the spatial projects being currently examined by the European community.

Determination of the cosmological parameters

The determination of the Hubble constant and of the deceleration parameter may benefit from various kinds of observations. In short, new kinds of objects may be used as distance indicators. Also, we will gain a better knowledge of objects already observed, up to larger distances, so that they may become efficient cosmological tools and be used for calibration.

Among expected improvements the nearest will come from the determination of new parallaxes by HIPPARCOS (presently flying). It is not certain if the HST will be able to provide new calibrations of indicators in nearby galaxies, as originally planned. Supernovae surveys would provide a class of absolute calibrators ; although there are actually several projects from ground, a spatial Schmidt telescope would be very interesting for this purpose. Also, the study of gravitational lensing may in principle allow to measure the geometry of the universe and to deduce H_0 and q_0 (as well as the dark matter). For this task a future spatial interferometer will certainly be very interesting. Simultaneous observations of the Sunyaev-Zeldovich effect and of the X-ray gas in galaxy clusters may provide their size and thus transform these objects into efficient calibrators. More generally, any class of objects observed from space may provide, if they can be selected in a sufficiently homogeneous and bias-free manner, a sample to study the geometry of the universe (infrared galaxies / X-ray quasars / X-ray clusters ....)

Deuterium and helium observations (in the UV range) will provide a better knowledge of the process of primordial nucleosynthesis and of the cosmic parameters that it helps to constrain. This is also the case for the problem of dark matter.

Formation and past evolution of objects

Probably the main output of spatial observations will concern the universe between recombination and now, a range of special interest for the study of the formation, and the first stages of evolution, of the structures that we observe now.

Such observations may be classified into three categories : 1) observations of objects that we cannot see from ground ; 2) observations providing a better knowledge, and an extension to larger redshifts, of objects that we already know ; and 3) the diffuse backgrounds.

1) The first category includes the protogalaxies and the galaxies underlying formation. Although we do not know precisely what appearance should present these objects, they will almost certainly be more prominent in non visible ranges : we could hope to detect UV light from young stars redshifted in the IR range ; also to see directly young galaxies in the UV range, if they are not too remote. We also expect to

see the thermal emission from dust [around 100μm] in the star formation regions of forming galaxies.

2) The second class involves most objects that we presently observe : ordinary and non ordinary galaxies [at any wavelength] in which we observe stellar evolution. Also hot gas in elliptical galaxies and clusters of galaxies in which the metal evolution is apparent [in X-rays]. Old stars in elliptical galaxies [observed around few μm] will provide information about the first (and following) stages of evolution of these objects.

Absorption clouds before quasars, infrared bright galaxies, remote quasars (in X-rays), X-ray clusters ... will be observed in all spectral ranges and their evolution better understood.

3) The Extragalactic backgrounds provide a very important information concerning the universe between recombination and now. They allow to test models for galaxy and structure formation. They can be formed by a superposition of sources of a type already known, or of sources of a new kind. They can also be caused by true diffuse processes (a distribution of gas or dust, or of uniformly distributed particles). In any case, we will soon or later discriminate between these possibilities. This will be of very high importance to understand the universe at high redshifts and to put constraints on the processes of formation of structures, mainly galaxies.

This will of course include the observations of CMB distortions and fluctuations [infrared, submillimetric, Sunyaev-Zeldovich effect]. But this will also concern the X-ray background (XRB) : the analysis of its spectrum and fluctuations ; and simultaneously the spectra and luminosity functions of the objects which may contribute to it (AGN's, clusters, young galaxies, objects to be discovered?). In any case, very important constraints will be derived concerning the formation of objects and the matter distribution. This is also true for the gamma-ray background. Possibly, the UV background also contains an extragalactic part which may be useful for cosmology (intergalactic gas?, decay lines?). Finally, the IR background is also full of promises, and will be covered by the ISO satellite (see the talk by C. Cesarsky in this conference).

The structure of the universe

Spatial observations will contribute to the exploration of the structure of the universe. Presently, our knowledge of the structure beyond a few Mpc comes almost entirely from optical observations. This introduces a bias of unknown characteristics and magnitude : the massive universe probably strongly differs from the visible one. It may be that the X-ray universe is less biased. In any case it is certainly differently biased so that it gives a complementary information. It will therefore be of a great importance to observe the large scale structures

(clusters, superclusters....) in the X-ray universe, as this is already started.

The new insights about large scale structures and matter distribution, obtained from the data of the IRAS satellite (see the talk by M. Davis) provide a good illustration of the usefulness of space observations. Quasars, AGN's, absorbing clouds, IR galaxies... are potential revelatories of the large scale matter distribution.

The problem of dark matter

The issue of dark matter will also largely benefit from spatial observations. Gravitational lenses [which may be observed thanks to space interferometry and spectroscopy] are useful tools in this purpose.

Space observations help to unveil the presence of gas in galaxies, clusters, and maybe in intergalactic medium [UV and X-ray backgrounds]. They also provide means of observing possible forms of dark matter in baryonic [halos of weak stars, apparent in infrared] or non baryonic [decaying particles contributing to the UV background] form. This will complement ground observations.

GAMMA RAYS OBSERVATIONS

Gamma rays allow exploration of sites with very high energy transfer. Suffering very weak absorption, they constitute potentially a very interesting cosmological window. Very few extragalactic sources have been presently observed. The majority of sources in the gamma-ray sky are galactic and/or transient. In the extragalactic sky, AGN's emit a very large proportion of their radiation in the gamma range and thus constitute very good targets.

Imagery is very important to localize these processes : The SIGMA telescope is now flying and GRO will soon begin its observations. SIGMA intends to localize sources at few arcminutes (about 4 times better than previous missions).

Gamma ray spectroscopy must wait for next missions. The study of gamma-ray lines will allow to identify the chemical elements and their characteristics and to trace nucleosynthesis.

The normal galaxies (where sources like in our own can be observed) and the clusters of galaxies are possible targets for extragalactic gamma-ray astronomy. But the AGN's are the most interesting targets since a substantial fraction of their energy is emitted around 1 MeV. Since gamma-rays are penetrating, they allow to observe their innermost regions. High energy spectra and contributions to extragalactic background would be the most direct sources of information. The Cosmic diffuse background will also be an important subject of observations. The **SIGMA** telescope (URSS+France) is now flying aboard the soviet Granat satellite. Its specificity comes from a coded mask (in tungstene) which allows a better angular resolution than

previously achieved [about 13 ' with a point source location accuracy ≈ 2'], and a position-sensitive detector with NaI (PSD). This instrumentation is protected from background radiations by various active and passive shielding devices.

Its scientific goals are mainly galactic (survey of the galactic disk : observations of compact objects, binaries, active regions ; galactic center ; transient sources...). They also include the supernova 1987 in LMC. The extragalactic goals concern active galaxies and quasars.

SIGMA already gave results for the galactic center. Hard X-rays and low energy gammas are one efficient window to observe it through the dense clouds. SIGMA made an image of the region with few arcminute resolution (march 24,1990), in the range 40-120 keV : a strong source is identified at 45' away from the very center. Recent results are being under reduction by the SIGMA team.

GAMMA RAY SPECTROSCOPY

Balloon experiments, as well as the HEAO3 and SMM missions, have discovered the 511 keV line (from positrons annihilation), and the emission at 1.809 MeV (^{26}Al) from the galactic center. This raises many questions concerning the variability, the extension (out of the galactic center?) of the sources of these lines, as well as the contribution from nucleosynthesis (novae?, supernovae?).

To explore the line emission in the galactic center, a sensitivity of 5 10^{-6} photons cm^{-2} sec^{-1} is necessary. Potentially, other lines from radioactive chains may be observed [^{44}Ti (T = 78 yrs) maps recent SN's ; and ^{22}Na the nucleosynthesis in novae].

Two different spectroscopic missions have been under study : GRASP, an European Gamma-Ray Astronomy satellite, was combining spectroscopy and imagery. But, after phase A study, it was not selected. NAE [Nuclear Astrophysics Explorer], a project from NASA + France, with a spectrometer only, is still waiting selection. But the new project INTEGRAL (ESA + US) is now under study. Presently in assessment, it will probably get phase A in 1991.

The **INTEGRAL** project [INTErnational Gamma-Ray Astrophysical Laboratory] is a Gamma-ray Astronomy mission dedicated to the high resolution spectroscopy and positioning of sources in the range 15 keV - 30 MeV It gathers on the same platform an imager and a distinct spectrometer (analog to NAE). It would provide an order of magnitude improvement or more over GRO and SIGMA ; allow line spectroscopy with unequal resolution (to resolve gamma lines) and high sensitivity.

The spectroscopic part includes nine large Germanium detectors (cooled at 85 K), surrounded by anticoincidence shield. Imagery is performed by a scintillation detector, with a mask optimized for high resolution (CsI scintillation bars viewed by photodiodes)

This will be the first imager with high spectral resolution in the gamma range. Its large spectral range (15 keV - 100 MeV) will allows a connection between X and gamma-rays. It will have high resolution spectroscopy (1000 at 1 MeV) in the range 15 keV - 1 MeV,

Besides many galactic goals (Galactic center, ISM, compact galactic objects, novae and Supernovae), it will also perform extragalactic tasks : identification of AGN's and derivation of their gamma-ray luminosity function, redshifts, spectra (especially the positron annihilation line,....). This will provide insights of the nuclear and particle interactions.

More generally, line spectroscopy allows the study of nucleosynthesis and chemical evolution, as well as cosmochronology. The possibility of Imagery coupled with spectroscopy allows mapping of the galaxy diffuse emission, and the source positioning at the arcminute level.

X-RAYS OBSERVATIONS

X-ray astronomy seems becoming a challenger to optical astronomy, when one looks at the present and future missions (here more or less in chronological order) :

ROSAT (Germany/USA)

XTE (USA) dedicated to temporal studies (5 µsec ; sensibility ≈ 0.1 mCrab)

EUVE (USA) opens the window of extreme UV.

SAX (Italy/Netherlands/ESTEC) : if launched, will allow imagery at 1' (in 0.1-10 keV) (effective surface ≈ 300 cm2), broad band spectroscopy (0.5 - 10 keV), spectral and timing measurements (millisecond to months) for bright sources.

Spectrum X (URSS/Danmark/UK/Germany/Italy/USA) will be made of 2 telescopes with large surface (2000 cm2) but low resolution (2'), with many instruments (spectrometer with semiconductor mosaic) ; 2 smaller telescopes will provide a better resolution (30")

AstroD (Japan-USA) : spectroimagery with medium resolution (0.2-10keV) with GSPC's and CCD's.

SPEKTROSAT (Germany) : very similar to ROSAT, with possibility of high resolution spectroscopy (100 at < 2 keV)

AXAF (USA) will have both good spatial (0.5") and spectral resolutions around the Fe line, thanks to cool bolometers (at 0.1 K).

XMM (ESA) is described below.

The ROSAT mission (ROentgen SATellite), now flying, will provide the first all sky survey (during 6 months) in soft X-rays (0.1 - 2 keV). Its sensitivity is 2-3 orders of magnitude better than the previous complete surveys, comparable to the sensitivity of the partial surveys of EINSTEIN (with medium resolution) and EXOSAT for small fractions of the sky. 100 000 new sources are expected to be discovered and located with an accuracy better than 1'. After the survey, pointed observations will start for guest observers.

The instrument includes a Wolter type 1 mirror system (maximum aperture ≈ 63 cm / focal length = 2.4 m), 2 redundant PSPC (Position Sensitive Proportional Counters) with sensitive area of 8 cm diameter. The HRI (High Resolution Imager), based on microchannel plates, will have a sensitive area of 2.5 cm diameter [5" of angular resolution ; no spectral resolution]. The PSPC offers an angular resolution about 30" and an energy resolution near 40%, with a sensitivity 5 times that of Einstein IPC.

The all sky survey (with PSPC) will concern all kind of objects. Many are galactic [coronal emission from stars, galactic SNR's ... ; mapping of the local ISM (XUV survey) and the more distant ISM (X-ray survey)]. It will also detect various types of AGN's (allowing to better estimate their contribution to the XRB), and intracluster gas.

The pointed observations will provide the structural, temporal and spectral characteristics of the various X-ray emitters (following EINSTEIN IPC and HRI observations). The sensitivity of PSPC is 5 times that of Einstein IPC (mainly due to the improved spatial resolution). That of the HRI (for point sources) is 3 times better than that of the EINSTEIN HRI.

The XMM mission is an ESA cornerstone, to be launched in 1998. It presents a large effective surface, and an excellent spectral resolution for soft X-rays (300 at < 2 keV).

It is made of 3 telescopes (7.5 m focal length) with 58 grazing mirrors. Its collectrice surface is very high (5000 cm^2) [4 times that of AXAF at low energy ; 10 times at ≈ 6keV, near the iron line]. It will have a good sensitivity at high energy (up to 10 keV) allowing detailed spectroscopy, or variability study of faint sources. Its eccentric orbit (T = 24 h) will allow long exposures (up to 20 h). The energy range (0.1 - 10 keV) allows the study of astrophysical plasmas above 10^6 Kelvin.

The angular resolution will reach 30", with a large field of 30' (for each telescope), allowing the study of extended sources (SNR's, clusters of galaxies). The sensitivity of the EPIC instrument (European Photon Imaging Camera, comprising 3 spectro-imagers with mosaics of CCD) will allow, in 60 000 sec , the detection of sources 2 10^{-15} erg cm^{-2} sec^{-1} in the 0.5 - 5 keV range. About 100 weak sources are expected in one field (confusion limited beyond).

The spectral resolution ranges from 8 (at 0.5 keV) to 50 (at 6.7 keV). This will allow to separate "hydrogenoid and heliumoid" lines (oxygen to iron). High spectral resolution (300 at 1.5 keV) will be also possible at < 2 keV thanks to reflection gratings.

The scientific objectives include galactic targets [stellar spectra ; spectroimagery of SNR's ; spectral variability of X-ray binaries and cataclysmic variables ; observation of isolated neutron stars ; of the galactic center].

Extragalactic observations will concern the contributions to the XRB (galactic and extragalactic), and also the study of its granularity at

an angular scale of about 1' ; the spectra of AGN's (up to z ≈ 3 - 3.5) ; the gas haloes of elliptical galaxies ; the intracluster gas and the Fe line inside clusters (evolution with z [for z<1], giving information concerning the past nucleosynthesis, the interactions of galaxies inside clusters).

ULTRAVIOLET COSMOLOGY IN SPACE

The LYMAN project will be an international observatory facility, in the spirit of the IUE mission, devoted to high resolution spectroscopy (30 000) ; its range (91.2 - 121.6 nm) is largely unexplored because of insufficient transparence of optical material and insufficient reflecting coatings. LYMAN will bring a gain by 10 000 in sensitivity, with respect to Copernicus.

This 80 cm telescope, with a prime spectrograph (dual echelle type ; effective area ≈ 100 cm^2) will provide very high spectral resolution (30 000 in the far UV from 90 to 120 nm), allowing to detect weak narrow IS absorption lines, and to split between Lyman lines of H and D. It has also a secondary Extreme UV spectrograph (10-90 nm), with low spectral resolution and imagery capacity.

The spectral range of LYMAN concerns the plasmas and chemical elements at 10^5 -10^6 K. It contains most important transitions of atomic and molecular hydrogen and deuterium, and numerous resonance lines of other abundant elements in various stages of ionization. The scientific goals of LYMAN, concerning cosmology, will be mainly : the deuterium abundance in local galaxies and galactic halos, as well as in intergalactic medium (in front of AGN's) ; and the helium abundances in front of AGN's (z ≈ 2)

This will provide information concerning the primordial nucleosynthesis (and thus the derived constraints on cosmological parameters), and the cosmic story of these elements (the history of nucleosynthesis in the Universe)

Of more indirect concern for cosmology, the study of the H_2 molecule [in galactic sources like planetary atmospheres, dense galactic clouds, star forming regions] will help to understand better the process of star formation. Also, the study of ionized oxygen (and other atoms, ions and molecules) will increase our knowledge of hot plasmas, and thus help to understand the origin of excitation in AGN's.

Absorption observations will be possible in front of stars or quasars, allowing the study of haloes of galaxies, absorbing clouds ; and to study the ionization of the IGM at high redshift (HEII Gunn-Peterson test in z ≈ 2 quasars). It will also allow to observe the interstellar medium of our and external galaxies. Finally, LYMAN will be able to observe almost all kinds of astronomical objects

Another project [**CUBE**] is devoted to spectroscopy of the diffuse background in the far UV (90-200 nm). This background includes many galactic contributions, like retrodiffusion by dust ; emission from hot gas ; H_2 fluorescence and emission lines from shocks. Extragalactic

contributions are badly known. They possibly include : radiative decay of particles ; resonance lines of IGM at 10^3-10^5 K [H Lyα at 121.6 nm and HeII at 30.4 nm ; redshifted, but probably very weak if IGM is ionized by quasars] ; galaxies on the line of sight ; a possible contribution by forming galaxies ($z \approx 3$) in the extreme UV (30 nm), if it can be seen through the neutral gas of these objects.

The high resolution (0.1 nm) will allow to separate the lines. Observations at low resolution and high sensitivity will allow the study of the continuum. This instrument would also permit the spectroscopy of weak and extended objects (galaxies, disks, cooling flows in clusters).

COSMOLOGY IN THE SUBMILLIMETRIC RANGE

It covers the decade 100 μm to 1 mm, between IR and millimetric and the relevant information is potentially comparable to the UV+visible range. This is the last unexplored important part of the spectrum (because of atmosphere opacity, only few windows being observable from ground ; and of the difficult detector technology). For this range, a large passively cooled antenna is most efficient than a cryogenic small telescope.

ESA prepares the big project FIRST (large deployable antenna ; comparable to LDE). Before that, the french balloon project PRONAOS has been selected to dynamize the submmillimetric community and to prepare FIRST. Another project - the NASA submillimetric explorer - is under discussion.

Scientific interest of submillimetric : the cold universe:

The submillimetric concerns many galactic fields : the abundances of molecules in the ISM, including cosmologically significant species like HD and LiH ; the identification of large molecules and/or grains (dust at $10 < T < 1000$ K provides the largest part of ISM energy) : the exploration of dense phases of ISM and star forming regions, like protostellar condensations, shocked regions in molecular clouds, protoplanetary disks, stellar regions...

For extragalactic research, the CMB is the most important target. Galaxies are also relevant to this range : star formation in external galaxies [spectroscopy and mapping of molecular and atomic lines] ; study of IRAS galaxies [with good spatial resolution and sensitivity] ; evolution of high z galaxies ; galaxy clusters, quasars , AGN...

The submillimetric spectroscopy (300 GHz $< \nu <$ 1000 GHz) mainly concerns the ISM in our and external galaxies. Many lines of specific transitions interesting ISM [CI, CII, OI may unveil the kinematics of far galaxies]. Rotation lines of light molecules allow the exploration of the dense and hot phases of ISM [water / HD].

Continuum observations allow to explore the regions of thermal dust (star formation regions ; AGN's) and the condensations in molecular

clouds. This domain is also well adapted to the study of protoplanetar disks. The imagery of nearby galaxies will unveil their structure and the distribution of star formation...(100 μm) ; also for AGN's and IRAS galaxies. The detection of galaxies at $z \approx 3$ (5 mJy at 350 μm) will help to better understand evolution effects. Finally the study of the submillimetric background and its angular fluctuations will be very important.

The FIRST project (Far Infrared and Submillimeter Space Telescope) will probably be selected in 1992 as the third ESA cornerstone, to fly around 2003. It has a big deployable antenna (between 4 m and 8 m) and will operate at 0.1 - 1 mm, with high efficiency heterodyne spectroscopy. The cooling will be ensured by a mechanical cooler or a large cryostat.

The LDE (Large Deployable Reflector) project of the NASA involves a still larger deployable antenna (20 m).

PRONAOS (France) is a 2m pointed telescope (balloon borne), with the main goal to prepare the technology of large spatial light reflectors. It comprises a multiband photometer (200 μm to 1.5 mm) with helium cooled bolometers, an heterodyne spectrometer (R=106). It will fly 20 h, with 5" pointing ability.

The Submillimetric explorer is an other possible project, (NASA+France), intermediary before large antennas (FIRST, LDE), following PRONAOS. Its 2 goals would be : a complete spectroscopic survey of a large number of sources (100 - 500 μm) ; and the ability of very sensitive (better than ISO or SIRTF), good resolution (6" at 100 μm) imaging of continuum radiation.

The 4 m non deployable mirror would be passively cooled with superconducting detectors (SIS) and bolometers at the cryogenic focal plane. Incoherent and heterodyne spectroscopy would be available.

The targets would be : dust with large column density in galaxies or AGN's ; star forming regions and molecular clouds in nearby galaxies ; protoplanetar disks ; AGN's and IRAS galaxies ; detection of galaxies at $z \approx 3$ [5 mJy at 350 μm], and study of evolution effects ; observations of the submillimetric background and its fluctuations.

Finally it may be useful to mention the project **QUASAT** devoted to radio interferometry in space. Many possible observations would be of interest for cosmology. Concerning the AGN's, QUASAT may help to answer the following questions : the nature of the compact radio-sources and of the central engine ; the physics of jets and relativistic motions ; the origin of the radio continuum and of the optical broad line emission ; the cosmological evolution of compact sources ; the origin of the synchrotron radiation, and the inverse Compton emission. QUASAT will also observe extragalactic masers in the arms and nuclei of nearby spiral galaxies. There is substantial hope that these objects may then be

used as distance indicators (the study of proper motions may be of interest for this task).

CONCLUSION

A potential information will become available in new domains, which is, quantitatively and qualitatively comparable to that already at our disposal in the visible range. It will be for instance possible to observe in X-rays with the same precision that very recently in optical (also think to spatial interferometry). As a personal opinion I would emphasize the following points which seems particularly promising :

A better knowledge of the backgrounds (luminosity, spectra and fluctuations) will teach a lot about the universe between decoupling and now.

A better knowledge of clusters of galaxies will provide information about the cosmological parameters (SZ effect) ; the structure of the universe (complete samples) ; the dark matter (gas in gravitational potential) ; the evolution of galaxies and clusters.

New objects, homogeneous samples of already known objects, new (bias free?) calibrations will probably permit a better exploration of the structure of the universe.

Observations of various components of galaxies and active objects, at various stages of their evolution will help to understand their formation and evolution.

useful references :

The high throughput X-ray mission XMM A. Peacock and J. Ellwood Space Science Review **48** (1988) 343-365

Medium-Sized astronomy Missions under Study for ESA's Horizon 2000 Programme, S. Volonté, ESA bulletin **51**, p.22

European Space science, Horizon 2000, ESA publications SP-1070, December1984

European Space science, Horizon 2000, report of the Survey Committee, ESA publications, 1984

ESA's Report to the 28th COSPAR Meeting, ESA publication SP-1124, May 1990

Space Astronomy and Solar System exploration, ESA publication SP-268, May 1987

Report on ESA's Scientific Satellites, ESA publication SP-1110, May 1989

Séminaire de Prospective du CNES, Deauville, octobre 1985, CNES, 1985

Catherine Cesarsky, Michel Spiro and Lucienne Norry

THE INFRARED SPACE OBSERVATORY

Catherine J. CESARSKY
Service d'Astrophysique/CE-SACLAY
91191 Gif sur Yvette Cedex, France

The Infrared Space Observatory (ISO), a fully approved and funded project of the European Space Agence (ESA), is an astronomical satellite, which will operate at wavelengths from 3-200 µm. ISO will provide astronomers with a unique facility of unprecedented sensitivity for a detailed exporation of the universe ranging from objects in the solar system right out to distant extragalactic sources. The satellite essentially consists of a large cryostat containing at launch about 2300 litres of superfluid helium to maintain the Ritchey-Chrétien telescope, the scientific instruments and optical baffles at temperatures between 2K and 8K. The telescope has a 60-cm diameter primary mirror and is diffraction-limited at a wavelength of 5 µm. A pointing accuracy of a few arc seconds is provided by a three-axis-stabilisation system consisting of reaction wheels, gyros and optical sensors. ISO's instrument complement consists of four instruments, namely : a camera (3-17 µm), a short wavelength spectrometer (3-45µm), a long wavelength spectrometer (45-180 µm) and a photo-polarimeter (3-200µm). These instruments are being built by international consortia of scientific institutes and will be delivered to ESA for in-orbit operations. ISO will be launched in 1993 by an Ariane 4 into an elliptical orbit (apogee 70000 km and perigee 1000 km) and will be operational for at least 18 months. In keeping with ISO's role as an observatory, two-thirds of its observing time will be made available to the european and american astronomical community.

INTRODUCTION

The Infrared Space Observatory (ISO), is a fully approved mission, currently under development by the European Space Agency. ISO was selected in 1983, just as the first data sent by the IRAS satellite was reaching the earth. IRAS has demonstrated the great advantage of space cryogenic missions for infrared astronomy : by getting rid of the absorption and emission of the earth atmosphere, and by limiting the emission from the telescope and the instruments, cooled down to superfluid helium temperature, it becomes possible to explore the infrared universe in unprecedented ways. Throughout its 10 months lifetime, IRAS has surveyed the whole sky in four wide bands around 12, 25, 60 and 100 μm. IRAS has revealed the richness of the infrared sky, and shown the relevance of infrared observations for the study of virtually all branches of astrophysics, from comets and interplanetary phenomena to galaxies and cosmology. Many unexpected discoveries were made : cometary trails, dust disks around main sequence stars, large number of bright IR stars in the galactic bulge, diffuse emission of the interstellar medium at 12 and 25 μm, ultrabright infrared galaxies.. Exciting as they are, the IRAS results suffer from many limitations, which most often make it difficult to interpret them unambiguously through physical models. We are left wondering about the emissivities of IRAS sources in the wavelength ranges outside the IRAS bands ; we would like to know in more detail the spatial and spectral distribution of the radiation, in some cases its degree of polarization ; and of course we would welcome an increment in sensitivity to be able to detect remote bright sources, such as far away starburst galaxies, and to explore better the realm of intrinsically faint sources, such as brown dwarfs.

Hence the necessity of a versatile mission such as the Infrared Space Observatory, with a wider wavelength coverage (2.5 to 200 μm), improved angular resolution (by a factor of about 10), and enhanced sensitivity (by 2 to 3 orders of magnitude), a variety of spectral resolutions and polarimetric capabilities. With ISO, it will be possible for the first time to image the infrared sky from space with array detectors at various spatial resolutions, and to draw medium ($\Delta\lambda/\lambda$~200 to 1000) and high resolution ($\Delta\lambda/\lambda$~10^4 to 3.10^4) spectra over the range 3 μm to 180 μm. ISO will help to elucidate many of the problems revealed by IRAS, and the potential for discovery is clearly high as well.

SATELLITE AND MISSION DESIGN

The satellite[4], consisting of a payload module and a service module, is 5.3 m high, 2.3 m wide and will weigh around 2400 kg at launch. The basic spacecraft functions such as data handling, power conditioning, telemetry and telecommand, and attitude and orbit control are provided by the service module. The nominal down-link bit rate is 33 kbps of which about 24 kbps are dedicated to the scientific instruments.

The payload module (figure 1) is essentially a large cryostat. Inside the vacuum vessel is a toroidal tank filled with about 2300 litres of superfluid helium, which will provide an in-orbit lifetime of at least 18 months. Some of the infrared detectors are directly coupled to this helium tank and are at a temperature of around 2K. Apart from these, all other units are cooled using the cold boil-off gas from the liquid helium. Mounted on the outside of the vacuum vessel is a sunshield, which prevents the sun from shining directly on the cryostat. The solar cells are carried by this sunshield.

Suspended in the middle of the main helium tank is the telescope, which has a Ritchey-Chrétien configuration with an effective aperture of 60cm and overall f/ratio of 15. A weight-relieved fused-silica primary mirror and a solid fused-silica secondary mirror have been selected as the telescope optics. The optical quality of these mirrors is adequate for diffraction-limited performance at a wavelength of 5μm. Stringent control of straylight, particularly from bright infrared sources outside the telescope's field of view, is necessary in order to ensure that the system sensitivity is not degraded. This control is accomplished by imposition of viewing constraints and by means of the sunshade, the Cassegrain and main baffles, and an additional light-tight shield around the instruments.

The scientific instruments are mounted on the opposite side of the optical support structure to the primary mirror, each one occupying an 80° segment of the cylindrical volume available. The 20 arc minute total unvignetted field of view of the telescope is split up between the four instruments by a pyramidal mirror. Thus, each instrument simultaneously receives a 3 arc minutes unvignetted field centred on an axis at an angle of 8.5 arc minutes of the telescope optical axis; to view the same target with different instruments, the satellite has to be repointed.

ISO will be launched by an Ariane-4 rocket. Its orbit will be elliptical, with an apogee height of 1000 km and a perigee height of about 70000 km.

SCIENTIFIC INSTRUMENTS

The ISO scientific payload consists of four instruments which although being developed separately, have been designed as a package to offer complementary facilities to the observers. Each instrument is being built by a consortium of scientific institutes using national non-ESA funding and will be delivered to ESA for in-orbit operation. Details of the individual instruments and of their capabilities are given in table 1. The four instruments view different adjacent patches of the sky, but, in principle, only one will be operational at a time. However, when the camera is not the prime instrument, it can be operated in a so-called parallel mode, either to gather additional astronomical data or to assist another instrument in acquiring and tracking its target. In order to maximise the scientific return of the mission, the ISOPHOT instrument will be operated during as many satellite slews as possible so as to make a partial sky survey at a wavelength of 200 μm, a region not explored by IRAS.

The ISOCAM (figure 2) instrument[1] consists of two optical channels, each with a 32x32 element detector array, operating in the wavelength ranges 2.5-5.5 μm and 4-17 μm. The short wavelength array uses an InSb detector with a CID readout and the long wavelength detector is made of Si:Ga with a direct read out (DRO). Each channel contains a wheel for selecting various filters (including circular variable filters, CVF, with a resolution of 45) and a second wheel for choosing a pixel field of view of 1.5, 3, 6, or 12 arc secs. Polarisers are mounted on an entrance wheel common to both channels. A sixth wheel carries mirrors for selecting between the channels, of which only one is operational at a time.

The LWS (fig. 3) instrument[2] consists of a reflection diffraction grating used in 1st and 2nd order with an array of 10 discrete detectors to provide a spectral resolving power of ~200 over the wavelength range from 45 μm to 180 μm. The detectors are made of Ge:Be and Ge:Ga (stressed and unstressed) material. Two Fabry-Pérot interferometers are mounted in a wheel and either can be rotated into the beam to increase the resolving power to ~10^4 across the entire wavelength range.

The SWS (figure 4) instrument[3] provides a resolving power of between 1000 and 2000 across the wavelength range from 2.4 μm to 45 μm by means of two reflection diffraction gratings used in 1st, 2nd and 3rd orders. Filters for order-sorting are placed at the instrument's various entrance apertures. Detectors made from InSb, Si:Ga, Si:P and Ge:Ga material are used . Over a part (14-30 μm) ofthe SWS's operating range, the resolution can be increased to ~$2x10^4$ by directing the incident radiation through either of two Fabry-Pérot interferometers.
The ISOPHOT (figure 5) instrument[5] consists of three sub-systems :

. ISOPHOT-C : a photopolarimeter which also provides imaging capability at close to the diffraction limit in the wavelength range from 40μm to 200μm.

. ISOPHOT-P : a multi-band, multi-aperture photopolarimeter for the wavelength range from 30 μm to 110 μm.

. ISOPHOT-S : a dual grating spectrophotometer which provides a resolving power of ~ 90 in two wavelength bands simultaneously (2.5-5 μm and 6-12 μm).

A focal plane chopper with a beam throw of up to 3' is also included in ISOPHOT. Selection between the different modes of the various sub-systems is achieved with appropriate setting of three ratchet wheels. ISOPHOT contains several types of infrared detectors made of Si:Ga and Ge:Ga (stressed and unstressed). These detectors are read out by specially designed cryogenic electronics, which exists in both multiplexed and "un-multiplexed" versions.

ISO OBSERVATIONS

The two thirds of ISO's observing time will be available to the scientific community via the submission and selection (by peer review) of proposals. In addition to this Open Time, there will also be Guaranteed Time for the groups who provide the instruments, for the five Mission Scientists (T. Encrena, H. Habing, M. Harwit, A. Moorwood, J.L. Puget) and for the Observatory Team, who will be responsible for all scientific operations. For most of the mission (at least 15 months), 65% of the time will be open time.

The programme to be carried on during the guaranteed time is currently being defined by the instrument groups, the mission scientists and the ESA Project Scientist (M. Kessler). It will include a number of fundamental observations which may require long observing times, but which are indispensable outputs of a mission such as ISO. For example, complete spectra of a number of bright objects will be drawn over the whole range available to ISO ; these will allow to explore unknown wavelength domains and will be used as templates for more reduced observations of fainter sources. Low resolution spectra of the diffuse interstellar medium at wavelength below 15μm will be obtained with the ISOCAM CVF and/or with ISOPHOT-S ; in this way, it will be possible to test the hypothesis that this emission is due to the same kind of very small grains or large molecules that emit bright "unidentified" lines in reflexion or planetary nebulae. Star formation regions will be mapped with various ISOCAM filters and in fine structure lines (CII and OI) with the long wavelength spectrometer, to study both star formation processes, and the structure of molecular clouds. The distribution of the main constituents of comets will be determined, and the deuterium abundance of Uranus and Neptune will be measured precisely, with the consequent cosmogonical implications. There will be a variety of programmes on normal galaxies, studying the dust in them through their far infrared emission, the distribution and excitation of very small grains and PAH, molecules which emit mid infrared photons, the cooling of the gas through the emission of far IR fine structure lines, the chemical abundances, the regions of star formation, the nuclei at various wavelengths.

The programs with greatest cosmological significance are likely to be the deep surveys that ISOCAM and ISOPHOT will carry out in chosen regions of the sky, devoid of cirrus ; the aim is to establish the luminosity fnction of galaxies and active nuclei in spectral intervals where it is unknown at present.

The waveband of the ISOCAM long wavelength channel is particularly well suited for the study of faint active galactic nuclei ; this mid-infrared range may be in fact the only one where it is possible to pick out the nuclear component, unhampered by the stellar and dust emission from the galaxy[6]. The deep surveys in empty fields will be complemented by deep survey of clusters of galaxies, up to z~1. The results will be useful for studies of galaxy evolution, and in particular for an assessment of the frequency of galaxy encounters and starbursts at various epochs in various environments.

ISOCAM and ISOPHOT may also be useful to measure the intensity and granularity of the infrared background. Finally, ISOCAM may detect brown dwarfs in the solar neighborhood, or, at least, set meaningful upper limits on their number.

The first call for Observing Proposals will be issued 18 months before launch. It will contain details of expected instrument performances and the program for the guaranteed time, and will sollicit proposals for observations to be carried out in the period from 3 to 10 months after launch.

CONCLUSION

ISO is a fully-approved and funded mission, which will offer astronomers unique and unprecedented observing opportunities at infrared wavelentths from 2.5-200 μm for a period of at least 18 months. Two thirds of the observatory's time will be available to the european and american astronomical community. Both the spacecraft and its selected complement of instruments are in their main development phase and the launch will take place in 1993.

REFERENCES

1) Cesarsky, C., Sibille, F. and Vigroux, L., "ISOCAM, a camera for the Infrared Space Observatory", New technnologies for Astronomy, Proc. SPIE **1130**, 202-213 (1989)

2) Emery, R.J. et al., "The Long Wavelength Spectrometer (LWS) for ISO", Proc. SPIE **589**, 194-200 (1985)

3) De Graauw, Th. et al. "The ISO Short Wavelength Spectrometer", Proc. 22nd ESLAB Symposium on Infrared Spectroscopy in Astronomy, ESA SP-290, 549-551 (1989)

4) Kessler, M.F., "The Infrared Space Observatory (ISO) and its instruments", New technologies for Astronomy, Proc. SPIE **1130**, 194-201 (1989)

5) Lemke, D., Burgdorf, M., Hajduk,Ch., and Wolf, J., "Dectectors and Arrays of ISO'S Photopolarimeter". New technologies for Astronomy, Proc. SPIE **1130**, 222-226 (1989)

6) Spinoglio, L. and Malkan, M.A., Ap. J. 342, 83, 1989.

Characteristics of the Instruments

Instrument and Principal Investigator	Main Function	Wavelength (Microns)	Spectral Resolution	Spatial Resolution	Outline Description
ISOCAM (C. Cesarsky, CEN-Saclay, F)	Camera and Polarimetry	3 - 17	Broad-band, Narrow-band, and Circular Variable Filters	Pixel f.o.v.'s of 1.5, 3, 6 and 12 arc seconds	Two channels each with a 32x32 element detector array
ISOPHOT (D. Lemke, MPI für Astronomie, Heidelberg, D)	Imaging Photo-polarimeter	3 - 200	Broad-band and Narrow-band Filters. Near IR Grating Spectrometer with R=100	Variable from diffraction - limited to wide beam	sub-systems: i) Multi-band, Multi-aperture photo-polarimeter (3-110 μm) ii) Far-Infrared Camera (30-200 μm) iii) Spectrophotometer (2.5-12 μm)
SWS (Th. de Graauw, Lab. for Space Research, Groningen, NL	Short-wavelength Spectrometer	3 - 45	1000 across wavelength range and $3x10^4$ from 15 - 30 μm	7.5x20 and 12x30 arc seconds	Two gratings and two Fabry-Pérot Interferometers
LWS (P. Clegg, Queen Mary College, London, GB)	Long-wavelength Spectrometer	45-180	200 and 10^4 across wave-length range	1.65 arc minutes	Grating and two Fabry-Pérot Interferometers

Table 1

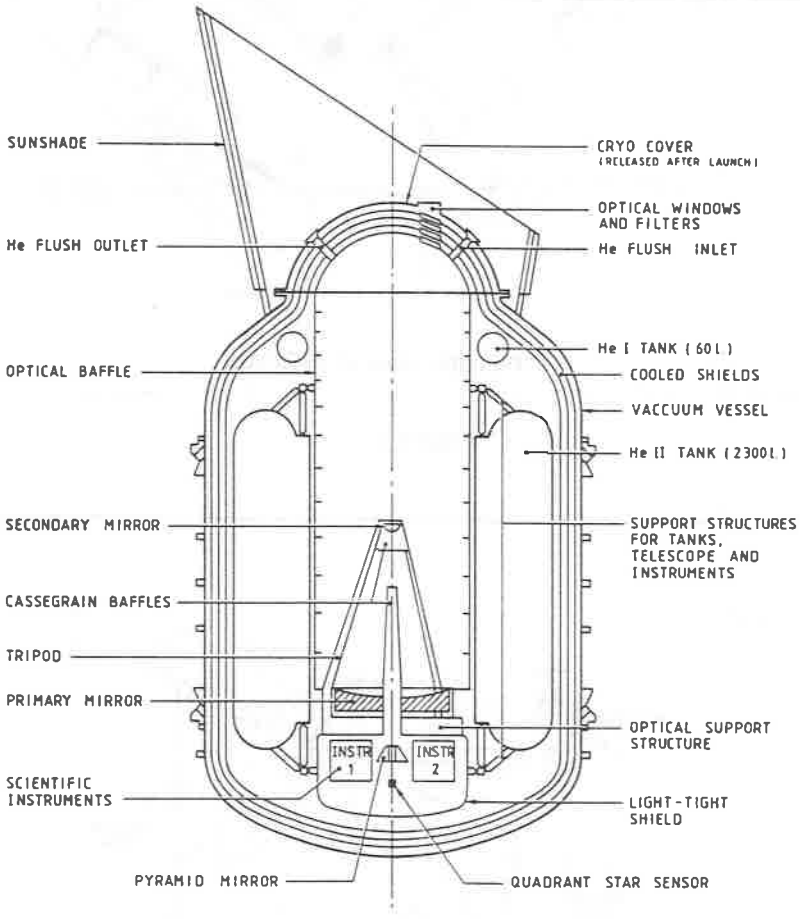

Schematic Diagram of Payload Module.

Figure 1

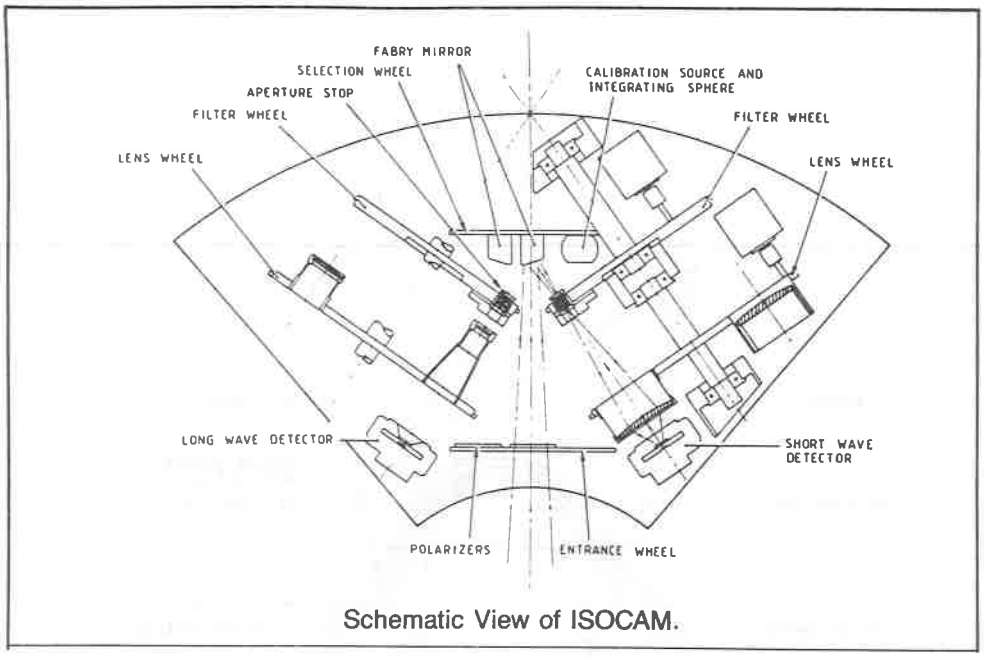

Schematic View of ISOCAM.

Figure 2

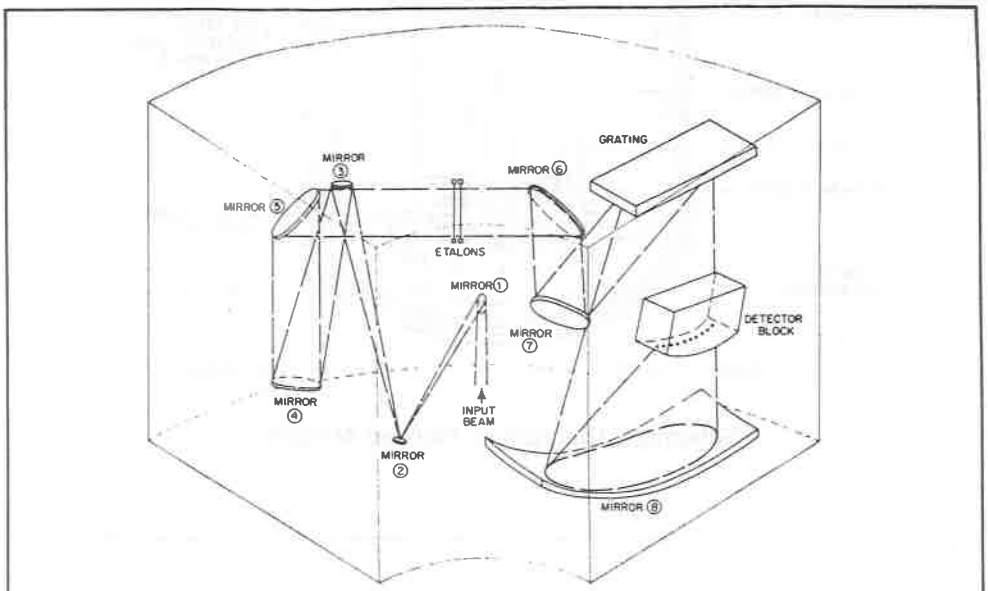

Schematic View of LWS.

Figure 3

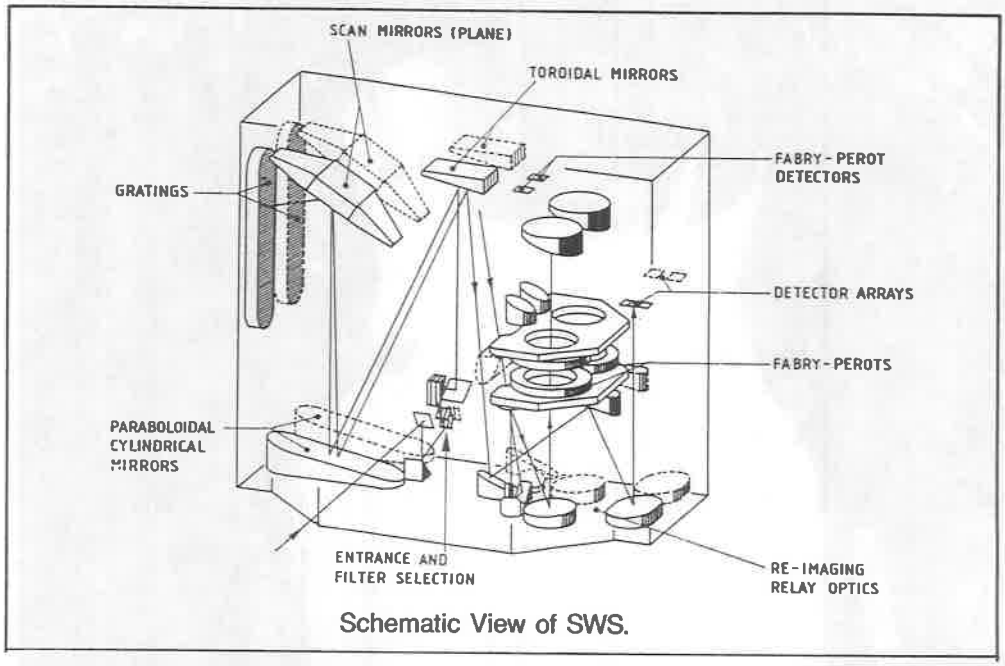

Figure 4

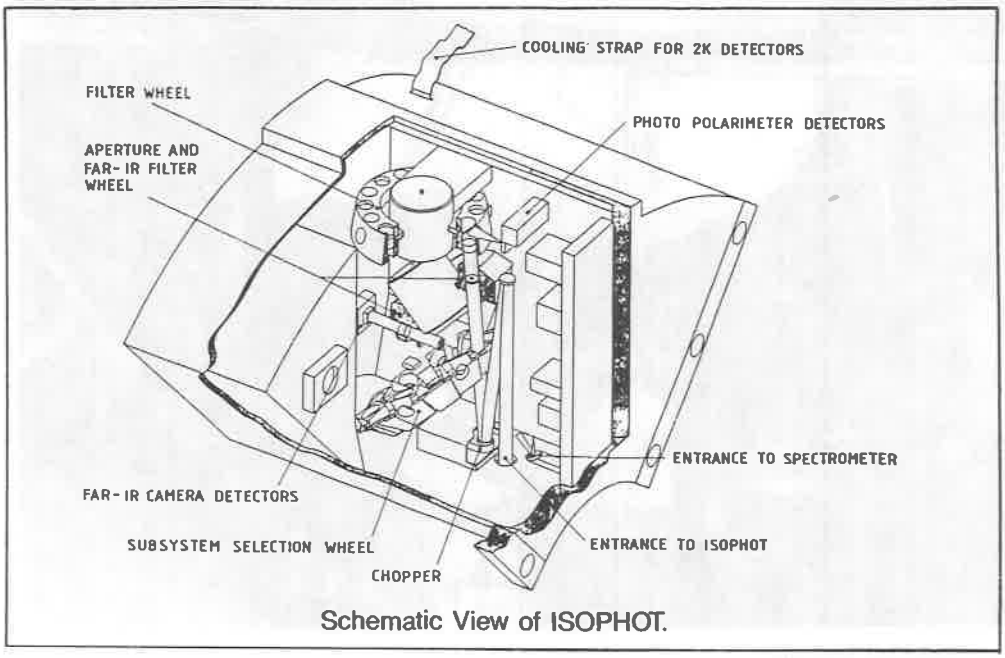

Figure 5

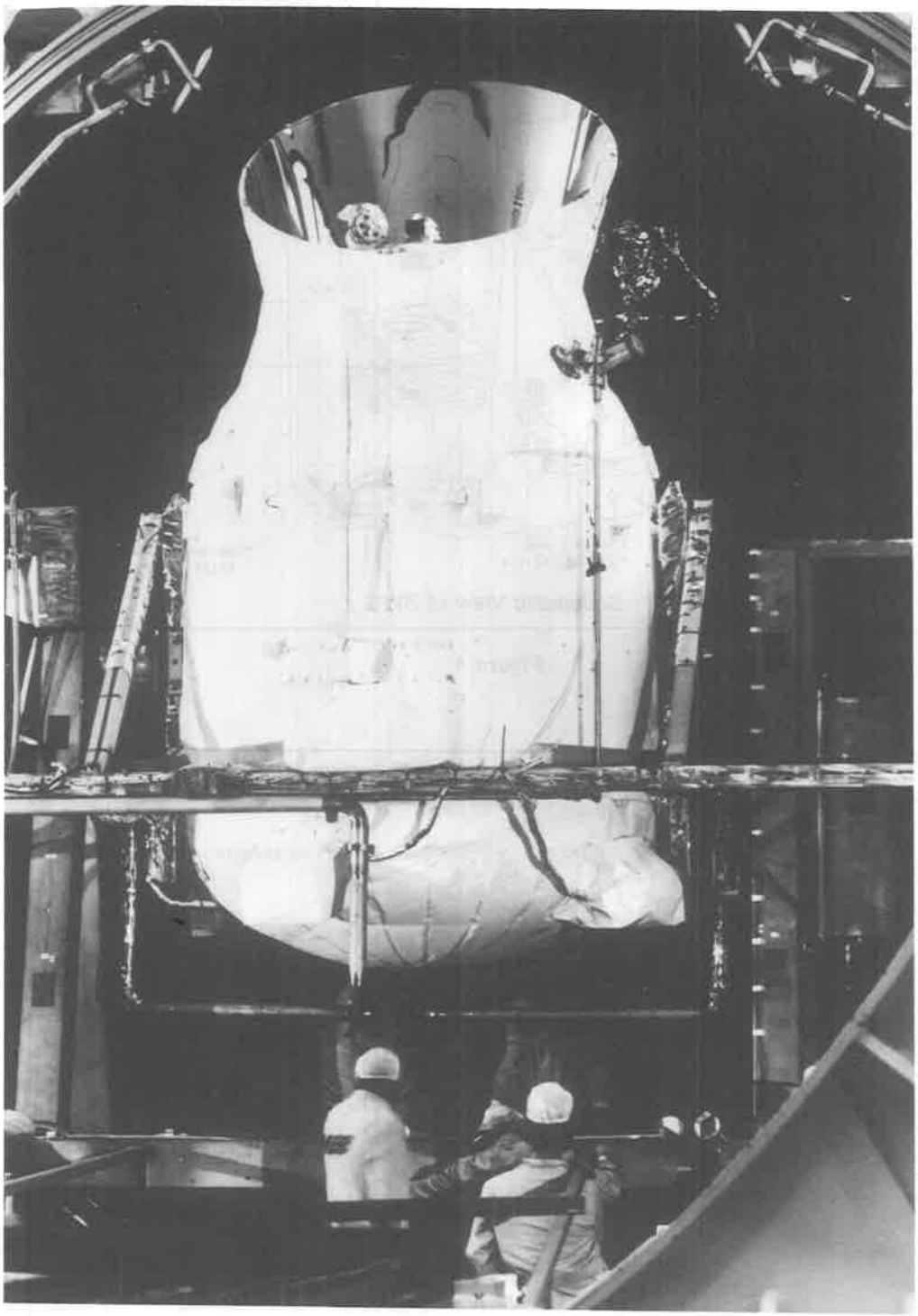

ISO payload module

ISOCAM qualifaction model

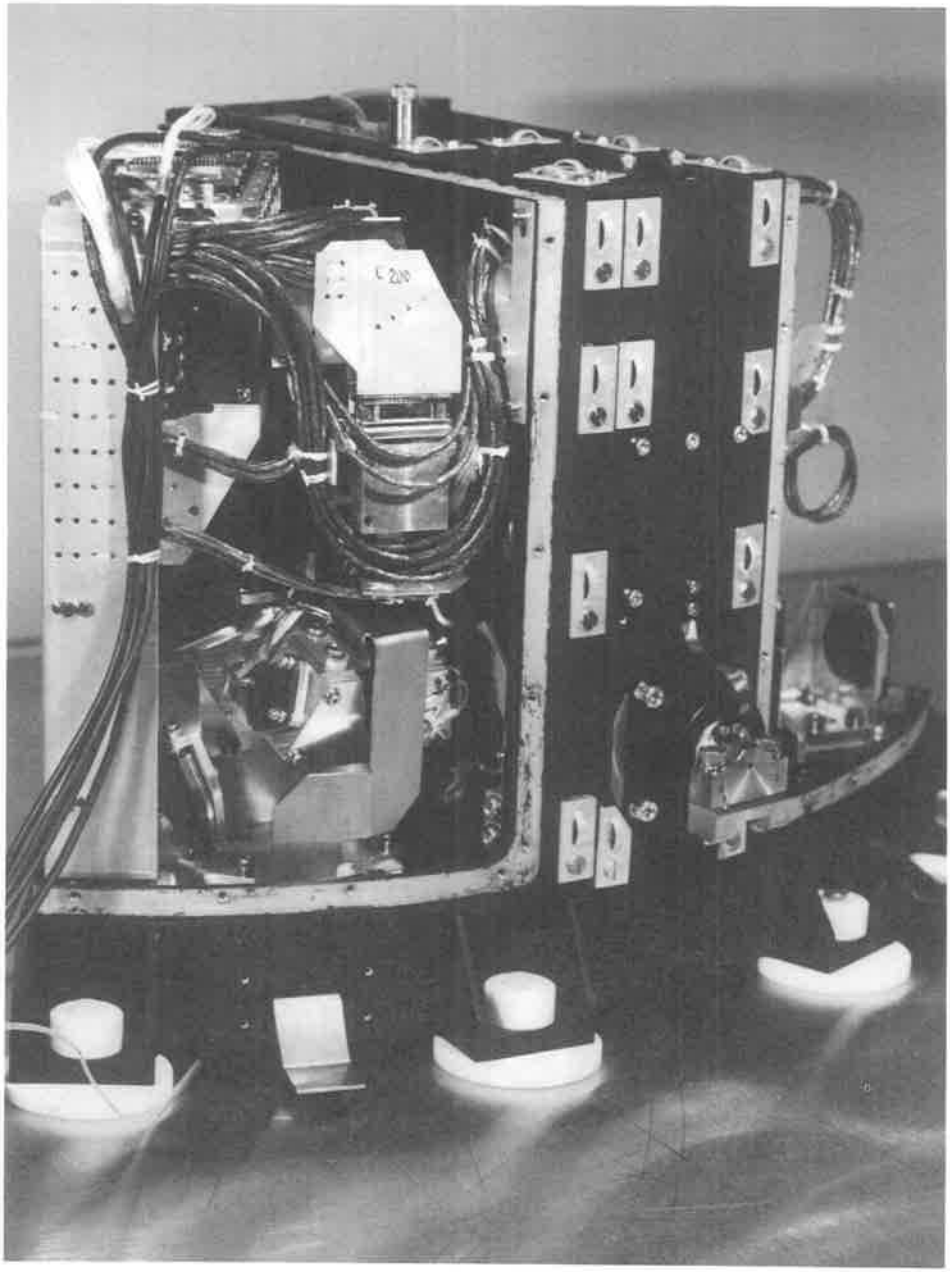

ISOPHOT qualifacation model

GROUND BASED OBSERVATIONS OF COSMOLOGICAL BACKGROUNDS

P. de Bernardis, M. De Petris, S. Masi, B. Melchiorri* and F. Melchiorri
Dipartimento di Fisica - Università "La Sapienza" - P.le A.Moro,2 - I00185 - Roma - ITALY
* Istituto di Fisica dell'Atmosfera - C.N.R. - P.le L.Sturzo,31 - I00144 - Roma - ITALY

ABSTRACT

We study in this paper the role of ground based millimetric telescopes in the Cosmic Background Cosmology. We describe an experiment consisting in a telescope and a detector devoted to the study of mm and sub-mm cosmic backgrounds. Maximum sensitivity has been obtained using incoherent detectors with a throughput of $\sim 1 cm^2 sr$. Beam switching and a two wavelengths correlation technique are used to avoid fluctuating gradients of atmospheric emission.

TARGETS OF MM and SUB-MM COSMOLOGY

Two main targets can be individuated which are suitable to be studied by millimetre and sub-millimetre ground based telescopes: the anisotropies of the Cosmic Background Radiation (CBR) and the anisotropies in the background generated by unresolved extragalactic sources. There is no need to repeat here the importance of a detection of CBR anisotropies; we only have to recall the relation between the observable quantity, which is the power on the detector ΔI, and the relative fluctuations of the CBR temperature field $\Delta T/T$:

$$\Delta I_{CBR} = A\Omega \cdot BB(T_{CBR}) \frac{xe^x}{e^x - 1} \frac{\Delta T_{CBR}}{T_{CBR}} \tag{1}$$

where $A\Omega$ is the detector throughput, $x = hc/kT\lambda$, and BB is the Planck function. The spectrum of ΔI_{CBR} is plotted in fig.1.

Outside our galaxy, other sources of submm radiation are present, mainly galaxies (active and not) and QSOs. The fluctuations in the detected signal due to unresolved sources (US) could limit, in principle, the search for CBR anisotropies in an apparently empty deep sky region. On the other hand, the detection of these fluctuations should provide important information on the early evolution of galaxies and QSOs. A theoretical estimate[1)] of the mm and submm fluctuations has been performed using galaxies with dust thermal emission to compute the fluctuation level σ at wavelengths shorter than 1.5 mm which are of interest here. This estimate is quite preliminary, because the catalogue of observations of these sources in the mm/submm region is quite poor. Non-evolving spirals, evolving ASF and Seyferts have been used. In fig.2 we plot the expected signal ΔI_{US} detectable using telescopes with different sizes: these estimates have been obtained from the formula

$$\Delta I_{US} = A\Omega \cdot BB(T_{CBR}) \left.\frac{\Delta T}{T}\right|_{US} \frac{xe^x}{e^x - 1} \tag{2}$$

where $\Delta T/T_{US}$ has been estimated from the model[1)]. We consider a survey for deep sky submm emitters necessary, as a key program for the new generation of ground based large telescopes.

The spectrum of CBR anisotropies is compared to the spectrum of atmospheric emission in a high mountain site in fig.1. It is evident that three millimetric windows are present, where a large fraction of the CBR anisotropy power can be detected from the ground: the windows are located in the bands $(2.4 \div 3.5)\ cm^{-1}$, $(4.4 \div 5.6)\ cm^{-1}$, $(6.7 \div 10.2)\ cm^{-1}$, and the fractions of power available are 4%, 10%, 32% respectively. In order to collect energy from the CBR anisotropy spectrum efficiently, wide band bolometric detectors with mesh

filters matching the atmospheric windows must be used. A large throughput $A\Omega$ is also useful, to get maximum sensitivity for diffuse radiation. These two requirements, however, increase the background level on the detector, thus degrading its responsivity. Therefore, we must look for the best compromise between high responsivity and large powers on the detector. In other words we have to maximize the detected signal $S = R(B) \cdot \Delta I$, where R is the detector responsivity, which is a function of the background B from the optics and the atmosphere, and ΔI is the signal from CBR anisotropies. Using the spectra plotted in fig.1 for the atmosphere and the CBR anisotropies, we have maximized the signal S under variations of bandwidth and throughput $A\Omega$. Using the best possible NEP of a bolometer[2)] optimized for work at 0.3 K, with a modulation frequency higher than 5 Hz, and a site with 1 mm of precipitable water vapour (pwv), it is possible to compute the S/N ratio for observation of CBR anisotropies (with $\Delta T/T = 10^{-5}$ and 1 s of integration time). This is plotted in fig.3 for different bands as a function of the throughput. Since the power from diffuse radiation increases linearly with throughput, while the NEP increases quite slowly, it is evident that large throughput bolometers have to be preferred. The maximum value of the throughput is constrained by other parameters depending essentially on telescope optimization: the size of the focal plane region free from excessive aberrations; the maximum beamsize compatible with the beam switching amplitude etc.. We also have to take into account the fact that the CBR anisotropy level expected in standard scenarios[3)] is an increasing function of the angular scale: this is another reason for preferring large values of the throughput. On the other hand, atmospheric noise increases with angular scale too: this effect limits the ratio between modulation amplitude and beamsize (and, as a consequence, the $A\Omega$) if correction methods are not available to avoid it. We will discuss this problem later.

Following the previous arguments, we have decided to optimize our telescopes in order to use a detector throughput which is as large as possible, and minimize atmospheric fluctuations using a correlation technique.

ATMOSPHERIC EMISSION FLUCTUATIONS IN THE MM-SUBMM RANGE

Atmospheric fluctuations can represent the main source of noise in ground based searches for CBR anisotropies at mm wavelengths. Their level is widely variable and depends on many parameters, the most important being the precipitable water vapour (pwv) content ant its variability. Little data has been published on this topic [4,5,6,7)] but it is a common experience that submm and mm observations must be carried out from very cold and dry sites, with $pwv \lesssim 1mm$. Moreover, the fluctuation level increases strongly with the angular scale of

the modulation, being irrelevant for large telescopes with few arcsec beams[8], and dominant for beams larger than 1^o. A correlation technique taking advantage of the simultaneous observation of 2 or more wavelengths has been proposed by some groups[7,9,10]. In order to have this technique working well, it is important that the two considered wavelengths have comparable absorption in the atmosphere: in this way the two detectors sample the same depth in the atmosphere and are equally sensitive to uncorrelated fluctuations occurring at different heights. This is not the case if one of the detectors is observing an atmospheric line while the other is matched to an atmospheric window. A simple analysis of the line profile formulas[10] shows that the previous condition is fullfilled if the two observation wavelengths are symmetrically displaced with respect to the centre of the emission line. However the atmospheric emission spectrum results from the overposition of a large numer of lines from H_2O, O_2 and O_3, and a numerical simulation is required in order to decide which is the best pair of wavelengths to use. We used the atmospheric model of Liebe[11]: this has been widely tested[12,13] and is a good description of the atmospheric emission in the wavelength range of interest here. We divided the atmosphere into 45 layers, each with a height between 300 m (for the lower layers) and 3 km (for the higher layers up to 30 km). For each layer the U.S. standard atmosphere parameters were assumed, and the contribution to the total atmospheric emission from a set of 30 H_2O lines, 32 O_3 lines and 48 O_2 lines in the range from 50 to 1000 GHz was computed, using the Rosenkranz[14] line profile formula. An empirical continuum term was added to describe the contribution from other lines. Three examples of atmospheric emission spectra from this model are presented in fig.1. Atmospheric noise was obtained by means of gaussian fluctuations of the atmospheric parameters: for each layer we assumed uncorrelated fluctuations around the average values of Temperature, Pressure, Water Vapour partial pressure and Ozone partial pressure. The variances of these fluctuations are strongly dependent on the specific climatic conditions but we will make only relative estimates, which are independent of the absolute values of the variances. These are only assumed to be much smaller than the corresponding averages squared. For each pair of frequencies, 100 independent realizations of the two atmospheric signals I_{1i} and I_{2i} were obtained, together with the corresponding atmospheric transmissions T_{1i}, T_{2i}, and we computed the correlation coefficient $R(I_1, I_2)$ (see fig.4), the rms of the two signals, the best regression line (with slope B) and the rms of the residuals. From fig.4 it is evident that the correlation is very bad when one of the wavelengths coincides with an atmospheric line, due to the different depths observed; on the other hand R can be very much closer to 1 when a suitable pair of frequencies is selected. In order to obtain a real advantage from this technique, we must also choose the

two frequencies in such a way that the ratio between the source emission in the two bands is very different from the ratio between atmospheric emission fluctuations; otherwise we will cancel out not only the atmospheric fluctuations but also the signal from the source. So we computed the S/N gain obtainable using the correlation method as follows: we assumed that the observed signals are $S_{1i} = I_{1i} + T_{1i} \cdot A_1$ and $S_{2i} = I_{2i} + T_{2i} \cdot A_2$, where A_1 and A_2 are the signals expected from CBR anisotropies at the top of the atmosphere. In the hypothesis that the atmospheric fluctuations are higher than the CBR anisotropies, we have

$$\frac{S/N(corrected)}{S/N(uncorrected)} = \frac{\langle S_1 - B \cdot S_2 \rangle}{\sqrt{var(S_1 - B \cdot S_2)}} \Big/ \frac{\langle S_1 \rangle}{\sqrt{var(S_1)}} \qquad (3)$$

this quantity is plotted in fig.5. It is evident again that a significant increase in the S/N is possible using this method at suitable wavelengths: using $\sigma_1 = 5cm^{-1}$ and $\sigma_2 = 10cm^{-1}$ the S/N gain is ~ 5; using $\sigma_1 = 10cm^{-1}$ and $\sigma_2 = 12cm^{-1}$ the gain can be as large as ~ 50 (a precipitable water vapour content of 1 mm was assumed in the previous estimates).

OPTIMIZED TELESCOPES FOR SUB-MILLIMETRE COSMOLOGY

Submillimetre telescopes have a lot of constraints to respect in order to obtain the best performances. To reduce atmospheric fluctuations we usually refer to differential meausurements. In our telescopes we adopt the optical solution of a wobbling secondary element in a Cassegrain type configuration. This efficient scheme of modulation is widely used (see *e.g.*,the 30-m Millimeter Radio Telescope (MRT) at Pico Veleta, the 15-m James Clerk Maxwell Telescope (JCMT) at Mauna Kea, the 1.5-m Italian National IR Telescope at Gornergrat (TIRGO) etc.). The severe geometrical aberrations present in the off-axis position are minimized by tilting the subreflector around the neutral-point. In this way we reach diffraction-limited performances even if large angles in the sky are explored with a high magnification factor telescope. The strategy used in the optical optimization procedure is described elsewhere[15]. The 2.6-m Infrared Telescope (TIR) is studied for balloon-borne observations but it operates equally well at ground stations. Its intrinsic characteristics are compactness, due to the high optical velocity of the primary mirror, and a free-vibration modulator. The peculiarity of the modulation system is a torque cancelling design to minimize any possible acoustic coupling between the nutation mechanism and the detector[16]. It is possible to refocus and correct the modulation axis by remote control[17]. Two electrodynamic low power dissipation vibrators wobble the subreflector at 10 HZ frequency in a push-pull configuration.

Two different configurations are employed in different cosmological topics. The first one, as flux collector (TIR FC), is devoted primarily to search for anisotropies of CBR or in

general for diffuse radiation. A 4-channel photometer with a large throughput is matched on the focal plane[18]. A second configuration (TIR AR) operates with a smaller beam divided into a 3×3 bolometer's array[19]. The higher angular resolution, due to a shorter wavelength, permits the study of molecular clouds or other IR sorgents. It is possible to change the configuration by substituting only the subreflector. Each mirror is a single aluminium alloy fusion and the structure is a light stiff ribwork. In this way the weights do not exceed 100 Kg and 1 Kg for primary and secondary mirrors respectively. The reachable surface roughness is about 15 μm after the polishing stage. In fig.6 the axial gain, function of the reflector surface r.m.s. error and diameter[20], for TIR and other millimetre telescopes is shown. In a prototype 1.2-m telescope[21], a flux collector with a large beam, we also tested two baffles to reduce stray radiation, unwanted radiation coming from an external out-of-field source. The baffle of the secondary mirror is designed specifically to vignette the subreflector. This trick prevents the photometer from collecting radiation directly from the hot vibrators behind the secondary mirror and the diffracted radiation from the edge of the wobbling subreflector. The other baffle, the conical primary one, extends from the focal plane towards the subreflector with an angle equal to that of acceptance. The length of this baffle is carefully chosen to vignette radiation from the secondary baffle with the right incidence angle. The back side of the secondary baffle is covered with a neoprene sheet. As regards the conical primary baffle, it has an Eccosorb AN72 lining to reduce stray radiation. All these apertures are sources of diffracted radiation but this does not affect our measurements too much because this is only a further background removed by the lock-in demodulation technique. A possible source of spurious signal is the anisotropic thermal emission from the surface of the primary mirror. A set of thermometers on the back side of the mirror monitors its temperature distribution.

REFERENCES

1) Franceschini A., Toffolatti L., Danese L., De Zotti G., 1989, *Ap.J.* , **344** ,35.

2) Mather J.C., 1984, *Appl.Opt.*, **23**, 584.

3) Vittorio N., Silk J., 1984, *Ap.J.Letters*, **285**, L39.

4) Clements D.L., Chase S.T., Joseph R.D., *Sensitivity of millimetre wave continuum observations over long integration times*, 1990, *M.N.R.A.S.*, in press

5) G. Dall' Oglio, P. de Bernardis, S. Masi, B. Melchiorri, A. Moleti, W. Pecorella, L. Pizzo, *Atmospheric transmission and noise measurements in Antarctica*, 1988, *Ir. Phys.*, **28**, 155.

6) Lombardini P.P., Melchiorri F., Salio G., Dall' Agnola L., *Atmospheric transmittance in the far IR at Testa Grigia*, 1975, *Ir.Phys.*, **15**, 73.

7) Meyers S.S., Jeffries A.D., Weiss R., *A search for the Sunyaev Zeldovich effect at millimeter wavelengths*, 1983, *Ap.J.Letters*, **271**, L1.

8) Kreysa E., Chini R., *Small scale anisotropy of the CMB at 230 GHz*, 1988, in *Particle Astrophysics: Forefront Experimental Issues*, E.B.Norman ed., World Scientific, pg.149.

9) Andreani P., Dall'Oglio G., Martinis L., Piccirillo L., Pizzo L., Rossi L., Venturino C., *Search for intermediate-scale CBR anisotropy from Antarctica*, 1990, *Astron. Astrophys. accepted.*

10) Boynton P., Lombardini P.P., Melchiorri F., 1974, *proposal to NSF and CNR*

11) Liebe H.J., *An Atmospheric millimeter wave propagation model*, *NTIA Report*, **83-137**, 1983.

12) Danese L. and Partridge B., *Atmospheric emission models: confrontation between observational data and predicitions in the 2.5-300 GHz frequency range*, 1989, *Ap.J.*, **342**, 604.

13) G. Dall' Oglio, B. Melchiorri, P. de Bernardis, S. Masi, A. Moleti, *Ground based atmospheric radiometry in the far infrared*, 1986, *Ir. Phys.*, **26**, 227.

14) Rosenkranz P.W., *Shape of the 5 mm oxygen band in the atmosphere*, 1975, *IEEE Trans. Ant. Prop.*, **AP-23**, 498.

15) De Petris M., Gervasi M., Liberati F., *New far IR and mm telescopes for differential measurements with large chopping angles in the sky*, 1989, *Appl. Opt.*, **28**, 1785.

16) Radford S.J.E., *Observation at mm wavelengths of small angular scale isotropy in the CBR*, 1986, **Ph.D. Thesis**, Washington D.C.

17) de Bernardis P., Masi S., Perciballi M., Romeo G., *A resonance wobbling secondary mirror for balloon - borne IR telescopes*, 1989, *Ir. Phys.*, **29**, 1005.

18) de Bernardis P., De Petris M., Gervasi M., Masi S., Cardoni M., De Ninno A., Scaramuzzi F., *A high throughput, multiband photometer for the TIR project*, 1990, *contributed paper to 29th Liége International Astrophysical Colloquium.*

19) Natale V., *A ^{3}He cooled bolometer array for mm and submm continuum observations*, 1990, *Mem.S.A.It.*, **61**, 247.

20) Ruze J., *Antennas Tolerance Theory - A Review*, 1966, *Proc. IEEE*, **54**, 633.

21) de Bernardis P., Amicone L., De Luca A., De Petris M., Epifani M., Gervasi M., Guarini G., Masi S., Melchiorri F., Natale V., Boscaleri A., Natali G., Pedichini F., *A short wavelength measurement of the CBR anisotropy* 1989, *Ap.J.Lett.*, **360**, L31.

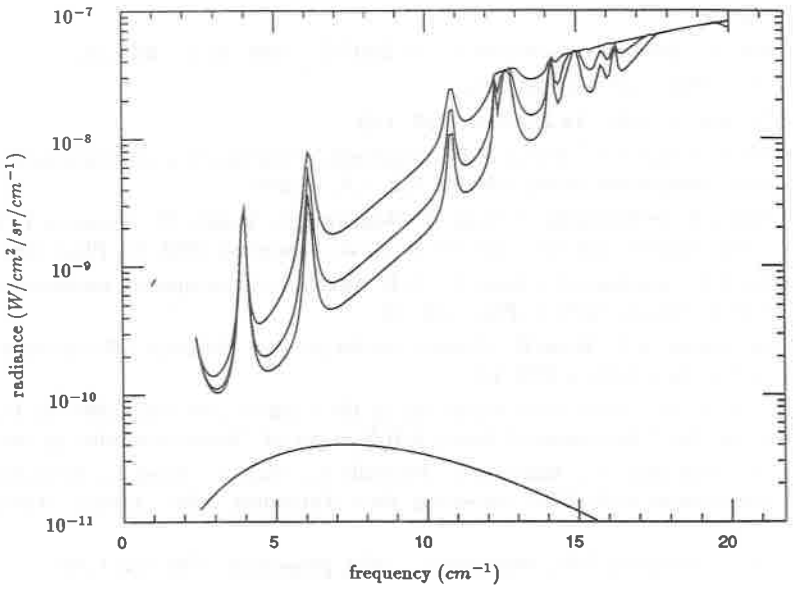

Figure 1 : The spectrum of atmospheric emission (for precipitable water vapour levels of 0.5 mm, 1 mm, 3 mm) is compared to the spectrum of CBR anisotropies (with $\Delta T/T = 1$). The three millimetric windows at 1.2, 2, 3.6 mm are evident.

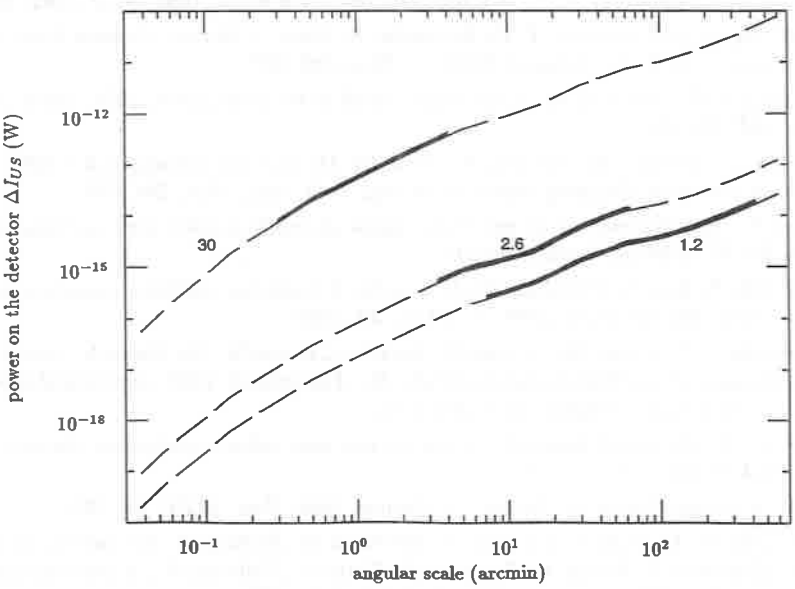

Figure 2 : Signal from unresolved extragalactic submm sources in the 800 μm window as expected from the model[1]). The three curves are labelled with the diameter (in meters) of the primary mirror of the telescope. The bold sections of the curves are those effectively observable using each telescope (angular scales larger than the diffraction limit and smaller than the maximum available modulation amplitude).

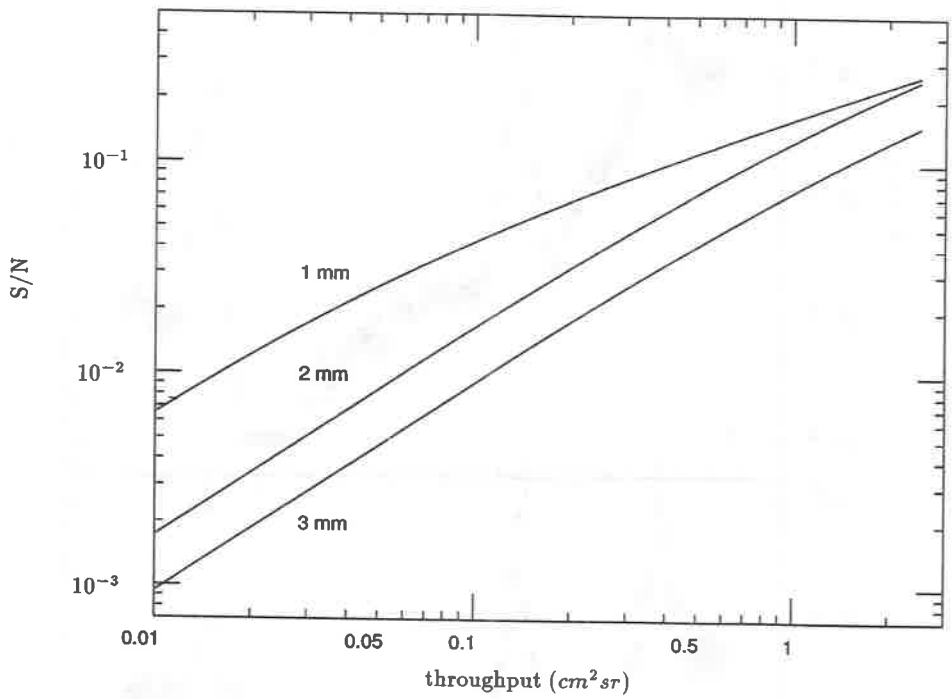

Figure 3 : S/N ratio for observations of CBR anisotropies ($\Delta T/T = 10^{-5}$, $\tau = 1s$), using bolometers optimized for different throughputs $A\Omega$. The optimized detector noise was computed using the formulas quoted in ref. 2) and is the quadrature sum of Johnson, Phonon and Photon noises. A precipitable water vapour content of 1 mm was assumed for the computation of the background and photon noise from the atmosphere; the three curves are labelled with the central wavelength of the atmospheric window.

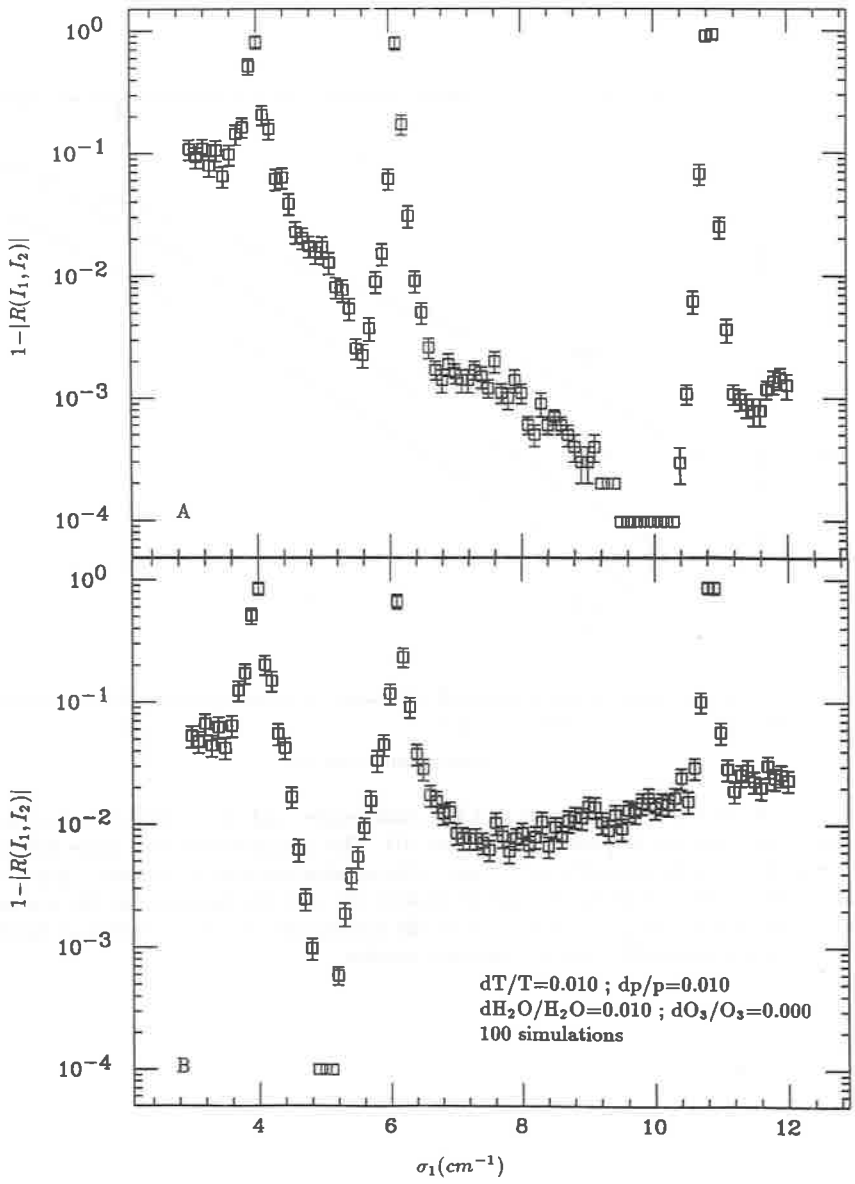

Figure 4: Correlation coefficient of atmospheric FIR signals at two different frequencies. In fig. 4*a* the first frequency σ_1 spans the range $2.5 \div 12 cm^{-1}$ while the second frequency is kept fixed at $\sigma_2 = 10 cm^{-1}$; in fig. 4*b* the second frequency is $\sigma_2 = 5 cm^{-1}$. A precipitable water vapour content of 1 mm was assumed. The ordinate is the difference between the correlation coefficient R and unity.

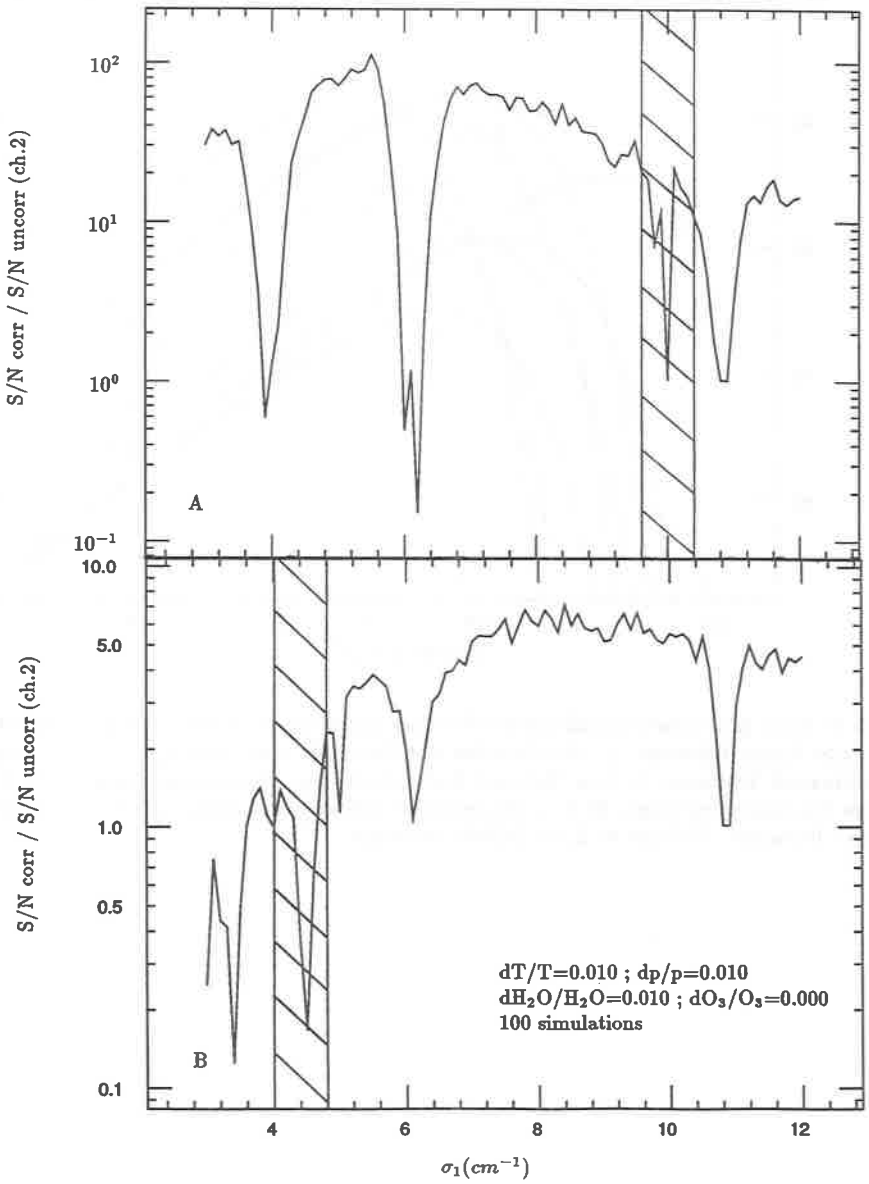

Figure 5: S/N ratio gain obtainable using the two frequencies correlation technique outlined in the text. The panels *a* and *b* are obtained with the same parameters of fig.4 *a* and *b*. An increase as large as a factor 50 can be obtained using suitable pairs of frequencies, for example by correcting data taken at 10 cm^{-1} by means of data taken at 5 cm^{-1}.

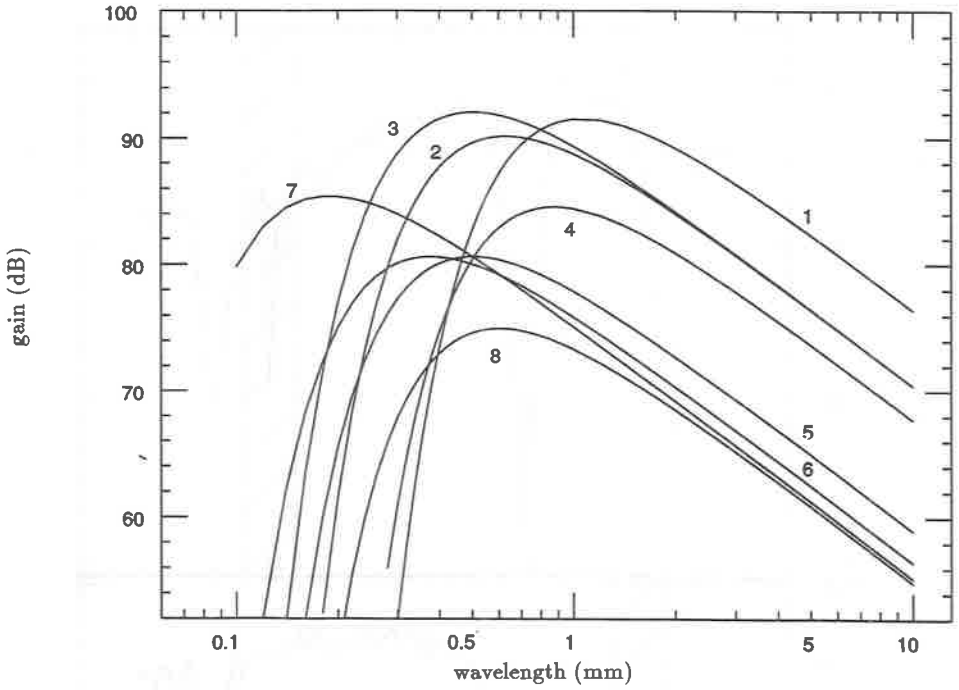

Figure 6: Axial gain of several millimetre telescopes (based on published estimates): 1) 30-m Millimeter Radio Telescope, 2) 15-m Swedish-ESO Submillimetre Telescope, 3) 15-m James Clerk Maxwell Telescope, 4) 11-m National Radio Astronomy Observatory telescope, 5) 4-m Nagoya University telescope, 6) 3-m University of Cologne-Gornergrat telescope, 7) 2.6-m Infrared Telescope -TIR and 8) 2.5-m POM-2 telescope.

André Rousset

Aerospatiale
37 Bd Montmorency
75016 Paris

I am happy to say a few words about AEROSPATIALE, which helped to sponsor this meeting.

AEROSPATIALE is of course well known to you through the AIRBUS aircraft, through the ECUREUIL and GAZELLE helicopters, and through the ARIANE spacecraft launchers. However, we are also active in certain aspects of astronomy, and I would like to note a few examples of our involvement in this area.

Our space division is prime contractor for the ISO program and is building a telescope which will be used to observe the infrared emission of stars and galaxies. The orbital instrument will be operated at the temperature of liquid helium, which is a source of unique problems.

AEROSPATIALE is willing to participate in the VLT, a European project which involves the construction of 4 big telescopes. Together with FRAMATOME, a common subsidiary compagny called TELAS is proposing to make an 8 metre mirror out of aluminium : this new idea would be cheaper, quicker and safer than a mirror made out of glass, the conventional material. A 1.8 metre prototype has now been built : its optical quality is good.

Finally, I would like to mention our recent involvement with lasers. The rencently created LASERDOT company, which is the old "OPTRONIC division" from MARCOUSSIS, has extensive competence in adaptive optics. As you probably know, such devices can be used advantageously in astronomy to eliminate the deleterious effect of atmospheric turbulence on telescopic images. A first experiment was conducted at the Haute Provence Observatory by a team led by Professor Pierre Léna, with the cooperation of ONERA ; the results were very satisfactory, since the diffraction limit was attained. A second experiment carried out at La Silla with the European telescope has also successfully obtained images at the diffraction limit, and half the size of the Haute Provence images.

Perhaps I should mention that I am here not only as a representaive of AEROSPATIALE, but also as an old neutrino physicist ; I have always been interested in the relation between astrophysics and particle physics. It was a pleasure to be with you during this week.

I thank you for your attention.

Trân Thanh Vân and André Rousset

Posters

Xavier Barcons and Martine Mouchez

INFLATION AND THE COBE SATELLITE

Robert K. Schaefer

Bartol Research Institute
Univ. of Delaware
Newark, Delaware, 19711
U.S.A.

ABSTRACT

The predictions of the inflationary cosmology are compared with the expected sensitivity of the COBE satellite. We explicitly display the 1 σ *prediction* error bars due to the Gaussian nature of the inflationary density fluctuations. In the usual biased cold dark matter version of inflation, the predicted large angle temperature fluctuations are close to the COBE theoretical sensitivity limit. Noting that this version of inflation is inconsistent with some recent large scale structure observations, we consider other forms of dark matter which are seen to be more easily detectable by COBE.

The inflationary model of the early universe provides an explanation for two fundamental cosmological puzzles, the horizon and flatness problems, as well as providing a mechanism for generating large scale primordial density fluctuations. The appeal of this model is that It also makes some strong predictions. These predictions are: that space is "flat" ($\Omega = \frac{\rho}{\rho_{crit}} = 1$) and Gaussian density fluctuations are produced which have a scale independent amplitude $\left[\frac{\delta\rho}{\rho}\right]^2_{t_{HOR}} = \epsilon_H^2 =$ constant. The amplitude ϵ_H is not well predicted from the particle physics of inflation, so we normalize ϵ_H to the observed structure in the universe.

The inflationary power spectrum gets modified on small scales by temporal evolutionary effects, which are dependent on the properties of the dark matter; hence, the value of ϵ_H depends on the type of dark matter. The smallest ϵ_H, found using cold dark matter, is further reduced by the use of "biasing", which assumes that structure represents $b\sigma$ peaks ($b > 1$), implying the underlying fluctuations are even smaller.

Using the inflationary spectrum one can calculate the amplitude of multipoles[1] of the temperature distribution produced via the "Sachs-Wolfe" effect. The relative values of the large angle moments (see Figure 1) are independent of the dark matter, but their overall magnitude depends on the value of ϵ_H. To compare predicted values of the moments in different dark matter scenarios, we scale the COBE sensitivity curves instead of the moments.

Using the 1 year 1 frequency theoretical COBE sensitivity limit[2], we see that COBE will need to reduce systematic errors to about the level of the detector's sensitivity in order to see temperature fluctuations produced by the highly biased ($b = 2.5$)

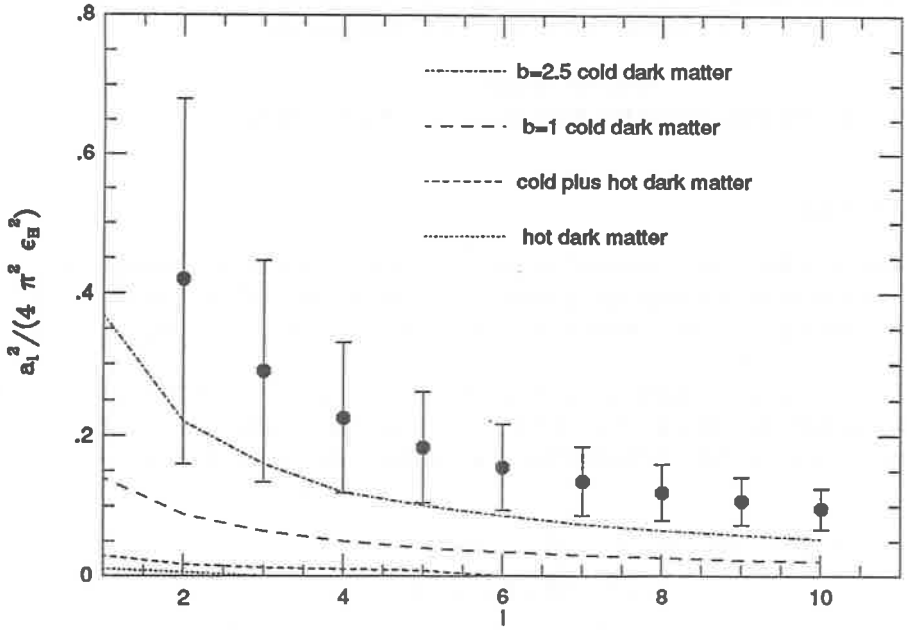

Fig. 1). The first ten inflationary multipole moments (excluding the dipole). The sensitivity of COBE is represented by curves scaled for the models indicated. The biased $b = 2.5$ cold dark matter model is the most difficult for COBE to detect. The cold plus hot dark matter model has a cold dark matter density which is 3 times that of hot dark matter. This ratio was chosen because it gives excellent agreement[3] with both the small scale galaxy correlations and the large scale velocity fields of the POTENT analysis (see talk by Bertschinger, this conference). A pure hot dark matter model, using the unbiased normalization of ref. 4, would give an easily detectable COBE signal.

1. L.F. Abbott and M.B. Wise, 1984, *Astrop. Jour. Lett.*, **282**, L47.
2. J. Mather, 1982, *Optical Engineering*, **21**, 749.
3. R.K. Schaefer, Q. Shafi, and F.W. Stecker, 1989, *Astrop. Jour.*, **347**, 575.
4. E. Braun, A. Dekel, P.A. Shapiro, 1988, *Astrop. Jour.*, **328**, 34.

Some Remarks on the Generation of Density Fluctuations in Inflationary Universe Models

Gerhard Börner and Kay Pirk
Max-Planck-Institut für Astrophysik, D-8064 Garching b. München

Introduction

The chaotic inflationary universe[1] relies on certain properties of a classical scalar field. Quantum fluctuations are thought to be responsible for the generation of a definite spectrum of density fluctuations. We want to investigate this aspect in some detail.

The scalar quantum field $\hat{\phi}$ is split into $\hat{\phi} = \phi + \delta\phi$ where $\phi := \langle\hat{\phi}\rangle$ denotes the C-number-valued expectation value of $\hat{\phi}$ in a yet unspecified quantum state; $\delta\phi$ is the remaining operator-valued distribution. The formal semiclassical Einstein equations are

$$-\Box\phi + \zeta R\phi + U_\phi(\phi) + \frac{1}{2}U_{\phi\phi\phi}(\phi)\left\langle\delta\phi^2\right\rangle = 0, \tag{1}$$

$$[-\Box + \zeta R + U_{\phi\phi}(\phi)]\,\delta\phi = 0, \tag{2}$$

$$(8\pi)^{-1} G_{\mu\nu} = T_{\mu\nu}(\phi) + \left\langle\hat{T}_{\mu\nu}(\delta\phi)\right\rangle. \tag{3}$$

Here we have made use of the *one-loop approximation.*

In this approximation $\delta\phi$ is understood as a free quantum field with time-dependent mass, ($U_{\phi\phi}$: the second derivative of the arbitrary potential U with respect to ϕ), and $\left\langle\hat{T}_{\mu\nu}(\delta\phi)\right\rangle$ as the expectation value of the stress-energy of this field. Therefore the system of eqn.(1–3) can be treated by the standard methods of a linear Quantum Field Theory.

The quantities $\left\langle\delta\phi^2\right\rangle$ and $\left\langle\hat{T}_{\mu\nu}(\delta\phi)\right\rangle$ have to be renormalized. We assume a *Hadamard* type singularity structure of the twopoint function[2] which allows us to define regularized quantities as C^∞ functions over spacetime.

Then a linearly perturbed spatially flat *Robertson-Walker* spacetime

$$g_{\mu\nu} = a(\eta)diag(-1,1,1,1) + \delta g_{\mu\nu} \tag{4}$$

is considered, and $\delta g_{\mu\nu}$ is decomposed into the eigenmodes[3] of the spatial *Laplacian*, denoted bei k. The classical field ϕ is decomposed similarly (the gaugeinvariant eigenmodes denoted by χ), as well as the renormalized quantum fluctuations w_0 (eigenmodes denoted by δw_0).

De Sitter Symmetric Case

If the quantum state exhibits the *de Sitter* symmetries, then $w_0 = const.$; we may further assume

$$U = \frac{1}{2}m^2\phi^2 + U_0 \quad \text{and} \quad \phi = 0, \quad U_0 = const. \tag{5}$$

Since $a^2 = 12/R\eta^2$, where R is a constant, the equations simplify considerably.

Shifting to variables

$$x = \frac{k\eta}{\sqrt{3}} \quad \text{and} \quad s = \frac{R}{384\pi^2}\frac{\delta w_0}{(1+\delta_{an})}, \tag{6}$$

and introducing the abbreviations

$$\delta_{an} = \frac{R}{72\pi}\left((6\zeta-1)^2 - \frac{1}{30}\right) + \frac{m^2}{12\pi}(6\zeta-1) \quad \text{and} \quad \mu^2 = 12\frac{m^2}{R}, \tag{7}$$

the equation for the density fluctuation Δ is

$$\begin{aligned}&\Delta'' - \frac{8}{x}\Delta' + \left(1 + \frac{18}{x^2}\right)\Delta = \\ &(6\zeta-1)\left\{x^2 s'' - 2xs' + 3x^2 s\right\} + 2\mu^2 s + \frac{2}{x}\Pi' + 2\left(1 - \frac{6}{x^2}\right)\Pi\end{aligned} \tag{8}$$

ζ is the coupling; $\zeta = 1/6$ for conformal coupling. The density perturbation is determined by the quantum fluctuations.

Non de Sitter Invariant Quantum State

We still use the potential U as above, but we drop the condition $\phi = 0$. The ansatz for w_0 will be now

$$\frac{w_0}{32\pi^2} = \frac{\bar{w}_0}{32\pi^2} - \frac{\phi^2}{2}; \tag{9}$$

$\bar{w}_0$ is meant as a constant. The equation governing the perturbation changes substantially:

$$\begin{aligned}&\Delta'' - \frac{8}{x}\Delta' + \left(1 + \frac{18}{x^2}\right)\Delta = \\ &\quad (6\zeta-1)\left\{x^2 s'' - 2xs' + 3x^2 s\right\} + 2\mu^2 s + \frac{2}{x}\Pi' + 2\left(1 - \frac{6}{x^2}\right)\Pi \\ &+ \quad (6\zeta-1)\left\{x^2\phi\chi_R'' + 2\left(x^2\phi' - x\phi\right)\chi_R' + 3\left(x^2 - 4\zeta\right)\chi_R\right\} \\ &- 3(2\zeta-1)\phi\mu^2\chi_R,\end{aligned} \tag{10}$$

where $\chi_R = R/12(1+\delta_{an}) \times \chi$.

It seems to us that this more general case has enough freedom to allow an arbitrary spectrum of density fluctuations Δ to be generated from χ and δw_0.

References

1)Linde, A.D.; 1984, Rep. Prog. Phys. **47**, 925

2)Kay, B.S.; Wald, R.M.; 1988, *Theorems on the uniqueness and thermal properties of stationary, nonsingular, quasi-free states on spacetimes with a bifurcate Killing horizon* Preprint

3)Kodama, H.; Sasaki, M.; Prog. Theor. Phys. Suppl. **78**

COSMOLOGICAL LIMITS ON CHERN-SIMONS ELECTROMAGNETISM

Sean M. Carroll and George B. Field
Harvard-Smithsonian Center for Astrophysics
Cambridge, MA, 02138, USA

ABSTRACT

Inspired by work in 2+1 dimensional physics, we investigate the behavior of a novel addition to Maxwell electrodynamics, an interaction Lagrangian known as the Chern-Simons term. Such an addition has many possible interpretations: as a parameterization of Lorentz invariance, as the coupling of axions to electromagnetism, and as a CP-violating term in QCD, to name a few. In this paper we focus on a specific application of Chern-Simons electromagnetism to testing the Principle of Equivalence, the cornerstone of modern theories of gravity. In this theory, a pseudoscalar (parity-violating) coupling of electromagnetic fields to gravitational fields leads to a rotation of the polarization vector of radiation emitted from distant galaxies. We have searched for such an effect and found none; we therefore conclude by placing strict limits on the existence of this term.

INTRODUCTION

Modern theories of gravitation are founded upon the Principle of Equivalence, which comes in three forms: the Strong Equivalence Principle (SEP) states that all experiments will give the same results when performed in any freely falling rest frame. The Einstein Equivalence Principle (EEP) states that all ***non-gravitational*** experiments give the same results in all freely-falling frames. The Weak Equivalence Principle (WEP) states that the trajectory of a test body will be independent of its composition. Any theory which obeys the EEP is a "metric theory," such as general relativity or Brans-Dicke thery, in which gravitation may be thought of as the curvature of spacetime through a metric $g_{\mu\nu}$.

Schiff has conjectured that any consistent theory which obeys the WEP must necessarily obey the WEP. In an attempt to prove this conjecture, Ni considered a general framework of electromagnetism coupled to gravity.[1] He was able to find a counterexample, an interaction Lagrangian $\mathcal{L} = \frac{1}{4}\phi\epsilon^{\alpha\beta\gamma\delta}F_{\alpha\beta}F_{\gamma\delta}$, where $F_{\alpha\beta}$ is the electromagnetic field strength tensor, ϕ is a scalar function of the gravitational fields, and $\epsilon^{\alpha\beta\gamma\delta}$ is the completely antisymmetric tensor. Furthermore, this is the ***unique*** counterexample to Schiff's conjecture, if we limit ourselves to Lagrangians which are gauge-invariant and quadratic in $F_{\alpha\beta}$, and exclude couplings to derivatives of the gravitational fields. Therefore, limits on Ni's counterexample serve as tests of the EEP.

OBSERVATIONAL LIMITS

This Lagrangian was studied in a different context by Carroll, Field and Jackiw,[2]

who showed that any non-constant ϕ would lead to a rotation in the polarization angle of radiation from distant radio galaxies. If we model the universe as homogeneous and isotropic, then ϕ will only vary with time. In this case, one can derive a simple expression between the change in polarization angle θ and the change in ϕ: $\Delta\theta = \frac{1}{2}\Delta\phi$.

Carroll, Field and Jackiw searched catalogues of radio galaxies for evidence of rotation in polarization angle between the source and us. Such rotation is not observed, to an accuracy of ~ 0.1 radians for galaxies at an average redshift $z \sim 1$. With this information, we can place limits on the variation of ϕ. If we assume that the time elapsed since radiation with $z \sim 1$ was emitted is of order $H_0^{-1} \sim 10^{17}$sec, then we obtain $|\dot{\phi}(\text{today})| < 9 \times 10^{-18}\text{sec} = 6 \times 10^{-42}\text{GeV}$. This upper limit is extremely small, superior to (for example) tests of gauge invariance set by the mass of the photon. We therefore conclude that violation of the EEP by Ni's counterexample (over cosmological scales) is effectively ruled out. Since Ni's Lagrangian is a unique counterexample to Schiff's conjecture (with some assumptions), this allows us to take accurate tests of the WEP by Eötvös experiments as evidence for the accuracy of the EEP, as well.

REFERENCES

1. W.-T. Ni, *Phys. Rev. Lett.* **38**, 301 (1977).

2. S.M. Carroll, G.B. Field and R. Jackiw, *Phys. Rev. D* **41**, 1231 (1990).

PRODUCTION OF ^{9}Be AND HEAVY ELEMENTS IN THE INHOMOGENEOUS UNIVERSE

Nobuo Terasawa
The Institute of Physical and Chemical Research,
Hirosawa 2-1, Wako-shi 351-01, Japan

Abstract

While ^{9}Be is expected to provide a test of inhomogeneous models of primordial nucleosynthesis, we show that the previous estimate by the simplified two-zone model of neutron diffusion overestimated the ^{9}Be abundance at least two orders of magnitude. The abundances of CNO elements expected to be the seeds of cosmic r-process are very small in the proper range of parameters consistent with the abundances of light elements.

It has been suggested, recently, that ^{9}Be may provide a test of inhomogeneous model of nucleosynthesis (Boyd and Kajino 1989), and efforts to find metal-poor population-II stars with lower ^{9}Be abundance were made (Ryan et al. 1990). Another interest in the inhomogeneous models of nucleosynthesis is the cosmological r-process suggested by Applegate, Hogan, and Scherrer(1988).

In this paper, we show the abundances of ^{9}Be and CNO elements in the inhomogeneous universe calculated with extended network including elements up to ^{22}Ne in the multi-zone scheme. Some neutron-rich nuclei which are important to estimate the abundances of these elements are added to the network.

The dependence of the ^{9}Be abundance on the scale of fluctuations is shown in Figure 1 as contour on the $d-R$ plane for $f_\nu = 0.11$. The recent observations of several population-II stars have placed the upper limit on the primordial ^{9}Be abundance to $\log \mathrm{B/H} = -13.7$ (Ryan et al. 1990), which is two orders of magnitude greater than the predicted abundance in the present work. The constraints on the parameters from other light elements, D, ^{3}He, ^{4}He, and ^{7}Li are more stringent than those placed by the ^{9}Be abundance.

The total abundance of heavy elements ($A > 7$) is at most $\sim 10^{-13}$ by mass fraction for $\eta_0 = 4\times10^{-10}(\Omega = 0.014h^{-2} = 0.056h_{50}^{-2})$ and $\sim 10^{-11}$ for $\eta_0 = 7\times10^{-9}(\Omega = 0.25h^{-2} = 1.0h_{50}^{-2})$ in the ranges of parameter calculated in the present study which is dominated by ^{11}B and CNO elements produced in the inner high density shells.

In summary, we have calculated the abundances of elements up to ^{22}Ne in the inhomogeneous universe with the extended network in the multi-zone scheme. The ^{9}Be abundance is two orders of magnitude smaller than that calculated in the simplified two-zone model in the calculated ranges of parameters. Further observational efforts seem to be needed to say something about the inhomogeneous cosmological models basing on the ^{9}Be abundance. Cosmic r-process proposed previously seems not to work in the proper range of parameters consistent with the light element abundances.

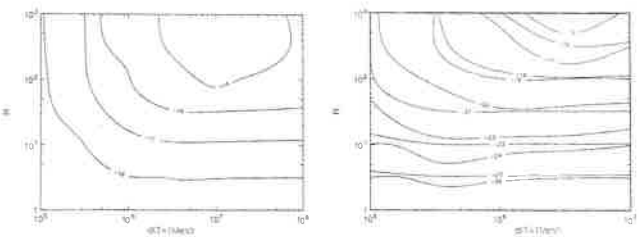

Figure 1. The contour of the average abundances of ^{9}Be on the $d-R$ plane for $\eta_0 = 4\times10^{-10}$(left) and $\eta_0 = 7\times10^{-9}$(right). Contour levels are log(^{9}Be/H).

THREE ISOTROPIC MODELS FOR UNIVERSE
(the universe is 40 billions years old)

Michel Mizony
Labo. d'analyse harmonique
bat 101, Université Lyon1
43 bd. du 11 novembre 1918
69622 VILLEURBANNE Cedex

ABSTRACT

We describe, by mean of the notion of Lie causality semigroup, the three kinds of homogeneous and isotropic models for universe coming from a big-bang event. For each of these models (expanding, flat or oscillating), we show the space-part of the underlying manifold is always open and otherwise the Lorentz homogeneous (hyperbolic) space.

Here's why, following I. Segal, P.A.M. Dirac, H. Bacry and J.M. Levy-Leblond, we suppose that these models are consistent with electromagnetism.

The main features of these models are in first part, to explain easily the isotropy of the background cosmic radiation, and in the second part not to introduce a horizon problem (no causally independant events) contrary to the Robertson-Walker standard models.

Besides, the cosmological constant appears as an initial condition, and of course, the present models are compatible with all cosmological observations, which implies that the universe is 40 billions years old. Starting from electromagnetism instead of thermodynamics, we justify the old hypothesis that V. Fock proposed to build cosmological models: he said that the isotropic group of an isotropic cosmological model is the Lorentz group itself.

§1 Definition of a model for the universe.

In literature there are two kinds of isotropic universe models: in one hand the usual "standard" model based on thermodynamics (the cosmic fluid is a perfect fluid), in the other hand the ones that have been elaborated to glue together gravitation and electromagnetism. In the same vein we find V. Fock[1] (the isotropic subgroup is nothing else than the Lorentz group itself), I. Segal[2] (the underlying manifold is an open set of the universal covering Σ of the conformal compactification of the Minkowski space), P.A.M. Dirac and others[3] who underline the notion of conformal factors for the metric, and so ever.

Our starting point is the H. Bacry and J.M. Levy-Leblond[4] or I. Segal theorem: there are three kinematical groups which are compatible with electromagnetism, i.e. three ten-dimensional subgroups of the conformal group that is the invariance group of the Maxwell equations: in fact the two de Sitter groups and the Poincaré group. Taking into account causality, the study of the three kinematical (causality) semigroups, spanned by Lorentz transformations and non negative time translations[5] leads us to postulate the following definition.

Definition: An homogeneous and isotropic universe model $(\mathbf{U},\eta)$ is an open set $\mathbf{U}$ of Σ, invariant under one of the three kinematical semigroups, endowed with a metric η that is conformally invariant under this semigroup (so the isotropic group is the Lorentz group).

§2 A particular case: models arising from a big-bang event.

Let us suppose that the big-bang event is a point singularity, so the underlying space-time is the future cone of a point of Σ, under one of the three kinematical semigroups; If we note $\mathbf{X}$ the upper half-part of the two sheets hyperboloïd endowed with the Lorentz invariant metric $d\sigma^2$, the three models obtained, using the structure of the kinematical semigroups, are the following.

For $\lambda^2 \in \mathbb{R}$ we define $(U_\lambda , \eta_\lambda)$ by:

a) For $\lambda^2>0$, it is the expanding model with $U_{+,\lambda} = \{(\tau,\sigma) \in]0, +\infty[\times \mathbf{X}\}$,

b) For $\lambda = 0$, it is the "flat" model with $U_0 = \{(\tau,\sigma) \in]0, +\infty[\times \mathbf{X}\}$,

c) For $\lambda^2<0$, it is the oscillating model with $U_{-,\lambda} = \{(\tau,\sigma) \in]0, \pi/2|\lambda|[\times \mathbf{X}\}$, (the expanding phase of an oscillating universe);

For these three models the metric is defined in the cosmic coordinates system (τ,σ) as follows:

$ds^2 = d\tau^2 - (sh^2\lambda\tau/\lambda^2)\, d\sigma^2$.

So, for each of these models (either expanding, flat or oscillating), the isotropy subgroup is the Lorentz group, the isotropy of the 3°K cosmic background radiation is obvious and there are no causally independant events (or horizon problem), contrary to the standard Robertson-Walker model.

The cosmological redshift is given by $1 + z = \text{sh } c\lambda\tau_0 / \text{sh } c\lambda\tau_e$, where c is the speed of light and τ_0 is the time at which the radiation emitted at the time τ_e is received. The Hubble "constant" is $H(\tau) = c\lambda \coth c\lambda\tau$ and the deceleration parameter is $q(\tau) = - \text{th}^2 c\lambda\tau$. We apply the Einstein equations and we obtain: $T_0^0 = 3c^2|\lambda|^2 = 8\pi G\rho^*$, where ρ^* is the constant density of the universe in the cosmic coordinates system (τ,σ); (we neglect the cosmological constant Λ because it appears as an initial condition). Given that the observed mean density ρ of the universe is around 10^{-31} , 10^{-30} g/cm^3, and the observed Hubble constant H is between 50 and 100 km/s/mpc, the two formula $8\pi G\rho = 3c^2|\lambda|^2 (c\lambda\tau)^3/(\text{sh } c\lambda\tau)^3$ and $H(\tau) = c\lambda \coth c\lambda\tau$ lead us to the conclusion that universe is between 25 and 60 billions years old as shown by figure 1.

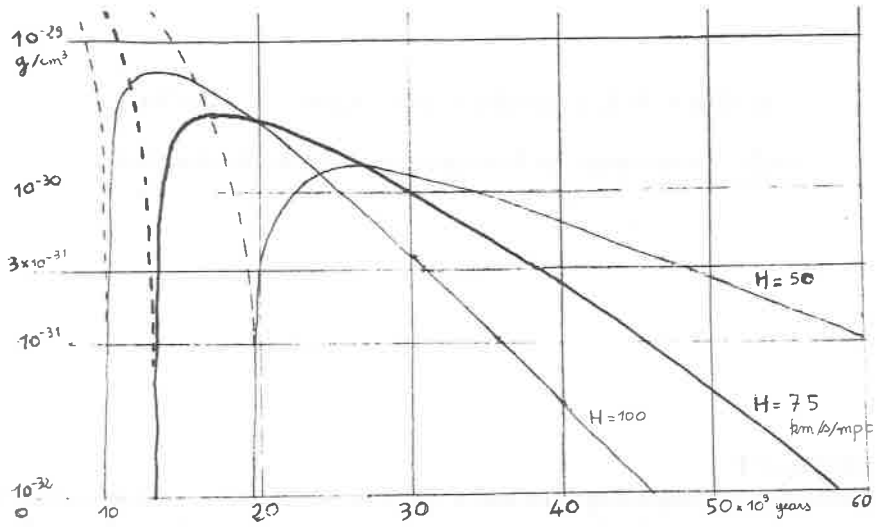

Figure 1: The three curves (H = 50, 75 or 100 km/s/mpc) give the mean density according to the age of the universe; the solid curves correspond to the expanding models, the dashed lines to the oscillating ones. The horizontal line at $\rho = 3\ 10^{-31}$ g/cm^3 shows that the universe should be from 30 to 50 billions years old.

Bibliography:

1) V. Fock, the theory of space, time and gravitation, Pergamon Press, London, 1964

2) I. Segal, Mathematical cosmology and extragalactic astronomy, Acad. Press, New-York 1976.

3) V. Canuto and all, Phys. Rev D. 16, 1643 (1977).

4) H. Bacry and J.M. Levy-Leblond, J. Math. Phys. 9, 1605 (1968).

5) M. Mizony, Publ. Dep. Math. Lyon 3/B, 1 (1982) and 3, 47 (1984).

HYDRODYNAMICAL SIMULATIONS FOR COSMOLOGICAL FLOWS

E. DUCLOUX, J. LEORAT, D. GERBAL, G. ALECIAN

DAEC, Observatoire de Paris-Meudon, F-92195 Meudon Cedex

ABSTRACT

Simulations are beginning to be one of the most useful way to understand the formation of structures in the Universe, mostly for the approach of the nonlinear effects. In the standard scenario, cosmological structures form from weak perturbations of the initialy hot and dense cosmological plasma. The evolution of this plasma encounter several phases until the actual distribution of matter and radiation. We simulate here hydrodynamicaly the whole evolution from the early universe (redshift$\approx 10^5$) until the formation of the first nonlinear structures.

INTRODUCTION

The study of the formation of structures (galaxies, clusters...) in the Universe has revealed the important role of the numerical simulations. Two kind of simulations are presently available: N-body or hydrodynamical. The first one is well represented in the literature[1)] and is necessary to describe the clustering in a gas of galaxies whereas the second one is quite new in cosmology and has a great interest in following continuously the perturbations from the early universe until the formation of the first generation of nonlinear objects. We report here some results of a plane parallel hydrodynamical simulation for a mixture of matter and radiation, which represents the cosmological medium.

THE CODE

All quantities are discretized on a one dimensionnal periodical grid with a typical number of points by period lying between 64 to 512. The resolution acts through semi spectral methods using Fourier transforms with FFT algorithms for spatial differentiation and the Adams-Bashforth scheme for the temporal evolution[2)]. We solve simultaneously the hydrodynamical equations, including radiation and gravitation (Newtonian) terms, and the radiation transfer equation. The radiation angular dependence is expanded into Legendre polynomials. The closure relation changes along the evolution to follow the strong variation in the opacity, from a completly thick universe to a transparent one. Dark matter is included as a classical gas with a given temperature. The ionisation and the cosmological scale factor are calculated numerically along the evolution for any value of the baryonic and dark matter densities.

RESULTS

The code has been applied to describe different kinds of evolutions for mass scales lying between 10^{-2} and $10^{18} M_{\odot}$. Any initial condition (redshift $\approx 10^5$) can be set here: adiabatical, isothermal, isocurvature, ...

As the first aim, the simulation tries to answer how the first generation of nonlinear seeds did form, whatever their mass is. The full nonlinear treatment in the pre-recombination area is then motivated by the small acoustic time and the unknown amplitudes for the smaller scales perturbations.

We have first checked the consistency between the simulation and the linear theory for small amplitudes fluctuations (see fig 1). Nonlinear interactions occur all along the evolution depending on the amplitude of the perturbations and on the ratio (acoustic time) / (Hubble time), and lead to a redistribution of the perturbation Fourier spectrum, partly from larger to smaller scales. Before recombination, nonlinearities induce shocks and large gradients and may provide a mechanism for a production of isothermal perturbations from initialy adiabatical ones. With the help of the code, we have shown that the choc waves present before decoupling progressively diminished until complete desappearance, for masses lower than $10^9 M_{\odot}$, due to the radiation damping. For greater masses, the constraints given by the CBR observations exclude any pre-recombination shock waves. Figure 2 shows the typical evolution of an adiabatical perturbation with the three phases: acoustic, decoupling, collapse.

REFERENCES

1) see for example White,S.: 1990, in this volume
2) Alecian,G., Léorat,J.: 1988, *Astron. Astrophys.* **196**,1

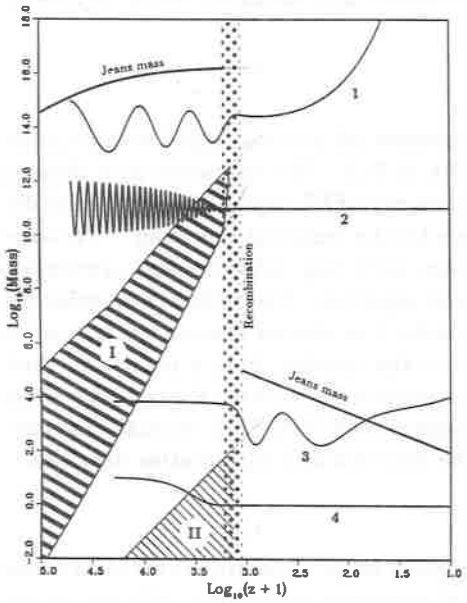

Fig 1 : Main features of the evolution of baryonic perturbations. Notice the two damping areas, for adiabatical (I) and isothermal (II) perturbations. The evolution is illustrate by 4 examples: **1** and **2** are adiabatical perturbations of masses $10^{14}M_\odot$ and $10^{11}M_\odot$, **3** and **4** are isothermal perturbations of masses $10^3M_\odot$ and $1M_\odot$. $\Omega_0h^2 = 1$.

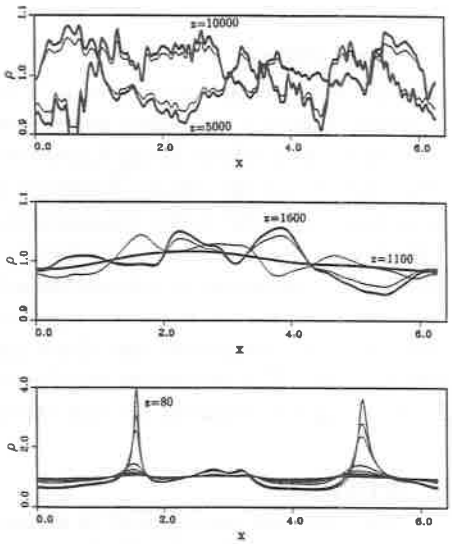

Fig 2 : Evolution of an adiabatical perturbation through recombination (Mass range: 10^9–$10^{15}M_\odot$). We recover in this example the classical features of the evolution. Thick line: radiation energy density. Thin line: matter density. $\Omega_0h^2 = 1$.

FORMATION OF LARGE-SCALE STRUCTURE BY THE WAKE OF OPEN COSMIC STRING

Tetsuya HARA, Shorji MORIOKA and Shigeru MIYOSHI

Department of physics, Kyoto Sangyo University, Kyoto 603, JAPAN

ABSTRACT. The large scale distributions of dark matter and galaxies are simulated under the open cosmic string model. Patterns by a slice selection of the wakes around a rich cluster are compared with the CfA observations.

1. Introduction and assumptions

According to open cosmic string model, sheetlike structures are wakes which are traces of cosmic strings, filaments are intersections of such wakes, and rich clusters of galaxies are high density regions where three wakes intersect. It follows[1] that the typical surface density of sheets, line density of filaments and mass of clusters are $\sim 10^{12}(G\mu\beta\gamma/2\cdot 10^{-6})M_\odot/\mathrm{Mpc}^2$, $\sim 5\cdot 10^{13}(G\mu\beta\gamma/2\cdot 10^{-6})^2 M_\odot/\mathrm{Mpc}$ and $\sim 3\cdot 10^{15}(G\mu\beta\gamma/2\cdot 10^{-6})^3 M_\odot$ where μ and β are the line density and the velocity of the string in units of c=1, and $\gamma=(1-\beta^2)^{-1/2}$.

Thus it is expected that a typical high density region will have extended features such as three sheets, six filaments and be surrounded by eight empty regions (voids).[1] Numerical calculations are performed with 32^3 particles and 32^3 cells in a cube with comoving length $L=45.6(M/2.10^{11}M_\odot)^{1/3}h_{50}^{2/3}\mathrm{Mpc}$, where each particle represents the mass of $M=2.10^{11}M_\odot$ ($M=\rho_b r_0^3$, where ρ_b is the background mean density and r_0 is the length of the cell, so $L=32r_0$).

2. Results and Discussions

The case for orthogonal intersections of three wakes is calculated and the cone diagrams are also shown in Fig.a) The CfA observations are also shown in Fig. b. The similarity between Fig.a) and Fig.b) around rich cluster seems to be very encouraging for the cosmic string model.

The characteristic feature in Figs.a) is that one line which represents the sheet structure, in the cone diagram, becomes discontinuous at the center, according to the crossing of the sheets. This is due to the situations that, galaxies in the sheet move into the center (other sheet). The galaxies on the other side fall toward the observer and, on the other hand, the galaxies on this side moves apart from observer . In Fig. b), it seems that, near the Coma Cluster, there is a discontinuity of filaments which represent the great wall. The characteristic value for the infall velocity of the sheet onto the other sheet is

$$v\simeq 240\cdot(G\mu\beta\gamma/2\cdot 10^{-6})\cdot((1+z_i)/6.10^3)^{1/2}/(1+z)\ \mathrm{km/sec}.$$

The velocity difference of the filaments in the center would be twice of the above value and which is not inconsistent with the observation ($\Delta v \simeq 300 \sim 400$km/sec).

It could be speculated that the objects of dark matter has been clustering within the wake. So, under the cosmic string scenario, it must be explained that the characteristic masses of light emitting objects are formed by thermal process.

One of the important thermal process in the expanding universe after recombination is the cooling by H_2 molecules at $1+z \simeq 10^2$. The mass scale of baryon component at this stage is $\simeq 3 \cdot 10^6 (\Omega_b/0.1)(G\mu\beta\gamma/10^{-6})^3 M_\odot$ which, interestingly, corresponds to the mass scale of globular clusters.

Other characteristic stage for thermal process is at $1+z \simeq 8$ where Compton cooling time becomes longer than the expansion time. Before $1+z \simeq 8$ the gas cools rather rapidly due to this cooling so the fragmented mass is small as order $10^5 \sim 10^6 M_\odot$.[8] At $1+z \simeq 8$, the fragmented mass of dark matter is $\simeq 6 \cdot 10^{10} (G\mu\beta\gamma/10^{-6})^3 M_\odot$ and the Jeans mass is also of the order as

$$M_J \simeq 5 \cdot 10^{10} (T/10^4)^{1/2} (\Omega_b/0.1)^{-1/2} ((1+z)/8)^{-3/2} M_\odot \quad ,$$

where we adopt the gas temperature as 10^4K for the cooling increases above this value rather rapidly.

It is concluded that the scenario of open cosmic string with cold dark matter is a good candidate for understanding the origin of large-scale structure. It is interesting to investigate the distribution of clustering dark matter objects around the wake and detailed thermal process for the formation of galaxies.

References

1) T. Hara and S. Miyoshi, Prog. Theor. Phys. 81(1989),1187.
T. Hara and S. Miyoshi, Prog. Theor. Phys. 77(1987),1152.

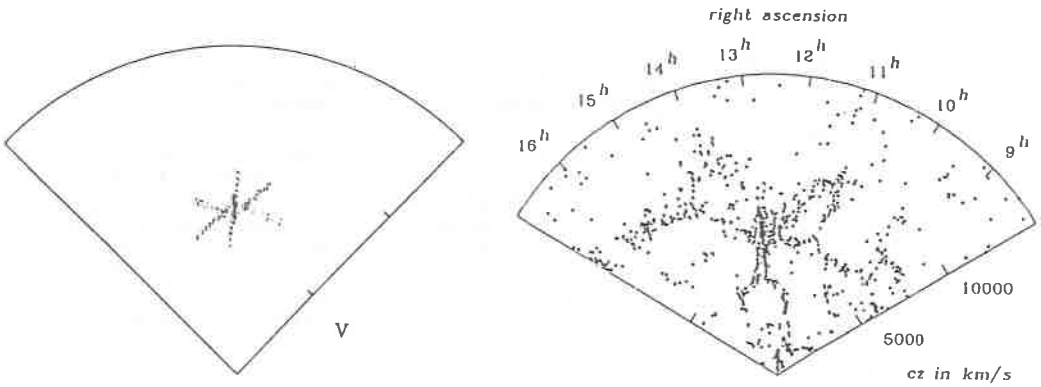

a) b)

Patterns by a slice selection of the wakes around a rich cluster are compared with CfA observations.

FRAGMENTATION AND CLUSTERING IN THE WAKE FORMED BY COSMIC STRING

Tetsuya HARA and Shigeru MIYOSHI
Department of physics, Kyoto Sangyo University, Kyoto 603 ,JAPAN

ABSTRACT. Numerical calculations are performed for the fragmentation, clustering and merging of dark matter under the open cosmic string model. Both the fragmentation in one dimensional collapse of pancake scenario and clustering theory from small scale to large scale within a wake are realized.

1 Introduction

Sheet-like structures in a large scale distribution of galaxies seem to be simply explained by open cosmic strings, for matter accumulates the traces of the string. According to this scenario, the characteristic size and the typical surface density of sheets are $\sim 10^2 \mathrm{Mpc} \times 10^2 \mathrm{Mpc}$ and $\sim 10^{12} (G\mu\beta\gamma/2\cdot 10^{-6}) M_\odot/\mathrm{Mpc}^2$,[1] where μ and β are the line density and the velocity of the string in unit of c=1, and $\gamma=(1-\beta^2)^{-1/2}$.

The accumulated dark matter in the plane may be fragmented due to the plane instability. The representative mass fragmented at 1+z is[1]

$$M \simeq 2\cdot 10^{14} (G\mu\beta\gamma/2\cdot 10^{-6})^3 \cdot ((1+z_i)/6.10^3)^{3/2}/(1+z)^3 M_\odot \ .$$

Then the mass sacle of galaxies is formed around $1+z \simeq 10$ and the typical mass at present is the order of group of galaxies.

Numerical calculations are performed with 32^3 particles and 32^3 cells in a cube with comoving length $L=45.6(M/2.10^{11} M_\odot)^{1/3} h_{50}^{2/3} \mathrm{Mpc}$.

2. Results of numerical calculations and discussions

The scale expansion of the factor e^4 ($\simeq 54.6$) is computed by 1000 time steps. At the first time, the fragmentation occurrs randomly, and small density peaks appears almost every where within the wake. As time has passed, the number of the density peak has decreased due to clustering and merging. The clustering and merging occur within the wake and, in the end, almost the regular stable configuration of finite numbers of fragments is realized, which may be due to the boundary condition of periodicity.

Under the cosmic string scenario, it could be explained the mass scale of group of galaxies through clustering of dark matter. However, mass scale of galaxies must be investigated through thermal process. The characteristic stage for thermal process is at $1+z \simeq 8$ when Compton cooling time due to 3K backgound radiation becomes longer than the expansion time. The Jeans mass at this stage is as

$$M_J \simeq 5 \cdot 10^{10} (T/10^4)^{1/2} (\Omega_{bm}/0.1)^{-1/2} ((1+z)/8)^{-3/2} M_\odot \quad .$$

The detail thermal process for the formation of galaxies must be pursued.

References

1) T. Hara and S. Miyoshi, Prog. Theor. Phys. 77(1987),1152.
T. Hara and S. Miyoshi, Prog. Theor. Phys. 81(1989),1187.

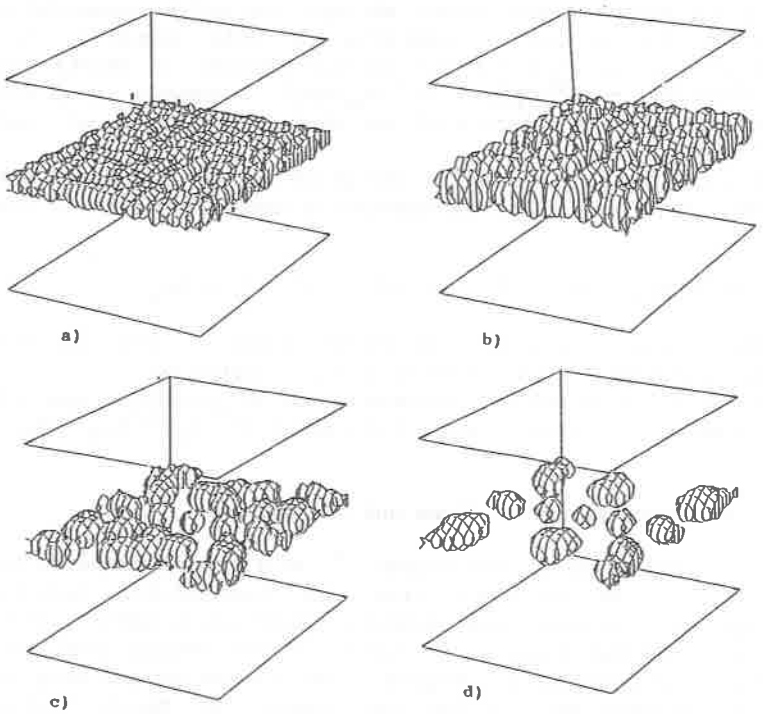

Fig. 1 Comparison of the morphology of the same density contrast surface ($\rho = 4 \times \rho_b$) to the background density. The universe has expanded from initial stage e times for a), e^2 times for b), e^3 times for c) and e^4 times for d).

CAN MORPHOLOGICAL SEGREGATION OF GALAXIES EXIST ON $10h^{-1}$Mpc SCALES?

H.J.MO[1], M.EINASTO[2]

[1]Max-Planck-Institut für Astrophysik, 8046 Garching, Germany
[2]Tartu Astrophysical Observatory, 202444 Toravere, Estonia

ABSTRACT

To test possible morphological segregation of galaxies on large scales, we have used pair-count ratio (between early type and late type galaxies) and clustering analysis to galaxy redshift samples formed in supercluster regions and in regions where there is no apparent large concentration of galaxy distribution, and to galaxy samples in which galaxies in clusters and groups of galaxies are removed. We find that systematic segregation by morphology exists on scales up to $\sim 10h^{-1}$Mpc.

Morphological segregation of galaxies (called MS) in clusters and groups of galaxies has been studied by a number of authors (e.g. Dressler 1980; Postman, Geller 1984). Davis, Geller (1976) and Giovanelli et al. (1986) demonstrated that elliptical and lenticular galaxies are more correlated than spiral galaxies in their two dimensional samples, suggesting MS on larger scales (see Mo 1989 for a review). Here we report briefly our consideration of this problem by using redshift samples and methods that are sensitive to the difference in the distributions of galaxies with different types.

Homogeneous samples are constructed from the CfA redshift survey (Huchra et al. 1983) in the northern hemisphere in different redshift ranges (indicated in the figures) Data is reduced in the same way as in Einasto et al (1984). These samples are divided further into two morphology subsamples of early type (elliptical and lenticular, i.e. $T \leq 0$) and later type ($T > 0$).

First we calculate the pair-count-ratio between late- and early- type galaxies. A total sample S_t is divided into two morphology subsamples (of early and late type galaxies) $S_e + S_l = S_t$, with the numbers of galaxies in the samples related by $N_e + N_l = N_t$ (here $N_l > N_e$). Let $S_l^{\rm diluted}$, $S_t^{\rm diluted}$ be two diluted samples obtained by randomly discarding the exceeding number of galaxies in S_l and in S_t so that $N_l^{\rm diluted} = N_e = N_t^{\rm diluted}$. We define the following pair-count ratio: $\mathcal{R}_{ll/ee}(r) \equiv P_{ll}(r)r^2dr/P_{ee}r^2dr$ and corresponding $\mathcal{R}_{le/ee}(r)$ and $\mathcal{R}_{tt/ee}(r)$, where P_{ll}, P_{ee}, P_{tt} are respectively the numbers of galaxy pairs with separation $r \to r + dr$ in $S_l^{\rm diluted}$, S_e and $S_t^{\rm diluted}$; $P_{le}(r)$ is the number of cross pairs between S_e and $S_l^{\rm diluted}$. These ratios are related to two-point correlation functions of different populations. The results are presented in Fig. 1. Error bars are 1σ among 20 realizations of the dilution. If early- type galaxies are more clustered on a scale r, then $\mathcal{R}_{ll/ee} < 1$ on this scale and vise versa. We see that early type galaxies are systematically more clustered on scales up to $\sim 10h^{-1}$Mpc.

In order to show that the deviation on larger scale is not due to the feature on small scales, we use a population analysis to the same samples. Each galaxy is divided into clustered (CL) or isolated (I) component according to whether or not it has a neighbor with distance smaller than a given radius R. The fraction of early-type galaxies in both the clustered and isolated components are calculated as a function of R. The result is shown in Fig. 2. The fraction of early-type galaxies in the isolated component decreases with R up to $R \approx 6 - 10h^{-1}$Mpc. At these radii there is no dense clusters in the isolated component. The result means that the morphological segregation continues outside of clusters and extends perhaps to filamentary structure of galaxy distribution.

In conclusion we can say that MS can exist in a wide range of densities of density distribution from high-density clusters to low-density regions.

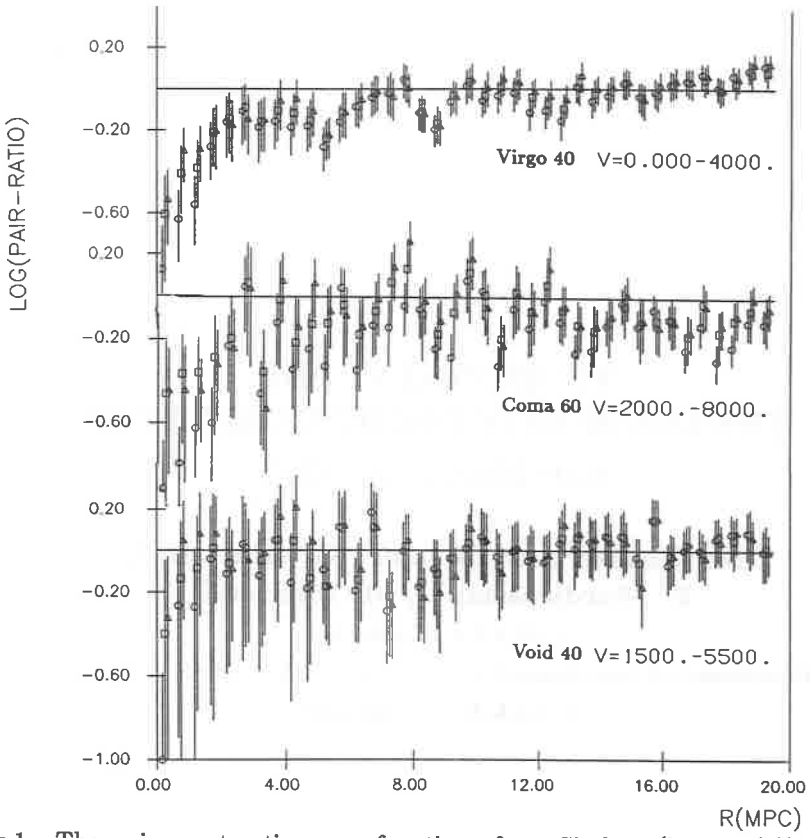

Fig.1. The pair-count ratios as a function of r. Circles: (late-late)/(early-early); triangles: (late-early)/(early-early); squares: (total-total)/(early-early).

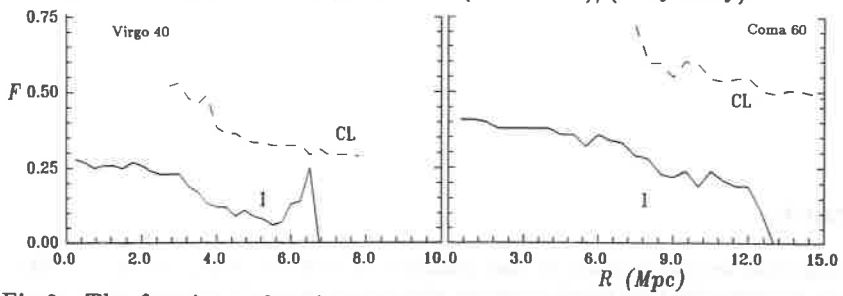

Fig.2. The fractions of early-type galaxies in the clustered (CL, dashed lines) and isolated (I, solid lines) components as a function of neighbourhood radius R.

REFERENCES

Davis M., Geller M., 1976, *Astrophys.J.* **208**,13.
Dressler,A.,1980,*Astrophys.J.* **236**,351.
Einasto J., Klypin A., Saar E., Shandarin S., 1984, *MNRAS*, **206**, 529.
Giovanelli R., Haynes M., Chincarini G., 1986, *Astrophys.J.*, **300**, 77.
Huchra J., Davis M., Latham D., Torry J., 1983, *Astrophys.J. Suppl.*, **52**, 89.
Mo H.J., 1989, in Max-Planck-Inst. für Astroph. Report, No. P3, p24.
Postman M., Geller M.J., 1984, *Astrophys.J.*, **281**,95.

ENVIRONMENT AND THE LUMINOSITY-DIAMETER RELATION FOR DISK GALAXIES

M. Girardi[1], A. Biviano[2], G. Giuricin[2,3], F. Mardirossian[2,3], M. Mezzetti[2,3]

1: S.I.S.S.A., Trieste, Italy

2: Dipartimento di Astronomia, Università degli Studi di Trieste, Trieste, Italy

3: C.I.R.A.C., Trieste, Italy

Abstract

We have collected several samples of disk galaxies, in order to study, in each of them, the relation between the blue total corrected absolute magnitude and the absolute corrected isophotal diameter. These Luminosity-Diameter relations have been compared, in order to detect a possible dependence on the density of the galaxy environment. No significant differences have been found among the several relations, especially if selection criteria relative to the various samples are taken into account. This result is in disagreement with several previous claims.

The tightness of the relationship between luminosity and the absolute diameters of galaxies (hereafter referred to as L-D relation) suggests that possible environmental effects should be detectable from the analysis of its shape in different samples.

We collected data samples from the literature. We looked for two basic parameters, the isophotal diameter D_{25} and the total blue magnitude B_T, both corrected and then transformed to absolute quantities M_B and Δ_{25}. We investigated the L-D relation in its logarithmic form M_B vs. $\log \Delta_{25}$. To each data sample we fitted the straight regression line. The comparison of different lines was given a statistical meaning via the use of the *Welch* test or the *Homogeneity* (*Variance-ratio*) test. These test yielded the probabilities that the differences in the intercepts and slopes of the compared fitting lines are significant. First, we compared Aaronson's clusters [1]. Then we compared Virgo[2] different shells, that is three subsamples of galaxies located at different projected distances from the cluster center; the same was performed to Hydra and Fornax clusters[3]. We compared also all cluster and field samples together. We performed other comparisons among samples by NBG[4]. No significant differences have been found among all the several relations, although they were chosen so as to span a large range of galaxy densities. As regard the previous findings[5],[6],[7] concerning the L-D relation for disk galaxies, we are led to say that any previous found difference in the L-D relations can be ascribed to the poor sample, and/or statistics differences in the sample selection criteria, and/or to an incorrect choice of the statistical tool used in the comparison analyses.

Our result can be restated by saying that the environment has a negligible effect on the L-D relations, either because these are physically unaffected by the local density, or because the scatter in the relations is too large and the accuracy in the data is too low, to allow us to detect any significant deviation from sample to sample. Lastly, we may remark that our conclusion on disk galaxies is in line with the recent finding by Giuricin et al.[8] on elliptical galaxies, and the theoretical work by Aguilar and White[9].

[1] Aaronson, M., Bothun, G., Mould, J.R., Huchra, J., Schommer, R.A., and Cornell, M.E. 1986, *Ap.J.*, **302**, 536.

[2] Binggeli, B., Sandage, A., and Tammann, G.A. 1985, *A.J.*, **90**, 1681.

[3] Lauberts, A., and Valentjin, E. 1989, *The Surface Photometry Catalogue of the ESO-Uppsala Galaxies* (European Southern Obs.).

[4] Tully, R.B. 1988, *Nearby Galaxy Catalog* (Cambridge Univ. Press) – "NBG".

[5] Peterson, B.M., Strom, S.E., and Strom, K.M. 1979, *A.J.*, **84**, 735.

[6] Giuricin, G., Mardirossian, F., and Mezzetti, M. 1985, *Astr.Ap.Suppl.*, **62**, 157.

[7] Giuricin, G., Mardirossian, F., and Mezzetti, M. 1988, *Astr.Ap.Suppl.*, **72**, 151.

[8] Giuricin, G., Mardirossian, M., Mezzetti, M., and Pisani, A. 1989, *Ap.J.*, **345**, 101.

[9] Aguilar, L.A., and White, S.D.M. 1986, *Ap.J.*, **307**, 97.

SCALE-INVARIANCE AND SELF-SIMILARITY INDUCED BY GRAVITATIONAL INSTABILITY IN EXPANDING UNIVERSE.

Jean-Michel Alimi, Fabien Moutarde
Département d'Astrophysique Extragalactique et de Cosmologie,
Observatoire de Paris-Meudon, Meudon, France.

François R. Bouchet
Institut d'Astrophysique de Paris,
Paris, France.

René Pellat
Centre de Physique Théorique de l'Ecole Polytechnique,
Palaiseau, France.

We investigate numerically and analytically the nonlinear gravitational collapse of collisionless matter in an $\Omega=1$ expanding universe.We focused on the collapse of a single smooth maximum of the density field resulting from the growth of a two- or three-dimensional overdensity, i.e., two or three plane wave density enhancement at right angle, with equal initial amplitude and wavelength, and velocities set to zero initially. We performed high resolution particle-in-cell simulations (up to 256^3particles in a 128^3mesh in three dimensional case). We observed the formation of a core-halo radial density profil. The existence of a virialized core, as well as its size, are determined by the properties of the initial state, i.e., its temperature and homogeneity level (see the discussion about the influence of the initial conditions in Alimi *et al.* 1990). On the contrary, the halo is characteristic of the collapse process itself. For homogeneous and low-temperature initial conditions, a scale-invariant density profile establishes progressively until the collapse time. We emphasize that the power law profile is established before shell-crossing, indicating that it results from the early infall. At early times the power law part is limited to a small range of scales, as the system evolves the scale invariance propagates toward smaller and smaller scales; at the collapse time the density profile is purely scale invariant on more than two decades of scales. The halo density profile is then well-fitted by a

power law of index -1.1 ± 0.05 in two-dimensional case and -1.8 ± 0.1 in three-dimensional case (Figure 1).

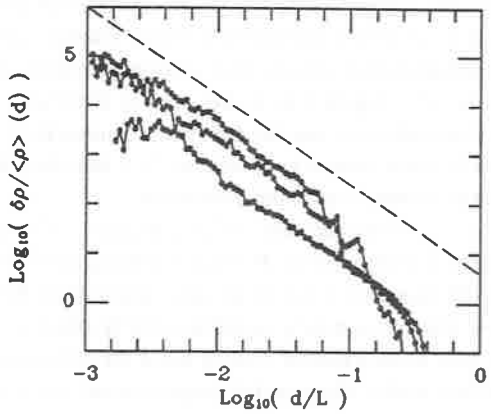

Figure 1: comoving density profiles at different times after the collapse ($a \approx a_{coll}$, lower curve , $a \approx 1.7 a_{coll}$ middle curve , $a \approx 3.3 a_{coll}$, upper-curve) in 3-dimensional case. A $\rho \propto d^{-1.8}$ dashed line is given for comparison.

We can derive analytically the establishment of these power-law profiles. For this purpose, we derived a new analytical approximation of the collapse using a perturbative development starting from the "Zeldovich approximation" (Moutarde *et al.* 1990). After the collapse the system soon reaches a self-similar regime, therefore conserving the same power-law profile (Figure 1). The amplitude increases with the expansion factor a approximatively as $a^{0.55}$ in two-dimensional case, as $a^{1.2}$ in three-dimensional case. Preliminary results concerning the superposition of caustics with unequal amplitudes (corresponding to ellipsoidal initial perturbations), or compensated "hatbox" type overdensities suggest that the aforementioned precollapse scale invariance and self-similarity evolution are generic for structures resulting from gravitational instability in $\Omega=1$ expanding universe, only the power-law index depends on the shape of the initial perturbation. The evolution of the velocity distribution also becomes self-similar both in two- and three-dimensional cases (Figure 2).

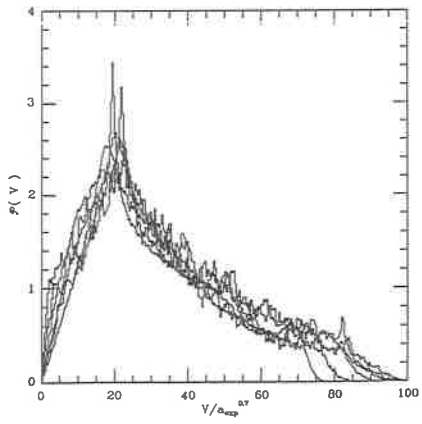

Figure 2: Velocity probability density in the cold and warm cases in 2-dimensional case, at $a \sim 1.6 a_{coll}$, $2.5 a_{coll}$ and $4 a_{coll}$, versus the scaled velocity $V/a^{0.7}$. Apart from the low end, where some evolution is still visible, the distribution evolves self-similarly.

Even though the velocity distribution are very different up to the collapse time, they relax to fairly similar shapes after the collapse by developping a high-velocity tail. The further evolution suggests as expected a self-similar evolution. In order to find the appropriate scaling variable, we simply computed the second velocity moment as a function of the expansion factor, the typical peculiar velocity then scales respectivilely in two- and three-dimensional case as $\sim a^{0.7}$ and as $\sim a^{1.2}$. Figure 2 shows the velocity distribution versus "renormalized" velocity for both the cold and warm case for different expansion facrtor after the collapse (cold and warm case refer to initial kinetic temperature). It is then clear that the high-velocity tail created by the collapse follows a self-similar evolution.

Gunn and Gott (1972) and Gunn (1977) suspected such a self-similarity but had to assume it in their works. Fillmore and Goldreich (1984) and Bertschinger (1985) proved that the self-similarity solutions do exist, and studied them semi-analytically. But they could not prove that such a regime would actually be attained. The precollapse scale-invariance pointed out here gives a natural starting point for self-similarity which was the missing link in the previous works. Moreover the conjectures and predictions of Fillmore and Goldreich (1984) on such a regime have been tested and mostly verified, except that in our case the slope is not an asymptotic value, but is conserved from the precollapse phase, keeping some memory of the initial overdensity.

REFERENCES

Alimi, J.-M., Bouchet, F., Pellat, R., Sygnet, J.-F. and Moutarde, F. 1990, *Ap.J.*, **354**, 3.
Bertschinger, E. 1985, *Ap.J.Suppl.*, **58**, 39.
Fillmore, J.A. and Goldreich, P. 1984, *Ap.J.*, **281**, 1.
Gunn, J.E. and Gott III, J.R. 1972, *Ap.J.*, **176**, 1.
Gunn, J.E. 1977, *Ap.J.*, **218**, 592.
Moutarde, F., Alimi, J.-M., Bouchet, F.R., Pellat, R. and Ramani, A. 1990, *in preparation.*

MOTIONS AND ACCUMULATION OF THE MATTER IN THE NEAR UNIVERSE

J. M. Martín-Mirones[1,2] and L. J. Goicoechea[1]

[1]Departamento de Física Moderna, Universidad de Cantabria, Avda. de Los Castros s/n, E-39005 Santander, Spain.

[2]Osservatorio Astronomico di Padova, Vicolo dell'Osservatorio 5, I-35122 Padova, Italy.

Abstract.

By using data about the motions of the Local Group with respect to 11 different reference frames placed at distances $< 40h^{-1}$ Mpc, we can obtain an effective dynamical spectrum $P_v(k) \propto k^{-2}$, which is valid on scales $5h^{-1} - 40h^{-1}$ Mpc. This spectrum reproduces (as typical values) both the data obtained by de Vaucouleurs and Peters[5)] and the new results derived by us from a sample of 300 elliptical galaxies. The behaviour proportional to k^{-2} can account for the observations by references 1 and 6 at 90% confidence level. Moreover, this phenomenological result suggests that the dark matter dominates on scales $< 40h^{-1}$ Mpc (the dynamical behaviour associated with the luminous matter must be characterized by the spectrum $P_v(k) \propto k^{-3.2}$). To do this analysis, we have considered the dispersion in the estimation of the redshifts due to the peculiar (gravitational and "thermal") motions of the galaxies; so, in order to calculate expected values and to normalize the spectra, we have used the Gaussian window $W_G(kR) = \exp(-k^2R^2)$ instead of the standard one (associated with the "top hat" model). On the other hand, by using again this Gaussian window, we have obtained that a universe dominated by adiabatic cold dark matter ($\Omega = 1$, $h = 0.5$) agrees well with the dynamical data when the bias parameter is $b = 2 - 2.5$. Finally, the observed correlation for Abell clusters (at separations $< 25h^{-1}$ Mpc) can be reproduced by means of the models derived from the dynamical observations. We have considered the data obtained in reference 13 as a lower limit and the correlation suggested in reference 2 as an upper limit.

1.The Data.

In order to study the large-scale structure and motions of the matter in the local universe ($< 40h^{-1}$ Mpc), we have used two sets of data. Firstly, the Local Group velocities with respect to 6 concentrical shells placed at distances between ≈ 600 km s^{-1} and ≈ 3600 km s^{-1} obtained by de Vaucouleurs and Peters[5)] from a sample of 600 galaxies of all types whose distances have been measured by means of different estimators: luminosity indices, Tully-Fisher relation, Faber-Jackson relation and diameters of inner ring structures in galaxies.

Secondly, the spectroscopic and photometric data for 300 elliptical galaxies out to ≈ 6000 km s^{-1} obtained in references 3 and 4 from which we have carried out a new analysis of the Local Group motion. The sample has been divided into 10 concentrical subsamples whose mean distances go from 1000 km s^{-1} up to 5500 km s^{-1} (width =1000 km s^{-1}). In order to calculate the distances, we have used a new estimator based on the relation $\sigma - D_n$[9], where D_n is the diameter within which the corrected mean surface brightness of a galaxy is 20.75 B mag arcsec^{-2} and σ is the velocity dispersion in the galaxy. The corrections made are: galactic extinction, K-correction and $(1+z)^4$ correction to aperture magnitudes in D_n, change in the linear aperture size as a function of the distance and redshift effects in σ and cosmological and Malmquist effects in the obtained distance. The magnitude of the error in the determination of Ln(distance) is $\Delta = 0.2$[9]. The solutions for the Local Group motion have been obtained by using the maximum likelihood procedure assuming the standard behaviour for the ith galaxy: $z_i = d_i - \vec{\Delta v} \cdot \vec{n}_i$, ($z_i$ =redshift, d_i =distance [in km s^{-1}], $\vec{n}_i$ =angular position and $\vec{\Delta v}$ =relative motion of the Local Group with respect to the concentrical shell). We have excluded the galaxies close to the Virgo cluster and the Hydra-Centaurus supercluster to remove the quadrupole moments in the surroundings of those regions and the galaxies whose residues $|z_i - d_i| \geq 2\sigma$, where σ^2 is a "mean" dispersion of the residues in the shell. Besides using individual galaxies, we have also grouped the data into regions of approximately equal sky areas, treating all the areas with equal weights irrespective of their population.

2.Results and Theoretical Implications.

In general, the dynamical data obtained by using galaxies and areas agree. In Table 1, the adopted solutions for $\vec{\Delta v}$ appear (in Galactic coordinates; Rn refers to the shell whose mean distance is nh^{-1} Mpc). We see that the value of Δv increases when the mean distance increases. Moreover, the angle formed by $\vec{\Delta v}$ and $\vec{v}_{dip}$ decreases gradually. The increase of α at R35 and R40 may be due to an infall of the galaxies toward a region in the surroundings of these shells. The vector $\vec{\Delta v}$ for R30 is clearly coincident with $\vec{v}_{dip}$. So, our new dynamical data confirm the trend reported by de Vaucouleurs and Peters[5]: the shell of galaxies at a distance of ≈ 3000 km s^{-1} is at rest with respect to the CMB, and consequently, a very local attractor (distance < 4000 km s^{-1}) is compatible with this fact. The comparison of these results have been made with the phenomenological velocity power spectra $P_v(k) \propto k^n$ (n =0, -1, -2, -3.2; the latter value is obtained from the autocorrelation function for galaxies and clusters[7]), the standard model dominated by adiabatic cold dark matter (CDM) ($\Omega = 1$, $h = 0.5$) and the mix model constituted by adiabatic CDM and non-gravitational "thermal" motions. The normalization is: for $P_v(k) \propto k^n$, $v_{rms}(R_{LG} = 5h^{-1}$ Mpc)=650 km s^{-1}, (peculiar motion of the Local Group with respect to the CMB), for the standard model, $\delta_{gal}(R) = b(R)\delta_{rms}(R) = 1$ [$R = 8h^{-1}$ Mpc and b(R)=bias parameter] and for the mix model, we use both conditions. In these normalizations, we have considered the dispersion in the estimation of the redshifts due to the peculiar (gravitational and "thermal") motions of

Table 1.- Adopted solutions for the motion of the Local Group

shell	Δv[a]	Δv_x[a]	Δv_y[a]	Δv_z[a]	α[b]	$\cos\alpha$[b]
R10	160	39	111	-107	158°	-0.93
R15	363	-315	-165	72	68°	0.37
R20	532	-424	-310	82	63°	0.45
R25	519	-324	-316	255	46°	0.70
R30	570	94	-294	480	20°	0.94
R35	602	470	-52	372	57°	0.55
R40	651	424	-66	490	51°	0.63
R45	704	-173	-287	619	34°	0.83
R50	834	-311	-731	256	35°	0.82
R55	852	-90	-847	32	39°	0.78

[a] km s^{-1}.
[b] α =angle formed by $\Delta v = (\Delta v_x, \Delta v_y, \Delta v_z)$ and the velocity of the Local Group with respect to the CMB: $v_{dip} = (83, -504, 403)$.

the galaxies; so, we have used the Gaussian window $W_G(kR) = \exp(-k^2R^2)$ instead of the standard one (associated with the "top hat" model). The main conclusions of the comparison of the theoretical results with the observational ones are:

(a) The effective dynamical spectrum that describes the observations in a better way is $P_v(k) \propto k^{-2}$ (this spectrum is compatible with the observations that appear in references 1 and 6 at 90% confidence level). This fact suggests that the non-galactic dark matter dominates the local universe on scales $< 40h^{-1}$ Mpc. If we admit a cutoff $k_o^{-1} \approx 20h^{-1}$ Mpc, the relative motions of the Local Group can be reproduced by means of the spectrum $P_v(k) \propto k^{-3.2}$. However, the observed correlation function for Abell clusters (at $r > 20h^{-1}$ Mpc) is consistent with the existence of wavenumbers $k^{-1} > 20h^{-1}$ Mpc.

(b) A standard universe is also consistent with the dynamical data if the bias parameter (on a scale of $8h^{-1}$ Mpc) is $b = 2$ or $b = 2.5$ (the latter, when we consider a mix model with adiabatic CDM and "thermal" motions). In previous studies[8,10] based on the standard window, the bias parameter $b = 2$ was rejected; these previous results are not surprising since the constants of normalization verify A(Gaussian)$\approx$4 A(standard).

(c) In order to obtain information about the large-scale structure of the matter, we have used the effective dynamical spectrum $\propto k^{-2}$. Then, the power spectrum of the density fluctuations is approximately constant (white noise). On scales of $\approx 10h^{-1}$ Mpc, the bias parameter predicted by the dynamical data is $b \approx 2.6\Omega^{0.6}$ (so, $b \approx 2.6$ if $\Omega = 1$ [which agrees with the observational result of $b \approx 3$ on scales of ≈ 1000 km s^{-1} for $\Omega \approx 1$ obtained from the Local Supercluster] and $b < 1$ if $\Omega = 0.1$). Moreover, at separations $r < 25h^{-1}$ Mpc, the two-point correlation for clusters (coherence length$= 17h^{-1} - 18h^{-1}$ Mpc) is consistent with the observed correlation for Abell clusters.

(d) Finally, the observed correlations at $r < 25h^{-1}$ Mpc for Abell clusters can be reproduced by means of a biased ($b = 2 - 2.5$) standard model (coherence length$\approx 20h^{-1}$ Mpc). We have used both the correlation function $\xi_c(r) = \left(\frac{r}{14h^{-1}\mathrm{Mpc}}\right)^{-1.8}$ obtained in reference 13 from the Struble and Rood catalogue[12] (588 Abell clusters with richness class ≥ 0) restricted to $|b| \geq 30°$ and $z \leq 0.3$ and the two-point correlation function (richness class $=1$) $\xi_c(r) = \left(\frac{r}{25h^{-1}\mathrm{Mpc}}\right)^{-1.8}$ suggested in references 2 and 11.

References.

[1] Aaronson, M., Huchra, J., Mould, J., Schechter, P. L., and Tully, R. B. 1982, *Ap. J.*, **258**, 64.

[2] Bahcall, N. A., and Soneira, R. M. 1983, *Ap. J.*, **270**, 20.

[3] Burstein, D., Davies, R. L., Dressler, A., Faber, S. M., Stone, R. P. S., Lynden-Bell, D., Terlevich, R. J., and Wegner, G. 1987, *Ap. J. Suppl.*, **64**, 601.

[4] Davies, R. L., Burstein, D., Dressler, A., Faber, S. M., Lynden-Bell, D., Terlevich, R. J., and Wegner, G. 1987, *Ap. J. Suppl.*, **64**, 581.

[5] de Vaucouleurs, G., and Peters, W. L. 1984, *Ap. J.*, **287**, 1.

[6] Hart, L., and Davies, R. D. 1982, *Nature*, **297**, 191.

[7] Kaiser, N. 1984, *Ap. J. Letters*, **284**, L9.

[8] Kaiser, N. 1988, *M. N. R. A. S.*, **231**, 149.

[9] Lynden-Bell, D., Faber, S. M., Burstein, D., Davies, R. L., Dressler, A., Terlevich, R. J., and Wegner, G. 1988 *Ap. J.*, **326**, 19.

[10] Martín-Mirones, J. M., and Goicoechea, L. J. 1990, *Ap. J.*, submitted.

[11] Postman, M., Geller, M. J., and Huchra, J. P. 1986, *A. J.*, **91**, 1267.

[12] Struble, M. F., and Rood, H. J. 1987, *Ap. J. Suppl.*, **63**, 543.

[13] Sutherland, W. 1988, *M. N. R. A. S.*, **234**, 159.

The Edinburgh Infrared Survey.

K. Glazebrook,
Department of Astronomy, University of Edinburgh, Edinburgh EH9 3HJ.

J.A. Peacock, L. Miller and C.A. Collins,
Royal Observatory, Edinburgh EH9 3HJ.

Abstract

We have completed a blank field infrared survey to a depth of K = 17.5 covering 575$\Box'$ of sky resulting in a sample of 450 objects. The prelimnary 2μm galaxy counts from one of our fields is presented and compared with the optical b_j counts. The predicted counts from different cosmological models are discussed.

Infrared Galaxy Counts

Faint samples of field galaxies provide an important tool in the study of the evolution of galaxies at large lookback times. In recent years various workers have shown that the slope of the B band galaxy galaxy counts from B = 18 to B = 28 is too steep to be explained by simply redshifting the local galaxy population. The obvious explanation was luminosity evolution at early epochs, however this has been shown to be inconsistent with deep redshift surveys. For example Colless *et al.* (1990) showed that even at $b_j = 22$ the mean galaxy redshift was only $\overline{z} = 0.312$, consistent (apart from the normalisation) with the no-evolution model and not showing the high-redshift tail which would be expected from simple luminosity evolution. Another possible explanation would be *number density* evolution of field galaxies, perhaps via some merging model. This would be less satisfactory as it requires a large change in the number of galaxies (by a factor of 2) in the very recent past (2–4 Gyr).

By observing in the infrared it is possible to disentangle the effects of luminosity and number density evolution. The B-band light is dominated by the light of massive short-lived O and B stars and so is very sensitive to the continuing star-formation history of the galaxy. The

K band (2 μm) light comes mainly from the old red stellar population and is less sensitive to star-formation. Thus the K band provides a much better tracer of the bulk mass of galaxies.

Figure 1 shows the K galaxy counts from several of our fields (354 $\Box'$) where we have performed star-galaxy seperation on R band CCD images of our infrared objects resulting in 182 galaxies. These define the bright end on the K counts down to K = 17. Also shown are the deep K counts of Cowie *et al.* (1990) from 1.6 $\Box'$ of sky which define the faint end down to K = 21 and the *bj* galaxy counts compiled from a number of studies.

Non-evolving models have been constructed using galaxy templates for K-corrections (Guideroni & Rocca-Volmerange, 1988) and an infrared luminosity function for each Hubble type based on the B band one shifted by zero redshift B − K colours. This agrees with the infrared luminosity function derived from the Durham/AAT redshift survey (Sharples, R.M., 1990, private communication). Non-evolving curves are shown for $\Omega_0 = 0$ and $\Omega_0 = 1$ cosmologies; it can be seen that while they seriously underpredict the B band data they provide a good fit in K.

Alternative World Models

Galaxy counts can in principle be used to differentiate between Friedmann models and alternative cosmologies such as the "tired light" model (Hubble & Tolman, 1935). Unfortunately this is seriously compromised in the optical by luminosity evolution and in fact tired light provides an embarassingly good fit to the $N - m$ and $N - z$ data! As the infrared light is insensitive to luminosity evolution the K galaxy counts allow a better test to be made. Figure 1 also shows the predictions of a non-evolving tired light cosmology and that of a cosmology where the energy density of the universe is dominated by the cosmological constant. If the curves are normalised at K = 16 using our data then the faint end prediction is inconsistent with the deep counts of Cowie *et al.*

References

Colless, M.M., Ellis, R.S., Taylor, K. & Hook, R., 1990. *Mon. Not. R. Astr. Soc.* **244**, 408.

Cowie, L.L., Gardner, J.P., Lilly, S.J. & McLean, I.S., 1990. *Astrophys. J.*, **360**, L1–L5.

Hubble, E.P. & Tolman, R.C., 1935. *Astrophys. J.* **82**, 302.

Lilly, S.J., Cowie, L.L. and Gardner, J.P., 1990. Preprint.

Metcalf, N., Shanks, T., Fong, R. & Jones, L.R., 1990. Preprint.

Rocca-Volmerange, B. & Guideroni, B., 1988. *Astr. Astrophys. Suppl. Ser.* **75**, 93.

Tyson, J.A., 1988. *Astr. J.*, **96**, 1.

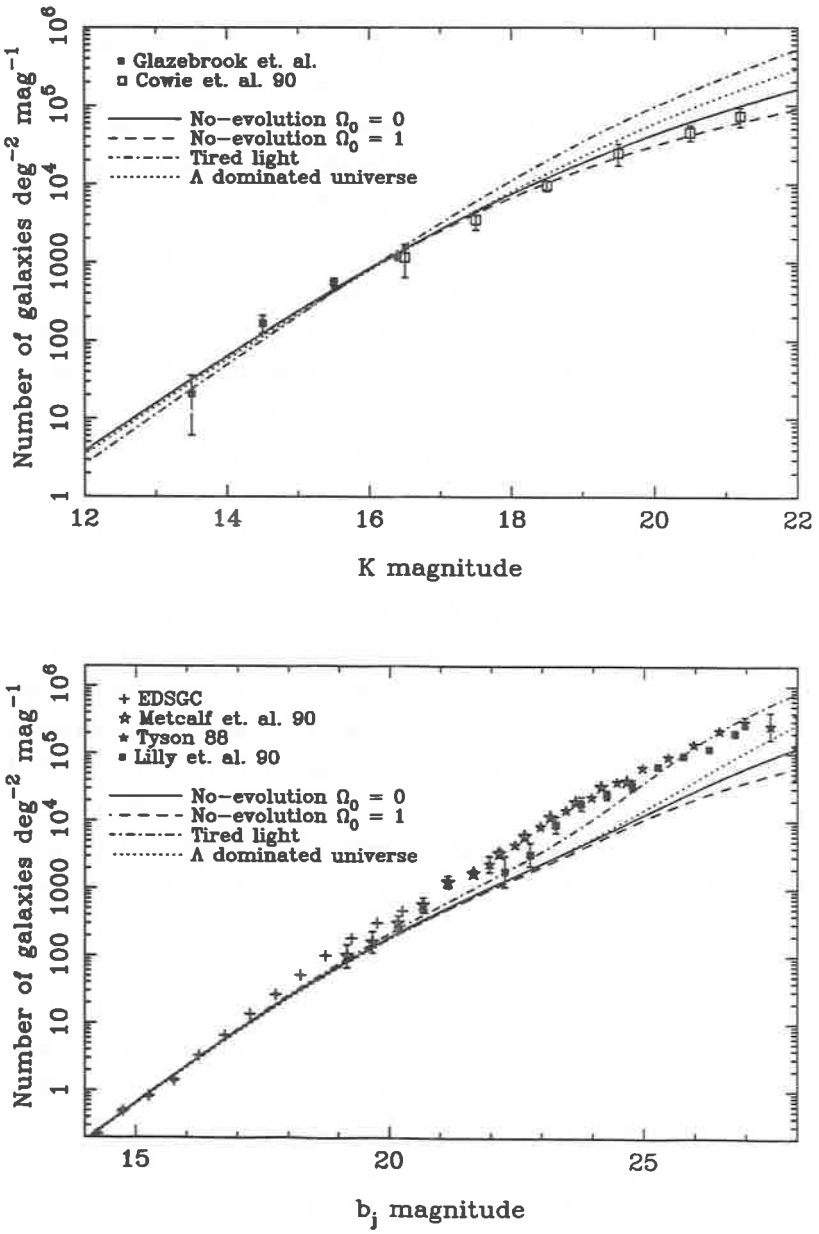

Fig. 1. The K band (top) and B band (bottom) galaxy counts compared with different cosmological models.

EVIDENCE FOR EXTINCTION IN THE VIRGO CLUSTER

A. Biviano[1], G. Giuricin[1,2], F. Mardirossian[1,2], M. Mezzetti[1,2], Y. Rephaeli[3]

1: Dipartimento di Astronomia, Università degli Studi di Trieste, Trieste, Italy

2: C.I.R.A.C., Trieste, Italy

3: School of Physics and Astronomy, Tel Aviv University, Tel Aviv, Israel

Abstract

We report the results of an analysis of color excesses and distance moduli of a sample of spiral galaxies in the Virgo cluster area. A significant correlation was found between color excesses and distance moduli obtained via the blue Tully-Fisher relation. No such correlation was found in a comparison sample of isolated galaxies. We checked for, but did not find any obvious selection bias to explain this correlation. A possible, though perhaps not the only interpretation is intracluster (IC) extinction of galactic light. If so, the required extinction is estimated to be $A_V \simeq 0.45$ mag, after correcting for the color-magnitude relation. The possibility that this extinction is due to IC dust is marginally acceptable.

The possible existence of dust in clusters of galaxies is of great interest[1]. Therefore, we have began a study of the colors of cluster galaxies in order to see if a systematic change is discernable, perhaps due to intracluster (IC) dust. Here we report the results of an analysis of a sample of spiral galaxies in the Virgo region. We have taken from the literature the data relevant to our analysis, i.e. the color-excesses, defined by $E_{B-V} \equiv (B-V)^0_T - <(B-V)^0_T>$, where $<(B-V)^0_T>$ is the mean, total, standard corrected color per morphological type[2], and the distance-moduli, obtained using the blue Tully-Fisher relation[3].

A strong correlation has been found between color-excesses and distance-moduli of the galaxies in the Virgo region, with significance $> 99\%$. A sample of isolated galaxies far from the Virgo region has been considered as well, in order to have an independent check of this result; no significant correlation was found in this comparison sample. Interestingly enough, improving the mean data quality (via a stricter selection criterion) improves the correlation in the Virgo area, yet does not affect the scatter in the sample of isolated galaxies. We have examined possible biases in the corrections applied to the colors, or in the determination of the distance-moduli. Only the known Color-Magnitude relation[4], was found to affect the correlation somewhat; we have corrected for this relation.

The correlation found can be interpreted as evidence for extinction in the Virgo cluster itself, since no such correlation is evident in the comparison sample of isolated galaxies. The extinction induced by the cluster can be estimated to be: $E^{Virgo}_{B-V} = 0.15 \pm 0.06$, corresponding to a visual extinction: $A^{Virgo}_V = R_V\ E^{Virgo}_{B-V}$ mag, R_V ranging from 1 to 3.

A physical explanation for the deduced extinction could be IC dust in Virgo. However, the deduced extinction implies that the effective time during which dust has been sputtered at the present rate by the hot IC gas, should be $\leq 3 \times 10^9$ years. The implied ratio of dust to gas densities is a few times larger than the Galactic value, assuming the same radial distribution. It is difficult to see how the IC value of this ratio can be higher than in the Galaxy. Thus, the deduced correlation may either have a different origin, or the required level of extinction by dust is somehow significantly lower. If this dust is at an effective temperature between 10 – 20 K (see reference 1), its Infra-Red emission could be detected by DIRBE, aboard COBE, at a few 100 μm.

[1] Dwek E., Rephaeli Y., and Mather J. 1990, *Ap. J.*, **350**, 104.

[2] de Vaucouleurs G.: 1977, in: *The Evolution of Galaxies and Stellar Populations*, ed.: B.M. Tinsley and R.B. Larson, Yale Univ. Obs.

[3] Biviano, A., Giuricin, G., Mardirossian, F., and Mezzetti, M. 1990, *Ap. J. Suppl.*, in press.

[4] Griersmith, D. 1980, *A. J.*, **85**, 1295.

ENVIRONMENT AND THE TULLY-FISHER RELATION

A. Biviano[1], G. Giuricin[1,2], F. Mardirossian[1,2], M. Mezzetti[1,2]

1: Dipartimento di Astronomia, Università degli Studi di Trieste, Trieste, Italy

2: C.I.R.A.C., Trieste, Italy

Abstract

We investigate the Blue and the IR Tully-Fisher relations (TFR's) in 10 cluster and three field samples, spanning a large range of galaxy densities. The TFR's fitted on these samples are not found to be signficantly different, given the present data-accuracies. Samples of galaxies with different environment related properties yield non significant different TFR's, as well. The Blue and the IR TFR's are found to give similar accuracies in the galaxy distance estimate.

In order to test the *universality* of the Tully-Fisher relation[1] (TFR in the following), we have collected data from the literature, for 10 samples of galaxy clusters and three "field" samples; these samples span the whole range of galaxy densities. We have studied the TFR using two 21 cm line width parameters corrected for non-rotational motions of the spiral galaxy, V_{max}, and W_R^i (see references 2,3), and two magnitude systems, B_T^0 and $H_{-0.5}^c$. We have scaled all the magnitude axes at the same distance, using the corrected mean velocity of each cluster. The absolute magnitudes of the field galaxies have been rescaled at the clusters distance scale, by minimizing the dispersion of the "field" galaxy magnitudes from the TFR fitted on the cumulative sample of all the cluster galaxies.

The statistical test for homogeneity is passed both by the 10 TFR's fitting the cluster samples alone, and by all the 13 TFR's fitting the cluster and field samples, despite a different degree of "incompleteness bias"[4] affects our samples. Moreover, we do not find any difference when comparing the TFR's for galaxies at different distances from their cluster center, nor do we between the TFR's for galaxies with low and normal HI-content (in accordance with reference 5); the claimed dependence of the TFR on morphological type[6] is not confirmed in our data-samples.

These results indicate that the TFR does not depend on the local galaxy density, nor on related properties. This result holds both for the Blue and the IR TFR's, and does not depend on the choice of the line-width parameter. As a by-product of this analysis, we have estimated that the Blue and the IR TFR's give similar accuracies in the distance-estimates, i.e. $\sim 20\%$. In conclusion, we can say that *we have not found any evidence for an environmental dependence of the TFR.* Environmental effects may possibly be present, but are not seen at the present level of data-accuracy. Our analysis strenghtens the credit of the TFR as a distance-indicator.

[1] Tully, R.B., and Fisher, J.R. 1977, *Astr. Ap.*, **54**, 661.

[2] Bottinelli, L., Gouguenheim, L., Paturel, G., and de Vaucouleurs, G. 1983, *Astr. Ap.*, **118**, 4.

[3] Tully, R.B., and Fouqué, P. 1985, *Ap. J. Suppl.*, **58**, 67.

[4] Bottinelli, L., Gouguenheim, L., and Teerikorpi, P. 1988, *Astr. Ap.*, **196**, 17.

[5] Guhatakurta, P., van Gorkom, J.H., Kotany, C.G., and Balkowski, C. 1988, *A. J.*, **96**, 851.

[6] Rubin, V.C., Burstein, D., Ford, W.K., and Thonnard, N. 1985, *Ap. J.*, **289**, 81.

X-RAY PROPERTIES OF SPIRAL GALAXIES WITH NORMAL AND LOW-ACTIVITY NUCLEI

G. Giuricin[1,2], G. Bertotti[3], F. Mardirossian[1,2], M. Mezzetti[1,2]

1: Dipartimento di Astronomia, Università degli Studi di Trieste, Trieste, Italy

2: C.I.R.A.C., Trieste, Italy

3: Center for Advanced Research in Space Optics, Padriciano 99, Trieste, Italy

Abstract

A statistical analysis of the soft X-ray emission of about 100 spiral galaxies with normal and low-luminosity active nuclei (LINERs and Seyferts 2) – derived from published observations obtained with the "Einstein Observatory" – has revealed that Seyfert 2 galaxies turn out to be, on average, stronger X-ray sources (per unit light) than non-Seyfert galaxies. Galaxies with LINER nuclei and HII region-like nuclei display X-ray emissions of comparable strength. More enhanced X-ray emission has been found in interacting galaxies compared to normal galaxies.

Introduction

We have done a statistical analysis of the soft ($\sim$ 0.5-4.0 kev) X-ray data – compiled from published observations in the soft X-ray band of the "Einstein Observatory" – of $\sim$ 100 bright ($B_T^0 \leq 13.5$) spiral galaxies with normal and low-luminosity active nuclei (LINERs and Seyferts 2). We have treated the upper limits on the X-ray emission by using techniques typical of the field of survival analysis.

Results

The major results of our study, which has revealed a number of previously unrecognized features of the soft X-ray emission, can be summarized as follows:

i) the Seyfert 2 galaxies (the least powerful class of X-ray sources of the Seyfert sequence) appear to be, on average, stronger soft X-ray emitters (per unit light) than non-Seyfert galaxies; on the contrary, Seyfert 2 galaxies have normal X-ray-to-radio luminosity ratios. Our finding is consistent with the recent claim[1)] – based on the scans of HEAO-1 A2 data – of a positive average hard X-ray signal (in the 2-10 kev range) for Seyfert 2 galaxies selected from a flux-limited (at 12 μm) sample of active galaxies. Nevertheless, the same authors reported no positive average X-ray signal from the sample of spectroscopically-selected Seyferts 2 of the Center for Astrophysics redshift survey.

ii) Among non-Seyfert galaxies, the two classes of galaxies with LINER and HII region-like nuclei display X-ray emission of comparable strength (per unit optical and radio luminosities). This finding does not seem to be trivial, since the former class of galaxies exhibit, on average, weaker radio emission than the latter class[2)] .

iii) "Arp-atlas" galaxies and interacting galaxies are characterized by an excess of X-ray emission (per unit light) with respect to normal galaxies; however, they have normal or relatively low X-ray-to-radio luminosity ratios, probably because of a corresponding appreciable increase in the radio emission. This result, which is in line with the general results of radio surveys which show an excess of radio emission in paired,interacting, and peculiar galaxies when compared with samples of relatively isolated and normal galaxies, sounds like a strong confirmation of some earlier suggestions (based on poor statistics) indicating enhanced soft X-ray emission in peculiar galaxies[3)] .

[1] De Zotti,G.,Danese,L.,Franceschini,A.,Persic,M.,Toffolatti, L.,1989, Proceedings of the 23rd ESLAB Symp. on Two Topics in X-ray Astronomy (Bologna,Italy), p.737.

[2] Giuricin,G.,Mardirossian,F.,Mezzetti,M.,1988, Astron. Astrophys. 203, 39.

[3] Fabbiano,G.,Feigelson,E.,Zamorani,G.,1982, Astrophys. J. 256, 397.

CLUSTER DIPOLE ANISOTROPY ON LARGE SCALES

Manolis Plionis and **Riccardo Valdarnini**
S.I.S.S.A., International School for Advanced Studies, Strada Costiera 11,
I–34014 Trieste, Italy

ABSTRACT

We have analysed two whole-sky samples of the combined Abell-ACO cluster catalogue; one with $m_{10} \leq 16.4$ which is 80% redshift complete and one with $m_{10} < 17$ which is $\sim$ 55% redshift complete. We have calculated the peculiar acceleration induced by the cluster distributions on the Local Group. The cluster dipole points within $\lesssim 10°$ of the CMB dipole direction which indicates that clusters trace the mass. The dipole amplitude converges at $\sim 150\ h^{-1}\ Mpc$, within the completeness limit of the catalogue. Most of the Local Group peculiar velocity is induced by matter fluctuations within $\sim 50\ h^{-1}\ Mpc$. The Shapley's concentration (else known as 'Giant-Attractor' or 'alpha region') at a depth of $\sim 140\ h^{-1}\ Mpc$, is responsible for $\lesssim 20\%$ of the Local Group's peculiar velocity. Using linear perturbation theory we find $4.5 \lesssim b\Omega_o^{-0.6} \lesssim 6$ (with b the biassing factor). We also find that the dipole anisotropy extends in depth and has a scale-length of $\sim 300\ h^{-1}\ Mpc$. Dividing the survey volume (up to $\sim 300\ h^{-1}\ Mpc$) into equal-volume shells of $\delta V \sim 4 \times 10^6\ h^{-3}\ Mpc^3$ we obtain that out to $\sim 160\ h^{-1}$ Mpc the acceleration induced by each shell is roughly aligned with the CMB dipole direction. The probability of this being due to chance is only $\sim 10^{-6}$.

1. INTRODUCTION

We analyse here the optical dipole for clusters of galaxies. This calculation is now possible thanks to the recently published southern extension of the Abell cluster catalogue ([1], hereafter ACO) which enables one to attempt to construct a homogeneous whole-sky cluster catalogue. Under the assumption that light traces the mass and because both fluxes and gravity fall as r^{-2}, the dipole moment is a measure of the peculiar force acting on the LG.

Up to now various populations have been used in this procedure : optical galaxies [2] [8], IRAS galaxies [13], X-ray clusters [4] and X-ray AGNs [6]. The optical and IRAS dipole (samples with characteristic depths of $\sim 60\ h^{-1}\ Mpc$) are aligned with the CMB dipole [3] [5] and the source of the LG motion is found to be within $\sim 3500\ km/sec$. However there is evidence for large mass aggregates at much larger distances [12].

2. METHOD

We have calculated the dipole moment ($\propto$ peculiar acceleration) of the cluster distributions (*using estimated redshifts only when the observed z's were not available*), *i.e.*;

$$\mathbf{D} = \frac{3}{4\pi} \sum_i W(r_i) \frac{\delta M_i}{r_i^2}\, \mathbf{r}_i \qquad (1)$$

where $\mathbf{g} = \frac{4\pi}{3} G\mathbf{D}$, $\mathbf{D}$ is the dipole moment of the cluster distribution and $W(r_i)$ is a radial function that equates the mass densities of the Abell and ACO samples (details will appear in [10]). We model Galactic obscuration effects by using various masks the choice of which does not alter our main results. The best mask, in the sense that it takes into account all the available data, models in more detail the obscuration effects and which also gives the best directional agreement between the CMB and the cluster dipole, is a coupled mask that accounts for the fact that we have a limited sample to $|b| \sim 13°$ and also for the usual smooth $cosec|b|$ dependence of the data with $|b| > 13°$.

3. MAIN RESULTS

(i) We find the cluster dipole pointing within $\lesssim 10°$ of the CMB dipole direction which indicates that clusters trace the mass. The dipole amplitude converges at $\sim 150\ h^{-1}\ Mpc$, within the completeness limit of the catalogue.

(ii) Most of the Local Group peculiar velocity is induced by matter fluctuations within $\sim 50\ h^{-1}\ Mpc$. The 'Giant-Attractor' or 'alpha region' [12], at a depth of $\sim 140\ h^{-1}\ Mpc$, is responsible for $\lesssim 20\%$ of the Local Group's peculiar velocity (in agreement with [11]).

(iii) Using linear perturbation theory [7], $\mathbf{v}_p = \frac{2}{3} H_\circ^{-1} \Omega_\circ^{-0.4} \mathbf{g}$, with $\mathbf{g}$ the gravitational acceleration induced by the distribution of clusters onto the Local Group of

galaxies, we find the Universe to be open with $\mathbf{4.5 \lesssim b\Omega_o^{-0.6} \lesssim 6}$.
(iv) Dividing the survey volume (up to $\sim 300\ h^{-1}\ Mpc$) into equal-volume shells of $\delta V \sim 4 \times 10^6\ h^{-3}\ Mpc^3$. we find that out to $\sim 160\ h^{-1}$ Mpc the peculiar acceleration induced by three shells is aligned (within $\lesssim 26°$) with the CMB dipole direction while in one (the 99 - 125 $h^{-1}\ Mpc$ shell) it is 56° away, pointing roughly towards the Centaurus direction. The random joint probability that the acceleration induced by the 4 equal-volume shells is aligned with the CMB dipole direction is $\sim 9 \times 10^{-7}$! This result supports the suggestion of [8] [9] that **the same anisotropy, which is responsible for the Local Group motion extends in depth much further $\sim 50\ h^{-1}$ Mpc.**

References

[1] Abell, G.O., Corwin, H.G. & Olowin, R.P. 1989, *Astrophys.J. Suppl.* **70**,1

[2] Lahav, O. 1987, *Mon. Not. R. astr. Soc.* **225**, 213

[3] Lahav, O., Rowan-Robinson, M., and Lynden-Bell, D. 1988, *M.N.R.A.S.*, **234**, 677

[4] Lahav, O., Edge, A.C., Fabian, A.C. & Putney, A. 1989, *Mon. Not. R. astr. Soc.* **238**, 881

[5] Lynden-Bell, D., Lahav, O. & Burstein, D. 1989, *Mon. Not. R. astr. Soc.*, **241**, 325

[6] Miyaji, T & Boldt, E. 1990, *Astrophys.J.*, **353**, L3

[7] Peebles, P.J.E. 1980, *The Large-Scale Structure of the Universe*, Princeton University press

[8] Plionis, M. 1988, *M.N.R.A.S.*, **234**, 401

[9] Plionis, M. 1989, *M.N.R.A.S.*, **238**, 417

[10] Plionis, M. & Valdarnini, R. 1990, *M.N.R.A.S.*, submitted

[11] Raychaudhury, S. 1990, *Nature*, **342**, 251

[12] Scaramella, R., Baiesi-Pillastrini, G., Chincarini, G., Vettolani, G. & Zamorani, G. 1989, *Nature*, **338**, 562

[13] Strauss, M.A. & Davis, M. 1989, *Large Scale Motion in the Universe*, eds V.C.Rubin & G.Coyne, Princeton University press, pp 255

MICROLENSING IN THE EINSTEIN CROSS 2237+0305

Hans-Jörg Witt Rainer Kayser Sjur Refsdal

Hamburger Sternwarte
Gojenbergsweg 112
D-W2050 Hamburg 80
Germany

Abstract

We present predictions of the frequency of high amplification events for the four images of 2237+0305. The expected mean frequency is 0.3–0.6 events per year for each image. The probability to obtain *no* event in all four images during one year is only about 4 per cent.

From the observed rapid change in brightness of image A in October 1988 ($\Delta m = 0.4^m$ in 12 days), we obtain a source size of about 10^{-4} pc (transverse velocity 3000 km/s assumed). Our simulations show that it is not necessary to assume a lens mass below 0.1 $M_\odot$ to explain this event.

1. Introduction

From theoretical considerations it has been clear that the quadruple *Einstein Cross* quasar 2237+0305 is the most promising candidate for the observation of microlensing events (Kayser and Refsdal 1989, see also Wambsganss *et al.* 1990). Indeed, a rapid change in the luminosity of image A was recently reported (Irwin *et al.* 1989), which is most likely a high amplification event (HAE) due to the crossing of a (micro-)caustic by the compact optical continuum source of the quasar.

In this contribution we present predictions of the frequency of high amplification events for the four images of 2237+0305, based on the macromodel of Schneider *et al.* (1988), see also Kayser and Refsdal (1989), with all matter condensed in stars.

2. Microlensing Parameters

We here use the notation introduced by Paczyński (1986) and Kayser, Refsdal and Stabell (1986), i.e. σ is the normalized surface density in stars (which is equivalent to the optical depth used by some authors), and γ is the normalized shear. For our calculations we have used a standard Friedmann cosmology ($\Omega = 1, \Lambda = 0$) with $H_0 = 75\mathrm{km/s\,Mpc}$. The redshift of 2237+0305 is $z_s = 1.7$, and the redshift of the lens galaxy is $z_d = 0.039$. This corresponds to a unit length in the source plane of $\zeta_0 = 0.04\mathrm{pc}$. Since the distance ratio D_s/D_d equals approximately 10 for this exceptional object, it seems plausible to assume that the transverse velocity between the source and the caustic network is relatively large due to the projection effect. We here use $V_t = 6000\frac{\mathrm{km}}{\mathrm{s}}$. The unit length then corresponds to a time scale of $\Delta t = 6.7$ years.

3. HAE Classification

During an HAE two microimages either appear or disappear. We denote the events with a plus sign (two images appear) or a minus sign (two images disappear). Two HAE in sequence are then of the kind $+-$, $-+$ or $++$ ($--$), and the corresponding distances between these two events are denoted Δl_{+-}, Δl_{-+}, and $\Delta l{+}{+}$ (Δl_{--}), respectively. Note that $\langle \Delta l_{++} \rangle = \langle \Delta l_{--} \rangle$, since the sequence $--$ is simply obtained by a time reversal of $++$.

4. Numerical Method

We have used the new method of Witt (1990) to analyse the caustic network for a sample of $10,000$ stars (point mass microlenses). For the mass spectrum of the stars we have used the standard Salpeter mass function for a range of 0.1 to 10 solar masses. About $2,000,000$ points of the caustic network were evaluated and stored on tape. These data were then used for a fine analyses of the distribution of the HAEs. The calculation of the caustic network took 2–3 hours per model on a Siemens 7.882 mainframe computer.

5. Results

In the tables we give the mean values of the distances between neighboring high amplification events (in dependence of the angle between the transverse velocity and the shear), as well as the distances within which to expect a HAE with a probability of 50 and 90 per cent, respectively.

For component C the highest frequency of HAE is expected. However, the HAEs will occur very irregularly due to the high tendency for clustering of the caustics. It is, e.g., possible that for a time scale of 5–10 years no event occurs. In contrast, if the source crosses a caustic cluster, 3–5 events per year are expected. The mean frequency for C is 0.5–0.6 events per year. The lowest frequency of HAEs is expected for component A: 0.3–0.5 events per year, depending on the direction of V_t.

The probability to obtain *no* event in all four images during one year is only about 4 per cent, which demonstrates again that 2237+0305 is an outstanding object for monitoring programs.

image A	$\sigma = 0.36$		$\gamma = 0.44$	image B	$\sigma = 0.45$		$\gamma = 0.28$
	0°	45°	90°		0°	45°	90°
$\langle \Delta l_{+-} \rangle$	0.200	0.163	0.136	$\langle \Delta l_{+-} \rangle$	0.157	0.137	0.124
$\langle \Delta l_{-+} \rangle$	0.850	0.640	0.523	$\langle \Delta l_{-+} \rangle$	0.812	0.683	0.584
$\langle \Delta l_{++} \rangle$	0.319	0.250	0.200	$\langle \Delta l_{++} \rangle$	0.248	0.221	0.191
$\langle \Delta l_{tot} \rangle$	0.468	0.347	0.279	$\langle \Delta l_{tot} \rangle$	0.413	0.342	0.293
$l_{tot}(50\%)$	0.184	0.150	0.125	$l_{tot}(50\%)$	0.144	0.130	0.116
$l_{tot}(90\%)$	1.16	0.88	0.72	$l_{tot}(90\%)$	0.99	0.83	0.74

image C	$\sigma = 0.88$		$\gamma = 0.55$	image D	$\sigma = 0.61$		$\gamma = 0.66$
	0°	45°	90°		0°	45°	90°
$\langle \Delta l_{+-} \rangle$	0.104	0.098	0.091	$\langle \Delta l_{+-} \rangle$	0.133	0.113	0.100
$\langle \Delta l_{-+} \rangle$	0.595	0.574	0.521	$\langle \Delta l_{-+} \rangle$	0.679	0.601	0.521
$\langle \Delta l_{++} \rangle$	0.183	0.173	0.148	$\langle \Delta l_{++} \rangle$	0.235	0.197	0.159
$\langle \Delta l_{tot} \rangle$	0.301	0.282	0.252	$\langle \Delta l_{tot} \rangle$	0.355	0.297	0.250
$l_{tot}(50\%)$	0.100	0.096	0.090	$l_{tot}(50\%)$	0.131	0.117	0.097
$l_{tot}(90\%)$	0.706	0.660	0.590	$l_{tot}(90\%)$	0.803	0.677	0.573

6. The October 1988 Event

The rapid change in the luminosity of image A reported by Irwin *et al.* (1989) is most likely a HAE. In October 1988 image A has changed its brightness by $\Delta m = 0.4^m$ on a time scale of 12 days (Irwin, private communication). This time scale corresponds to a source radius of

$$R_s \approx 10^{-4}\,\mathrm{pc}\,\frac{V_t}{3000}\,\mathrm{km/s} \quad . \tag{1}$$

Since microlensing in image A of 2237+0305 can not be treated in the small optical depth approximation, it is not possible to draw any conclusion on the mass of the microlens involved (as, e.g., done by Irwin *et al.* (1989)). From our numerical simulations (Witt *et al.* , in preparation; see also Wambsganss *et al.* 1990) it is, however, clear that it is not necessary to assume a lens mass below $0.1 M_\odot$.

REFERENCES

Irwin,M.J., Webster,R.L., Hewett,P.C., Corrigan,R.T., Jedrzejewski,R.I.: 1989, *Astron. J.* **98**, 1989

Kayser,R., Refsdal,S. and Stabell,R. : 1986, *Astron. Astrophys.* **166**, 36

Kayser,R., Refsdal,S. : 1989, *Nature* **338**, 745

Kayser,R., Witt,H.J. : 1989, *Astron. Astrophys.* **221**, 1

Paczyński,B. : 1986 *Astrophys. J.* **301**, 503

Schneider,D.P., Turner,E.L., Gunn,J.E., Hewitt,J.N., Schmidt,M., Lawrence,C.R. : 1988, *Astron. J.* **95**, 1619

Wambsganss,J., Paczyński,B., Katz,N. : 1990, *Astrophys. J.* **352**, 407

Witt,H.J. : 1990, *Astron. Astrophys.* **236**, 311

DYNAMICAL THRESHOLDING OF PANCAKE MODELS

1. Dynamical Thresholding

T. BUCHERT

Max-Planck-Institut für Astrophysik
D-8046 Garching/Munich, F. R. G.

Abstract

This consideration summarizes the beginning of a detailed study of Lagrangian selection methods to discriminate among *luminous* and *dark* matter, we call this 'Lagrangian biasing'. This appears to be necessary in view of recent results by Kates et al. (1990), who found a striking disagreement between modelled galaxy distributions and distributions traced from initial peaks of the density field (we call the latter 'Eulerian biasing'). It continuous work which has been done in that direction e.g. by Braun et al. 1988, Doroshkevich et al. 1989 and parallels work on Lagrangian selection criteria in numerical simulations like that of Klypin et al. (1989), Kates et al. (1990); (see also the related contribution by T. Buchert, R. Klaffl and references therein as well as Martinez 1989).

Acknowledgements

This work has been performed on the background of a fruitful collaboration with B.J.T. Jones and L. Appel. I am thankful to H.J. Mo and V.J. Martinez for helpful exchange of experience on the correlation function and to A. Schott for plotting Fig.1. I acknowledge financial support by DFG (Deutsche Forschungsgemeinschaft).

References

Braun E., Dekel A., Shapiro P.R. (1988): Ap.J. **328**, p.34.

Doroshkevich A.G., Klypin A.A., Khlopov M.U. (1989): M.N.R.A.S. **239**, p.923.

Martinez V.J. (1989): Ph.D.-thesis, Valencia, p.139ff.

Klypin A.A., Kates R.E., Kotok E.V. (1989): MPA-Report No. 474.

Kates R.E., Kotok E.V., Klypin A.A. (1990): Astron. Astrophys., in press.

Figure Captions

Fig.1: Different "dynamical thresholds":

Fig.1a shows a typical evolution profile of the Lagrangian density contrast $\chi = (1+\delta)(t)$ along one particle trajectory. Below, we shall illustrate differences of thresholding by indicating the corresponding branch of the modulus of this profile. Chosen are three types of threshold to give examples:

Fig.1b: **"P-threshold"**: We take all particles as luminous if $|\chi| > \chi_c$ or $\chi < 0$. Its meaning is that "galaxies" remain luminous after beeing lighted up. This type selects all internal points of pancakes if χ_c is chosen appropriate. In general, it also selects some peripheric points.

Fig.1c: **"A-threshold"**: We paint all particles *luminous* which obey the criterium $|\chi| > \chi_c$. Thus, we select a subbranch of **"P"**: The "galaxy" lights up at this density threshold, but as soon as this formation condition is violated ($-\chi < -\chi_c$), the "galaxy" extinguishes again, (destabilizes), i.e., is formally removed from the sample. This type selects points around the pancake ridge and thus gives results similar to 'Eulerian biasing' at $Z = 0$.

Fig.1d: **"D-threshold"**: Both methods above guarantee early formation of "galaxies", depending only on the local density surroundings, χ_c determines the onset of the formation epoch to be subjected to Quasar constraints. Another possibility is to

delay galaxy-formation according to intrinsic formation time scales, which gives late formation of a "second generation" of objects (late galaxy formation). Here the threshold selects a late branch of the profile. In contrast to type **"A"**, which emphasizes the filamentary structures, **"D"** shifts the topology of the smoothed sample to that of a cluster-pattern. Thus, different methods of selection induce differences in local structure characteristics (see part 2 of this contribution).

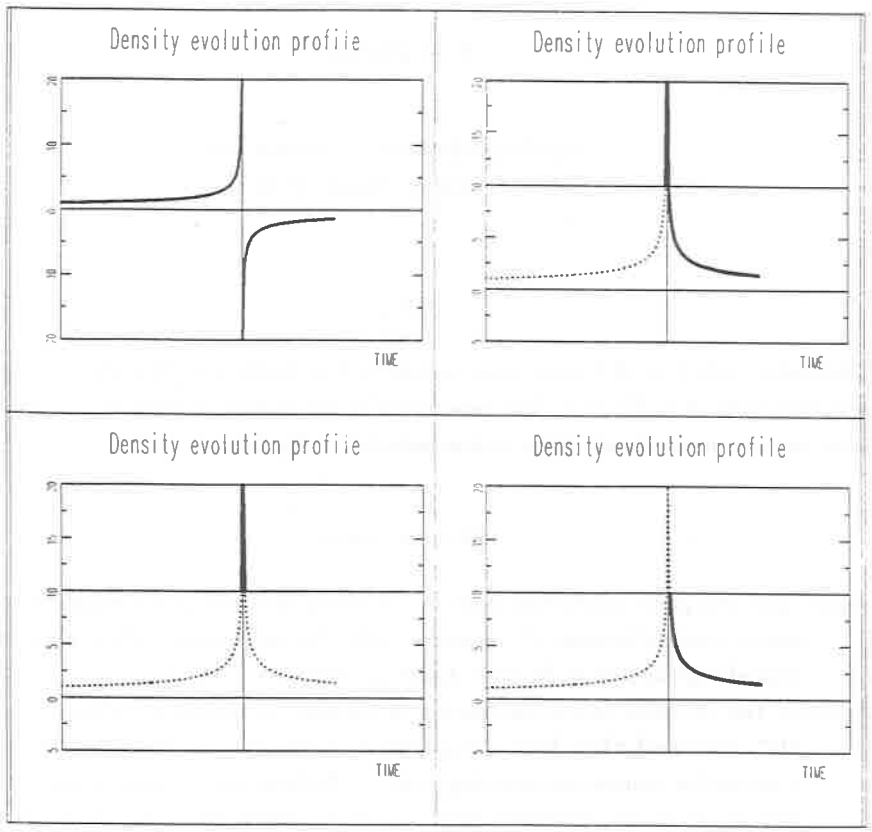

Figure 1: Different dynamical thresholds: Density profile and selected branches

DYNAMICAL THRESHOLDING OF PANCAKE MODELS

2. The Two-point Correlation Function

T. BUCHERT

Max-Planck-Institut für Astrophysik
D-8046 Garching/Munich, F. R. G.

Abstract

The scaling behaviour of the two-point correlation function is tested for different threshold selection methods in *Fig.2a-c*. The dependence of the correlation function amplitude and slope on 'dynamical thresholding' is demonstrated in *Fig.2d-i*.

Figure Captions

Fig.2: The two-point correlation function of thresholded samples obtained from two-dimensional realizations of a pancake model (for explanations of the model see the related contribution by Buchert, Klaffl and references therein).

Fig.2a-c: The two-point correlation function of samples thresholded according to the types **"P", "A" and "D"**. Here, the amplitude of the reference function $5.7(r/r*)^{-1.77}$ is chosen for comparison of scaling regimes. Different spatial regimes can be distinguished, where the correlation function obeys a scaling law of the observed slope.

Fig.2d-i: The two-point correlation function of samples thresholded according to the types **"P", "A" and "D"** and for different threshold values. Here, the amplitude of the reference function $0.176(r/r*)^{-1.8}$ is chosen according to the correction obtained by Kates et al. (1990) to relate the 2D calculation to the observed 3D correlation length $r* = 5$ Mpc/h. All figures (except *Fig.2i*) correspond to boxes with 12 cutoff lengths boundaries. *Fig.2h* shows the result for *dark* matter and *Fig.2i* shows the result for a larger realization (see part 3 of this contribution).

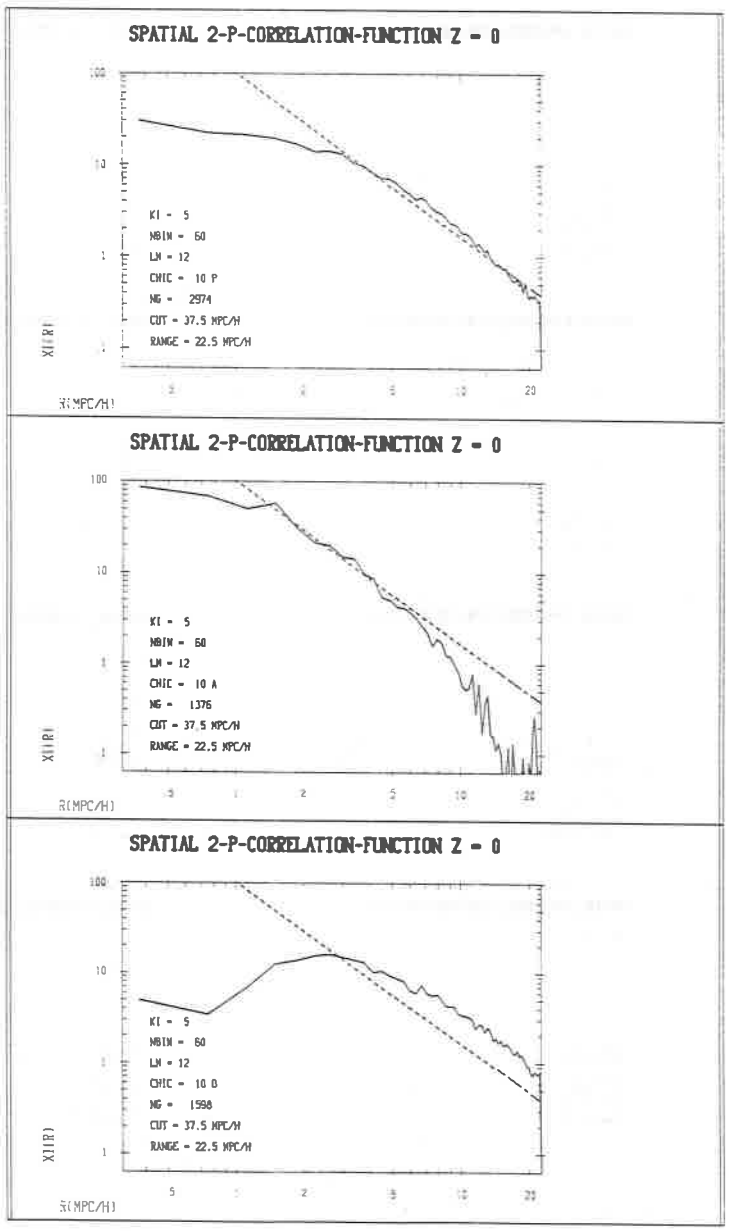

Fig. 2a-c: Two-point correlation function for various threshold types

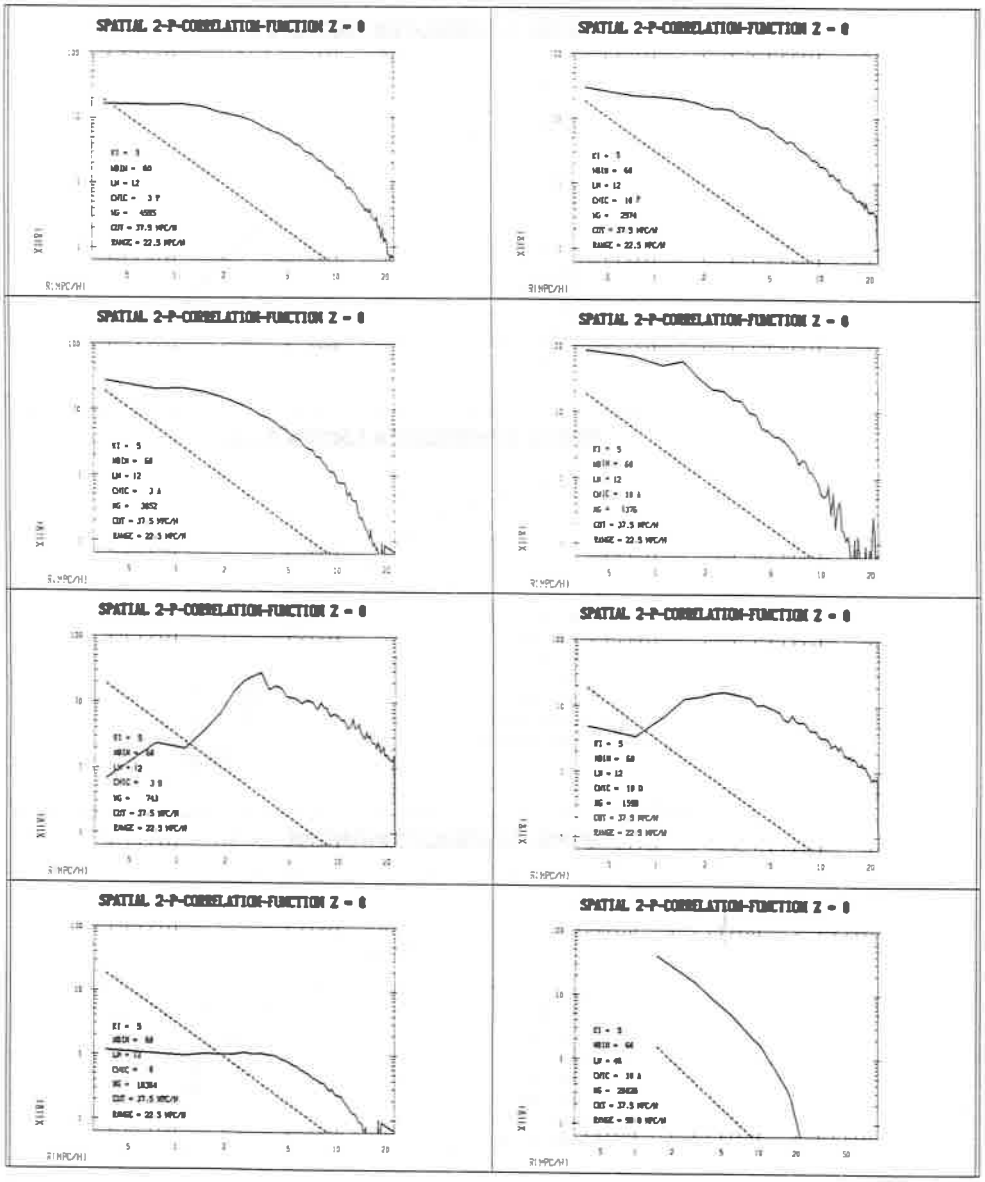

Fig.2d-i: Two-point correlation function for various threshold values and types

DYNAMICAL THRESHOLDING OF PANCAKE MODELS

3. Large 2D-Realizations and Subsampling

T. BUCHERT

Max-Planck-Institut für Astrophysik
D-8046 Garching/Munich, F. R. G.

Abstract

A large two-dimensional realization of a dynamically thresholded pancake model is shown. It demonstrates the 'statistical fairness' of the whole sample compared to subsamples of approximate size 200 Mpc/h, which manifestly differ with respect to number density of modelled galaxies and clusters. Results on the correlation function (Buchert; Martinez in prep.) show strong dependence of slope and amplitude on the choice of the subsample.

Figure Captions

Fig.3: Large 2D realizations of a pancake model thresholded at $\chi_c = 10$ according to method **"A"** together with subsamples; (n=0 power law spectrum with cutoff, 512^2 particles, sample size is 48 cutoff lengths, $\delta_{lin}(Z=0)=1$, $\delta_{rms}(Z=0)=1$ on the scale $\approx \lambda_{cut}/5$):

Fig.3a: Whole sample (26025 "galaxies" $\approx 1/10$ of all baryonic tracers of the density field).

Fig.3b: Some subsamples of size $(6\lambda_{cut})^2$.

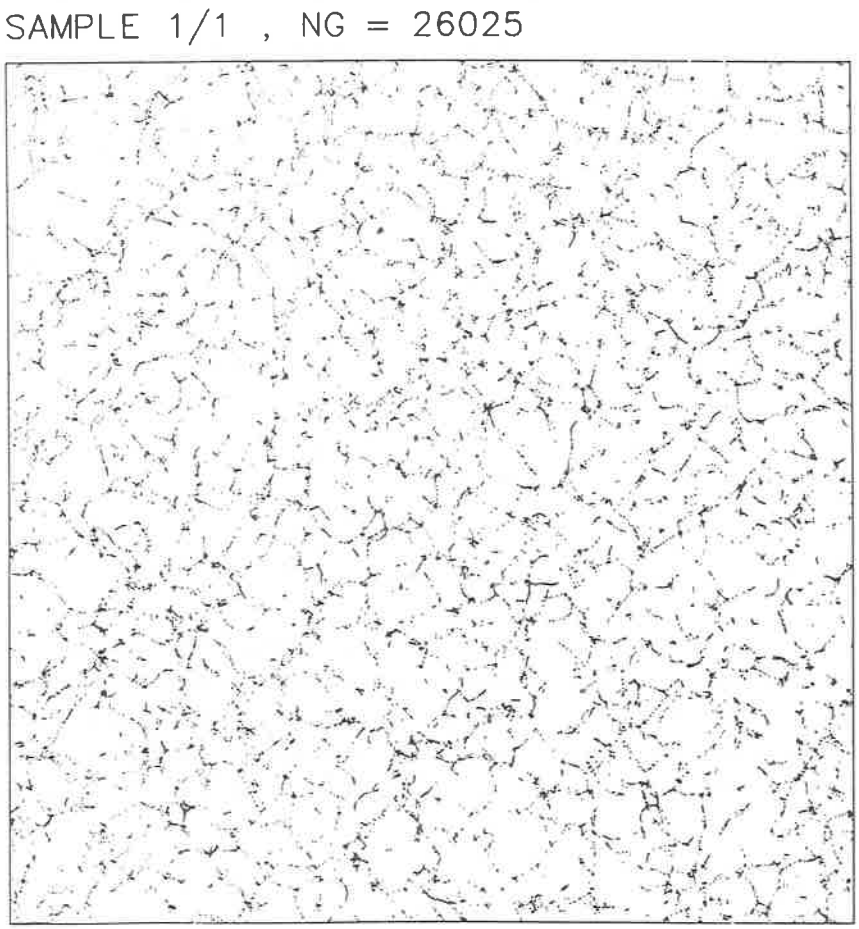

Fig.3a

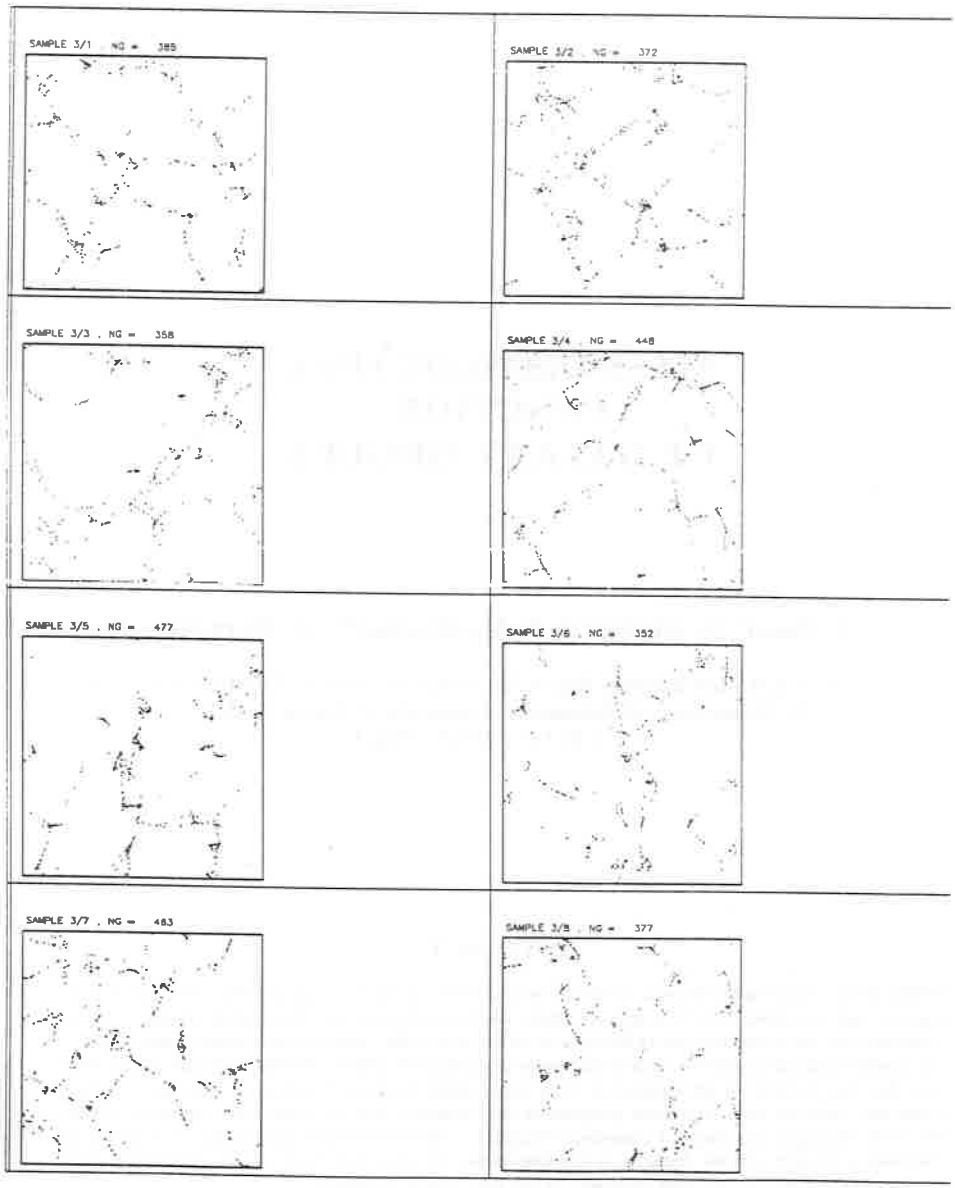

Fig. 3b: ZA2D/realization A(243)B(253),N=512,LM=48,P=8,Z=0,C=10,ΛBS

MASS DISTRIBUTION FUNCTION OF GALAXY GROUPS

A. Pisani[1], G. Giuricin[2,3], F. Mardirossian[2,3], M. Mezzetti[2,3]

1: S.I.S.S.A.-International School for Advanced Studies, Trieste (Italy);
2: Department of Astronomy, University of Trieste (Italy);
3: C.I.R.A.C., Trieste (Italy)

ABSTRACT

Within every cosmological scenario it should be possible to predict the probability that objects with a given mass are present within a given volume. Hence a constrain on cosmological scenario may be obtained from the mass multiplicity function of cosmic structures. Moreover the mass of these systems is a fundamental parameter for their dynamical evolution and formation as well. The aim of this work is to face the problem of estimating the mass distribution function of groups of galaxies. We have considered different mass estimators proposed in the literature, and, as a first step, we have analysed the C.f.A. catalogue of groups. A procedure is applied to account for those groups that are missed by observation because of their distance or low brightness. We also have examined the dynamical state of groups and corrected the mass estimate for the case of non-virialization.

ANALYSIS

We have analysed the groups of the C.f.A. catalogue[2] (GH) rejecting the groups that are parts of well-known clusters or are too much contaminated by interloper galaxies as already discussed in the literature[2,6].

In order to reduce the observational biases as much as possible without loosing too much information, we have decided to consider only groups in GH within 20 Mpc from us (namely 38 groups). In this way the spurious correlations between some physical parameters of groups and their distance were significantly reduced.

On the basis of the data listed in GH it is possible to estimate the mass of each group using different estimators. We considered the virial mass estimator, specifically the unweighted (i.e., equal mass members) virial mass M_{V_u} and the luminosity-weighted virial mass is considered M_{V_l}. Moreover, we have considered other unweighted mass estimators introduced, tested and discussed in a previous work[5]: the projected, average and median mass estimators, M_P, M_{Av}, M_{Me}, respectively. The basic assumptions concerning the derivation of these estimators are: 1) the system is a bound and isolated collection of point-like bodies, 2) the system is in a steady state.

We have estimated the effect of the non-stationary dynamical state of the mass distribution[4], assuming $\Omega = 0.2$, but the main general conclusions hold also for $\Omega = 1$ We have obtained that $\sim 90\%$ of the GH groups have not yet reached the virial equilibrium condition. The application of the correction for the non-virialisation to the mass of GH groups causes no strong effect. The distribution of the group mass corrected for the non-virialised dynamical state goes from $\log M_{V_u} = 12.04$ (in solar units) to $\log M_{V_u} = 14.41$, with a mean value of 13.58, standard deviation 0.77 and median 13.63. The various mass distributions obtained via different mass estimators have been found to share the same underlying, parent distribution, according to the Kolmogorov-Smirnov and Kruskal-Wallis statistical tests. In other words the mass estimators constitute an homogeneous set of estimators for GH groups. However the detected homogeneity may be related to the fairly small number of available groups[7]. In table 1 we list the main statistical parameters of the mass of GH groups obtained by using different estimators. Some of the GH groups would not be observed if they were moved far away enough from us, but still within the adopted limit distance of 20 Mpc. This leads us to suspect that an unknown amount of similar (but unobserved) groups could be present within the considered volume, but it is unobservable. In order to estimate the effect of the unobserved groups on the observed mass distribution, a procedure to recover these groups is necessary. Our approach is based on a model assumed for the spatial distribution of groups. As a first step, we have assumed that the number density of groups is proportional to the number density of galaxies and hence inversely proportional to the square distance from the Virgo cluster[8]. It is assumed also that each group disappears from the catalogue at the distance D where its third-ranked galaxy would have its apparent magnitude equal to the completeness limit of the galaxy sample. If $D < 20\ Mpc$, then the number of unobserved groups is estimated integrating the number density distribution in the region between D and $20\ Mpc$. If D turns out to be greater than the limit distance of $20\ Mpc$ then there are no unobserved, similar groups. In this way it was possible to estimate the number of unobserved, similar groups in the catalogue. The mass of the unobserved groups is supposed to fall around the observed value. The law of distribution of the mass of the recovered groups around the value of the mass of each observed group is obtained on the basis of numerical simulations[1,3]. The shape and statistical behavior of the mass distribution was not significantly affected by the procedure of recovering unobserved groups, but the global quantities like the total number and total mass of groups estimated to be present within 20 Mpc is strongly sensitive to the adopted model for the spatial distribution of groups.

A similar analysis for other group catalogues is in progress.

Table 1: The parameters and confidence intervals of different mass estimators for GH nearby groups.

m. est.	min.	max.	mean	median
$\log M_{Vu}$	11.54	14.03	13.04	13.19
$\log M_{VI}$	11.67	14.93	13.18	13.28
$\log M_P$	11.58	14.23	13.03	13.10
$\log M_{Mc}$	11.59	14.09	13.06	13.18
$\log M_{Av}$	12.11	14.17	13.14	13.19

CONCLUSIONS

The main results of our analysis of GH nearby groups are the following:

- A large fraction of the GH groups has not yet reached the dynamical equilibrium and hence they are not yet virialised. However their mass distribution is not significantly altered by the correction for non-virialisation.
- The observed mass distribution of groups is stable against variations in the choice of the mass estimator; all mass estimators (i.e., unweighted and luminosity-weighted virial mass, projected, median and average mass) lead to essentially the same mass distribution.
- A procedure to recover the groups that are not observed because of their distance or low brightness has been applied. We have found that the observed mass distribution is not significantly altered by this correction.

REFERENCES

1: Aarseth S.J. and Saslaw W.C. 1972: *Astrophys J.*, **172**, 17.
2: Geller M. and Huchra J.P. 1983 (GH): *Astrophys. J. Suppl. S.*, **52**, 61.
3: Giuricin G., Mardirossian F., Mezzetti M., Santangelo P. 1984: *Astrophys. J.*, **277**, 38.
4: Giuricin G., Gondolo P., Mardirossian F., Mezzetti M., Ramella M. 1988: *Astron. & Astrophys.*, **199**, 85.
5: Heisler J.N., Tremaine S. and Bahcall J.N. 1985: *Astrophys J.*, **298**, 8.
6: Mezzetti M., Pisani A., Giuricin G., Mardirossian F. 1985: *Astron. & Astrophys.*, **143**, 188.
7: Perea J., del Olmo A. and Moles M., 1990: *Astrophys. J.*, in press.
8: Tully R.B. 1982: *Astrophys. J.*, **257**, 389.

LUMINOSITY SEGREGATION AND DYNAMICAL EVOLUTION IN RICH GALAXY CLUSTERS

R. Domínguez-Tenreiro and G. Yepes.

Departamento de Física Teórica C-XI
Universidad Autónoma de Madrid
Cantoblanco-28049 Madrid SPAIN

ABSTRACT

An analysis of the luminosity segregation in several galaxy clusters has been carried out by means of the intergalactic distance distribution function, corrected from the masking effects of field galaxies. The clusters present different degrees of luminosity segregation, ranging from appreciably segregated to virtually not segregated.

Simulations of the dynamical evolution of galaxy clusters by means of the *Fokker-Planck equation moments method*, lead us to the conclusion that the previous situations can be interpreted as due to dynamical evolution during the two-body relaxation phase, and that the differences reflect the different initial conditions present at the onset of this phase.

I. LUMINOSITY SEGREGATION IN OBSERVED CLUSTERS

The distribution function of projected intergalactic distances, $P(s)ds$, has been used as statistical descriptor to quantify luminosity segregation (LS) in galaxy clusters. This method has been introduced by Capelato *et al.* (1980). Its formulation, when the effect of field galaxies in the LS determination is taken into account, has been made by Domínguez-Tenreiro and Del-Pozo-Sanz (1988), who show that field galaxies do strongly mask LS. This method has been applied to the study of the LS of four rich clusters of galaxies whose name and some of their characteristics are given in Table 1. (Yepes and Domínguez-Tenreiro 1990).

The main results of our analysis is that *the degree of LS decreases from the A2218 cluster to the A2111 cluster*, which shows no substantial LS.

II. THEORETICAL SIMULATIONS

The *Fokker-Planck equation* has been used to study the dynamical evolution of galaxy clusters. It has been solved by means of the distribution function moments method. We have developed a generalization of Larson's method (Larson 1970) which includes the two indispensable elements in any realistic description of galaxy clusters: i) *anisotropy of the distribution function in the momentum space*, treated in a self-consistent manner, and ii) *a mass spectrum*, which in particular allows us to consider the effects of a *continuous distribution of dark matter*.

A King model (King 1966) has been taken as initial configuration of the clusters. The observed differential luminosity function of galaxy clusters is well fitted by the Schechter (1976) luminosity function.

Several simulations for different models have been carried out. The $P(s)$ curves have been calculated directly from the outputs of the theoretical simulations through the projected number density. We have found different degrees of mass segregation which mimics, even at a quantitative level, what was found in our data analysis. Some simulations have been carried out with a tidal limited mass spectrum (Merritt 1984). In this case the mass segregation is slightly less than in the case of Schechter mass spectrum models.

III. CONCLUSIONS

From our data analysis we conclude that:

a) Due to the masking effect of field galaxies, distant galaxy clusters are more luminosity segregated than what is commonly measured by methods which do not take into account this masking effect.

b) The degree of LS is different for different galaxy clusters.

The theoretical simulations lead to the conclusions :

c) The LS found in galaxy clusters could be explained as a result of dynamical evolution in the two-body relaxation or post-virialization phase.

d) The variety of situations found in the data analysis concerning LS could be interpreted as due to the different initial conditions present at the onset of two-body relaxation as measured by the model parameters. Low LS in clusters could also be explained as due to the competing effects of two-body relaxation and post-virialization tidal stripping in low density inter-cluster medium environments.

References

Capelato, H., Gerbal, D., Mathez, G., Mazure, A. Salvador-Solé, E., and Sol, H. 1980, *Ap. J.*, **241**, 521.

Domínguez-Tenreiro, R. and Del-Pozo-Sanz, R. 1988, *Ap. J.*, **324**, 677.

King, I. R. 1966, *A. J.*, **71**,64.

Larson, R. 1970, *M.N.R.A.S.*, **147**,323.

Merritt, D. 1984, *Ap. J.*, **276**, 26.

Schechter, P. L. 1976, *Ap. J.*, **203**, 297.

Yepes, G. and Domínguez-Tenreiro, R. 1990, *Ap. J.*, in press.

TABLE 1. Some characteristics of the analyzed clusters.

Cluster name	z	R_{max}(Mpc)	R_c(Mpc)	NPG*
A2218.....	0.171	0.87	0.43	306
A1758.....	0.280	1.25	0.72	320
0004.8 − 3450..	0.114	1.87	1.20	333
A2111.....	0.23	1.08	0.94	269

* Total Number of Plate Galaxies in the circular region of radius R_{max}.

NUMERICAL STUDY OF THE EVOLUTION OF GALAXY CLUSTERS WITH DARK MATTER

G. Yepes. and R. Domínguez-Tenreiro

Departamento de Física Teórica C-XI
Universidad Autónoma de Madrid
Cantoblanco-28049 Madrid SPAIN

ABSTRACT

A self-consistent generalization of Larson's model based on the *Fokker-Planck equation moments method* has been developed in order to study the two-body relaxation phase of the dynamical evolution of anisotropic, multimass self-gravitating spherical systems. The model has been applied to the study of the main features of the dynamical evolution of galaxy clusters with a Schechter-like mass spectrum and a continuous background of dark matter. An isotropic King model has been taken as initial configuration for the clusters. The main result of our simulations is that the final state of the dynamical evolution of these systems is always a situation of *Gravothermal Catastrophe*, with a high degree of mass segregation. The influence of the model parameters on the characteristic collapse time has been analyzed. The effects of tidal stresses have also been studied . We have found that the final situation of gravothermal collapse is not avoided by considering these effects. They only slow down the onset of the gravothermal instability.

I. DESCRIPTION OF THE MODEL

We present the model and results of a systematic study of the dynamical evolution of rich galaxy clusters in the two-body relaxation phase, which includes two fundamental ingredients in any realistic description of these systems: i) anisotropy of the distribution function in the momentum space, treated in a self-consistent manner, and ii) a mass spectrum, which in particular allows us to analyze the dynamics of a continuous background of dark matter.

We have developed a generalization of Larson's moment method (1970) to the anisotropic multimass case. (Yepes and Domínguez-Tenreiro 1990).

As an initial model for the cluster we have taken the output of the violent relaxation period (Lynden-Bell 1967): isotropic and mass independent distribution functions with zero odd order moments. The King model (King 1966) fulfills these requirements and has been chosen because the present density profiles of rich galaxy clusters are well fitted by these models (Kent and Gunn 1982; Kent and Sargent 1983). Two different populations are present in the clusters: dark matter and galaxies. The galaxy population is endowed with a mass spectrum. Two different kinds of mass spectra have been considered: i) Schechter like (Schechter 1976), ii) Tidal limited (Merritt 1984).

II. RESULTS OF THE SIMULATIONS

The fundamental feature of the models we have analyzed is that the simulated systems never attain a state of thermodinamical equilibrium where the distribution functions become Maxwellians and the energy equipartition among the different subsystems is complete. On the contrary, the result of the evolution is always a process of gravothermal catastrophe. This process is accelerated relative to the monomass case by the lack of energy equipartition among the more massive galaxies and the lighter particles.

We have obtained the collapse times, t_{cc}, for different initial King models. Tidal limited mass spectra slightly slow down the evolution rate relative to a Schechter like mass spectrum. A complete equipartition is never reached. Only when the amount of dark matter,η, is high, the most massive galaxies tend to an energy equipartition. From an observational point of view, the study of the Coma cluster by des Fôrets *et al.* (1984) seems to indicate that bright galaxies (within 2 magnitudes from the brightest one) show energy equipartition, while the fainter ones do not show it.

The distribution functions f^a are isotropic at the onset of the two-body relaxation. As a consequence of the evolution, an anisotropy develops. This process is more important around $r/R_c \simeq 1$ and when η is high. Massive galaxies preferently

move in the transverse direction and light galaxies in the radial direction in this region. The central regions remain isotropic along the evolution. Except for the most massive galaxies, the collapse is not self-similar.

The projected velocity dispersion profile, $\sum(s)$ of the massive galaxies present a central diminution by an amount similar to some observations (Kent and Gunn 1982). By contrast, $\sum(s)$ for less massive galaxies is almost constant. The $\sum(s)$ profiles are in fact very sensitive to the model parameters and they carry a lot of information on the dynamical age of the cluster.

Energy equipartition among the most massive galaxies, the central decrease of the $\sum(s)$ profiles and mass segregation are indications of the dynamical evolution of the cluster, and, consequently, should be observed at the same time in rich evolved clusters of galaxies.

References

Des Forêts, G., Domínguez-Tenreiro, R., Gerbal, D., Mathez, G., Mazure, A. and Salvador-Solé, E. 1984, *Ap. J.*, **280**, 15.

Kent, S. M. and Gunn, J. E. 1982, *A. J.*, **87**,945.

Kent, S. M. and Sargent, W. L. W. 1983, *A. J.*, **88**,697.

King, I. R. 1966, *A. J.*, **71**,64.

Larson, R. 1970, *M.N.R.A.S.*, **147**,323.

Lynden-Bell, D. 1967, *M.N.R.A.S.*, **136**,101.

Merritt, D. 1984, *Ap. J.*, **276**, 26.

Schechter, P. L. 1976, *Ap. J.*, **203**, 297.

Yepes, G., Domínguez-Tenreiro, R. 1990, *Ap. J.*, submitted.

OBSERVATIONS IN THE SUBMILLIMITER RANGE OF THE SUNYAEV-ZELDOVICH EFFECT WITH THE SPM-PRONAOS BALLOON EXPERIMENT

F. PAJOT[1], J.-P. BERNARD[2], F.-X. DÉSERT[3] AND J.-M. LAMARRE[1]

[1] Institut d'Astrophysique Spatiale, Campus d'Orsay, Bt. 120
91405 Orsay Cedex, France

[2] California Institute of Technology, MC 320-47
Pasadena CA 91125, USA

[3] DEMIRM, Observatoire de Meudon,Place Jules Janssen
92195 Meudon Principal Cedex, France

ABSTRACT. The focal plane instrument SPM (Système de Photométrie Multibande) will be flown on the French submillimeter balloon program PRONAOS (PROgramme NAtional d'AstrOnomie Submillimétrique) in 1992. The operation of a four channel photometer (^{3}He cooled bolometers) with a 2-meter telescope at stratospheric altitudes (40 km) will allow to map the continuum emission of extended sources with a high sensitivity at the arc minute resolution level, in a wavelength range mostly unaccessible from the ground. The scientific objectives for the program are the observation of the cold dust emission of our and external galaxies in the 200 μm-700 μm range, and the detection of the positive part of the Sunyaev-Zeldovich effect towards distant clusters of galaxies between 700 μm and 1.3 mm. This might bring an unambiguous confirmation of the negative part of the effect already observed at radio wavelength, and can potentially give unique informations on important cosmological parameters when combined to X-ray measurements.

1. THE PRONAOS PROJECT

The submillimeter (submm) spectral range is almost completely absorbed by the atmosphere and can only be accessed with planes ($14\,km$), stratospheric balloons ($40\,km$) or satellites.

The balloon program PRONAOS is a preparatory mission to the big satellite submm observatories of the end of the century. This program is funded by the Centre National d'Etudes Spatiales and directed by the Centre National de la Recherche Scientifique (P.I. is G.Serra). The first flight is scheduled in July 1992 from Sicily to Spain.

PRONAOS consists of a 2-meter Cassegrain telescope mounted on a stabilized gondola, and two focal instruments, SPM (Submm multiband photometer) or alternatively SMH (Heterodyne submm spectrometer). The telescope is composed of 6 gold-coated carbon fiber petals which are dynamically adjusted during the flight (MATRA responsibility). The gondola provides a 5 arcsec rms pointing accuracy to the telescope-focal instrument ensemble and transmits telemetry and telecommands for the experiment. Total payload weighs $2300\,kg$ and the overall height is $7\,m$ (CNES direction). The volume of the helium-filled balloon is $800000\,m^3$ at the cruising altitude of $38\,km$ (pressure $3\,mb$).

2. THE SPM INSTRUMENT

The SPM submm multiband photometer is realized under the responsibility of the Institut d'Astrophysique Spatiale (Orsay - P.I. is J.M.Lamarre), in cooperation with the C.E.S.R. (Toulouse), the I.A.P. (Paris) and the S.A. (Verrires). The instrument is based upon 4 bolometers in a a ^{3}He cryostat. Dichroic and bandpass filters define the photometric channels between $180\,\mu m$ and $1200\,\mu m$. The warm optics provides an internal modulation (typically 8 arcmin on the sky) and an absolute calibration system.

3. THE SUNYAEV-ZELDOVICH EFFECT

The Cosmic Microwave Background (CMB) is distorted when passing through a cluster of galaxies: the hot electrons of the cluster interact with the CMB photon via inverse Compton scattering (Sunyaev and Zeldovich 1970). The Rayleigh-Jeans part ($h\nu \ll kT_{CMB}$) of the CMB is decreased whereas the Wien part is enhanced (see figure 1). While the negative part of the Sunyaev-Zel'dovich effect may have already been detected (see Birkinshaw, this conference), PRONAOS-SPM will attempt to measure the

positive part of the effect. The long wavelength channel (4: $540 - 1200\,\mu m$) is optimised for this detection whereas the 3 others (1:180-240, 2: 240-340, and 3: 340-540 μm) will detect a possible dust emission component from the cluster. For the best candidates (Abell85, A1795, A2029, A2218, A2319, 0016+16), an expected typical 5σ detection time is 3 to 4 hours.

Possible implications of this measurement include the determination of the peculiar velocity of the cluster (Sunyaev and Zeldovich 1980), and combined with X-ray data, of the Hubble constant. The experiment can also provide interesting constraints on the small scale (8 arcmin) CMB anisotropy as well as on submillimeter interstellar dust emissivity properties.

REFERENCES

Sunyaev, R. A., and Zeldovich, Ya. B., 1970, *Astrophys. Sp. Sc.*, **7**, 3

Sunyaev, R. A., and Zeldovich, Ya. B., 1980, *M.N.R.A.S.*,**190**, 413

QUASI-PERIODICITY IN DEEP REDSHIFT SURVEYS

Rien van de Weygaert
Sterrewacht Leiden
P.O. Box 9513
2300 RA Leiden
The Netherlands

ABSTRACT

The surprising recent result of Broadhurst *et al.*[1] , a very regular clumpy redshift distribution in deep pencil-beam redshift surveys towards the North- and South Galactic Pole, is explained within the context of Voronoi foams. This geometrical model describes the cellular or foam-like galaxy distribution on large scales, of which it can be considered to be the skeleton. Putting in only one length-scale, the mean distance between Abell clusters, it gives both a cluster-cluster correlation function in agreement with the observations (ie. both slope and amplitude of the power law), as well as a scale of clumping in pencil-beam surveys of around $100 - 130h^{-1}$ Mpc, consistent with the observations[1].

In this short contribution a Monte-Carlo study of galaxy clustering within Voronoi foams is presented. The used Voronoi tessellation is generated by Poissonian distributed seeds (expansion centres). Deep narrow pencil-beam surveys through these Voronoi foams were simulated. These simulations show that around 15% of beams with an opening angle of 20 arcmin and out to a redshift of 0.5 show a periodic clumping of galaxies (while the cellular structure itself is intrinsically non-periodic, because based on Poissonian distributed seeds).

THE VORONOI FOAM

The Voronoi foam is the simplest statistical model for a distribution of galaxies that is confined to sheets, filaments, and clusters surrounding voids. It is physically motivated by the notion that structure formation under the influence of gravity can be described by looking to the evolution of underdense regions in the mass-density, which will expand with respect to the background and become more and more spherical[2,3]. A Voronoi tessellation in three dimensions is the tiling of space into convex polyhedral cells, each cell consisting of that part of (here: comoving) space closer to its expansion centre than to any of the other expansion centres. The interior of the cell is considered to be an underdense region from which matter streams away towards the planes bounding the cell, identified with the "walls" in the galaxy distribution. The walls intersect in edges, the filaments in the galaxy distribution, while the edges come together in the vertices of the tessellation, where the clusters in the galaxy distribution will be found.

The only scale which comes into the model is the mean distance between the vertices, which is put equal to the mean distance between the Abell clusters. Using this scale it was shown[4] that the vertices have a power-law two-point correlation function with slope and amplitude equal to the correlation function of Abell clusters.

THE PENCIL-BEAM SIMULATION

We set a Voronoi tessellation consisting of 2500 cells generated by 2500 Poissonian distributed expansion centres, in a box with side ratios of $2 : 1 : 1$. Using the described scale normalization this means the box has comoving sides of $2240h^{-1} \times 1120h^{-1} \times 1120h^{-1}$ Mpc. Through this box narrow opposite cones are cut, both to a depth of $z = 0.5$. In a completely geometrical way the Voronoi walls lying within the cones are determined.

The spatial distribution of galaxies is taken to be uniform within the Voronoi walls. Although observations show this not to be the case, we do this to control the simulation with as few parameters as possible. Perpendicular to the plane the galaxy distribution is taken to be Gaussian with a $\sigma = 2.5h^{-1}$ Mpc. The number of galaxies differs from wall to wall, being proportional to the distance between seed and wall and to the surface area of the wall (which determines the amount of matter which will stream out of the cell into the wall). Multiplying the average number density of galaxies by the "influence volume" of the wall gives the number of galaxies within the wall. The number of galaxies within the wall is then a Poisson variate with that expectation value. The galaxies in the simulation have absolute magnitudes between $M_{B_T} = -17$ and $M_{B_T} = -22$, and have a Schechter luminosity function with the parameters

determined by Efstathiou *et al.*[5]. The luminosity of each galaxy in the cone is determined by random sampling from the specified luminosity function. Having the distance and luminosity of each galaxy within the cone its apparent magnitude is determined. Galaxies with apparent magnitudes in excess of $m_{B_T} = 21.5$ are taken out of the survey. In this way we end up with a redshift survey through the Voronoi foam.

RESULTS

The final result, the redshift distribution of galaxies is shown in Fig. 1. Positive redshift means the galaxy is in the cone pointing in one direction, while negative redshift means the galaxy is situated in the opposite pencil beam. The example redshift distribution indeed shows a striking regularity, with a peak-to-peak distance in the order of $107h^{-1}$ Mpc. This regularity is confirmed by the corresponding pair number count shown in Figure 2. However, although all pencil-beam survey simulations do show clustering on roughly the same scale, most of them do not show regularity. On the basis of some 30 realizations it is estimated that approximately 1 in every 6 to 7 show regularity. This agrees roughly with the analytical estimate in Ref. 6.

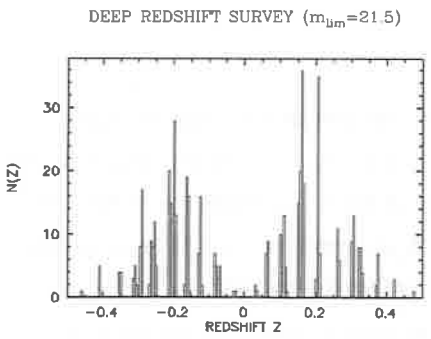

FIGURE 1. The redshift distribution for pencil beam surveys through a 3-D Voronoi tessellation.

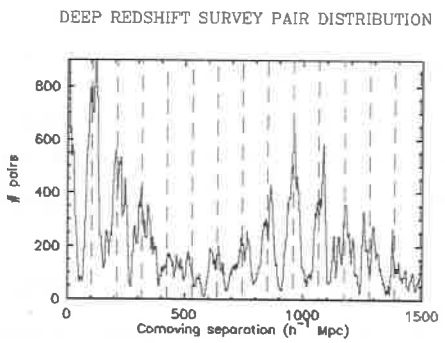

FIGURE 2. The pair-count correlation diagram for all redshift data in Fig. 1

REFERENCES

1. Broadhurst, T.J., Ellis, R.S., Koo, D.C., & Szalay, A.S., 1990. *Nature*, **343**, 726.
2. Icke, V., 1984. *Mon. Not. R. astr. Soc.*, **206**, 1P.
3. Icke, V., & van de Weygaert, R., 1987. *Astron. Astrophys.* **184**, 16.
4. van de Weygaert, R., & Icke, V., 1989. *Astron. Astrophys.* **213**, 1.
5. Efstathiou, G., Ellis, R.S., & Peterson, B.A., 1988. *Mon. Not. R. astr. Soc.*, **232**, 431.
6. Coles, P., 1990. *Nature*, **346**, 446.

FORMATION AND EVOLUTION OF EARLY DISTORTIONS OF THE MICROWAVE BACKGROUND SPECTRUM: A NUMERICAL STUDY

C. BURIGANA[1], L. DANESE[1], and G. DE ZOTTI[2]

[1] Dipartimento di Astronomia, Vicolo dell'Osservatorio 5, I–35122 Padova, Italy

[2] Osservatorio Astronomico, Vicolo dell'Osservatorio 5, I–35122 Padova, Italy

We have completed (Burigana et al., 1990) an extensive numerical study on the formation and evolution of early distortions of the microwave background spectrum.

The thermalization redshift, z_{therm}, of arbitrary distortions has been determined by integrating the system of ordinary differential equations for the chemical potential μ and the electron temperature T_e. A least square fit to the numerical results for $T_0 = 2.74\,K$, $\kappa = 1.68$ and $\widehat{\Omega}_b \leq 0.3$, where radiative Compton dominates over bremsstrahlung, yields:

$$z_{therm} \simeq \begin{cases} 2.46\,10^6 \mu^{0.11} \widehat{\Omega}_b^{-0.39} & \text{if } \mu \leq 1 \\ 2.90\,10^6 \widehat{\Omega}_b^{-0.36} & \text{if } \mu \geq 2.5. \end{cases}$$

Also we have obtained a simple analytic formula allowing to estimate the upper limits on the fractional amount of energy $\Delta\epsilon/\epsilon_i$ released at any redshift z, from the observational limits on the chemical potential μ_0.

The time required for a distorted spectrum to relax to a stationary, Bose–Einstein like shape, was found to be independent of the details of the heating process. We confirm

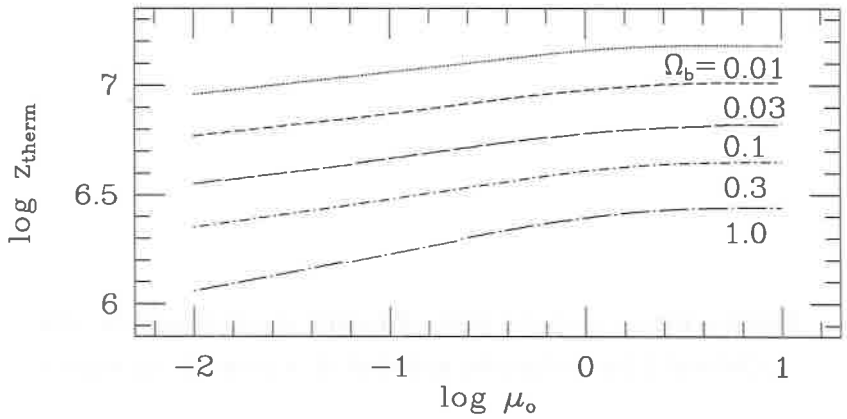

that such spectrum is formed, for $h\nu/kT_r \geq 1$ ($T_r = T_0(1+z)$), in a time corresponding to $y_e \simeq 0.25$, y_e being the comptonization parameter (Zeldovich and Sunyaev, 1969) , while, at longer wavelengths, a longer time is required. At variance with earlier estimates, however, the critical value of y_e, y_1, for relaxation of the long wavelength portion of the spectrum, turned out to be essentially independent of $\widehat{\Omega}_b$. Another new result is that y_1 increases with decreasing $\Delta\epsilon/\epsilon_i$: we find $y_1 \simeq 2.5$ if $\Delta\epsilon/\epsilon_i = 0.15$; $y_1 \simeq 4$ if $\Delta\epsilon/\epsilon_i = 0.03$; $y_1 \simeq 5$ if $\Delta\epsilon/\epsilon_i \leq 0.001$.

Moreover have obtained a simple analytic formula providing a remarkably accurate description of the final spectrum, in presence of an early energy injection (i.e. occuring at $y_e \gtrsim y_1$). For an energy injection occurring at $y_1 \gtrsim y_e \gtrsim 1$ the wavelength where the maximum distortion occurs does not change with y_e; however the amplitude of the maximum distortion, for given $\Delta\epsilon/\epsilon_i$, increases as y_e approaches y_1. For $1 \gtrsim y_e \gtrsim 0.1$ there is no a well defined minimum in the brightness temperature but, rather, a broad depression.

Finally we note that a superposition of blackbody spectra provides an accurate solution of the Kompaneets equation up to $y_e = 0.15$ in the case of $T_e \gg T_r$ (reheating of the intergalactic plasma at low redshifts); in the case of early distorsions (i.e. $T_e \simeq T_r$), however, this approximation begins to fail when y_e is larger than a few percent.

References

Burigana, C., Danese, L., De Zotti, G.: 1990, *Astron. Astrophys.*, submitted.

Zeldovich, Ya. B., and Sunyaev, R.A.: 1969, *Ap. Space Sci.*, 4, 301.

COSMIC X-RAY BACKGROUND NOT FROM CLUMPED HOT GAS

R.D. ROGERS and G.B. FIELD
Harvard-Smithsonian Center for Astrophysics
60 Garden Street, Cambridge, MA 02138

ABSTRACT

Because the spectrum of the cosmic x-ray background (XRB) fits thermal bremsstrahlung with $T \sim 30$ keV, it has been suggested that the XRB is due to diffuse hot gas, possibly intergalactic gas that would contribute signficantly to Ω. If smoothly distributed, the gas would violate the upper limit on the Compton y-parameter from COBE. Gravitational clumping would avoid this problem, and also provide a heating mechanism. However, we show here that models in which the gas is gravitationally confined in condensations of stable dark matter are not consistent with the spectrum and isotropy of the XRB as well as with constraints from gravitational lensing and the isotropy of the cosmic microwave background. We conclude that the XRB is not due to gravitationally clumped hot gas.

INTRODUCTION

The cosmic x-ray background, discovered in 1962, has not yet been explained definitively. Its energy density is 3×10^{-4} of that of the cosmic microwave background (CMB); it is isotropic on both large and small scales; and there is a break in its spectrum at 30 keV which is well fitted by thermal bremsstrahlung.

Because AGNs are x-ray sources, it is natural to assume that the XRB is due to numerous faint AGNs that remain unresolved. The expected number of faint AGNs is adequate to account for the XRB at energies of about 3 keV if evolution is taken into account. However, bright AGN x-ray sources do not appear to have the same spectrum as the XRB.[1)]

Alternatively, one could account for the XRB by thermal bremsstrahlung from smoothly distributed gas heated at redshifts about 3 if the density parameter of the gas is $\Omega_g = 0.5$ ($h = 1/2$ here and hereafter), but this possibility has been ruled out by COBE's finding that the Compton y-parameter is $< 10^{-3}$, rather than the predicted 0.03.

A model based on smoothly distributed gas has other difficulties: Ω_g exceeds $\Omega_b \simeq 0.06$ from primordial nucleosynthesis, and the energy requirements for heating the gas are unrealistic (10^{10} $M_\odot c^2$ per L_* galaxy). Both difficulties would be alleviated if the gas is heated by falling into deep potential wells ("condensates"), perhaps associated with large-scale structure. Such a model would account for the high temperature of the gas, and because the emission is proportional to n_e^2, the resulting clumpiness would greatly reduce the required value of Ω_g. If the gravitational potential is supplied by baryons alone, the anisotropy of the XRB would exceed observed limits.[2)] However, the condensates might be constituted of stable dark matter with $\Omega \simeq 1$ (the case in which the dark matter is unstable has been considered earlier[3), 4)]). Here we show that this hypothesis is ruled out because no combination of parameters can simultaneously meet constraints imposed by the isotropy of the XRB, the isotropy of the CMB, and the number of gravitationally lensed quasars.

OBSERVATIONAL CONSTRAINTS

Emission by condensates results in fluctuations in the XRB. The lack of observable fluctuations in *Einstein* survey data of the XRB implies that there must be $> 5,000$ sources deg^{-2}. The application of this constraint depends on the assumed cooling time of the gas, t_c. If t_c is a small fraction of t_0, the age of the Universe, each source contributes little to the surface density, so the space density of condensates n_c must be large to account for a large surface density, but if t_c is large, n_c can be small. This

constraint on t_c/t_0 as a function of n_c is plotted as the dash-dot line in Figure 1, which applies to an assumed emission redshift $z_e = 2$. Here $n_{77} = n_c/10^{-77}$ cm^{-3}.

It has been shown[6] that fluctuations in the CMB on arc-minute scales are $< 2 \times 10^{-5}$. The Sunyaev-Zel'dovich effect of each condensate contributes an average Compton parameter $< y >$ that depends on the redshift z_e when emission starts and the redshift z_f when it finishes. Finite numbers of condensates cause fluctuations. Again, large n_c is required to avoid the isotropy constraint. This is plotted as the dotted line in Figure 1. From the isotropy constraints on the XRB and CMB, n_{77} must exceed 1.

If there are large numbers of condensates, a few should show up as gravitational lenses. Any condensate with a virial temperature of 30 keV would gravitationally deflect light through a typical angle $\alpha = \frac{8kT}{\mu m_H c^2} = 30$ arcsec Searches for gravitationally lensed quasars with separations in the range 2-120 arcsec give a conservative upper limit of 6×10^{-3} on the fraction of quasars that are lensed.[7] This allows us to put a constraint on the local number density of condensates which is plotted in Figure 1 as the solid line.

GRAVITATIONAL HEATING

Condensates consistent with the constraints can be gravitationally bound all right, as they lie above the dashed line for gravitational binding in Figure 1. However, the conservative upper limit on n_{77} from gravitationally lensed quasars conflicts with the lower limit from isotropy. Hence gravitational heating cannot explain the XRB for z_e=2. We find the same thing for all values of z_e in the range from 1 to 4. (The case $z_e = 1.1$, in which the condensates are assumed to have formed in the recent past, barely satisfies the constraints considered so far, but is ruled out by the low number of individually detectable sources in the *Einstein* Deep Survey.) We conclude that gravitational infall into condensates of stable particles cannot account for the XRB.

REFERENCES

1. Schwartz, D.A., Qian, Y., and Tucker W.H. 1989, *Proc. 23rd ESLAB Symposium: "X-Ray Astronomy: X-Ray Binaries, AGN and the X-Ray Background,"* Bologna, Italy, September 1989.
2. Field, G.B., and Perrenod, S.C. 1977, *Ap.J.*, **215,** 717.
3. Daly, R.A. 1987, *Ap.J.*, **322**, 20.
4. _____1988, *Mon. Not. R.A.S.*, **232,** 853.
5. Hamilton, T.T. and Helfand, D.J. 1987, *Ap.J.*, **318**, 93.
6. Readhead, A.C.S., Lawrence, C.R., Myers, S.T., Sargent, W.L.W., Hardebeck, H.E., and Moffet, A.T. 1989, Caltech Preprint, to appear in *Ap.J.*
7. Webster, R.L., Hewitt, P.C., and Irwin, M.J. 1988, *Ap.J.*, **95**, 19.

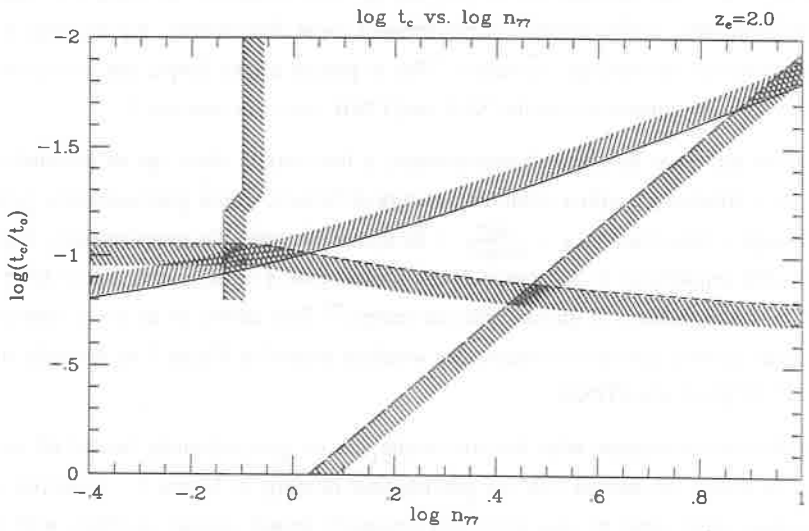

Figure 1

Constraints on the space density of condensates $n_c = 10^{-77} n_{77}$ cm^{-3} as a function of cooling time t_c, expressed as a fraction of t_0, the age of the Universe, all for z_e, the redshift at which emission begins, equal to 2. Cross hatching indicates regions not allowed by the constraints. The curves indicated have these interpretations:

(——) Isotropy of the XRB.

(- - -) Isotropy of the CMB.

(— —) Gravitational binding of hot gas.

(·····) Fraction of quasars that are gravitationally lensed.

As the conservative upper limit on n_c from gravitational lensing is below the lower limit from isotropy, there is no solution consistent with gravitationally bound hot gas.

TEMPERATURE AND IRON ABUNDANCE OF THE DISTANT GALAXY CLUSTERS A2507 AND A483

M. LACHIEZE-REY[1], M. ARNAUD[1,2], R. ROTHENFLUG[1], K. YAMASHITA[3,4], I. HATSUKADE[3,5]

[1] Service d'Astrophysique, CEN Saclay, 91191 Gif sur Yvette Cedex FRANCE

[2] Present address : Harvard-Smithsonian Center for Astrophysics, 60, Garden Street, Cambridge MA02138 U.S.A.

[3] Department of Physics, Osaka University, Toyonaka, Osaka, 560 JAPAN

[4] Present address: Institute of Space and Astronautical Science, Sagamihara, Kanagawa 229 JAPAN

[5] Present address: Faculty of Engineering, Miyazaki University, Miyazaki, 889-20 JAPAN

ABSTRACT

We observed with the GINGA LAC experiment the 2 distant clusters of galaxies A483 (z=0.28) and A2507 (z=0.196). We measured their X-ray spectra in the energy range 1-17 keV and deduced their temperature and iron abundance . They are the most distant clusters for which such measurements exist. Our results show no significant difference from nearby clusters.

GINGA (=Astro C) is a japanese satellite of X-ray astronomy launched in february 1987.The **LAC (Large Area Counter)** experiment [Turner et al, 1989] covers the energy range 1 keV to 37 keV, with an energy resolution about 18% at 6 keV. With its large effective area over a wide energy range, it is particularly well suited for the study of temperature and iron abundance in galaxy clusters

For each source, one day was devoted to the source pointed observation, and the adjacent day to a nearby blank field, used for background subtraction. Background subtraction was particularly tricky since the measured fluxes are typically 10 times fainter than the background. Moreover the background varies in a complex fashion round the orbit (Hayashida et al. , 1989).

We fitted the spectra with theoretical isothermal thin plasma emission models at ionization equilibrium, convolved with the LAC response function (taking into account efficiency, energy resolution, nonlinearity and X-ray scattering by the collimator). Line and continuum emissions were computed following Mewe et al (1985,1986) with the ionic fractions from Arnaud and Rothenflug (1985). Other models (Masai and Raymond) for the underlying atomic physics also give excellent agreement in their predictions . Hydrogen column density value was fixed according to21 cm measurements [Heiles, 1975], although our results are quite insensitive to absorption. The redshifts are fixed at the optical value. Only 3 free parameters remain: the temperature T, the emission measure EM (or normalization) and the iron abundance.

Derived physical parameters from plasma model fits

(with H_0=50km/s/Mpc, q_0=0.5)

	A2507	A483	
$\int n_e n_H dv$ =	15.3 ± 1.4	18.7 ± 2.5	10^{67} cm^{-3}
T =	9.1 [-1.9,+2.6]	8.4 [-2.1,+3.3]	keV
[Fe/H] =	0.30 [-0.30,+0.36]	0.30 [-0.30,+0.49]	* 4 10^{-5}
χ_ι^2 =	0.85	0.52	
Iron line EW =	260.	280.	eV
L_X (2-10keV) =	1.73± 0.08	2.06 ± 0.14	10^{45} ergs/s

DISCUSSION

Good fit are obtained for both clusters although the iron abundance is poorly determined. Uncertainties just reflect the statistics of the measures. Note that the luminosities in the 2-6 keV for A2507 and for A483 are respectively 3.6 and 2.3 fainter than the luminosity measured by HEAO A-1. Such overestimation by HEAO was already reported by Henry et al. (1982) for some distant clusters.

We emphasize that these 2 clusters are the most remote ones for which such spectroscopic quantities have ever been determined. They are in accordance with the general correlation between temperature and luminosity for nearby clusters (Edge, 1989). Thus they do not seem to differ from nearby clusters.

In the frame of a hierarchical scenario for the formation of structures (cold dark matter or other), convenient assuptions allow to derive the average temperature of clusters as a function of redshift (depending on Ω and the index n of the primordial spectrum of fluctuations).

The figure gives the predicted T^* (the maximum of the temperature distribution) as a function of the redshift, for various models, as well as the temperatures for all clusters with $L_X > 0.9\ 10^{45}$ ergs/s, for which temperature measurement exist. Even if a very good fit cannot expected (broad dispersion; unknown selection effects), it seems that recent data (from Exosat and Ginga) do not support a decrease of temperature with z and seem to exclude the possibility of an high Ω universe, although the shape of the initial fluctuation spectrum cannot be constrained very much. Of course the cosmological implication of this result should not be overrated in view of both uncertainties in data and the simplicity of the underlying model.

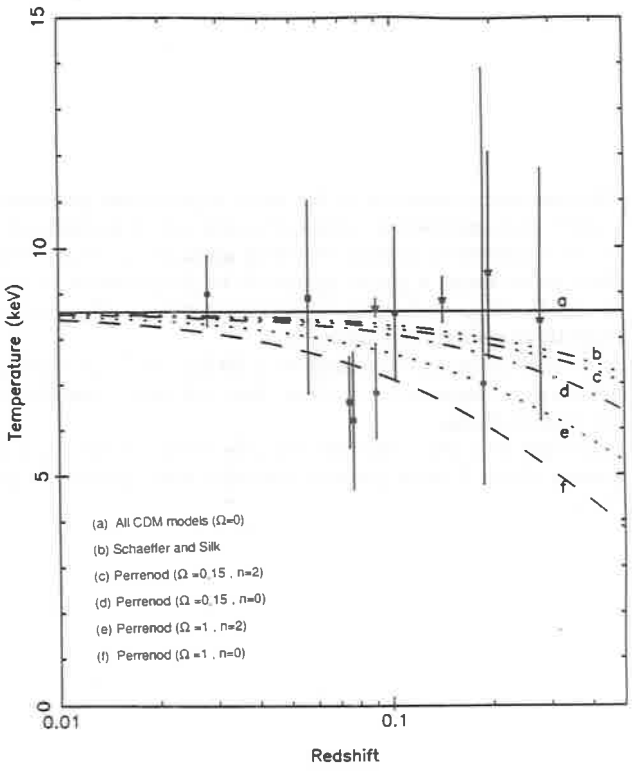

DISTANT CLUSTERS OF GALAXIES AS TRACERS FOR THE COSMOLOGICAL MODEL

A. Buzzoni, G. Chincarini
E. Molinari and D. Pedrana

Osservatorio Astronomico di Brera, Milano
Via Brera, 28 - 20121 Milano, Italy

Photometric properties of the early-type galaxy population in distant clusters are discussed and analysed in terms of a new set of models for galaxy evolution. The goal is to use confidently normal elliptical galaxies as tracers for the cosmological model.
Here we attempt a global approach to the problem, which requires at a time the study of the fundamental cosmological parameters (H_o and q_o), and the knowledge of the redshift of galaxy formation (z_f).
A Hubble constant consistent with 50 km/sec/Mpc, and a low value for the cosmological deceleration parameter q_o (less than 1/2 and, possibly, close to zero) are suggested by the observations.
Although in a less confident way, we evidence the possibility that z_f might be (much) greater than 3, with present-day elliptical galaxies (and the Universe) older than 16 Gyrs.

1. Introduction

Evolutionary status of elliptical galaxies can be easily understood in terms of a simple scenario involving one initial burst of star formation which drives any subsequent photometric evolution of the galaxies (Tinsley and Gunn 1976; Arimoto and Yoshii 1986; Buzzoni 1988). Furthermore, ellipticals populate the bright tail of the cluster luminosity function (Binggeli, Sandage and Tammann 1988), and are rather well segregated in color.

For these reasons, they are an ideal candidate to which address our analysis in order to use properties of the cluster galaxy population for cosmological tests. In particular, in this work we compared observed color-redshift relationship for elliptical galaxies in clusters with the theoretical models for evolutionary stellar population synthesis (Buzzoni 1989), attempting a more effective approach to the definition of the cosmological model. Our observational data base concerns five distant clusters of galaxies and was collected since 1986 at the ESO 3.6m telescope in La Silla, Chile (see, for details, Buzzoni *et al.* 1988; Molinari, Buzzoni and Chincarini 1990, Pedrana 1989).

2. Testing the Cosmological Model

Two different sets of cosmological models have been considered, according to relevant values for the deceleration parameter (i.e. $q_o = 0$, and $1/2$). Each set assumes for the Hubble constant both $H_o = 50$ and 100 km/sec/Mpc, and four possible values for the redshift of galaxy formation: $z_f = 2.5, 5, 10, \infty$. Results are summarized in Fig.1.

Here, we added to our observations also those by Schneider, Gunn and Hoessel (1983), which were made in a nearly similar photometric system. It is worth stressing, however, that they concern only the first-ranked galaxies in clusters, and not the whole early-type galaxy population, as it is our case. Therefore, some cautions are needed, in order to compare consistently the different sets of data. Actually, a subtle bias would be induced when using colors for these galaxies. Since at large distances we detect preferentially compact clusters (Cappi *et al.* 1989), their first-ranked galaxies will be sistematically brighter (Sandage and Hardy 1973), and therefore redder due to the Visvanathan and Sandage (1977) c-m effect. As a consequence, ranking apparent colors with redshift, we would expect a steeper trend, as shown in Fig.1.

The major conclusion stemming from our approach is that photometric properties of elliptical galaxies at different redshifts converge toward a value of 16 ± 2 Gyr for their age at present time. It is worth stressing, of course, that the validity of our inference implicitly rests on the accepted canonical scenario for stellar evolution. In this sense, therefore, it is not surprising that our estimate for the age of the galaxies closely matches that derived for the Galactic globular clusters.

Accordingly, the Hubble constant could hardly exceed 70 km/sec/Mpc, and in facts the value inferred from Fig.1 seems to prefer 50 rather than 100 km/sec/Mpc. The

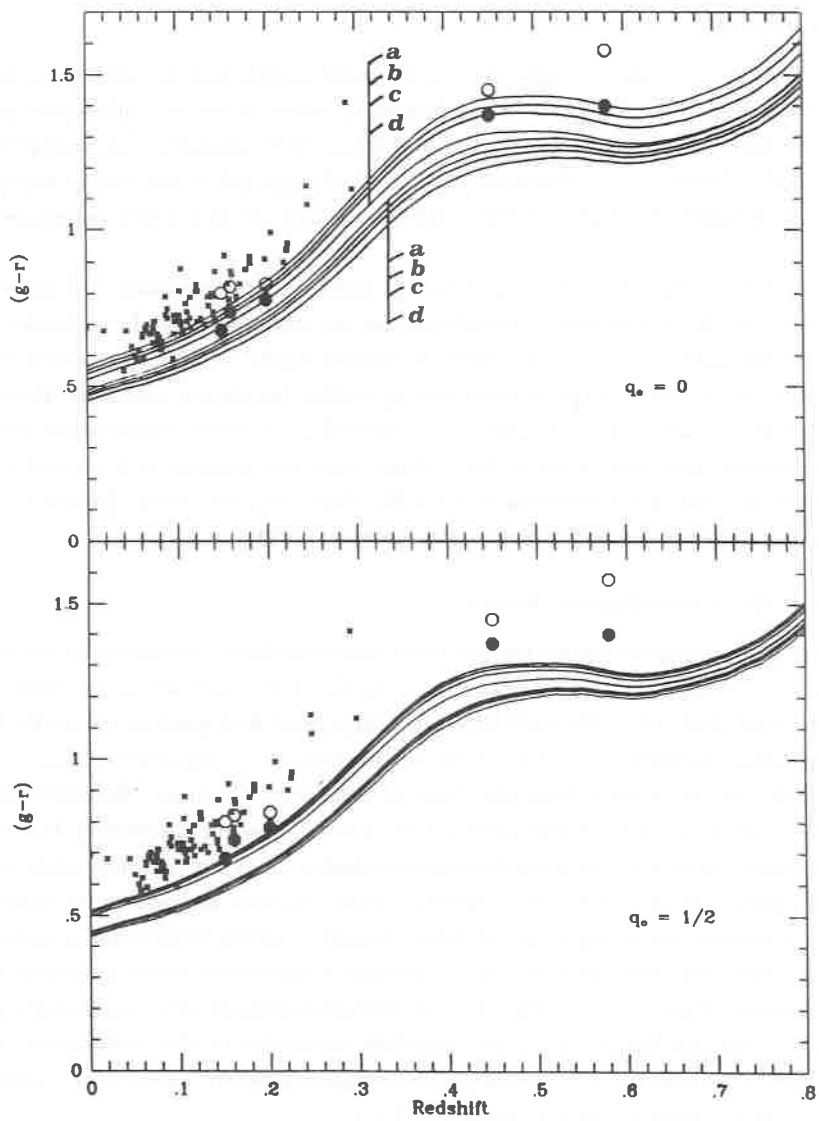

Fig. 1. Mean colors for observed early-type galaxy population (•) and first-ranked galaxies (○) in clusters at different redshift. Included are also colors for first-ranked galaxies in the Schneider *et al.* (1983) clusters (×). These have been increased by 0.04 mag in $(g-r)$ to match our photometric system. All the data are corrected for Galactic reddening via the Burstein and Heiles (1982) sky reddening map. The two panels are labelled with their value of q_o. In each one two families of four reference curves are displayed, accounting for $H_o = 50$ (upper set) and $H_o = 100$ (lower set), and different redshifts for galaxy formation, z_f: a=∞, b=10, c=5, and d=2.5.

deceleration parameter, q_o, better agrees with a value less than 1/2 suggesting a low-density open model for the Universe. Observed colors seem too red for an Einstein-De Sitter model (possibly relevant in the inflationary scenario), and either a substantial increase in the correction for Galactic reddening or an unusually low value for H_o (i.e. less than 40) would be required to support this case.
Finally, the redshift for galaxy formation, z_f, directly stems from the combined action of the other two cosmological parameters. Although in a less confident way, Fig.1 helps setting limits for it too. One sees that $z_f > 3$ would be preferred with the (H_o,q_o) = (50,0) combination, and this limit would even increase for any other combination involving higher values for H_o and/or q_o.

References

Arimoto, N. and Yoshii, Y., 1986, *Astr.Ap.*, **164**, 260.

Binggeli, B., Sandage, A., and Tamman, G.A., 1988, *Ann.Rev.Astr.Ap.*, **26**, 509.

Burstein, D. and Heiles, C., 1982, *Astr.J.*, **87**, 1165.

Buzzoni, A., 1988, *Erice Workshop, Towards Understanding Galaxies at Large Redshift*, eds. R. G. Kron,and A. Renzini (Dordrecht: Kluwer), p.61.

Buzzoni, A., 1989, *Ap.J.Suppl.*, **71**, 817.

Buzzoni, A., Molinari, E.C., Manousoyannaki, I., and Chincarini, G., 1988, *The Messenger*, **53**, 50.

Cappi, A., Chincarini, G., Conconi, P., and Vettolani, G., 1989, *Astr.Ap.*, **223**, 1.

Molinari, E., Buzzoni, A., and Chincarini, G., 1990, *M.N.R.A.S.*, **244**, in press.

Pedrana, D., 1989, Thesis dissertation, Univ. of Milano.

Sandage, A. and Hardy, E., 1973, *Ap.J.*, **183**, 743.

Schneider, D.P., Gunn, J.E., and Hoessel, J.G., 1983, *Ap.J.*, **264**, 337.

Tinsley, B.M. and Gunn, J.E., 1976, *Ap.J.*, **203**, 52.

Visvanathan, N. and Sandage, A., 1977, *Ap.J.*, **216**, 214.

ALIGNMENT OF BRIGHTEST GALAXIES IN CLUSTERS

Piotr Flin † and Ronald P.Olowin ‡

† Center for Interdisciplinary Studies, Pontifical Academy, Cracow, ul. Kanonicza 20, Poland.

‡ Department of Mathematical Sciences, Saint Mary's College of California, Moraga, CA 94575, USA.

Numerous studies revealed the existence of the alignment of the brightest cluster galaxy with the long axis of the parent cluster (Sastry 1968, Carter and Metcalfe 1980, Binggeli 1982, Struble and Peebles 1985, Struble 1987,1988,1990). The above mentioned papers were based on the analysis of Abell clusters located mainly in the northern hemisphere. We investigated the relation for southern clusters.

The observational basis consists of 49 clusters of galaxies located in the southern hemisphere, which have been analyzed by Olowin (1985) and they are incorporate in the ACO Catalogue (1989).

In each cluster the rectangular coordinates of galaxy, the extension of galaxy image and the position angle of the major axis were measured using a back -lit digitizer. The cluster center was determined as the arithmetic means of the x and y coordinates. For determination of the cluster shape the method of dispersion ellipse was applied, which gives the values of the semi axes a and b of the cluster, as well as the inclination of the major axis a with respect to the x-axis. The known reference objects allowed to determine the position angle of the cluster major axis p_c.

We analyzed the acute angle between the galaxy position angle p_g and the long axis of the cluster:

$$\Delta p_1 = p_c - p_{g1} \quad \text{and} \quad \Delta p_2 = p_c - p_{g2}$$

where indices 1 and 2 corresponds to the brightest and the second brightest cluster member.

The distribution of the analyzed angles Δp_1 and Δp_2 is presented in the fig. 1 and fig. 2 respectively.

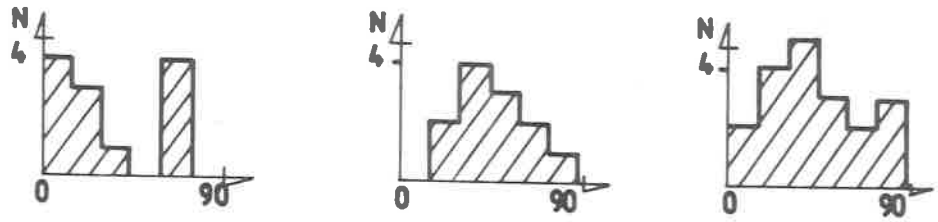

BM types: I + I-II | BM type II | BM types: II-III + III

Fig. 1. The distribution of the Δp_1 angle

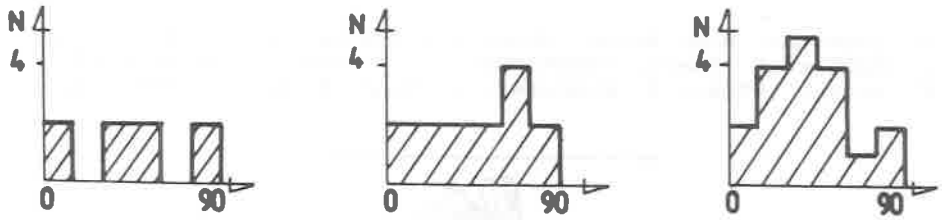

BM types: I + I-II | BM type II | BM types: II-III + III

Fig. 2. The distribution of the Δp_2 angle

From the fig.1 follows that the distribution is different for BM clusters with type $\leq$ I-II and the remaining types. It appears that in the case of BM types $\leq$ I-II there is preferred orientation; the brightest cluster members tend to be aligned to long axis of the parent clusters. For cluster with BM type = II the distribution is perfectly random. The distribution of the Δp_2 does not show an alignment.

The additional considerations allow us to conclude that our result is due to neither observational errors nor the applied method of observational data analysis.

References

Abell, G.O., Corwin, H.G.,& Olowin, R.P., 1989. Astrophys.J.Suppl.**70**,1.
Binggeli, B., 1982. Astron.Astrophys. **107**,338.
Carter, D., & Metcalfe, N., 1980. Mon.Not.R.astr.Soc. **191**,325.
Olowin, R.P., 1985. PhD, University of Oklahoma, Norman.
Sastry, G.N., 1968. Publ.Astr.Soc.Pacific **80**, 252.
Struble, M.F., 1987. Astrophys.J. **317**, 668.
Struble, M.F., 1988. Astron.J. **96**, 1534..
Struble, M.F., 1990. Astron.J. **99**, 743..
Struble, M., & Peebles, P.J.E., 1985. Astron.J. **90**, 542.

CALIBRATION OF THE COBE FAR INFRARED ABSOLUTE SPECTROPHOTOMETER (FIRAS)

R. Isaacman, R.E. Eplee (General Sciences Corp.), E. Cheng, J. Mather, R. Shafer (NASA/GSFC), S. Meyer, R. Weiss (MIT) E. Wright (UCLA), R. Kummerer, S. Read, L. Olson (STX Corp.)

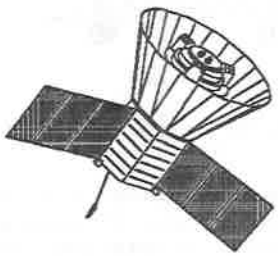

COSMIC BACKGROUND EXPLORER

The Far Infrared Absolute Spectrophotometer (FIRAS) instrument aboard NASA/GSFC's Cosmic Background Explorer (COBE)* satellite is designed for precision measurements of the absolute sky spectrum between 1 and 100 inverse cm (1 to 0.01 cm wavelength). This is achieved by a combination of (1) design of a null spectral comparison that is insensitive to instrument gains; (2) in-flight calibration that allows an accurately-measured blackbody source to be substituted for the sky; and (3) sophisticated analysis software. Initial calibrations have allowed measurements of the cosmic background spectrum to better than 1% of the peak intensity. We present the calibration techniques used, together with a discussion of current limitations and improvements for reaching 0.1% accuracy.

*NASA/GSFC is responsible for COBE with the scientific guidance of the COBE Science Working Group.

The FIRAS External Calibrator is an Eccosorb cone ($e > 0.999$) that fills the sky aperture and is controlled to within a millikelvin of the nominal cosmic background temperature. FIRAS is thus a substitution experiment whose accuracy is only weakly dependent upon the instrument gains.

However, in searching for departures from a Planck curve it is necessary to know the optical efficiency and internal emissivities of the instrument. To achieve this, the calibrator is inserted in the sky horn and it, the sky horn, an internal blackbody, and the internal reference horn are driven independently between 2.2 K and 20 K. The resulting ensemble of spectra, after correction for the effects of cosmic ray hits and the responses of the bolometer and electronics, provide the input for a fit at each frequency to the overall optical throughput, the emissivities of the horns and internal calibrator, and an offset term.

There are subtleties in this approach. (1) An a priori bolometer model determines the detector gain; (2) untreated cosmic ray hits will corrupt the data; (3) baseline subtraction and apodization must not introduce spurious responses; (4) we need accurate thermometry over a very large dynamic range; and (5) we must account for internal emission.

Current studies address all of these issues. Most importantly, the volume of calibration data from the mission allows inclusion of thermometry corrections and bolometer parameters in the calibration model. An improved optical model also accounts for internal emission. We thus expect to reach accuracies of 0.1% of the peak flux of the Planck curve.

A DEEP WESTERBORK SEARCH FOR HIGH REDSHIFT HI

Mark Wieringa[1], Ger de Bruyn[2] and Peter Katgert[1]
[1]Leiden Observatory and [2]NFRA Dwingeloo

ABSTRACT

The formation of large scale structure in the universe, spanning the range from galaxies to superclusters, can in principle be observed by detecting the redshifted 21 cm 'background radiation' due to neutral hydrogen in the forming structures. A number of such searches have been made, spanning redshifts from 3 to 8, all yielding upper limits to the HI content of the early universe. We present the results of a more sensitive, large search for cosmological neutral hydrogen at a redshift around 3.4. We have used the Westerbork SRT to extend our previous search with 2 new, deeper fields at 325 MHz, spanning a combined area of $\sim$ 11 sq. degrees to half power. The velocity depth of the observations is 4000 km/s. No significant positive detections were made at spatial resolutions of $1'$–$8'$ and velocity resolutions of 200–1200 km/s. Corresponding limits on HI masses range from 4×10^{13} to $1.4 \times 10^{14} M_{\odot}$. Implications are that ionization (by shock heating and/or the first formed galaxies) has efficiently ionized most protoclusters around $z = 3.4$.

INTRODUCTION

An approach to study the formation of large scale structures in the universe, first proposed by Sunyaev&Zel'dovich[1], is a search for 21 cm line emission (redshifted to meter wavelengths) due to neutral hydrogen in the precursors of current structures. They considered the possibility of observing 'pancake'-like structures. In this picture they propose structures of $3 \times 10^{14} M_{\odot}$ with a diameter of 2 Mpc containing $10^{14} M_{\odot}$ of neutral hydrogen. The velocity width of the structure is estimated to be less than the virial width $(GM/R)^{1/2}$, the line of sight velocity width will be a factor $1/\sqrt{3}$ lower, about 600-700 km/s. However, expected signals for realistic HI masses are low (mJy range) and all attempts so far are aimed at just detecting any signal, to determine if large HI masses are observable in the formation history of current structure.

The first search for cosmological HI was conducted by Davies et. al.[2] with the Jodrell Bank Mk IA telescope at 328 and 240 MHz, corresponding to z =3.33 and 4.92 respectively; Bebbington [3] used the Cambridge 6C array at 151 MHz ($z = 8.4$) to map the sky North of $\delta = 82^{\circ}$ differentially in frequency ; Hardy&Noreau [4,5] used the VLA at 327 MHz ($z = 3.34$) in D-configuration to map 5 fields (25 sq. degrees). In 1985 we used the WSRT at 327 MHz to map two fields (11 sq. degrees) reaching the lowest limits at the time [6]. All searches failed to detect any significant signal, setting interesting limits on the HI contents of the early universe. We now report an extension of our search with two new fields.

OBSERVATIONS

We have used the WSRT at 325 MHz to observe two new fields. Our first observations in 1985 were somewhat limited in velocity range (2000 km/s), lowering the sensitivity to 1000 km/s structures. In our new observations (1987/88) we eliminated this problem by doubling the frequency range, in addition the integration times are longer.

One of our fields (at $\alpha = 6^h 45^m, \delta = 45^{\circ}$, integration 8×12^h per channel) contains the quasar OH471 which has a redshift $z = 3.4$, at that z HI falls within our bandpass. Because quasars point to the sites where the first luminous structures form, one might expect large structures nearby. On the other hand the quasar will ionize surrounding neutral hydrogen and thus reduce the probability of a detection. Our second field (at $\alpha = 8^h 36^m, \delta = 70^{\circ} 28'$, integration 12×12^h per channel) observed in this period is therefore located in a region void of known quasars near $z = 3.4$; also strong galactic emission and strong continuum sources were avoided.

The calibration and reduction of the observations was done using DWARF, the WSRT reduction package which uses the redundant baseline information available in Westerbork observations to determine telescope based calibration factors[7]. The spectral channels were then selfcalibrated using the continuum model, which was subsequently subtracted from the u-v-data. All data clearly influenced by interference were deleted.

After these steps the resulting maps were nearly free from systematic structure, although some low level ($\lesssim 1\sigma$) 'striping' due to missing data is visible in most maps. We made maps spanning $6^{\circ} \times 6^{\circ}$ at resolutions of $1'$, $2'$, $4'$, the half-power radius is at $\sim 1.3^{\circ}$

ANALYSIS and CONCLUSIONS

We inspected the data for any coherent structure in position-velocity space by scanning through the available channels. Maps at resolutions from $\sim 1'$ to $8'$ were inspected and we made velocity smoothed versions of the datacubes as well, probing the range from 200 to 1200 km/s. No significant detections, corresponding to 4–5σ peaks (depending on resolution), were made and no large coherent structures were found. The resulting limits for the deepest field are given in Table 1, for the other field the values are 20% higher. No correction has been applied for the average attenuation of ~ 1.4. A histogram and power spectrum analysis also yielded no significant detections.

The expected signal for a HI-mass with velocity width ΔV within the beam is given by:

$$S_\nu[\mathrm{mJy}] = 11.7h^2 \left(\frac{M_{HI}}{10^{14}M_\odot}\right)\left(\frac{\Delta V}{10^3\mathrm{km/s}}\right)^{-1} \frac{\Omega_0^4(1+z)}{\left[\Omega_0 z + (\Omega_0-2)(\sqrt{1+\Omega_0 z}-1)\right]^2}.$$

For $\Omega_0 = 1, h = 0.5, z = 3.4$, we obtain the mass-limits given in Table 1 (the masses are 3 times larger for $\Omega_0 = 0.1$.)

Table 1. Upper limits (4–5σ) for the field at $\alpha = 8^h36^m, \delta = 70°28', z = 3.4$ ($\Omega_0 = 1, h = 0.5$).

Angular resolution	$2'$	$2'$	$2'$	$4'$	$4'$	$8'$
ΔV [km/s]	200	400	1200	400	1200	1200
S[mJy]	5.0	3.5	2.0	4.9	2.8	3.0
$M_{HI}/10^{14}M_\odot$	0.4	0.6	0.9	0.8	1.3	1.4

The comoving volume per 4000 km/s field is $3.0 \cdot 10^5 h^{-3}\mathrm{Mpc}^3$ for $z = 3.4$ and $\Omega_0 = 1$. Using a comoving density of rich clusters[8] of $1.2 \cdot 10^{-6}h^3\mathrm{Mpc}^{-3}$ this results in an expected number of 0.4 clusters per field. Including the somewhat less rich clusters (richness class ≥ 1) this value is about 4 times larger: 1.5. Combining all 4 fields yields expected numbers of ~ 1 rich cluster and 5 $R \geq 1$ clusters (for $\Omega_0 = 0.1$ these values are 5.5 times larger). Preliminary analysis of 3 new fields reaching similar depths has also yielded no detections so far.

We have surveyed a limited volume of the universe around $z = 3.4$ and find no evidence for neutral structures with masses above 5×10^{13}–$1.4 \times 10^{14}M_\odot$ and velocity widths of 200-1200 km/s. Combined with the evidence from quasar spectra this probably means that no or very few large, neutral structures survived until this epoch.

REFERENCES

1) Sunyaev, R.A., Zel'dovich, Ya.B., 1975, M.N.R.A.S., 171, 375
2) Davies, R.D, Pedlar, A., Mirabel, I.F., 1978, M.N.R.A.S., 182, 727
3) Bebbington, D.H.O., 1986, M.N.R.A.S., 218, 577
4) Hardy, E., Noreau, L., 1987, Astron. J., 94, 1469
5) Noreau, L., Hardy, E., 1988, Astron. J., 96, 1845
6) de Bruyn, A.G., Wieringa, M.H., Katgert, P. & Sancisi, R., 1988, *Large Scale Structure of the Universe, IAU Symp. 130*, p 211, eds. Audouze, J., Pelletan, M.-C. & Szalay, A., Kluwer, Dordrecht
7) Noordam, J.E., de Bruyn, A.G., Nature, 299, 597
8) Kaiser, N., 1986, M.N.R.A.S., 222, 323

EVIDENCE FOR A SCALING LAW IN THE DISTRIBUTION OF GALAXY CLUSTERS

A. CAPPI[1], S. MAUROGORDATO[2] AND M. LACHIÈZE-REY[3]

[1]Osservatorio Astronomico di Bologna, Via Zamboni 33, 40100 Bologna, Italy

[2]CNRS UA 173; DAEC, Observatoire de Paris, Section de Meudon, F-92195 Meudon Principal cédex, France

[3]CNRS Service d'Astrophysique, CEN Saclay, 91191 Gif sur Yvette, France

Abstract

We have analyzed the dependence of the spatial void probability function ϕ_0 on the scaling variable $q = nV < \xi >$ for different galaxy cluster samples. We used the tridimensional distance-limited sample defined by Postman, Huchra and Geller (1986), and Tully's catalog (1987). Within the distance for which they are reasonably complete ($z \leq 0.08$), these cluster samples appear to follow a general scaling invariance law, up to $q \sim 2$, corresponding to void radii of $\sim 50h^{-1}\ Mpc$ ($h = H_0/100$). This scaling law is consistent, within the statistical uncertainties, with the law followed by galaxies in the Center for Astrophysics and Southern Sky Redshift Survey catalogs.

1. Introduction

The 2-point correlation function ξ_{cc} of clusters seems to follow the same power-law as ξ_{gg} of galaxies, but with a larger correlation radius r_0 [1] It has been shown that the cluster 3-point correlation function ζ_{cc} is related to the ξ_{cc} by the same relation as for galaxies [2),3)], and galaxy distributions obeying scaling relations, generalizing to the n-th order the observed relation between ξ and ζ have been studied [4),5)]. The void probability function ϕ_0 [6)] provides a sensitive test of the existence of a scaling law, which has been found in the galaxy distribution [7),8)]. The constant slope in the power-law behaviour of ξ suggests a scaling invariance in the galaxy formation, while the similarity of the dimensionless amplitudes of ξ_{cc} for clusters with different richness indicates a scaling invariance in the clustering process [9)]. Therefore we analysed the distribution of galaxy clusters through the statistics of voids, searching for a scaling law in the distribution of clusters and a possible relation between the scaling of galaxy and cluster distributions, and testing cluster segregation as a function of richness [10)].

2. Void Probability Function and scaling

We used the distance-limited sample of Postman et al. [11)] (hereafter PHG), which includes all Abell clusters belonging to the statistical sample [12)] having a measured or estimated redshift ≤ 0.1, a richness class $R \geq 1$, and a cutoff in absolute magnitude of the tenth brightest galaxy $M_c \leq -19.38$; and the Tully sample [13)], which includes all Abell clusters with measured redshifts $z \leq 0.1$. We cut at $z = 0.06$ and $z = 0.07$ the PHG sample, and at $z = 0.07$ and $z = 0.08$ the Tully sample; we cut also at $b_{II} = 40$, to avoid galactic absorption. We calculated $\phi_0(r, n)$ for each sample of density n, by measuring the probability of finding a sphere of radius r without clusters. Beyond 50 h^{-1}Mpc, the statistics fails because of the limited size of the sample. We calculated also $q = nV < \xi >$ using the J_3 integral, $J_3 = 4\pi \int r^2 \xi(r) dr$ [14)] and we used the density independent normalized function $\chi(q) = Log(\phi_0(r, n))/nV$. Fig.1 shows the J_3 integral, which is a measure of the mean number of neighbours in excess of random. This indicator shows the higher clustering of the PHG catalog relatively to the Tully catalog, which includes richness 0 clusters. Our results are consistent with Bahcall's results showing an increasing correlation radius with richness class. In Fig.2 we plot the Tully sample limited at $z = 0.08$ and the PHG sample limited at $z = 0.06$, compared to the behaviour of the CfA galaxy sample analysed by Maurogordato and Lachiéze-Rey. ϕ_0 has values higher than in the case of a random distribution, reaching a value of ~ -0.55 at $q \sim 2$ ($r \sim 50 h^{-1}\ Mpc$). χ is similar for the two cluster samples and for galaxies up to $q \sim 2$. This result is strengthened by the fact that the involved scales and density are extremely different.

3. Conclusions

We have shown that the scaling invariance, which extends to void radii of about $12\ h^{-1}\ Mpc$ in the case of galaxies (CfA and SSRS samples), is still present in the cluster distribution up to void radii of $\sim 50\ h^{-1}\ Mpc$. Jing [15)] has recently examined the bidimensional ACO cluster distribution, finding a scaling relation similar to that of galaxies. The two complementary works point to the same conclusion.

References

1) Bahcall, N.A., Soneira,R.M.: 1983, *Astrohpys. J.* **270**, 20
2) Jing, Y., Zhang, J.: 1989, *Astrohpys. J.* **342**, 639
3 Tóth, G., Hollósi, J., Szalay, A.S.: 1989, *Astrohpys. J.* **344**, 75
4) Fry, J.N.: 1984, *Astrohpys. J. Letters* **277**, 5
5) Schaeffer, R.: 1984, *Astron.Astrophys.* **134**, L15
6) White, S.D.M. 1979, *Mon.Not.R.astr.Soc.* **186**, 145
7) Bouchet, F.R., Lachièze-Rey, M.: 1986, *Astrohpys. J. Letters***302**, 37
8) Maurogordato, S., Lachièze-Rey, M.: 1987, *Astrohpys. J.* **320**, 13
9) Szalay, A.S., Schramm, D.N.: 1985, *Nature*, **314**, 718
10) Cappi, A., Maurogordato, S., Lachièze-Rey, M.: 1990, *Astron.Astrophys.*,in press
11) Postman, M., Geller, M.J., Huchra, J.P.: 1986, Astron.J. **91**, 1267
12) Abell, G.O.: 1958, *Astrohpys. J. Suppl.* **3**, 211
13) Tully, R.B.: 1987, *Astrohpys. J.* **323**, 1
14) Maurogordato, S., Schaeffer, R., Da Costa, L.N.: 1989, *preprint*
15) Jing, Y.: 1990, *Astron.Astrophys.* **233**, 309

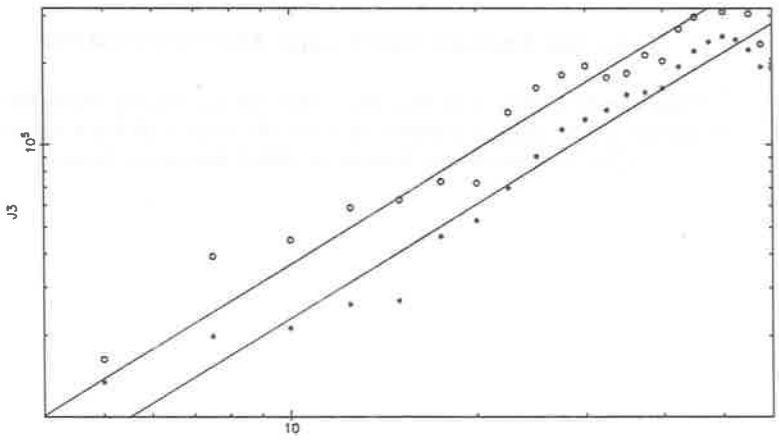

Figure 1

J_3 integral as a function of the sphere radii (in Mpc), for PHG (circles) and Tully (stars) samples ($z \leq 0.07$). Fits follow a power law with $\gamma = -1.6$ and r_0 respectively 24 and 18 Mpc.

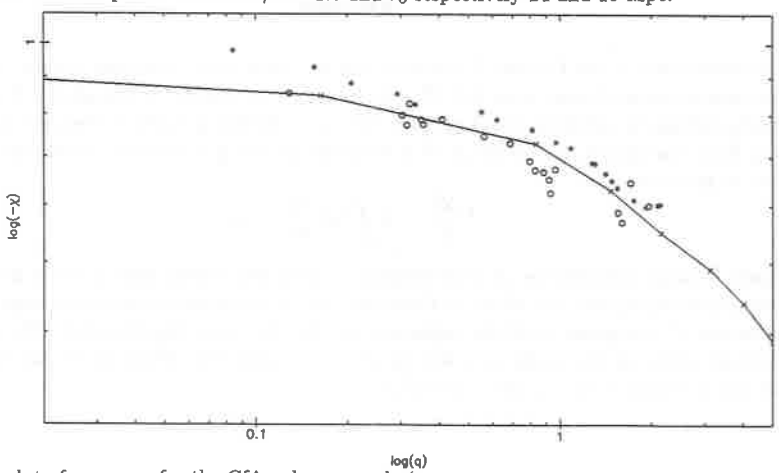

Figure 2

Logarithmic plot of $-\chi$ vs. q for the CfA galaxy sample (crosses connected by lines), the Tully sample, $z \leq 0.08$ (stars) and the PHG sample, $z \leq 0.06$ (circles).

Gravitational CMBR temperature fluctuations from non-linear structures: N-body simulations

Eelco van Kampen[1] and Enrique Martínez-González[2]

[1] Sterrewacht Leiden, P.O. Box 9513, 2300 RA Leiden, the Netherlands
[2] Instituto de Estudios Avanzados en Física Moderna y Biología Molecular, CSIC-Universidad de Cantabria, 39005 Santander, Spain

Abstract

Anisotropies of the Cosmic Microwave Background Radiation are usually characterized by the temperature fluctuations $\Delta T/T$, which consist of several terms arising from a number of effects acting on photons coming from the last-scattering surface towards us. The term arising from the gravitational effect of non-linear evolving structures along the path of the photon is given by:

$$\cdot \frac{\Delta T}{T} = 2 \int_e^o d\tau \frac{\partial \phi}{\partial \tau}(\tau, \vec{x})$$

We used N-body simulations of cosmological objects like voids, rich clusters and Great Attractors, and calculated the effect of these objects by shooting photons through an evolving distribution of computer particles representing the real mass distribution. For rich clusters we find an effect on the order of a few times 10^{-7}, while the effect for Great Attractor-like structures is found to be on the order of 2×10^{-6}.

The integrated gravitational effect

In this paper, we study the integrated gravitational influence of non-linear structures on the temperature of the microwave photons. An estimation of this effect for a Swiss-cheese model was first given by Rees and Sciama (1968). More extensive work was done by Dyer (1976), Nottale (1984) and Thompson and Vishniac (1987). In order to be realistic, the non-linear evolution of the structure is followed by N-body simulations.

The gravitational effect on $\frac{\Delta T}{T}$ in the general case of a photon propagating in a non-static linear gravitational potential has recently been given by Martínez-González, Sanz and Silk (1990). The result for the case of an Einstein-de Sitter universe can be expressed as:

$$\frac{\Delta T}{T} = \frac{1}{3}(\phi_e - \phi_o) + 2\int_e^o d\tau \frac{\partial \phi}{\partial \tau}(\tau, \vec{x}) + \vec{n} \cdot (\vec{v}_o - \vec{v}_e)$$

While the first and third terms are the known Sachs-Wolfe (Sachs and Wolfe 1967) and Doppler terms respectively, the second term is the integrated gravitational effect given by the rate of change of the potential ϕ with time from the emitting point to the observer. This is the term we are interested in and it is calculated for several structures.

Results of the integrated gravitational effect have already been given for the Bootes void, assuming the thin shell approximation to describe its evolution, and for the Great Attractor modelled either with a Swiss-cheese or with an uncompensated secondary infall collapse (Martínez-González and Sanz 1990). In all cases the effect analytically found is at most a few times 10^{-6}.

Numerical calculation of the effect

Instead of using a model for non-linear structures encountered by photons coming towards us, we calculate the effect using the potentials obtained for a distribution of particles by an N-body integrator. The code used was a slightly adapted version of the Barnes & Hut treecode (1986), with initial conditions produced by a beautiful code deviced by Bertschinger (1987) based on a path integral method (see the *acknowledgements*). We first considered the most simple and popular case of an $\Omega = 1$ Einstein-de Sitter universe with a Cold Dark Matter spectrum.

As a first but already good approximation we shoot a two-dimensional grid of 64^2=4096 photons through an evolving N-body distribution, with the photons just travelling on parallel lines at the speed of light. This is justified for our intermediate scale objects at $z = 0.6$ because they measure about 1^o on the sky. For larger objects, like our Great Attractor at $z = 0.6$ as shown below, zero geodesics should be used, needing more extensive software (future work).

Results and discussion

We calculated the effect for several objects. We define our objects using Gaussian window functions, i.e. an object has an amplitude $\nu\sigma$ in the smoothed density field $\delta^W(\vec{x})$, obtained by convolving $\delta(\vec{x})$ with a window function $W(r) = exp - r^2/2R^2$, with σ being the r.m.s. of this field δ^W. So an object is defined by R and its density excess ν expressed in $\sigma(R)$. The code deviced by Bertschinger (1987) can produce initial conditions constrained to form any desired object. Very useful indeed !

We placed several 'intermediate scale' objects at $z = 0.6$, and calculated the effect using $\approx$ 17500 particles (a sphere cut out of a 32^3 particles cube). We chose 4 objects defined by a smoothing length of $R = 10$ Mpc (we use $H_o = 50$ km/s/Mpc) with amplitudes -2σ, 0σ,

2σ and 3σ. All objects give an effect on the order of their amplitude ν times 10^{-7}. This will hardly be measurable. The resulting map on the sky for the 3σ peak (a rich cluster) is shown in figure 1[a].

$\Delta T/T$ due to a Great Attractor or a Cosmic Void could be measurable. To test this, we calculated the effect due to a Great Attractor of the type claimed to exist by the Seven Samurai. Such a Great Attractor can be defined as a 2.1σ-peak for $R = 28$ Mpc (Bertschinger *et al.* 1990). We produced such an object within a sphere of radius 150 Mpc, and placed it at $z = 0.6$. The amplitude of the effect is almost redshift independent from $z = 0$ to $z = 2$, so also valid for the Seven Samurai Great Attractor. The resulting temperature fluctuations are about 2×10^{-6}, as shown in figure 1[b]. This might once be measurable.

More details on this research can be found in van Kampen and Martínez-González 1991.

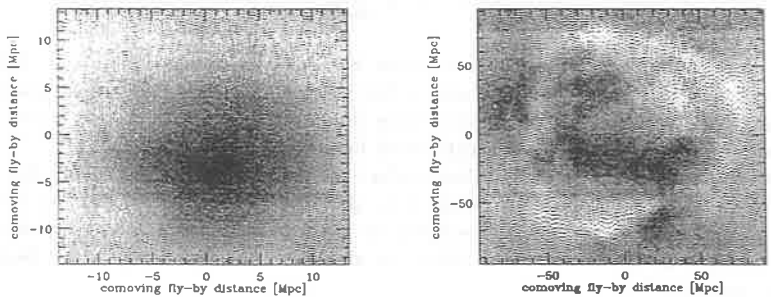

Maps of a patch of microwave background sky for photons which have traversed a rich cluster (on the left) or a Great Attractor-like structure (on the right). Both structures are at $z = 0.6$, so the cluster measures about 1° on the sky, and the G.A. spans about 6°. The gray-scales for the cluster: white=$+10^{-7}$, black=-4×10^{-7}. For the G.A.: white=$+2 \times 10^{-6}$, black=-3×10^{-6}. The maximum fluctuations are -3.5×10^{-7} and -2.5×10^{-6} respectively.

Acknowledgements

First of all we like to thank Bernard Jones, for supplying so much enthousiasm, energy and help. Rien van de Weygaert was essential for supplying us with realistic initial conditions, which he obtained from the beautiful code and method deviced by Bertschinger (1987). Vincent Icke deserves many thanks for useful comments on the physics and the numerical method. One of us (EvK) likes to acknowledge the Leids Kerkhoven-Bosscha Fonds and EelcoSoft Software Services for providing financial support.

References

Barnes, J. and Hut, P. 1986, *Nature* **324**, 446
Bertschinger, E. 1987, *Ap.J.Lett.* **323**, L103
Bertschinger, E., Dekel, A., Faber, S.M. and Dressler, A. 1990, *submitted to Ap.J.*
Dyer, C.C. 1976, *M.N.R.A.S.* **235**, 895
van Kampen, E. and Martínez-González, E. 1991, *submitted to M.N.R.A.S.*
Martínez-González, E. and Sanz, J.L. 1990, *M.N.R.A.S., in press*
Martínez-González, E., Sanz, J.L. and Silk, J. 1990, *Ap.J.Lett.* **355**, L5
Nottale, L. 1984, *M.N.R.A.S.* **206**, 713
Rees, M.J. and Sciama, D.W. 1968, *Nature* **217**, 511
Sachs, R.K. and Wolfe, A.M. 1967, *Ap.J.* **147**, 73
Thompson, K.L. and Vishniac, E.T. 1987, *Ap.J.* **313**, 517

STOCHASTIC FIELD FLUCTUATIONS IN GALAXIES AND CLUSTERS.

V. Antonuccio-Delogu and *F. Atrio-Barandela.*
NORDITA, Blegadamsvej 17, DK 2100 Copenhagen, **DENMARK**

Abstract.
Stochastic fluctuations of the gravitational field in a forming protostructure are induced by small radius, high density peaks. We compute the probability distribution of the gravitational field induced by a population of randomly placed peaks, for a power law spectrum of density fluctuations. **A net enhancement of the probability for large F is produced by the clustering.** We shortly stress the consequences of this on the dynamical evolution of forming protostructures.

Stochastic force fields.

In any model of structure formation in the Universe, peaks in the density field arise and are believed to be the primordial seeds of the observed objects. In this work, we study the dynamical influence that small-scale, high density peaks have on the collapsing protiostructures, through the gravitational field they engender. Chandrasekhar and Von Neumann (1942) and Kandrup (1980) have considered the random force field generated by a population of randomly placed pointlike objects. They give a probability distribution of a random stochastic force field W(F), measuring the probability that a test mass randomly placed feels a gravitational force of modulus F (**Holtsmark's Law**). In a context of biased galaxy formation, high peaks in the density field are strongly correlated: we calculate the modification of the Holtsmark law introduced by this effect. One can prove that the probability distribution of the force induced by the objects in a clustered system having a two–point correlation function $\xi(|\mathbf{r}_1 - \mathbf{r}_1|)$ is given by:

$$W(F) = \frac{2F}{\pi} \int_o^\infty dk \sin(kF) A(k)$$

where:

$$A(k) = \exp\left[-\frac{\alpha}{2}(G\langle m\rangle_p|\mathbf{k}|)^{\frac{3-p}{2}}B(p)\right]\cdot\left[1+\frac{\Sigma(k)}{A^2_{(1)}(k)}\right],$$

and one has defined: $\alpha = \rho_{tot}(3-p)/R_1^{-p}$, $\langle m\rangle_p^{(3-p)/2} = \int_0^\infty dm\mu(m)m^{\frac{3-p}{2}}$ and

$$\Sigma(k) = \langle m\rangle_p^{(3-p)}\int d\mathbf{r}_1\int d\mathbf{r_2}\exp[i\cdot\mathbf{kF}(\mathbf{r}_1)]\exp[i\cdot\mathbf{kF}(\mathbf{r_2})]\xi(|\mathbf{r_2}-\mathbf{r}_1|)\tau_M(\mathbf{r}_1)\tau_M(\mathbf{r_2})$$

$$A_{(1)} = \frac{3-p}{4\pi R_1^{3-p}}\int_0^{R_1} drd\Omega r^{2-p}\exp(i\mathbf{k}\cdot\mathbf{F})$$

In Figs. 1a–b we plot the resulting W(F) for two different values of the index of the power spectrum. As is evident, the clustering results in an enhancement of the probability of interaction at small distances and on average the resulting forces are larger.

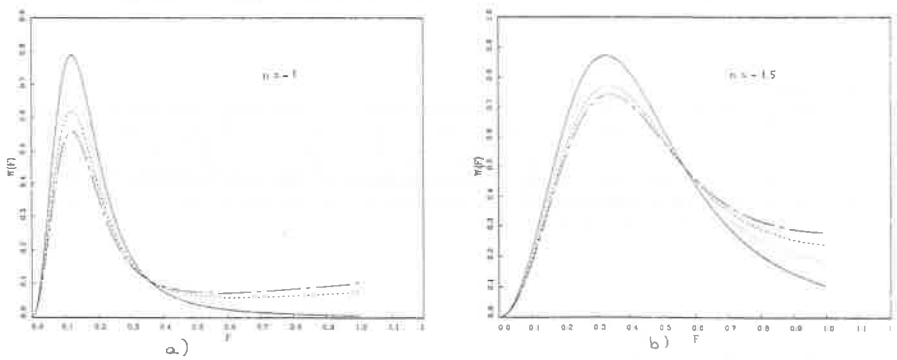

Figure 1. Probability distribution of the force F experienced by a random test particle, for two power spectrum: (a) n = -1, (b) n = -1.5. The force is in units of GM/R^2. The continuous solid curve is for an uncorrelated system. Dotted, dashed and long–dashed curves are for progressively increasing values of ξ_o. The values are separated by $\Delta\xi_o = 0.1$.

We can also obtain an expression for the probability distribution of the induced torques, and to study the angular momentum exhange between small–scale and structures and collapsing peaks. All this results in a readjustement and inner transport of angular momentum: for more details, we refer to a forthcoming paper (Antonuccio–Delogu and Atrio–Barandela (1990))

References.

Antonuccio–Delogu,V. and Atrio–Barandela,F., submitted to *Ap. J. Letters*(1990)

Chandrasekhar,S. and Von Neumann,J., *Asrophys. J.* 95, 489 (1942)

Kandrup.H., *Phys. Rep.* 63,1 (1980)

THE DISTRIBUTION OF LYMAN LIMIT ABSORBERS: IMPLICATIONS FOR THE LYMAN VALLEY

Palle Møller
European Southern Observatory
Karl-Schwarzschild-straße 2, D-8046 Garching bei München
Federal Republic of Germany

ABSTRACT

An analysis of the redshift evolution of Lyman limit absorbers in quasar spectra is presented. The analysis includes 5 new low redshift IUE quasars, and employs a strict and conservative optical depth lower limit of $\tau \geq 1.5$ at the Lyman limit.

A redshift evolution parameter of $\gamma = 1.52 \pm 0.66$ is found. This is somewhat higher than previous results, but still compatible with $\gamma = 1$. The reason for the steeper redshift evolution found in this $\tau \geq 1.5$ sample is, that most of the Lyman limit absorbers reported in IUE quasars at low redshifts, and included in earlyer samples, have $\tau < 1.5$.

The implications of the steeper redshift evolution, for the prediction of the *'Lyman valley'* absorption, are discussed. In particular it is found that $\approx$7% of all $z_{em} \geq 3.1$ quasars should be less than 50% absorbed, and $\approx$25% less than 90% absorbed, at the redshifted HeII λ304 Å line. This provides a far more optimistic estimate of the probability of carrying out the HeII Gunn-Peterson test for intergalactic helium with the *Hubble Space Telescope* than previously reported.

1. INTRODUCTION

The current intense interest in the determination of the number density and redshift evolution of the different classes of quasar absorption systems, stems in part from the direct implications for the cosmological models and evolutionary scenarios, but also in part from the realization that the interpretation of the extreme UV spectra of high redshift quasars, relies heavily upon the access to realistic models of the absorption by intervening matter.

In the line of sight to a high redshift quasar there will always be a *large* number of intervening clouds with optical depth at the Lyman limit $\tau < 1$; the accumulated absorption due to these clouds is well understood and easily predicted. The **total** mean absorption, however, is very sensitive to the number and exact distribution of the scarce but heavily absorbing Lyman limit systems (LLSs). For a detailed discussion of the statistics of the accumulated absorption by neutral hydrogen along the line of sight to high redshift quasars, see Møller and Jakobsen (1990).

Following Peterson (1978), it is customary to parameterize the evolution of the number of Lyman forest clouds per unit redshift as $\frac{dn}{dz} = A(1+z)^{\gamma}$, where the currently favored value of the evolution parameter $\gamma \approx 2.3$ (Hunstead, 1988) indicates an evolution strongly in excess of a constant comoving density. A constant comoving density of absorbers with constant mean cross-section, would require $\gamma = 1$ for $q_o = 0$ and $\gamma = \frac{1}{2}$ for $q_o = \frac{1}{2}$.

Tytler (1982), and Bechtold *et al.* (1984), both found that the distribution of LLSs is fully compatible with constant comoving evolution. This result was recently confirmed by Sargent, Steidel and Boksenberg (1989) who found $\frac{dn}{dz} = 0.76(1+z)^{0.68\pm0.54}$.

The purpose of this paper is to set realistic upper and lower limits on the density of LLSs, and hence on the accumulated Lyman continuum absorption (the *'Lyman valley'*).

2. THE SAMPLE

The sample compiled by Sargent, Steidel and Boksenberg (1989) was combined from their own observations of 59 high redshift quasars, 9 low redshift quasars observed by Bechtold *et al.* (1984), and the sample of Tytler (1982); in all 54 LLSs in 90 quasars. To improve on the statistics at the low redshift end, I have expanded the sample by including the IUE data from Gondhalekar, O'Brien, and Wilson (1986). The quasars for this study were all selected without any prior knowledge of their absorption spectra (O'Brien, 1990).

Sargent, Steidel and Boksenberg chose to maintain a conservative optical depth completeness limit of $\tau \geq 1.5$ for their own data, and I shall hence adopt this limit for the total sample. Imposing this requirement, it was in 3 cases (Q1247+268, Q1317+277, and Q2228-403) necessary to examine the original data. For all three I estimate that the strength of the continuum jump is compatible with $\tau \geq 1.5$. Finally I have chosen to keep a constant $z_{min} = 2.510$ for *all* quasars observed by Sargent, Steidel and Boksenberg. The total sample then contains 46 LLSs, with optical depth $\tau \geq 1.5$, in 95 quasars. In cases where a metal system associated with the LLS has been found, the reshift of the metal system has been adopted as the true redshift of the system.

3. ANALYSIS

Using the maximum likelihood method formulated by Sargent, Steidel and Boksenberg (1989), I obtain $\gamma = 1.52 \pm 0.66$, suggesting a much steeper redshift evolution than the $\gamma = 0.68 \pm 0.54$ found by them, but still compatible with $\gamma = 1$. If LLSs make up a non evolving class of absorbers, this then is slightly in favor of an open universe ($q_o < \frac{1}{2}$), whereas $q_o = \frac{1}{2}$ would require $\gamma = \frac{1}{2}$.

The maximum likelihood fit to the evolution law of Lyman limit absorbers with $\tau \geq 1.5$ is given by

$$\frac{dn}{dz} = 0.21(1+z)^{1.52}. \qquad (1)$$

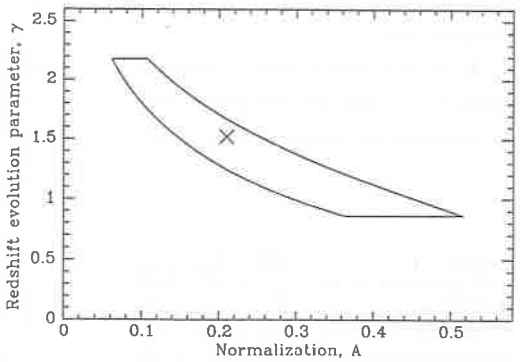

Figure 1. *Maximum likelihood model (×), and the enclosing 1σ curve in the (A, γ) parameter space.*

The reason for the steeper redshift evolution in this $\tau \geq 1.5$ sample is, that most of the low column LLSs included in the original sample, were found in IUE quasars at low redshifts.

In Figure 1 the maximum likelihood fit (×), and the area of the (A, γ) plane enclosed by the 1σ curve, are shown. Of the models inside the 1σ curve, the ones giving rise to the weakest, and the strongest, cumulated Lyman limit absorption are given by $\frac{dn}{dz} = 0.061(1+z)^{2.18}$ and $\frac{dn}{dz} = 0.40(1+z)^{1.13}$ respectively.

The maximum likelihood redshift evolution law, given by equation (1), corresponding lower and upper limit, and the data, are shown in Figure 2.

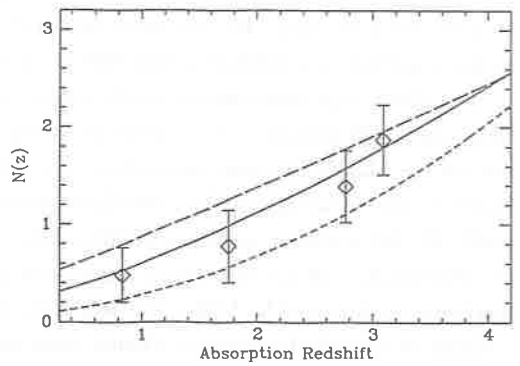

Figure 2. *The maximum likelihood model (full curve), its 1σ lower limit (short dash), and 1σ upper limit (long dash) to the data. The data (◇) have been rebinned for display purposes.*

4. IMPLICATIONS FOR THE LYMAN VALLEY ABSORPTION

I shall define Lyman forest systems as absorbers having column density in the range $10^{13}cm^{-2} - 10^{17}cm^{-2}$, a column density spectrum $f(N) \propto N^{-1.51}$, and a redshift distribution law $\frac{dn}{dz} = 14(1+z)^{2.3}$, and LLSs as absorbers in the range $10^{17}cm^{-2} - 10^{22}cm^{-2}$, with a column density spectrum $f(N) \propto N^{-1.39}$. Rescaling the distribution law given by equation (1), and its lower and upper 1σ limits, to the defined column density range for Lyman limit absorbers, gives A = 0.086, 0.29, and 0.56 for $\gamma = 2.18$, 1.52, and 1.13 respectively.

The expected mean transmission spectra of the intervening medium out to a redshift of $z_{em} = 2.72$, for these 3 distribution laws of the Lyman limit systems, and also including the Lyman forest systems, are plotted In Figure 3. Superimposed on the model spectra is the IUE spectrum of HS1700+6416 obtained by Reimers *et al.* (1989). This is so far the only quasar spectrum, in which the gentle slope of the far side of the Lyman valley has been seen. The spectrum has been smoothed and divided by the power law continuum found by Reimers *et al.*

It is seen from Figure 3 that the **mean** transmission in the Lyman valley is known to within a factor of ≈2.

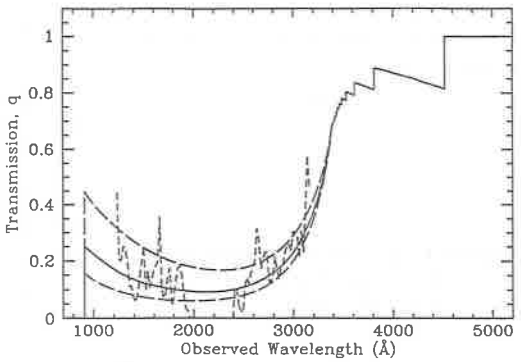

Figure 3. *Lyman valley transmission spectrum of the $z_{em} = 2.72$ QSO HS1700+6416 (short dash), expected mean transmission spectrum for the distribution law given by equation (1) (full curve), and its 1σ lower and upper limit (long dash).*

A detailed Monte Carlo analysis, identical to the one described by Møller and Jakobsen (1990), has been carried out for the maximum likelihood model. This analysis confirms that our previous estimate of the number of $z_{em} \geq 3.1$ quasars suitable for a HeII Gunn-Peterson test with HST, has been far too pessimistic. The original estimate of ≈7% of the $z_{em} \geq 3.1$ quasars being less than 90% absorbed, and ≈1% less than 50% absorbed, for this revised model translates into ≈25% less than 90% absorbed, and ≈7% less than 50% absorbed.

The rather large uncertainties on the mean transmission spectrum, even from this quite large sample (95 quasars in all), reflects the strong dependence of the expected mean absorption on the LLS distribution parameters γ and A. However this strong dependence can be turned to our advantage, in the sense that observations of the full Lyman valley in a fairly small (10 - 20) sample of medium redshift quasars at low resolution, will provide a much better determination of the distribution parameters (including the power of the column density spectrum, as discussed by Møller and Jakobsen, 1990), than is currently available from the counting of individual systems in a much larger sample.

5. SPECTRA OF QUASARS WITH VERY HIGH REDSHIFT

Since a statistically interesting number of quasars with $z_{em} > 4$ has now been found, it is interesting also to see how well the model accounts for the observed properties at $z_{em} > 4$. A simulated spectrum combined from a power law continuum ($f_\nu \propto \nu^{-0.7}$), typical emission lines, and the maximum likelihood transmission spectrum, is seen in Figure 4. The spectrum is made for a redshift of 4.1. Note that in the calculation of the accumulated Lyman limit absorption, **only** the Lyman forest absorbers have been included. The residual flux shortward

of 4650 Å in the spectrum shown in Figure 4, is hence the signal against which one would have to detect a Lyman limit absorber, to expand the redshift coverage of the LLS sample, into this region.

Comparing Figure 4 to the spectra of 10 quasars with $z_{em} > 4$ obtained by Schneider, Schmidt and Gunn (1989), it seems that the observed line blanketing in the Lyman forest is stronger than expected from the model. This could suggest that the redshift evolution of the Lyman forest absorbers is even stronger than $\gamma = 2.3$. Alternatively an increase in the velocity dispersion of the clouds at higher redshifts, or the existence of a diffuse Gunn-Peterson medium at high redshifts, could account for the enhanced Lyman line blanketing.

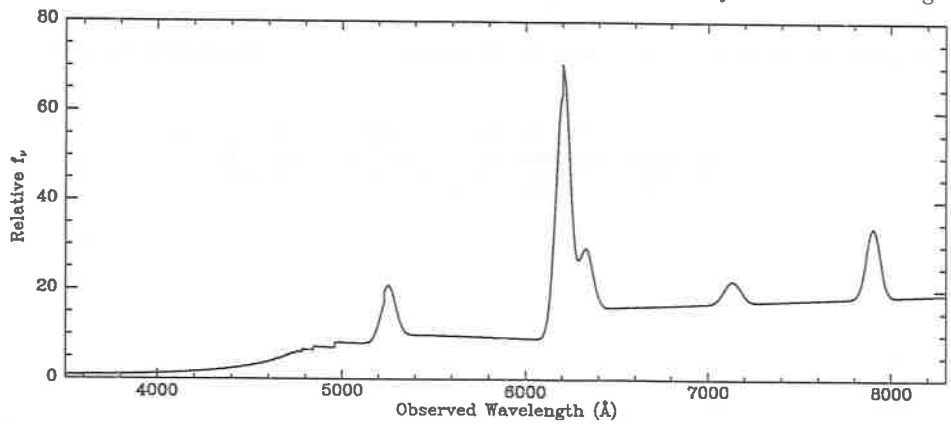

Figure 4. *Simulated mean quasar spectrum at $z_{em} = 4.1$. Expected Lyman continuum absorption from LLSs has not been included.*

Acknowledgements

I am grateful to W. L. W. Sargent for making a copy of the extended Sargent, Steidel and Boksenberg LLS sample available, and to Reimers *et al.* for providing a copy of their data on HS1700+6416. I am indebted to Peter Jakobsen for many stimulating discussions.

REFERENCES

Bechtold, J., Green, R. F., Weymann, R. J., Schmidt, M., Estabrook, F. B., Sherman, R. D., Wahlquist, H. D., Heckman, T. M.: 1984, *Astrophys. J.*, **281**, 76.

Gondhalekar, P. M., O'Brien, P., Wilson, R.: 1986, *Monthly Notices Roy. Astron. Soc.*, **222**, 71.

Hunstead, R. W.: 1988, in *QSO Absorption Lines: Probing the Universe*, p. 71, eds. J. C. Blades, D. A. Turnshek, C. A. Norman, Cambridge University Press, Cambridge.

Møller, P., Jakobsen, P.: 1990, *Astron. Astrophys.*, **228**, 299.

O'Brien, P. T.: 1990, *Private communication.*

Peterson, B. A.: 1978, in *Large Scale Structure of the Universe*, IAU Symp. No. 79, p. 389, eds. J. Einasto, M. S. Longair, Reidel, Dordrecht.

Reimers, D., Clavel, J., Groote, D., Engels, D., Hagen, H. J., Naylor, T., Wamsteker, W., Hopp, U.: 1989, *Astron. Astrophys.*, **218**, 71.

Sargent, W. L. W., Steidel, C. C., Boksenberg, A.: 1989, *Astrophys. J. Suppl.*, **69**, 703.

Schneider, D. P., Schmidt, M., Gunn, J. E.: 1989, *Astron. J.*, **98**, 1507.

Tytler, D.: 1982, *Nature*, **298**, 427.

COLLAPSE OF POPULATION III OBJECTS INDUCED BY COLD COLLISIONLESS DARK MATTER

J.C.N. de Araujo and R. Opher
Instituto Astronômico e Geofísico da USP
C.P. 30.627, 01051 São Paulo, SP - Brasil

ABSTRACT

We study the formation of Population III Objects that can be formed by cold collisionless dark matter. We take into account photon drag, photon-cooling, recombination, photoionization, collisional ionization, Lyman - α cooling and the formation and cooling of hydrogen molecules in the barionic matter. We previously showed that the minimum mass to collapse from the recombination era without dark matter was $\sim 10^4 M_\odot$ [1]; we show here that our calculations indicate that with dark matter the minimum mass is reduced to $\sim 10^3 M_\odot$ if virialization occurs $\sim 0.01\ r_{ta}$, and is $\sim 10^4 M_\odot$ if virialization occurs at $\sim 0.5\ r_{ta}$, where r_{ta} is the turn-around radius.

INTRODUCTION

We are interested here in the role of the cold collisionless dark matter on the formation of Population III Objects.We study the influence of the dark matter perturbations on the barionic matter starting from the beginning of the recombination era.

A detailed calculation of the role of cold dark matter on the formation of Population III Objects, taking into account relevant physical processes for the barionic matter, is absent in the literature.

Following our previous studies[1-3],we take into account in the present investigation a series of physical processes for the barionic matter lacking for the dark matter: photon-cooling (heating), collisional ionization, photoionization, Lyman-α cooling and the formation and cooling of H_2 molecules.

CALCULATIONS AND DISCUSSION

We treat the cold dark matter and the barionic matter as two independent fluids coupled only by gravity. We choose, similar to our previous articles[1-3],a square density profile for the density, and a linear dependence for the velocity (which is consistent with the density profile). We take $\Omega_b = 0.1$ and $\Omega_d = 0.1$, 0,5 and 0.9 and for the Hubble constant $H = 100$ km s^{-1} Mpc^{-1}. We present here preliminary results of our calculations (in another paper a more detailed discussion will be presented[4]).

We begin the calculations at the recombination era T_r=4000K($z_{rec}\cong$1482).

As a function of the dark matter mass $M_d/M_\odot = 10^4$-10^8, we calculate:a) the turn around redshift, z_{ta} for the dark matter (when $d\bar{r}_d/dt = 0$); b) the initial (at the beginning of recombination) barionic mass, M_{bi}, that follows the dark matter perturbations; c) the collapse redshift, z_c, (defined when $\bar{r}_d/\bar{r}_{ta} \cong 10^{-2}$); d) the barionic mass, M_{bc}, at z_c; and e) the Jeans mass just for barionic matter (also at z_c).

We are interested in the formation of Population III Objects and study clouds of dark matter $M_d = 10^4$-$10^8 M_\odot$ and a spectrum of perturbations of the

form

$$\delta = (M/M_o)^{-\alpha} \quad (1 + z_{rec})^{-1} \tag{1}$$

at recombination, where M_o is the mass scale and z_{rec} is the redshift at recombination. We assume here different values for α and M_o.

We performed calculations considering virialization at $\bar{r}_d/r_{ta}=0.5$ (as suggested in reference 5) and examined the way the results are modified as compared with virialization at $\bar{r}_d/r_{ta} \sim 0.01$. The results are significantly different only for $M_d \lesssim 10^5\ M_\odot$.

We previously showed that the minimum mass to collapse from the recombination era without dark matter was $\sim 10^4\ M_\odot$ [1]; we found here that our calculations indicate that with dark matter the minimum mass is reduced to $\sim 10^3\ M_\odot$ if virialization occurs $\sim 0.01\ r_{ta}$, and is $\sim 10^4\ M_\odot$ if virialization occurs at $\sim 0.5\ r_{ta}$.

ACKNOWLEDGEMENTS

One of the authors (J.C.N.A.) would like to thank the brazilian agencies FAPESP and CNPq for support, and the other author (R.O.) the brazilian agency CNPq for partial support. We both would like to thank Joel Primack , David Schramm and Gary Steigman for helpfull discussion.

REFERENCES

1. de Araujo, J.C.N. and Opher, R. 1988, M.N.R.A.S., 231, 923
2. de Araujo, J.C.N. and Opher, R. 1989, M.N.R.A.S., 239, 371
3. de Araujo, J.C.N. and Opher, R. 1990a, Ap. J. 350, 502
4. de Araujo, J.C.N. and Opher, R. 1990b, Ap. J. (submitted)
5. Steigman, G. Sarazin, C.L., Quintana, H. and Faulkner, J. 1978, Astron. J., 83, 1050

NON-ISOTHERMAL X-RAY EMISSION FROM RICH CLUSTERS OF GALAXIES: EVIDENCE FOR AN INTRACLUSTER MEDIUM HEATED BY GALAXY EJECTION?

Mark J. Henriksen
Applied Research Corporation
8201 Corporate Drive, Suite 920
Landover, MD 20785

We have studied the X-ray spectra and images of 10 rich clusters of galaxies. We fit an empirical model to the data which includes fully hydrostatic as well as partially non-hydrostatic gas distributions. Six out of 10 clusters are better fit by models with a non-isothermal intracluster medium. Using the available theoretical simulations of cluster formation and evolution, we interpret this as evidence of an intracluster medium initially heated to ~10^8 °K by galaxy ejection rather than infall. The observed gas density profile requires a low (<1.5) biasing parameter.

Fe abundances are derived and marginal evidence is found (60 percent confidence) for a deviation from constant abundance (1/2 solar). The trend is that hotter, clusters with a more massive (>$2x10^{14}M_o$) intracluster medium tend to have less than 1/2 solar iron abundance and those with a less massive intracluster medium, though undersampled in the current data, appear to have relatively more iron. If we assume that the gas mass and iron abundance difference is due to primordial material left over from galaxy formation, roughly 10 percent of the cluster mass is left over after the galaxies are formed.

If the hot gas is in hydrostatic equilibrium, then we can determine a meaningful total mass distribution and put constraints on the amount and distribution of dark matter. In general, the clusters with non-isothermal temperature profiles (such as Coma and A85) require relatively less dark matter than those which may be nearly isothermal (A2199). The dark matter is also more concentrated to the center of the cluster than the X-ray or galaxy light distribution for the non-isothermal cluster giving a mass-to-light ratio which is higher in the center and decreases with radius. The statistically acceptable range of temperature and density profiles for some clusters includes a central, hydrostatically bound region of gas surrounded by a slowly expanding region. This solution typically requires a small ($5x10^{14}M_o$) centrally concentrated dark matter component.

The reduction in dark matter results in the X-ray emitting gas making up a more significant fraction (20-50 percent) of the total mass than was believed based on the optically derived virial mass.

THE EPOCH OF COOLING FLOW FORMATION IN CLUSTERS OF GALAXIES

The Dirth of Cooling Flows in Merging Clusters

How likely is it that none of the 14 clusters in the 7 bimodal X-ray systems have cooling flows? To calculate an expected frequency of cooling flows we use a complete subsample of the Abell catalog. These are rich nearby clusters; all have been detected by the Einstein or HEAO-1 observatories. Because of observational uncertainties, mass inflow rates larger than about 25 solar masses per year are most reliable. We find 8 out of 24 clusters in the complete subsample have an inflow of greater than 25 solar masses per year. This gives a probability of 0.33 that a rich cluster will have a cooling flow.

On hundred and twenty seven clusters have been detected in the X-ray imaging surveys. The probability that 14 clusters randomly chosen out of 127 do not have cooling flows (using a probability of .33 that a cluster will have a cooling flow) is .0016. Thus clusters in bimodal systems are less likely to have a cooling flow than rich nearby clusters. This implies that either the stage in the merging process seen in bimodal systems is one in which the cooling flow has been disrupted or a cooling flow is a latter stage of cluster evolution.

Simple Dynamical Arguments on Tidal Disruption

These systems have a lower limit to a merge time of about a billion years. This assumes that they are initially at rest and uses their projected separation to calculate a lower limit. Calculation of the tidal forces on these systems for a typical separation 1-1.5 Mpc and roughly equal masses shows that the gas at the maximum cooling flow radius has about a 10 times stronger force from its own potential than from the other cluster. In a pressure driven flow, the self-gravity is negligible compared to the external gas pressure so that the flow is even more stable. The lateral component to the tidal force is a factor of 10 less than any self-gravity making it unlikely that the lateral force has any effect.

Optical Substructure and Cooling Flows

Clusters with optical substructure frequently have smooth X-ray emission. This implies a later stage of cluster evolution than that seen in the bimodal X-ray distributions since there is a single potential rather than two. The data of Geller and Beers (1982) and Baier (1977 and later) contain 30 clusters which have X-ray images. Six have cooling flows greater than 25 solar masses per year making the incidence slightly less frequent than in the complete sample (20 percent as opposed to 33 percent). However, 15 of the clusters appear to have substructure and 3 of the 15 have cooling flows. On the other hand, 15 do not have substructure and of these there are 3 with cooling flows. In this data there is no evidence then that optical substructure on scales of .25-1. Mpc anticorrelates with the presence of a cooling flow.

Summary of Cooling Flows and Merging Systems

Compared to nearby rich clusters (including unrelaxed clusters), pre-merger clusters are less likely to have cooling flows. Simple dynamical calculations show that it is unlikely that these clusters have had their cooling flows tidally disrupted. Thus we conclude that the development of cooling flows is generally an occurrence late in the evolution of a rich cluster (post-merger). The optical data implies that cooling flows are established after the individual potentials have merged but are independent of whether the galaxies have reached a smooth, equilibrium distribution. This would require that mass deposition occurs over a shorter time than the cluster lifetime since n-body simulations show that roughly z=.2 is the epoch of subcondensation mergers. Calculations of the total mass deposition are overestimated by a factor of 10 or so unless the flow rates were much higher in the past. This impacts the significance of the role of cooling flows in making centrally dominant galaxies in clusters or alternatively requires much higher cooling flow rates in the past.

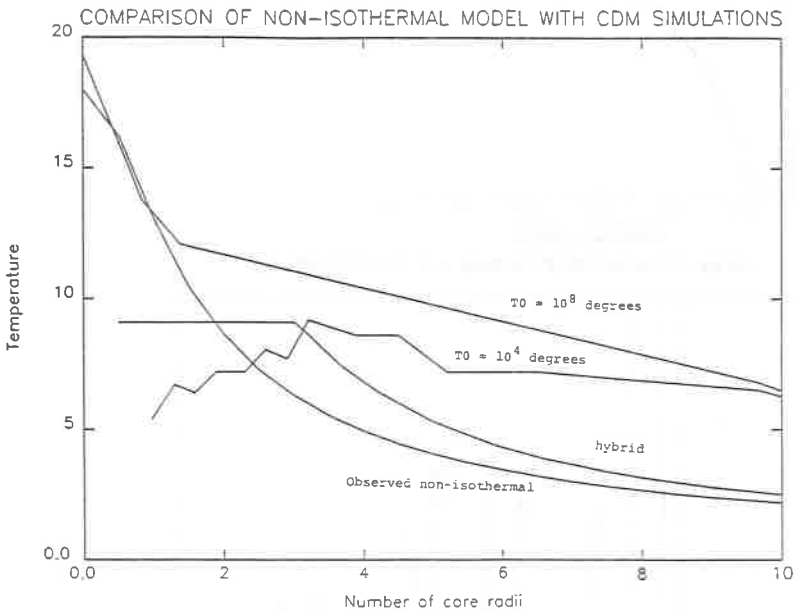

Four temperatures (KeV) profiles are shown for the Coma cluster (core radius of 0.34 MPc). Two simulations (Evrard) of a gas which has evolved in a cold dark matter dominated cluster are shown: one with high initial gas temperature (10^8 °K) and one with an initially low temperature (10^4 °K). The low temperature gas is heated by infall. The high temperature gas more closely resembles the non-isothermal temperature profile which Henriksen and Mushotzky (1987) found for Coma. The energy requirements for the metal abundance of the intracluster medium based on a supernove origin for the metals is consistent with a gas heated to 10^8 °K at an early epoch. One explanation for the non-isothermal temperature profiles we find is that they are evidence of this enrichment stage.

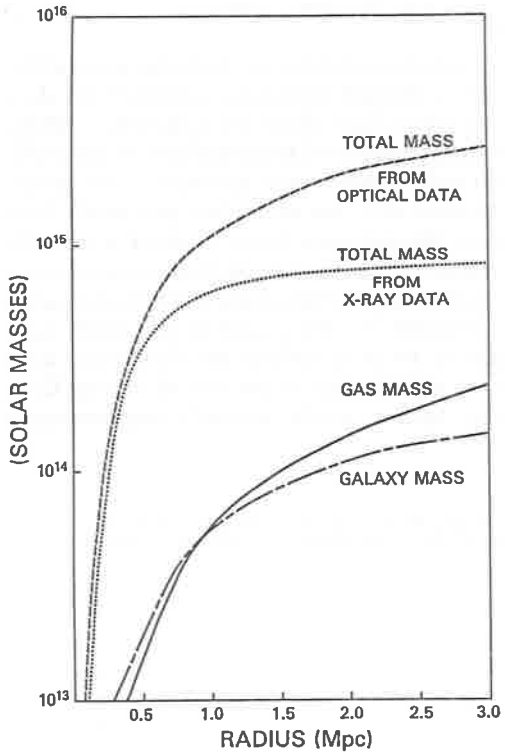

If the gas is in hydrostatic equilibrium, the total cluster mass can be calculated as a function of radius. The non-isothermal temperature profiles reduce the amount of mass (Dark Matter) in excess of the gas and galaxies and show that it is more concentrated to the center than either the galaxies or the gas. Our survey included 10 clusters, this figure is for the Coma cluster.

IRON ENRICHMENT IN GAS VS. TEMPERATURE

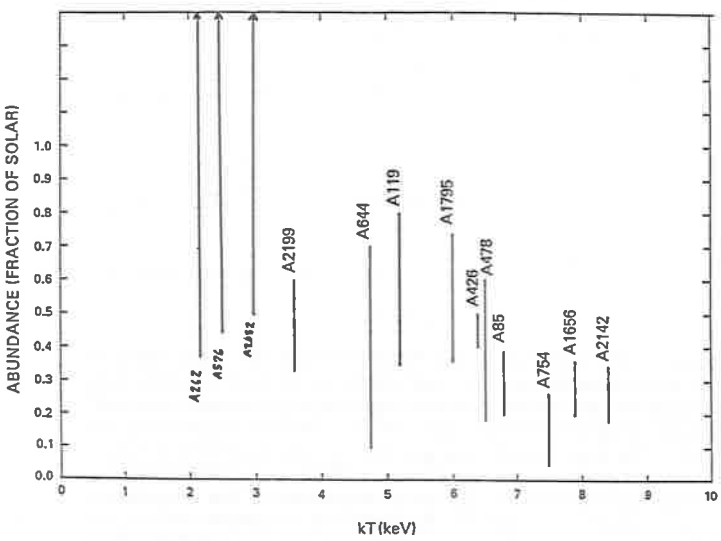

At the 60 percent confidence level, there is a deviation from constant abundance. Hotter clusters have a lower average abundance than cooler clusters.

EVIDENCE FOR SCALE-INVARIANT CLUSTERING ON LARGE SCALES

Luigi Guzzo[1], Angela Iovino[1], Guido Chincarini[1,2]
Riccardo Giovanelli[3] & Martha P. Haynes[4]

[1] *Osservatorio Astronomico di Brera, Milano*
[2] *Universitá di Milano*
[3] *N.A.I.C. - Arecibo Observatory*
[4] *N.A.I.C. - Cornell University*

ABSTRACT

We have explored the scaling properties of galaxy clustering at large separations using the Perseus-Pisces region redshift catalogue[1)]. The analysis reveals that clustering shows a scale-invariant character also on scales much larger than the correlation length and it is not negligible up to separations as large as $\sim 30\ h^{-1}\ Mpc$. A well defined scaling range characterized by a fractal dimension $D \simeq 2.2$ is present for $4 < hr < 30\ Mpc$, while for $hr < 4\ Mpc$ the simmetry is broken into the 'standard' small-scale range with $D \simeq 1.2$, the region usually evidenced by two-point correlation function analyses. Comparison with other surveys shows that this behaviour is not a peculiarity of the sample used, but on the contrary represents a general feature of clustering. Remarkably, the breakpoint between these two ranges is located at separations where the correlation function $\xi(r) \sim 1$, i.e. around the expected transition between large-scale linear density fluctuations ($\delta\rho/\rho < 1$) and nonlinear clustering at smaller radii. We argue that this result could point towards a scenario similar to that suggested by Szalay and Schramm[2)], where a scale-invariant process of galaxy formation created an initial pattern with fractal dimension $D \sim 2$ on all scales up to (at least) $\sim 30\ h^{-1}\ Mpc$. The enhanced clustering observed at small separations could then be explained as the consequence of the nonlinear effects of gravity, which has modified the initial scale-free distribution introducing a characteristic length at $r_b \simeq 4\ h^{-1}\ Mpc$.

It is a well known fact that the distribution of galaxies on relatively small scales looks very similar to a fractal[3,4]. This means that the clustering pattern obeys to a very simple scaling relation, at least inside a certain range of separations. A formal evidence for this property is given by the power-law shape of the two-point correlation function $\xi(r)$, that *on small scales* provides a measure of the fractal *correlation* dimension $D \simeq 1.2$. In general, the scaling properties of a set can be analysed by looking at the way it fills the ambient space. In the presence of a fractal range the mean number of objects in volumes of increasing radius is expected to grow as $N(r) \propto r^D$ and accordingly the mean density goes as $\langle n(r) \rangle \propto r^{D-3}$. The correlation dimension can thus be calculated from the logarithmic slope of these functions. A useful estimator for this purpose is the *conditional density* function[5] $\Gamma(r) = \langle n(\mathbf{x}) \cdot n(\mathbf{x}+\mathbf{r}) \rangle / \langle n \rangle$ that also follows a power law $\propto r^{D-3}$ for a scale-invariant set. It is simply related to the usual two-point correlation function as $\Gamma(r)/\langle n \rangle = 1 + \xi(r)$. This relation shows that a scale-invariant range will show up as a power law $\propto r^{D-3}$ in a plot of $1 + \xi(r)$, but in general not of $\xi(r)$. Only at small separations, where $\xi(r) \gg 1$ and thus $\xi(r) \simeq \Gamma(r)/\langle n \rangle$, the power-law behaviour is mapped directly into $\xi(r)$ (justifying the $D \simeq 1.2$ usually inferred from $\xi(r)$).

In Fig.1 we show the plots of $\Gamma(r)$ for three different volume limited samples extracted from the Perseus-Pisces catalogue. Note: (1) the two well behaved power laws with indexes $\gamma_1 \simeq 1.8$ and $\gamma_2 \simeq 0.8$ corresponding to $D \simeq 1.2$ and $D \simeq 2.2$ respectively; (2) the sharp break between the two ranges at $r_b \simeq 4\ h^{-1}\ Mpc$; (3) the flattening of the curves for $r > 30\ h^{-1}\ Mpc$, a possible evidence for a crossover to homogeneity. This result implies that galaxy clustering retains a scale-invariant character also on scales much larger than $\sim r_o$, even if with a different scaling law. This is not in full agreement neither with recent results claiming a single fractal range on all scales[6], nor with the conclusion from other works that the scaling range is limited to $r < 5\ h^{-1}\ Mpc$ (ref. 7).

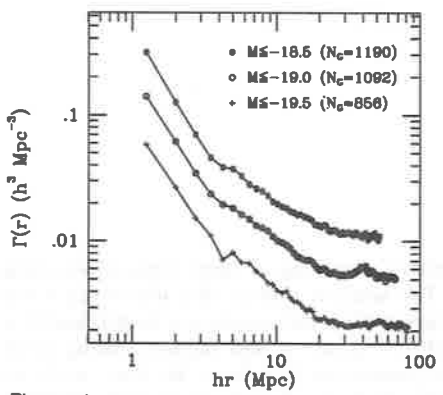

Figure 1

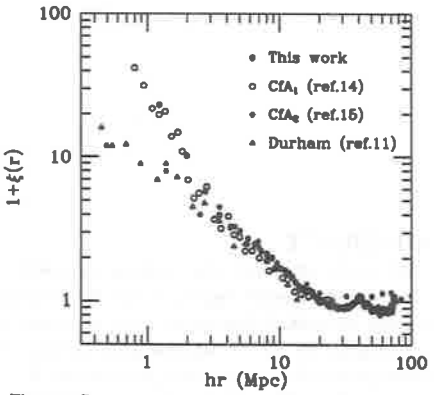

Figure 2

The break at $r_b \simeq 4\ h^{-1}\ Mpc$ and the large-scale $D \simeq 2.2$ range show up clearly also in the data from previous works, when the appropriate quantity $1 + \xi(r)$ is plotted (Fig.2). This general agreement confirms the universal character of these features. The 'two-power-laws' behaviour of $1 + \xi(r)$ was already noticed previously[8], but not discussed from the point of view of scale-invariance.

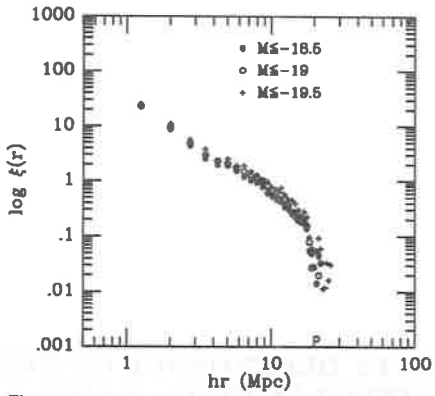

Figure 3

When $\xi(r)$ is plotted (Fig. 3), the $D \simeq 2.2$ scaling range appears only as an excess over the small-scale power law, the well known 'shoulder'. This feature, widely debated in the literature[8-11] is then simply the fingerprint of the change in the geometry of the distribution, which can be fully evidenced only when looking at $1 + \xi(r)$. The small-scale power law is on the other hand preserved since at these separations $\xi(r) \simeq 1 + \xi(r)$. Notice how the correlation length $r_o \simeq r_b$, i.e. $\xi(r)$ is of the order of unity around the breakpoint between the two scaling ranges. This suggests that the steeper logarithmic slope at small scales could be simply the result of gravitational amplification on an initial $D \sim 2$ pattern, which is still visible in the linear regime ($r \gg r_o$). Further details can be found in ref. 12. It looks remarkable that the large-scale correlation dimension $D \simeq 2.2$ found here is close to the value of the Hausdorff dimension $D_H \simeq 2.1$ determined in recent analyses[7,13] that evidenced the multifractal character of clustering. Since these two dimensions are expected to be equal only for homogenous self-similar fractals, this fact could be evidence of a simple geometry as such on large scales. In this view the multifractal nature observed today when analyzing the galaxy distribution as a whole could be the consequence of the small-scale gravitational amplification of the initially scale-invariant pattern.

We thank J. Huchra and M. Geller for supplying unpublished redshifts.

References

(1) Haynes, M.P. & Giovanelli, R. in *Large-Scale Motions in the Universe* (eds Rubin V.C. & Coyne G.V.) 31-70, (Pontificia Academia Scientiarum, Vatican City & Princeton University Press, Princeton, 1988).
(2) Szalay, A.S. & Schramm, D.N., 1985: *Nature* **314**, 718
(3) Mandelbrot, B.B. *The Fractal Geometry of Nature* (Freeman, San Francisco, 1982).
(4) Peebles, P.J.E. *The Large Scale Structure of the Universe* (Princeton University Press, Princeton, 1980).
(5) Pietronero, L., 1987: *Physica* **144a**, 257
(6) Coleman, P.H., Pietronero, L. & Sanders, R.H., 1988: *Astron. Astrophys.* **200**, L32
(7) Martinez, V.J. & Jones, B.J.T., 1990: *Mont. Not. R. Astr. Soc.* **262**, 517
(8) Dekel, A. & Aarseth, S.J., 1984: *Astrophys. J.* **283**, 1
(9) Shanks, T., *et al.*, 1983: *Astrophys. J.* **274**, 529
(10) Peebles, P.J.E. in *Large-Scale Motions in the Universe* (eds Rubin V.C. & Coyne G.V.) 31-70, (Pontificia Academia Scientiarum, Vatican City & Princeton University Press, Princeton, 1988).
(11) Shanks, T., *et al.*, 1989: *Mont. Not. R. Astr. Soc.* **237**, 589
(12) Guzzo, L., Iovino, A., Chincarini, G., Giovanelli, R. & Haynes, M.P.: *Nature* (submitted)
(13) Martinez, V.J., *et al.*, 1990: *Astrophys. J.* **357**, 50
(14) Davis, M. & Peebles, P.J.E., 1983: *Astrophys. J.* **267**, 465
(15) de Lapparent, V., Geller, M.J., & Huchra, J.P., 1988: *Astrophys. J.* **332**, 44

RADIO-LUMINOSITY DEPENDENCE OF THE IR-RADIO ALIGNMENT EFFECT IN HIGH-z RADIO GALAXIES

J. S. Dunlop* **& J. A. Peacock†**

**Dept. of Physics & Astronomy, Lancashire Polytechnic, Preston PR1 2TQ, U.K.*

†Royal Observatory, Blackford Hill, Edinburgh EH9 3HJ, U.K.

ABSTRACT

We present intial results from a K-band imaging study of a subsample of radio galaxies from the $S_{2.7GHz} > 0.1$ Jy Parkes Selected Regions (PSR), along with a comparison sample of 3CR galaxies which are a factor ~ 10 more radio luminous. Our K-band images of 3CR galaxies at $z \simeq 1$ show that i) the established optical-radio alignment effect is still sufficiently apparent at K to have been easily discovered in the near-IR, and ii) our IRCAM images are certainly deep enough to reveal comparable distortions in the PSR galaxies, should they exist.

However, we find no evidence for a comparable IR-radio alignment effect in the PSR sample, and also find the PSR galaxies to be generally less elongated and have redder R-K colours than their 3CR counterparts. The only significant *a priori* difference between the two subsamples of objects appears to be radio luminosity.

These preliminary results indicate that, at least at K, radio-induced contamination of the light of the underlying galaxy may only be a significant problem for the most extreme radio luminosities. This suggests that radio galaxies may still be relevant probes of galaxy evolution in general, provided one avoids the most extreme radio luminosities found in the 3CR galaxies at $z \sim 1$.

We present preliminary results from a near-infrared study of radio galaxies from the Parkes Selected Regions (PSR) sample[1] , along with a control sample of the more powerful 3CR galaxies. At a given redshift, the PSR galaxies have radio luminosities a factor ~ 10 lower than the powerful 3CR radio galaxies, and hence provide an opportunity to separate radio luminosity effects from genuine epoch-dependent effects which might apply to massive galaxies in general. Of particular interest is the investigation of the prevalence and possible radio-luminosity dependence of elongation and alignment with the radio axis at near-IR wavelengths. We now possess IRCAM K-band images of 38 PSR galaxies and 18 3CR galaxies, with integration times of between 27 and 54 minutes.

Infrared-radio alignments in the 3CR sample

The first question to address is whether or not the well-established tendency for the *optical* images of 3CR galaxies with $z \geq 0.8$ to be elongated and aligned with the radio axis is also prevalent at 2.2 μm. McCarthy *et al.* (1987)[2] quote optical position angles for 11 of the 3CR galaxies in our sample, and so, for these objects we show (Figure 1) the optical-radio alignment histogram compared with the IR-radio alignment histogram derived from our IRCAM data using contours at 30% of peak brightness. Although the extent of the elongation is generally slightly less than in the optical, this diagram shows that the alignment effect is still sufficiently clear to have been 'discoverable' at K (in both cases, comparison with a uniform distribution using the KS test gives a significance level $p << 0.01$). This indicates that, even at K, a significant fraction of the light from these galaxies is being influenced by the passage of the radio source (most probably through stimulation of large-scale star-formation activity).

Lack of infrared-radio alignments in the PSR sample

In contrast to the 3CR sources, we find no clear evidence for an IR-radio alignment effect in our sample of PSR galaxies (comparison with a uniform distribution gives $p > 0.2$). However, whereas our 3CR sample is very strongly peaked around $z \sim 1$, the PSR sample contains a much wider range of redshifts, raising the worry that any alignment effect could be diluted. For this reason, and also to remove any confusing epoch dependence, the comparison of the two samples is clarified by confining attention to two 'matched' galaxy subsamples with $0.8 \leq z \leq 1.3$.

Comparison of 3CR and PSR subsamples at $z \sim 1$

Selecting only those objects with redshifts in the range $0.8 \leq z \leq 1.3$ produces two well-

matched subsamples of galaxies – 13 3CR galaxies and 12 PSR galaxies (the PSR redshifts have to be estimated from their K magnitudes, but this is still a reasonably reliable procedure at $z \sim 1$ - see *e.g.* refs. **1** & **3**). These subsamples are statistically indistinguishable in redshift distribution, distribution of radio angular size, and distribution of radio spectral index. This leaves radio luminosity as the only significant *a priori* difference between the subsamples, but three other important differences are revealed by our K-band imaging, namely: **i)** virtually all the PSR galaxies are less elongated than those in the 3CR subsample, **ii)** as before, the 3CR subsample shows clear evidence of an IR-radio alignment effect, while the PSR subsample shows none, **iii)** the PSR galaxies at $z \sim 1$ generally have redder R–K colours than their 3CR counterparts.

Conclusion

These initial results imply that, at least at K, pollution of the light of the underlying galaxy by radio-induced effects may well be only significant for the most extreme radio luminosities. This suggests that, despite some scaremongering in the literature, radio galaxies may still be relevant probes of galaxy evolution in general, provided one steps down from the most extreme radio luminosities found in the 3CR sample at $z \sim 1$.

REFERENCES

1. Dunlop, J.S. *et al.* 1990. *M.N.R.A.S.*, **238**, 1171.

2. McCarthy, P.J. *et al.* 1987. *Ap. J.*, **321**, L29.

3. Lilly, S.J., Longair, M.S. & Allington-Smith, J.R., 1985. *M.N.R.A.S.*, **215**, 37.

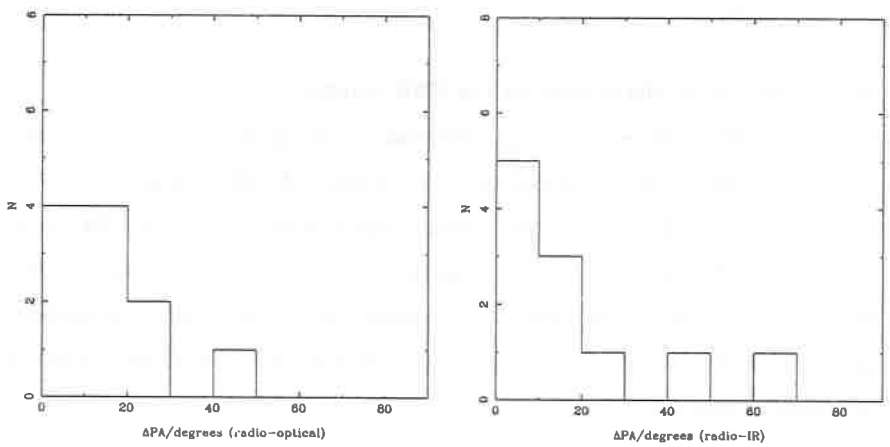

Figure 1 Comparison of the optical–radio and K-band–radio alignment histograms for 11 3CR galaxies.

POWER SPECTRA OF REDSHIFT SPIKES

J. A. Peacock & N. Kaiser

CIAR Cosmology Program, CITA, Toronto M5S 1A1, Canada

Abstract. We consider the power-spectrum analysis of one-dimensional redshift surveys such as that performed recently by Broadhurst *et al.* (1990). Our conclusion is that such surveys are not a powerful way of discriminating between competing models for large-scale structure, for the following reasons. The number density fluctuations in a 1D 'skewer' survey are dominated by the true 3D clustering on the scale of the transverse dimension of the tube; any search for large-scale structure must deal with a high background of aliased small-scale noise. The power spectra of such surveys are random fields whose properties may be found analytically via the central limit theorem. The frequency and height of power-spectrum spikes depend mainly on the rms density variation plus the survey selection function, and are very insensitive to the true level of 3D power on large scales. We find that apparent periodicity in the form of high isolated power-spectrum spikes can often arise in such surveys, independent of the nature of the 3D density field.

1 Random power spectra in one dimension

The one-dimensional redshift survey by Broadhurst *et al.* (1990; BEKS) has generated considerable controversy through the apparent regular spacing of clumps of galaxies $128h^{-1}$ Mpc apart. We report here some results of an investigation designed to assess whether this effect forces a drastic revision of our ideas on large-scale structure, or whether it could arise in more conventional models. As it seems the most appropriate statistic, we have concentrated on the power spectrum of such a survey. For more details and derivations, see Kaiser & Peacock (1991).

First, what is the ensemble average 1D power spectrum? Suppose we have a tube with selection function $w(z)W(r)$; in terms of $\Delta^2_{1D} \equiv kP_{1D}/\pi$ and $\Delta^2_{3D} \equiv k^3P_{3D}/2\pi^2$, we have

$$\Delta^2_{1D}(k) = k\int_k^\infty \Delta^2_{3D}(y)\tilde{W}^2\left(\sqrt{y^2-k^2}\right)y^{-2}dy. \tag{1}$$

If we take the Gaussian $\tilde{W} = \exp -(kR)^2/8$ (approximately right for $W(r)$ a disc of radius R) then, with a pure power-law correlation function: $\xi(r) = (r/r_0)^{-\gamma}$, $\Delta^2_{3D} \equiv \beta(kr_0)^\gamma$ ($\beta = 0.903$ if $\gamma = 1.8$), we get

$$\Delta^2_{1D}(k) \to \beta\, kR(r_0/R)^\gamma\, 2^{\gamma-2}\Gamma\left(\frac{\gamma-1}{2}\right) \tag{2}$$

as $k \to 0$. Clearly, the 1D power is dominated by the 3D power at about the cutoff R; for the BEKS survey with $R \simeq 3h^{-1}$ Mpc, we expect $\Delta^2_{1D} \sim 1$ at $\lambda = 128h^{-1}$ Mpc, even if $\Delta^2_{3D} = 0$ there.

What about the *texture* of the power spectra? Here we may use the central limit theorem (whose applicability requires only a few independent clumps in the survey), and apply some of the classic techniques for analysing random noise in 1D (Rice 1954). The sine and cosine transforms of the data ($s(k)$, $c(k)$) and their derivatives are Gaussian random fields which are correlated via the redshift selection function w:

$$\begin{aligned}\langle c(k)c(k')\rangle &= \frac{\langle f_k^2\rangle}{2}\int dz\; w^2(z)\cos([k-k']z)\\ \langle s(k)c'(k')\rangle &= \frac{\langle f_k^2\rangle}{2}\int dz\; z\; w^2(z)\cos([k-k']z)\quad etc.\end{aligned} \tag{3}$$

By generating Gaussian fields with the appropriate correlations, we can make some power-spectrum realisations designed to match the BEKS data, shown in figure 1. These allow for the actual multi-conical survey geometry, which complicates things only a little. Clearly, random fluctuations can produce spikes in the power spectrum quite as isolated as that seen by BEKS.

The height distribution of spikes can also be found in the high-peak limit:

$$N(>P) = \frac{\gamma}{\sqrt{\pi}\,k_*}\sqrt{P/\langle P\rangle}\,\exp\left(-P/\langle P\rangle\right), \tag{4}$$

where, for a uniform tube of length L, the coherence wavenumber $k^* = 2\pi/L$ and the spectral parameter $\gamma = \sqrt{5}/3$. Application of this formula to the BEKS data yields a probability of 6% for the observed peak in the velocity-undamped range $k < 0.1h\,\mathrm{Mpc}^{-1}$

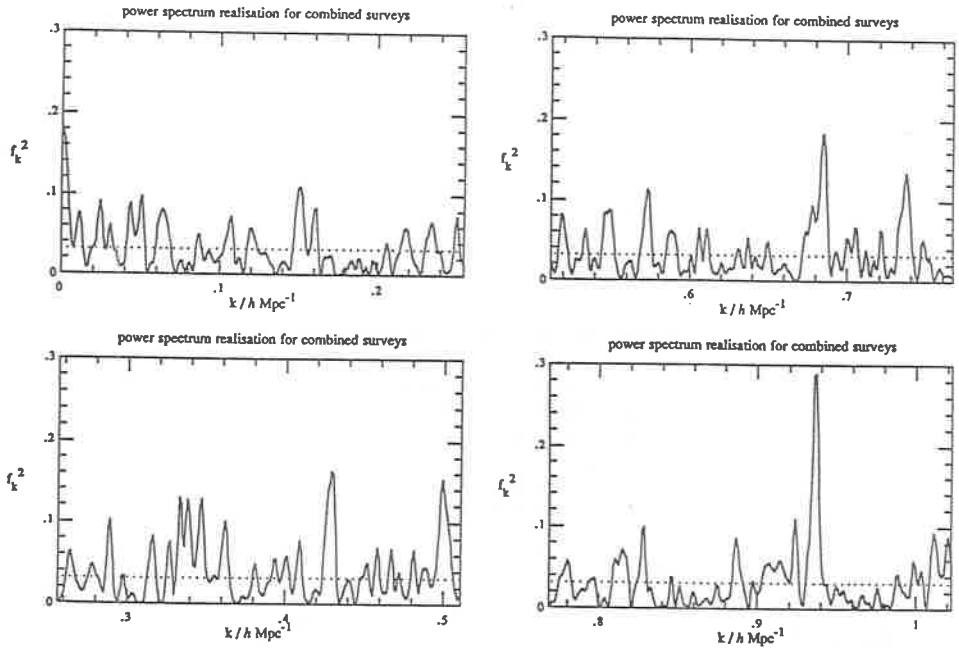

Figure 1. *Realisations designed to match the BEKS composite sample; to be compared with Figure 2 or Figure 2b of BEKS – the realisation here corresponding to about 10 times their useable bandwidth (peculiar velocities damp their power spectrum for $k \gtrsim 0.1$). Despite having no intrinsic periodicity, the texture of the field matches well what is observed, producing spectacular cases of high isolated spikes (for comparison, the BEKS spike has $f_k^2 = 0.21$).*

2 Conclusions

The properties of spikes in 1D power spectra are rather generic and insensitive to the details of the 3D density field. The BEKS apparent periodicity could quite plausibly arise in a model where there was no real large-scale non-uniformity. The correct interpretation of their data may well be in terms of the survey beam intersecting a quasi-periodic cellular structure. However, the 1D data alone do not seem capable of distinguishing between this and other alternative models.

References

Broadhurst, T.J., Ellis, R.S., Koo, D.C. & Szalay, A.S., 1990. *Nature*, **343**, 726. (BEKS)

Kaiser, N. & Peacock, J.A., 1991. *Astrophys. J.*, in press.

Rice, S.O., 1954. *Selected papers on noise and stochastic processes*, p. 133, ed. Wax, N. Dover, New York.

A 100-200 MPC GROUP OF QUASARS

LUIS E. CAMPUSANO*
Departamento de Astronomía
Universidad de Chile, Santiago

ROGER G. CLOWES
Royal Observatory, Edinburgh

ABSTRACT

We have discovered a very large, elongated group of quasars with size 100-200/h Mpc at z~1.3, in the direction of ESO/SERC field 927 which has the field center 10h 40m(1950)+05° 00'. Our group, which is already known to involve at least 10-13 quasars, seems to be quite similar in size and number of quasars to that found by Crampton et al.[1] : 23 quasars with size of at least 60/h Mpc at z~1.1. The fact that two groups with these characteristics have been detected so far is evidence that the distribution of quasars is not so simple as was previously thought: at large scales (>10/h Mpc) the majority of quasars may be distributed uniformly and at random, but rare, large groups also occur.

Large groups of quasars, like the 1040+0500 reported here, may be large physical structures. However, their apparent scarcity makes doubtful a strong association of them with the large structures of galaxies, because the latter - such as the "great wall" - seem to be emerging as commonplace features of the universe.

We intend to carry out further spectroscopy in the ESO/SERC field 927, including absorption-line spectroscopy of background quasars, to improve our knowledge of the claimed quasar group.

Full details of the present evidence for the 1040+0500 group are given in Clowes & Campusano[2].

---

* Visiting astronomer, Cerro Tololo Inter-American Observatory, National Optical Astronomy Observatories, operated by the Association of Universities for Research in Astronomy, Inc., under cooperative agreement with the National Science Foundation.

QUASARS AS SIGNPOSTS OF LARGE-SCALE STRUCTURE IN THE UNIVERSE

Since the initial search for quasar clustering by Osmer[3], much effort has been devoted to this question. Osmer searched for structure of redshift 2 quasars down to scales of 50/h Mpc and found no deviation from randomness. Later on, however conclusive evidence for some clustering was finally revealed thanks to the progressive availability of larger and more refined samples of quasars. We will name this evidence in two steps and include only a few key results. On the one hand, there is: strong evidence for clustering on scales of $<10/h$ Mpc[4]; further evidence found by Iovino & Shaver[5] for clustering at the same scale together with the suggestion that such clustering disappears for $z>1.5$; no clustering detection in an automated grism-sample[6] containing mostly objects with $z>1.5$. On the other hand, lies the supporting evidence for the existence of, apparently, very rare, isolated, large groups[7,1], like the one reported in this paper.

Several research topics can be extracted from the situation described, like: What is the relation between the small-scale clustering of quasars and the large groups? Does small-scale clustering occur only inside the large groups? What is the most efficient strategy to reveal large groups? Are they really so rare? Is there any relation of these large groups with the large scale structures of galaxies that have found in the local universe? Do these groups follow the suggested relation of Iovino & Shaver, i.e., they do not exist at redshifts larger than 1.5?

We intend to carry out some of the proposed research on the 1040+0500 group.

REFERENCES

1. Crampton, D., Cowley, A.P. & Hartwick, F.D.A., 1989. Astrophys. J., **345**, 59.
2. Clowes, R.G. & Campusano, L.E., 1991. Mon. Not. R. astr. Soc., in press.
3. Osmer, P.S., 1981. Astrophys. J., **247**, 762.
4. Shanks, T., Boyle, B.J. & Peterson, B.A., 1988, A.S.P. Conf. Series, 2, 154.
5. Iovino, A. & Shaver, P., 1988. Astrophys. J., **330**, L13.
6. Osmer, P.S. & Hewett, P.C., 1990. Astrophys. J. Suppl., submitted.
7. Webster, A., 1982. Mon. Not. R. astr. Soc., **199**, 683.

ACKNOWLEDGEMENTS

The work of LEC was partially funded by FONDECYT-Chile (grant 487/88) and DTI-Universidad de Chile (grant 2828-89).Fundación Andes gave finantial support for the participation of LEC at this conference.

DISTRIBUTION OF DYNAMICAL MATTER IN ABELL85, USING X-RAY DATA

D. GERBAL[1], F. DURRET[1,3], G.B. LIMA-NETO[2], & M. LACHIEZE-REY[4]
[1] DAEC, [2]DEMIRM , Observatoire de Paris-Meudon, F-92195 Meudon Cedex
[3] Institut d'Astrophysique de Paris, CNRS, 98bis Bld Arago, F-75014 Paris
[4] Service d'Astrophysique, C.E.N. Saclay

PRESENTATION

We have developed a method to extract both spectral and spatial information from IPC data on galaxy clusters .We are able to derive from the data, independently of any model, the density and temperature profiles of the intra-cluster gas. This in turn allows us to estimate: the temperature and mass of the X-ray emitting gas, the cluster dynamical mass the radial dependence of these quantities. The method is applied to Abell85. First results are given.

METHOD

A85 has been observed by the Imaging Proportional Counter (IPC) on the Einstein Observatory in three energy bands [(0.5-2), (0.5-3), (0.5-4.5keV)] therefore giving spectral information. We wrote a code to emulate the IPC properties: the equivalent surface (efficiency) per pixel in each energy channel and the point spread function.

We then constructed a "synthetic cluster" with parametrized form for the density and temperature profiles. The aim of this procedure is to find the optimal functional form, i.e. the parameters which best fit the data. From the considered functions, assuming a hydrogen plasma and allowing for the inclusion of the Gaunt factor (Mewe et al., 1986), we have calculated a volume emissivity as a function of the distance to the cluster centre. This volume emissivity

was then "convolved" with the emulated IPC response: we thus obtained the expected counts per pixel.

These three synthetic images are then compared to the actual IPC images, pixel per pixel. Minimizing the $\chi 2$ between the calculated and observed counts gives the best fit density and temperature profiles. The minimization is performed using the MINUIT program from the CERN library, and the images were processed with the eVe software.

DISCUSSION

Preliminary results are summarized in Table 2:Parameters for different fits

Model	n(0) (10-3 cm-3)	beta	Rc (kpc)	T(0) (keV)	Rt (kpc)	Gas Mass (10**13 Mo)	Dyn. Mass (10**13 Mo)
1	9.4	0.50	102	8.7	...	6.0	48
2	19	0.47	54	9.5	...	6.0	50
3	11	0.50	94	10.2	495	5.9	86
4	34	0.41	26	10.3	108	6.7	83

Models 1,2 Isothermal, central region (1 - excluded), (2 - included)

Models 3,4 Modified Hubble law, central region (3 - excluded), (4 - included)

$n(r) = n_0 [\ 1 + (\frac{r}{r_c})^2\ ]^{-3\beta/2}$, $T(r) = T_0 [\ 1 + (\frac{r}{r_T})^2\ ]^{-0.5}$ (modified Hubble law)

The present method indeed allows us to derive the X-ray emitting gas temperature and its radial dependence.

Runs have been performed with isothermality imposed, but the value of the temperature and the density profile remaining free (model 1, model 2) . The temperatures found are ≈ 9keV, comparable to other determinations through spectrometers. Moreover the density profile

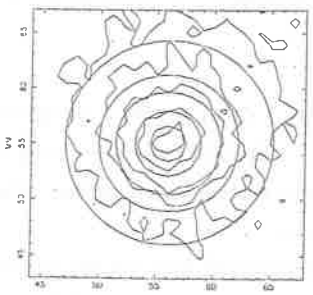

Isophotes of IPC data superimposed on an isothermal fitting

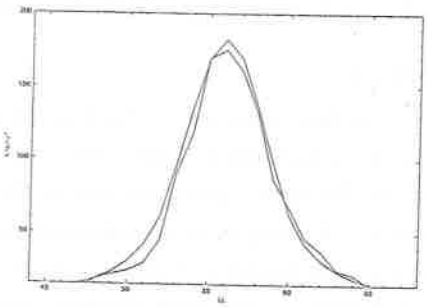

Cuts of the image superimposed on a synthetic image

obtained, agrees well with those given by Jones & Forman. This established the validity of our method.

The central part of A85 is overluminous (it is classified as xD by Jones & Forman). Fits lead to very high central values of the density (Model 2, Model 4). However a single Hubble profile is too rough to account for the central part.

For temperature profiles showing gradients, the central temperature is higher than for isothermal ones. However, the gradients turned out to be very weak (the temperature core radius is ≈ 4 times the density core radius).

For each type of model, the temperature is the same whether the centre is taken into account or not. The central region seems therefore isothermal.

We give the mass of the X-ray emitting gas, M_{gas}, and the dynamical mass M_{dyn}, assuming hydrostatic equilibrium within 1 Mpc (in solar units). We find the ratio M_{dyn} / M_{gas} to range between 8 and 15. The central density and temperature behaviours do not influence strongly the global dynamics. (When the centre is taken into account, the central density is roughly about twice the value obtained when it is excluded from the fit. On the other hand, the core radius and the b parameter are smaller in the first case, so the mass of the gas remains constant).

We show the relative distribution of dynamical density/ICM density:

Typical relative ratio (dynamical matter/ICM):

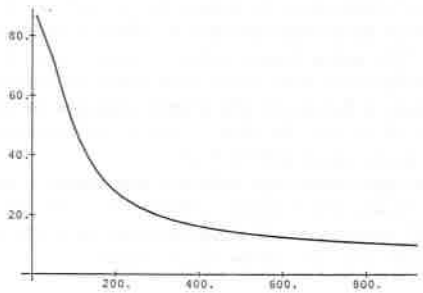

Radius (kpc)

Clearly, the unseen matter is more concentrated than the gas which represents the bulk of the bayonic matter.

THE DISTANCE OF THE VIRGO CLUSTER VIA IMAGE SHARPENING

N.R.TANVIR[1] and T.SHANKS[1],
J.V.MAJOR[1], A.P.DOEL[1], R.M.MYERS[1] and C.DUNLOP.[1]
([1]University of Durham, England.)

M.REDFERN[2], N.DEVANEY[3] and P.O'KANE[2],
([2]University College, Galway, Ireland.)
([3]RGO, Cambridge, England.)

1. Introduction

Recently, image sharpening cameras on ground based telescopes have been used to attain $\sim 0.3''$resolution[1,2,3]. We have investigated the technique of image sharpening using two different prototype instruments on the 4.2m William Herschel Telescope on La Palma. One, the MARTINI instrument, employs real-time adaptive optics and integrates six, independently corrected, apertures directly onto a CCD[2]. The other is the Galway ISCAM which gathers data with a photon counting IPD device. In this case the data is subsequently computer processed to achieve the seeing improvement[3].

We have turned these techniques to the challenging problem of resolving Virgo Cluster galaxies sufficiently to identify their brightest stars. Hitherto, the furthest galaxy in which Cepheids have been found is M101[4]. They give a distance modulus for that galaxy of $\mu_0 = 29.3$. This compares to distance estimates to the Virgo Cluster generally in the range $30.5 < \mu_0 < 32$. Since M101 is very readily resolved in $1.2''$seeing, Virgo galaxies should have a similar appearance in seeing of $0.7''$to $0.3''$. The motivation behind this is to obtain new estimates of the distance to this cluster which is pivotal in the extragalactic distance scale. Our preliminary results are presented in section 3.

2. Technical Results

We first used bright time observations to investigate the parameters of image sharpening. Our aim here was to test theoretical predictions and also to optimise the cameras for faint object work.

a) seeing improvement. The seeing improvements we have found are broadly in line with predictions [5,6]. In particular performance does indeed peak when the entrance pupil is around $4r_0$ and the improvement is then about a factor$\sim$ 2. On several occasions we have experienced very good intrinsic seeing in the region $0.5''$to $0.8''$. On these occasions both cameras have produced sharpened pictures with stellar images in the range $0.25''$to $0.4''$.

b) isoplanatic patch; the area around the reference star which is well sharpened. Observations of double star systems have shown that in good conditions there can be strong correlation of image motion for separations of $20''$. Since the monitoring star is at the centre of the $\sim 1'$ field, we expect the isoplanatic patch to extend over most of the target galaxy.

3. Virgo Observations

We had several nights in February 1990 to attempt this project, although the weather was generally poor allowing only half a night on our object. We had identified a short-list of Virgo galaxies as candidates based on the availability of a nearby star, the brightness of the galaxy and the likelihood that it was indeed a cluster member. The intrinsic seeing conditions dictated that we restrict the the six apertures to $89cm$. Our final choice of best candidate was IC3583, which has a monitoring star of magnitude $B = 13.5$ at its edge. This is a dwarf galaxy with an apparent magnitude of $B = 13.9$ and a recession velocity close to the cluster mean.

With the MARTINI camera we took eight exposures of IC3583 with a total exposure time of $4500s$. We observed in the R band to utilise the peak CCD efficiency. The final sharpened image is

shown in figure 1. The final seeing we obtained was 0.65″FWHM. A slight pattern across the centre of the image is a by-product of a Fourier plane mask used to remove a CCD pickup pattern.

The resulting limiting magnitude was around $R \sim 22.5$ in the outskirts of the galaxy. Several objects are visible in the image as well as some knotty structures. The brighter ones are extended, probably HII regions, but one of the fainter images is point-like.

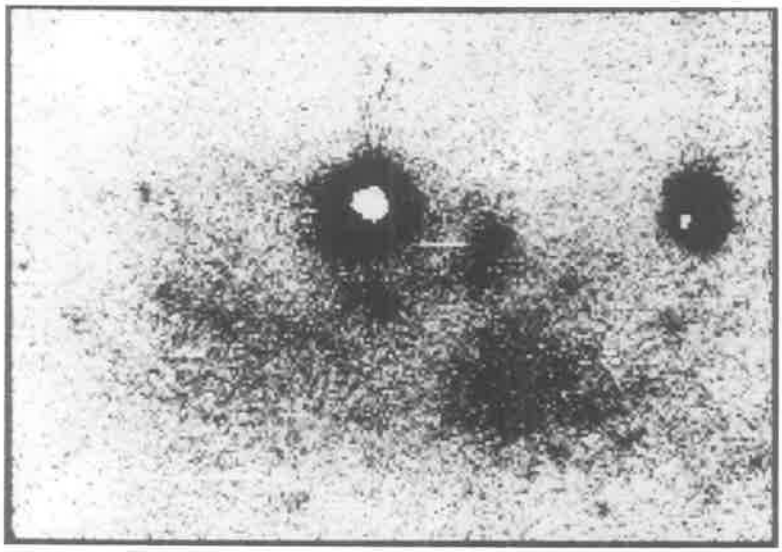

Figure 1. Sharpened image of IC3583 with 0.65″resolution. The hexagonal shape is a ghost image and the saturated object is the monitoring star. The whole picture is $\sim 1'$ wide.

4. Conclusions

We are very encouraged that we managed to obtain a high quality image even in poor conditions for image sharpening. It is as yet too early to assess the full significance of our results for IC3583. The data itself must be examined in more detail and quantitative comparisons made with nearer galaxies for which we also have CCD images (specifically M101 and M81).

Subjectively it does not appear as if IC3583 is as resolved in 0.65″as M101 is in 1.2″. This would tend to contradict shorter Virgo distances of $\sim 12Mpc$. There is one individual object which is still point like in our high resolution image. It would, however, be uncomfortably bright for a star in IC3583, hence we must investigate other possibilities such as it being a faint foreground star.

Finally, we are planning to continue this project next year using redesigned optics to increase S/N by a factor$\sim$ 3, and with the hope of finding occasions of better starting seeing in which to work.

References

1) Racine, McClure, P.A.S.P., 1989, **101**, 731.
2) Doel, Ph.D. Thesis, University of Durham, 1990.
3) Redfern, Devaney, Rosa, O'Kane, Ramirez, Rosa, 1989, MNRAS, **238**, 791.
4) Cook, Aaronson, Illingworth, 1986, Ap.J.Let., **301**, L45.
5) Fried, 1978a, J.Opt.Soc.Am., **68**, 1651.
6) Fried, 1978b, IAU.Col.50, 4.1.

A FAMILY OF FRACTAL CASCADING MODELS FOR THE LARGE SCALE GALAXY DISTRIBUTION

A. PROVENZALE

Istituto di Cosmogeofisica del CNR, Corso Fiume 4, 10133 Torino, Italy

ABSTRACT

We consider a family of fractal cascading models which describe the large scale galaxy distribution. These fractal cascades are based on appropriate modifications of the β-model which has been introduced in the study of turbulence. In particular, we consider cascading processes which generate a scale-dependent scaling exponent and provide a smooth transition from small-scale fractality to large-scale homogeneity. In this context, the notion of "dressed" fractal dimension is discussed. We also introduce a simple model which produce a two-point correlation function with two different scaling regimes, as recently observed in the analysis of galaxy catalogs.

Several observational evidences now suggest an approximate fractal behavior for the large-scale distribution of luminous matter. Direct estimates from three-dimensional catalogs furnish a correlation dimension $\nu \approx 1.2$ for the galaxy distribution. Several models based on the notion of self-similarity have then been proposed in order to describe these observed fractal properties. In particular, an interesting way of modelling a self-similar fractal distribution is to use the classic version of the β-model, which is based on a self-similar fragmentation cascade.[1] A basic object with size l_0 breaks into M smaller objects with size $l_1 = l_0/2$. Each one of the "son" objects has a probability p of surviving and breaking again. At the k-th iteration, each survived object breaks down into M smaller objects with size $l_0/2^k$. In the self-similar version, the survival probability p is the same for all objects and for all iterations. It is easy to show that the fractal dimension of the point distribution generated by such a cascade is $D = \log(pM)/\log 2$. Thus the dimension is fixed by the value of p.

In contrast to the picture of a simple self-similar galaxy distribution, however, we recall that: (a) there is apparent evidence of a multifractal behavior of the galaxy distribution;[2,3] (b) the scaling properties of the galaxy distribution seem to be scale-dependent;[4] and (c) there are both observational evidences and theoretical reasons for an homogeneous matter distribution at sufficiently large scales. One possibility for modelling a distribution of galaxies with scale-dependent fractal behavior is to use a cascading β-model with a scale-dependent survival probability.[5-8] In this case, the survival probability p is a function $p(l_k)$ of the linear size l_k of the breaking object. At very large scales, $p(l_k)$ tends to one, which corresponds to a space-filling, homogeneous galaxy distribution. At small scales, $p(l_k)$ asymptotes to a value p_o corresponding to an asymptotic dimension D_{as}. In [5-7] we have considered different functional forms for the survival probability $p(l_k)$ which provide a smooth transition from small-scale fractality to large-scale homogeneity. The distributions generated by these fractal cascades are characterized by an homogeneity scale L, such that a well-defined power-law dependence of the two-point correlation function, $1+\xi(r) \approx r^{-\gamma}$, is observed for scales smaller than L. At larger scales, $\xi(r) \approx 0$, as it is typical for uniform random distributions. The correlation dimension $\nu = 3-\gamma$ which is computed in the scaling range of the function $1+\xi(r)$ is an "effective" value $\nu(L)$ which is larger than the asymptotic value D_{as}, owing to a "dressing" mechanism generated by the varying survival probability.

The cascading β-model introduced in [5-8] has been proposed mainly as a phenomenological description of the galaxy distribution, whose possible relevance relies upon its capability of reproducing the properties of real galaxy catalogs. Even with the simple choice of $p(l_k)$ used in [5,6] we have obtained point distributions characterized by large voids, clusters and filaments which resemble the observed distributions. However, there are physical motivations and justifications which suggest the use of a cascading β-model. These are discussed in detail in [6,7]. Here we only recall that the most natural interpretation of the β-model is in the framework of a fragmentation cascade in a hot dark matter universe. We also note that the cascading β-model introduced above may be easily extended and that the dependence of the survival probability on the size as well as on

the mass of the fragmenting object may be chosen in such a way as to reproduce the properties of the observed galaxy distribution. In particular, the family of cascading β-models introduced here may be used to physically generate a correlation function with two different scaling regimes, as it has been recently observed in the analysis of the Perseus-Pisces region redshift data.[9] Figure 1a reports a slice of a three-dimensional galaxy distribution generated by the cascading β-model with survival probability p=1 at the largest scales, p=1/2 at intermediate scales and p=1/4 at small scales. This corresponds to a dimension D=3 at the largest scales, D=2 in the intermediate regime and D=1 at small scales. This type of distribution may be physically generated by a fragmentation process at large scales associated with non linear gravitational clustering at small scales.[8] Figure 1b reports the function $1+\xi(r)$ for this distribution. Two well-defined scaling regimes are clearly visible, as observed in [9]. In addition, Figure 1b shows also the more standard function $\xi(r)$. In this representation, the second scaling regime at large scales is almost completely lost, again as shown by Guzzo et al.[9] Thus, in this context the fractal β-model may be used as a quantitative tool to study the properties of real galaxy catalogs and to test data analysis methods on synthetic catalogs with a controllable fractal behavior.

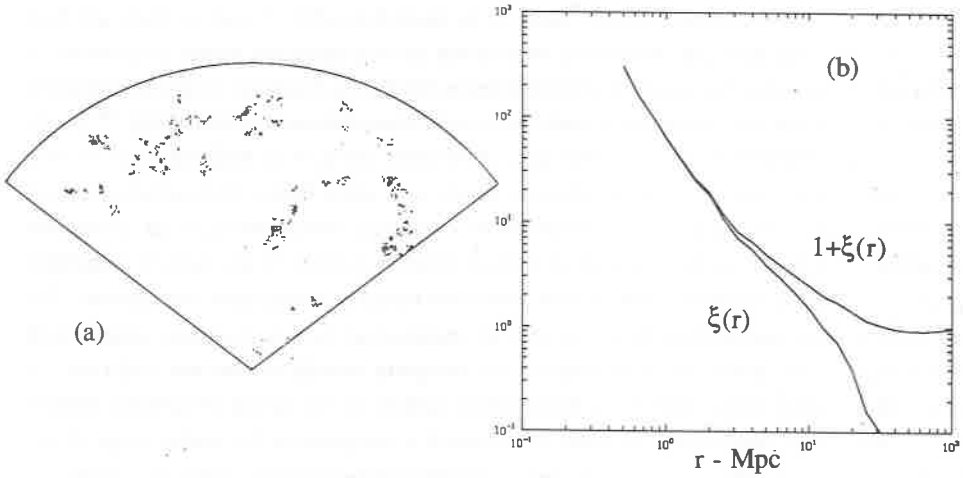

Figure 1. (a) A slice of a three-dimensional galaxy distribution generated by the β-model; (b) the two-point correlation functions $1+\xi(r)$ and $\xi(r)$. The length scales are only indicative.

References
1) Frisch, U., Sulem, P., Nelkin, M.: 1978, *J. Fluid Mech.* **87**, 719.
2) Jones, B. J. T., Martinez, V. J., Saar, E., Einasto, J.: 1988, *Astrophys. J. (Lett.)* **332**, L1.
3) Martinez, V., Jones, B. J. T., Dominguez-Tenreiro, R., van de Weygaert, R.: 1990, *Astrophys. J.*, **357**, 50.
4) Lukash, V. N., Novikov, I. D.: 1988, Acad. Sciences USSR - IKI preprint.
5) Castagnoli, C., Provenzale, A.: 1990, *Vistas in Astronomy*, to appear.
6) Castagnoli, C., Provenzale, A.: 1990, *Il Nuovo Cimento*, to appear.
7) Provenzale, A.: 1991, in *Applying Fractals in Astronomy*, A. Heck and J. Perdang Ed., Springer, in press.
8) Provenzale, A.: 1991, *sub judice*.
9) Guzzo, L., Iovino, A., Chincarini, G.: 1991, this volume.

OBSERVATIONS OF THE SKY AND COSMIC BACKGROUND RADIATION TEMPERATURE AT 36 CM AND 12 CM WAVELENGTH FROM THE SOUTH POLE

G.Sironi, G.Bonelli, M.Limon^

Dipartimento di fisica dell'Universita' - Milano - Italy
Istituto Fisica Cosmica - CNR - Milano - Italy
(^) Now at LBL- University of California/Berkeley

ABSTRACT

We report a new measure of the sky and Cosmic Background Radiation temperature made at .82 and 2.5 GHz from the Amundsen-Scott base at the South Pole.

Over the last five years our knowledge of the Cosmic Background Radiation (CBR) frequency spectrum has improved dramatically (for a review see, for example, Sironi and Celora, 1990).

Above 30 GHz 1% upper limit to the amplitude of the deviations from a pure planckian distribution has been set by the COBE collaboration (Mather et al., 1990); between 2.5 and 30 GHz the 5% upper limit set by the White Mountain collaboration (Smoot et al., 1985) is still valid.

Below few GHz, where deviation from a Planck spectrum are expected too, our knowledge of the CBR spectrum is, however, still poor.

Because the detection of these distortions is an important clue to our understanding of the physical processes which gave rise, starting from a uniform universe, to the matter condensations we see today, a program of observations at different frequencies between 0.5 and 10 GHz has been prepared by a Milano-Berkeley collaboration (Kogut et al., 1989).

Here we present the result of the observations made in december 1989 at 0.82 and 2.5 GHz by the Milano group. Simultaneous observations at 1.4, 3.8 and 7.5 GHz made by the Berkeley colleagues are reported elsewere. All The observations have been made from the Amundsen-Scott base at the South Pole.

Table 1 shows the measured values of the zenith temperature, sky temperature (obtained after subtraction of the atmospheric,

ground and sun contributions) and the resulting value of the CBR antenna and thermodinamic temperature (obtained after subtraction of the galactic contribution and of the blend of extra-galactic unresolved sources).

The astrophysical implications of these data will be discussed in a future paper when the simultaneus data collected at the Pole by our US colleagues will be presented.

Table 1

	0.82 GHz	2.5 GHz	
T zenith	6.7 ± 1.5	3.73 ± 0.15	K
T gr	0.03 ± 0.03	0.03 ± 0.03	K
T atm	0.90 ± 0.35	1.15 ± 0.30	K
T sun	0.08 ± 0.08	0.00 ± 0.01	K
T sky	5.7 ± 1.6	2.57 ± 0.34	K
T gal	2.67 ± 0.33	0.12 ± 0.03	K
T ex	0.34 ± 0.07	0.02 ± 0.01	K
T CBR	2.7 ± 1.6	2.44 ± 0.34	K
T CBR (thermodynamic)	2.7 ± 1.6	2.50 ± 0.34	K

REFERENCES

Mather J.C. et al. 1990: Ap.J. Letters 354, 37

Smoot G.F. et al.: Ap.J. Letters 291, 23

Kogut A. et al. 1989: AIP Conf. Proc. 198 156

Sironi G, Celora L. 1990: Nuovo Cimento B, 105, 1031

CLUSTERING OF GALAXIES AS A FUNCTION OF MORPHOLOGY AND LUMINOSITY

A. Iovino[1], G. Chincarini[2],
R. Giovanelli[3], L. Guzzo[1], M. Haynes[4]

[1] Osservatorio Astronomico di Brera, Milano
[2] Universita' di Milano
[3] Arecibo Observatory
[4] Cornell University

The aim of this paper is to study the space distribution of galaxies, to determine whether the known morphology-density relationship and the luminosity-density relationship are unrelated or a consequence of the different luminosity functions for different morphological types. It is found that morphology and luminosity are two independent parameters affecting both the clustering properties of galaxies, and their distribution as a function of the local density.

It has been shown by various authors and there is fair agreement in the literature that:
a) the distribution of galaxies obey a morphology-density relation (eg. Dressler, 1980, *Ap. J.*, **236**, 351, Postman, Geller, 1984, *Ap. J.*, **281**, 95).
b) there are indications of a luminosity-density relation (eg. Hamilton, 1988, *Ap. J.*, **331**, L59) and
c) there is evidence of a luminosity-morphology relation: that is different morphological types have different luminosity functions (eg. Binggeli et al., 1988, *Ann.Rev.Astr.Ap.*, **26**, 509). In brief we have a hierarchical clustering which is "aware of" types and luminosity.
It is not clear, however, how to unravel the interplay of the three effects mentioned above. In fact since the galaxy population changes with the density we could ask, for instance, whether the luminosity-density relation could be due to the combined effect of population and luminosity function (which is different for different morphological types) or it is real and a secondary effect, unrelated to the galaxy population.
To better understand this matter we used the Pisces-Perseus survey (~ 2500 galaxies up to $m_l \sim 15.7$, Giovanelli, Haynes, 1990, priv. comm., Geller, Huchra, 1990, priv. comm.) to answer the following specific questions:
1) At a given luminosity do we have an explicit dependence of the clustering properties on the morphological type?
2) On the other hand, are clustering properties related to the luminosity for each morphological type? and
3) is the mean luminosity function, for a given morphological type, a function of the local density?
Our analysis shows that (we adopted $H_o = 100h\ Km/sec\ Mpc^{-1}$):
1) The clustering properties are a strong function of the morphological types. The autocorrelation analysis on a sample at fixed absolute luminosity ($-19.0 \leq M \leq -20.0$) shows that the effect is particularly strong up to a scale length of about $10h^{-1}$ Mpc and that it is not a luminosity effect (Fig. 1).
2) Within each morphological type the bright objects are more strongly clustered that the faint ones. This result was obtained by comparing for different morphologies the magnitude distribution of the objects having at least one neighbour in the sphere of radius $3h^{-1}$ Mpc, and one of the objects having at least one neighboor at larger distances.
3) The luminosity segregation, that is brighter objects cluster in regions of higher density, is not due to the morphology-density relation, and it is rather an independent fact in the distribution of galaxies. Fig. 2 displays the number of all neighbours within $2h^{-1}$ Mpc as a function of the absolute magnitude for each type grouping.

Aknowledgements: We thank M. Geller and J. Huchra for kindly supplying part of the unpublished redshifts in the Pisces-Perseus region.

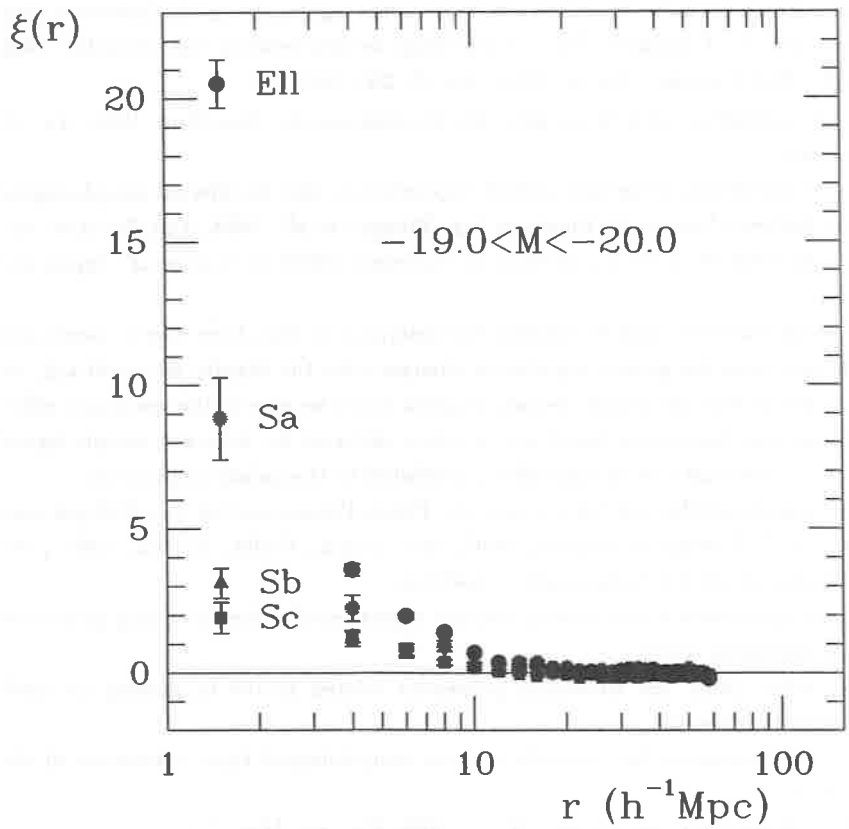

Fig. 1. Correlation function for different morphological types in the absolute magnitude bin $-19.0 \leq M \leq -20.0$.

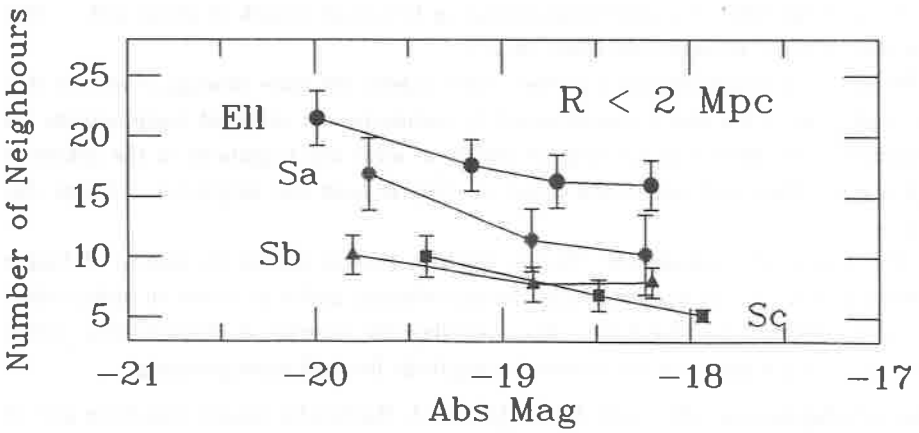

Fig. 2. Mean number of neighbours whithin a sphere of radius $R = 2h^{-1}Mpc$ as a function of the morphological type and of the absolute magnitude of the center galaxy.

The Problems in Assessing the Galactic Synchrotron Contribution to the Tenerife CMB Experiments.

R.A.Watson,[1] and C.Gutiérrez de la Cruz[2],
1. NRAL, Jodrell Bank, University of Manchester, UK.
2. Instituto de Astrofisica de Canarias, Tenerife, Spain.

ABSTRACT

The two surveys carried out in Tenerife on the anisotropy of the Cosmic Microwave Background at 10.45GHz on two intermediate angular scales of 8.4 and 5.6 degrees (FWHM) have shown weak structures of $\delta T/T = 4 - 7 \times 10^{-5}$. The interpretation of this is made difficult by the unknown contribution of weak non-uniform synchrotron emission at high galactic latitudes. Here we demonstrate that simple linear spectral index extrapolations made from the 408MHz all sky survey and the 1420MHz Bonn survey to 10.45GHz are dominated by survey baseline uncertainties at high galactic latitudes of amplitude ≈0.25mK. Preliminary limits from a new experiment at 15GHz suggests that the spectrum of the observed structure is more compatible with galactic synchrotron than with the intrinsic CMB thermal spectrum. Therefore we conclude that there may still be a significant galactic signal, but that artificial spectral index variations between the two surveys mask possible true variations.

Introduction

In our original paper[1] we reported sensitive measurements on the anisotropy of the Cosmic Microwave Background (CMB) made with drift scans at declination +40° with a triple-beam radiometer using 8.4° FWHM beams with 8.1° separation at a frequency of 10.45GHz. At this frequency, our tentative detections could contain a component of high-latitude radio continuum from the galaxy. An extrapolation to 10.45GHz made directly from the 408MHz survey with a single spectral index of $\alpha = 2.8$ ($T(\nu) \propto \nu^{-\alpha}$) convolved with our experimental beam profile lead to a comparatively small predicted signal of 70μK, which did not match the detected signal in position.

A further experiment made in Tenerife with smaller beams of 5.6° FWHM found a larger more significant signal at the same frequency[2,3]. An example of this was a 'hot spot' of 0.3mK found at declination +40° and Right Ascension 15^{hr}, although similar spots can now be seen in other parts of the data set. The problem now is to explain that observed structure, which seems in conflict with theoretical predictions for intrinsic CMB anisotropies.

The Surveys and the Extrapolation to 10.45GHz

The two surveys we have used are the 408MHz all sky survey[4] and the 1420MHz northern sky survey[5,6], which was limited to declinations $\delta \gtrsim -19°$. The problem of these surveys occurs in the slight offsets between adjacent scans due to changes in weather, receiver and ground pick-up. Corrections had been made to reduce these effects by using overlapping scans made in different directions, but these become more difficult at higher frequencies where the drifts are comparatively larger. In the 408MHz survey these effects appear as small vertical bands, while in the 1420MHz survey they appear as curving ripples sloping at approximately 45° to declination.

Both the surveys were convolved to the same resolution of 1° and baselevels were removed of 5.89K at 408MHz and 2.93K at 1420MHz. This is required to remove non-galactic components such as atmospheric emission, the CMB and an extragalactic component due to discrete sources. The next step was to convolve both surveys with a 5.6° FWHM Gaussian, which represents a single beam. A spectral index map was made from both survey and used to extrapolate to 10.45GHz.

At this stage the baseline ripples seem to have been removed, but when this map is convolved with 3 delta functions ($-\frac{1}{2}$,+1,$-\frac{1}{2}$) with separations of 8.1° to represent the beam switching geometry, the ripples are seen again with typical amplitude 0.25mK and are shown in Figure 1, where black represents $\lesssim$−0.3mK and white $\gtrsim$0.7mK. The smooth fall off in galactic emission with latitude has been removed by the beam switching, leaving the weak structure on the scale-size of the beam. This structure, which is mostly the result of residual baseline errors left after the 5.6° smoothing, is magnified by the extrapolation because of the large factor (8.9) in the

ratio of the frequency differences between 408, 1420 and 10450MHz.

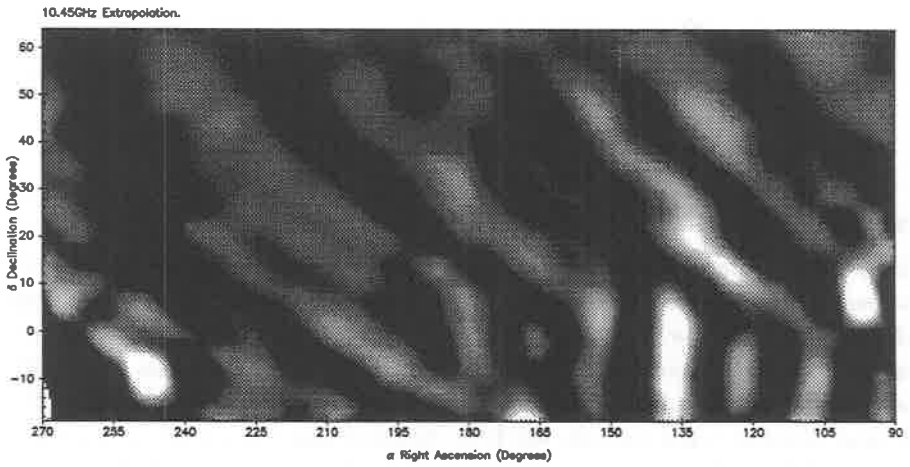

Figure 1: Extrapolation to 10.45GHz convolved with experimental triple beam.

Conclusions.

A simple extrapolation between the 408 and 1420MHz surveys does not appear good enough to establish the likely synchrotron contribution at 10.45GHz at our sensitivity and with our beam geometry. Our recent measurements at 15GHz have reached a sensitivity better than any of our 10GHz scans and show no detected structure. This suggests that whatever is the cause of the 10GHz structure it is non-thermal (and therefore non-CMB), but there remains a strong possibility that galactic emission is the cause. In that case we require a good galactic assessment in order to assess the probable contributions at 15GHz for our present experiment, and so we are continuing the 10GHz experiment to provide such a survey. We wish to acknowledge an Acciones Integradas award from the British Council for providing funds for us to meet our collaborators.

References

1) Davies, R.D., Lasenby, A.N., Watson, R.A., Daintree E.J., Hopkins, J., Beckman, J.E., Sanchez-Almeida, J. and Rebolo., R. 1987, Nature, **326**, 611

2) Watson, R.A., Rebolo, R., Beckman, J.E., Davies, R.D. and Lasenby, A.N.,1988, in *Large*, eds Mezzetti *etal.* , Kluwer Academic Publishers.

3) Watson, R.A. 1989, *Ph.D. thesis*, University of Manchester.

4) Haslam, C.G.T., Salter, C.J., Stoffel, H. and Wilson, W.E.,1982,*Astr.Astrophys.Suppl*, **47**,1

5) Reich, W., 1982, *Astr.Astrophys.Suppl.*, **48**, 219

6) Reich, P. and Reich, W., 1986, *Astr.Astrophys.Suppl.*, **63**, 205

Ω FROM THE GREAT ATTRACTOR

A.F. Heavens
Department of Astronomy, University of Edinburgh,
Royal Observatory, Edinburgh, U.K.

SUMMARY

Large-scale peculiar velocities can be used as an effective tool to estimate the density parameter of the Universe. This can be done in a number of ways, such as calculating dipoles[1] or by using $\nabla.\mathbf{v}$ to estimate a mass overdensity (Bertschinger, this volume). These methods allow an estimate of Ω because the relationship between mass overdensity $\delta\rho$ and peculiar velocities induced involves $\Omega^{0.6}$, if the perturbations are gravitational[2]. This paper describes a new method, which involves analysing 'attractors'– points where there is infall from all directions (in the microwave background frame). The two main results are that for CDM models, Ω must exceed about 0.5, and that, if Ω is high, one should not expect a large mass concentration at the Great Attractor.

MINIMA IN THE PECULIAR VELOCITY POTENTIAL

The growing mode of gravitational perturbations is irrotational, so the velocity field can be expressed as the gradient of a potential field. Using galaxies as tracers of the velocity field, and smoothing on a large scale ($\gtrsim 12h^{-1}$ Mpc), Bertschinger *et al.* (1990) have constructed[3] this potential within a distance of about $60h^{-1}$ Mpc. The Great Attractor appears as a local minimum of the potential, indicative of infall from all directions. Assuming the field is Gaussian, it is possible[4] to analyse the properties of local minima, using an extension of the theory of density maxima[5,6] The main result is that the joint number density distribution of potential drop and overdensity has a relatively simple form

$$n_{ga}(\varphi,\nu;r)d\varphi d\nu = \frac{f(\nu)}{(2\pi)^{5/2}R_\Phi^3\beta_1}\exp\left[-\frac{1}{2\beta_1^2}\left(\varphi^2 - 2\varphi\nu\beta_2 + (\beta_1^2+\beta_2^2)\nu^2\right)\right]d\varphi d\nu$$

where $\nu \equiv \delta/\sigma_0$, where $\delta \equiv \delta\rho/\rho$ and $\sigma_0 \equiv \langle(\delta\rho/\rho)^2\rangle^{1/2}$. $f(\nu)$ is defined in Bardeen *et al.* (1986)[6], and the $\beta(r)$ depend on the fluctuation spectrum with the autocorrelation function of the field. R_Φ is related to the smoothing length. Full details may be found in Heavens (1991)[4]. The variable φ is related to the potential drop $\Delta\Phi$ by $\varphi \propto -\Delta\Phi/(\Omega^{0.6}\sigma_0)$, so increasing Ω or σ_0 has the effect of allowing deeper potential wells. This distribution, combined with the known depth and distance of the Great Attractor gives likelihood estimates for the parameter(s) Ω (and ν) if σ_0 can be found by other methods. For example, using the microwave background to constrain σ_0 for particular fluctuation spectra[7] gives

a likelihood function for CDM shown in Fig. 1. Alternatively, σ_0 may be estimated using one of the IRAS surveys[8], assuming the IRAS galaxies form a biased tracer of the mass: $\delta N/N = b\delta\rho/\rho$. In this case, we estimate the overdensity from the IRAS counts[9] to get $\nu \simeq 2$, and obtain the likelihood for $\Omega/b^{5/3}$ (Fig. 2). Again, we see that, if $b \sim 1$, $\Omega \gtrsim 0.5$ is indicated. We may put these two methods together to constrain $0.7 \lesssim b \lesssim 1.4$, for the bias parameter on a scale of $12h^{-1}$ Mpc.

In conclusion, this is a very clean test for Ω and the power spectrum, relying on very few assumptions and with no major uncertainties.

1. Strauss, M.A. & Davis, M., 1988. In *Large Scale Motions in the Universe.* Ed. Rubin, V.C. & Coyne, G.V. Princeton University Press, Princeton.
2. Peebles, P.J.E., 1980. *The Large Scale Structure of the Universe*, Princeton University Press.
3. Bertschinger, E., Dekel, A., Faber, S.M., Dressler, A., & Burstein, D., 1990. *Astrophys. J.*, in press.
4. Heavens, A.F., 1991. Submitted to *Mon. Not. R. astr. Soc.*.
5. Peacock, J.A. & Heavens, A.F., 1985. *Mon. Not. R. astr. Soc.*, **217**, 805.
6. Bardeen, J.M., Bond, J.R., Kaiser, N. & Szalay, A.S., 1986. *Astrophys. J.*, **304**, 15.
7. Vittorio, N., Meinhold, Muciaccia, Lubin & Silk 1990. Preprint.
8. Saunders, W.S., Frenk, C.S., Rowan-Robinson, M., Efstathiou, G.P., Lawrence, A., Kaiser, N., Ellis, R.S., Crawford, J., Xiao-Yang, X. & Parry, I., 1990. Preprint.
9. Yahil, A., 1990. *Proceedings of Les Arcs meeting. Rencontres de Moriond.*

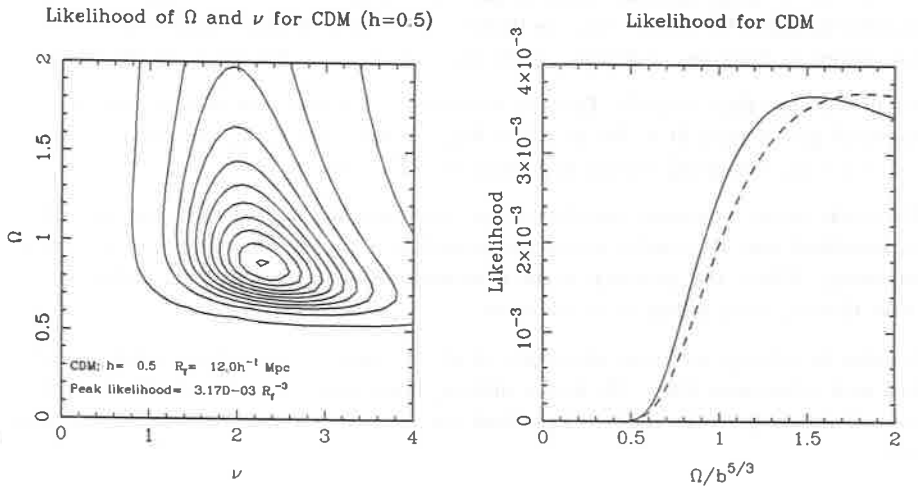

Figure 1. The likelihood as a function of Ω, using the UCSB South Pole microwave background experiment to constrain σ_0, for CDM with $h = 0.5$. This assumes that σ_0 is as large as possible, with marginal consistency with the 95% upper limit of $\Delta T/T$. Contours at 1%, 10%, 20% ... 90% and 99% of peak.

Figure 2. The likelihood distribution for CDM, using IRAS galaxies to obtain σ_0, for two values of $hb^{5/3}$, 0.5 and 1.0, shown full and dashed.

Exact hierarchical clustering in one dimension

Brian Williams & Alan Heavens *Department of Astronomy, University of Edinburgh, Royal Observatory, Edinburgh, U.K.*

John Peacock *Royal Observatory, Edinburgh, U.K.*

Sergei Shandarin *Department of Physics and Astronomy, University of Kansas, U.S.A.*

We have used the adhesion (or Burgers') model[1] as a basis for numerical simulations in one dimension (in which case it is exact) and used the resulting catalogue of bound objects to test analytic theories of the mass function and two-point correlation function.

The adhesion model is an extension of the well-known Zel'dovich[2] approximation into the non-linear regime by treating the particles as 'sticky'. This forbids the crossing of particle trajectories; particles move together after collision.

We limit ourselves to one-dimensional simulations as here the model is exact and we can obtain the large dynamic range in mass necessary to test thoroughly the various analytic theories. We believe that the theories we test are equally valid in one and three dimensions as there are no features in the theories that are dimension-specific.

We have found that both the Press & Schechter[3] mass function and the Peaks mass function[4] give a good fit to the data (see Fig. 1) over a wide range of spectral indices ($-1 < n < 3$). The peaks theory in general provides a better fit.

The peaks theory two-point correlation function[5] provides a good fit to the data (Fig. 2), provided that the initial power spectrum has a significant amount of statistical clustering. Where the majority of the clustering arises from dynamical evolution the peaks theory proves a poor fit to the data.

In order to attempt to locate structures of given mass, we smooth the initial density field with a low-pass filter. We tested different functional forms for the filter, finding that a Gaussian provides the best fit to both the mass function and correlation function data.

References

1) Gurbatov, S.N., Saichev, A.I., & Shandarin, S.F., 1989, *Mon. Not. R. astr. Soc.*, **236**, 385.

2) Zel'dovich, Ya. B., 1970, *Astron. Astrophys.*, **5**, 84.

3) Press, W.H. & Schechter, P., 1974, *Astrophys. J.*, **187**, 425

4) Peacock, J.A. & Heavens, A.F., 1990, *Mon. Not. R. astr. Soc.*, **243**, 133

5) Lumsden, S.L., Heavens, A.F., & Peacock, J.A., 1989, *Mon. Not. R. astr. Soc.*, **238**, 293.

A full account of ths work has been submitted to MNRAS.

1. Mass function, $M^2 f(M)$, showing data from adhesion model simulations (data points), Press-Schechter (solid line) and peaks theory (broken line) for three different values of the scale factor, a.

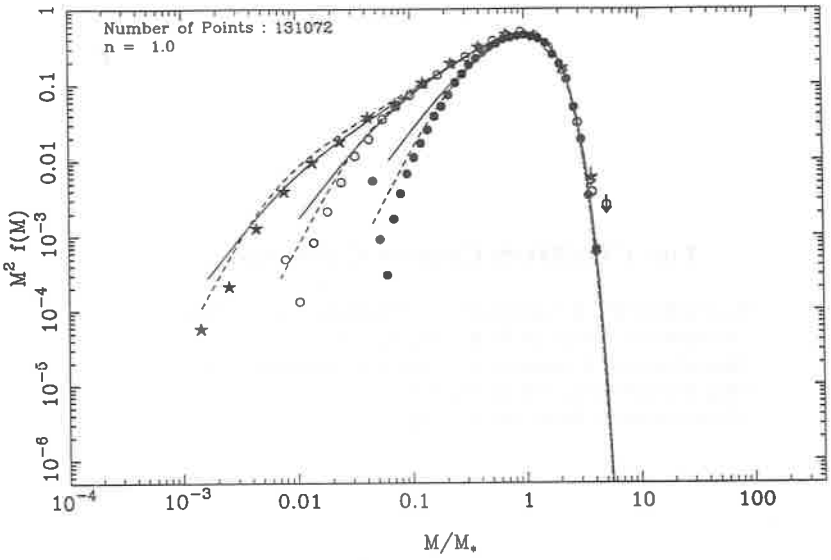

2. Two-point correlation function, showing data from adhesion model simulations (data points) and peaks theory (solid line) for different thresholds.

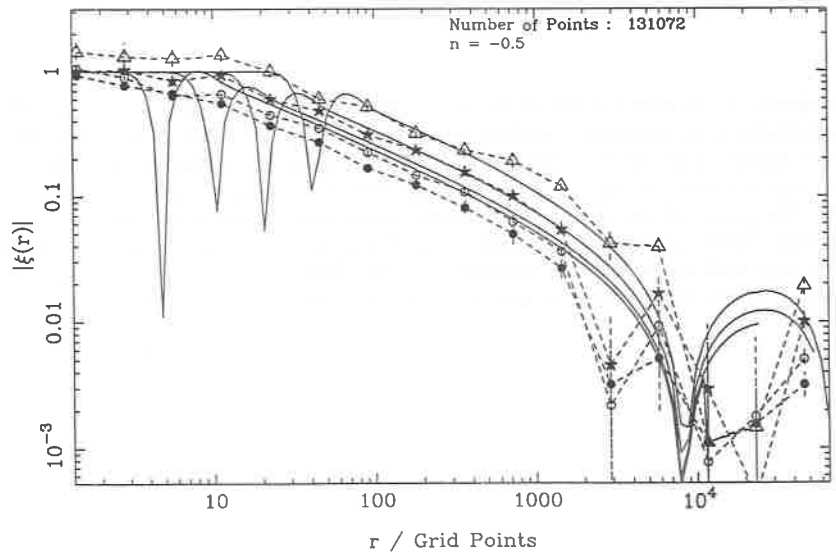

The COSMOS Cluster Catalogue

S.LUMSDEN[1], R.NICHOL[2], C.COLLINS[3], L.GUZZO[4]
[1] *Astrophysics Group, ICSTM, London, U.K.*
[2] *Department of Astronomy, University of Edinburgh, U.K.*
[3] *Royal Observatory, Edinburgh, U.K.*
[4] *Osservatorio di Brera, Milan, Italy.*

Abstract
Clusters of galaxies can be used to trace the large scale density field. They also provide a powerful test of galaxy evolution and enviromental effects through the luminosity function. However, previous large scale cluster catalogues have been based on unquantifiable, 'eye-balled' surveys. Because the selection bias in these catalogues is inherently unknown, they do not provide a statistically complete set. The recent advent of objective, machine based galaxy catalogues allows a new, objectively selected cluster catalogue to be constructed. Below, we present details of the selection procedures we have used to create such a catalogue from the EDSGC. Furthermore, since the Abell catalogue has previously been extensively used, we show what errors might arise from this use.

Construction of the Catalogue

The EDSGC[1] comprises data on 1.5 million galaxies, 95% complete to a limit of $b_j \sim 20.5$ and with less than 10% stellar contamination, covering an area of 0.5 steradian centred on the SGP. The production of the cluster catalogue falls into two stages. The first provides candidate clusters; the second is a modified Abell[2] type analysis of these candidates.

The EDSGC was binned into equal area square bins. This process was carried out three times for three different magnitude limits ($b_j < 18.5, 19.5, 20.5$). The bins were then lightly smoothed using a Shectman[3] filter to reduce binning noise. They were further smoothed on a scale of 1° to create a 'sky' frame. This was subtracted from the original image and peaks located in the difference frame. This prevents clusters only being found preferentially in areas of high projected surface density. These peaks were located and deblended[4] to provide a complete set of candidates. Extensive checking showed these procedures were reliable.

The candidates were subjected to a modified Abell analysis. For this procedure all the galaxies in the EDSGC were used. The major modification to the Abell procedure was to use background information to provide 'true' estimates of m_3, m_{10} and the richness count, c. The background was determined by using data from a $4° \times 4°$ region, centred on the cluster. An iterative approach was used to determine m_{10}. This involved calculating the number of background galaxies within the Abell radius, r_A. This radius was then re-evaluated for the new value of m_{10} and so on until the value of r_A was constant to 1% between iterations. Similarly the values of m_3 and c were corrected for the background.

The result of this analysis were three lists for each of the three initial bin sizes. These lists are merged into one by considering overlapping Abell radii to indicate the possibility of a single cluster. The background corrected magnitude distributions were compared using a KS test. Clusters failing at the 90% confidence level were deemed to be distinct. The galaxies from all the merged clusters were used to determine the parameters for this single new cluster. The last step was to test this distinct set of clusters for overlaps to check for blends. A deblended dataset in which any galaxy

could only belong to one cluster was created. This process reduces projection effects of the form previously noted[5] as a problem in cluster catalogues.

Comparison with the Abell Catalogue

The final catalogue was matched with the clusters from the same area in the southern extension of the Abell catalogue[6]. Since magnitudes quoted there are in V, a constant conversion factor of $b_j - V = 0.742$ was applied to our catalogue. Of those clusters found in common, the scatter in the values of m_{10} was found to be 0.6 mags, and in the richness 30 galaxies. These values are large enough to represent a shift in richness or distance class of ± 1, leading to the conclusion that the Abell catalogue is unlikely to be complete when sub-samples selected according to richness or distance class are used. About half of our clusters are in the Abell catalogue: the others, including several rich clusters are not listed by Abell. Similarly, we find only 30% of the listed Abell clusters: some of those missing are beyond our completeness limit ($m_{10}(b_j) \sim 19.5$), but many on visual inspection must be classed as very poor. Again, the conclusion must be that the Abell catalogue is not complete in any sense (as Abell noted himself in his original paper), and should not be used as such.

Summary

Our catalogue provides an objective sample of clusters near the SGP, complete within the selection criteria outlined. In future, we shall use it to calculate both angular and spatial cluster correlation functions (based on a multi-object spectroscopic study of 100 of the richer systems) and to determine the LF for these clusters.

References

1: Heydon-Dumbleton, N.H., Collins,C.A., & MacGillivray, H.T., 1989. *Mon. Not. R. astr. Soc.*, **238**, 379.
2: Abell, G.O., 1958. *Astrophys. J. Suppl.*, **3**, 211.
3: Shectman, S.A., 1985. *Astrophys. J. Suppl.*, **57**, 77.
4: Beard, S.M., MacGillivray, H.M. & Thanisch, P.F., 1990. *Mon. Not. R. astr. Soc.*, in press.
5: Sutherland, W., 1989. *Mon. Not. R. astr. Soc.*, **234**, 159.
6: Abell, G.O., Corwin, H.G. & Olowin, R.P., 1989. *Astrophys. J. Suppl.*, **70**, 1.

Can the X-ray Background originate from Massive X-Ray Binaries?

Marie-Agnès Treyer [1,2] , Martine Mouchet [1,3] , Alain Blanchard [1,3] , Joseph Silk [2,4]

[1] DAEC, Observatoire de Meudon, 92190 Meudon, France.
[2] Astronomy Department, U.C. Berkeley, CA 94720 USA.
[3] Université Paris VII, 2 Place Jussieu, 75251 Paris Cédex 05, France.
[4] Mount Stromlo, Private Bag, Weston Creek PO, ACT 2611, Australia.

Abstract: It has been suggested that MXRB in star-forming galaxies could be the main contributor to the X-ray background (Bookbinder et al., 1980, Griffiths, 1989). This idea is appealing as there is a well defined correlation between X-ray luminosity and IR luminosity for IRAS galaxies and star-forming galaxies. Such a possibility has been investigated in some detail by Griffiths and Padovani (1990). By taking the observed $L_X - L_{IR}$ correlation and a fit of the luminosity function of IRAS galaxies and an evolution law, it is possible to estimate the amplitude of the X-ray background. We have modelled the resulting spectrum by taking a composite X-ray spectrum from MXRB in our Galaxy. It appears that this spectrum fails to reproduce the observed hard tail of the X-ray background when evolution is required to match the flux at 10 keV. On the other hand, we find better agreement if an important contribution from fainter galaxies is assumed.

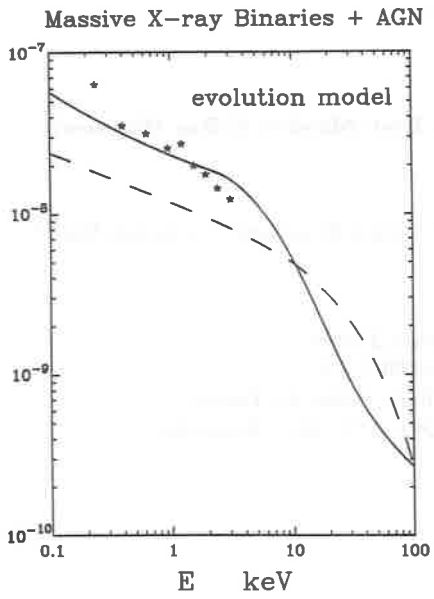

Figure 1 : The X-ray spectrum (full line) obtained by adding the contribution of MXRB and from AGN compared to the fit of the observed background spectrum (dashed line) and the recent soft X-ray spectrum as deduced by Wu et al, 1990 (stars). An evolution law $\exp(t/\tau)$ with $\tau \approx 0{\cdot}15$ is necessary in order to reproduce the flux at 10keV.

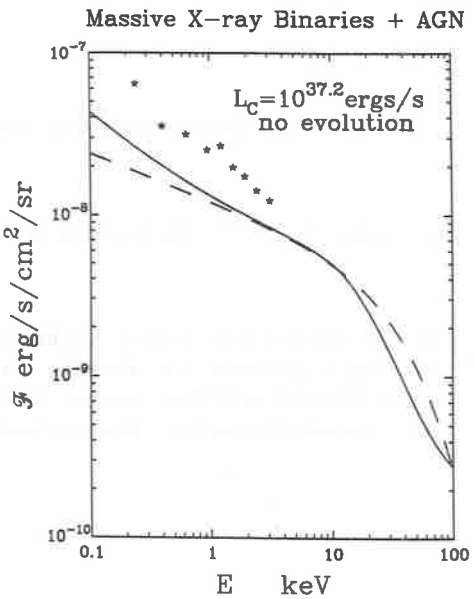

Figure 2 : As in Figure 1, without evolution and using the IR luminosity function from Soifer et al. (1987). A cut-off L_c at the faint end of the X-ray luminosity function is chosen in order to fit the flux at 10keV.

Spectrum from MXRB: an evolution model

We have computed a composite spectrum for the MXRB present in our Galaxy using sources for which spectra were fitted by White et al.(1983). Although the number of these MXRB is small, we have verified by bootstrap resampling that the uncertainty in this composite spectrum is small. Following Griffiths and Padovani (1990) we used the $L_X - L_{IR}$ correlation and the IR luminosity function of IRAS galaxies (Saunders et al., 1990) to derive the X-ray contribution of these galaxies. Without evolution the total contribution represents typically 10% of the total background. In order to produce most of the background, we have therefore assumed a luminosity evolution model $L \propto \exp(t/\tau)$ and we have determined τ so that the total flux fits the observed flux at 10 keV. An additional contribution from AGNs is assumed with a spectral index of 0.7 in order to fit the observed flux at 100 keV. The resulting spectrum is presented in Figure 1. As one can see, it does not reproduce the observations very well.

Another possibility: faint galaxy contribution

The total flux from IRAS galaxies from the Soifer et al. (1987) IR luminosity function is mathematically divergent at the faint end. This seems to be due to the absence of correction for inhomogeneities in the sample. Actually, recently Saunders et al. (1990) found that the luminosity function of IRAS galaxies does not lead to such a surprising effect. However, we investigated a rather extreme model in which most of the contribution to the X-ray luminosity comes from faint star-forming galaxies at low redshift. Using the Soifer et al. luminosity function, we assume a low luminosity cut-off faint enough to reach the total X-ray contribution at 10 keV without significant evolution. As in the previous case an additional contribution from AGNs is assumed. The resulting spectrum is given in Figure 2. It is in reasonably good agreement with the observations.

Conclusions

Our main conclusion is that MXRB do not seem very appropriate for reproducing the spectral shape of the observed X-ray background when substantial evolution is advocated to produce the observed flux. However, the possibility remains that most of the background may originate from a faint population of star-forming galaxies with no significant evolution. A fluctuation analysis is under investigation and should exclude such a possibility, as the background is known to be highly isotropic (Hamilton and Helfand, 1987; Barcons and Fabian, 1989).

References

Barcons, X., and Fabian, A.C. : 1989, *M.N.R.A.S.* **237**, 119.
Bookbinder et al.: 1980, *Ap.J.* **237**, 647.
Griffiths, R.E.: 1989, in "The epoch of galaxy formation", eds. Frenk et al, p 235.
Griffiths, R.E. and Padovani, P.: 1990, preprint.
Hamilton, T. and Helfand, D.J., : 1987; *Ap.J.*, **318**, 93.
Saunders et al.: 1990, M.N.R.A.S., in press.
Soifer et al.: 1987, *Ap.J.*, **320**, 238.
White, N.E., Swank, J.H., Holt, S.S.: 1983, *Ap.J.*, **270**, 711.
Wu, X, Hamilton, T., Helfand, D.J., Wang, Q., et al.: 1990, preprint.

QUASAR'S PECULIAR VELOCITY

Yaoquan Chu
Center for Astrophysics
University of Sci. & Tech. of China
Hefei, Anhui 230026, China
and
Li-Zhi Fang
Institute of Astronomy
University of Cambridge
Cambridge CB3 OHA, UK

Peculiar velocity of quasars is among the needed extremely to be sought out in the observational cosmology. The information about the distribution of peculiar velocity at high redshift are of fundamental importance for models of formation of galaxies and large-scale structure in the universe. Up to now we know little about the peculiar velocity of quasar. The difficulty of derterming quasar peculiar velocity is that there is no methods independent of redshift to determine the distance of quasar. This paper discusses a methods for determining an upper limit to the peculiar velocity of quasar by means of statistical analysis of quasar pair.

We conside a sample of quasar pairs, if distribution of quasars is randomly homogeneous in space, then the orientation of the pairs should also be isotropic. We have

$$N(D_r)\, dD_r = \frac{3}{2} N_T \left(1 - \frac{D_r^2}{D_{max}^2} \right) d\left(\frac{D_r}{D_{max}}\right) \qquad (1)$$

$$D \cong \frac{1}{N_T}\int_0^{D_{max}} D_r N(D_r)\, dD_r = \frac{3}{8} D_{max} \qquad (2)$$

where the D_r is the radial projections of the distance between two quasars in a pairs and N_T is the total number of pairs in the sample. The quasar clustering and peculiar velocity would lead to deviation from the above distribution.

As we know, the clustering of quasar at high redshift is very weak[1]. Here we conside a simple model in which we assume that two quasars in every pairs are approching each other at average speed of V. Then the deviation of $\overline{D}_r$ due to the peculiar velocity is show as

$$\overline{D}_r = \frac{3}{8} D_{max}\left(1 - \frac{1}{3}\frac{V}{c}\frac{c}{H_0}\frac{1}{D_{max}}\right) \qquad (3)$$

For statistical analysise, we use the quasar sample given by Savage & Bolton[2], which includes quasars in two $5^\circ \times 5^\circ$ regions around respectively $(02^h, -50^\circ)$ and $(22^h, -18^\circ)$ in the southern hemisphere. For the sake of comparison we also calculate the distribution of the Monte Carlo sample which is given by avarage of 10 Monte Carlo results of randomizations of angular coordinates of each quasar. The results of $\overline{D}_r$ are listed in the Table in which the upper limit V_{up} to peculiar velosity is obtained by:

$$V_{up} = 8H_0\left|\overline{D}_r - \frac{3}{8} D_{max}\right| \qquad (4)$$

Sample	D_{max} (Mpc)	$\overline{D}_r$ (Mpc)	$\frac{\overline{D}_r - \frac{3}{8}D_{max}}{\frac{3}{8}D_{max}}$	V_{up} (km/s)
$(02^h, -50^\circ)$	50	19.8	5.6%	888
$(02^h, -50^\circ)$	100	35.9	4.2%	1280
$(22^h, -18^\circ)$	50	18.0	4.0%	576
$(22^h, -18^\circ)$	100	39.7	5.9%	1760

All results of V_{up} for the four subsamples are around 1000km/s Therefore, if all deviations of $\overline{D}_r$ from that given by Eq.(2) are due to the motion of two quasars in a pair to approach each other, such peculiar velocity should have the order of 1000km/s.

REFERENCE:
1) Chu Y., and Fang L., 1987, in"Observational Cosmology",p.627, ed. by A. Hewitt, G. Burbidge and L. Fang, Reidel.
2) Savage A. and Bolton J.G., Mon. Not. R. Astr. Soc., vol.188 (1979), p.599.

LARGE-SCALE STRUCTURES

A.P. FAIRALL AND G. KAUFFMANN
Department of Astronomy, University of Cape Town,
Rondebosch, 7700, South Africa

ABSTRACT

We have merged the almost-complete updated Catalogue of Radial Velocities of Galaxies[1] and an updated version of the Southern Redshift Catalogue[2] to form a database of 22000 galaxy redshifts. Plots of this database (slices in R.A. and Declination) confirm many known features, but also reveal many new features, including a wall having two sharp bends and a total length > 20 000 km s^{-1} (in redshift space). We have also used Monte-Carlo simulations of the data to identify more than a hundred significant voids. A spectrum of void sizes is presented.

The limited space available here allows us to include only a small sample of the plots displayed at the conference; (Figure 1), but the full set is being published in reference 3. We have also identified 129 voids, each having >85% statistical significance of being real. We use these to drive a spectrum of sizes (Figure 2). Details are given in reference 4.

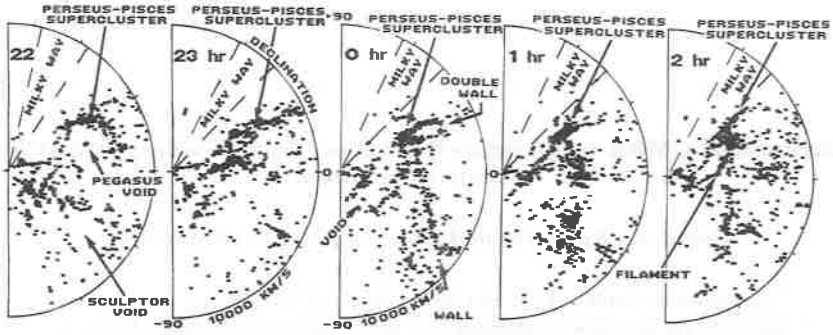

Figure 1. Sample sequence of R.A. slices. Whilst the Perseus-Pisces supercluster is well known, new wall-like features are apparent in the central plot. One exhibits two right-angled bends (and extends beyond the diagram). The "Pegasus" void (left-hand diagram) has three Markarian galaxies at its centre.

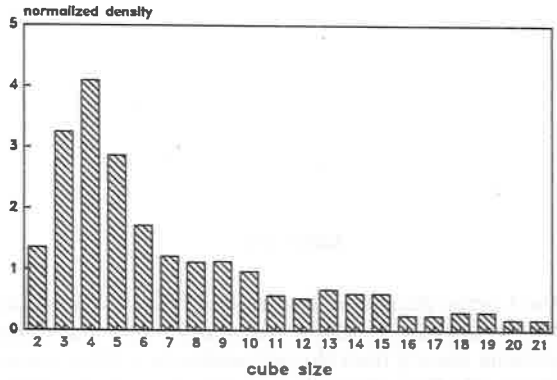

Figure 2. Void size spectrum. The numbers on the y axis indicate the relative percentage of the total volume occupied by each size class, the size is in units of 200 km s^{-1}.

REFERENCES

1. Palumbo, G.G.C., Vettolani, G., Baiesi-Pillastrini, G. and Fairall, A.P., in preparation.
2. Fairall, A.P. and Jones, A., *Publ. Dept. Astr. Univ. Cape Town*, No. 10 (1988).
3. Fairall, A.P., Palumbo, G.G.C., Vettolani, G., Kauffmann, G., Jones, A. and Baiesi-Pillastrini, G., *Mon. Not. R. astr. Soc.*, in press.
4. Kauffmann, G. and Fairall, A.P., *Mon. Not. R. astr. Soc.*, in press.

Gravitational CMBR temperature fluctuations from non-linear structures: N-body simulations

Eelco van Kampen[1] **and Enrique Martínez-González**[2]

[1] Sterrewacht Leiden, P.O. Box 9513, 2300 RA Leiden, the Netherlands
[2] Instituto de Estudios Avanzados en Física Moderna y Biología Molecular, CSIC-Universidad de Cantabria, 39005 Santander, Spain

Abstract

Anisotropies of the Cosmic Microwave Background Radiation are usually characterized by the temperature fluctuations $\Delta T/T$, which consist of several terms arising from a number of effects acting on photons coming from the last-scattering surface towards us. The term arising from the gravitational effect of non-linear evolving structures along the path of the photon is given by:

$$\frac{\Delta T}{T} = 2 \int_e^o d\tau \frac{\partial \phi}{\partial \tau}(\tau, \vec{x})$$

We used N-body simulations of cosmological objects like voids, rich clusters and Great Attractors, and calculated the effect of these objects by shooting photons through an evolving distribution of computer particles representing the real mass distribution. For rich clusters we find an effect on the order of a few times 10^{-7}, while the effect for Great Attractor-like structures is found to be on the order of 2×10^{-6}.

The integrated gravitational effect

In this paper, we study the integrated gravitational influence of non-linear structures on the temperature of the microwave photons. An estimation of this effect for a Swiss-cheese model was first given by Rees and Sciama (1968). More extensive work was done by Dyer (1976), Nottale (1984) and Thompson and Vishniac (1987). In order to be realistic, the non-linear evolution of the structure is followed by N-body simulations.

The gravitational effect on $\frac{\Delta T}{T}$ in the general case of a photon propagating in a non-static linear gravitational potential has recently been given by Martínez-González, Sanz and Silk (1990). The result for the case of an Einstein-de Sitter universe can be expressed as:

$$\frac{\Delta T}{T} = \frac{1}{3}(\phi_e - \phi_o) + 2\int_e^o d\tau \frac{\partial \phi}{\partial \tau}(\tau, \vec{x}) + \vec{n} \cdot (\vec{v}_o - \vec{v}_e)$$

While the first and third terms are the known Sachs-Wolfe (Sachs and Wolfe 1967) and Doppler terms respectively, the second term is the integrated gravitational effect given by the rate of change of the potential ϕ with time from the emitting point to the observer. This is the term we are interested in and it is calculated for several structures.

Results of the integrated gravitational effect have already been given for the Bootes void, assuming the thin shell approximation to describe its evolution, and for the Great Attractor modelled either with a Swiss-cheese or with an uncompensated secondary infall collapse (Martínez-González and Sanz 1990). In all cases the effect analytically found is at most a few times 10^{-6}.

Numerical calculation of the effect

Instead of using a model for non-linear structures encountered by photons coming towards us, we calculate the effect using the potentials obtained for a distribution of particles by an N-body integrator. The code used was a slightly adapted version of the Barnes & Hut treecode (1986), with initial conditions produced by a beautiful code deviced by Bertschinger (1987) based on a path integral method (see the *acknowledgements*). We first considered the most simple and popular case of an $\Omega = 1$ Einstein-de Sitter universe with a Cold Dark Matter spectrum.

As a first but already good approximation we shoot a two-dimensional grid of 64^2=4096 photons through an evolving N-body distribution, with the photons just travelling on parallel lines at the speed of light. This is justified for our intermediate scale objects at $z = 0.6$ because they measure about 1^o on the sky. For larger objects, like our Great Attractor at $z = 0.6$ as shown below, zero geodesics should be used, needing more extensive software (future work).

Results and discussion

We calculated the effect for several objects. We define our objects using Gaussian window functions, i.e. an object has an amplitude $\nu\sigma$ in the smoothed density field $\delta^W(\vec{x})$, obtained by convolving $\delta(\vec{x})$ with a window function $W(r) = exp - r^2/2R^2$, with σ being the r.m.s. of this field δ^W. So an object is defined by R and its density excess ν expressed in $\sigma(R)$. The code deviced by Bertschinger (1987) can produce initial conditions constrained to form any desired object. Very useful indeed !

We placed several 'intermediate scale' objects at $z = 0.6$, and calculated the effect using $\approx$ 17500 particles (a sphere cut out of a 32^3 particles cube). We chose 4 objects defined by a smoothing length of $R = 10$ Mpc (we use $H_o = 50$ km/s/Mpc) with amplitudes -2σ, 0σ,

2σ and 3σ. All objects give an effect on the order of their amplitude ν times 10^{-7}. This will hardly be measurable. The resulting map on the sky for the 3σ peak (a rich cluster) is shown in figure 1[a].

$\Delta T/T$ due to a Great Attractor or a Cosmic Void could be measurable. To test this, we calculated the effect due to a Great Attractor of the type claimed to exist by the Seven Samurai. Such a Great Attractor can be defined as a 2.1σ-peak for $R = 28$ Mpc (Bertschinger *et al.* 1990). We produced such an object within a sphere of radius 150 Mpc, and placed it at $z = 0.6$. The amplitude of the effect is almost redshift independent from $z = 0$ to $z = 2$, so also valid for the Seven Samurai Great Attractor. The resulting temperature fluctuations are about 2×10^{-6}, as shown in figure 1[b]. This might once be measurable.

More details on this research can be found in van Kampen and Martínez-González 1991.

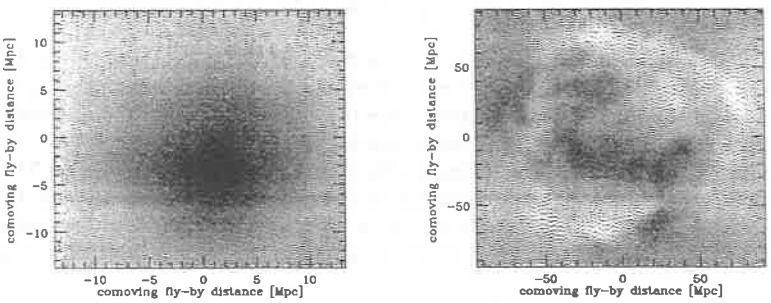

Maps of a patch of microwave background sky for photons which have traversed a rich cluster (on the left) or a Great Attractor-like structure (on the right). Both structures are at $z = 0.6$, so the cluster measures about 1° on the sky, and the G.A. spans about 6°. The gray-scales for the cluster: white=$+10^{-7}$, black=-4×10^{-7}. For the G.A.: white=$+2 \times 10^{-6}$, black=-3×10^{-6}. The maximum fluctuations are -3.5×10^{-7} and -2.5×10^{-6} respectively.

Acknowledgements

First of all we like to thank Bernard Jones, for supplying so much enthousiasm, energy and help. Rien van de Weygaert was essential for supplying us with realistic initial conditions, which he obtained from the beautiful code and method deviced by Bertschinger (1987). Vincent Icke deserves many thanks for useful comments on the physics and the numerical method. One of us (EvK) likes to acknowledge the Leids Kerkhoven-Bosscha Fonds and EelcoSoft Software Services for providing financial support.

References

Barnes, J. and Hut, P. 1986, *Nature* **324**, 446
Bertschinger, E. 1987, *Ap.J.Lett.* **323**, L103
Bertschinger, E., Dekel, A., Faber, S.M. and Dressler, A. 1990, *submitted to Ap.J.*
Dyer, C.C. 1976, *M.N.R.A.S.* **235**, 895
van Kampen, E. and Martínez-González, E. 1991, *submitted to M.N.R.A.S.*
Martínez-González, E. and Sanz, J.L. 1990, *M.N.R.A.S., in press*
Martínez-González, E., Sanz, J.L. and Silk, J. 1990, *Ap.J.Lett.* **355**, L5
Nottale, L. 1984, *M.N.R.A.S.* **206**, 713
Rees, M.J. and Sciama, D.W. 1968, *Nature* **217**, 511
Sachs, R.K. and Wolfe, A.M. 1967, *Ap.J.* **147**, 73
Thompson, K.L. and Vishniac, E.T. 1987, *Ap.J.* **313**, 517

QUASARS AS COSMOLOGICAL PROBES AN ESO KEY-PROGRAMME

C. Barbieri[1], *S. Cristiani*[1], *P. Andreani*[1,2], *R. Clowes*[3], *A. Gemmo*[1], *H. MacGillivray*[3], *C. Gouiffes*[2], *A. Iovino*[4], *F. La Franca*[1,5], *M. Sanvico*[1], *A. Savage*[6], *R. Vio*[1].

[1]Department of Astronomy, Padova; [2]European Southern Observatory; [3]Royal Observatory, Edinburgh; [4]Brera Observatory; [5]Institute of Radio Astronomy, Bologna; [6]UK Schmidt Telescope Unit, AAO.

The aim and the problems

A number of quasar surveys have provided considerable information about the distribution in time and space and the evolutionary history of this important constituent of the Universe. The main limitation, and a well known one for decades, is the statistical significance of the available samples: subtle selection effects, photometric errors, incompleteness of the spectroscopic data, etc. are among the many causes of uncertain or unfounded conclusions.

The field of the SA 94 as a diagnostic tool

One way out of this limitation is to obtain information with many independent but complementary techniques; an example is our own study of the field of SA 94 ($2^h53^m+0°20'$), where we have applied the methods of multi-colour photometry, slitless spectroscopy, optical variability, cross examination of radio and X catalogues to derive a deep and numerous sample. Our claim is to have obtained in that area a practically complete and unbiased ensemble. In turn, the study of this field has provided a well calibrated and tested set of criteria and working procedures that have been applied to a search of bright quasars over a large area of sky developed in the context of an ESO Key-Programme.

Three papers (Barbieri and Cristiani, 1986; Barbieri et al., 1987; Cristiani et al., 1989) have been already published; a summary of these papers can be found in Barbieri

et al., 1989, where also an analysis of the quasar counts in the range $16.5 < B < 22.4$ is carried out. A fourth paper discussing the automatic search on objective prism plates is in preparation (Cristiani, La Franca, Barbieri, Clowes, Iovino, 1990). At present, about 180 QSOs candidates have been confirmed by slit spectroscopy, mostly with the ESO telescopes. The central 10 deg^2 of the area provide a sample complete to B=19.9 and $z < 2.1$, whilst over 21 deg^2 the search is complete to B=19.4 and $1.8 < z < 3.2$.

Some results

a) Spectra. The spectral properties of the QSOs affect both photometric and spectroscopic surveys with subtle effects; to model as accurately as possible these effects, Cristiani and Vio (1990) have calculated a composite spectrum of quasars. The Principal Component Analysis was then applied, showing that UBVRI photometry is not well suited fort the selection of complete samples in the redshift interval 2.5-3.3, because of the great similarity with colours of A-F stars. Slitless spectroscopy, variability, or as yet unused narrower filters must then complement the multi-colour search.

b) Variability. The study of the optical variability of QSOs has long been a standard study at the Observatory of Asiago; a first study of the variability of 11 SA94 QSOs was already performed by Barbieri and Romano (1987). Subsequently, a very careful analysis, specifically aimed at the definition of criteria able to provide complete samples, has been performed by Cristiani, Vio and Andreani (1990) on 15 plates spanning a time interval of 7 years. The result is that variability is a powerful tool to derive complete (albeit not numerous) samples over a large range of redshifts, provided the study is continued for some years.

c) Clustering. An analysis of clustering has been carried out by Iovino et al. (1989), who found a significant excess of pairs with separations $< 10h^{-1}Mpc$ at $z < 1.5$; this work is now being extended to higher redshift QSOs. The three point correlation has also been examined (Pons et al. 1990), with the result that its value is lower than that of normal galaxies; however, the small number of available triplets calls for a future revision of the work with more quasars.

The ESO Key-Programme.

All studies of the bright end of the luminosity function ($B < 18.0$) are affected by a further difficulty, namely by the low surface density of objects; several hundred square degrees of sky must be searched in order to derive a meaningful number of objects. We have undertaken such difficult task in the framework of an ESO Key-Programme (An Homogeneous Bright Quasars Survey) which has obtained a considerable support of telescope and machine time at several institutions. A detailed description of this Key-Programme is given by Barbieri *et al.*(1989), so it suffices here to recall some salient features:

- planned area 2000 deg^2 at galactic latitudes $b < -60°$
- limiting magnitudes $16.0 < B < 18.25$
- $z < 2.2$ (in some areas the search has been extended up to $z = 3.2$).

The basic search is done by multi-colour (UBVRI) photometry on Schmidt plates obtained at UKSTU and at ESO, with the aid of objective-prism Schmidt plates examined with the AQD software (Clowes, 1986a) for selecting QSO candidates.

The Key-Programme started in 1989; As of today, 6 fields of 25 deg^2 each have already UBVRI (or UJVRI) photometry, obtained by scanning two plates for each colour and referring the magnitudes and colour indices to our own CCD photometric standards. The faint limit of the photometry varies from field to field from B=19.5 to B=21.0; the accuracy is 0.1 mag both in mag and colour index. For 3 out of 6 fields we also have the AQD data, down to B=19.4. Of the several hundreds of candidates so identified, some 300 have already been examined spectroscopically. The success rate is about 50%, extremely encouraging. In the same time, the sample of SA 94 is continually increased and perfected by additional spectra. As expected, most quasars turn out to have $z < 2.2$, although a fair number of higher redshift quasars is also obtained.

At the end of the year we expect to have reasonably complete data for at least 5 fields (125 deg^2) to be used for a first significant improvement in the study of the luminosity function. The rest of the programme should follow smoothly; actually, up to now we have spent a good amount of time on the candidates in the fainter apparent luminosity bins for which an area much smaller than 2000 deg^2 will provide significant statistics. Therefore, the subsequent stages could be speeded up, to reach the goal in 5 years.

REFERENCES

Barbieri, C., and Cristiani, S., 1986, *Astron. Astrophys. Suppl.* **63**, 1

Barbieri, C., Cristiani, S., Iovino, A., and Nota, A., 1987, *Astron. Astrophys. Suppl.* **67**, 551

Barbieri, C., Cristiani, S., La Franca, F., 1989, invited talk at the VIII Convegno Nazionale di *Relatività Generale e Fisica della Gravitazione*, Cavalese (Trento), ed. Cerdonio, Cianci, Francaviglia, Toller, pg. 20

Barbieri, C., Cristiani, S., Andreani, P., Clowes, R., Gemmo, A., Gouiffes, C., Iovino, A., La Franca, F., Savage, A., Vio, R. 1989, *ESO Messenger* **58**, 22

Barbieri, C., Romano, G., 1987, *Acta Astronomica*, **37**, 275

Clowes, R.G., 1986, *Mon. Not. R. astr. Soc.* **218**, 139

Cristiani, S., Barbieri, C., Iovino, A., La Franca, F., and Nota, A., 1989, *Astron. Astrophys. Suppl.* **77**, 161

Cristiani, S., and Vio, R., 1990, *Astron. Astrophys.* **227**, 385

Cristiani, S., Vio, R., Andreani, P., 1990, *Astron. J.* **100**, 56

Iovino, A., Shaver, P.A., Osmer, P.S., Hewitt, P., Crampton, D., Cowley, A.P., Hartwick, F.D.A., Barbieri, C., Cristiani, S. 1989, in *Large Scale Structure and Motion in the Universe*, Mezzetti *et al.*eds., pg. 369

Pons Borderia, M., Iovino, A., Bonometto, S. 1990, Search of the 3-point Correlation Function for Quasars, submitted to *Astron. J.*

THE SELECTION OF EXTRAGALACTIC SOURCE SAMPLES FROM THE IRAS DATABASE

E.J.A. Meurs[1], H.-M. Adorf[2]

[1]Max-Planck-Institut für Extraterrestrische Physik
Giessenbachstraße
D-8046 Garching b. München, FRG

[2]Space Telescope - European Coordinating Facility
European Southern Observatory
Karl-Schwarzschild-Straße 2
D-8046 Garching bei München, FRG

ABSTRACT

A very homogeneous and almost complete view of the sky at infrared wavelengths was provided by the IRAS sky survey. For infrared studies of the large-scale structure in the distribution of galaxies it is important to establish samples of extragalactic sources which are as unbiased and complete as possible. We discuss the selection of such samples from the IRAS Point Source Catalog, employing methods from multivariate statistics and decision theory. An essentially unbiased and complete selection may be used to assess features present in the large-scale structure of galaxies, to attempt to include regions near the Galactic Plane, to determine the IRAS dipole and to address further cosmological questions.

Introduction

The study of the large-scale distribution of galaxies requires a galaxy sample with a high degree of homogeneity as well as large sky coverage. The infrared sky survey carried out by the IRAS satellite provides a database with such properties and it is obviously interesting to extract the extragalactic sources it contains using a suitable selection method. On the basis of their infrared colours several object categories may, in fact, be distinguished among the IRAS sources. The application of statistical inferencing techniques allows to discriminate between different categories in a fairly objective way.

Studies of the overall contents of the IRAS Point Source Catalog (IPSC) have shown that stars generally are bright at 12 and 25 μm, while galaxies rather show up at 60 and 100 μm (see ref. 3, hereafter MH). Thus we selected from the IPSC (Version II) the sources with high or moderate quality fluxes at 60 and 100 μm. The resulting distribution of data points can be broken up into distinct categories of sources (stars, "Cirrus", "Thin Plane" and extragalactic sources) by putting limits to the IRAS colours and including the flux at 100 μm (utilizing their distribution in galactic coordinates, see MH for details). An objective discrimination between these different types of sources may be obtained by applying multivariate statistical techniques combined with methods from decision theory.

Source selection

Sets of sources representative of the different source categories were used to train a Bayesian statistical classifier[1,4]. We employed as "features" the three flux ratios ("colours") 12/25, 25/60, 60/100 and the flux at 100 μm. Here the colours are defined as $C_{mn}=\log(F_m/F_n)$, where F_1 is the flux in band 1 (12 μm), etc. The maximum likelihood (ML) classification criterion was invoked to determine (hyper-)surfaces discriminating between the class-specific distributions of these data points in feature space. After this, all 33435 pre-selected IPSC sources could be classified into the relevant source categories. The resulting classification can be judged from the class-specific distributions on the sky and in feature space.

The classification errors were further reduced (in a statistical sense) by using the maximum a-posteriori (MAP) classification strategy, capable of taking into account the relative importance of each category, as specified by the number of sources selected by the ML-classifier. For illustration, the following table details the number of sources that changed class, from the ML-class given by the column to the MAP-class given by the row.

#ML / #MAP	1	2	3	4	total	
1	14192	30	314	68	14604	**1: Galaxies**
2	0	5603	0	20	5623	**2: Thin Plane**
3	0	522	10547	148	11217	**3: Cirrus**
4	0	0	0	1991	1991	**4: Stars**
total	14192	6155	10861	2227	33435	

The region of the feature space where extragalactic objects occur is characterized by the centre coordinate (C_{12}, C_{23}, C_{34}, log F_4) = (-0.0507, -0.492, -0.337, 0.349) and the variance-covariance matrix of the Gaussian density function fitted to the distribution of data points in this class.

Extragalactic sources

The sky distribution of our MAP-selected extragalactic objects (ref. 5, Fig. 1) shows several larger features which are also visible on maps constructed from optical data (see also MH): galaxy chains and clusters, and the Supergalactic Plane. The zone of avoidance (probably originating from source confusion rather than extinction) is restricted to an elliptically shaped region with semi-axes of ~90° and ~12°, much smaller than in the optical, where the zone is a ~15° wide band extending all over the sky. The IRAS extragalactic sky displays a high degree of homogeneity, whereas optically the boundaries between different catalogues are discernible (cf. MH, Fig. 2f). The impression of homogeneity is enhanced by two other factors, namely that the IPSC data refer almost exclusively to spirals, which are less clustered than ellipticals, and that the infrared luminosity function of galaxies is broader than the corresponding optical one. MH discuss, for a selection closely resembling the present one, how the success rate of a classification of extragalactic objects may be estimated.

Applications, including cosmological issues

A selection as derived here may be used (i) to assess large-scale structure in the distribution of galaxies, (ii) to follow such structures closer to the Galactic Plane than is possible with optical data, (iii) to address cosmological questions, and (iv) to select conveniently samples for observations at other wavelengths. Examples of cosmological studies on the basis of a sample of extragalactic IPSC objects include determination of the dipole anisotropy in the distribution of galaxies (e.g. ref. 2), determination of the total infrared background due to galaxies, a search for any Great Attractor, the relation of the IRAS galaxy distribution to the Supergalactic Plane, and comparative studies of IR and optical galaxy correlation functions. In general, the homogeneity of an extragalactic IPSC sample should be a feature of interest when considering observational work at other wavelengths. Note that a greater range of subjects may be studied when redshifts become available (cf. the contributions by Davis and Bertschinger).

References

1) Adorf, H.-M., Meurs, E.J.A., 1988, in: "Large-Scale Structures in the Universe --- Observational and Analytical Methods", W.C. Seitter, H.W. Duerbeck and M. Tacke (eds), Lecture Notes in Physics 310, Springer-Verlag Heidelberg, p. 315.
2) Harmon, R.T., Lahav, O., Meurs, E.J.A., 1987, *Mon. Not. Royal Astron. Soc.* **228**, 5P.
3) Meurs, E.J.A., Harmon, R.T., 1988, *Astron. Astrophys.* **206**, 53.
4) Meurs, E.J.A., Adorf, H.-M., Harmon, R.T., 1988, in: *Proc. ESO Conf. "Astronomy from Large Databases: Scientific Objectives and Methodological Approaches"*, Garching, Oct. 1987, F. Murtagh and A. Heck (eds), p. 49.
5) Meurs, E.J.A., Adorf, H.-M., Harmon, R.T., 1990, in: *"The Galactic and Extragalactic Background Radiation"*, S. Bowyer and Ch. Leinert (eds), IAU Symp. **139**, Kluwer Academic, p. 383.

THREE-DIMENSIONAL REALIZATIONS OF DYNAMICALLY THRESHOLDED PANCAKE MODELS

T. BUCHERT & R. KLAFFL

Max-Planck-Institut für Astrophysik
D-8046 Garching/Munich, F. R. G.

Abstract

We present first results of a three-dimensional simulation of pancake models for galaxy formation that is large enough to allow the study of both large- and small-scale cosmogonic features. The inherent flexibility of the model allows the construction of a phenomenological link between large-scale structure and the galaxy formation process itself.

Pictures are shown for different possibilities of density thresholding implying different assumptions for the formation history of a galaxy.

1. The Model

The model is based on two extensions of the standard pancake picture:

First, we add parameter freedom on small scales by introducing a local (Lagrangian) control parameter space (δ,τ,b): It controls the formation of luminous matter in the model. As structural discriminators between dark and luminous matter we use the density contrast (δ) together with a characteristic time of formation (τ), both determined along particle trajectories. The characteristic scale (b) of luminous objects is determined by the spatial resolution of the large-scale model and can be related to the size and/or the spatial separation of thresholded objects (see Buchert 1990a,b; Buchert et al. 1990). The characteristic time is mapped, for simplicity, into different types of threshold selection methods, which are related to different assumptions for the formation process into luminous lumps. Results of a two-dimensional calculation show that not only the amplitude, but also the slope of the two-point correlation function is affected and changes with different threshold values as well as different selection methods. Moreover, different threshold mechanisms give different spatial regimes, where the correlation function can be considered to obey a scaling law with power index -1.8 (see the related contribution by T. Buchert).

Second, we prefer to consider very large samples (Gpc scales) to assure 'statistical fairness' in order to match normalizations to the spatial distribution of clusters properly. We then adjust the small-scale structure characteristics like the correlation function or the density contrast of galaxies by using control parameters. The resulting effect of phase correlations of a large number of harmonics in the spectrum gives very extended structures as well as considerable deviations of statistical properties of CfA-sized subsamples compared to the whole sample. This again adds *flexibility* to the model with respect to the measurement of structures (see Buchert et al. 1990).

Both extensions might rescue the neutrino-model from oblivion. They imply that we can assign mildly non-linear stages to the present epoch (not later than the starting time of back-oscillation of particles onto pancakes at the border of validity of 'Zel'dovich-type' approximations).

2. Three-dimensional Realizations

Pictures of some first three-dimensional realizations (n=+1 power law spectrum with cut-off (at wavelength λ_{min}), 128^3 particles, $\delta_{lin}(Z=0)=1$, $\delta_{rms}(Z=0)=1$ on the scale $\lambda_{min}/5$) give an impression of the distribution of thresholded particles according to three different selection methods (*Fig.1*). We plan to enlarge the total box size as well as the particle resolution in order to extract ensembles of subcubes from the whole sample for the purpose of statistical comparison. Thereby we use advantages of the analyticity of the model, which needs e.g. only about 1 minute CPU-time on a CONVEX C220 using FFT to realize a box of the sort shown in *Fig.1*. Note that even in the comparatively small box

volume with $\lambda_{box} = 12\lambda_{min}$ and the "harmless" $n = +1$ power spectrum, we observe *walls* with extensions up to $4\frac{1}{2}$ cut-off lengths.

We like to thank P. Schiller for helpful discussions during the planning stage of this work and G. Börner for stimulating remarks. TB likes to thank B.J.T. Jones for fruitful cooperations concerning this project. TB acknowledges financial support by DFG (Deutsche Forschungsgemeinschaft).

References

Buchert T. (1990a): Rev. Mod. Astron. **2**, p.267.
Buchert T. (1990b): Astrophys. Sp. Sci., in press.
Buchert T., Jones B.J.T., Appel L. (1990): in preparation.

Figure Captions

Figs.1a,b,c: Shown is the whole box containing a thresholded sample (threshold was 50 - only bright galaxies) using the types P,A and D (see the related contribution by T. Buchert).

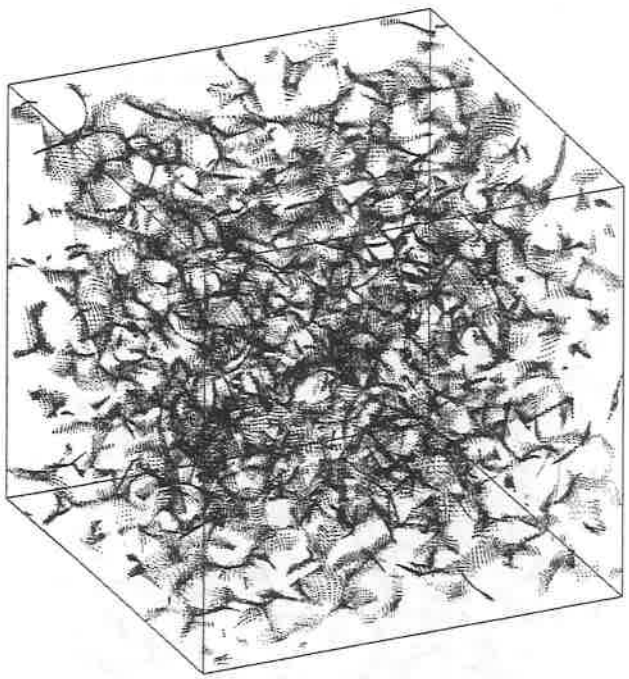

Fig.1a: Threshold type P

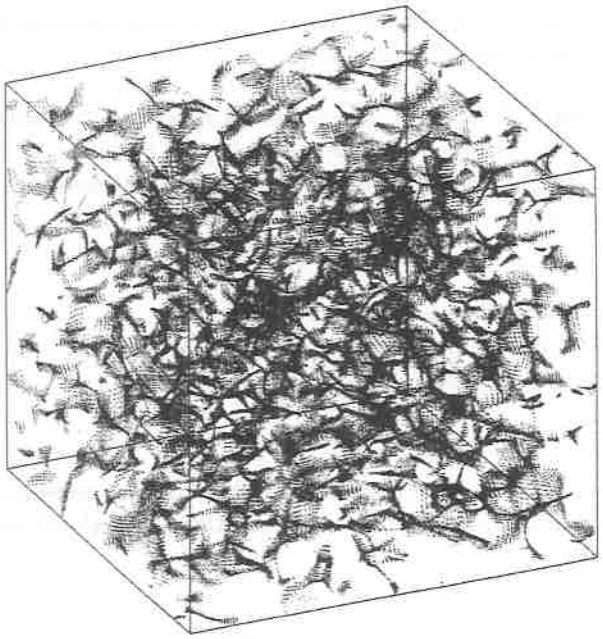

Fig.1b: Threshold type A

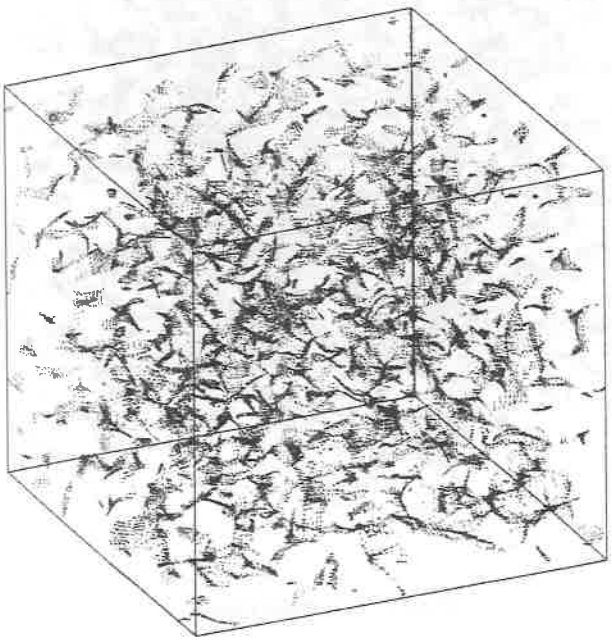

Fig.1c: Threshold type D

THE LAS CAMPANAS DEEP REDSHIFT SURVEY

Robert P. Kirshner
Harvard-Smithsonian Center for Astrophysics

Augustus Oemler, Jr.
Yale University Observatory

Paul L. Schechter
Massachusetts Institute of Technology

Stephen A. Shectman
The Observatories of the Carnegie Institution of Washington

Douglas L. Tucker
Yale University Observatory

ABSTRACT

We have begun a large-scale survey of the distribution of galaxies using a multi-object fiber spectrograph on the Las Campanas 2.5 meter DuPont Telescope. When complete, this survey will map the distribution of galaxies to redshifts of 0.2 in a pattern of fields, each 1.5^{o} x 3.0^{o} in size, which cover both galactic polar caps with a filling factor of about 25 percent.

As of the Fall of 1990, we have obtained photometry, using CCD drift scans, of 130 fields. We have measured redshifts of about 3600 galaxies in 40 fields. These delineate voids, lumps, and filaments with scales up to at lease $50h^{-1}$ Mpc. A preliminary calculation of the two-point galaxy correlation function suggests $\xi(r) \sim (r/r_o)^{-1.8}$, where $r_o \sim 6h^{-1}$ Mpc. This is similar to previous determinations, but has much greater reliability, because of the very long baseline of separations available in this survey.

MOTIVATION

The spatial distribution of galaxies remains both the prime motivation and the primary test of theories of the origin and growth of structure in the universe. Over the past fifteen years, great effort has been devoted to characterizing that distribution with larger and larger surveys of the redshifts of galaxies. This effort has revealed many intriguing features of the galaxy distribution, but has not, so far, contributed much to our understanding of the formation of structure. It is clear that much more data are needed, including data on the very large-scale distribution of galaxies. Such large-scale information will greatly improve constraints on the shape of the density fluctuation spectrum. It can provide a direct test of the cosmological principle. The large volumes encompassed by such observations allow one to study the occurrence of rare features, such as large voids, whose incidence may vary dramatically between clustering models.

TECHNIQUE

Surveying large volumes requires redshifts of large numbers of rather faint galaxies. Obtaining such data has been made practical by the recent introduction of multi-object fiber spectrographs, capable of observing tens of spectra at a time. The Las Campanas 2.5 meter DuPont Telescope, with a field of view of 2.1^{o}, is unexcelled in its potential for such work. We have constructed a multi-object fiber system for this telescope to carry out a redshift survey covering the two galactic polar caps to redshifts of about 0.2. When complete, this survey will include redshifts for between 15,000 and 20,000 galaxies, and will provide information on structures with scales of up to $1000h^{-1}$ Mpc.

Despite the increased efficiency of fiber systems, we cannot hope to survey all of both galactic caps to these depths. Instead, we have covered the caps with an array of fields whose covering factor is about 25 percent. Each field is 3^{o} wide and 1.5^{o} high, twice the area of the DuPont fiber field. The fields are laid out in a checkerboard pattern, with several declination strips completely filled to provide continuous sampling. Galaxy photometry and astrometry in the fields is performed from CCD drift scans, obtained using TI 800 x 800 and, more recently, Ford 2048 x 2048 detectors on the Swope 1.0 meter telescope. Each field is covered by 7 overlapping strips. From these, we obtain R photometry of the galaxies, accurate to about 0.07 mag, and equatorial coordinates, with accuracy in each axis of about 0.1 arc sec. Calibration of the positional system is performed using the HST Guide Star Catalog.

Redshifts are measured on the DuPont Telescope using a fiber system which feeds the standard Boller and Chivens spectrograph with 2D-Frutti detector. Our present system is based on plug-plates and permits the use of 60 fibers: 50 for galaxies and 10 for sky background. Next year we expect to increase that number to 100 fibers, and, in two years, after construction of a new spectrograph, to 200. With 2 hour exposures per field, we can typically observe 4 fields per night. Our present redshift yield is between 85 and 90 percent.

The selection of the galaxy sample is somewhat different than that in most redshift surveys, because of the desirability of maximizing the efficiency of the fiber spectroscopy. We want to always observe as many galaxies as there are fibers, and want them to have a small range of brightness, so that good spectra of all can be obtained with one exposure. Our sample is drawn from all galaxies with $16.0 < R < 17.3$, excluding a small (~15%) fraction of very low central surface brightness. If the number of such objects per DuPont field is larger than the number of fibers, we choose a random subset. If it is smaller, we enlarge the magnitude range to produce the required number.

PRELIMINARY RESULTS

As of November 1990, we had obtained photometry of 130 fields, and had measured the redshifts of about 3600 galaxies. Only a preliminary analysis of the data has been undertaken. One difficulty with this analysis has been in the determination of the galaxy luminosity function, which is needed before any study of the galaxy space distribution can be performed. Our rejection of the lowest surface brightness objects has produced a sample with a luminosity function different than that usually found, because of the systematic exclusion of low luminosity spirals and irregulars. Furthermore, the narrow magnitude range of our sample has significantly reduced the efficiency of the methods we have previously used[1] to determine the luminosity function. As a result, our present estimate of $\phi(L)$ is rather uncertain, despite the large sample size.

Despite this, the basic properties of the galaxy clustering are clear. The two-point correlation function is well fit by the usual $r^{-1.8}$ power law, with a correlation length of approximately $6h^{-1}$ Mpc. The very long baseline of pair separations available in this deep three-dimensional sample will permit us to delineate the large-scale behavior of $\xi(r)$ much better than any previous survey. What that behavior will turn out to be is not yet clear: our present data show very different behavior on scales greater than $15h^{-1}$ Mpc in the two galactic polar caps. Whether this is due to sampling statistics, or to a real difference in clustering in these two volumes of the universe has not yet been established.

The qualitative nature of the galaxy distribution is very similar to that previously delineated in much smaller volumes by Geller and Huchra[2]. There are lumps, voids, filaments and sheets with scales of at least $50h^{-1}$ Mpc, and perhaps much more. There are hints of very large scale ($200h^{-1}$ to $500h^{-1}$ Mpc) density variations, but confirmation of these will require many more redshifts, and a firmer determination of the luminosity function.

REFERENCES

1) Kirshner, R.P., Oemler, A., and Schechter, P.L. 1979, *Astron. J.*, **84**, 951.

2) Geller, M.J., and Huchra, J.P. 1989, *Science*, **246**, 897.

A VLA HI SURVEY OF THE PERSEUS-PISCES REGION: STUDYING LOW-LUMINOSITY DWARF GALAXIES

P. GUHATHAKURTA[1]

Institute for Advanced Study
Olden Lane, Princeton, NJ 08540, USA.

ABSTRACT

We present preliminary results of a VLA 21-cm survey of the Perseus-Pisces supercluster and a foreground void. The survey is aimed towards detecting gas-rich dwarf galaxies that may be optically faint. Equal volumes ($\sim 100\mathrm{Mpc}^3$) were searched in each of the supercluster and void, down to a conservative detection threshold of about $10^8 M_\odot$ of neutral hydrogen (HI). A total of 17 objects were detected in the supercluster, ten of these being previously uncatalogued dwarf galaxies. No galaxies were detected in the void. This indicates that dwarfs have a large-scale distribution similar to that of bright galaxies, although our data does not rule out a moderate "bias" between dwarf and bright galaxy spatial number density contrasts. The dwarfs in the supercluster show a clear preference for being near bright galaxies. The number of galaxies detected in the supercluster is somewhat smaller than that expected from a naive extrapolation of the optical (Schechter) luminosity function. Our results do not allow the existence of a large population of HI-rich dwarfs that could have been missed by conventional, optical galaxy catalogues. Even the uncatalogued objects mostly have optical counterparts that are barely visible on the Palomar Sky Survey plates.

[1] In collaboration with D. H. Weinberg (Univ. of California, Berkeley), A. Szomoru (Univ. of Groningen), and J. H. van Gorkom (Columbia Univ.).

Our VLA 'D' array survey covers two regions: (1) 12 $1° \times 1°$ fields, each spanning $1000\,\mathrm{km\,s^{-1}}$, centred on the velocity of the Perseus-Pisces supercluster ($5100\,\mathrm{km\,s^{-1}}$), and (2) 30 similar sized fields centred on the redshift ($3500\,\mathrm{km\,s^{-1}}$) of a foreground void. No galaxies were detected in the void; Table 1 shows the detections in the supercluster. Thus, dwarfs do *not* fill in the void delineated by bright galaxies. The observed number of dwarfs in the supercluster is somewhat smaller than that predicted by extrapolating the Schechter luminosity function. Our results appear *not* to support scenarios where a significant fraction of these dwarfs are missed by existing optical catalogues because they are in a faint, dormant state between starbursts. A more complete report of our survey will appear in a future paper[1].

1. Weinberg, D. H., Szomoru, A., Guhathakurta, P., van Gorkom, J. H., Fruchter, A. S., and Gunn, J. E. 1991, *Ap. J. (Lett.)*, in preparation.

No.	v_{hel} km s^{-1}	Δv km s^{-1}	M_{HI} $10^8 M_\odot$	V_{det} Mpc^3
1[a]	4948	100	5.6	66
2	4994	140	3.4	54
3[b]	4962	311	52.6	87
4	4850	120	5.3	65
5	5226	42	1.0	18
6[b]	5070	469	29.9	85
7	4998	100	3.6	56
8	5110	81	2.0	40
9	5477	102	4.9	63
10	5326	75	3.9	58
11[b]	5017	295	5.4	66
12[a]	5224	222	5.1	64
13[a]	4843	115	24.2	84
14[b]	4976	465	44.4	86
15	4882	58	5.4	66
16	4792	155	6.1	68
17	5046	66	2.2	42

[a] optically catalogued galaxy
[b] target galaxy (optically bright)

Table 1: The HI detections in the 12 supercluster fields. Five of these fields contain a bright target galaxy. All but the last three dwarfs were detected in the targeted fields. The last column shows the survey volume within which a galaxy of this mass *could* have been detected.

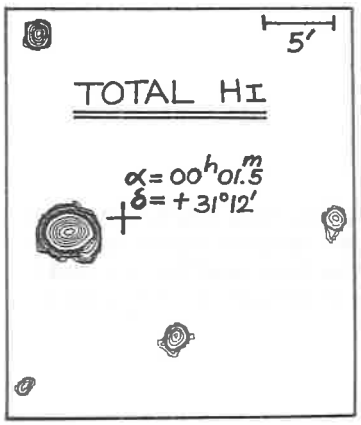

Figure 1: An HI column density map of one of the supercluster fields. The big galaxy (UGC26) contains $5 \times 10^9 M_\odot$ of gas, while the smallest of the four dwarf galaxies has $10^8 M_\odot$. The dwarfs follow the large-scale structure defined by the bright galaxies (none detected in the void), and live near bright galaxies in the supercluster.

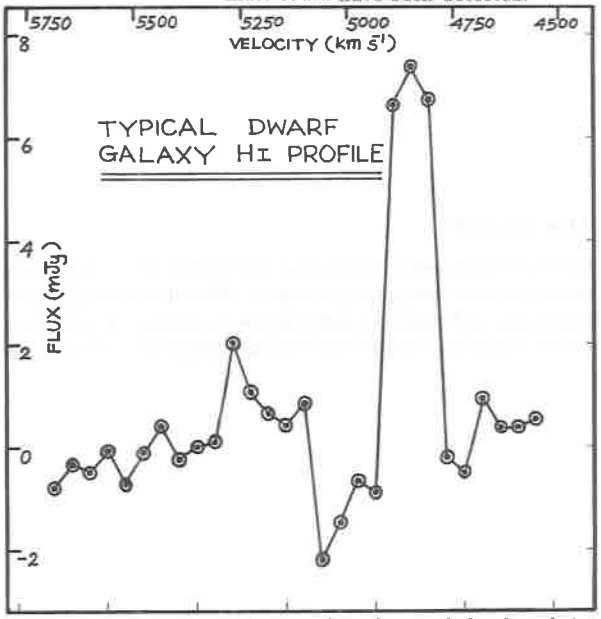

Figure 2: The 21-cm line profile of one of the dwarfs in Figure 1 that contains $5 \times 10^8 M_\odot$ of HI. Its line shape, velocity width, and HI mass are typical of the dwarf galaxies found in our survey. Of the 10 uncatalogued dwarfs detected, most have faint, but visible optical counterparts.

SEGREGATION ANALYSIS OF THE CfA CATALOGUE

R. DOMINGUEZ-TENREIRO [1] and V.J. MARTINEZ [2]

[1] Departamento de Física Teórica, Universidad Autónoma de Madrid, Cantoblanco, 28049 Madrid, Spain.
[2] Departament de Matemàtica Aplicada i Astronomia, Universitat de València, Burjassot, 46100 València, Spain.

ABSTRACT

The luminosity and morphological segregation of several galaxy samples drawn from the CfA redshift survey has been analyzed by means of different statistical descriptors: correlation function, generalized dimensions and minimal spanning tree technique. In any case, it has been found that these samples exhibit luminosity and morphological segregation, and both kinds of segregation are not correlated.

Large-scale segregation of luminosity is an important observational test for some biased galaxy formation models [1,2]. An exhaustive study of the CfA galaxies segregation (both morphological and of luminosity) has been carried out by means of the following statistical descriptors:

a) Two-point correlation function.

b) Generalized dimensions [3].

c) Minimal spanning tree technique (MST for short).

The MST of a set of N points is the unique network of $N-1$ edges (each linking two points) such that it provides a path between any pair of points without closed loops and satisfies the condition that the sum of the lengths of the edges is minimum. The MST has been introduced in Astronomy in the study of large-scale filamentary structures [4]. Here we use this technique in the study of the clustering properties of galaxies with different luminosity and morphological type. We present the histograms corresponding to the distribution of the MST branches for the galaxy samples specified in Table 1 (luminosity segregation analysis, Figures 1a and 1b) and Table 2 (morphological segregation analysis, Figures 2a and 2b).

Table 1: *Samples for the study of the luminosity segregation.*

sample	$V_{\rm min}$	$V_{\rm max}$	$M_B^{\rm max}$	$M_B^{\rm min}$	n. gal.
$S0017B$	0	1,700	-18.10	$-\infty$	251
$S0017F$	0	1,700	-16.65	-18.10	255
$S1765B$	1,700	6,500	-19.94	$-\infty$	179
$S1765F$	1,700	6,500	-19.56	-19.94	180

Table 2: *Samples for the study of the morphological segregation.*

sample	$V_{\rm min}$	$V_{\rm max}$	T (type)	n. gal.
$S0017E$	0	1,700	$T \leq 0$	157
$S0017S$	0	1,700	$T \geq 1$	349
$S1765E$	1,700	6,500	$T \leq 0$	115
$S1765S$	1,700	6,500	$T \geq 1$	244

Luminosity segregation is apparent in Figure 1b corresponding to the distant sample. Brighter galaxies are more clustered than fainter ones. No significative segregation appears in Figure 1a (close sample). By contrast, both the close and the distant sample exhibit morphological segregation, with the $T \leq 0$ type galaxies more clustered than the $T \geq 1$ type galaxies. The results of the analysis by means of the statistics a) and b) are in agreement with these Figures and suggest that:

i) A critical absolute magnitude exists $M_c \approx -20$ ($H_0 = 100$ km s^{-1} Mpc $^{-1}$) such that galaxies brighter than M_c are more clustered than fainter ones.

ii) Luminosity and morphological segregation are statistically independent.

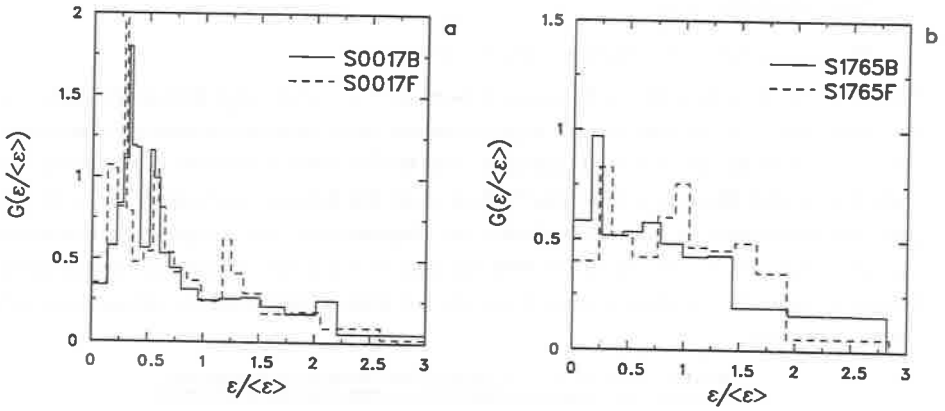

Figure 1: *Histogram of the distribution function of the MST branches for the analysis of the luminosity segregation, a: close sample, b: distant sample.*

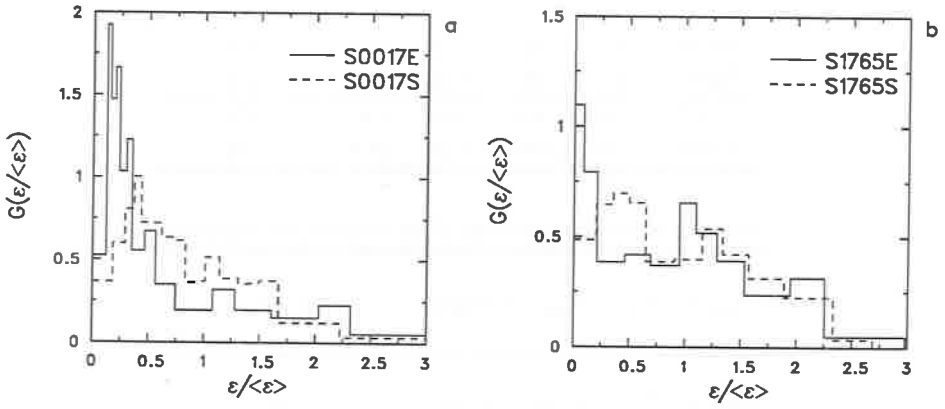

Figure 2: *Histogram of the distribution function of the MST branches for the analysis of the morphological segregation, a: close sample, b: distant sample.*

REFERENCES

1) Kaiser, N., 1984 *Ap. J. Lett.* **284**, L9.

2) Bardeen, J.M., Bond, J.R., Kaiser, N., and Szalay, A.S., 1986, *Ap. J.* **304** , 15.

3) Domínguez-Tenreiro, R., and Martínez, V.J., 1989, *Ap. J. Lett.* **339**, L9.

4) Barrow, J.D., Bhavsar, S.P., and, Sonoda, D.H., 1985 *M.N.R.A.S.* **216**, 17.

MEAN FIELD CORRELATIONS IN THE CORE OF RICH GALAXY CLUSTERS

V. J. MARTINEZ [1], J. A. LOPEZ [2], B.J.T. JONES [3] and E. SAAR [4]

[1] Departament de Matemàtica Aplicada i Astronomia, Universitat de València, 46100 Burjassot, València, Spain.
[2] The Niels Bohr Institute, Blegdamsvej 17, DK-2100 Copenhagen, Denmark.
[3] NORDITA, Blegdamsvej 17, DK-2100 Copenhagen, Denmark.
[4] Tartu Astrophysical Observatory, Toravere 2202444, Estonia, USSR.

ABSTRACT

We develop a theory for the contribution to the clustering correlation function from gravitational interactions of neighboring pairs of galaxies in clusters. If the galaxies are merely test particles, then we would expect their distribution to be a Poisson distribution, following the mean cluster density profile. If on the other hand all of the mass lay in the galaxies, they would interact pairwise and we might hope to see that as a non-Poisson contribution to the distribution of pairs of galaxies in the cluster core. This would manifest itself as a non-zero two point correlation function of the galaxy distribution relative to the smoothed out cluster background.

The problem is to quantify the effect: by how much is the two point correlation function (measured relative to the mean cluster background) enhanced by galaxy - galaxy interactions? The following simple argument motivates our approach. By measuring the small scale excess clustering due to gravitational interactions between galaxies one can estimate the mass to light ratio of individual galaxies in the core of rich clusters. For this purpose we exploit a technique used in statistical physics which is consistent even without the assumption of thermal equilibrium. This is based on the "hypernetted chain equation", a self-consistent integral equation relating the correlation function to the interaction potential.

The "Hyper-netted Chain" equation (HNC for short) gives an approximation to the induced two-point correlation function as an easily solvable integral equation involving the interparticle potential. The basic idea behind the HNC approximation comes from the ansatz of Ornstein and Zernike [1] that the correlation function for a system of N particles could be represented by an integral equation

$$\xi(r_{12}) = c(r_{12}) + \rho \int c(r_{13})\xi(r_{23})d\vec{r}_3 \tag{1}$$

Here $c(r_{12})$ describes the effect of the short ranged two body correlations, it is the so-called direct correlation function. The second term is a convolution of correlation functions and measure the influence between the two particles through a third one, which represents the medium, by averaging over all its possible positions and weighting with the number density ρ. This term contains the effect of long ranged correlations. Equation (1) is open in the sense that it involves two unknown correlation functions, $c(r)$ and $\xi(r)$. We need to express one in terms of the other in order to give self-consistency to equation (1). The HNC ansatz is

$$c(r_{12}) = g(r_{12}) - 1 - \ln(e^{\Phi(r_{12})/T} g(r_{12})) \tag{2}$$

where $g(r) = \xi(r) + 1$ and $\Phi(r)$ and T stand for the interaction potential and temperature of the system. By substituting (2) in equation (1) we get the hyper-netted integral equation,

$$g(r_{12}) = \exp\left\{-\Phi(r_{12})/T + \rho \int [g(r_{13}) - 1 - \ln g(r_{13}) - \Phi(r_{13})/T]\,[g(r_{23}) - 1]\,d\vec{r}_3\right\} \tag{3}$$

Using an iterative method one can solve this integral equation to find an approximation to $\xi(r_{12})$. Rewriting this expression as

$$g(r_{12}) = e^{-\Phi(r_{12})/T} e^{N_{12}} \tag{4}$$

where

$$N_{12} = \rho \int [g(r_{13}) - 1 - \ln g(r_{13}) - \Phi(r_{13})/T]\,[g(r_{23}) - 1]\,d\vec{r}_3 = \rho \int [g(r_{13}) - 1 - N_{13}]\,[g(r_{23}) - 1]\,d\vec{r}_3 \tag{5}$$

We can now Fourier transform this last result to obtain, after some manipulation,

$$\overline{N} = \rho \left[\overline{g - 1 - N}\right]\,\overline{[g - 1]} \tag{6}$$

where the bar denotes the Fourier transform. The HNC integral equation (3) can then be solved for $g(r)$ using expressions (4) and (6) iteratively. For example, setting $N^{(o)} = 0$ as an initial guess, we obtain $g^{(o)} = \exp(-\Phi(r)/T)$ and get the next approximation

$$N^{(1)} = \overline{\rho \left[g^{(o)} - 1\right]^2} \tag{7}$$

This iteration is continued until convergence on $g(r)$ is obtained. This method allows us to calculate $g(r)$ for given values of ρ and T which are the only input parameters aside from the shape of the gravitational potential.

In summary, we think of the central regions of a cluster as an ensemble of galaxies, each of mass m, with overall number density ρ and temperature T, and use the HNC equation to obtain the corresponding $g(r)$ of this body. Next we apply this formalism to the core of Coma cluster. We select our galaxy sample from the CfA redshift survey [2] as consisting of the 260 galaxies within 4 degrees of

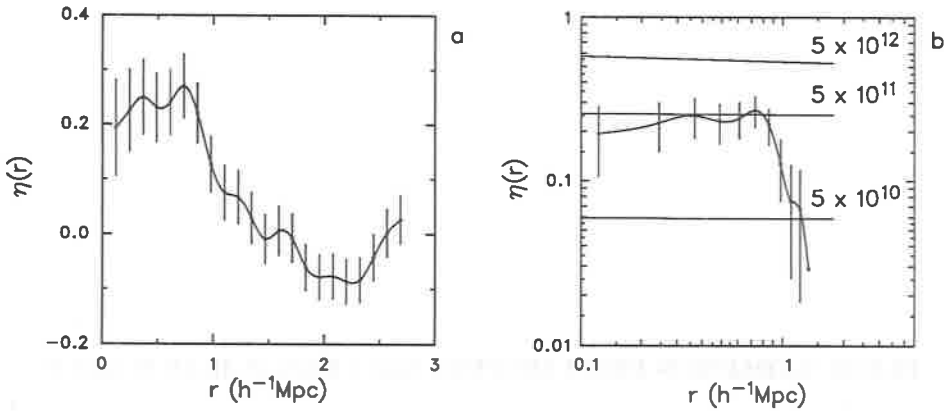

Figure 1: a: *Projected two-point correlation function of the Coma cluster.* b: *Comparison of projected HNC correlations with the observed one.*

the cluster center having velocity in the range $3650 + 500\theta < v < 10000 - 500\theta$, θ being the projected distance from the cluster center in degrees.

In Fig. 1a we show the projected two-point correlation function $\eta(r)$ calculated for our data sample. This calculation has been performed using a larger catalog with the radial profile chosen to fit the observed one. $\eta(r)$ is clearly seen to be positive in the core region. To apply the HNC formalism to the Coma cluster we use the values of the data sample: $\rho = 18$ gal/Mpc^3 and a temperature T corresponding to a dispersion velocity [3], $\sigma = 861$ km s^{-1}. We have calculated the three dimensional correlation function $\xi(r)$ using the HNC formalism for three values of the temperature corresponding to setting the mass per galaxy equal to 5.8×10^{10}, 5.8×10^{11}, and 5.8×10^{12} $M_\odot$. $\xi(r)$ always falls off approximately as $r^{-\gamma}$ with γ slightly larger than 1, but the amplitude depends on the choice of the galaxy mass. Its amplification effect will allow us to estimate the dynamical mass attached to the galaxies in the core of the clusters. The uniformity of the slope reflects the gravitational power law and the fact that at those temperatures the density term plays little role.

In order to compare these three dimensional results with the two dimensional excess correlations seen in Fig. 1a, it is necessary to project the theory onto the plane of the sky. We do that by means of the Limber equation. For our case, in which the spatial correlation function can be fitted to a power law of the kind $\xi(r) = Ar^{-\gamma}$ the projected correlation function is given directly by the method of Fall and Tremaine [4]. The projected correlations and the excess correlation are plotted in Fig. 1b. It is clear from this figure that the best fit to the data is provided by a mass per galaxy slightly less than 5.8×10^{11} $M_\odot$. Since the mean luminosity of the galaxies in our sample is 7.4×10^9 $L_\odot$, this gives a mass to B-light ratio of around 80 for our adopted Hubble constant of $H_0 = 100$ km s^{-1}Mpc^{-1}.

REFERENCES

1) Ornstein, L.S., and Zernike, F., 1914, *Pub. Acad. Sci. Amsterdam.*, **17**, 793.

2) Huchra, J., Davis, M., Latham, D., and Torny, J., 1983, *Ap. J. (Suppl.)*, **52**, 89.

3) Rood, H.J., Page, T.L., Kinter, E.C., and King, I.R., 1972, *Ap. J.*, **175** 627.

4) Fall, M. S., and Tremaine, S., 1977, *Ap. J.*, **216**, 682.

FAR-IR RADIATION FROM SEYFERT GALAXIES IN IRAS SURVEY

Wang Tinggui[1], Cheng Fuzhen[1,2], Zhang Jialu[1]
[1] Center for Astrophysics, University of Science and Technology of China, Hefei, China
[2] Center of Astronomy and Astrophysics, CCAST (World Lab.)

Data and Analysis

IRAS observation of active galaxies has already revealed the complication for the infrared radiation from Seyfert galaxies, besides thermal and nonthermal radiation from the active nuclei, there are two important non-nucleus components: contribution from cold matter in the host galaxy disk and star-forming region surrounding the active nuclei (Rodriguez-Espinosa et al. 1986, Helou 1988). But the rule of these components to the IRAS flux is still an open question.

In order to provide some clues to the answer of this question, we collected infrared data of Seyfert galaxies from IRAS observation (Lonsdale et al. 1989), and roughly classify them into four subclasses (cf. Fig.1): (a) straight flat spectra; (b) flat spectra with a bump around 25 μm; (c) straight steep spectra with a bump around 60 μm; (d) steep turnover spectra. The classification shows that Sy2 has higher fraction of B and C than Syl has; the B, C rate as high as 21% and 72% in Sy2 in comparison with 11% and 44% in Syl; Sy2 has similar rate of subclass D as Syl, but lack of subclass A. After classifying IRAS spectra we plot the $\alpha(12/25)$ vs. $\alpha(60/100)$ (Fig.2). It is further illustration of our classification. In the Fig.2 starbursts are also plotted, and obviously they occupy the same region as subclass C.

To support our classification, we also make statistical comparison of the X-ray, broad line and narrow line properties of these subclasses. The results show that the ratios of X-ray, high ionized [OIII], broad lines to far-IR radiation of subclass A,B are higher than those of C,D for both Syl and Sy2 (except that Sy2 has no broad lines), on average. The subclass B shows the same ratios of the X-ray, broad lines to far-IR radiation as subclass A, but higher

$\log([OIII]/L_{fir})$, reddening; subclass C shows some higher ratios of X-ray and lines to far-IR radiation than D. Subclass C, D also show lower ionization than A,B. In far-IR luminosity, subclass D has the lowest value. Subclass C has the same value of the ratio of low ionized narrow lines to far-IR radiation as starbursts, but A,B higher and D lower.

Conclusions and Discussions

We suggest that these statistical results imply: (1) infrared flux of subclass A,B is dominated by nucleus radiation , and of C,D by non-nucleus emission; (2) bump in subclass B is produced by hot dust in NLR; (3) most of far-IR radiation of subclass C may comes from star-forming region; (4) infrared emission of subclass D is strongly influenced by cold matter and cirrus in galactic disk; (5) as compared with Sy1, Sy2 show relative bigger starburst region and more, warmer dust.

As a result of above conclusions, the contribution of non-nucleus components should be subtracted when computing luminosity function of AGNs, and it is not a trivial task. Another consequence is when searching for starforming region around the nucleus, the best candidates may be the subclass C.

Acknowledgements. C.F.Z. would like to thank Profs. Danese and De Zotti for useful discussions and hospitality during his stay at the Padova Observatory. This project was supported in part by the National Natural Science Foundation of China.

REFERENCES

Rondriguez-Epinosa J.M., Rudy R.J. & Jones B. (1986) Ap.J., 309, 76.
Helou G. (1988), In Interstellar Dust, IAU Symposium 135, Santa Clara, July 1988.
Catalogued Galaxies and Quasi-stellar Objects Observed in the IRAS Survey, 1989, eds. Lonsdale C.J., et al.

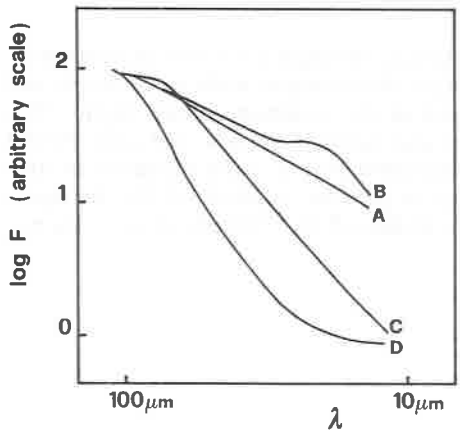

Fig 1. Sketch of four far-IR emission components. A. QSO, B. Hot dust reradiation, C. Starburst, D. Galactic disks.

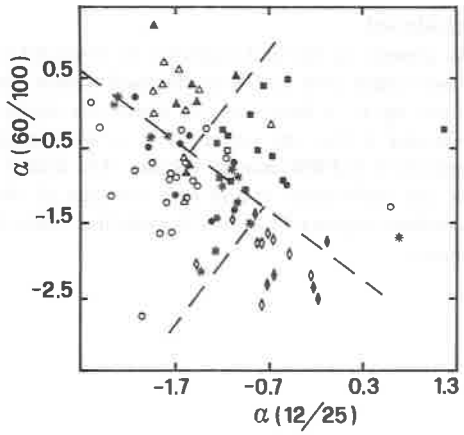

Fig 2. Far-IR color-color plot, $\alpha(12/25)$ vs. $\alpha(60/100)$. The filled symbols refer to Sy1,the open symbols to Sy2. Squares, triangles, circles and diamonds refer to subclasses A, B, C, and D, respectively; asterisks denote starbursts. The dashed lines approximately divide the region into four parts.

THE DISTRIBUTION OF CLUSTERS OF GALAXIES AND THE ISOTROPY OF THE UNIVERSE

R. Scaramella[‖], *G. Vettolani*[†], *G. Zamorani*[◇],

[‖] *Osservatorio Astronomico di Roma, Monteporzio, Italy.*

[†] *Istituto di Radioastronomia CNR, Bologna, Italy.*

[◇] *Osservatorio Astronomico di Bologna, Italy.*

Abstract

We present for the first time firm evidence for the spatial convergence of a cosmological dipole, which bends over and stays flat well within the depth of the sample, while the monopole still grows up to a factor of ~5 times the dipole level at the maximum sample depth. This behavior is the one expected in a homogeneous and isotropic universe and gives further support to a FRW model, besides that from Cosmic Backgrounds. After suitable correction for the differences in the two catalogs of clusters of galaxies (Abell & ACO), the dipole direction appears to be stable pointing towards $\approx$ 25 degs off the CMB dipole apex (LG rest frame).

Sample: Abell & ACO with $z \leq 0.1$ (beyond this distance estimates for Abell become unreliable –see Scaramella *et al.* 1990), $|b| \geq 20^o$, and $R \geq 0$ (~ 860 clusters).

"Monopole" [$\mathcal{M}$] and "Dipole" [$\vec{\mathcal{D}}$] computed by:

$$\mathcal{M} \equiv \sum_i W_i \frac{1}{|\vec{r}_i|^2} \qquad \vec{\mathcal{D}} \equiv \sum_i W_i \frac{\hat{r}_i}{|\vec{r}_i|^2}$$

Weights: $W_i = 1$ (number); $W_i = \phi^{-1}(\hat{r}_i)$ (inverse of selection function); $W_i = N_{g,i}/100$ (Richness w.r.t. a Coma–like cluster — Coma has $N_g = 106$); $W_i = \phi^{-1}(\hat{r}_i)N_{g,i}/100$ (combination of the last two). Correction for obscuration and incompletness: we subtract from $\vec{\mathcal{D}}_{raw}$ the correction $\vec{\mathcal{D}}_{rand}$ obtained from the average of 100 random samples which have same biases as the data have.

RESULTS:

a) A very good convergence of $|\vec{\mathcal{D}}|$ is obtained within the sample depth ($\approx$ 80 % complete in redshift within the convergence length, $\approx 180\, h^{-1}\, Mpc$), while $\mathcal{M}$ keeps steadily growing. That is, **the value of $|\vec{\mathcal{D}}|$ is basically unchanged by adding twice as many clusters as those (~ 300) responsible for the signal.** As seen in Fig. 1, *the general behavior is basically unchanged even when discarding the $R = 0$ class clusters, i.e. by halving the sample.*

b) The correction given by subtracting the random samples changes little the behavior of $|\vec{\mathcal{D}}(r)|$, but nicely fixes its direction: $\hat{\mathcal{D}}$ *stays almost constant even after adding twice as many clusters.* It must be noticed also that this direction happens to be within 25^o from CMB dipole.

DISCUSSION: Much effort has been devoted in the recent past to study the inhomogeneities and anisotropies in the distribution of galaxies surrounding us, especially in connection with the problem of large–scale peculiar flows (see Gunn 1988 for a review). The basic goal has been to determine the depth, d_{conv}, that contains all the matter fluctuations which are responsible for the peculiar motion of the LG w.r.t. the CMB rest frame. Here we want to stress that *the proof of the very same existence of d_{conv} for a set of cosmic objects has as a very important consequence that it is* **operationally** *reached the cross–over point to a homogeneous and isotropic Universe* (cf. Stoeger *et al.* 1987).

The basic problem is the connection between the unobservable matter distribution and that of the cosmic tracers used in the various analyses, i.e. the different amount of biases. This is of course the weakest point in trying to map medium and large scales with clusters of galaxies. These, in fact, can trace only part of the galaxy distribution (the densest spots), and very sparsely. Indeed rich clusters do not trace our nearby surroundings. Clusters are also more correlated among themselves than galaxies are and therefore than matter. However, the non–zero galaxy–cluster correlation function (Seldner and Peebles 1977) indicates that each rich cluster has related to it a large cloud of galaxies and hence traces a mass perturbation

much larger than the typical cluster virialized core. This fact is much more enhanced in the phenomenological model proposed by Bahcall (1986) to explain the difference in amplitude of correlation function of clusters and that of galaxies, although they have same slope.

All the above considerations, however, just strengthen the principal point we made. Indeed **the fact that the distribution of clusters of galaxies is proven to become homogeneous and isotropic on the large scales implys that the same happens to the matter distribution, because the former constitutes a biased subset of latter.**

A fuller discussion of these points, with indications about a low value of Ω_0 will be given elsewhere.

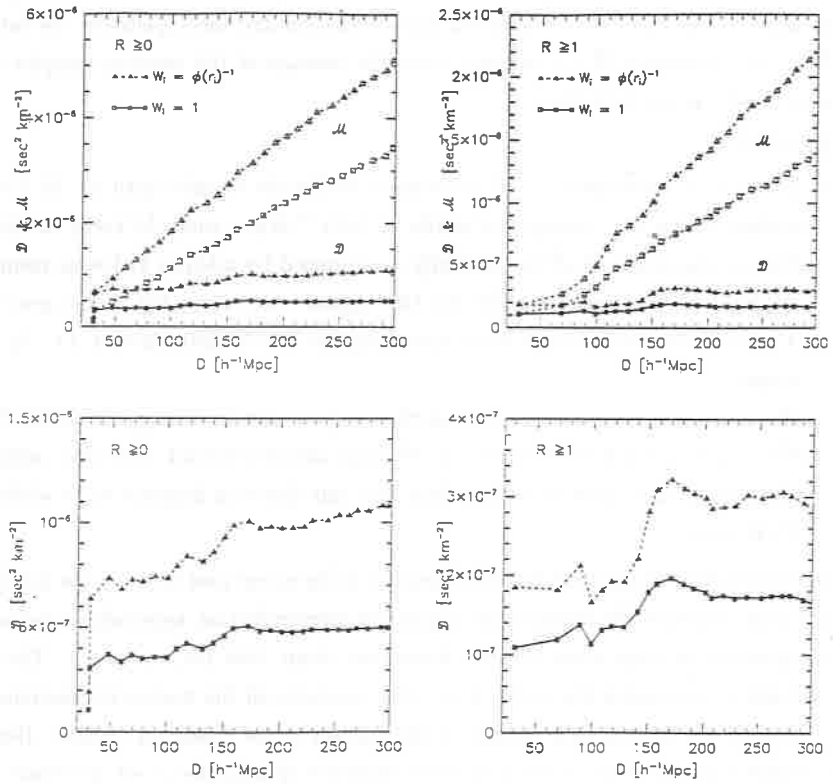

CAPTION Upper panels: both monopole ($\mathcal{M}$) and dipole ($\mathcal{D}$) run with radial distance are shown for two different weights. Only the dipole is shown on an expanded scale on lower panels. Left panels refer to clusters with richness class $R \geq 0$, right panels to those with $R \geq 1$.

REFERENCES

Bahcall, N.A., 1986, *Ap. J. (Lett.)* **302**, L41.

Gunn, J.E., 1988, in *"The Extragactic Distance Scale"*, van den Bergh, S., and Pritchet, C.J., (eds.), ASP Conference Series, 344.

Scaramella, R., Zamorani, G., Vettolani, G., and Chincarini, G., 1990, *A. J.* , in press.

Seldner, and Peebles, P.J.E., 1977, *Ap. J.* **215**, 703.

Stoeger, W.R., Ellis, G.F.R., and Hellaby, C., 1987, *M.N.R.a.S.* **226**, 373.

Author Index

List of Participants

ALIMI Jean-Michel	Observatoire de Meudon D.A.E.C F- 92195 MEUDON PRINCIPAL Cedex FRANCE
ANTONUCCIO Vincenzo	NORDITA Nordisk Inst. für Teor. Atomfysik DK- 2100 COPENHAGEN O DENMARK
BABUL Arif	University of Cambridge Inst of Astronomy CAMBRIDGE CB3 OHA UNITED KINGDOM
BANDAY Anthony	University of Durham Dept of Physics DURHAM DH1 3LE UNITED KINGDOM
BARBIERI Cesare	Osservatorio Astronomico Vicolo Osservatorio, 5 I- 35122 PADOVA ITALY
BARCONS Xavier	Universitad de Cantabria Departamento de Fisica Moderna E- 39005 SANTANDER SPAIN
BARRABES Claude	UFR Sciences Dept de Physique F- 37200 TOURS FRANCE
BENNETT David	University of California Lawrence Livermore Nat. Lab. LIVERMORE CA 94550 USA
BERNARDEAU Francis	CEN Saclay DPhT F- 91191 GIF sur YVETTE Cedex FRANCE
BERTSCHINGER Edmund	M. I. T. Dept of Physics CAMBRIDGE MA 02139 USA
BIRKINSHAW Mark	Harvard University Dept. of Astronomy CAMBRIDGE MA 02138 USA
BIVIANO Andrea	Universita di Trieste Dipartimento di Astronomia I- 34131 TRIESTE ITALY

BLANCHARD Alain	Observatoire de Paris-Meudon Service d'Astrophysique F- 92195 MEUDON PRINCIPAL Cedex FRANCE
BORNER Gerhard	Max Planck Institut für Astrophysik D- 8046 GARCHING FEDERAL REP. OF GERMANY
BOUCHET François	Institut d'Astrophysique de Paris 98 bis Boulevard Arago F- 75014 PARIS FRANCE
BOUQUET Alain	Université Paris VII LPTHE - Tour 16 F- 75251 PARIS Cedex 05 FRANCE
BUCHERT Thomas	Max Planck Institut für Astrophysik D- 8046 GARCHING FEDERAL REP. OF GERMANY
BURBIDGE Geoffrey	University of California San Diego Center for Astrophysics & Space Science LA JOLLA CA 92093 USA
CAMPOS AGUILAR Ana	Instituto de Astrofisica de Andalucia E- 18080 GRANADA SPAIN
CAMPUSANO Luis E.	Universidad du Chile Observatorio Astronomico Nationale SANTIAGO CHILE
CANIZARES Claude	M. I. T. Dept of Physics CAMBRIDGE MA 02139 USA
CARLBERG Raymond	University of Toronto Dept of Astronomy TORONTO M5S 1A1 CANADA
CARR Bernard	Queen Mary & Westfield College Dept of Physics LONDON E1 4NS UNITED KINGDOM
CARROLL Sean	Harvard Smithsonian Center for Astrophysics CAMBRIDGE MA 02138 USA

CESARSKY Catherine	C E N Saclay DPhG/SAp F- 91191 GIF sur YVETTE Cedex FRANCE
CHAMBERS Kenneth	Sterrewacht Leiden Dept of Astrophysics NL- 2300 RA LEIDEN NETHERLANDS
CHENG Fu-Zhen	Univ. of Science & Technology of China Center for Astrophysics HEIFEI Anhui REPUBLIC OF CHINA
CHENG Edward	NASA/Goddard Space Flight Center Code 660 GREENBELT MD 20771 USA
CHU Yaoquan	Univ. of Science & Technology of China Center for Astrophysics HEIFEI Anhui REPUBLIC OF CHINA
COLLINS Christopher	University of Edinburgh Royal Observatory EDINBURGH EH9 3HJ UNITED KINGDOM
COLOMBI Stéphane	Institut d'Astrophysique de Paris 98 bis Boulevard Arago F- 75014 PARIS FRANCE
CORON Noel	Institut d'Astrophysique Spatiale B. P. 10 F- 91371 VERRIERES LE BUISSON FRANCE
DAVIS Marc	University of California Dept of Astronomy BERKELEY CA 94720 USA
de BELLEFON Alain	Collège de France Lab. de Physique Corpusculaire F- 75231 PARIS Cedex 05 FRANCE
DE GANDT François	Observatoire de Paris D A R C F- 92195 MEUDON PRINCIPAL Cedex FRANCE
DE RUJULA Alvaro	CERN TH Division CH- 1211 GENEVE 23 SWITZERLAND

DEKEL Avishai	Hebrew University Recah Institut of Phsyics 91904 JERUSALEM ISRAEL
DEN HARTOG Roland	Sterrewacht Leiden Dept of Astrophysics NL- 2300 RA LEIDEN NETHERLANDS
DOMINGUEZ-TENREIRO Rosa	Universidad Autonoma de Madrid Depto de Fisica Teorica - Mod C-XI E- 28 049 MADRID SPAIN
DOROSHKEVICH Andrei	Institute of Applied Mathematics Miusskaya Square 4, 125047 MOSCOW U S S R
DUBROVICH Victor	Institute of Applied Mathematics Miusskaya Square 4, 125047 MOSCOW U S S R
DUBRULLE Bérengère	Observatoire de Toulouse 14 avenue E. Belin F- 31400 TOULOUSE FRANCE
DUCLOUX Eric	Observatoire de Paris Meudon F- 92195 MEUDON PRINCIPAL Cedex FRANCE
DUNLOP James	School of Physics & Astronomy Faculty of Science PRESTON PR1 2TQ UNITED KINGDOM
FAIRALL Tony	Cape Town University Dept of Astronomy RONDEBOSCH 7700 SOUTH AFRICA
FANG Li Zhi	University of Cambridge Institute of Astronomy CAMBRIDGE CB3 OHA UNITED KINGDOM
FERREIRA Jonathan	Université de Grenoble Groupe d'Astrophysique F- 38041 GRENOBLE FRANCE
FLIN Piotr	Center for Interdisciplinary Studies PAT ul. Augustianska, 7 PL- KRAKOW POLAND

FONG Richard	University of Durham Dept of Physics DURHAM DH1 3LE UNITED KINGDOM
FORT Bernard	Observatoire de Toulouse 14 avenue E. Belin F- 31400 TOULOUSE FRANCE
FORTINI Pierluigi	Universita di Ferrara Istituto di Fisica I- 44100 FERRARA ITALY
FRENK Carlos	University of Durham Dept of Physics DURHAM DH1 3LE UNITED KINGDOM
GELLER Margaret	Harvard College Observatory Center for Astrophysics CAMBRIDGE MA 02138 USA
GERBAL Daniel	Observatoire de Meudon D.A.E.C F- 92195 MEUDON PRINCIPAL Cedex FRANCE
GERBIER Gilles	CEN Saclay DPhPE F- 91191 GIF sur YVETTE Cedex FRANCE
GIRARDI Marisa	SISSA-ISAS Strada Costeria 11 I- 34014 TRIESTE ITALY
GIURICIN Giuliano	Universita di Trieste Dipartimento di Astronomia I- 34131 TRIESTE ITALY
GLAZEBROOK Karl	University of Edinburgh Department of Astronomy EDINBURGH Scotland G 12 8QQ UNITED KINGDOM
GÖKALP Ahmet	Middle East Tech. University Dept of Physics ANKARA TURKEY
GROTH Edward	Princeton University Dept of Physics PRINCETON NJ 08544 USA

GUALDI Carlo	Universita di Ferrara Istituto di Fisica I- 44100 FERRARA ITALY
GUHATHAKURTA Puragra	Institute for Advanced Study School of Natural Sciences PRINCETON NJ 08540 USA
GUNZIG Edgard	Université Libre de Bruxelles Faculté des Sciences BL- 1050 BRUXELLES BELGIUM
GUTIERREZ DE LA CRUZ Carlos M.	Universidad de la Laguna Instituto de Astrofisica de Canarias E- ISLAS CANARIAS SPAIN
GUZMAN DE LA SELVA Enrique	Ruhr-Universität Bochum Institut für Theor. Physik II D- 463O BOCHUM 1 FEDERAL REP. OF GERMANY
GUZZO Luigi	Osservatorio di Breda Via E. Banchi 46 I- 22055 MERATE ITALY
HALPERN Mark	University of British Columbia Dept. of Physics VANCOUVER BC V6T 2A6 CANADA
HARA TeTsuya	University of Kyoto Sangyo Dept of Physics 603 KYOTO JAPAN
HEAVENS Alan	University of Edinburgh Royal Observatory EDINBURGH EH9 3HJ UNITED KINGDOM
HENDRY Martin	University of Glasgow Dept of Physics and Astronomy GLASGOW G12 8QQ UNITED KINGDOM
HENRIKSEN Mark	Applied Research Corporation 8201 Corporate Drive, LANDOVER MD 20785 USA
HICKSON Paul	British Columbia University Dept of Geophysics & Astrophysics VANCOUVER BC V6T 1W5 CANADA

IOVINO Angela	Osservatorio Astronomico di Brera Via Brera 28 I- 20121 MILANO ITALY
ISAACMAN Richard	General Sciences Corp. 6100 Chevy Chase Dr. LAUREL MD 20707 USA
JONES Bernard	Sterrewacht Leiden Dept of Astrophysics NL- 2300 RA LEIDEN NETHERLANDS
KATZ Neal	University of Arizona Steward Observatory TUCSON AZ 85721 USA
KAUFFMANN Guinevere	Cape Town University Dept of Astronomy RONDEBOSCH 7700 SOUTH AFRICA
KLAFFL Robert	Max Planck Institut für Astrophysik D- 8046 GARCHING FEDERAL REP. OF GERMANY
KOCH-MIRAMOND Lydie	C E N Saclay DPhG/SAp F- 91191 GIF sur YVETTE Cedex FRANCE
KRAUSS Lawrence	Yale University Center for Theoretical Physics NEW HAVEN CT 06511 USA
KUZMIN Vadim	Academy Science USSR Inst. for Nuclear Research (INR) 117 312 MOSCOW U S S R
LACEY Cedric	Oxford University Department of Astrophysics OXFORD 0X1 3RH UNITED KINGDOM
LACHIEZE-REY Marc	CEN Saclay Dept d'Astrophysique F- 91191 GIF sur YVETTE Cedex FRANCE
LENA Pierre	Observatoire de Paris Meudon F- 92195 MEUDON PRINCIPAL Cedex FRANCE

LI Shu Xian	University of Cambridge Inst of Astronomy CAMBRIDGE CB3 OHA UNITED KINGDOM
LINDE Andrei	Academic Science USSR (FIAN) P. N. Lebedev Inst. of Physics 117 924 MOSCOW U S S R
LONGARETTI Pierre-Yves	Observatoire de Toulouse 14 Avenue E. Belin 31400 TOULOUSE FRANCE
LUMINET Jean-Pierre	Observatoire de Paris D A R C F- 92195 MEUDON PRINCIPAL Cedex FRANCE
LUMSDEN Stuart	Imperial College Blackett Laboratory LONDON SW7 2BZ UNITED KINGDOM
MADDOX Steve	Oxford University Department of Astrophysics OXFORD 0X1 3RH UNITED KINGDOM
MARTIN-MIRONES Jose Maria	Universitad de Cantabria Departamento de Fisica Moderna E- 39005 SANTANDER SPAIN
MARTINEZ Vicent J.	Universitat de Valencia Depto de Matematica Aplicada i Astronomi E- 39005 SANTANDER SPAIN
MARTINEZ-GONZALEZ Enrique	Facultad de Ciencas Avda. Los Castros Sin Spain 39005 SANTANDER SPAIN
MASANI Alberto	Universita di Torino Istituto di Fisica I- 10125 TORINO ITALY
MATRAVERS David	Portsmouth Polytechnic School of Mathematical Studies PORTSMOUTH PO1 ZEG UNITED KINGDOM
MELCHIORRI Francesco	Universita di Roma "La Sapienza" Dipt di Fisica I- 00100 ROMA ITALY

MELLIER Yannick	Observatoire de Toulouse 14 avenue E. Belin F- 31400 TOULOUSE FRANCE
MEURS Evert	Max Planck Institute for Extraterrestrial Physics D- 8046 GARCHING FEDERAL REP. OF GERMANY
MEYER Stephan	M. I. T. Lab. for Nuclear Science CAMBRIDGE MA 02139 USA
MIRABEL Felix I.	CEN Saclay Dept d'Astrophysique F- 91191 GIF sur YVETTE Cedex FRANCE
MIZONY Michel	Université Lyon I Institut de Mathématiques F- 69622 VILLEURBANNE FRANCE
MO Houjun	Max Planck Institut für Astrophysik D- 8046 GARCHING FEDERAL REP. OF GERMANY
MOLINARI Emilio	Osservatorio Astronomico di Brera Via Brera 28 I- 20121 MILANO ITALY
MOLLER Palle	Copenhagen University Observatory Oster Voldgade 3 DK- 1350 COPENHAGEN DENMARK
MORRISON Douglas	CERN European Organization for Nuclear Res. CH- 1211 GENEVE 23 SWITZERLAND
MOUCHET Martine	Observatoire de Meudon D.A.E.C F- 92195 MEUDON PRINCIPAL Cedex FRANCE
NASH Thomas	FERMILAB Dept of Physics BATAVIA IL 60510 USA
NOTTALE Laurent	Observatoire de Meudon D.A.E.C F- 92195 MEUDON PRINCIPAL Cedex FRANCE

OEMLER Augustus	Yale University Dept of Astronomy NEW HAVEN CT 06511 USA
ORTOLAN Antonello	Universita di Ferrara Istituto di Fisica I- 44100 FERRARA ITALY
PARTRIDGE Bruce	Harverford College Dept of Astronomy HAVERFORD PA 19041 USA
PEACOCK John	University of Edinburgh Royal Observatory EDINBURGH EH9 3HJ UNITED KINGDOM
PEEBLES Jim	Princeton University Dept of Physics PRINCETON NJ 08544 USA
PEOPLES John	FERMILAB Dept of Physics BATAVIA IL 60510 USA
PICHON Christophe	Observatoire de Paris-Meudon Service d'Astrophysique F- 92195 MEUDON PRINCIPAL Cedex FRANCE
PINEAU DES FORETS Guillaume	Observatoire de Paris-Meudon Service d'Astrophysique F- 92195 MEUDON PRINCIPAL Cedex FRANCE
PISANI Armando	SISSA-ISAS Strada Costeria 11 I- 34014 TRIESTE ITALY
PLIONIS Manolis	SISSA-ISAS Strada Costeria 11 I- 34014 TRIESTE ITALY
PONS-BORDERIA Maria Jesus	NORDITA Nordisk Inst. für Teor. Atomfysik DK- 2100 COPENHAGEN O DENMARK
PORTILLA Miguel	Universidad de Valencia Fac. de Ciencias Fisicas E- BURJASOT Valencia SPAIN

PROKOPEC Tomislav	Brown University Dept of Physics PROVIDENCE RI 02912 USA
PROVENZALE Antonello	CNR Istituto di Cosmo-Geofisica I- 10133 TORINO ITALY
PUY Denis	Observatoire de Paris-Meudon Service d'Astrophysique F- 92195 MEUDON PRINCIPAL Cedex FRANCE
RADFORD Simon	I.R.A.M. 300, rue de la Piscine F- 38406 SAINT MARTIN D'HERES FRANCE
RHIE Sun Hong	University of California Lawrence Livermore Nat. Lab. LIVERMORE CA 94550 USA
RIEUTORD Michel	Observatoire de Toulouse 14 avenue E. Belin F- 31400 TOULOUSE FRANCE
ROCCA-VOLMERANGE Brigitte	Institut d'Astrophysique de Paris 98 bis Boulevard Arago F- 75014 PARIS FRANCE
ROUSSET André	Aerosptatiale F- 75781 PARIS Cedex 16 FRANCE
SADAT Rachida	Observatoire d'Alger C.R.A.A.G. BOUZAREAH ALGERIA
SCARAMELLA Roberto	Osservatorio Astronomico di Roma Via Dell'Osservatorio, 5 I- 00040 MONTEPORZIO CATONE ITALY
SCHAEFER Robert	University of Delaware Bartol Research Foundation NEWARK DE 19716 USA
SCHAEFFER Richard	CEN Saclay DPhT F- 91191 GIF sur YVETTE Cedex FRANCE

SCHRAMM David	University of Chicago Dept of Astronomy and Astrophysics CHICAGO IL 60637 USA
SIRONI Giorgio	Universita di Milano Istituto di Fisica I- 20133 MILANO ITALY
SMOOT George	University of California Lawrence Livermore Nat. Lab. LIVERMORE CA 94550 USA
SPIRO Michel	CEN Saclay DPhPE F- 91191 GIF sur YVETTE Cedex FRANCE
STEIGMAN Gary	Ohio State University High Energy Physics Lab. COLUMBUS OH 43210 USA
TANVIR Nial	University of Durham Dept of Physics DURHAM DH1 3LE UNITED KINGDOM
TAVKHELIDZE Albert	Academy of Sciences of Georgian SSR Institut of Physics 380008 TBILISI U S S R
TERASAWA Nobuo	Institut of Physical and Chemical Res. 2-1 Hirosawa 351-01 SAITAMA JAPAN
TRAN THANH VAN Jean	Université Paris Sud LPTHE F- 91405 ORSAY Cedex FRANCE
TREYER Marie Agnès	Observatoire de Paris-Meudon Service d'Astrophysique F- 92195 MEUDON PRINCIPAL Cedex FRANCE
TRIAY Roland	CNRS Centre de Physique Théorique F- 13288 MARSEILLE Cedex 9 FRANCE
TRINH XUAN Thuan	University of Virginia Dept of Physics CHARLOTTESVILLE VA 22901 USA

VAN DE WEYGAERT Rien	Sterrewacht Leiden Dept of Astrophysics NL- 2300 RA LEIDEN NETHERLANDS
VAN HAARLEM Michiel	Sterrewacht Leiden Dept of Astrophysics NL- 2300 RA LEIDEN NETHERLANDS
VAN KAMPEN Eelco	Sterrewacht Leiden Dept of Astrophysics NL- 2300 RA LEIDEN NETHERLANDS
VIDAL-MADJAR Alfred	Institut d'Astrophysique de Paris 98 bis Boulevard Arago F- 75014 PARIS FRANCE
VITTORIO Nicola	Univ. degli Studi di l'Aquila Dipart. di Fisica I- 67100 L'AQUILA ITALY
VON LINDE Joachim	Hamburger Sternwarte Bergedorf Gojenbersweg 112 D- 2050 HAMBURG 80 FEDERAL REP. OF GERMANY
WATSON Robert A.	Nuffield Radio Astronomy Labs Jodrell Bank MACCLESFIELD SK11 9DL UNITED KINGDOM
WHITE Simon	University of Arizona Steward Observatory TUCSON AZ 85721 USA
WIERINGA Mark	Sterrewacht Leiden Dept of Astrophysics NL- 2300 RA LEIDEN NETHERLANDS
WILKINSON David	Princeton University Dept of Physics PRINCETON NJ 08544 USA
WILLIAMS Brian	University of Edinburgh Royal Observatory EDINBURGH EH9 3HJ UNITED KINGDOM
WILSON Robert	AT & T Bell Laboratories Crawford Hill Lab. HOLMEDEL NJ 07733 USA

WITT Hans-Jörg	Hamburger Sternwarte Bergedorf Gojenbersweg 112 D- 2050 HAMBURG 80 FEDERAL REP. OF GERMANY
YEE Howard K. C.	Université of Toronto Dept. of Astronomy Toronto Ontario M5S 1A7 CANADA
YEPES Gustavo	Universidad Autonoma de Madrid Depto de Fisica Teorica - Mod C-XI E- 28 049 MADRID SPAIN